GEOLOGICAL SURVEY OF CANADA
COMMISSION GÉOLOGIQUE DU CANADA

**PAPER/ÉTUDE
91-1E**

CURRENT RESEARCH, PART E

RECHERCHES EN COURS, PARTIE E

1991

Energy, Mines and Resources Canada
Énergie, Mines et Ressources Canada

THE ENERGY OF OUR RESOURCES - THE POWER OF OUR IDEAS

L'ÉNERGIE DE NOS RESSOURCES - NOT

NOTICE TO LIBRARIANS AND INDEXERS

The Geological Survey's Current Research series contains many reports comparable in scope and subject matter to those appearing in scientific journals and other serials. Most contributions to Current Research include an abstract and bibliographic citation. It is hoped that these will assist you in cataloguing and indexing these reports and that this will result in a still wider dissemination of the results of the Geological Survey's research activities.

AVIS AUX BIBLIOTHÉCAIRES ET PRÉPARATEURS D'INDEX

La série Recherches en cours de la Commission géologique contient plusieurs rapports dont la portée et la nature sont comparables à ceux qui paraissent dans les revues scientifiques et autres périodiques. La plupart des articles publiés dans Recherches en cours sont accompagnés d'un résumé et d'une bibliographie, ce qui vous permettra, on l'espère, de cataloguer et d'indexer ces rapports, d'où une meilleure diffusion des résultats de recherche de la Commission géologique.

GEOLOGICAL SURVEY OF CANADA
COMMISSION GÉOLOGIQUE DU CANADA

PAPER / ÉTUDE
91-1E

CURRENT RESEARCH, PART E
RECHERCHES EN COURS, PARTIE E

Includes/comprend:

Cordillera and Pacific Margin
Cordillère et marge du Pacifique

Interior Plains and Arctic Canada
Plaines intérieures et région arctique du Canada

Canadian Shield
Bouclier canadien

Eastern Canada and National and General Programs
Est du Canada et programmes nationaux et généraux

1991

Available in Canada through

authorized bookstore agents and other bookstores

or by mail from

Canada Communication Group — Publishing
Ottawa, Canada K1A 0S9

and from

Geological Survey of Canada offices:

601 Booth Street
Ottawa, Canada K1A 0E8

3303-33rd Street N.W.,
Calgary, Alberta T2L 2A7

100 West Pender Street,
Vancouver, B.C. V6B 1R8

A deposit copy of this publication is also available for reference in public libraries across Canada

Cat. No. M44-91/1E
ISBN 0-660-56535-8

Price subject to change without notice

Cover photo

Slope failures in high ice content deposits at Hot Weather Creek, Ellesmere Island. Photo by D.A. Hodgson.

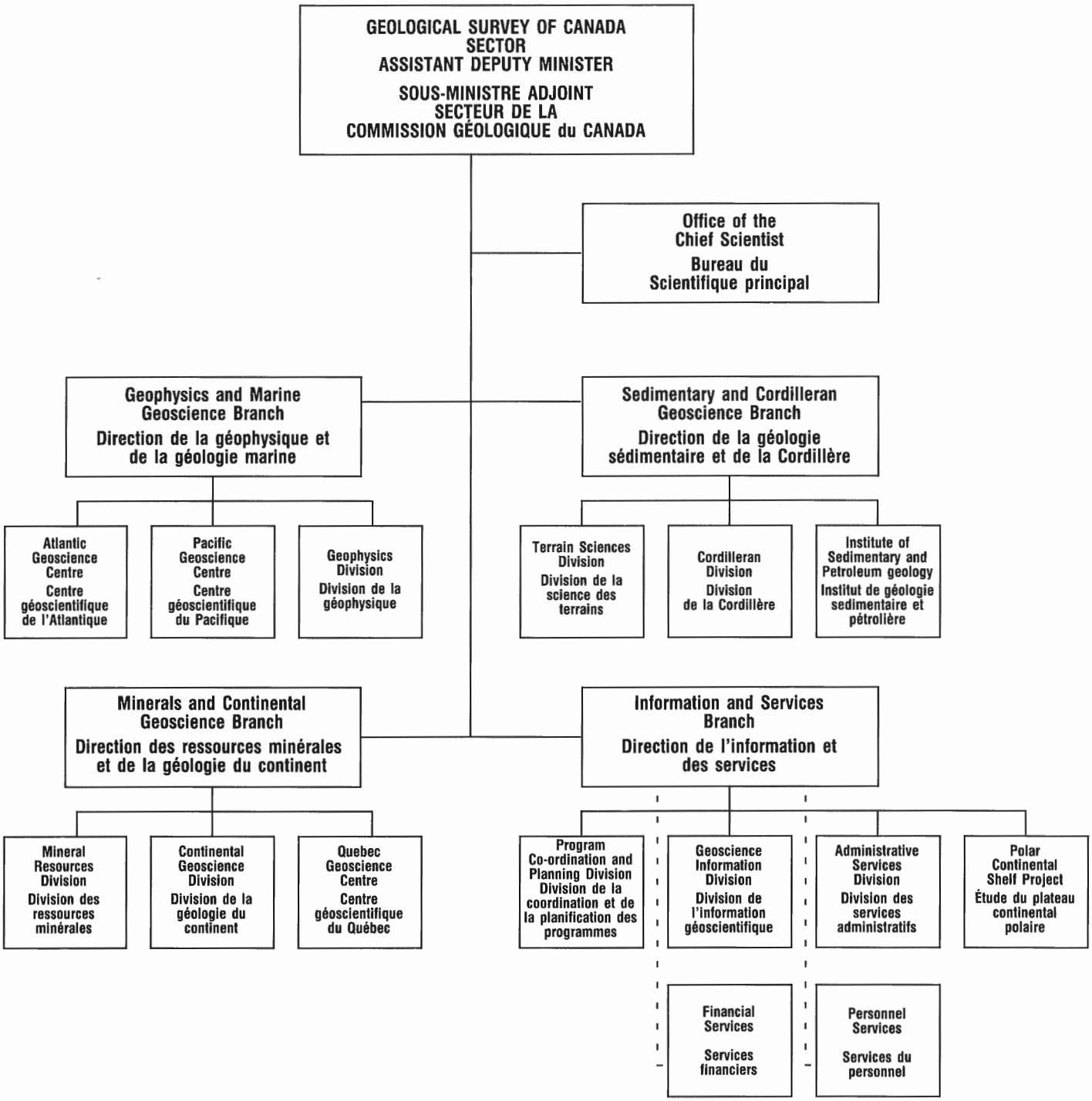
GEOLOGICAL SURVEY OF CANADA
SECTOR
ASSISTANT DEPUTY MINISTER
SOUS-MINISTRE ADJOINT
SECTEUR DE LA
COMMISSION GÉOLOGIQUE du CANADA
Office of the
Chief Scientist
Bureau du
Scientifique principal
Geophysics and Marine
Geoscience Branch
Direction de la géophysique et
de la géologie marine
Sedimentary and Cordilleran
Geoscience Branch
Direction de la géologie
sédimentaire et de la Cordillère
Atlantic
Geoscience
Centre
Centre
géoscientifique
de l'Atlantique
Pacific
Geoscience
Centre
Centre
géoscientifique
du Pacifique
Geophysics
Division
Division de la
géophysique
Terrain Sciences
Division
Division de la
science des
terrains
Cordilleran
Division
Division
de la Cordillère
Institute of
Sedimentary and
Petroleum geology
Institut de géologie
sedimentaire et
pétrolière
Minerals and Continental
Geoscience Branch
Direction des ressources minérales
et de la géologie du continent
Information and Services
Branch
Direction de l'information et
des services
Mineral
Resources
Division
Division des
ressources
minérales
Continental
Geoscience
Division
Division de la
géologie du
continent
Quebec
Geoscience
Centre
Centre
géoscientifique
du Québec
Program
Co-ordination and
Planning Division
Division de la
coordination et de
la planification des
programmes
Geoscience
Information
Division
Division de
l'information
géoscientifique
Administrative
Services
Division
Division des
services
administratifs
Polar
Continental
Shelf Project
Étude du plateau
continental
polaire
Financial
Services
Services
financiers
Personnel
Services
Services du
personnel

Separates

A limited number of separates of the papers that appear in this volume are available by direct request to the individual authors. The addresses of the Geological Survey of Canada offices follow:

601 Booth Street
OTTAWA, Ontario
K1A 0E8
(FAX: 613-996-9990)

Institute of Sedimentary and Petroleum Geology
3303-33rd Street N.W.
CALGARY, Alberta
T2L 2A7
(FAX: 403-292-5377)

Cordilleran Division
100 West Pender Street
VANCOUVER, B.C.
V6B 1R8
(FAX: 604-666-1124)

Pacific Geoscience Centre
P.O. Box 6000
9860 Saanich Road
SIDNEY, B.C.
V8L 4B2
(Fax: 604-363-6565)

Atlantic Geoscience Centre
Bedford Institute of Oceanography
P.O. Box 1006
DARTMOUTH, N.S.
B2Y 4A2
(FAX: 902-426-2256)

Québec Geoscience Centre
2700, rue Einstein
C.P. 7500
Ste-Foy (Québec)
G1V 4C7
(FAX: 418-654-2615)

When no location accompanies an author's name in the title of a paper, the Ottawa address should be used.

Tirés à part

On peut obtenir un nombre limité de «tirés à part» des articles qui paraissent dans cette publication en s'adressant directement à chaque auteur. Les adresses des différents bureaux de la Commission géologique du Canada sont les suivantes:

601, rue Booth
OTTAWA, Ontario
K1A 0E8
(facsimilé : 613-996-9990)

Institut de géologie sédimentaire et pétrolière
3303-33rd St. N.W.,
CALGARY, Alberta
T2L 2A7
(facsimilé : 403-292-5377)

Division de la Cordillère
100 West Pender Street
VANCOUVER, British Columbia
V6B 1R8
(facsimilé : 604-666-1124)

Centre géoscientifique du Pacifique
P.O. Box 6000
9860 Saanich Road
SIDNEY, British Columbia
V8L 4B2
(facsimilé : 604-363-6565)

Centre géoscientifique de l'Atlantique
Institut océanographique Bedford
B.P. 1006
DARTMOUTH, Nova Scotia
B2Y 4A2
(facsimilé : 902-426-2256)

Centre géoscientifique de Québec
2700, rue Einstein
C.P. 7500
Ste-Foy (Québec)
G1V 4C7
(facsimilé : 418-654-2615)

Lorsque l'adresse de l'auteur ne figure pas sous le titre d'un document, on doit alors utiliser l'adresse d'Ottawa.

CONTENTS

CORDILLERA AND PACIFIC MARGIN
CORDILLÈRE ET MARGE DU PACIFIQUE

INTERIOR PLAINS AND ARCTIC CANADA
PLAINES INTÉRIEURES ET RÉGION ARCTIQUE DU CANADA

CANADIAN SHIELD
BOUCLIER CANADIEN

EASTERN CANADA AND NATIONAL AND GENERAL PROGRAMS
EST DU CANADA ET PROGRAMMES NATIONAUX ET GÉNÉRAUX

Cordillera and Pacific Margin
Cordillère et marge du Pacifique

New placer gold anomalies in the northern Liard Range – southern Ram Plateau area, South Nahanni River region, District of Mackenzie, Northwest Territories[1]

C.W. Jefferson and D. Paré[2]
Mineral Resources Division

Jefferson, C.W. and Paré, D., 1991: New placer gold anomalies in the northern Liard Range – southern Ram Plateau area, South Nahanni River region, District of Mackenzie, Northwest Territories; in Current Research, Part E; Geological Survey of Canada, Paper 91-1E, p. 1-4.

Abstract

About 450 bulk stream silt samples were collected from 1985 to 1987 for a resource assessment of proposed extensions of the Nahanni National Park Reserve. For the study reported here, 211 of these samples were passed on a water-fed concentrating table to recuperate heavy mineral concentrates (HMCs) for neutron activation analysis. Results were compared with previous analyses of standard stream silts and HMCs prepared from sandy gravels taken at the same sites. The HMCs from silts confirmed a gold anomaly at Wretched Creek which had been identified by the HMCs from sandy gravels but missed by standard silt samples. The HMCs from silts also identified 6 new placer gold anomalies: Jackfish River, Windy Creek in Liard Range, a small tributary to Nahanni River at the south end of Nahanni Karst, and 3 tributaries in Ram Plateau. Base metal values from the two different sets of HMCs parallel those of the standard silt samples and spring waters.

Résumé

Environ 450 échantillons de silt fluviatile en vrac ont été prélevés de 1985 à 1987 pour une évaluation des ressources des prolongements proposés pour la réserve du parc national de Nahanni. Dans la présente étude, 211 de ces échantillons ont été passés à la table de concentration alimentée à l'eau pour en récupérer des concentrés de minéraux lourds destinés à des analyses par activation neutronique. Les résultats ont été comparés à des analyses antérieures de silts fluviatiles ordinaires et des concentrés de minéraux lourds préparés à partir de graviers sablonneux prélevés aux mêmes endroits. Les concentrés de minéraux lourds provenant des silts ont confirmé la présence d'une anomalie aurifère au ruisseau Wretched, laquelle a été indiquée par les concentrés de minéraux lourds provenant des graviers sablonneux, mais ne l'a pas été par les échantillons de silt ordinaire. Les concentrés de minéraux lourds provenant des silts ont aussi indiqué 6 nouvelles anomalies d'or alluvionnaire: la rivière Jackfish, le ruisseau Windy dans le chaînon Liard, un petit affluent de la Nahanni à l'extrémité sud du karst de Nahanni, et 3 affluents sur le plateau Ram. Les concentrations de métaux communs des deux différents ensembles de concentrés de minéraux lourds se comparent à celles des échantillons de silt ordinaire et des eaux de source.

[1] Canada-Northwest Territories Mineral Development Agreement 1987-1991. Project C1.2.3, Nahanni Tungsten and Rare Metals Corridor, carried by GSC; Supply and Services Canada Unsolicited Proposal No. C7-050; GSC Contract No. 232233-8-1919/01-SZ.

[2] Consorminex Inc., 11-1695, rue Atmec, Gatineau (Québec) J8P 7G7

OBJECTIVES

This project was designed to further document the occurrence of tungsten, gold and other metals in the South Nahanni River area, and to experiment with sampling techniques for exploration geochemistry by analyzing heavy mineral concentrates (HMCs) from bulk, silt-sized, stream-sediment samples. Preparation of HMCs was to be contracted out. This project was designed to enhance the mineral resource assessment of proposed extensions to the Nahanni National Park Reserve (Spirito et al., 1988; Hamilton et al., 1988; Scoates et al., 1986) and contribute to a metallogenic transect across the southern Mackenzie Mountains.

METHOD

During 1985 to 1987 field work for the mineral resource assessment of South Nahanni region (Spirito et al., 1988), about 450 large samples of stream silt (1.5-3 kg) were collected in addition to sieved (<1 cm) sandy gravels (1.5-3 kg) for preparation of HMCs. For the resource assessment, small splits of the silt samples were routinely analyzed for a large suite of elements by ICP and neutron activation, and the <850μmportions of the gravels were passed on a Deister concentrating table (Stewart, 1986) to prepare HMCs. This project used the remaining large splits of the silt samples to test two techniques: a) the efficiency and effectiveness of the Deister concentrating table in preparing HMCs from large silt samples; and b) the comparability of geochemical results from silt HMCs, standard 30 g silt samples and sieved-gravel HMCs. If the results were favourable, a new exploration technology would have been developed, making it possible to sample stream sediments for heavy minerals and standard silt samples in one, less expensive step.

The size of this project was increased due to two factors: a) On-going preparations of HMCs from stream gravels for the resource assessment showed great success at separating

Table 1. Comparison of gold from silt HMCs with gold from standard silt samples and from sandy gravel HMCs, eastern Nahanni Karst (Ram Plateau) and northeastern Tlogotsho Plateau (northern Liard Range). The net ppb Au in silt HMCs and sandy gravel HMCs is a calculated[4,6] value which combines weights of separated gold flakes (determined by J.C. Bisson on a Perkins-Elmer ultramicrobalance with AD-6 autobalance, giving precisions of +/-0.0005 mg on samples of <2 mg and +/-0.001 mg on samples up to 20 mg.) with the ppbs of gold determined by neutron activation of the remaining HMC. Gold in silts was determined by neutron activation of whole standard samples[5].

Creek/ River	Sample Number	Silt (g)[1]	Silt HMC (g)[2]	Au flakes #	Au flakes (mg)	Silt HMC Au (ppb)[3]	Net ppb Au in three media: silt-HMC[4]	silt[5]	gravel-HMC[6]
Wretched	6237	2575	27.00	1	0.0409	360	1,875	<5	77,000
Wretched	6239	2100	20.75	2	0.0411	<5	1,981	<5	<5
Tetcela	6242	2000	14.25	7	0.4741	180	33,450	<5	22
Tetcela	6243	1800	24.05	6	0.0528*	<5	2,195*	<5	<11
Windy	6244	2775	20.80	17	0.1641*	330	8,219*	<5	<5
Jackfish	6249	2100	27.95	11	0.1785	705	7,091	<5	7
N. Yohin	6273	2275	16.90	0	0.0	<5	<5	<5	31,000*
Ram	6276	3300	13.35	3	0.3328	<5	24,929	<5	<5
Wretched	7065	2550	11.80	0	0.0	<16	<16	<5	4,750*
Wretched	7066	3025	11.25	0	0.0	N/A	N/A	<5	41,400*

[1] weight of standard silt (<80 mesh = <177μm) bulk sample.
[2] weight of heavy mineral concentrate (HMC) made on Deister concentrating table from silt.
[3] determined by neutron activation on sample from which gold flakes have been removed.
[4] calculated ppb: [ppb by NAA] + 10^6[weight of gold flakes (mg) / weight of silt HMC (g)].
[5] ppb by neutron activation analysis of 30 g split of whole standard silt (<80 mesh) from stream.
[6] calculated ppb: [ppb by NAA] + 10^6[weight of gold flakes (mg) / weight of gravel HMC (g)]. Gravel HMC made on table from <850μm split of bulk sandy gravel sample.
* minimum value, because one or more grains of gold were lost before or during weighing.

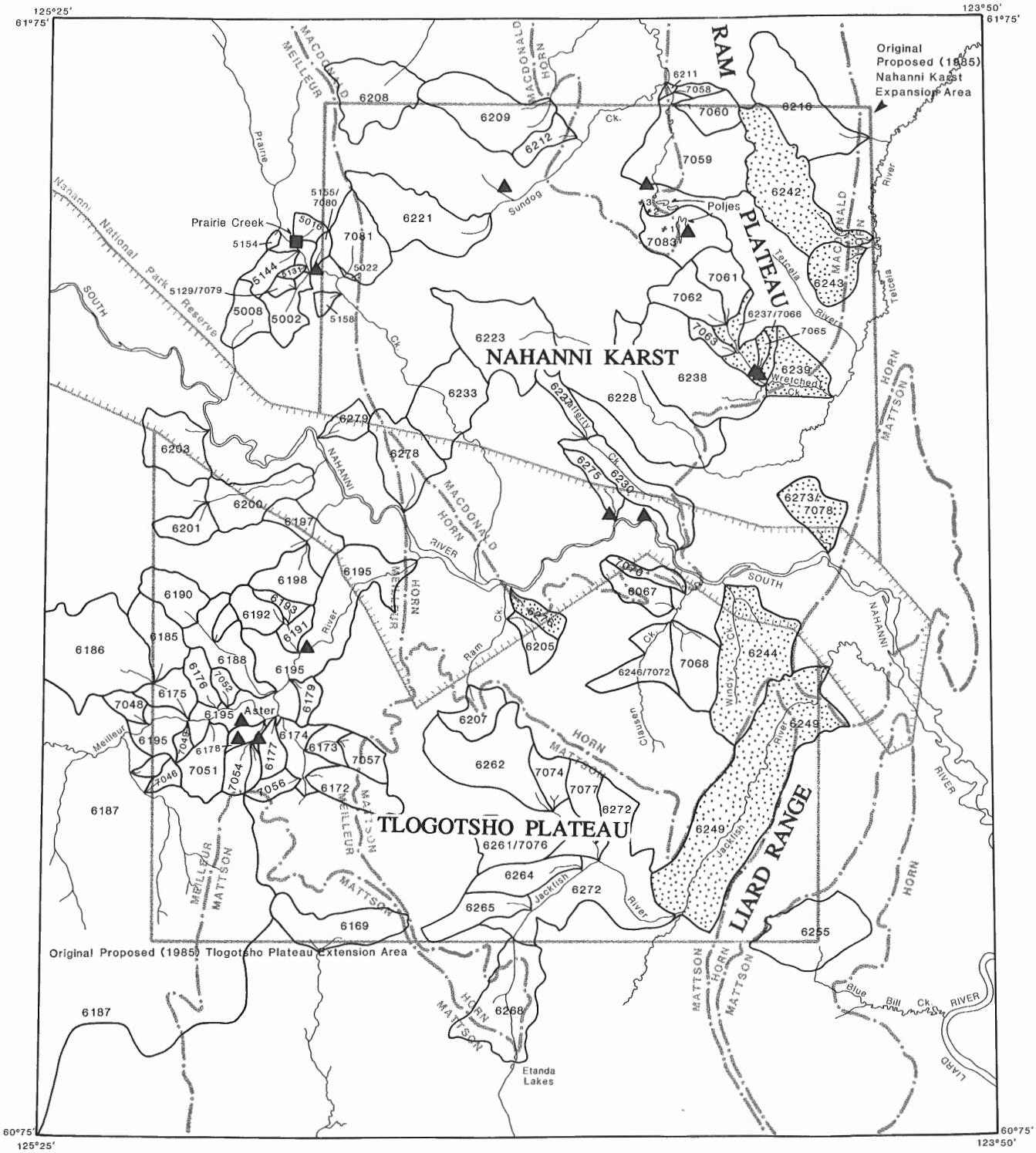

Figure 1. Locations of catchment basins (numbered polygons outlined by solid lines) which are anomalous in one or more elements in the eastern part of the South Nahanni River resource assessment region. Dotted polygons are those which yielded anomalous amounts of placer gold (Table 1) in heavy mineral concentrates made from stream sediment samples. Faint background lines and text outline the Nahanni National Park Reserve, earlier proposed park extensions, and various geological domains: HORN = Devonian and younger shales, MACDONALD = platformal carbonates, MATTSON = Mesozoic sandstones; MEILLEUR = Ordovician to Devonian shales of Selwyn Basin. Solid triangles indicate spring waters with anomalous zinc and associated metals; 3.7 ppt (above background) gold at Wretched Creek (Hamilton et al.; 1988, Hamilton, 1990). Solid square shows location of adit for Prairie Creek Ag-Pb-Zn vein.

free gold grains (up to 33 per sample and as small as 10μm) on a Deister concentrating table equipped with a black deck. Most of the gold grains were captured in a petri dish at the table and were not included in the HMCs sent for neutron activation. These grains were measured (most were flakes in the order of 100-300μm in diameter) and weighed (Table 1). A South American conical gold pan (batea) was used to immediately confirm the presence of very fine gold grains (>10μm) in the tabled HMC. Highly anomalous gold (calculated 30 000 ppb Au in HMC from gravel) was thus documented before neutron activation analysis in one stream of Ram Plateau, informally named Wretched creek for its rugged topography. Subsequent neutron activation analyses of a series of samples from which free gold had been removed yielded very low gold abundances, indicating that initial preparation of HMCs on the Deister table gave immediate results which were as useful for gold as the final neutron activation analyses (Table 1). Final analyses of standard silt samples and gravel HMCs were still useful for base metals and for accessory elements which helped to interpret the gold values. b) Consorminex Inc., which had been preparing the gravel HMCs, offered a proposal to the Department of Supply and Services Canada (DSS) to develop and test technology to extract HMCs from fine grained stream sediment samples in the same region. DSS supported the proposal, as did GSC through this project. A total of 211 HMCs were then prepared from the silt samples. With 26 standards and duplicates, the silt HMCs were analyzed by neutron activation for gold and 33 other elements.

Gravity table HMCs from 53 silt and 53 gravel samples from the same sites were further concentrated using methylene iodide (3.3 s.g.), thereby ensuring that virtually no minerals with densities <3.3 were left in the concentrate. Small splits (<.05g) obtained by coning and quartering were mounted in Araldite on 1" x 2" glass slides, so that the slides could be readily polished and would be compatible with microprobe and SEM stages. Relative percentages of heavy minerals were determined by counting 300 grains under a binocular microscope. The computer program used to enter the data was designed for 50 classes. Comparisons for this paper were made by visual scanning of the data. Rigorous statistical comparisons among the geochemical and mineralogical data sets from the three different sample media are in progress.

RESULTS

The HMCs from silt samples confirmed gold anomalies which had been identified using gravel HMCs (Spirito et al., 1988), and indicated 6 new highly anomalous placer gold localities: Jackfish River, Windy Creek in Liard Range, a small tributary of Nahanni River at the south end of Nahanni Karst, and 3 tributaries of Tetcela River in Ram Plateau (Fig. 1, Table 1).

All but one of these new localities are aligned north-south on a trend that appears to be independent of the distribution of glacial deposits. For example, sample 6238 from a tributary entering Wretched creek very close to sample 6237, and other streams such as Tetcela River and sample 6216 along the same belt revealed no gold despite very similar sediment compositions. Nevertheless, the possibility of gold concentration during deposition of exotic debris along a melting ice front cannot be discounted. Each auriferous locality coincides with an intersection of northerly and northwesterly trending faults. The provenance of this placer gold is being investigated in the resource appraisal. Inspection also shows that zinc values from silt HMCs parallel those from sieved-gravel HMCs. Informal discussions with Parks Canada officials have resulted in revision of proposed park boundaries to exclude the gold-bearing stream basins, as part of the on-going mineral and energy resource appraisal process (cf. Scoates et al., 1986).

ACKNOWLEDGMENTS

The above sample collection and processing could not have been accomplished without the assistance of W.A. Spirito who is preparing an M.Sc. thesis on spatial analysis and stream sediment geochemistry in the South Nahanni River area (Spirito et al., 1988). Polar Continental Shelf Project provided helicopter support for field work. B. Cooke and other staff of Consorminex Inc. provided invaluable assistance in the laboratory. S.B. Ballantyne and Y.T. Maurice provided advice on sampling techniques and on the design of the proposal. P.W.B. Friske and R.N.W. DiLabio co-supported the unsolicited proposal at GSC, making it possible for DSS to add its support. R.N.W. DiLabio critically reviewed this report.

REFERENCES

Hamilton, S.M.
1990: The application of spring water geochemistry and hydrogeology to a non-renewable resource assessment of the South Nahanni River area, NWT; M.Sc. thesis, Carleton University, Ottawa, 169 p.

Hamilton, S.M., Michel, F.A., and Jefferson, C.W.
1988: Groundwater geochemistry, South Nahanni resource assessment, District of Mackenzie; in Current Research, Part E; Geological Survey of Canada, Paper 88-1E, p. 127-136.

Scoates, R.F.J., Jefferson, C.W., and Findlay, D.C.
1986: Northern Canada mineral resource assessment; in Prospects for Mineral Resource Assessment on Public Lands: Proceedings of the Leesburg Workshop, (ed.) S.M. Cargill and S.B. Green; United States Geological Survey, Circular 980, p. 111-139.

Spirito, W.A., Jefferson, C.W., and Paré, D.
1988: Comparison of gold, tungsten and zinc in stream silts and heavy mineral concentrates, South Nahanni resource assessment area, District of Mackenzie; in Current Research, Part E; Geological Survey of Canada, Paper 88-1E, p. 117-126.

Stewart, R.A.
1986: Routine heavy mineral analysis using a concentrating table; Journal of Sedimentary Petrology, v. 56, p. 555-556.

Compressional and dextral motion along the Chatter Creek Fault, Main Ranges, British Columbia

Stephen E. Grasby[1] and Eric W. Mountjoy[1]
Institute of Sedimentary and Petroleum Geology, Calgary

Grasby, S.E. and Mountjoy, E.W., 1991: Compressional and dextral motion along the Chatter Creek Fault, Main Ranges, British Columbia; in Current Research, Part E; Geological Survey of Canada, Paper 91-1E, p. 5-11.

Abstract

The Chatter Creek Fault was examined in two areas west of Mallard Peak, immediately northwest of the Whirlpool River. Two phases of deformation occurred in this region; an early phase responsible for low-angle thrusting (D_1), and a second phase that folded these structures to produce major upright folds (D_2). The McGillivray Fault outcrops east of, and is cut by, the Chatter Creek Fault. The McGillivray Fault dips 20 to 30° southwest and may represent a minor splay from a D_2 thrust.

Slickensides and minor folds in the Chatter Creek fault zone, west of Mallard Peak, indicate two distinct stages of motion: 1) compressional, northeast-vergent; and 2) dextral. The relative timing of these two stages of motion is uncertain. The Chatter Creek Fault is likely a D_2 or later structure. A fold train, trending 20 to 35° more westerly than regional D_2 folds, may be related to dextral motion along the Chatter Creek Fault.

Résumé

La faille de Chatter Creek a été observée à deux endroits à l'ouest du pic Mallard, dans la région immédiate au nord-ouest de la rivière Whirlpool. À cet endroit, deux phases de déformation ont été notées : l'une précoce à l'origine du chevauchement à pendage faible (D_1) et l'autre qui a plissé les structures de la première pour former d'importants plis droits (D_2). La faille de McGillivray affleure à l'est de celle de Chatter Creek en plus d'être recoupée par cette dernière. Son pendage est de l'ordre de 20 à 30° vers le sud-ouest, ce qui signifie qu'on peut considérer cette structure comme une divergence mineure du chevauchement D_2.

Dans la zone de faille de Chatter Creek, à l'ouest du pic Mallard, les miroirs de faille et les plis mineurs permettent de distinguer deux étapes de mouvement : 1) une compression à direction nord-est et 2) un déplacement dextre. La relation de temps entre ces deux étapes de mouvement demeure incertaine. Il semble que la faille de Chatter Creek soit reliée à la phase D_2 ou à des événements plus tardifs. Une série de plis, dont l'orientation est de 20 à 35° plus à l'ouest que le plissement régional D_2, peut être associée au mouvement dextre le long de la faille de Chatter Creek.

[1] Department of Geological Sciences, McGill University, 3450 University St., Montreal, Quebec H3A 2A7

INTRODUCTION

The Chatter Creek Fault, and its equivalents, mark the boundary between the eastern and western Main Ranges of the southern Canadian Rocky Mountains. The Chatter Creek Fault was originally defined in the Rogers Pass map area by Wheeler (1963), as a nearly vertical fault that moved Lower Cambrian rocks on the west into juxtaposition with Middle Cambrian strata on the east. Cook (1975) suggested that the Chatter Creek Fault continues southward into the Martin Creek Fault, which eventually dies out just south of Kicking Horse Pass (lat. 51°15'N).

The Chatter Creek Fault can be traced north to the headwaters of the Fraser River and into the Moose Lake Thrust (McDonough and Simony 1988a; Dechesne and Mountjoy, 1990; McDonough and Mountjoy, 1990). Mountjoy and Forest (1986) and Mountjoy and Price (1989) have suggested that the Chatter Creek Fault at this latitude (52°30'N) accommodated shortening associated with the Fraser River Antiform and the Ptarmigan Creek thrust zone (see Fig. 1 for locations). However, Dechesne and Mountjoy (1988, 1990, in press) suggested that shortening on the Ptarmigan Creek thrust zone is too great to have been accommodated by the Chatter Creek Fault and, therefore, interpreted the Chatter Creek Fault as a late stage, out-of-sequence thrust.

Reported evidence of dextral oblique motion on thrust structures adjacent to the Southern Rocky Mountain Trench has been increasing (McDonough and Simony, 1988b; McDonough and Simony 1989). A north-trending splay of the Chatter Creek Fault, the Resplendant Fault, may dextrally offset the Mount Robson Syncline (Mountjoy 1964, 1980). Along strike 150 km, the Chatter Creek Fault can be traced into the Martin Creek Thrust (Price and Mountjoy, 1970), immediately to the east of which Cook (1975) observed dextral motion on the Cathedral-Stephen and Cataract Brook normal faults.

In the region studied, the trace of the Chatter Creek Fault follows valleys that are mostly covered by alluvium. The fault outcrops in only two areas between the headwaters of Hugh Allan Creek and Whirlpool River, immediately west of Mallard Peak (Fig. 1, 2). These areas were studied to help elucidate the true geometric and temporal relationships of the Chatter Creek Fault.

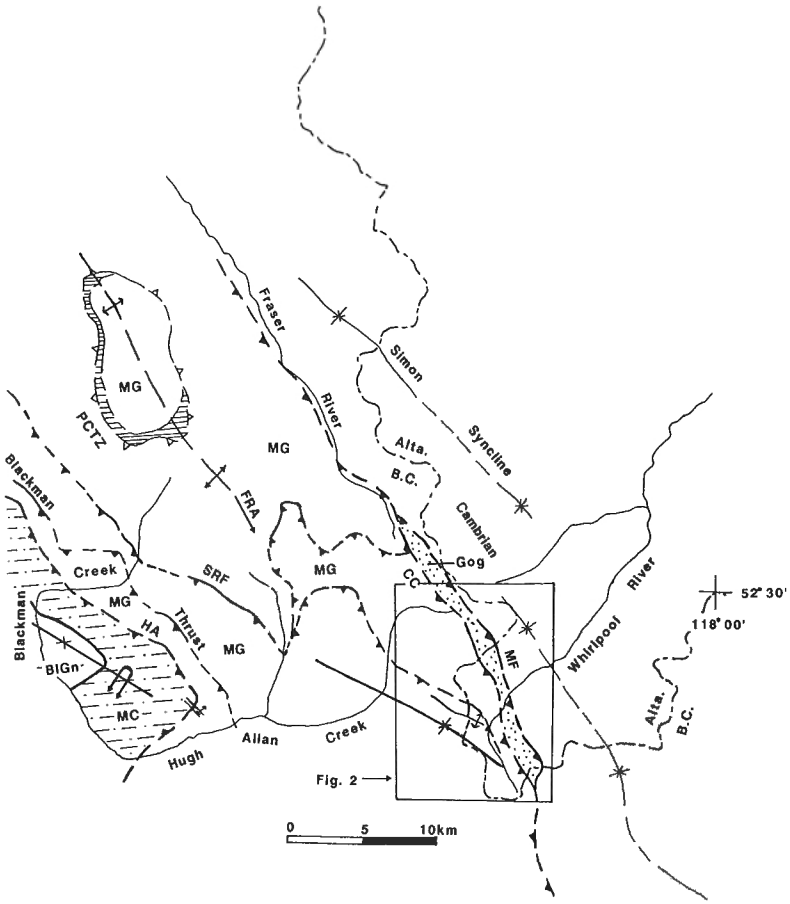

Figure 1. Simplified regional geological map of the southern Selwyn Range. BIGn = Blackman Gneiss, MC = Mica Creek Succession (McDonough and Murphy, 1990), HA = Hugh Allan Thrust, SRF = Selwyn Range Thrust, PCTZ = Ptarmigan Creek Thrust Zone, MG = Miette Group, CC = Chatter Creek Thrust, MF = McGillivray Fault, Cambrian = Cambrian undivided, Gog = Gog Group, FRA = Fraser River Antiform.

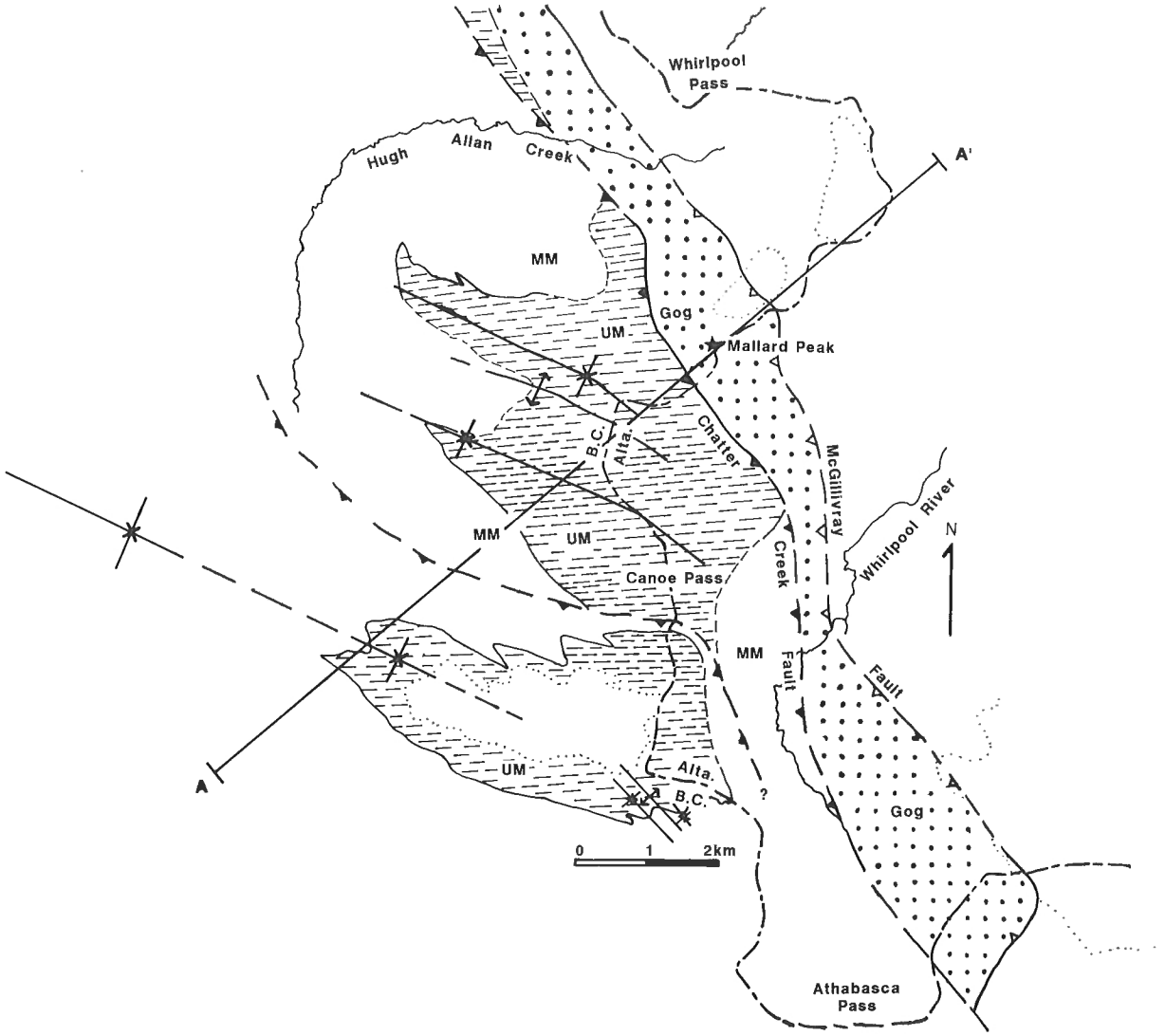

Figure 2. Geological map, between the headwaters of Hugh Allan Creek and Athabasca Pass. The Chatter Creek Fault is only exposed immediately west of Mallard Peak, at two localities. Gog = Gog Group, UM = upper Miette Group, MM = middle Miette Group.

REGIONAL GEOLOGY

Two main phases of deformation are recognized in the western Main Ranges near Jasper. The first phase (D_1)* is characterized by recumbent isoclinal folds, with an associated pervasive phyllitic to slaty cleavage subparallel to bedding. D_1 faults, as in the Ptarmigan Creek thrust zone in the Selwyn Range (Mountjoy and Forest, 1986), are low angle and commonly shear the limbs of associated folds. These early structures have been folded by later (D_2), open and upright, regional folds (Fraser River Antiform, Simon Syncline), and have an associated axial planar crenulation cleavage. A series of open, broad, regional-scale folds occurs near the headwaters of Whirlpool River. These folds are unique in that they trend to 295°, oblique to the regional trends of 330° in the southern Selwyn Range, and 315° in the eastern Main Ranges to the northeast (Fig. 1).

* West-verging structures earlier than D_1 have been noted by Mountjoy et al. (1985) and McDonough and Simony (1988b) in strata overlying the Blackman and Bulldog gneisses.

STRATIGRAPHY OF THE MALLARD PEAK AREA

Proterozoic upper Miette Group

The upper Miette Group consists of up to one kilometre of dark grey to black pelite, weathering grey to rusty brown, with abundant ripple laminated, light coloured silt layers

(millimetre- to centimetre-scale). A few beds of calcareous quartzite, up to one metre thick, occur in the upper part of the upper Miette Group and are more common at its base.

Lower Cambrian Gog Group

The Gog Group of the region is divided into three formations comprising (in ascending order): a coarse grained quartz sandstone unit (about 3000 m thick); a unit of light grey carbonate interbedded with shale and siltstone (about 165 m thick); and a fine grained, quartz sandstone unit (about 450 m thick) (Mountjoy and Price, 1989).

McNaughton Formation

McNaughton Formation strata are predominantly clean, white to pink quartzite with planar crossbedding. Composite beds are 10 to 30 cm thick, with scattered thin partings of green pelite (up to 5 cm thick). Clasts in the quartzite consist of green quartz, red quartz, and white quartzite in pebbles up to one centimetre long. Feldspar clasts are rare (<3%).

Mural Formation

The Mural Formation consists of massive, finely crystalline, grey, micritic limestone containing archaeocyathid and ollenellid fragments. Massive carbonates commonly occur at the top and bottom of the formation with silty to calcareous shale in the middle portion.

Middle Cambrian Snake Indian Formation

The Snake Indian Formation is a recessive weathering unit between the Gog Group and the overlying Eldon Formation. It consists of alternating resistant beds of grey argillaceous limestone, sandy dolomite, and recessive calcareous grey shale.

Figure 3. Photograph immediately southwest of Mallard Peak looking northwest at the Chatter Creek Fault (below arrow), placing upper Miette Group (left) against McNaughton Formation (right). White line marks bedding dipping steeply northeast.

STRUCTURE

Chatter Creek Fault

The Chatter Creek Fault juxtaposes Miette Group and lower Paleozoic to upper Proterozoic strata (mostly Gog Group) between Mount Robson and Wood River. Near Mallard Peak, the Chatter Creek Fault occupies a discrete zone, easily recognized by the juxtaposition of brown weathering upper Miette Group pelites and resistant Gog Group quartzites (forming a nearly vertical cliff face) (Fig. 3). Just north of Mallard Peak the vertical dip of the Chatter Creek Fault can be observed in a steep valley with over 500 m of vertical relief. In outcrop, the fault has produced a zone (up to one metre thick) of highly deformed upper Miette Group brown pelite and calcareous sandstone, with abundant chlorite- and carbonate-bearing quartz veins.

Two sets of folds (10 to 20 cm in amplitude) are observed within the Chatter Creek fault zone. One set is characterized by shear folds, defined by rotation of the vertical fault zone fabric on the long limbs, to horizontal on the short limbs, similar to the regional D_2 folds. A penetrative cleavage, in the fault zone and immediate footwall, is axial planar to these upright folds. The second set of folds are vertical (fold axes plunge at 90°), and show a dextral sense of shear. Overprinting of folds was not observed, so that their relative ages are uncertain and the folds may be coeval.

Footwall rocks contain a set of north-south trending vertical shear planes within 100 m of the Chatter Creek Fault. Spacing between shear planes decreases from 10 cm next to the fault zone, to 1 to 2 m away from the zone. These shear planes contain horizontal slickensides that consistently trend north-south, all showing steps in quartz fibers indicating dextral slip (Fig. 4). The spatial and angular relation of these shear planes with the strike of the Chatter Creek Fault (30°), suggest that they are R Riedel shears related to the dextral motion along the Chatter Creek Fault. Steeply dipping bedding planes near the fault contain slickensides with a similar orientation and sense of shear. Rare northeast trending slickensides occur on the bedding surfaces, indicating a top to the northeast compressional motion (Fig. 5).

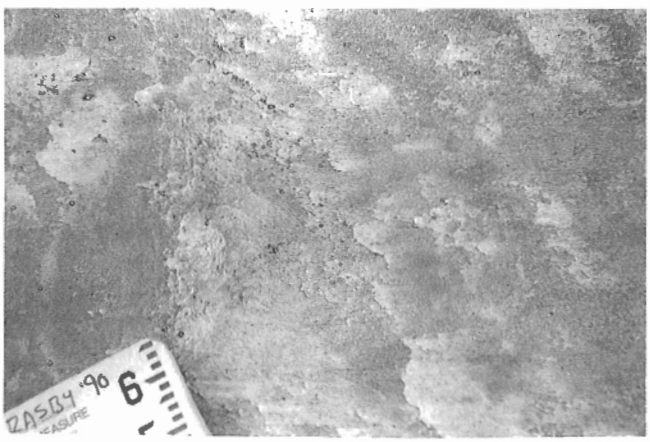

Figure 4. Looking east at a vertical joint surface with horizontal slickensides, indicating dextral offset.

McGillivray Fault

The McGillivray Fault outcrops immediately east of the Chatter Creek Fault (Fig. 2). It is a low-angle thrust (20-30°) displacing Gog Group quartzites over Middle Cambrian carbonate rocks at McGillivray Ridge, and at Mallard Peak along strike to the northwest. East of Mallard Peak the fault zone is covered, but immediately adjacent carbonate rocks of the Lower Cambrian Mural Formation are deformed into strongly developed, northeast-verging, recumbent folds with a pervasive axial planar cleavage. At Athabasca Pass, Shaw and Morton (1990) observed a 2 m thick, quartz-rich mylonite along the McGillivray Fault. They inferred that a series of west-dipping, hanging wall splays from the McGillivray Fault shear the thinned limbs of associated recumbent folds in the Gog Group quartzite. (Fig. 7 of Shaw and Morton, 1990). We did not see these relationships at Mallard Peak and the steeply dipping surfaces shown in Shaw and Morton's Figure 7 are apparently joints with little or no displacement at this locality, since bedding can be traced continuously across these structures at McGillivray Ridge.

Shaw and Morton (1990) interpreted the McGillivray Fault as a footwall splay of the Chatter Creek Fault. South of Athabasca Pass, the nearly vertical Chatter Creek Fault cuts the gently inclined McGillivray Fault at a high angle, making such a correlation unlikely (Fig. 2,6). The Chatter Creek Fault appears to be out of sequence with respect to the McGillivray Fault. There are no direct indications as to whether McGillivray Fault is a D_1 or D_2 structure.

Fold Train between Hugh Allan Creek and Whirlpool River

Broad, southeast-plunging, open folds between Hugh Allan Creek and Whirlpool River trend about 295°, compared to regional D_2 fold trends of 330° in the southern Selwyn Range and 315° in the eastern Main Ranges. This suggests that their origin is unrelated to the regional D_2 event, although no interference relationships were observed to support this interpretation. These folds are at an angle of about 35° to the trace of the more northerly part of the Chatter Creek Fault (Fig. 1).

DISCUSSION

Thrust displacement on the Chatter Creek Fault is approximately 3.5 km (Fig. 6). When this displacement is eliminated in a palinspastic restoration, the McGillivray Fault at Canoe Pass appears to connect with a fault that is correlated with another fault to the northwest (interpreted as a splay of the Selwyn Range Fault). The unnamed fault at Canoe Pass is associated with upright folds, consistent with D_2 structures in the western Main Ranges, suggesting that McGillivray Fault also may be a D_2 structure. The minimum displacements along the McGillivray and unnamed faults, near Mallard Peak, are about 1500 m (Fig. 6). The cutoffs of the McGillivray Fault, in the footwall of the Chatter Creek Fault, cannot be used to determine total dextral displacement, as Gog strata have been eroded in the hanging wall of the Chatter Creek Fault. If our correlation of the McGillivray Fault with the unnamed fault is correct, dextral motion on the Chatter Creek Fault would be minor, as the other two faults lie opposite each other on either side of the Chatter Creek Fault.

The near vertical dips on the Chatter Creek Fault constrain it to cut the gently dipping McGillivray Fault at a steep angle (Fig. 6), indicating that the Chatter Creek Fault is out of sequence relative to the McGillivray Fault. This crosscutting relationship indicates that the Chatter Creek Fault is at least a D_2 (or later) structure.

Two distinct phases of motion (compressional and dextral) are indicated by the two fold domains and slickensides in the Chatter Creek Fault zone; the relative timing of these phases is uncertain however. They could have developed at the same time, resulting from both dextral strike-slip and transpression along the Chatter Creek Fault. McDonough (1989) reported evidence of dextral motion along the Klapperhorn Thrust in the northern Selwyn Range (in about same structural position as the Chatter Creek Fault) that was late to post D_2. Therefore, the dextral motion on the Chatter Creek Fault in the Mallard Peak – Athabasca Pass area also may be the result of post-D_2 compression.

The fold train between Hugh Allan Creek and Whirlpool River does not appear to be related to the regional D_2 folds. The fold train's angular relationship with the Chatter Creek Fault is consistent with folds formed in a transpressional regime (Sanderson and Marchini, 1984), indicating that the folds may be related to dextral motion along the Chatter Creek Fault. The anomalous trends of the fold train are not likely to be related to paleobasin geometry, because they are

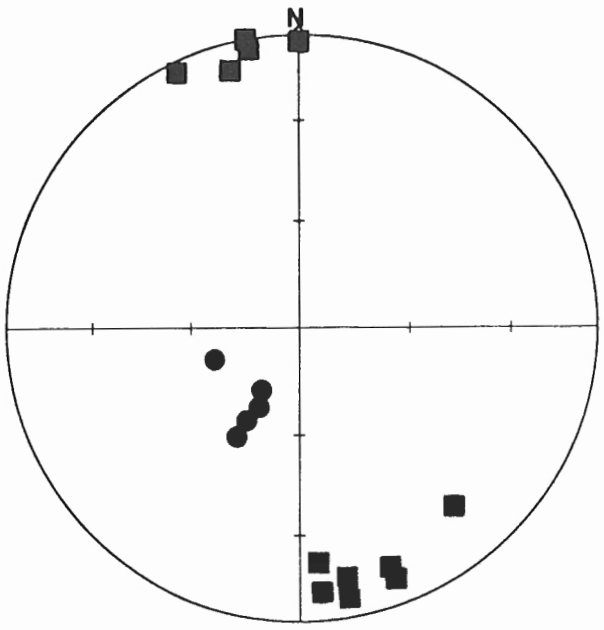

Figure 5. Equal area plot of slickensides in the immediate footwall of the Chatter Creek Fault, showing two distinct groupings. The subhorizontal slickenlines (squares) all show dextral offset. The steeply southwest dipping slickenlines (circles) all show top-to-the-east motion.

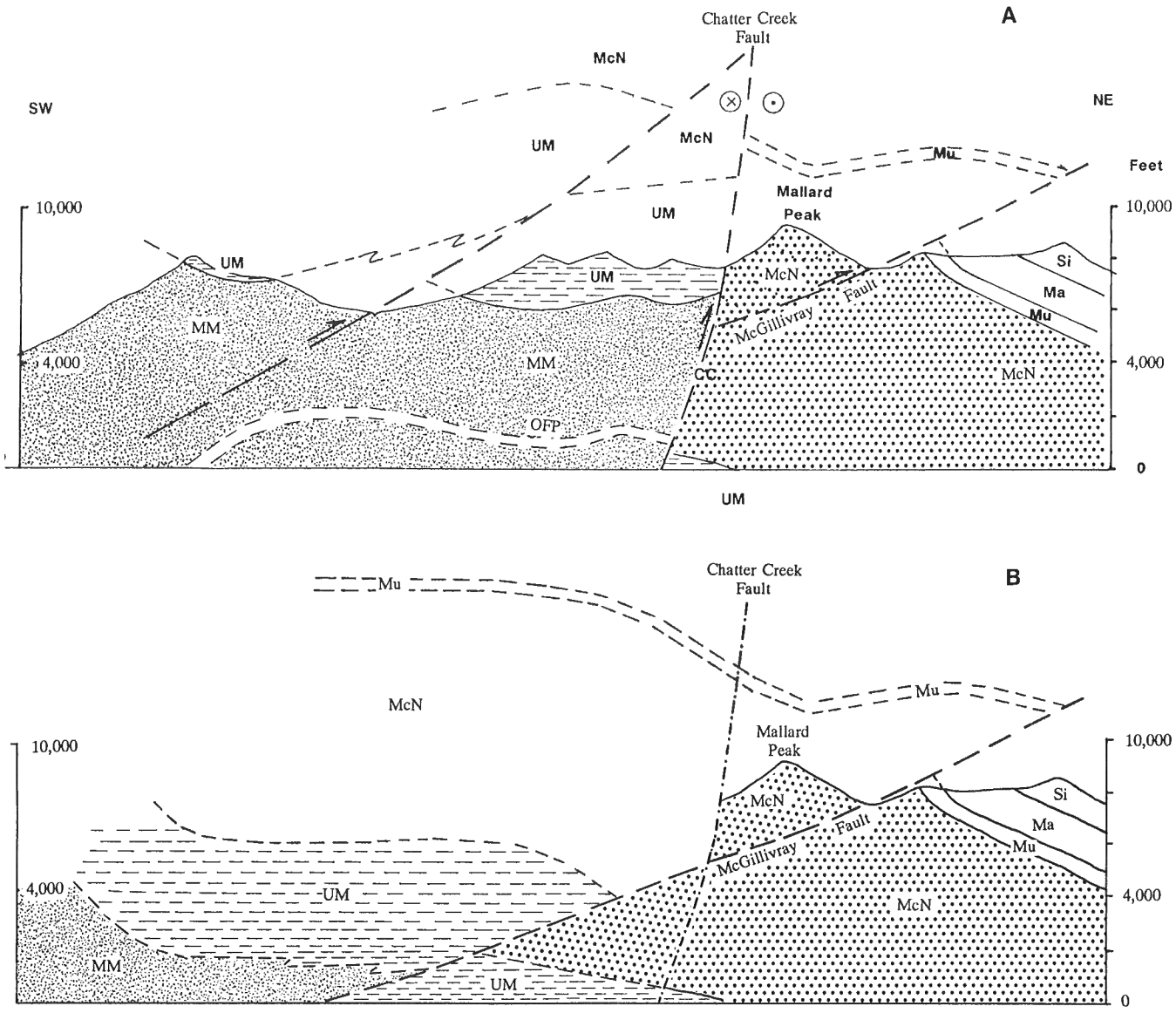

Figure 6. A. Structural cross-section through Mallard peak showing McGillivray Fault cut by the Chatter Creek Fault. **B.** Cross-section in A with vertical displacement on Chatter Creek Fault restored. CC = Chatter Creek Thrust, OFP = Old Fort Point Formation, MM = middle Miette Group, UM = upper Miette Group, McN = McNaughton Formation, Mu = Mural Formation, Ma = Mahto Formation, Si = Snake Indian Formation.

in an area where the Miette Group does not show marked changes in thickness and which is surrounded by regional folds consistently trending 20 to 35° more northerly.

ACKNOWLEDGMENTS

Financial support for this research comes from a contract with the Geological Survey of Canada in Calgary, EMR Research Agreement 90/4/250, and Mountjoy's NSERC grant (A2128). Amoco Canada's scholarship, awarded to S. Grasby, is gratefully acknowledged. We are grateful to Yellowhead Helicopters and Niki and Carl Forman for their service and expediting. T. Waller provided excellent field assistance. We appreciate the helpful comments on the manuscript by M. McMechan and M. McDonough.

REFERENCES

Cook, D.G.
1975: Structural style influenced by lithofacies, Rocky Mountain Main Ranges, Alberta – British Columbia; Geological Survey of Canada, Bulletin 233, 73 p.

Dechesne, R.G. and Mountjoy, E.W.
1988: Structural geology of part of the Main Ranges near Jasper, Alberta; in Current Research, Part E, Geological Survey of Canada, Paper 88-1E, p. 171-176.

1990: Geology of the Lucerne east-half map area, Rocky Mountain Main Ranges, Alberta and British Columbia; in Current Research, Part D, Geological Survey of Canada, Paper 90-1D, p. 95-100.
in press: Multiple décollements at deep levels of the southern Canadian Rocky Mountain Main Ranges, Alberta and British Columbia; in Structural Geology of Fold and Thrust Belts, edited by S. Mitra, Dave Elliott volume, Johns Hopkins University Press.

McDonough, M.R.
1989: The structural geology and strain history of the northern Selwyn Range, Rocky Mountains, near Valemount, British Columbia; Ph.D. thesis, University of Calgary, Calgary, Alberta, 290 p.

McDonough, M.R. and Mountjoy, E.W.
1990: Lucerne (west half), British Columbia (83 D/15); Geological Survey of Canada, Open File 2260, scale 1:50 000.

McDonough, M.R. and Murphy, D.C.
1990: Valemount, British Columbia (83 D/14); Geological Survey of Canada, Open File 2259; scale 1:50 000.

McDonough, M.R. and Simony, P.S.
1988a: Stratigraphy and structure of Late Proterozoic Miette Group, northern Selwyn Range, Rocky Mountains, British Columbia; in Current Research, Part D, Geological Survey of Canada, Paper 88-1D, p. 105-113.
1988b: Structural evolution of basement gneisses and Hadrynian cover, Bulldog Creek area, Rocky Mountains, British Columbia; Canadian Journal of Earth Science, v. 25, p. 1687-1702.
1989: Valemount strain zone: a dextral oblique-slip thrust system linking the Rocky Mountain and Omineca belts of the southeastern Canadian Cordillera; Geology, v. 17, p. 237-240.

Mountjoy, E.W.
1964: Geology, Mount Robson, Alberta – British Columbia; Geological Survey of Canada, Map 47-1963; scale 1 inch to 2 miles.
1980: Mount Robson, Alberta – British Columbia. Geological Survey of Canada, Map 1499A; scale 1:250 000.

Mountjoy, E.W. and Forest R.
1986: Revised structural interpretation, Selwyn Range between Ptarmigan and Hugh Allan creeks, British Columbia — an antiformal stack of thrusts; in Current Research, Part A, Geological Survey of Canada, Paper 86-1A, p. 177-183.

Mountjoy, E.W. and Price, R.A.
1989: Geology, Amethyst Lakes (83D/9); Geological Survey of Canada, Map 1657A; scale 1:50 000.

Mountjoy, E.W., Forest, R., and Leonard, R.
1985: Structure and stratigraphy of the Miette Group, Selwyn Range, between Ptarmigan and Hugh Allan creeks, British Columbia; in Current Research, Part A, Geological Survey of Canada, Paper 85-1A, p. 485-490.

Price, R.A. and Mountjoy, E.W.
1970: Geological Structure of the Canadian Rocky Mountains between Bow and Athabasca rivers, a progress report; Geological Association of Canada, Special Paper 6, p. 7-26.

Sanderson, D.J. and Marchini, W.R.D.
1984: Transpression; Journal of Structural Geology, v. 6, p. 449-458.

Shaw, P.G. and Morton, R.D.
1990: Gold mineralization in Lower Cambrian McNaughton Formation, Athabasca Pass, Canadian Rocky Mountains: structural, mineralogical and temporal relationships; Canadian Journal of Earth Sciences, v. 27, p. 477-493.

Wheeler, J.O.
1963: Rogers Pass map-area, British Columbia and Alberta (82 N west half); Geological Survey of Canada, Paper 62-32, Map 43-1962, scale 1 inch to 4 miles, 32 p.

Calcareous nannofossils from the Late Triassic-Early Jurassic of the Queen Charlotte Islands, British Columbia

Paul R. Bown[1]
Cordilleran Division

Bown, P.R., 1991: Calcareous nannofossils from the Late Triassic-Early Jurassic of the Queen Charlotte Islands, British Columbia; in Current Research, Part E; Geological Survey of Canada, Paper 91-1E, p. 13-18.

Abstract

Samples collected from the Triassic and Lower Jurassic sequences of the Queen Charlotte Islands during the 1990 field season have yielded the first early Mesozoic calcareous nannofossils from North America. The assemblages are generally poorly preserved but are comparable with those found in northwest Europe in the Lower Jurassic, and the rare Triassic nannofossil localities, in Austria, Indonesia, and northwest continental shelf of Australia. Paleobiogeographic observations are inconclusive but important features include the absence of Schizosphaerella punctulata *and* Mitrolithus jansae *in the Lower Jurassic, and the absence of* Eoconusphaera zlambachensis *in the Triassic.*

Résumé

Des échantillons prélevés dans des séquences du Trias et du Jurassique inférieur des îles de la Reine-Charlotte pendant la campagne de 1990 ont permis de mettre au jour les premiers nanofossiles calcaires du début du Mésozoïque en Amérique du Nord. Les assemblages sont en général mal conservés, mais sont compatibles avec ceux trouvés dans le nord-ouest de l'Europe dans le Jurassique inférieur et les rares localités de nanofossiles du Trias en Autriche, en Indonésie et dans le nord-ouest du plateau continental de l'Australie. Les observations paléobiogéographiques ne sont pas concluantes, mais il faut noter entre autres éléments importants l'absence de Schizosphaerella punctulata *et de* Mitrolithus jansae *dans le Jurassique inférieur, et l'absence de* Eoconusphaera zlambachensis *dans le Trias.*

[1] Department of Geological Sciences, University College London, Gower Street, London WC1E 6BT, United Kingdom

INTRODUCTION

The Late Triassic to Early Jurassic was an important interval in the history of calcareous nannofossils which saw their first appearance in the Carnian/Norian, extinctions at the Triassic/Jurassic boundary, and diversification through the Early Jurassic. This interval, however, is relatively poorly known compared to the later Mesozoic and Cenozoic. Early studies by Stradner (1963), Prins (1969), and Barnard and Hay (1974) were the first to utilize nannofossils for biozonation of the Early Jurassic and, more recently, Crux (1984, 1987), Bown (1987), and Bown et al. (1988) have further improved biostratigraphic resolution. Almost all the work undertaken in the Early Jurassic has been confined to northwest Europe and, to a lesser extent, circum-Mediterranean regions. Consequently, our knowledge of nannofossil paleobiogeographic and stratigraphic distribution away from these areas is limited. Even less is known about Triassic nannofossils, their existence having only been conclusively proven in the last decade, initially in material from the Kossen and Zlambach beds in Austria (Moshkovitz, 1982; Jafar, 1983; Bown, 1985) and more recently in coeval strata from Indonesia and the northwest continental shelf of Australia (Bralower et al., 1991).

The presence of calcareous nannofossils in the early Mesozoic sequences of the Queen Charlotte Islands is therefore of great interest and significance in terms of broadening our understanding of paleobiogeography for this time interval. These results also represent the first records of Jurassic calcareous nannofossils from North America, and the only record of Triassic nannofossils away from the tethyan region.

A total of 200 samples were collected from the Kunga and Maude groups (Upper Triassic to Middle Jurassic) during the 1990 field season. This preliminary report is based on 110 samples that have been processed for nannofossil extraction; 38 of these samples yielded nannofossil assemblages that were generally of low species diversity and moderate to poor preservation. The Peril Formation (Upper Carnian-Upper Norian) and Ghost Creek Formation (Lower Pliensbachian) yielded the best nannofossil assemblages; severely etched assemblages were recovered from the Whiteaves Formation (Toarcian); and complete absence or extremely impoverished assemblages were encountered in the Sandilands (Upper Norian-Sinemurian), Rennell Junction (Lower Pliensbachian), Fannin (Upper Pliensbachian-Lower Toarcian), and Phantom Creek (Upper Toarcian-Lower Aalenian) formations, and in a small number of Yakoun Group (Lower Bajocian) samples.

NANNOFOSSIL RESULTS

Triassic

The Peril and Sandilands formations of Late Triassic age were sampled on Frederick Island (Fig. 1), and at Kennecott Point (Fig. 1) and Sadler Point, northwest Graham Island. The lower part of the Peril Formation (Lower Norian) was barren of nannofossils, but grey and black shales, bearing abundant *Monotis,* yielded abundant nannofossil assemblages. These Middle-Upper Norian nannofossil assemblages are dominated by the nannolith *Prinsiosphaera triassica* Jafar and also contain rarer *Thoracosphaera geometrica* (Jafar) and *Thoracosphaera* spp., and the small coccolith *Crucirhabdus minutus* Jafar. Nannofossils are found as high as the middle Upper Norian but are absent from the Sandilands Formation in the interval adjacent to the Triassic/Jurassic boundary at Kennecott Point (Tipper and Carter, 1990).

Lower Jurassic

Lower Jurassic sediments of the Maude Group were sampled around Skidegate Inlet, Central Graham Island, and Kennecott Point.

Sandilands Formation

The Sandilands Formation at Kennecott Point was essentially barren of nannofossils, although rare fragments of *Thoracosphaera* sp. were observed in the Sinemurian. In Central Graham Island, a section on Ghost Creek Road (Fig. 2), transitional between the Sandilands and Ghost Creek formations, yielded assemblages typical of the Upper Sinemurian, including *Crepidolithus crassus* (Deflandre), *C. pliensbachensis* Crux, *Mitrolithus elegans* Deflandre, and *Parhabdolithus liasicus* Deflandre. These assemblages fall within the Crepidolithus crassus Nannofossil (NF) Zone (NJ3) (Upper Sinemurian-lowermost Pliensbachian) of Bown et al. (1988).

Ghost Creek Formation

The Ghost Creek Formation (Lower Pliensbachian) was sampled on Maude Island (Section 8 of Cameron and Tipper, 1985) (Fig. 2) and at Whiteaves Bay (Section 7 of Cameron and Tipper, 1985) (Fig. 2). The grey and black shales of this formation consistently yield poor to moderately preserved nannofossil assemblages. The assemblages are similar to those of northwest Europe and include the earliest species of *Biscutum, B. novum* (Goy), which has a first occurrence in the Jamesoni Ammonite Zone. The occurrence of *B. novum* and absence of the genus *Lotharingius* Noel places this formation within the Biscutum novum (NJ4) NF Zone (Bown et al., 1988). The presence of *Parhabdolithus robustus* Noel in many of the samples constrains the dating further to the Crepidolithus pliensbachensis NF Subzone (NJ4a), which is confined to the Jamesoni and Ibex Ammonite zones in the northwest European area. This is in good agreement with the ammonite biostratigraphy in the Queen Charlotte Islands (Smith and Tipper, 1989), which dates the Ghost Creek Formation as Imlayi to Whiteleavesi Ammonite zones (Jamesoni and Ibex Ammonite Zone equivalents). The assemblages are characterized by common *Crepidolithus crassus, Mitrolithus elegans*, and *Parhabdolithus liasicus*, along with rarer *Biscutum novum, Mitrolithus lenticularis* Bown, *Parhabdolithus robustus,* and *Tubirhabdus patulus* Prins *ex* Rood, Hay and Barnard.

FREDERICK ISLAND - SECTION C

AGE	FORMATION	SAMPLE NO. / SPECIES	Prinsiosphaera triassica	Thoracosphaera geometrica	Thoracosphaera sp.
E. NORIAN	PERIL	FI-8	.	.	.
		FI-6	.	.	.
		FI-5	.	.	.
		FI-4	.	.	.
		FI-3	C	C	C

FREDERICK ISLAND - SECTION D

AGE	FORMATION	SAMPLE NO. / SPECIES	Thoracosphaera sp. indet.	Prinsiosphaera triassica
E.-M. NORIAN	PERIL	10435	.	R
		10433	F	.
		10432	F	.

KENNECOTT POINT - SECTION KP-M

AGE	FORMATION	SAMPLE NO. / SPECIES	Prinsiosphaera triassica	Thoracosphaera sp. indet.	Crucirhabdus minutus	Crucirhabdus primulus
M.-L. NORIAN	SAN.	KP-9	.	.	.	.
	PERIL	KP-8	C	.	.	.
		KP-7	.	.	.	.
		KP-6	A	.	R	.
		KP-5	.	.	.	.
		KP-4	A	.	F	?
		KP-2	C	.	R	.
		KP-1	A	F	.	.

FREDERICK ISLAND - SECTION E

AGE	FORMATION	SAMPLE NO. / SPECIES	Prinsiosphaera triassica	Thoracosphaera geometrica	Thoracosphaera sp. indet.	Crucirhabdus minutus
M.-L. NORIAN	PERIL	10443	VA	.	.	F
		10442	A	.	.	.
		10441	C	?	?	.
		FI-13	.	.	.	.

KENNECOTT POINT - SECTION X

AGE	FORMATION	SAMPLE NO. / SPECIES	Crucirhabdus minutus	Prinsiosphaera triassica
L. NORIAN	SANDI-LANDS	KP-14	.	C
		KP-10	.	.
		KP-11	.	.
		KP-13	R	C

KEY

R = Rare (0-2 counts)
F = Few (3-5 counts)
C = Common (6-100 counts)
A = Abundant (101-1000 counts)
VA = Very abundant (>1001 counts)
? = Questionably present
. = Not present

Figure 1. Distribution of nannofossils in Triassic sections: Section C, Frederick Island; Section D, Frederick Island; Section E, Frederick Island; Section KP-M, Kennecott Point, northwest Graham Island; Section X, Kennecott Point, northwest Graham Island.

Rennell Junction and Fannin formations

These formations, of Early Pliensbachian to Early Toarcian age, are characterized by an increase in fine- to medium-grained clastic sediments. They were sampled on Maude Island and at Whiteaves Bay but all material was barren of nannofossils.

Whiteaves Formation

The Whiteaves Formation is of Early to Late Toarcian age and consists of greenish-grey silty shale with concretions and rare sandy beds. The formation was sampled at Whiteaves Bay (Section 7 of Cameron and Tipper, 1985) but all samples were barren of nannofossils (Fig. 2). A second section on the Yakoun River, Central Graham Island (Section 11 of Cameron and Tipper, 1985), yielded low diversity, low abundance, and etched assemblages, the clays having very little fine fraction carbonate content (Fig. 2). All assemblages contained *Lotharingius* , which has a Upper Pliensbachian first occurrence in European sections. Samples 13 to 20 also contained *Discorhabdus striatus* Moshkovitz and Ehrlich placing them within the Discorhabdus striatus NF Zone (NJ7) of Bown et al. (1988) (Bifrons-Levesquei Ammonite zones). The assemblages include *Biscutum novum*, *Discorhabdus criotus* Bown, *D. striatus, Lotharingius hauffii* Grun and Zweili, *L. barozii* Noel, and *L. sigillatus* (Stradner). The preservation state of the nannofossils suggests postdepositional diagenetic dissolution of the majority of the assemblages.

Phantom Creek Formation

The Phantom Creek Formation ranges in age from Late Toarcian to Early Aalenian and consists of green, medium grained sandstone. The formation was sampled on the Yakoun River (Section 11 of Cameron and Tipper, 1985); all samples are barren of nannofossils.

Yakoun Group — Graham Island Formation

The Graham Island Formation is of Early Bajocian age and consists of tuffaceous sandstone and rare shale interbeds. The formation was sampled on Branch Road 59, Central Graham Island (Section 13 of Cameron and Tipper, 1985). One sample yielded the dissolution resistant genus *Watznaueria* Reinhardt, which has a first occurrence in the Lower Bajocian in northwest Europe; the remaining samples were barren.

COMPARISON WITH EUROPEAN NANNOFLORAS

The nannofossil assemblages from the Queen Charlotte Islands are relatively poorly preserved and of low diversity and abundance. Although this appears wholly attributable to postdepositional etching and dissolution, not reflecting original assemblage features, the preservational bias somewhat limits comparisons with coeval assemblages from the European area and reduces our ability to make confident comments on paleobiogeography. In addition, our knowledge of paleobiogeographic patterns in the Lower Jurassic is still rudimentary, although significant differences between northwest European and circum-Mediterranean assemblages have been described (Bown, 1987); even less information exists for the Upper Triassic.

Triassic

The Triassic assemblages from the Queen Charlotte Islands are comparable to those observed elsewhere, i.e. Austria, northwest continental shelf of Australia, and Indonesia. In all cases the assemblages are of high abundance and low diversity (maximum of six species), and dominated by the nannolith *Prinsiosphaera triassica*. In addition, other calcispheres are present, e.g. *Thoracosphaera geometrica*, along with extremely small (2-3 microns) coccoliths, e.g. *Crucirhabdus minutus*. In contrast, the Queen Charlotte Island assemblages do not contain *Eoconusphaera zlambachensis* (Moshkovitz) which is an important component of the Austrian assemblages, and is rarely found in the Australian material. This suggests a distribution for *E. zlambachensis* which may have been limited to Tethys and particularly Western Tethys.

It should be noted that no Triassic nannofossils have yet been recorded from "Boreal" sections.

Lower Jurassic

The Lower Jurassic assemblages from the Queen Charlotte Islands are generally comparable with those of northwest Europe and are entirely compatible stratigraphically. The most significant difference is the absence of *Schizosphaerella punctulata* Deflandre and Dangeard, which is often a very significant component of Lower Jurassic assemblages, occurring in rock-forming abundance in the Tethyan region.

The presence of *Mitrolithus lenticularis* in the Ghost Creek Formation samples is suggestive of Tethyan affinities, although it is found rarely in the Boreal region during the Lower Pliensbachian.

A further significant paleobiogeographic feature is the absence of *Mitrolithus jansae* (Wiegand) from Queen Charlotte Island assemblages. The abundant presence of this species characterizes Tethyan assemblages in the European and Mediterranean region; it is generally absent in the Boreal area, but is also absent in samples from Timor and Argentina. The low latitude location of this region during the Lower Jurassic has been demonstrated using paleontological evidence which indicates strong Tethyan affinities (Smith and Tipper, 1986). The absence of *M. jansae* here and also from Timor and Argentina suggests that this species did not have a straightforward Tethyan distribution but may have been limited to Western Tethys and the proto-Atlantic ocean. Such a distribution is comparable with other later Mesozoic nannofossils, e.g. *Conusphaera mexicana* Trejo and *Nannoconus* Kamptner spp.

Figure 2. Distribution of nannofossils in Jurassic sections: Ghost Creek Road, Graham Island; Strat. Section 8, Maude Island; Strat. Section 7, Whiteaves Bay, Moresby Island; Strat. Section 15, Yakoun River, Graham Island (ammonite zone information from G. Jakobs, pers. comm., 1990). See Figure 1 for key to abbreviations.

REFERENCES

Barnard, T. and Hay, W.W.
1974: On Jurassic coccoliths: a tentative zonation of the Jurassic of Southern England and Northern France; Eclogae Geologicae. Helvetiae, v. 67, p. 563-585.

Bown, P.R.
1985: *Archaeozygodiscus* — a new Triassic coccolith genus; International Nannofossil Association Newsletter, v. 7, p. 32-35.
1987: Taxonomy, evolution, and biostratigraphy of late Triassic-early Jurassic calcareous nannofossils; Special Papers in Palaeontology, v. 38, p. 1-118.

Bown, P.R., Cooper, M.K.E., and Lord, A.R.
1988: A calcareous nannofossil biozonation scheme for the early to mid-Mesozoic; Newsletters in Stratigraphy, v. 20, p. 91-114.

Bralower, T., Bown, P.R., and Siesser, W.
1991: Significance of Upper Triassic nannofossils from the Southern Hemisphere (ODP Leg 122, Wombat Plateau, NW Australia); Marine Micropalaeontology, v. 17, p. 119-154.

Cameron, B.E.B. and Tipper, H.W.
1985: Jurassic stratigraphy of the Queen Charlotte Islands, British Columbia; Geological Survey of Canada, Bulletin 365, p. 1-49.

Crux, J.A.
1984: Biostratigraphy of Early Jurassic calcareous nannofossils from southwest Germany; Neues Jahrbuch fur Geologie und Palaontologie, Abhandlungen, v. 169, p. 160-186.
1987: Early Jurassic calcareous nannofossil biostratigraphic events; Newsletters in Stratigraphy, v. 17, p. 79-100.

Jafar, S.A.
1983: Significance of the Late Triassic calcareous nannoplankton from Austria and southern Germany; Neues Jahrbuch fur Geologie und Palaontologie, Abhandlungen, v. 166, p. 218-259.

Moshkovitz, S.
1982: On the findings of a new calcareous nannofossil (*Conusphaera zlambachensis*) and other calcareous organisms in the Upper Triassic sediments of Austria; Eclogae Geologicae Helvetiae, v. 75, p. 611-619.

Prins, B.
1969: Evolution and stratigraphy of coccolithinids from the Lower and Middle Lias; in Proceedings, First International Conference on Planktonic Microfossils, Geneva, (ed.) P. Bronnimann and H.H. Renz, v. 2, p. 547-558.

Smith, P.L. and Tipper, H.W.
1986: Plate Tectonics and Paleobiogeography: Early Jurassic (Pliensbachian) Endemism and Diversity; Palaios, v. 1, p. 399-412.
1989: Biochronology, stratigraphy and tectonic setting of the Pliensbachian of Canada and the United States; in 2nd International Symposium on Jurassic Stratigraphy, Lisboa 1987, (ed.) R.B. Rocha and A.F. Soares, v. 1, p. 119-138.

Stradner, H.
1963: New contributions to Mesozoic stratigraphy by means of nannofossils; Proceedings of the 6th World Petroleum Congress Section 1, p. 1-16.

Tipper, H.W and Carter, E.S.
1990: Evidence for defining the Triassic-Jurassic boundary at Kennecott Point, Queen Charlotte Islands, British Columbia; in Current Research, Part F; Geological Survey of Canada, Paper 90-1F, p. 37-41.

High resolution seismic and side-scan sonar mapping of the Fraser Delta front and adjacent Strait of Georgia, British Columbia

B.S. Hart, J.V. Barrie, R.G. Currie, J.L. Luternauer[1], D.B. Prior[2], and R.D. Macdonald
Pacific Geoscience Centre, Sidney

Hart, B.S., Barrie, J.V., Currie, R.G., Luternauer, J.L., Prior, D.B., and Macdonald, R.D., 1991: High resolution seismic and side-scan sonar mapping of the Fraser Delta front and adjacent Strait of Georgia, British Columbia; in Current Research, Part E; Geological Survey of Canada, Paper 91-1E, p. 19-23.

Abstract

Marine geophysical surveys of the delta front and prodelta regions of the Fraser Delta and Strait of Georgia are being carried out by the Geological Survey of Canada in response to growing public demand for information on the offshore geological processes and hazards potential. The surveys are a renewed effort to understand the characteristics and properties of the seafloor through collaboration among the Pacific and Atlantic Geoscience Centres, and Cordilleran Division. During PGC Cruise 91-01 we collected high resolution seismic records and side-scan sonographs of this region, and these data can be used to identify patterns of Quaternary sedimentation, seafloor deformation and erosion, and the effects of human use of the seafloor (e.g. dumping, power transmission routes). Sediment cores will be collected to determine the recent depositional history of the submarine delta, providing a framework within which observations of modern processes can be evaluated.

Résumé

Des levés géophysiques marins des régions du front et de l'avant du delta du Fraser sont menés par la Commission géologique du Canada en réponse à la demande publique croissante d'information sur les phénomènes géologiques extracôtiers et les dangers possibles qui y sont associés. Les levés constituent un nouvel effort de collaboration entre le Centre géoscientifique du Pacifique, la Division de la Cordillère et le Centre géoscientifique de l'Atlantique pour comprendre les caractéristiques et les propriétés du fond marin. Pendant la campagne de janvier 1991 du CGP, nous avons réalisé des enregistrements sismiques de haute résolution et des sonogrammes à balayage latéral du front du delta et du détroit adjacent de Georgie, et nous démontrons ici comment cette information peut être utilisée pour identifier des signes de sédimentation quaternaire d'une part, et de déformation, de mouvement de masse et d'érosion du fond marin d'autre part. Des images sonars peuvent aussi servir à reconnaître les effets d'utilisations humaines du fond marin (dépotoir, chalutage, lignes de transport d'énergie, etc.). Les levés acoustiques, complétés par le carottage des sédiments, permettront de retracer l'histoire récente de la formation des parties littorales du delta, constituant ainsi un cadre permettant de mieux évaluer les observations de phénomènes récents.

[1] Cordilleran Division, Vancouver, British Columbia
[2] Atlantic Geoscience Centre, Halifax, Nova Scotia

INTRODUCTION

The Fraser River is the largest river reaching the Canadian west coast. It discharges into the Strait of Georgia, and in the past 10 000 years has constructed a subaerial delta which covers approximately 1000 km^2 (Clague et al. 1983). The delta is located near British Columbia's main urban centre and so is subject to the pressures of development while directly affecting the development potential of the region. To ensure that human uses of the offshore portions of the delta are undertaken safely, efficiently, and with minimal disruption of the environment, it is essential that the delta's architecture, seafloor behaviour and hazards potential be evaluated (e.g. Luternauer and Finn, 1983; Luternauer and Macdonald, 1987; McKenna and Luternauer, 1987; Tarbotton and Murphy, 1987; Clague et al., in press).

The subaerial delta plain has been extensively studied (e.g. Luternauer, 1980), and many reports have been published describing specific aspects of the delta front and prodelta region (e.g. Pharo and Barnes, 1976; Hamilton and Luternauer, 1983; Kostaschuk et al., in press). Hamilton (in press) analyzed airgun seismic records to identify and map the distribution of the main seismostratigraphic packages in the Central Strait of Georgia. However, there has been no systematic mapping using marine high-resolution seismic data, side-scan sonar imagery, and submarine cores at scales and coverage consistent with the regional and local patterns of delta front processes. Consequently, our objective is to study the surface morphology and internal structure of the subaqueous portion (delta front and prodelta) of the Fraser Delta and adjacent Strait of Georgia in its entirety, while building upon the results of existing studies. The results should permit detailed reconstruction of the recent growth of the delta, while allowing identification of potential offshore hazards and the effects of human development on the seafloor.

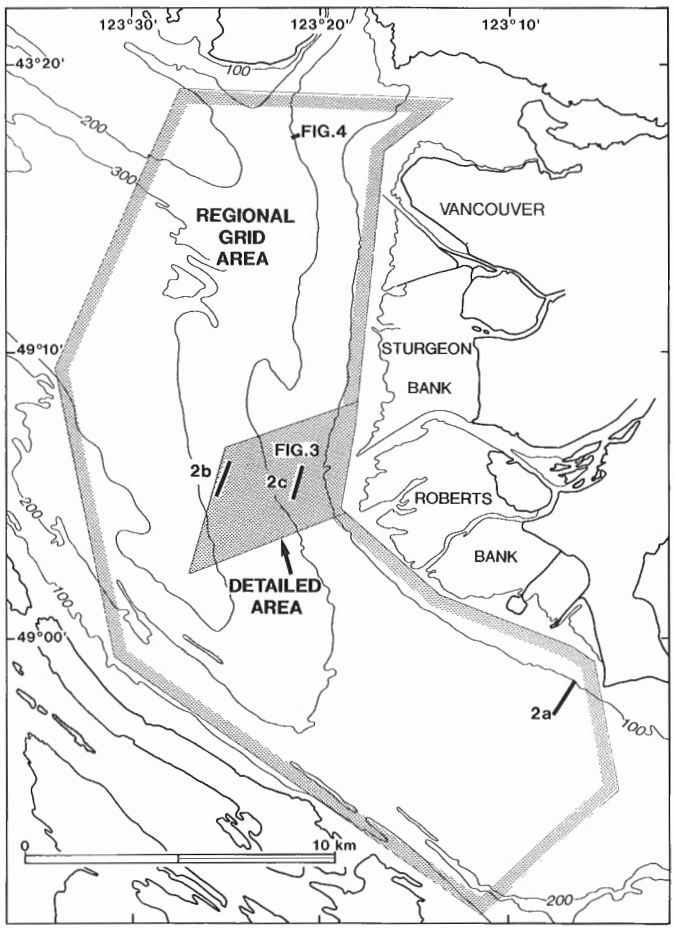

Figure 1. Study area showing areas covered by regional and detailed grids, and locations covered by seismic or side-scan images in Figures 2 to 4.

STUDY AREA AND METHODS

Two cruises were scheduled to collect data for this project: PGC Cruise 91-01 (C.S.S. Tully, 9-15 February 1991), and PGC Cruise 91-04 (C.S.S. Parizeau, 13-24 May 1991). Here we present results from the first cruise, where we collected side-scan sonar images (Klein Model 595 with correction for slant range distortion), Huntec Deep Tow Seismic (DTS) and 12kHz records.

Our study area covers that part of the Central Strait of Georgia within a radius of about 20 km of the break in slope between the relatively flat intertidal delta plain and the more steeply dipping subtidal delta front (Fig. 1). About 670 km of survey lines (including both strike and dip lines) cover the area on a regional scale (2 km spacing between strike lines), while another 25 lines, each about 8 km long and with about 200 m spacing between adjacent lines, provide detailed coverage of an area immediately offshore of the mouth of the main distributary channel of the Fraser River at Sand Heads.

Figure 2. (opposite) Sample Huntec DTS records showing characteristic reflection configurations. a) Continuous parallel reflectors (left) showing slight divergence into trough (centre) and onlapping relationship with underlying Pleistocene units (right). Note gas effects and internal angular discordance. Water depth in centre of trough is about 130 m. b) Debris lobe with chaotic reflectors overlying unit with continuous parallel reflectors in upper portions. A portion of Foreslope Hills (*c f.* Hamilton and Wigen 1987) visible on right. Water depth in centre of image is about 250 m. c) Main submarine channel (centre) offshore of main Fraser River distributary channel. Channel separates continuous parallel reflectors to north (off Sturgeon Bank) from broken reflector configuration to south (off Roberts Bank). Note truncation of reflectors along north margin of channel. Section crosses channel obliquely (see Fig. 3), explaining apparent asymmetric channel form. Water depth in centre of channel 165 m. The location of all images are shown in Figure 1.

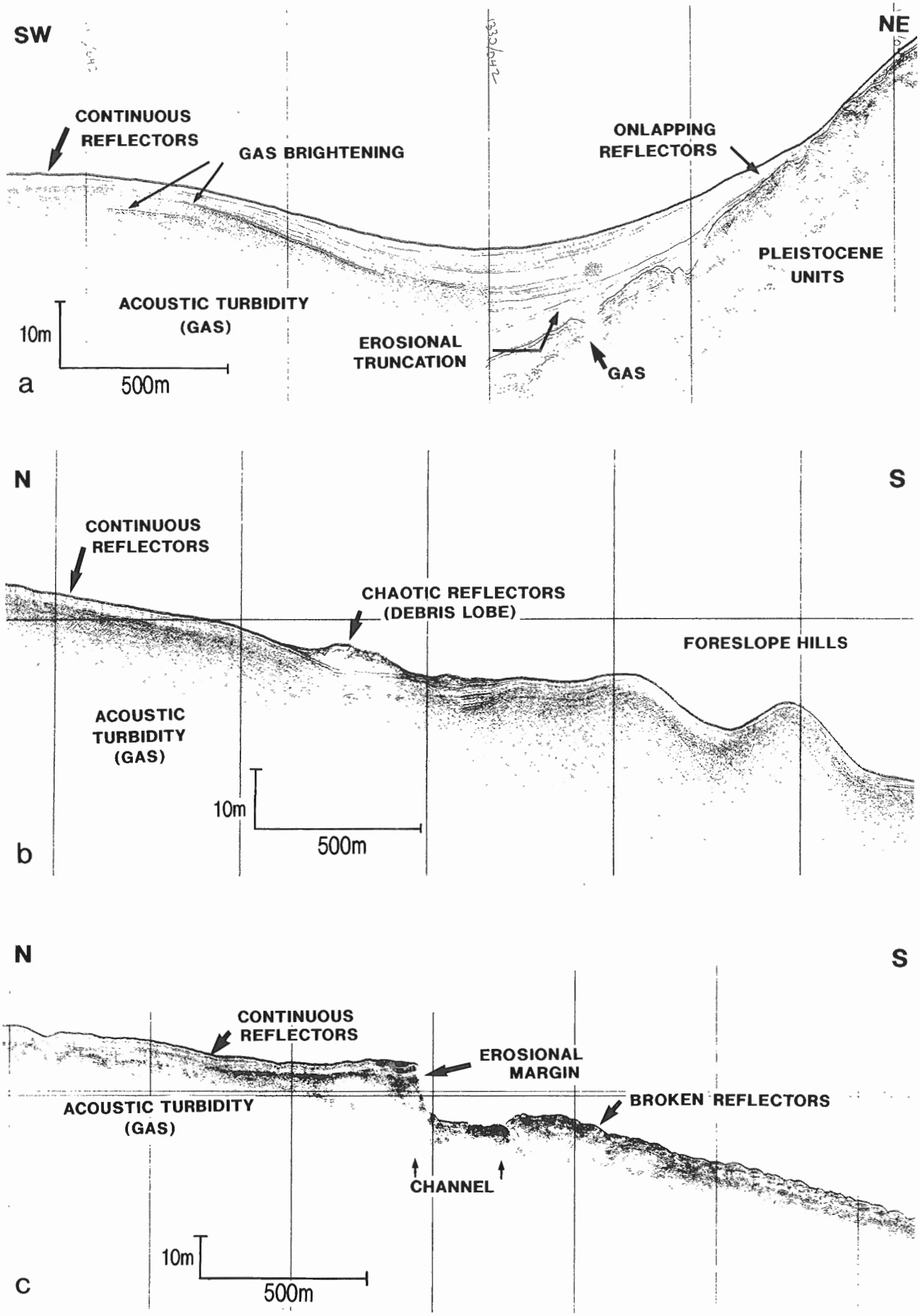
SW
NE
CONTINUOUS REFLECTORS
GAS BRIGHTENING
ONLAPPING REFLECTORS
PLEISTOCENE UNITS
ACOUSTIC TURBIDITY (GAS)
10m
500m
a
EROSIONAL TRUNCATION
GAS
N
S
CONTINUOUS REFLECTORS
CHAOTIC REFLECTORS (DEBRIS LOBE)
FORESLOPE HILLS
ACOUSTIC TURBIDITY (GAS)
10m
500m
b
N
S
CONTINUOUS REFLECTORS
EROSIONAL MARGIN
BROKEN REFLECTORS
ACOUSTIC TURBIDITY (GAS)
CHANNEL
10m
500m
c

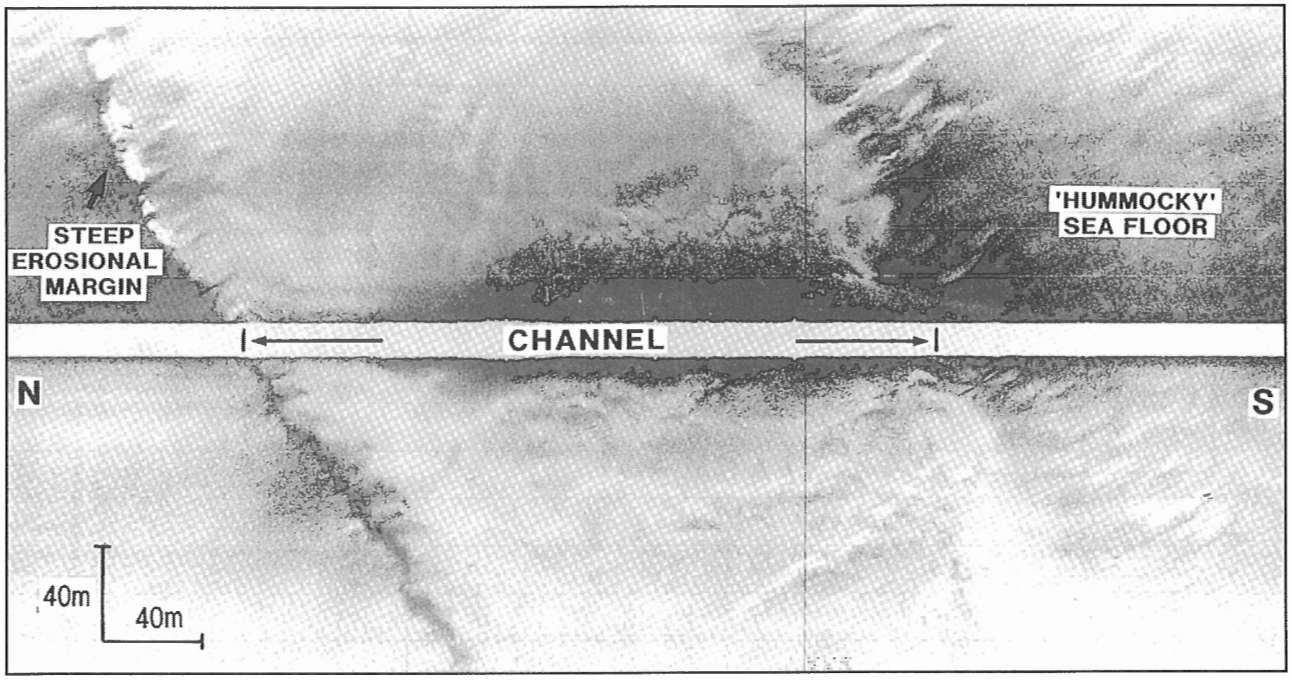

Figure 3. Side-scan sonograph illustrating portion of submarine channel shown in Figure 2c. Note the sharp northern channel margin and the difference in seafloor topography on either side of the channel.

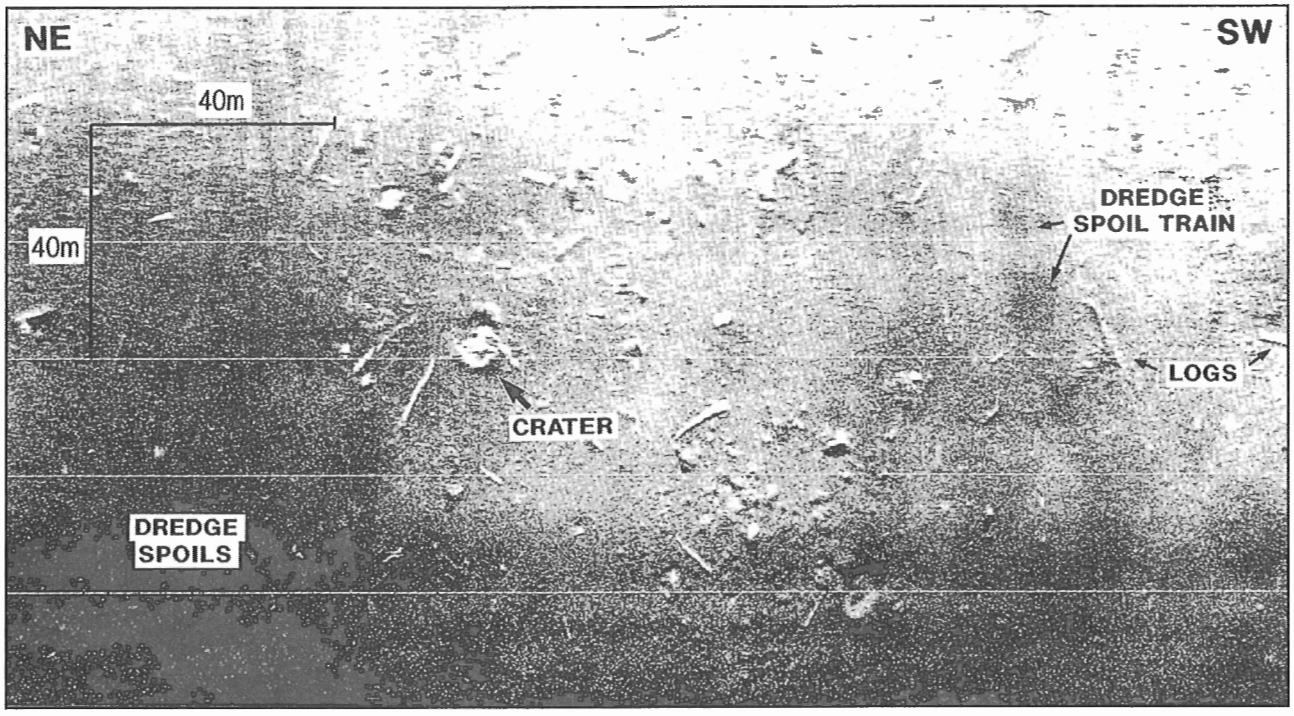

Figure 4. Side-scan sonograph illustrating a variety of anthropogenic debris on the seafloor in "Spoil Area" adjacent to Point Grey.

RESULTS

The side-scan images and Huntec records are used to recognize zones of undisturbed sediment accumulation, seafloor erosion, and instability. On the Huntec records, the former are characterized by continuous, parallel reflectors which drape underlying topography (Fig. 2a,b,c), and flat, relatively featureless seafloor on the side-scan images. This type of reflection configuration is typically found in the deep, axial portions of the strait (prodelta region) and on the delta front adjacent to Sturgeon Bank (Fig. 1). Acoustic scattering by interstitial gas masks reflectors at relatively shallow depths on many of the Huntec records, especially those collected close to the delta front (Fig. 2a,b,c). Seafloor erosion is indicated where continuous reflectors on high-resolution seismic records are abruptly truncated at the sediment surface (e.g. Fig. 2c). Zones of instability-related disturbance of the sediment column (common on the delta front adjacent to Roberts Bank) can be identified by the existence of broken-parallel or chaotic reflection configurations (Fig. 2b,c).

Side-scan images from the detailed grid area near Sand Heads (Fig. 1) provide plan views of features indicating active seafloor processes including collapse depressions, debris lobes, and rotational slumps. Most spectacular is a subaqueous channel (Fig. 2c, 3), traceable down to over 200 m below sea level, which has incised into the delta front immediately offshore of the main distributary channel of the river (Kostaschuk et al., in press). A sandwave field on the delta front west of the ferry terminal at Tsawwassen (Luternauer, 1980) can be delineated. Pockmarks on the seafloor, gas escape features best developed in the deep axial portions of the strait offshore of Sturgeon Bank, are also visible on sonographs.

The side-scan images also portray traces of human activity in this region. For example, the seafloor west of Point Grey is mantled with dredge spoils, sunken logs (possibly derived from a booming ground on the north channel), and various other unidentifiable refuse (Fig. 4). In this area, craters over 10 m in diameter possibly formed by the impact of large objects dumped on the muddy seafloor. Other anthropogenic features visible in the side-scan images elsewhere include trawler marks, a sewage outlet pipe (*cf.* Luternauer and Macdonald, 1987), and underwater transmission cables.

SUMMARY

We have begun a program of high resolution marine geophysical mapping of the Fraser Delta front and prodelta which complements and extends earlier studies in this region. Examination of high-resolution seismic records along with sonographs of the seafloor allows recognition of zones of sediment accumulation, erosion, deformation, and mass movements. The sonographs also permit identification of human disturbances of the seafloor. With completion of the regional survey grid, it will be possible to map the distribution of the major late Holocene seismostratigraphic packages. Integration of acoustic data with lithological and chronological control (radiocarbon dates, Cs^{137} dating) from cores will permit a detailed sequence stratigraphic reconstruction of the growth of the delta. This historical perspective should act as a framework within which observations of modern processes can be better evaluated.

ACKNOWLEDGMENTS

We thank Captain J. Anderson, the officers and crew of the C.S.S. Tully for their efforts during PGC Cruise 91-01. Bill Hill, Gerry Horel, Ivan Frydecky, Carl Amos, Kim Conway, Russ Parrot, and Harry Olynyk (Terra Surveys) are thanked for their competent technical support. Kim Conway and Tark Hamilton are thanked for their helpful reviews.

REFERENCES

Clague, J.J., Luternauer, J.L., and Hebda, R.J.
1983: Sedimentary environments and postglacial history of the Fraser Delta and lower Fraser Valley, British Columbia; Canadian Journal of Earth Sciences, v. 20, p. 1314-1326.

Clague, J.J., Luternauer, J.L., Pullan, S.E., and Hunter, J.A.
in press: Postglacial deltaic sediments, southern Fraser River delta, B.C.; Canadian Journal of Earth Sciences.

Hamilton, T.S.
in press: Seismic stratigraphy of unconsolidated sediments in the central Strait of Georgia: Hornby Island to Roberts Bank; Geological Survey of Canada, Open File 2350.

Hamilton, T.S. and Luternauer, J.L.
1983: Evidence of seafloor instability in the south-central Strait of Georgia, British Columbia: a preliminary compilation; in Current Research, Part A; Geological Survey of Canada, Paper 83-1A, p. 417-421.

Hamilton, T.S. and Wigen, S.O.
1987: The Foreslope Hills of the Fraser Delta: implications for tsunamis in Georgia Strait; The International Journal of the Tsunami Society, v. 5, p. 15-33.

Kostaschuk, R.A., Luternauer, J.L., McKenna, G.T., and Moslow, T.F.
in press: Sediment transport in a submarine channel system: Fraser River delta, Canada; Journal of Sedimentary Petrology.

Luternauer, J. L.
1980: Genesis of morphologic features on the western delta front of the Fraser River, British Columbia - status of knowledge; in The Coastline of Canada, (ed.) S.B. McCann; Geological Survey of Canada, Paper 80-10, p. 381-396.

Luternauer, J.L. and Finn, W.D.L.
1983: Stability of the Fraser River Delta front; Canadian Geotechnical Journal, v. 20, p. 603-616.

Luternauer, J.L. and Macdonald, R.D.
1987: Tractive flows adjacent to site for submarine sewage pipeline, Fraser River Delta slope, British Columbia, Canada; Coastal Zone '87, American Society of Coastal Engineers, Seattle, Washington, p. 1862-1873.

McKenna, G.T. and Luternauer, J.L.
1987: First documented large failure at the Fraser River delta front, British Columbia; in Current Researach, Part A; Geological Survey of Canada, Paper 87-1A, p. 919-924.

Pharo, C.H. and Barnes, W.C.
1976: Distribution of surficial sediments of the central and southern Strait of Georgia, British Columbia; Canadian Journal of Earth Sciences, v. 13, p. 684-696.

Tarbotton, M.R. and Murphy, D.S.
1987: An application of acoustic core analysis; Lighthouse, Edition 35, p. 7-11.

Preliminary studies of fluid inclusions in sphalerite from the Robb Lake Mississippi Valley-type deposit, British Columbia

D.F. Sangster and J.J. Carrière
Mineral Resources Division

Sangster, D.F. and Carrière, J.J., 1991: Preliminary studies of fluid inclusions in sphalerite from Robb Lake Mississippi Valley-type deposit, British Columbia; in Current Research, Part E; Geological Survey of Canada, Paper 91-1E, p. 25-32.

Abstract

Preliminary fluid inclusion and petrographic studies on sphalerite in breccias from the Muncho-Mc-Connell-Stone interval have determined an average homogenization temperature of 119°C and salinities from 16 to greater than 23 equivalent wt% NaCl for the ore forming fluid at Robb Lake. Eutectic temperatures of -24° to -36°C indicate the presence of other salt(s) besides NaCl. Most determinations were made on pseudosecondary inclusions occurring in planes or along healed fractures.

Résumé

Les premières études pétrographiques des inclusions de fluide dans la sphalérite bréchique de l'intervalle Muncho-McConnell-Stone ont révélé que le fluide minéralisant au lac Robb avait une température moyenne d'homogénéisation de 119 °C et des salinités de 16 à plus de 23 % en poids d'équivalent NaCl. Les températures eutectiques de -24 à -36 °C indiquent la présence d'un ou des sels autres que NaCl. La plupart des mesures ont été effectuées sur des inclusions pseudosecondaires dans des plans ou le long de fractures cicatrisées.

INTRODUCTION

Study of fluid inclusion geothermometry of the Robb Lake lead-zinc deposit is part of a larger research project to investigate the thermal history of carbonate-hosted lead-zinc deposits of the Mackenzie Platform of northern British Columbia, western Northwest Territories, and eastern Yukon. This report presents results of a preliminary study of fluid inclusions in Robb Lake sphalerites to determine the minimum formational temperature of the deposit and the salinity of the mineralizing fluid(s).

DEPOSIT GEOLOGY

The Robb Lake lead-zinc deposit, in northeastern British Columbia (56°56N, 123°43W; 94B/13), mainly occurs in dolostones of the Middle Devonian Stone Formation close to a major facies change westward to fine grained clastics (Fig. 1). Discovered in 1971, the deposit was eventually determined to contain reserves of 6.1 x 10^6 short tons of 7.3% combined lead-zinc (Northern Miner, Jan. 30, 1975).

Mineralization, consisting largely of brown sphalerite and white crystalline dolomite with lesser galena, pyrite, quartz, pyrobitumen, and calcite, occurs mainly as cement to dolostone fragments in breccia zones. Sulphides also occur as vein, vug, and fracture fillings, as fine grained replacements of host carbonate, and as massive crystalline pods.

In the breccia bodies, sphalerite displays "snow-on-roof" texture, a texture distinctive of Mississippi Valley-type (MVT) lead-zinc deposits (Sangster, 1985) wherein sulphide crystals or crystal aggregates occur predominantly on top of dolostone fragments (Fig. 2). Another characteristic MVT texture at Robb Lake are the "trash zones" consisting of angular fragments of sphalerite and galena in a matrix of fine grained dolomite sand and hydrocarbon-rich insoluble residue (Sangster, 1985). Trash zones at Robb Lake, as in other MVT deposits, are found at the base, or lower portions, of the breccia zones.

Robb Lake ore-hosting breccias have been described by Thompson (1972), Taylor et al. (1975), Sangster and Lancaster (1976), and Macqueen and Thompson (1978). The breccias comprise tabular and lenticular zones which may be both conformable or disconformable to bedding. The zones range from a few centimetres to as much as 50 metres thick and with lateral dimensions up to 300 m. Dolostone clasts are angular, with sharp boundaries, and range in size from a few centimetres to several metres. Boundaries of the breccias are very sharp in some places and gradational in others. Origin of the breccias has long been controversial and remains so, largely because of a lack of research on this important aspect of the deposit. Sangster and Lancaster (1976) favoured a paleokarst solution collapse origin, linked to an unconformity between the host Stone Formation and the overlying Pine Point Formation. Macqueen and Thompson (1978) rejected this hypothesis and ascribed the breccias to hydraulic fracturing accompanying compaction and dewatering of fine grained clastic sediments adjacent to the Robb Lake property.

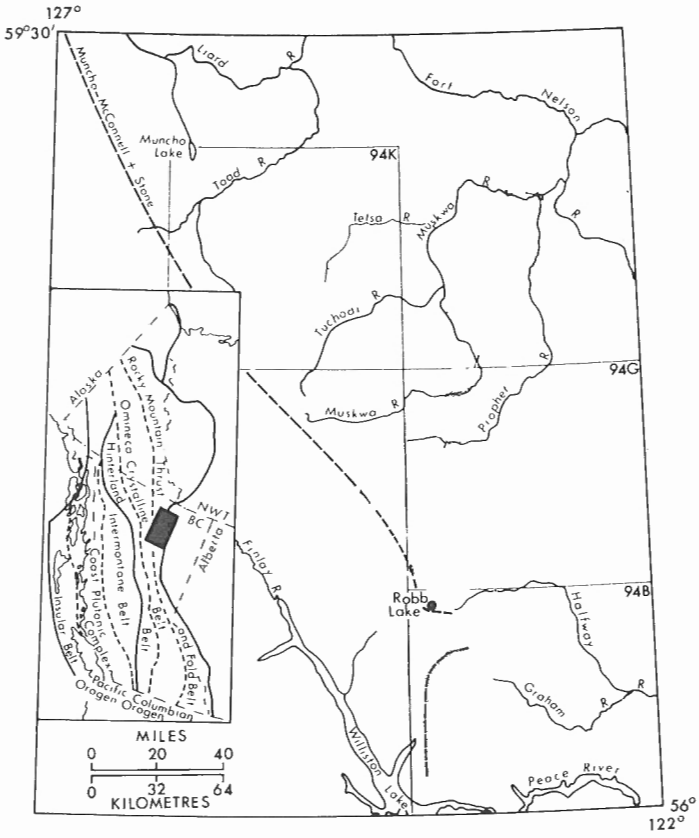

Figure 1. Location of Robb Lake deposit relative to position of Stone Formation carbonate-shale facies change (modified from Macqueen and Thompson, 1978).

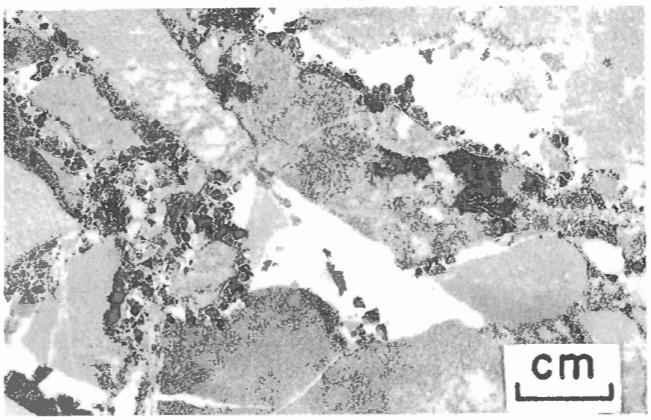

Figure 2. Sample SP2047, consisting of angular dolostone fragments cemented by white, coarsely crystalline sparry dolomite and sphalerite. Where both dolomite and sphalerite form the cement, note that sphalerite formed earlier than dolomite and occurs preferentially on top of the fragments ("snow-on-roof" texture) with dolomite filling the remainder of the cavity

FLUID INCLUSION STUDY

Material used

Samples of mineralization from existing GSC collections were selected on the basis of the size and colour of sphalerite crystals. The samples (Fig. 2 and 3) consist of aggregates of coarsely crystalline sphalerite, minor galena, and white dolomite occurring as cement in a dolostone breccia.

Petrography

Six fluid inclusion plates and two polished thin sections were prepared for study. Special care was taken during preparation of the fluid inclusion plates to minimize the possibility of erroneous results due to stretching caused by overheating. The plates for thermometric study were prepared by Vancouver Petrographics Ltd. and Atelier de Petrographie du Saguenay Inc.

Observed in thin section were dolostone, dolomite, sphalerite, galena, quartz and pyrite (Fig. 4a). Angular dolostone fragments are partially rimmed by irregular masses of sphalerite. Subhedral to euhedral sphalerite crystals and crystal aggregates occur in contact with the irregular sphalerite masses (Fig. 4b) as well as within the white sparry dolomite cement (Fig. 4c). The sphalerite is white, yellow, dark orange or brown; alternating colour bands are common. Many solid inclusions of carbonate rhombohedrons (probably calcite) are contained in the sphalerite.

Minor amounts of galena are associated with sphalerite. In places, galena occurs as veinlets cutting sphalerite or as masses surrounded by sphalerite. In other places sphalerite grains are completely enclosed by galena (Fig. 4d). Quartz is a minor constituent and, where present, is typically associated with galena, either in fractures cutting it (Fig. 4e) or as inclusions (Fig. 4f). Euhedral to subhedral fine grained pyrite is sparsely disseminated throughout.

The fluid inclusions observed were all two phase: liquid plus vapour. Homogenization by heating occurred by contraction of the vapour bubble to yield only a liquid phase (i.e. by the expansion of the liquid to eliminate the bubble). Many inclusions had irregular shapes, although negative crystal shaped inclusions were extremely common. The inclusions ranged in size from 5 to 20 m. Vapour bubbles were small, occupying 1 to 2 volume percent of the inclusions. Inclusions along healed fractures (Fig. 5) or in planes (Fig. 6) within a single crystal were interpreted as pseudosecondary. A small minority of inclusions was interpreted as primary using the criteria of Roedder (1976). Inclusions outlining growth zones were observed but were too small to yield results. The inclusion population was generally quite dense, but the majority of inclusions were either too dark or too thick-rimmed to allow observation of vapour bubble action.

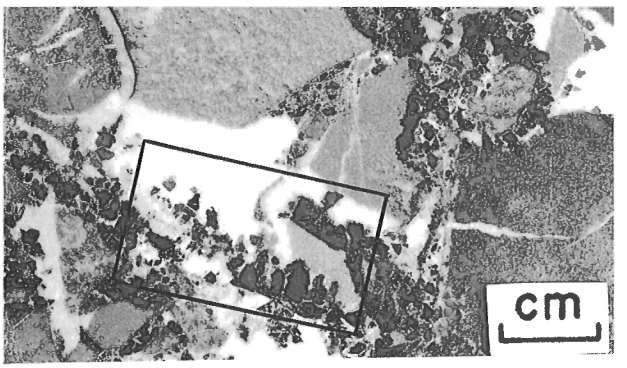

Figure 3. Crystal aggregates of sphalerite and galena in breccia matrix, adjacent to dolostone fragments. Fluid inclusion plate 2047D was cut from area indicated in photo.

Homogenization temperatures

Using a Linkam TH600 heating/freezing stage, homogenization temperatures were determined on 105 inclusions in sphalerite. The homogenization temperatures determined for the primary inclusions fall within the range of those for the pseudosecondary inclusions (Fig. 7). This supports the premise that both primary and pseudosecondary inclusions were contemporaneous and early-formed with respect to sphalerite growth.

Heating the inclusions until phase homogeneity was accomplished provided a minimum temperature of formation. The actual temperature of entrapment of the fluid inclusion is derived by adding a pressure correction to the temperature of homogenization. According to Macqueen and Thompson (1978), the Middle Devonian of the Robb Lake area reached a maximum burial depth of about 5 km during mid-Cretaceous time. However, because the timing (and hence the depth) of mineralization at Robb Lake is not known, no corrections were made to the determined temperatures but, at these low temperatures and high salinities, such corrections would be small, even at 5 km (Roedder, 1984).

The stage was calibrated both before and after measurements were made using SYN FLINC Temperature Calibration Standards and an additional four compounds of known melting points ranging from -56.6° to 200°C. The maximum error between theoretical and measured melting temperature was 2°C but, for the majority of standards, was less than 1°C. This is smaller than the errors inherent in the methods and thus no calibration correction was necessary. Sources of error included thermal lag and heat loss, but were due mainly to visual limitations. The poor optical characteristics of many inclusions and the rapid movement of the tiny bubbles near homogenization combined to give an average estimated precision ±3°C on most readings. Homogenization runs were repeated on many inclusions and results were duplicated to within 2°C.

Table 1 summarizes the fluid inclusion data for individual specimens. Primary and pseudosecondary fluid inclusions in the sphalerite examined have homogenization temperatures in the range of 87° to 154°C with a mean of 119°C. Inclusions in the same sphalerite crystal commonly show a wide range of formation temperatures (as much as 50°C), which could indicate rapidly fluctuating depositional conditions or extremely slow growth rates.

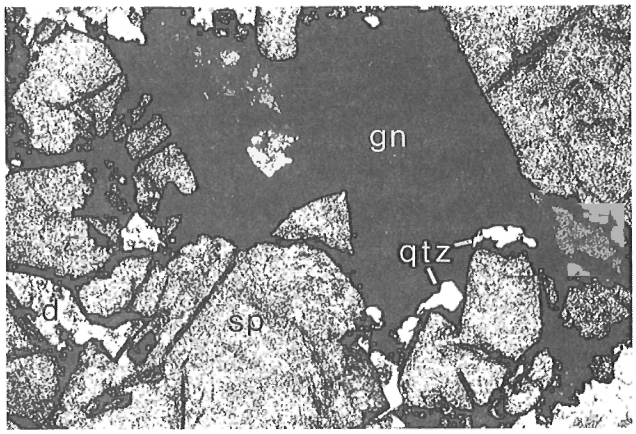

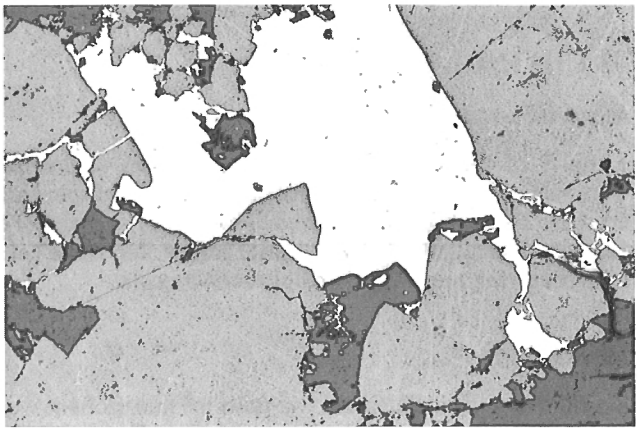

Figure 4a

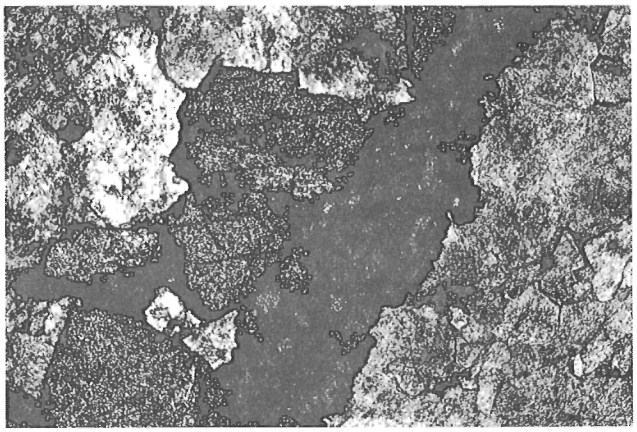

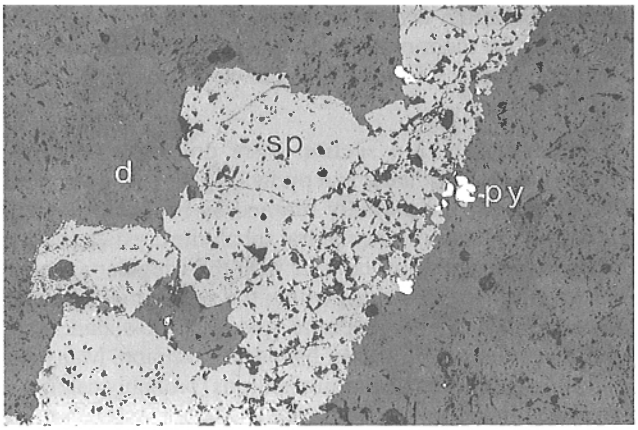

Figure 4b

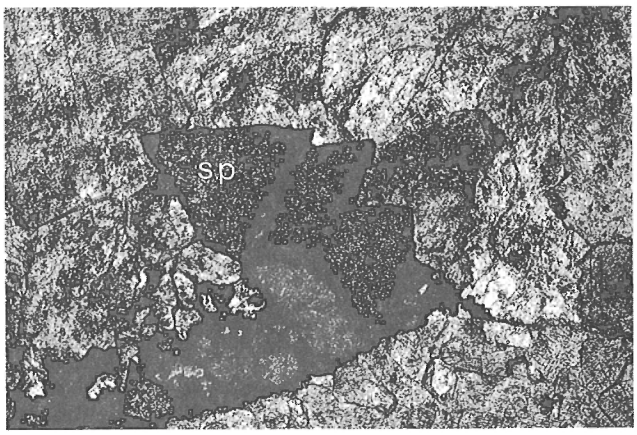

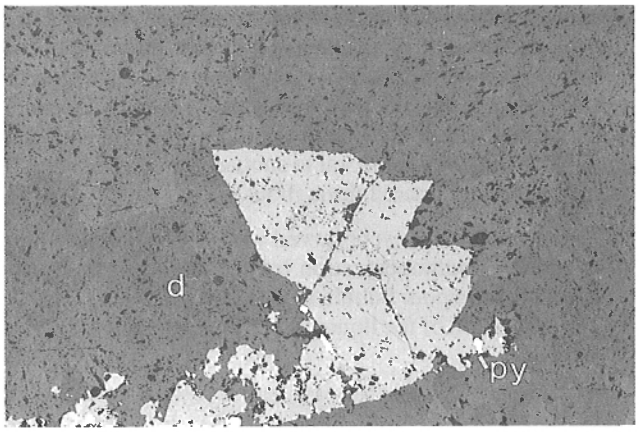

Figure 4c

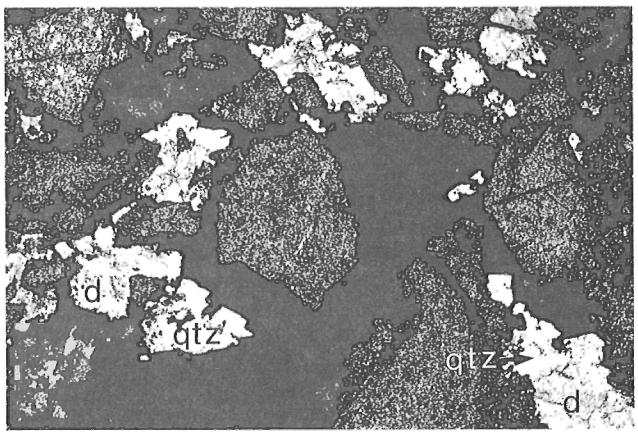

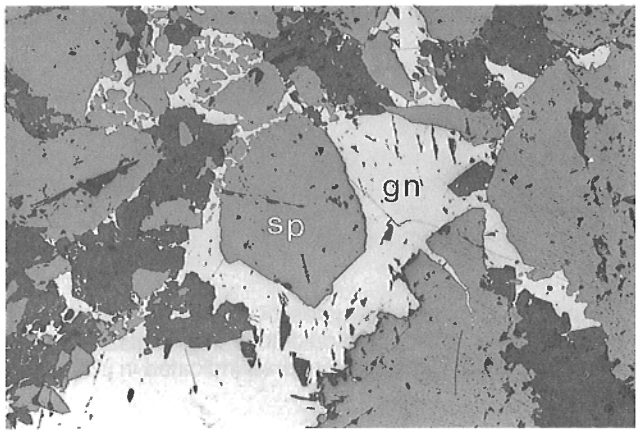

Figure 4d

Melting temperatures

Inclusions were cooled to -70 to -80°C with most inclusions freezing around -70°C. The vapour bubble contracted when liquid froze, indicating an H_2O-rich fluid. The first appearance of liquid upon heating was difficult to see, mainly due to the small size of the inclusions. The eutectic temperatures of only 23 inclusions were determined with certainty; these ranged from -36° to -24°C with a mean of -31°C. Because the eutectic temperature of a NaCl-saturated solution is -20.8°, the lower initial melting temperature indicated the presence of another salt, probably $CaCl_2$.

Melting temperatures, although difficult to obtain because of problems with metastability and limited optics, were determined for 41 of the 105 inclusions studied. The melting

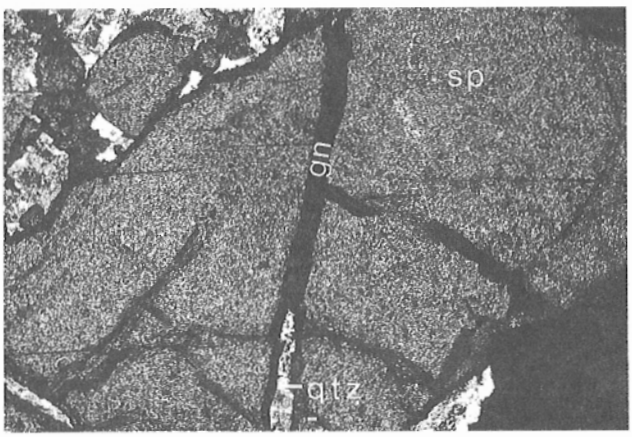

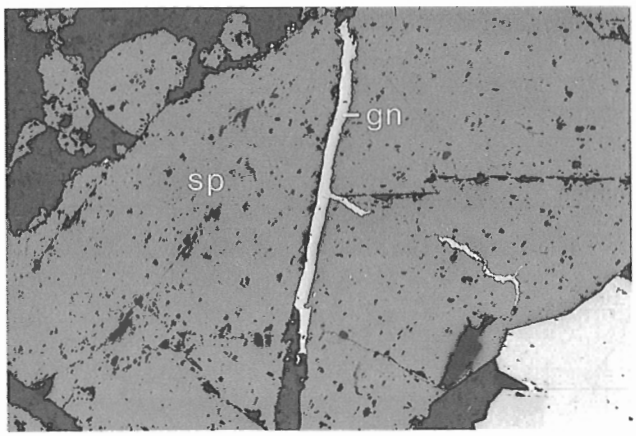

Figure 4e

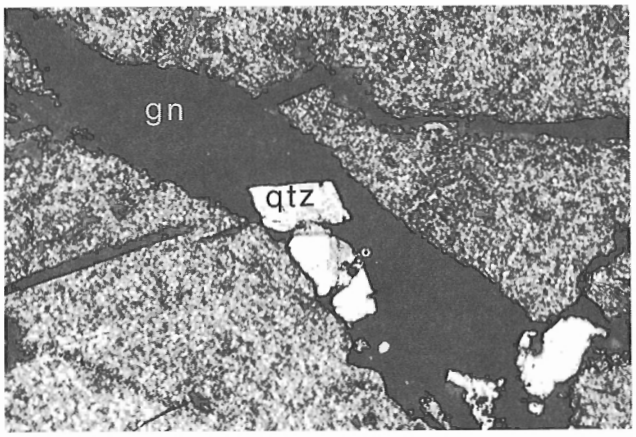

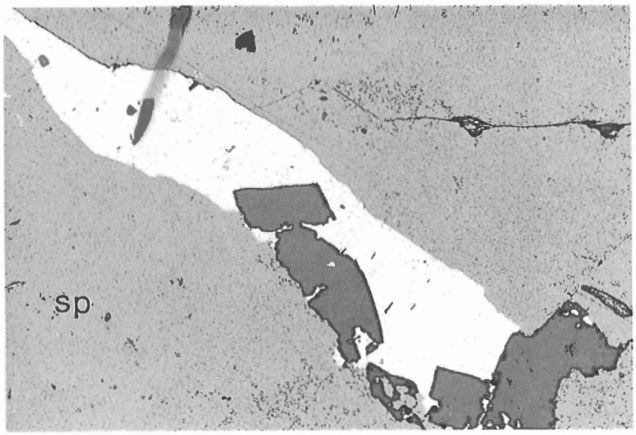

Figure 4f

a - Typical mineralogy includes galena containing small patches of quartz and surrounded by subhedral sphalerite. Small amounts of dolomite are also visible.

b - Irregular mass of sphalerite is more easily distinguished from the subhedral grains of sphalerite in transmitted light (left). Pyrite is obvious only in reflected light (right). Dolomite surrounds the sphalerite.

c - Aggregate of euhedral to subhedral sphalerite grains enclosed in dolomite. Sparsely disseminated pyrite grains are visible.

d - Sphalerite grains enclosed in galena which is surrounded by sphalerite. Note that quartz is confined to galena. Dolomite fills gaps.

e - Galena- and quartz-filled veinlet in sphalerite.

f - Quartz in galena, surrounded by sphalerite, contains fluid inclusions.

Figure 4. Minerals and textures found in Sample 2047 compared in photomicrograph pairs taken in transmitted light (left column) and reflected light (right column) with polars uncrossed. Abbreviations as follows: qtz, quartz; d, dolomite; sp, sphalerite; gn, galena, py, pyrite. Width of field = 2 mm.

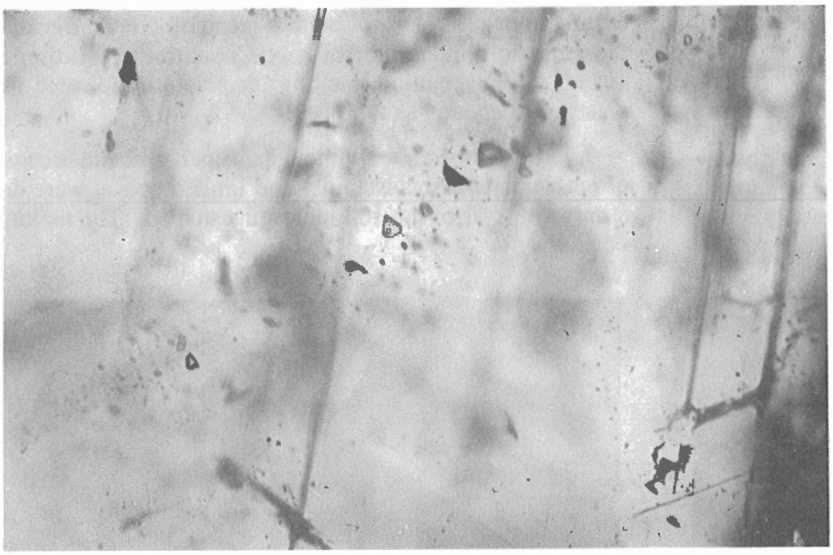

Figure 5. Trail of pseudosecondary inclusions within a single grain of sphalerite from sample 2047D. Clear inclusion in centre of trail is 6 μm long and yielded a Tm of -19.5°.

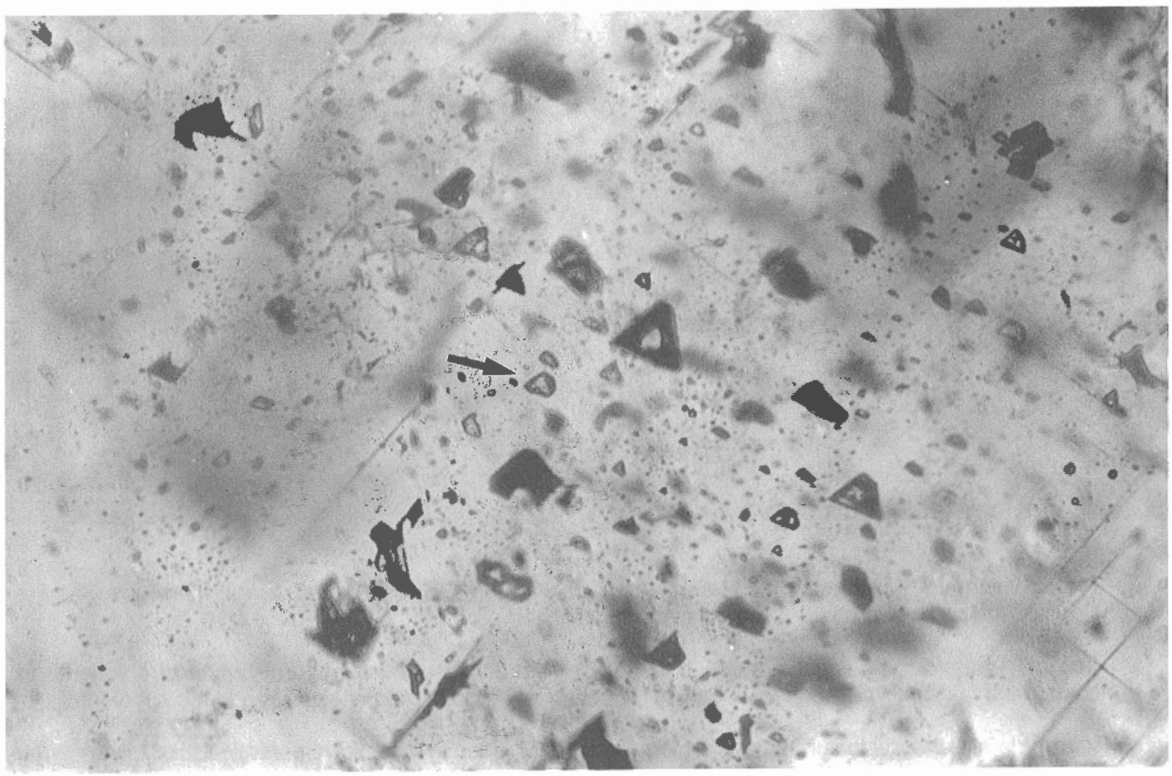

Figure 6. Plane of pseudosecondary fluid inclusions in sphalerite from sample SP2047D. The triangular shaped inclusion No. 6 (see arrow) is 8 μm wide. This photomicrograph was taken at -30.6°C just as initial melting was beginning. Ice is visible in most inclusions. Inclusion No. 6 yielded a Th of 127°C and Tm of -20.5°. These readings were duplicated within 1.5°C. Population density, strong negative crystal shapes and poor optical quality of the inclusions is well illustrated.

temperature determined ranged from -12°C to -26°C with a mean of -18°C (Table 1). This suggested that the mineralizing fluid was a brine containing 16 to greater than 23 equivalent weight percent NaCl. Salinity derived from tables calculated using the equation of Potter et al. (1978). Melting temperature data are reproduced in Figure 8 in histogram form and, as with the homogenization temperatures, data for primary and pseudosecondary inclusions are similar.

Table 1. Summary of fluid inclusion data, Robb Lake, British Columbia

HOMOGENIZATION TEMPERATURES (Th)				MELTING TEMPERATURES (Tm)		
Sample No.	**No. of inclusions**	**Range (°C)**	**Avg. (°C)**	**No. of inclusions**	**Range (°C)**	**Avg. (°C)**
SP 1943	16	88-154	111	7	-12 to -19	-16
SP 2047	20	90-143	119	5	-20 to -26	-22
SP 2047C	20	87-154	122	17	-15 to -26	-18
SP 2047D	17	91-136	115	8	-16 to -20	-18
SP 2054	25	91-153	120	2	-20	-20
SP 4233	7	105-144	136	2	-17 to -23	-20
SUMMARY	105	87-154	119	41	-12 to -26	-18

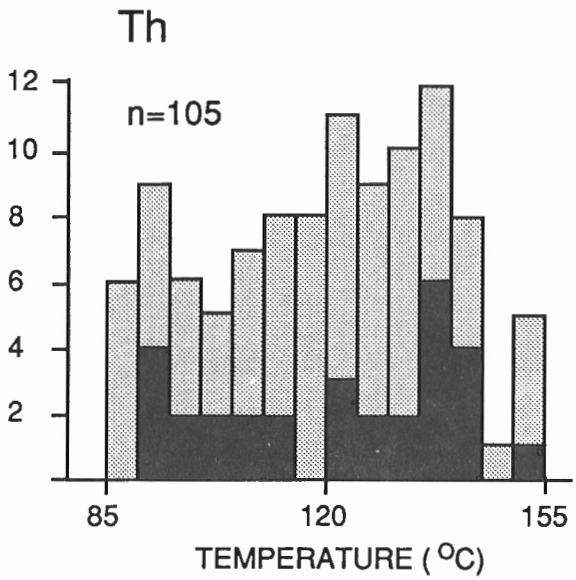

Figure 7. Homogenization temperatures of inclusions in sphalerite. Primary inclusions indicated by black bars; pseudosecondary are shaded.

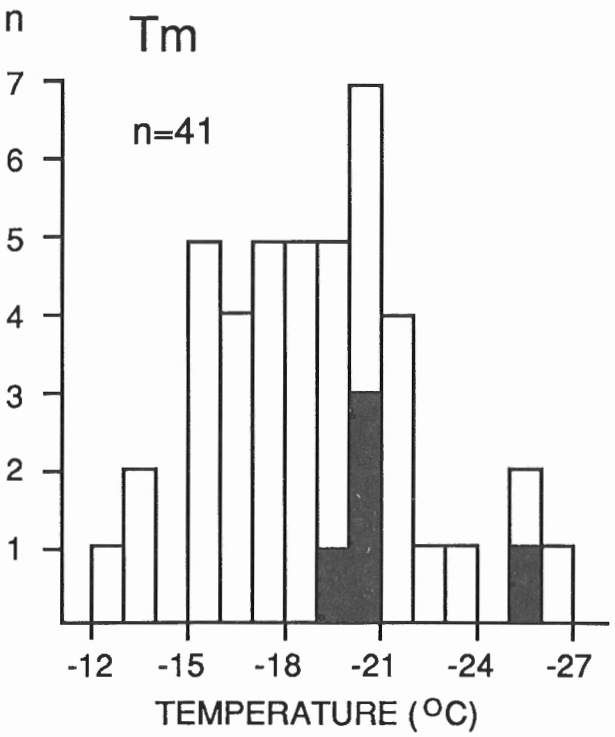

Figure 8. Melting temperatures of inclusions in sphalerite. Primary inclusions indicated by black bars; remainder are pseudosecondary.

DISCUSSION

Homogenization temperatures obtained for fluid inclusions in sphalerite in this study (average = 119°C) are at variance with those reported by Macqueen and Thompson (1978) for 20 inclusions in two quartz crystals in proximity to sphalerite. Values for this quartz ranged from 210-260°C "..with many grouped around a temperature of ~230°C" (ibid.). Although individual values in other MVT deposits in North America may be as high as these, as a group these temperatures are anomalously high for MVT deposits. For example, a compilation of over 1800 Th determinations in sphalerite from 14 North American MVT deposits yielded a range from 50-190°C with a mode of approximately 100-110°C. In the present study, quartz crystals, some with visible fluid inclusions, were observed but only embedded in galena (Fig. 4e and 4f) as opposed to the sphalerite-associated quartz of Macqueen and Thompson (1978). As paragenetic or petrographic details of the materials studied were not provided by Macqueen and Thompson (1978), the relationship between their quartz and mineralization and between their sphalerite-associated quartz and that observed by us in galena are uncertain. Hence, the discrepancy between the two data sets cannot be reconciled at present.

In the midcontinental area of the U.S.A., Leach and Rowan (1986) proposed a genetic and temporal link between uplift of the Ouachita foldbelt and the occurrence of several major MVT districts in the foreland platform carbonates to the north. Part of their evidence for this proposal was a progressive northward decrease in average homogenization temperatures in sphalerites of the MVT deposits. When integrated over the distances involved in a south-north transect, the lateral thermal gradient obtained was 0.09°C/km. If the same concept is applied in a west-to-east transect between Robb Lake (av. Th = 119°C) and Pine Point (av. Th = 80°C), an integrated lateral thermal gradient of 0.1°C/km is obtained. The similarity in lateral thermal gradients in the two regions is intriguing but requires further investigation before further inferences can be made.

ACKNOWLEDGMENTS

We are grateful to our colleague, François Robert, for his assistance on some of the microthermometric determinations.

REFERENCES

Leach, D.L. and Rowan, E.L.
1986: Genetic link between Ouachita foldbelt tectonism and the Mississippi Valley-type lead-zinc deposits of the Ozarks; Geology, v. 14, p. 485-504.

Macqueen, R.W. and Thompson, R.I.
1978: Carbonate-hosted lead-zinc occurrences in northeastern British Columbia with emphasis on Robb Lake; Canadian Journal of Earth Sciences, v. 15, p. 1737-1762.

Potter, R.W., Clynne, M.A., and Brown, D.L.
1978: Freezing point depression of aqueous sodium chloride solutions; Economic Geology, v. 73, p. 284-285

Roedder, E.
1976: Fluid-inclusion evidence on the genesis of ores in sedimentary and volcanic rocks. Chapter 4 in Handbook of Strata-Bound and Stratiform Ore Deposits (ed.) K.H. Wolf, v. 2, Geochemical Studies, p. 67-110. Elsevier, Amsterdam.
1984: Fluid inclusions; Mineralogical Society of America, Reviews in mineralogy, v. 12, 644p.

Sangster, D.F.
1985: Breccia-hosted lead-zinc deposits in carbonate rocks; in James, N.P. and Choquette, P.W., eds., Paleokarst, Springer-Verlag, New York, p. 102-116.

Sangster, D.F. and Lancaster, R.D.
1976: Geology of Canadian lead-zinc deposits; in Report of Activities, Part A; Geological Survey of Canada, Paper 76-1A, p. 301-310.

Taylor, G.C., Macqueen, R.W., and Thompson, R.I.
1975: Facies changes, breccias, and mineralization in Devonian rocks of Rocky Mountains, northeastern British Columbia (94B,G,J,N); in Report of Activities, Part A; Geological Survey of Canada, Paper 75-1A, p. 577-585.

Thompson, R.I.
1972: Robb Lake property; in Geology, Exploration, and Mining in British Columbia, 1972; British Columbia Department of Mines and Petroleum Resources, p. 463-472.

The vent complex of the Sullivan stratiform sediment-hosted Zn-Pb deposit, British Columbia: preliminary petrographic and fluid inclusion studies

Craig H.B. Leitch and Robert J.W. Turner
Mineral Resources Division, Vancouver

Leitch, C.H.B. and Turner, R.J.W., 1991: The vent complex of the Sullivan stratiform sediment-hosted Zn-Pb deposit, British Columbia: preliminary petrographic and fluid inclusion studies; in Current Research, Part E; Geological Survey of Canada, Paper 91-1E, p. 33-44.

Abstract

In the vent zone, quartz forms rare veins or a matrix cement of calcite-pyrrhotite-chlorite ±tremolite-dravite-biotite-muscovite-sphene-ilmenite, between variably chlorite, biotite, or tourmaline altered clasts in fragmental rocks ("conglomerate" and "breccia") commonly found at the base of the massive sulphide orebody. Fluid inclusions in the relatively rare quartz veins and stockworks, previously reported to be high temperature (415°C) and high salinity (35-40 wt.%) are here characterized as moderate temperature (300°C) and moderate salinity (15-32 wt.%), containing significant $CaCl_2$ and $MgCl_2$. In finely laminated ore at the southeastern fringe of the overlying bedded orebody, remnant framboidal pyrite is overgrown by coarse euhedral pyrite and poikilitic garnet, magnetite and quartz; pyrrhotite is remobilized into fractures. In this zone, pegmatitic sphalerite and quartz contain fluid inclusions of moderate temperature (165-295°C) and moderate salinity (20-25 wt.%).

Résumé

Dans la zone de cheminée, du quartz forme de rares veines ou un ciment matriciel de calcite-pyrrhotite-chlorite trémolite-dravite-biotite-muscovite-sphène-ilménite entre des fragments, plus ou moins altérés par de la chlorite, de la biotite ou de la tourmaline, de roches détritiques ("conglomérat" et "brèche") situées normalement à la base de la minéralisation sulfurée massive. Des inclusions fluides dans les veines et stockwerks de quartz relativement rares, initialement réputées de haute température (415 °C) et de salinité élevée (35 à 40 % en poids), peuvent maintenant être caractérisées comme étant de température de salinité moyennes (300 °C et 15 à 32 % en poids) et contenant beaucoup de $CaCl_2$ et de $MgCl_2$. Dans le minerai finement feuilleté à la bordure sud-est de la minéralisation litée sus-jacente, de la pyrite framboïde résiduelle présente un accroissement secondaire de pyrite automorphe grossière et de grenat, de magnétite et de quartz poecilitiques; la pyrrhotite est remobilisée en fractures. Dans cette zone, la sphalérite et le quartz pegmatitiques contiennent des inclusions fluides de température et de salinité moyennes (165 à 295 °C et 20 à 25 % en poids).

INTRODUCTION

Stratiform sediment-hosted Zn-Pb deposits consist predominantly of hydrothermal sediments that were exhaled from seafloor vents. Some vent complexes formed by reaction of hydrothermal fluids with sediments deposited above the fluid discharge conduit. The Sullivan deposit in southeastern B.C. is a classic stratiform deposit composed of such a vent complex and directly overlying bedded sulphides. The vent complex at the Sullivan deposit consists of a discordant, sulphide-poor breccia pipe of altered rock, and is overlain by a conformable massive pyrrhotite body that formed as a replacement of the sheet-like body of hydrothermal sediments (Hamilton and Shaw, 1986; Shaw and Hodgson, 1986). The Sullivan is unusual among sediment-hosted Pb-Zn deposits in that it also has an altered zone immediately overlying the stratiform deposit suggesting continued hydrothermal activity following burial of seafloor sulphide sediments.

Studies of vent complexes provide constraints on the temperature and chemistry of ore-forming fluids. To date, knowledge of the fluid chemistry related to formation of the Sullivan deposit has been limited. Oxygen isotope studies of the pre-ore footwall tourmalinite and post-ore albite-chlorite alteration suggest formation from fluids of <100°C and <200°C respectively (Nesbitt et al., 1984), or 200-250°C (Beaty et al., 1988). Preliminary fluid inclusion studies by Shaw and Hodgson (1986) suggested temperatures of 200-250°C and salinities of 22-29 wt.% for albite-chlorite alteration. Leitch (1991) described five fluid inclusion types found in quartz, carbonate, albite and cassiterite within the vent complex, although it is not clear whether they represent mineralizing or metamorphic fluids. Metamorphic grade is biotite-muscovite-albite-quartz±garnet greenschist facies (McMechan and Price, 1982).

Sullivan project is part of a multidisciplinary study organized by the Geological Survey of Canada and the B.C. Geological Survey Branch and includes researchers from industry, U.S. Geological Survey, Royal Ontario Museum, and various universities. This paper is a reconnaissance petrographic and fluid inclusion study based on a suite of samples collected underground in the fall of 1990 that are representative of the different components of the Sullivan vent complex (Fig. 1). Observations in this paper are based on study of 17 polished thin sections and 32 polished rock slabs and complementary petrographic studies of district-scale alteration in the Sullivan-North Star area (Leitch et al., 1991).

VENT COMPLEX

Tourmalinite, quartz- or sulphide-cemented fragmental, massive chlorite-pyrrhotite and massive pyrrhotite samples were all collected in the R-10-30 decline that passes through the base of the pyrrhotite body into the underlying footwall zone. Tourmalinite samples were also collected in the #2 Cut-out and P-10-4 areas, and hanging wall albite-chlorite samples were collected from the N-11 stope. Sample sites are located in Figure 1 and sample details are listed in Table 1.

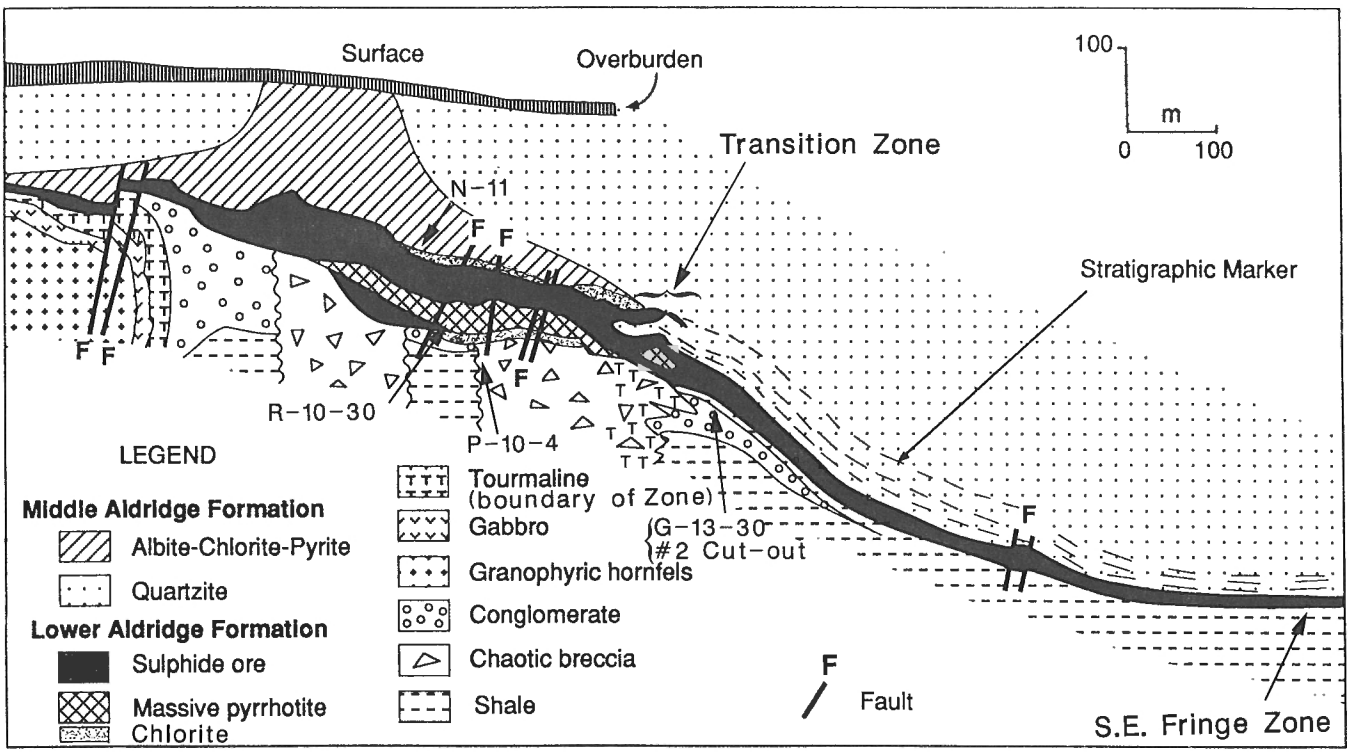

Figure 1. Geological cross-section of the Sullivan deposit, indicating the zones studied (W.D. Goodfellow, pers. comm., 1991, as modified from Morris et al., 1972 and Ransom et al., 1985).

Table 1. Summary of 1990 petrographic samples, Sullivan deposit

Sample[1]	Type[2]	Mineralogy[3]	Observations
90SVT2 R-10-30(#1)	Breccia (po matrix)	ms-qz-ch-ca-tm-gt po-cp-as-sl-gn-sp-il	Coarse tourmaline (dravite)
90SVT3,4 R-10-30(#1)	FW fragmental tourmalinite	tm-qz-ch-ca po-cp-sp-ru	Fine tourmaline replacing matrix
90SVT5 R-10-30(#1)	FW chlorite- pyrrhotite	ch-ca-qz-bi-ap-zr po-sp-gn-cp-mz-Bi	Possible volcanic protolith
90SVT6 R-10-30(#1)	Breccia (po matrix)	qz-ch-ms-ca-tm-gt-?ap po-sp-cp-as-il-gn-mz	Coarse tourmaline (dravite)
90SVT7 R-10-30(#1)	FW fragmental tourmalinite	tm-bi-qz-ca-ch-ms-tr-ap po-sp-sl-mz-ru-cp-gn-as	Coarse dravite + fine tourmaline
90SVL2 R-10-30	FW massive pyrrhotite	ch-qz-ca-ms-sp-?mz po-bl-sl-cp-gd-tt-fr-Sb-Bi	Boulangerite- chlorite vein
90SVL4 #2 Cut-out	FW fragmental tourmalinite	tm-qz-ca-ch po-cp-ru-gn	Hydrothermal Ti- minerals (as 5A)
90SVT9-12 90SVL5A,B P-10-4	FW tourmalinite	qz-tm-ch-ms-?ap-ca-zr po-as-sp-il-cp-ru-mz	Coarse dravite + fine tourmaline
90SVT13,14; 90SVL1 N-11	HW albitite, chlorite	ab-ch-hbi-do-qz-ms-?zr py-ru-sp	Prograde chlorite is magnesian
90SVT15 G-13-30	Moyie sill	hb-qz-ch-ep-do-pl-ms il-sp-po	Calcic plagioclase and amphibole
90SVT16-19 90SVL6 SE Fringe	Bedded pyrite ore	do/ca-gt-qz-ms-hbi-ch-tm py-po-sl-mt-sp-gn-lö-ap	Framboidal/collo- morphic pyrite
90SVL3 SE Fringe	Coarse quartz, sphalerite	qz-ch-bi-ab-ms sl-po-py-gn-sp	Type 1 and 2 fluid inclusions

[1] Collector (SVT=Turner, SVL=Leitch). Location in the mine underlined.
[2] Abbreviations: HW = hanging wall, FW = footwall, SE = southeast.
[3] Minerals are listed in approximate order of decreasing abundance. Transparent minerals are: ab=albite, ap=apatite, bi=biotite, ca=calcite, ch=chlorite, do=dolomite, ep=epidote, gt=garnet, hb=hornblende, hbi= hydrobiotite, ms=muscovite, mz=monazite, pl=plagioclase, qz=quartz, sp=sphene, tm=tourmaline, tr=tremolite, zr=zircon. Opaque minerals are: as=arsenopyrite, Bi=native Bi, bl=boulangerite, cp=chalcopyrite, fr=freibergite, gd=gudmundite, gn=galena, il=ilmenite, lö=löllingite, mt=magnetite, po=pyrrhotite, py=pyrite, ru=rutile, Sb=native Sb, sl=sphalerite, tt=tetrahedrite. Question marks indicate optical determination only.

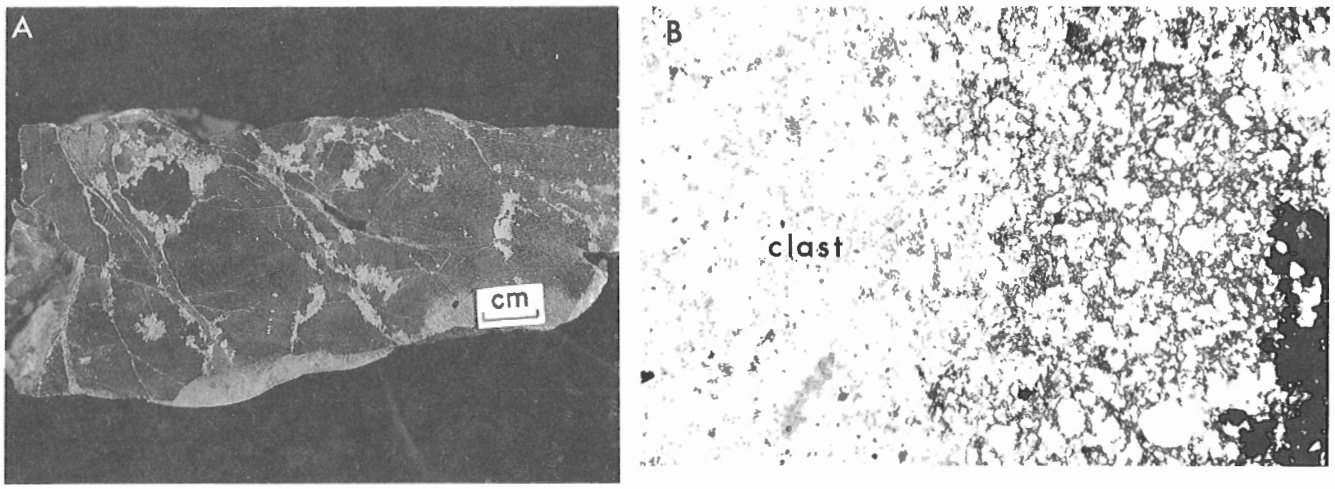

Figure 2. Tourmalinite zone. **A**) Almost massive tourmalinite in sample 90SVT9 with vague fragment outlines cut by stockwork of quartz-pyrrhotite-arsenopyrite. **B**) Tourmaline replacing mud fraction of matrix only (not clast). Transmitted light, uncrossed polars, field of view 5 mm wide.

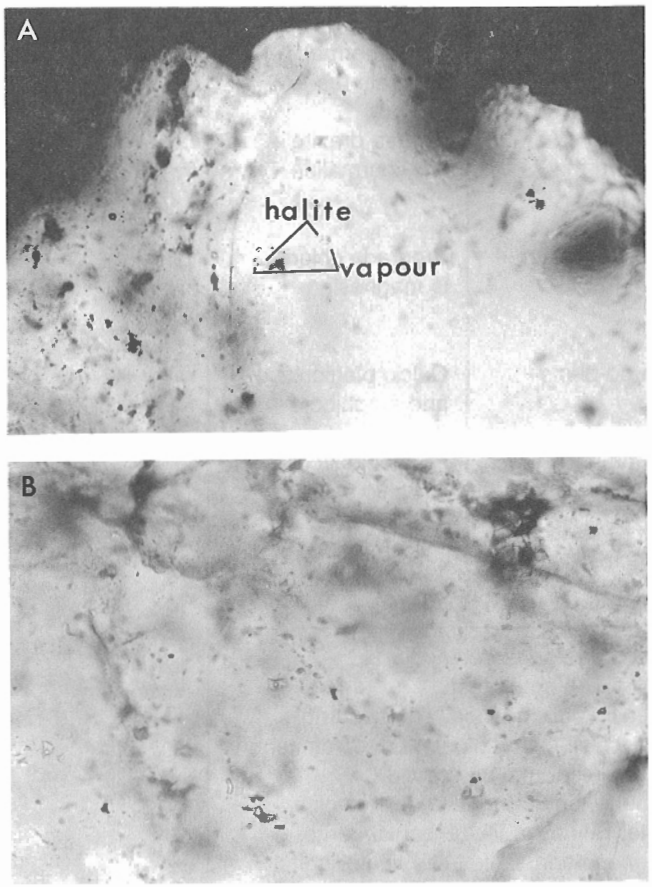

Figure 3. Fluid inclusions (classification in Leitch, 1991) in quartz of stockwork zone cutting tourmalinite. **A**) Halite daughter of same size as vapour bubble in 5-10 μm long Type 1 inclusions, sample G79SL4. **B**) 5-15 μm long Type 2a inclusions in sample 90SVL4 lacking halite daughter.

Footwall vent complex

Tourmalinite alteration

Dark brown to black, massive to fragmental, conchoidal-fracturing, intensely tourmalinized rocks underlying the western orebody contain bedding-parallel and transgressive pyrrhotite replacements. They are also cut in places by a stockwork of quartz-sulphide veins (Fig. 2A). A framework of detrital quartz grains is still apparent but detrital feldspar and clay/mica present regionally are largely replaced by tourmaline, magnesian chlorite and muscovite (Fig. 2B; cf. Leitch et al., 1991). Tourmaline displays two forms: major amounts of felted, extremely fine grained (5-15 μm) euhedral needles, typical of the hydrothermal alteration and probably replacing former feldspar; and minor 0.3 mm euhedral dravite with yellowish pleochroism that mimics the distribution of ?detrital schorl in regional Aldridge samples. These two tourmalines are also seen in the footwall fragmental rocks (see below) and in samples from North Star Hill (Leitch et al., 1991). Sulphides, including pyrrhotite, chalcopyrite and arsenopyrite, occur as clots, replacements and in vein stockworks; veins also contain pyrite, marcasite, galena, boulangerite and native Bi, plus ilmenite, sphene, rutile and ?apatite. The Ti-minerals in these samples are clearly hydrothermal, occurring with the sulphides in veins and bedding-parallel replacements, some of which cut veins. Rare subhedral ?zircon and monazite occur in chlorite, the latter with strong pleochroic haloes. Green clasts are richer in chlorite, muscovite and quartz compared to the rest of the rock, and are not tourmalinized (Fig. 2B).

Several specimens were collected from this zone to look at quartz in the pyrrhotite-arsenopyrite veins for Type 1 fluid inclusions of Leitch (1991: specimen G79SL4). Many of the inclusions stretched during heating and could not be homogenized even at 450-500°C, making the high temperatures of

Type 1 inclusions suspect. Repeat measurements on sample G79SL4 and this year's samples showed that although many of the Type 1 inclusions are highly saline, with the size of daughter halite cubes suggesting 35-45 wt.% NaCl equivalent (Fig. 3A; cf. Fig. 1C of Leitch, 1991), none have reliable homogenization temperatures over 320°C and they must therefore be redefined as differing from Type 2 by the presence of a halite daughter. Attempts to measure the salinity by the disappearance of the salt cube were not precise, with estimates ranging from 295 to 405°C suggesting salinities, if only NaCl were present, of 37 to 46 wt.% NaCl equivalent (Crawford, 1981). However, repeated eutectic temperatures of -55°C or below suggest the presence of $CaCl_2$; other melting events at -40 and -25°C suggest the possible presence of $MgCl_2$, with Na:Ca:Mg ratios possibly about 2:1:1 (Crawford et al., 1979a,b). Furthermore, the "salting-out" effect of Ca and Mg on NaCl (Roedder, 1984) means that the true salinity of these inclusions is possibly about 25-32 wt.% NaCl equivalent if only Ca is present, or 15-27 wt.% if Mg is also present. Type 2 inclusions in these quartz veins cutting tourmalinite (Fig. 3B) show lower salinities (10-25 wt.%) and temperatures (166-280°C), confirming results presented in Leitch (1991) and suggesting a continuum from Type 1 to Type 2 fluids.

Quartz ± sulphide-cemented footwall fragmental rocks

Variably tourmalinized fragmental rocks, characteristic of parts of the footwall to the massive sulphide body, are similar to breccias (see below), but lack a sulphide matrix. They are clast-supported and conglomerate-like, with pebbles (Fig. 4A) of Aldridge Formation in a siliceous and locally pyrrhotitic "matrix". Subangular clasts (to 4 cm) vary from silicate-rich (biotitized or variably tourmalinized: Fig. 4B), to semimassive or laminated pyrrhotite replacements (Fig. 4C). Some clasts contain abundant chlorite as euhedral, 0.05 mm flakes with a seriate texture, as in massive chlorite rock (see below). Clasts occur within clasts; in these the ratio of

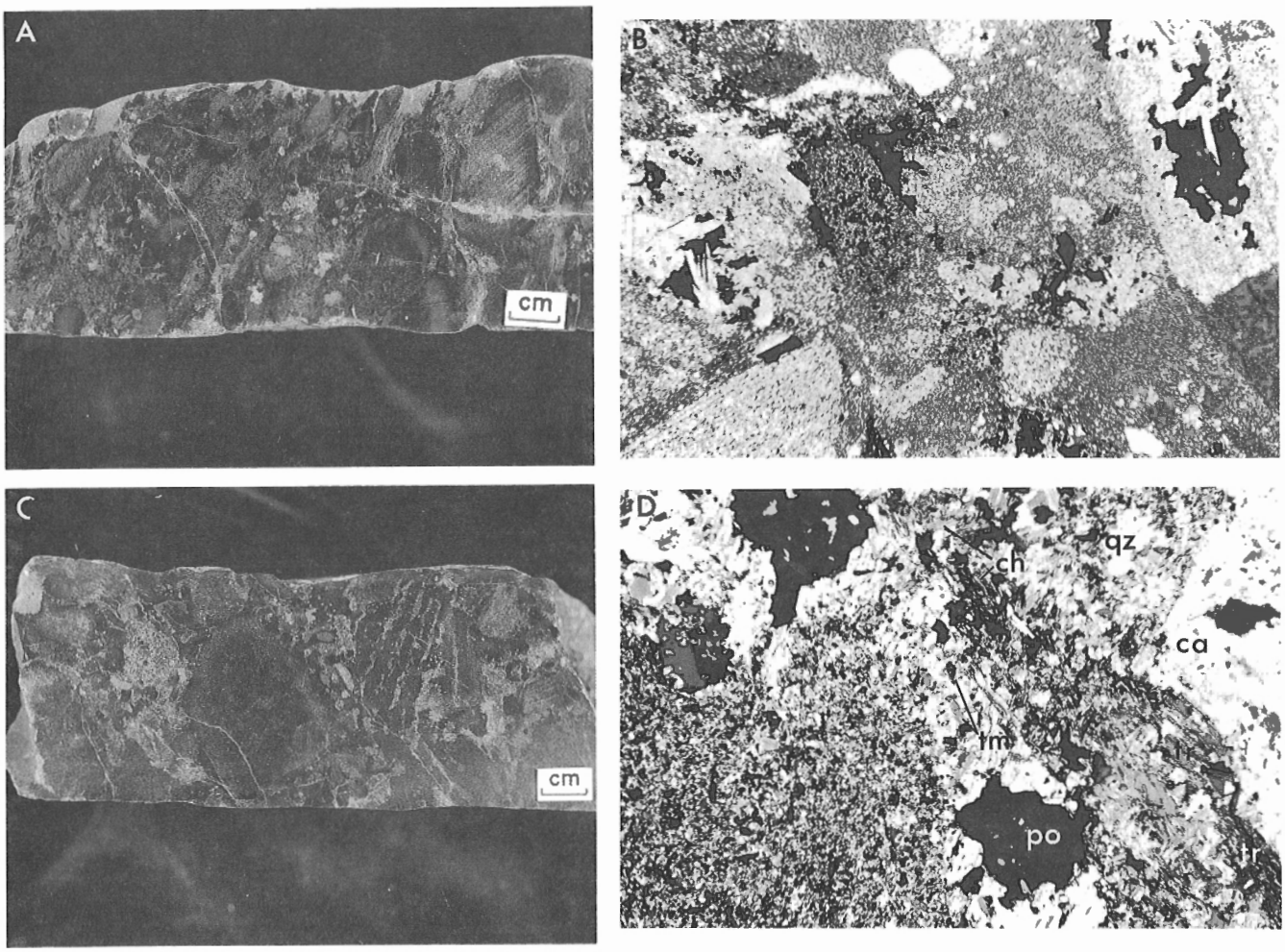

Figure 4. Variably tourmalinized footwall fragmental rocks. **A**) Rounded pebble-like clasts (cf. G.D. Delaney and K.L. Hauser, unpub. rep., 1983) in "conglomerate", sample 90SVT3. **B**) Subangular clasts, sample 90SVT4; some clasts and the matrix are highly tourmalinized. Transmitted light, uncrossed polars, width of view 5 mm. **C**) Laminated and massive pyrrhotite replacement of clasts, sample 90SVT4. **D**) Matrix minerals, including calcite (ca), chlorite (ch), pyrrhotite (po), tremolite (tr), quartz (qz), and tourmaline (tm); strongly tourmaline-biotite altered clasts. Transmitted light, crossed polars, width 5 mm.

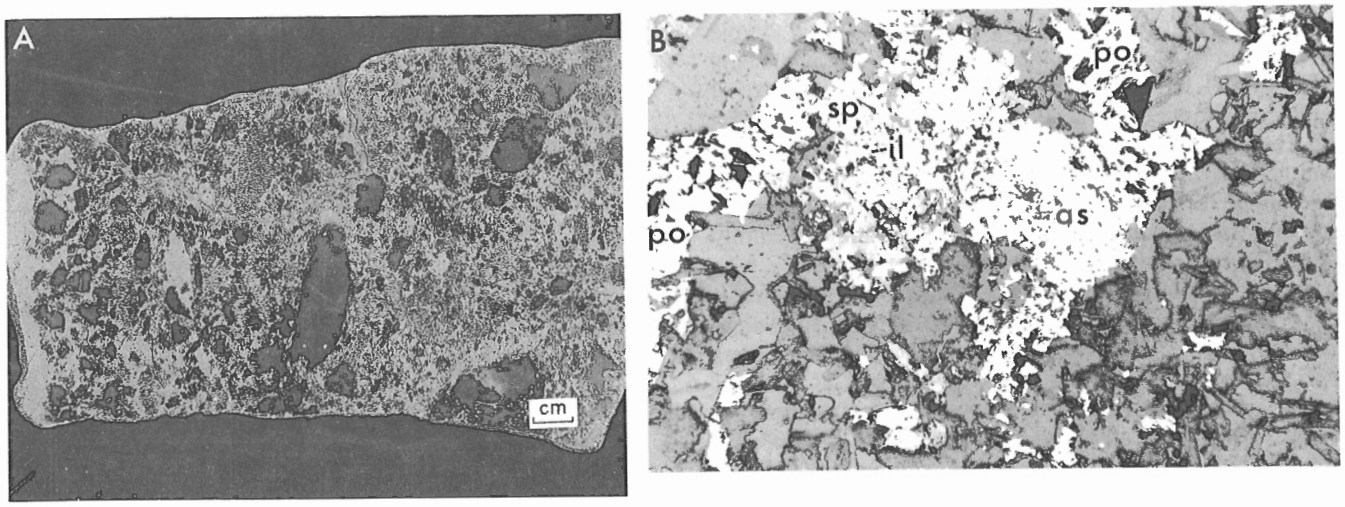

Figure 5. Pyrrhotite matrix "breccia". **A**) Subrounded dark green clasts in pyrrhotitic matrix, sample 90SVT6b. **B**) Opaque minerals in matrix of sample 90SVT2: pyrrhotite(po)-arsenopyrite(as), with ilmenite (il) grains in sphene (sp). Reflected light, uncrossed polars, field of view 1.3 mm.

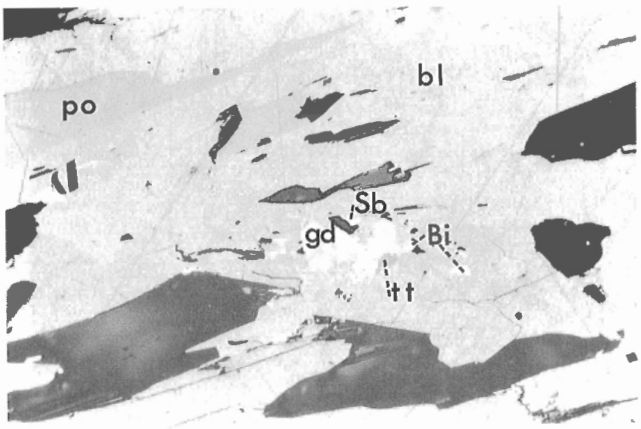

Figure 6. Composite 100 μm grain of gudmundite (gd), native Sb and Bi, tetrahedrite (tt), with pyrrhotite (po), in massive boulangerite (bl) of bedding-parallel vein, sample 90SVL2. Reflected light, uncrossed polars.

fragments to matrix is about 80 to 20. Tourmaline in the clasts forms randomly oriented euhedral crystals that are so fine (10 μm) that their colour is difficult to determine: it may be intermediate in composition between dravite and schorl (cf. Ethier and Campbell, 1977). It appears to be hydrothermal, replacing chlorite in places. Quartz occurs as fine rounded pebbles or angular clasts as well as finer anhedral matrix grains. The "matrix" between clasts (Fig. 4D) is composed of coarse, euhedral calcite-magnesian chlorite-pyrrhotite± quartz-tremolite-tourmaline-biotite-muscovite-sphene and traces of monazite-?apatite-sphalerite-galena-chalcopyrite-arsenopyrite. This assemblage locally corrodes clasts or occurs as irregular replacements or narrow quartz-chlorite stringers. Matrix tourmaline is coarse and euhedral, with the distinct yellow colour of dravite (cf. Taylor and Slack, 1984). Sphene is associated with pyrrhotite, and may contain small euhedral grains of rutile. The coarse grain size of sphene (1 mm) suggests it is hydrothermal; it contains trails of 7 μm long pseudosecondary fluid inclusions.

Sulphide-matrix breccias

These fragmental rocks, which occur in the R-10-30 decline adjacent and gradational to the quartz-cemented footwall fragmental rocks, consist of up to 5 cm subangular black to dark green clasts supported in a pyrrhotitic matrix (Fig. 5A). The clasts are not tourmalinized; they contain rounded ?detrital quartz up to 0.2 mm with scattered euhedral 0.1 mm muscovite and chlorite flakes. The matrix comprises subhedral pyrrhotite and coarse euhedral crystals of muscovite, quartz, magnesian chlorite and tourmaline, anhedral calcite, large garnets, and minor sphene and ilmenite ± traces of ?apatite and monazite. Pyrrhotite contains rounded inclusions of chalcopyrite, fine euhedral rhombs (rarely over 50 μm) of arsenopyrite, minor subhedral sphalerite, and traces of subhedral galena. The sulphides (Fig. 5B) are closely associated with or included in sphene, some of which contain cores of ilmenite. Tourmaline forms euhedral zoned crystals of dravite with distinctive yellow pleochroism as opposed to the blue to khaki pleochroism of the widespread ?detrital schorl found in all Aldridge sediments examined (Leitch et al., 1991). Garnets have sieve textures with silicate and sulphide inclusions; epidote is absent. Fluid inclusions in hydrothermal quartz of the matrix are Type 1, 2a or 2b (200-300°C, some with halite daughter), and calcite contains 4 μm pseudosecondary inclusions (Type 2a). No fluid inclusions were seen in tourmaline.

Massive chlorite-pyrrhotite footwall alteration

Massive chlorite-pyrrhotite rock in the immediate footwall of the western orebody, exposed underground in R-10-30, appears to grade into either massive pyrrhotite of the orebody or pyrrhotite-matrix breccia. Abundant irregular pyrrhotite

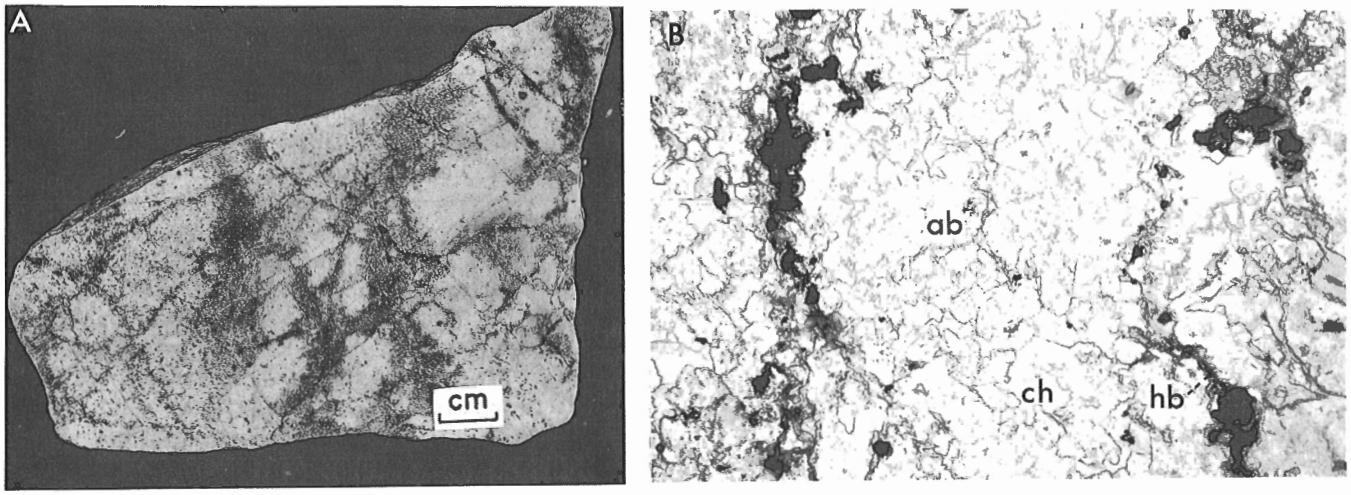

Figure 7. Hanging wall albite-chlorite zone, sample 90SVT13. **A**) Albitite cut by grey network of dolomite-hydrobiotite-ferrous chlorite-pyrite-minor quartz-sphene fractures. **B**) Thin section view (1.3 mm wide) of subhedral 0.1 mm albite (ab), magnesian chlorite (ch); fractures with dark hydrobiotite (hb), opaque pyrite. Transmitted, plane light.

blebs, coarse rounded grains of calcite and lesser quartz, plus euhedral crystals of sphene and rare brown euhedral biotite, are set in a matrix of nonoriented coarse euhedral Mg-chlorite flakes. Dark green pleochroic haloes in the chlorite surround euhedral 25 μm ?monazite crystals; euhedral ?zircon and apatite crystals are clearer and lack haloes. Large poikilitic quartz grains do not look detrital. Well-developed 120° triple junctions in pyrrhotite containing galena and chalcopyrite inclusions, indicate annealing. Galena contains minute inclusions of native Bi (confirmed by scanning electron microscope: cf. sample 89SVR1 in Leitch, 1991). Abundant sphene and magnesian chlorite could possibly suggest a mafic volcanic protolith. Rare calcite grains contain cores full of two-phase ?primary fluid inclusions up to 5 μm across, plus pseudosecondary trails of possibly three-phase, vapour-rich inclusions up to 7 μm (respectively Types 2a and 4: Leitch, 1991).

Intrusive Rocks

A specimen of Moyie sill that intrudes the vent complex in G-13-30 is a medium grained, altered, vaguely porphyritic rock. The sill, possibly an altered gabbro, now consists of 1-2 mm ragged hornblende relict phenocrysts in a fine grained matrix of quartz and relict plagioclase; the latter may originally have been 1 mm grains of calcic composition that were subsequently replaced by sericite, epidote, chlorite and quartz. Amphibole is replaced by epidote-chlorite-dolomite-pyrrhotite; relicts of ilmenite are found at centres of sphene grains.

Sulphosalt veinlets, massive pyrrhotite body

A sample from the base of the massive pyrrhotite orebody in R-10-30 contains a 2 cm thick bedding-parallel "vein" of boulangerite ($Pb_5Sb_4S_{11}$) and Mg-chlorite. Within the boulangerite are small anhedral grains up to 50 μm long of an Fe-Sb sulphosalt, probably gudmundite (FeSbS), that contains 1-10 μm inclusions of probable native Sb and native Bi (Fig. 6). Two varieties of tetrahedrite, a light grey argentian variety (freibergite) and an olive-grey more Fe-rich, Cu-poor variety lacking Ag, are found in association with these minerals. Generalizing from results obtained in preliminary scanning electron microscope work from this and other samples, the indications are of a Pb-Sb-Fe-Bi group of sulphosalts including tetrahedrite, boulangerite, gudmundite, and native Sb and Bi metals in the Sullivan ores. Silver appears to be mainly in tetrahedrite (although pyrargyrite is reported by Hamilton et al., 1983) and does not occur in Pb sulphosalts; arsenic appears to be restricted to arsenopyrite, tetrahedrite being As-free.

Hanging wall albite-chlorite-pyrite alteration

Altered rocks in this zone consist of two distinct rock types: dark green chlorite with up to 40% coarse cubic pyrite, or light grey to white, albite-chlorite rocks veined by an irregular network of dark grey carbonate-hydrobiotite-chlorite-pyrite±quartz-muscovite-sphene fractures (Fig. 7A). Albite (An_7) is subhedral, 0.1 mm, and slightly clouded by fine clay and fluid inclusions (Type 5 secondary: Leitch, 1991). Chlorite is interstitial and has little colour and high relief suggesting a Mg-rich variety such as ripidolite (Fig. 7B). Within the fractures some chlorite has distinct green pleochroism and purple anomalous birefringence that suggest retrograde higher-Fe chlorite (note that Mg-chlorite is stable to upper greenschist facies while Fe-chlorite is not: Winkler, 1971). Fine, ragged, brownish hydrobiotite accompanying the Fe-chlorite gives the dark colour to the pyritic fracture network. The stable Ti phase in this rock appears to be rutile, forming randomly oriented tiny euhedral needles replacing sphene. Carbonate, probably dolomite (not as common as calcite in the Sullivan system), is distributed mainly along the fracture system and may therefore be late. Coarse carbonate, quartz and muscovite occur in pressure shadows of the larger pyrite

cubes; rare veins with chlorite selvages consist of 3 mm long anhedral strained quartz grains with regular subhedral 50 μm inclusions of albite. The quartz contains abundant secondary fluid inclusions up to 7 μm long, some with possible halite daughters (probable Type 1 and 2a: Leitch, 1991).

BEDDED FACIES

Samples of finely bedded sulphides were collected from Stopes 1 and 3 of the Southeast (S.E.) Fringe Zone (Fig. 1). Footwall slate samples are from earlier collections not precisely located in the mine.

Southeast Fringe Zone bedded sulphides

Samples from this zone (see also SUL13: Leitch, 1991) are finely laminated, isoclinally folded pyritic ore (Fig. 8A). Beds up to 2 cm thick are composed of extremely fine grained pyrite with remnant framboidal and atoll texture, or balls of collomorphic pyrite, all overgrown by coarse euhedral pyrite. Some pyrite beds are graded with pyrite-rich bases overlain by increasing amounts of pyrrhotite and porphyroblastic garnet, quartz and magnetite, all with poikilitic pyrite inclusions. These pyrite beds are interlayered with beds of massive or euhedral lath-shaped pyrrhotite up to 1 cm thick (Fig. 8B) and thin (1-2 mm) sharply defined black layers of quartz-dolomite-calcite-garnet-hydrobiotite-green muscovite-Fe chlorite-sphene-rare schorl and sphalerite ± minor galena. During deformation, fine pyrite layers have fragmented (Fig. 8C) allowing more ductile pyrrhotite to flow into cracks in pyrite and magnetite. It is difficult to see how the euhedral pyrrhotite laths could survive deformation; they must represent syndeformation recrystallization or postdeformation deposition. Fold hinges are especially prominent in the

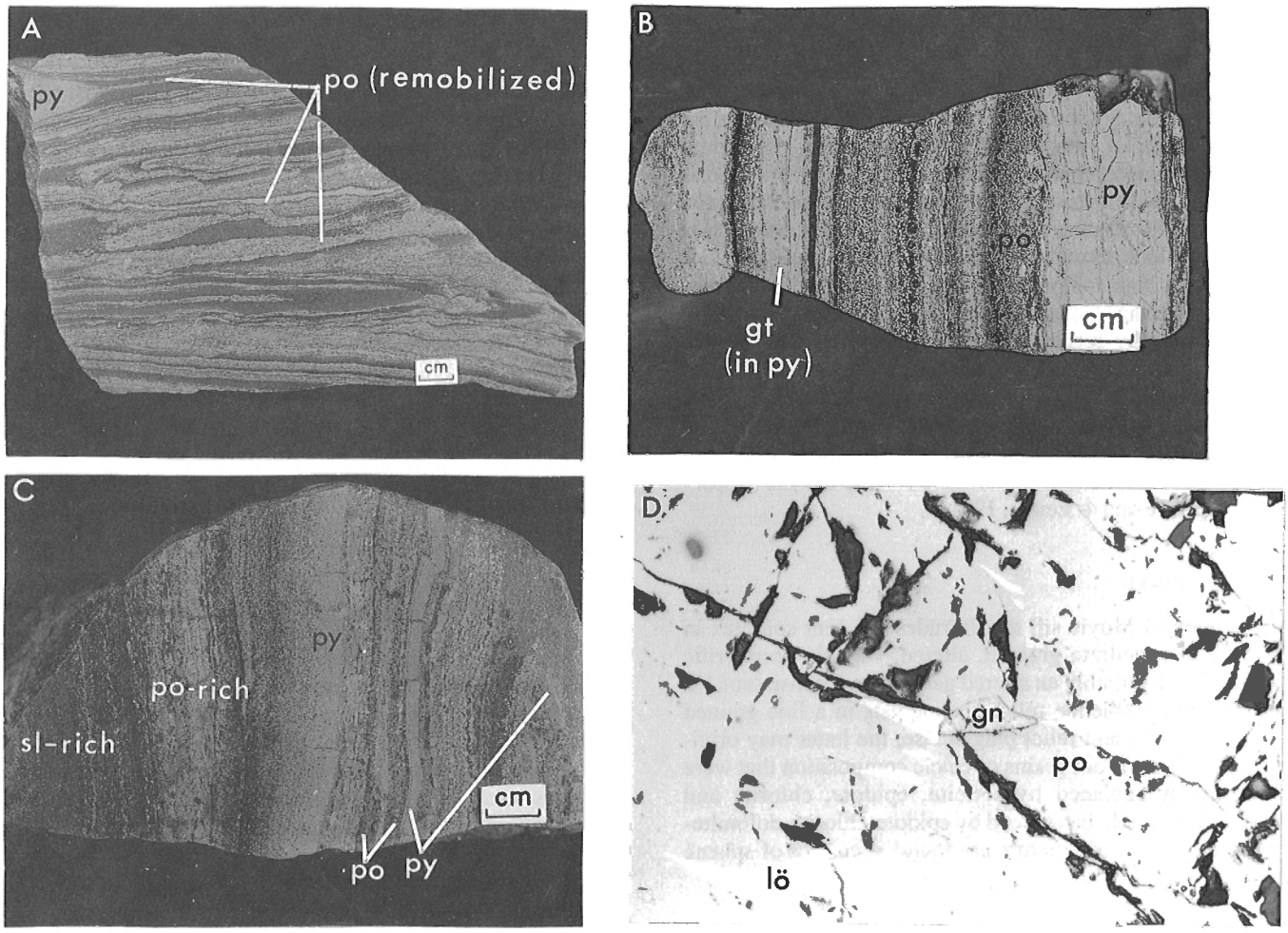

Figure 8. Southeast Fringe Zone laminated ores. **A**) Tightly folded thin beds of pyrrhotite and rare thicker beds of fine pyrite (py), cut by thin remobilized veins of pyrrhotite (po) in sample 90SVT18. **B**) Remnant atoll and collomorphic textures in pyrite (py), which also occurs in thick massive beds that are fractured and infilled by pyrrhotite (sample 90SVT16). Bladed laths of pyrrhotite (po) also visible to left of the scale; garnet (gt). **C**) Broken and boudinaged pyrite (py) beds in darker matrix of pyrrhotite (po), sphalerite (sl) and silicates, sample 90SVT19. **D**) Löllingite (lö) as wispy grains up to 60 μm long in remobilized pyrrhotite (po); minor galena (gn). Reflected light, uncrossed polars, sample 90SVT19.

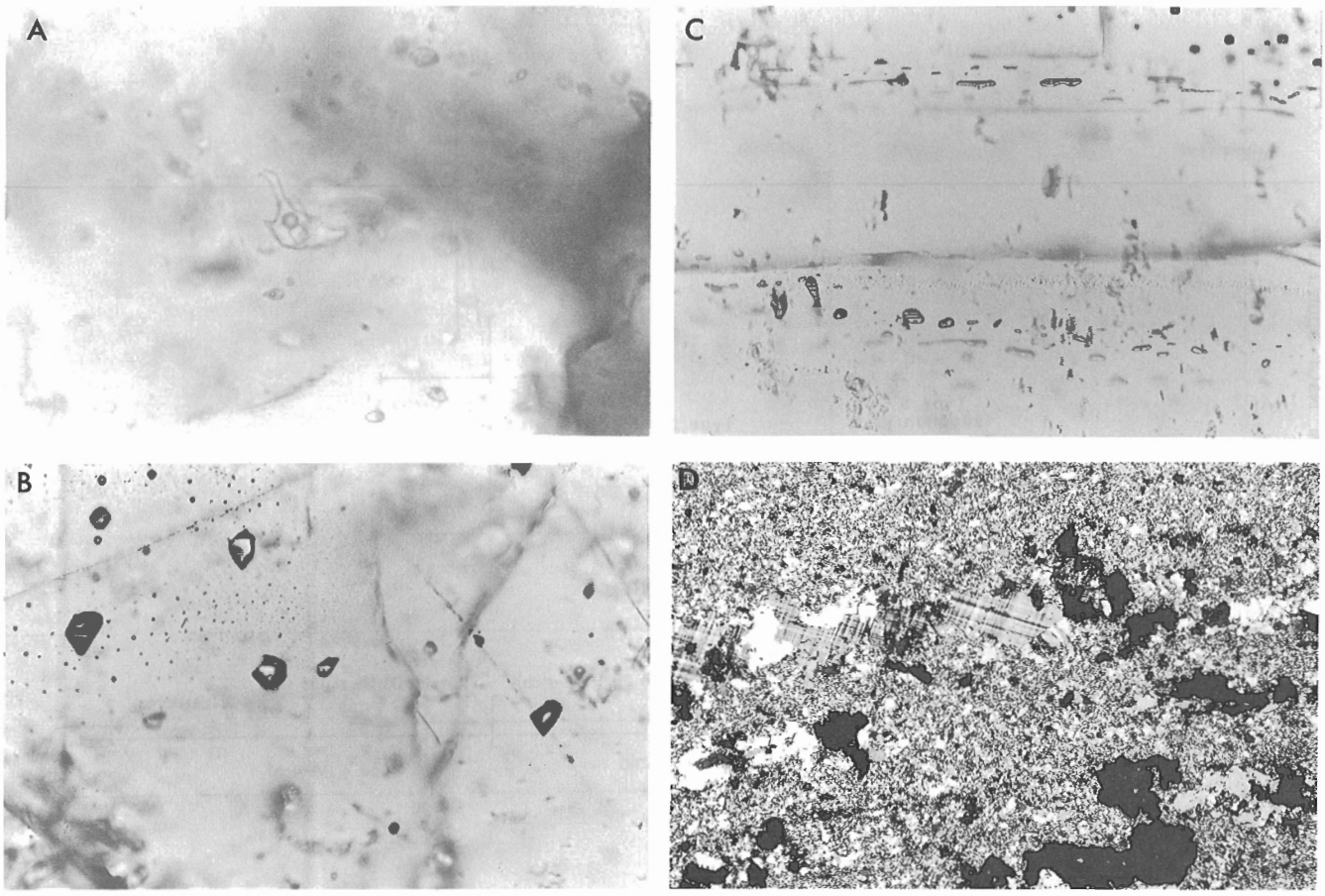

Figure 9. Fluid inclusions in coarse sphalerite "blow" containing quartz "augen" of Southeast Fringe Zone, sample 90SVL3. **A**) 5 μm halite daughter cube, larger than vapour bubble, in Type 1 inclusions in quartz. **B**) Type 2a pseudosecondary inclusions (dark, vapour bubble barely visible) up to 15 m across in sphalerite. **C**) Type 5 secondary inclusions as planar arrays with tubular shapes up to 20 m long in sphalerite. **D**) Bedding-parallel layer of quartz-microcline-sulphide in sericitized "footwall slate", sample 83SVT5; crossed polars, field of view 2.5 mm.

fine pyritic layer, in places apparently cut by thin veins of remobilized pyrrhotite ± minor sphalerite-galena-?löllingite ($FeAs_2$: Fig. 8D).

Carbonate and quartz in the bedded ore have trails of fine (2-3 μm) secondary/pseudosecondary fluid inclusions, probably Type 2b of Leitch (1991). However, quartz (Fig. 9A) and sphalerite (Fig. 9B) from a coarse pegmatitic pod in the southeast fringe zone contain abundant large pseudosecondary Type 1 and 2 inclusions respectively. The sphalerite also contains secondary inclusions (Fig. 9C) with salinities of about 10-15 wt.% NaCl and homogenization temperatures of 140-155°C. This pod also contains albite (An_{7-8}) similar in texture and size to that seen in hanging wall albitite, plus muscovite and dark brown biotite that is replaced by an Fe-rich chlorite. In quartz, most but not all inclusions contain a halite daughter (Fig. 9A), probably contain $CaCl_2$, and have salinities of around 20-30 wt.% NaCl equivalent. Inclusions in sphalerite are dark, but none appears to contain halite; salinities, including significant $CaCl_2$, are in the 20-25 wt.% range. Imprecisely measured clathrate melting at about +6 to +20°C suggests the presence of minor CO_2 in both quartz and sphalerite inclusions. Homogenization temperatures are difficult to measure due to stretching, leaking and decrepitation. Reliable estimates are confined to the range 165-295°C for sphalerite and 226-325°C for quartz, similar to inclusions from the stockwork zone.

Footwall slate

Samples of pale olive-green "footwall slate" appear to be sericite-chlorite-Kspar-albite-quartz altered equivalents of typical dark brown biotitic metasediments of the Lower Aldridge that contain a metamorphic assemblage of quartz-muscovite-biotite-garnet-tourmaline-pyrrhotite-monazite. The altered rocks contain relics of biotite, bedding-parallel layers of quartz and microcline (Fig. 9D) or albite (An_5), pyrite and minor sphalerite. As at North Star Hill (Leitch et al., 1991) feldspar in the altered rocks does not appear to be of primary detrital origin.

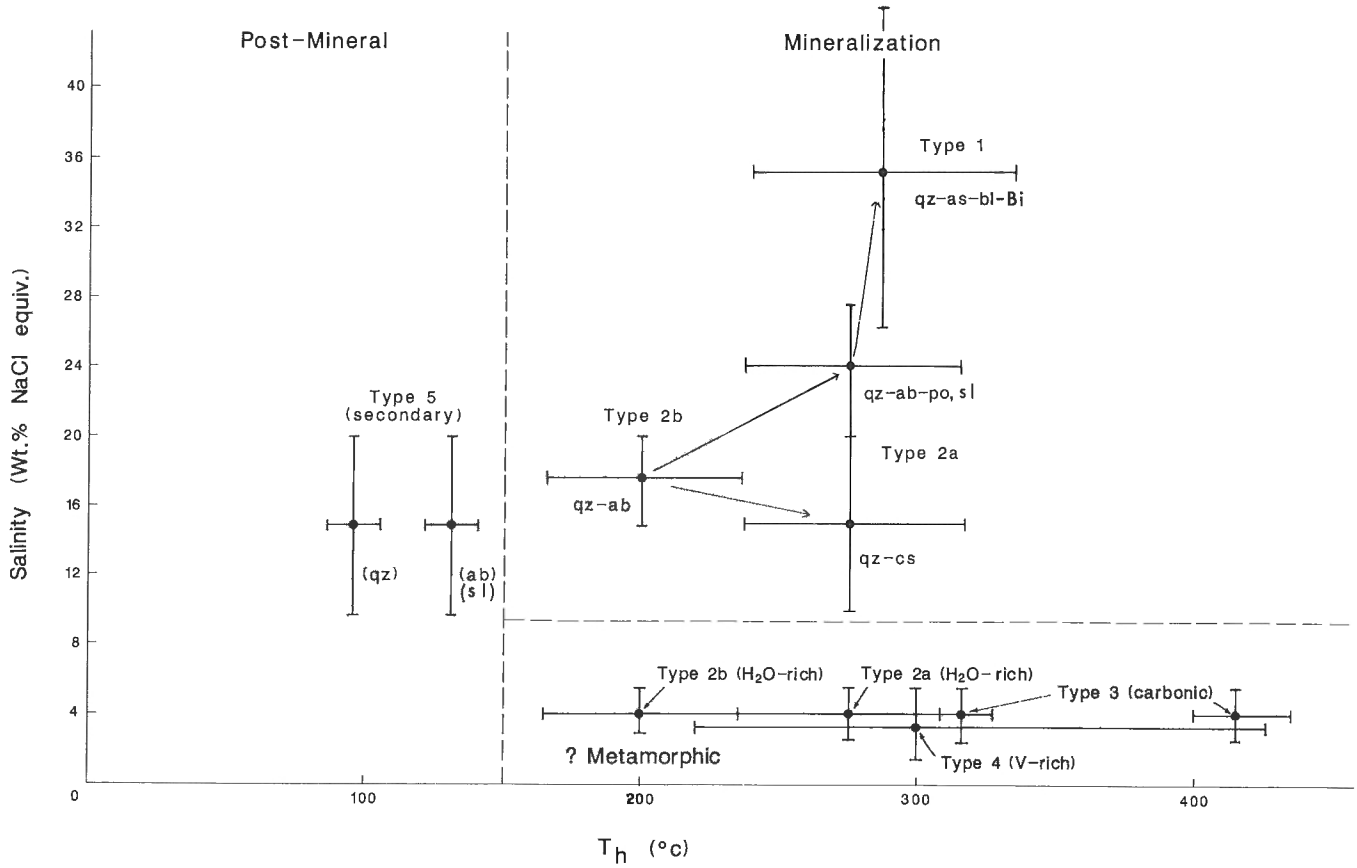

Figure 10. Salinity versus T_h (homogenization temperature) plot for the fluids observed at Sullivan; T_h values over 325°C are plotted but may be due to stretching. The division into metamorphic and mineralization related fluids is tentative, and is based on the difference in salinity between the two groups and the carbonic component of the latter. Parageneses of associated minerals suggest a progression from Type 2b to 2a to 1. Abbreviations are: ab=albite, as=arsenopyrite, bl=boulangerite, cs=cassiterite, po=pyrrhotite, qz=quartz, sl=sphalerite, V=vapour.

DISCUSSION

Petrographic and fluid inclusion studies of the western massive sulphide orebody and bedded sulphides from the Southeast Fringe zone at the Sullivan deposit have added to the data base for this important ore deposit and complement studies of the Sullivan-North Star zone (Leitch et al., 1991). Most chlorite in hanging wall and footwall alteration appears from its optical properties to be magnesian, and is therefore stable at middle and upper greenschist facies. An Fe-chlorite is seen rarely, always in late fractures of ?retrograde paragenesis such as fractures cutting hanging wall albite-chlorite alteration or in a coarse sphalerite-quartz pod in the Southeast Fringe ore zone. Chlorite in samples from North Star Hill and regional Aldridge rocks is also either a late Fe-rich variety replacing biotite and garnet, or Mg-rich where it forms part of the hydrothermal assemblage. Tourmaline associated with the hydrothermal assemblage is magnesian (dravite) where it is coarse grained enough to determine; the massive fine grained replacements are too fine to see the pleochroism properly and must await chemical analysis for identification. Schorl, or common iron tourmaline, is widespread in Aldridge rocks as coarse stubby euhedral grains that may be detrital, derived from acid igneous rocks, or a product of widespread hydrothermal activity in the basin.

The hydrothermal vent or feeder zone, marked by minor sulphide-quartz veining hosted in intensely tourmalinized rocks below the western orebody, appears to be manifested upward by fragmental rocks with cement or matrix that consists of quartz, calcite, pyrrhotite, tremolite, dravite, mica, sphene, garnet and minor sulphides. Some of these minerals may be metamorphic, but epidote, a possible metamorphic mineral seen regionally and on North Star Hill, is lacking at Sullivan. The matrix varies from silicate-rich to sulphide-rich, giving the footwall fragmental rocks the appearance of conglomerates and breccias, respectively. Similar minerals are found in massive chlorite-pyrrhotite rocks immediately below the massive orebody, implying they are also the product of hydrothermal activity. The occurrence of chlorite and sphene in footwall and hanging wall alteration zones near the deposit, in more distal stratigraphically equivalent "footwall slate", and in the Moyie sills (cf. Höy, 1989), may suggest a possible sill or tuff horizon just below the orebody or widespread alteration by magmatic fluids.

Re-evaluation and extension of fluid inclusion data show that Type 1 inclusions (Fig. 10; inclusion types defined in Leitch, 1991) in thin quartz veins of the feeder zone below the western massive sulphide body are of moderate temperature (300°C) and may contain significant divalent salts such as $CaCl_2$ and possibly $MgCl_2$, in addition to NaCl. They may therefore have lower salinities (15-32 wt.%) than indicated by the size or dissolution temperature of the halite daughter mineral (37-46 wt.%). These characteristics are transitional to those of Type 2 inclusions, which are distinguished by the absence of a halite daughter phase. The hottest, most saline fluids are associated with what appears to be the latest paragenesis (arsenopyrite-boulangerite-Bi), indicated by the arrows on Figure 10, but this requires further work.

Type 1 and 2 fluids are also found in coarse sphalerite-quartz pods in bedded sulphides from the Southeastern Fringe Zone. This coarse assemblage may represent distal vent complex alteration within the hydrothermal sediments, or metamorphic remobilization. The similarity of these fluids to those in minerals from the stockwork feeder zone below the western orebody suggests the former hypothesis is correct, but does not rule out a metamorphic origin for fluids in both areas. Only low salinity Type 2a and 2b fluids (Fig. 10), associated with Type 3 and 4 carbonic (CO_2 + CH_4 bearing) fluids, are suggested to be metamorphic. Prograde or retrograde metamorphic $CaCl_2$ bearing fluids similar to Sullivan Type 1 and 2 fluids have been described by Crawford et al. (1979a and 1979b respectively). Although the prograde fluids described are from a calc-silcate environment quite different from the Aldridge, the retrograde fluids are from amphibolite-grade greywackes and pelites. It remains ambiguous whether the fluids observed at Sullivan are related to ore deposition or later metamorphism. Further work on inclusions in unaltered metamorphic rocks is required to resolve this problem.

Bedded sulphides of the Southeastern Fringe Zone show traces of former framboidal, collomorphic and atoll textures preserved in the refractory pyrite, whereas the more ductile pyrrhotite has responded to stress by flowing. Boudinage of the pyritic layers and isoclinal folding suggests that stratigraphy in these layers has been modified by structural repetition, as suggested by McClay (1983).

ACKNOWLEDGMENTS

We are indebted to Cominco staff at the Sullivan mine for permission to visit and further sample the Sullivan deposit, access to drawings and information at the mine site, and valuable discussions; we particularly thank Norris del Bel Belluz for a tour of the mine. Wayne Goodfellow, John Hamilton and Dave Shaw are thanked for critical reading of the manuscript, and we are grateful to Richard Lancaster for preparing and photographing the polished slabs used in this study.

REFERENCES

Beaty, D.W., Hahn, G.A., and Threlkeld, W.E.
1988: Field, isotopic, and chemical studies of tourmaline-bearing rocks in the Belt-Purcell Supergroup; genetic constraints and exploration significance for Sullivan-type ore deposits; Canadian Journal of Earth Sciences, v. 25, p. 392-402.

Crawford, M.L.
1981: Phase equilibria in aqueous fluid inclusions; in Fluid Inclusions: Applications to Petrology; Mineralogical Association of Canada, Short Course Handbook, v. 6, p. 75-100.

Crawford, M.L., Filer, J., and Wood, C.
1979b: Saline fluid inclusions associated with retrograde metamorphism; Bulletin de Minéralogie, v. 102, p. 562-568.

Crawford, M.L., Kraus, D.W., and Hollister, L.S.
1979a: Petrologic and fluid inclusion study of calc-silicate rocks, Prince Rupert, British Columbia; American Journal of Science, v. 279, p. 1135-1159.

Ethier, V.G. and Campbell, F.A.
1977: Tourmaline concentrations in Proterozoic sediments of the southern Cordillera of Canada and their economic significance; Canadian Journal of Earth Sciences, v. 14, p. 2348-2363.

Hamilton, J.M. and Shaw, D.R.
1986: Evolution of source fluid and resulting deposits during genesis of the Sullivan orebody, Kimberley, B.C.; Geological Society of America, Abstracts with Programs, v. 18, p. 626.

Hamilton, J.M., Delaney, G.D., Hauser, R.L., and Ransom, P.W.
1983: Geology of the Sullivan deposit, Kimberley, B.C., Canada; in Sediment-Hosted Stratiform Lead-Zinc Deposits, (ed.) D.F. Sangster; Mineralogical Association of Canada, Short Course Handbook, p. 31-83.

Höy, T.
1989: The age, chemistry, and tectonic setting of the Middle Proterozoic Moyie sills, Purcell Supergroup, southeastern British Columbia; Canadian Journal of Earth Sciences, v. 26, p. 2305-2317.

Leitch, C.H.B.
1991: Preliminary fluid inclusion and petrographic studies of parts of the Sullivan stratiform sediment-hosted Pb-Zn deposit, southeastern British Columbia; in Current Research, Part A, Geological Survey of Canada, Paper 91-1A, p. 91-101.

Leitch, C.H.B., Turner, R.J.W., and Höy, T.
1991: The district-scale Sullivan-North Star alteration zone, Sullivan mine area, B.C.; A preliminary petrographic study; in Current Research, Part E, Geological Survey of Canada, Paper 91-1E (this volume).

McClay, K.R.
1983: Structural evolution of the Sullivan Fe-Pb-Zn-Ag orebody, Kimberley, British Columbia, Canada; Economic Geology, v. 78, p. 1398-1424.

McMechan, M.E. and Price, R.A.
1982: Superimposed low-grade metamorphism in the Mount Fisher area, southeastern British Columbia--implications for the East Kootenay orogeny; Canadian Journal of Earth Science, v. 19, p. 476-489.

Morris, H.C. and Geological Staff
1972: An outline of the geology of the Sullivan mine, Kimberley, B.C.; 24th International Geological Congress, Montreal 1972, Field Excursion Guidebook A24-C24, p. 26-34.

Nesbitt, B.E., Longstaffe, F.J., and Muehlenbachs, K.
1984: Oxygen isotopic geochemistry of the Sullivan massive sulfide deposit, Kimberley, British Columbia; Economic Geology, v. 79, p. 933-946.

Ransom, P.W., Delaney, G.D., and McMurdo, D.
1985: The Sullivan orebody; in Field Guides to Geology and Mineral Deposits in the Southern Canadian Cordillera, (ed.) D. Tempelman-Kluit; Geological Society of America Cordilleran Section Meeting, Vancouver, B.C., May 1985, p. 11-20 to 32.

Roedder, E.
1984: Fluid Inclusions; Mineralogical Society of America, Reviews in Mineralogy, v. 12, 644 p.

Shaw, D.R. and Hodgson, C.J.
1986: Wall-rock alteration at the Sullivan mine, Kimberley, B.C.; in The Genesis of Stratiform Sediment-Hosted Lead and Zinc Deposits: Conference Proceedings, (ed.) R.J.W. Turner and M.T. Einaudi; Stanford University Publications, School of Earth Sciences, v. 20, p. 13-21.

Taylor, B.E. and Slack, J.F.
1984: Tourmalines from Appalachian-Caledonian massive sulfide deposits: textural, chemical, and isotopic relationships; Economic Geology, v. 79, p. 1703-1726.

Winkler, H.G.F.
1971: Petrogenesis of Metamorphic Rocks; Third Edition, Springer-Verlag, New York, 237 p.

The district-scale Sullivan-North Star alteration zone, Sullivan mine area, British Columbia: a preliminary petrographic study

C.H.B. Leitch, R.J.W. Turner, and T. Höy[1]
Mineral Resources Division, Vancouver

Leitch, C.H.B., Turner, R.J.W., and Höy, T., 1991: The district-scale Sullivan-North Star alteration zone, Sullivan mine area, British Columbia: a preliminary petrographic study; in Current Research, Part E; Geological Survey of Canada, Paper 91-1E, p. 45-57.

Abstract

Lower Aldridge feldspathic greywacke, siltite, and argillite, within a zone extending 6 km south from and stratigraphically lower than the Sullivan orebody, are variably altered to muscovite-pyrite and tourmalinite assemblages which include variable quartz, muscovite, epidote, tourmaline, pyrite and pyrrhotite, lesser sphalerite and galena, and rare chalcopyrite and arsenopyrite. Metamorphic grade in these rocks is middle greenschist, as indicated by the assemblage quartz-muscovite-Mg chlorite-albite-microcline-biotite-epidote-garnet, whereas Fe-chlorite appears to be retrograde. Garnet, probably manganiferous, occurs only within altered rocks and likely reflects hydrothermal Mn enrichment of the original sediment. The presence of garnet provides an indicator of altered rocks, where other macroscopic criteria are lacking. Other more restricted exploration criteria such as abundant sulphides, tourmalinite, and massive nonbedded or fragmental rocks can focus exploration within the garnet-bearing zone. Epidote-tremolite "granophyric" alteration is developed adjacent to Moyie sills.

Résumé

Le grauwacke, la siltite et l'argilite feldspathiques de la formation inférieure d'Aldridge, à l'intérieur d'une zone s'étendant sur 6 km au sud du gisement Sullivan et lui étant stratigraphiquement inférieure, sont inégalement altérés en associations de muscovite-pyrite et de tourmalinite qui comprennent du quartz, de la muscovite, de l'épidote, de la tourmaline, de la pyrite et de la pyrrhotite, un peu de sphalérite et de galène, et très peu de chalcopyrite et d'arsénopyrite. Le degré de métamorphisme de ces roches a atteint celui du faciès intermédiaire des schistes verts, comme l'indique l'association quartz-muscovite-chlorite à Mg-albite-microcline-biotite-épidote-grenat, tandis que la chlorite à Fe semble rétrograde. Le grenat, probablement manganésifère, ne se trouve que dans les roches altérées et dénote vraisemblablement un enrichissement en Mn hydrothermal du sédiment original. La présence de grenat est un indice de roches altérées en l'absence d'autres indices macroscopiques. D'autres indices d'exploration plus restreints comme la présence de sulfures en abondance, de tourmalinite et de roches non stratifiées ou détritiques massives, peuvent orienter l'exploration à l'intérieur de la zone grenatifère. L'altération "granophyrique" en épidote-trémolite s'observe à proximité des filons-couches de Moyie.

[1] Ministry of Energy, Mines and Petroleum Resources, Geological Survey Branch, 200-756 Fort Street, Victoria, B.C. V8V 1X4

INTRODUCTION

Semiconformable zones of altered volcanic rocks kilometres in extent and hundreds of metres thick are associated with some volcanogenic massive sulphide districts. Such district-scale features, distinct from smaller alteration pipes underlying individual massive sulphide deposits, represent large-scale exploration targets. Alteration on a district scale associated with stratiform Zn-Pb deposits is less common, but has been described in the MacMillan Fold Belt, Yukon (Abbott and Turner, 1990). Höy (1984) described a zone of pyrrhotite alteration, tourmalinite, brecciation and loss of bedding definition in Aldridge strata in a zone that extends 5 km south of Sullivan Mine and includes the North Star Hill area. The Sullivan-North Star alteration zone shares similarities with altered and brecciated rock footwall to the Sullivan orebody (Hamilton et al., 1983; Shaw and Hodgson, 1986).

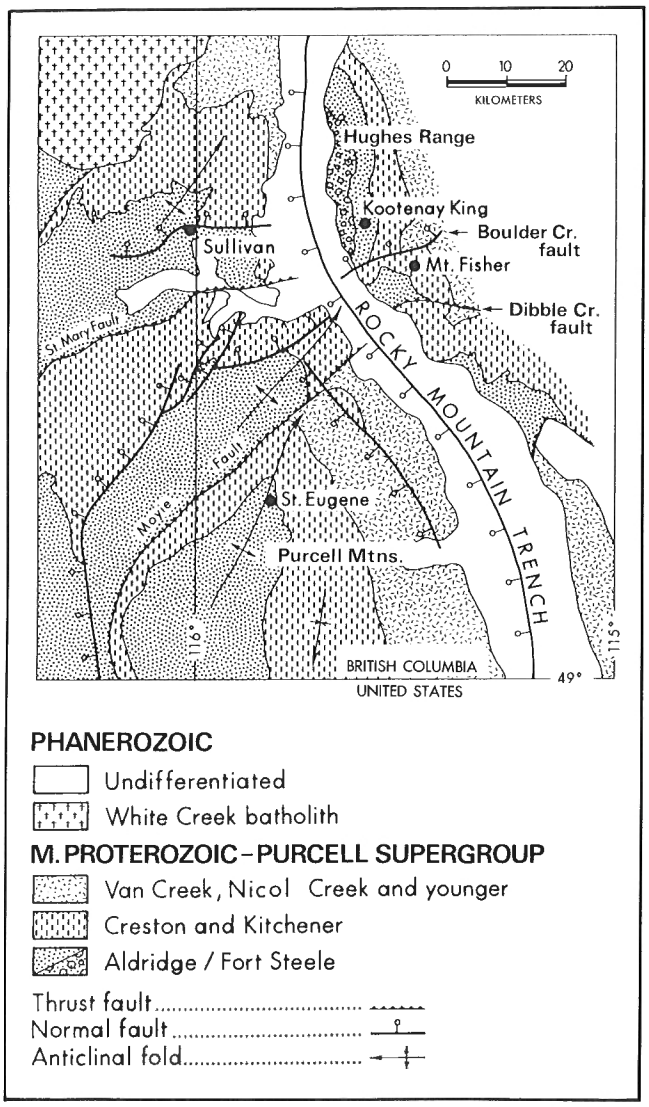

Figure 1. Regional map showing location of the Sullivan Mine in southeastern B.C. (from Höy, 1984).

Numerous zones of tourmalinite and albite-chlorite alteration occur in Aldridge strata in southeastern B.C. (Ethier and Campbell, 1977). Because of association of such alteration types with the Sullivan deposit, these alteration zones have been the target of much exploration effort over the years. However, the relationship of such alteration to Sullivan-type mineralization is poorly understood (e.g. Nesbitt et al., 1984; Beaty et al., 1988). This preliminary study is an attempt to document the petrographic character of the Sullivan-North Star alteration zone, and compare it to current studies of alteration at the Sullivan Mine (Leitch, 1991; Leitch and Turner, 1991). It lays the framework for our 1:2000 scale mapping of the Sullivan-North Star zone during 1991, part of the larger Sullivan project, an integrated multidisciplinary study that involves researchers from the Geological Survey of Canada, B.C. Geological Survey, the mining industry, Royal Ontario Museum, U.S. Geological Survey, and universities.

GEOLOGIC SETTING OF THE SULLIVAN-NORTH STAR ALTERATION ZONE

The Sullivan stratiform lead-zinc-silver orebody occurs in Middle Proterozoic Aldridge Formation turbidites in southeastern B.C. (Fig. 1). The Sullivan deposit occurs near the transition between laminated siltite and argillite of the Lower Aldridge Formation and overlying thicker bedded arenite, siltite, and argillite of the Middle Aldridge Formation (Hamilton et al., 1983; Höy, 1983). Aldridge strata near the Sullivan Mine form a gently-folded shallowly northeast-dipping homocline (Höy, 1984: Fig. 2) cut by a variably developed steep, west-dipping cleavage. Both east-trending (e.g. Kimberley) faults and younger north to northeasterly ("Sullivan-type") faults cut Aldridge strata in the Kimberley area (Fig. 2).

Sullivan-North Star alteration zone

A zone of alteration within the Lower Aldridge Formation 6 km long by up to 2 km wide extends south-southeastward from the Sullivan deposit to the North Star Hill area (Fig. 2). The north-dipping Kimberley fault, estimated to have over 2500 m of net normal slip, truncates this alteration zone to the north. The zone (Höy, 1984) is characterized by: (1) increased disseminated and irregularly laminated pyrrhotite and pyrite; (2) pyrite, galena and sphalerite-bearing veins; (3) stratiform Pb-Zn deposits; (4) zones of silicified and tourmalinized rock; (5) irregular zones of breccia or diamictite, with pyrite, pyrrhotite, and minor sphalerite and galena in the matrix; and (6) local obliteration of bedding associated with fragmental rocks. Lead-zinc deposits within the Sullivan-North Star alteration zone (Fig. 2) include the Sullivan and the smaller North Star high grade stratiform (Hamilton et al., 1983; Schofield, 1915) and Stemwinder vein deposits (Freeze, 1966).

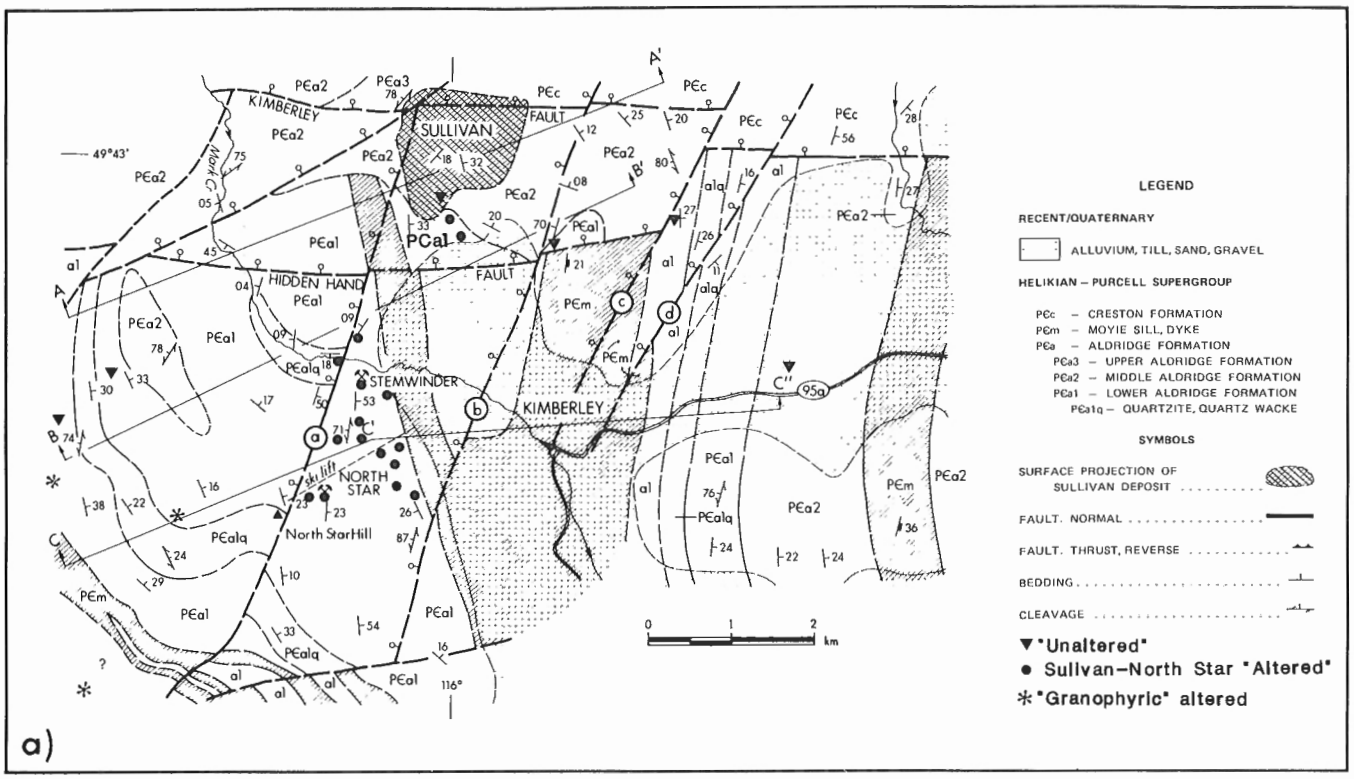

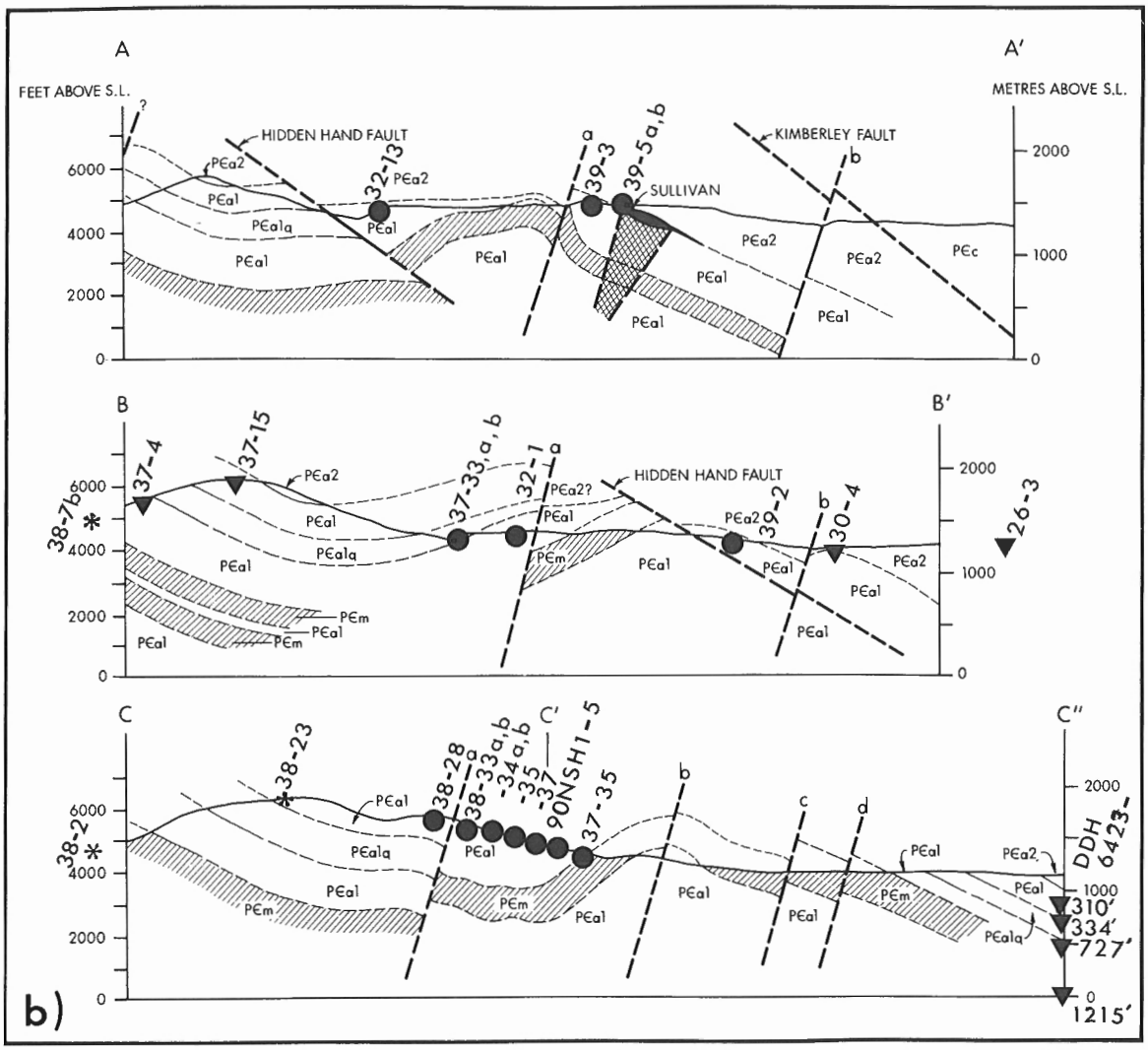

Figure 2. Geology in the vicinity of the Sullivan deposit, Kimberley (from Höy, 1984). Location of samples used in this study indicated.

Sample materials

Samples were collected on five traverses in the North Star Hill and Mark Creek areas, and from Cominco drill holes 3 km east of Kimberley, by Trygve Höy in 1981 (Fig. 2); further samples were collected on North Star Hill in October 1990. Petrographic study of 23 thin and 13 polished thin sections from these samples are the basis of this study.

"UNALTERED" ALDRIDGE METASEDIMENTARY ROCKS

Ten unaltered Lower and Middle Aldridge samples collected from outside the Sullivan-North Star trend provided a reference frame for altered samples from within the trend (Table 1; Fig. 3). Only one sample is well removed from the Sullivan area (90ALT1: 15 km south of Cranbrook); it is a finely laminated Middle Aldridge siltstone composed of quartz-biotite-feldspar-epidote-tourmaline-sphene-monazite-carbon (Fig. 4A, B; Table 1). Descriptions of regionally distributed Aldridge samples by Huebschmann (1973) and Edmunds (1977) also help establish protolith mineralogy; however, mineralogy of unaltered Lower Aldridge is not yet well established.

Mineral assemblage

The average modal composition of "unaltered" Lower Aldridge siltstones based on six samples (Table 1) is: quartz 40%, biotite 20%, muscovite 10%, K-feldspar 10%, plagioclase 7%, sphene 3%, tourmaline 2%, pyrite 2%, organic carbon 1%, pyrrhotite 1%, and trace amounts of chlorite, carbonate, epidote, monazite, apatite, rutile, and (?)zircon. These modal data compare well with data of Edmunds (1977), who found evidence of a bimodal population amongst his 95 samples of Aldridge rocks, leading him to classify them into "argillite" and "greywacke" with the average compositions shown in Table 1.

Interpreted sedimentary protolith

Based on their common occurrence as anhedral grains with a clast-like habit, we interpret the quartz, plagioclase, apatite, monazite and possibly some of the coarse muscovite to represent original detrital components (Fig. 4C). The increased abundance of organic carbon and monazite in the dark, finer grained beds suggests these are also of detrital origin (cf. Huebschmann, 1973). The dark laminae have a higher content of minerals such as monazite, sphene and organic carbon, yielding a distinctive Ca-Ti-P-C-REE (rare-earth elements) geochemical signature. Albitization of K-feldspar and plagioclase, common below 2500 m depth during sediment diagenesis (Boles, 1982), and metamorphism, account for the albitic feldspar; biotite is interpreted as metamorphosed detrital and authigenic clays. Tourmaline, characterized by coarse (0.1-0.2 mm) euhedral schorl (iron tourmaline), may be of detrital or diagenetic origin. Epidote replaces some plagioclase and may be related to the diagenesis or metamorphism of feldspars. Sphene appears detrital in unaltered sediments but also locally constitues part of the hydrothermal assemblage. Apatite may be detrital or metamorphic after an authigenic phosphatic mineral. Pyrrhotite and pyrite are common diagenetic minerals related to sulphate reduction in shallowly buried sediments.

METAMORPHOSED ALTERED ROCKS OF THE SULLIVAN-NORTH STAR TREND

Mineralogy

Altered rocks in the Sullivan-North Star trend are distinguished from unaltered equivalents by the near absence of feldspars and the collective abundance of chlorite, epidote, garnet, tourmaline, and sulphides (Fig. 3; Table 1). The major minerals present in almost all samples (altered and unaltered) are quartz, muscovite and biotite (Fig. 4A-F). The only exceptions are a suite of (clino)zoisite-tremolite bearing rocks (K38-2, 7b and possibly 23: Fig. 5A) that may have undergone "granophyre" alteration near a Moyie sill west of the Sullivan-North Star trend (Fig. 2, 3), and rocks where biotite has been converted to chlorite and/or muscovite.

Metamorphosed detrital component

Quartz grains, commonly 25 μm to 0.2 mm size (silt to fine sand; rarely to 0.8 mm), retain their detrital size and shape with only minor overgrowths and suturing of boundaries. There is no clear evidence for addition of hydrothermal silica to altered rocks. The stable detrital character of quartz is shown by its almost constant abundance in all samples (until swamped by hydrothermal input in the massive sulphides of the North Star deposit: Fig. 3). Muscovite most commonly occurs as abundant fine (50 μm) subhedral flakes interstitial to the quartz grains, forming a matrix to them (Fig. 5B) and locally imparting a weak to moderate foliation to the rock (Fig. 5C, D); minor coarse (0.1-0.5 mm) euhedral flakes are also scattered through the rock (Fig. 5E). Biotite is distinct by its occurrence as coarse (?porphyroblastic) 0.1-0.2 mm subhedral to euhedral books and flakes. It has deep brown pleochroism except where bleached or interleaved by muscovite and chlorite; aggregates of biotite and quartz locally create a "spotted" texture (Fig. 5B).

Feldspars (K-feldspar and plagioclase) locally form up to 20% of the unaltered rock, but are less abundant in altered rocks and massive sulphides, reflecting destruction/swamping by hydrothermal processes. Potassium-feldspar is microcline (Fig. 9D of Leitch and Turner, 1991); amounts were estimated by staining with sodium cobaltinitrite. In thin section, it has "grid" twinning and forms anhedral to subhedral, 25 μm to 0.1 mm grains concentrated along bedding-parallel "sweat" veins grading to "clots", disseminated, on crosscutting fractures, or in some samples, euhedral laths of uncertain origin. Plagioclase is rarely identifiable, except where polysynthetic twinning is visible in coarser (0.1 mm) grains in bedding-parallel "sweats" or between quartz grains. Grains large enough for optical determination of composition are limited, but where observed are albite (An_{5-8}). "Plagioclase", differentiated from albite in Table 1 by brackets,

appears to have a refractive index greater than quartz, but this may be due to incipient alteration to fine tourmaline, sericite, and possibly epidote.

Detrital accessory minerals such as sphene, monazite, apatite (Fig. 5B), rutile, and carbonaceous matter also appear to be less abundant in altered rocks. Sphene, as subhedral grains up to 0.25 mm diameter, averages 3% in unaltered rocks but only 1% in altered rocks. Rutile, which replaces sphene and quartz as minute (10-25 μ m) euhedral needles, is more common in the altered rocks. Ilmenite forms subhedral grains up to 0.1 mm, commonly associated with sphene and pyrrhotite in the most altered rocks such as tourmalinite. However, at Sullivan sphene is part of the alteration assemblage (Leitch and Turner, 1991), and, along with apatite, is possibly remobilized rather than destroyed by alteration.

Table 1. Summary of mineralogy (visually estimated modes)

Sample	Fm	Qz	Ms	Bi	(Hb) Ch	(Do) Ca	Ks	(Pl) Ab	(Dr) Tm	Gt	Tr	(Zo) Ep	Sp	Mz	(Mc) Po	(Lm) Py	Ap	C?	Zr	Ru	Sl	Cp	Gn	As	Bi	(Mt) Il
"UNALTERED" ROCKS																										
90ALT1	M	35	1	30	3		10		5			7	4	?3		tr		2								
-310'	?M	30	30	25	3M	tr			2				3	1	3		?2	1[1]	?ra	?tr						
-334'*	M	28	30	22	2M	(2)		5	1				2	1	3		?1	2		?<1	<1					
-727'	L	35	5	15	1M	15	5	10	1			1	5		3	2	1			?tr						
-1215'*	L	30	25	23	*2F	(5)	1	3	1				1	1	5	2		1			tr					
K26-3	*L	50	10	10	*5F	10		10	<1				3	<1		?2										
30-4?	L	35	10	15	1F		20	10	1				2	?3			?2			?1						
37-4	L	40	10	20			15	?5	3				2	1			1	2								
37-15	L	45		25			10	?5	5				5	?2		1	?<1	2								
38-2?	L	45	10		(1)		1				10	(20)	2		?3	?7	<1									
38-7b?	L	25					15				35	20	2	?1	?2			<1								
38-23?	L	40	6	15	5M		10	(?7)	1		2	3	2	1		?5		3								
Avg (6)	**L**	**40**	**10**	**20**	**2**	**1**	**10**	**7**	**2**			**1**	**3**	**1**	**1**	**2**	**1**	**1**		**?tr**						
Avg (3)	**M**	**31**	**20**	**25**	**3**	**1**	**3**	**2**	**3**			**2**	**3**	**2**	**2**	**tr**	**?1**	**2**	**?ra**	**?tr**						
Avg (47)	**A**	**35**	**26**	**15**	**0.7**	**1.1**	**1.5**	**(17)**	**0.5**			**0.3**			**tr**	**0.3**		**1.5**								**(1.1)**
Avg (46)	**G**	**60**	**9**	**6**	**0.5**	**0.6**	**0.3**	**(23)**				**0.2**						**0.1**								**(0.5)**
ALTERED ROCKS																										
K32-1	L	40	20	30			2		2	2			<1	2		2		<1								
32-13	*L	35	30	(5)	10M				5			1	1	1	10		?<1	2		?<1						
37-33	L	35	25	25	<1F				3	5		1		2	2	1	1			?<1		<1				
37-33a	L	25	25	25			2	7	3	3		<1	<1	1		1	<1				3		3			
37-33b*	L	25	37	25	<1F		1		1	7		<1	2	1		1	<1				<1					
37-35	ΦL	40	25	(5)	10M	(2)		2	1	2		2	1	1	(5)	2					2		tr			
38-28	L	45	30				3		(3)	5		3	5			?3	1	?2			tr					
38-33a	S	10	7		2F	(<1)	5		1	3			<1		60						5	<1	5	<1		
38-33b	S	5	3	7	1F	(7)	1			2	2		<1	tr	30,3	5					30		5			
38-34a	S	15	10	(3)	5F	(10)	1								(4)	1	<1				50	tr	tr			
38-34b	T	50	3	10	1M		<1	(5)	20*	1		3	1	tr	3	2	<1		<1	tr	<1					
38-35	L	40	15	15	2M		10		1	7		3	1	<1	2	1	<1	3		?tr	tr					
38-37	ΦL	35	25	15	3M		1		1	3		3	3	1	?7	?3	<1				<1					
39-2	L	30	35	10	2M		5		(3)		2		1	tr	?5	1,5		2		?tr						
39-3	L	60	20	10	2F	1	1		2			2	<1	?2			tr	tr	?<1							
39-5a	M	25	50	5	*10F	2			2			5	tr	<1					?tr							?1
39-5b	M	25	10	20	1M	35		(5)	1			2	?tr	<1		<1			?tr							?<1
90NSH1A	L	45	20	20	3M			(tr)	<1	<1		<1	<1	?tr		?10	<1				1					
B	L	40	20	15	trM				tr	<1			<1			?20	tr		?tr		tr					
C	L	35	35	15	1MF				(1),2	5			<1			?3	<1	?2								
2A	L	50	15	20					2	5		3				?5			?tr							
B	L	40	15	25	2MF				1	2		<1				?10			tr							
C	L	20	55	15	<1MF				1*	2		3				3,<1				?<1						
3B	L	50	15	20	2MF		5		1			3		?1			3									
C	L	40	20	(5)	15F				<1	5		10				5,tr										
4A	T	30	3	20	4M			(12)	7*	5		13	?<1		(1),3		2		tr			<1				
B	T	40		25					25*	2		5	<1		3				<1	<1			tr			
D	ΦL	35	25	(5)	15M				1*	5		5	2		(1),3	2				<1	<1	<1	<1		tr	
E	T	40	20	10	5M				5*	3	<1	7	<1		(7),1	1	<1			tr						(1)
F	T	35	10	25	<1MF			(5)	10*	1		3	tr		1	10			?tr	tr		tr				
5A	L	25	35	15	5F				2*	5		10		<1		?2				1						
B	ΦL	35	40		10?				5							10				tr						
C	ΦT	35	15	10	3M				25*	2	<1	5	1		(1),2	1	tr		?tr	tr		tr	tr			
Avg(22)	**L**	**38**	**26**	**14.5**	**4**		**tr**	**1.5**	**0.5**	**2**	**3**	**tr**	**2.5**	**1**	**0.5**	**1.5**	**4**	**0.5**	**0.5**	**tr**	**tr**	**0.5**	**tr**	**tr**		**ra**	
Avg(6)	**T**	**38**	**8**	**16.5**	**2**				**(4)**	**15***	**2**	**<1**	**6**	**0.5**		**4**	**2**	**0.5**		**tr**	**<1**	**tr**	**tr**		**tr**	**ra**	**(tr)**
Avg(3)	**S**	**10**	**7**	**3**	**3**	**(9)**	**2**		**tr**	**2**	**<1**		**<1**		**32**	**2**	**tr**				**28**	**<1**	**3**	**tr**	**ra**	
Avg(2)	**M**	**25**	**30**	**13**	***6F**	**18**		**(2)**	**1**				**3**	**tr**	**<1**		**tr**									**1**

Fm = Formation (M=Middle, L=Lower Aldridge; ΦL=fragmental; *L=lower quartzite; ?= ?unaltered sample; S=massive sulphides, T= tourmalinite; 310' etc. = depth in DDH 6423); * = average of several estimates for different layers. Amounts questioned where identification uncertain; tr=trace, ra=rare, [1] = percent of unidentified mineral. Averages A=argillite (n=47), G=greywacke (n=46) are from Edmunds (1977).
Abbreviations are: Qz=quartz; Ms=muscovite; Bi=biotite (bracketted if relict); Ch=chlorite (*=metacrysts, M=magnesian, F= iron-rich, Hb=hydrobiotite); Ca=calcite (Do=dolomite, ankerite, siderite); Ks=microcline; Ab=albite (Pl=plagioclase); Tm=tourmaline (*=2 types, see text; Dr=dravite, otherwise schorl); Ep=epidote, clinozoisite (Zo=zoisite); Sp=sphene; Mz=monazite; Po=pyrrhotite (± secondary marcasite, pyrite); Py=pyrite (Lm=limonite); Ap=apatite; C?=?carbonaceous matter; Zr=zircon; Ru=rutile; Sl=sphalerite; Cp=chalcopyrite; Gn=galena; Il=ilmenite (Mt=magnetite).

Apatite forms clouded, euhedral prisms up to 50 μ m long in unaltered sediments but, as at Sullivan, in altered rocks it forms coarser (to 0.1 mm) clear subhedral grains. Carbon is found as minute (often <5 μ m) grains interstitial to all other minerals, concentrated in layers in unaltered rocks but (?)re-mobilized into round clots or balls (Fig. 5A) in altered rocks; carbon abundances are slightly less in altered rocks. Zircon is difficult to identify due to similarity to monazite and sphene, but appears more common in altered rocks where it forms clear euhedral stubby prisms to 40 μ m long that lack pleochroic haloes in adjacent biotite or chlorite. Magnetite is not often identified in Lower Aldridge rocks (however, Edmunds, 1977 describes magnetite associated with chloritization and carbonation).

Chlorite occurs mainly as a retrograde replacement of biotite. It forms subhedral flakes interleaved with muscovite and relict biotite, lacking the distinctive anomalous birefringence or pleochroism that would suggest an Fe-rich or magnesian composition. In a few cases, marked with an asterisk in Table 1, Fe-chlorite occurs as euhedral metacrysts up to 2 mm long. Minor Fe-chlorite with purple anomalous birefringence is associated with iron sulphides, particularly pyrite; this probably is a retrograde equilibration around the sulphides. This effect is also seen in the radiation damaged haloes around monazite crystals.

Carbonate is more abundant in unaltered rocks, where it occurs as subhedral 0.25 mm grains that are mainly calcite or dolomite. In altered rocks it is absent; however, in massive sulphides it is present as inclusions of anhedral ankerite and

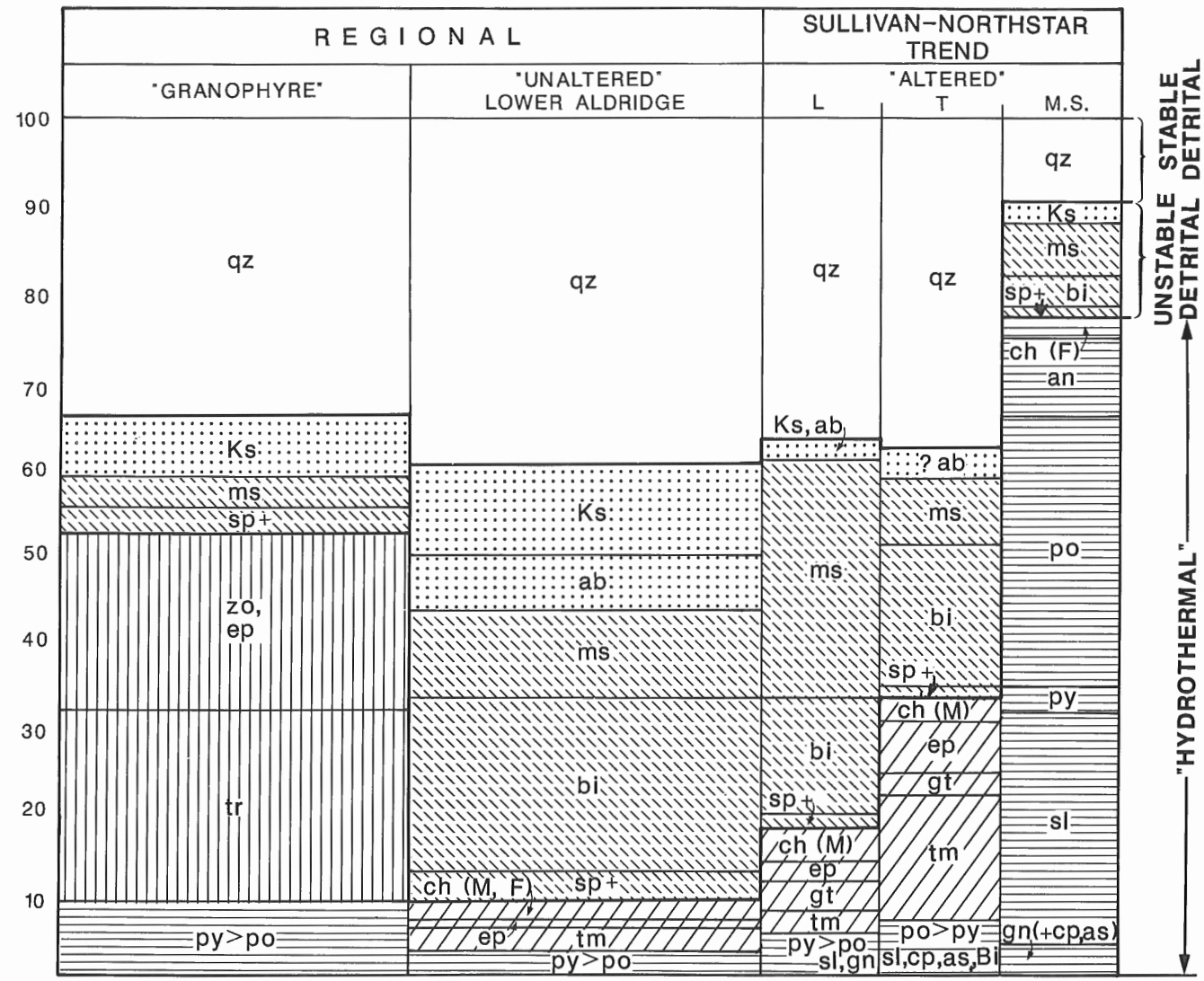

Figure 3. Schematic diagram of averaged modal mineralogy (abundances in per cent) for altered and unaltered rocks in the vicinity of Sullivan-North Star trend (see Table 1 for mineral abbreviations; L=Lower, T=tourmalinite; MS=massive sulphide). Note the trend to increased muscovite, sulphide, epidote, garnet, and tourmaline in altered rocks.

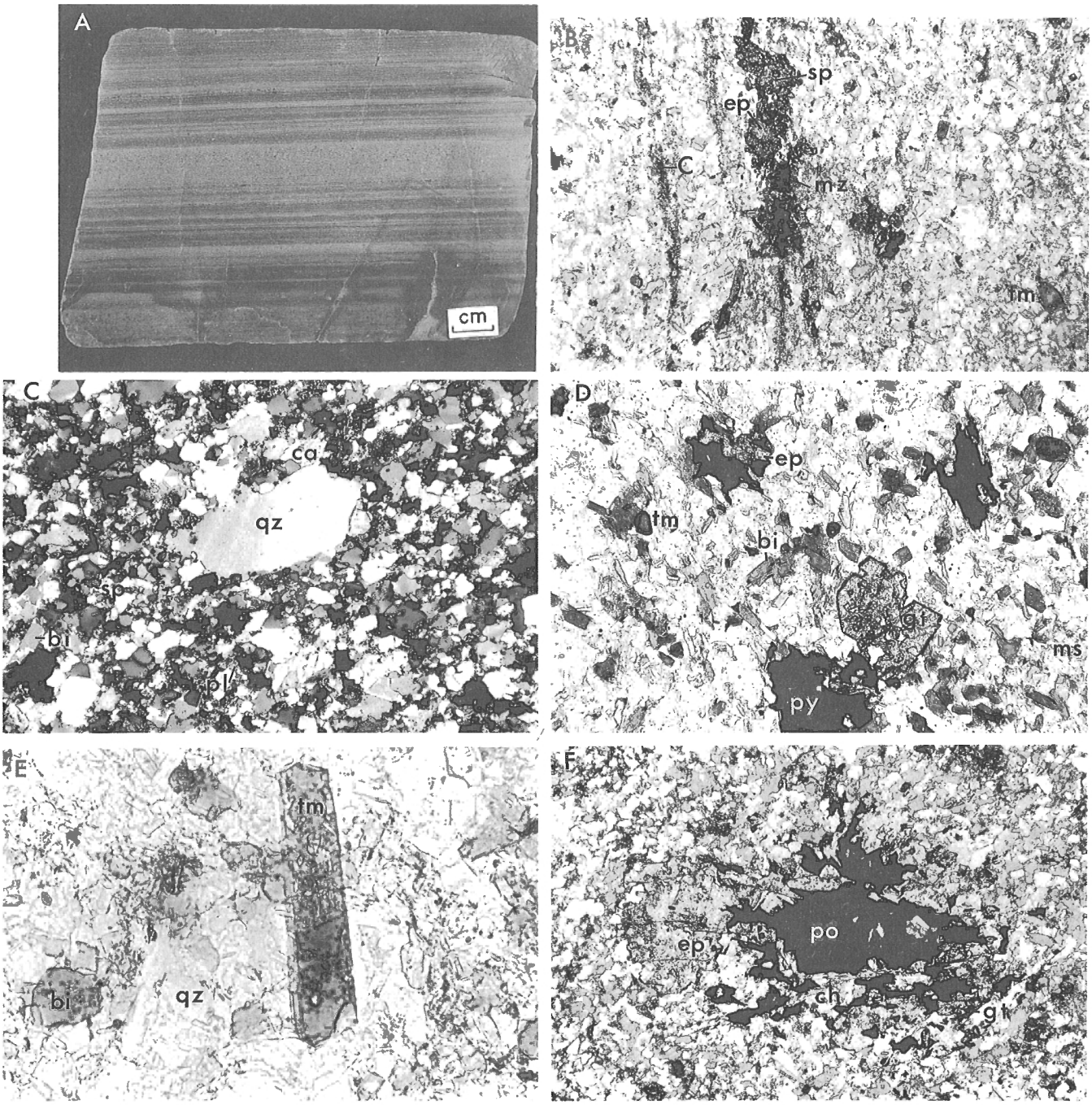

Figure 4. "Unaltered" and biotite-garnet altered rocks from the Sullivan-North Star trend (photomicrographs in plane polarized light except for C, width of view in mm; mineral abbreviations in Table 1). **A)** Finely laminated marker horizon in Middle Aldridge siltstone (90ALT1). **B)** Sphene-monazite-epidote and fine carbon causing "dark" layers in 90ALT1; euhedral tourmaline crystals (1.25 mm). **C)** Coarse detrital quartz showing minor overgrowths, fine grained interstitial plagioclase, calcite, biotite, sphene, and apatite (2.5 mm, K-26-3). **D)** Euhedral garnet in quartz-biotite-muscovite matrix; epidote-pyrite clots, tourmaline crystals (1.25 mm, 90NSH2A). **E)** Euhedral tourmaline prism in quartz-muscovite-biotite matrix (0.3 mm, 6423-334'). **F)** Epidote-pyrrhotite-garnet-quartz-chlorite clot (2.5 mm, 90NSH4A).

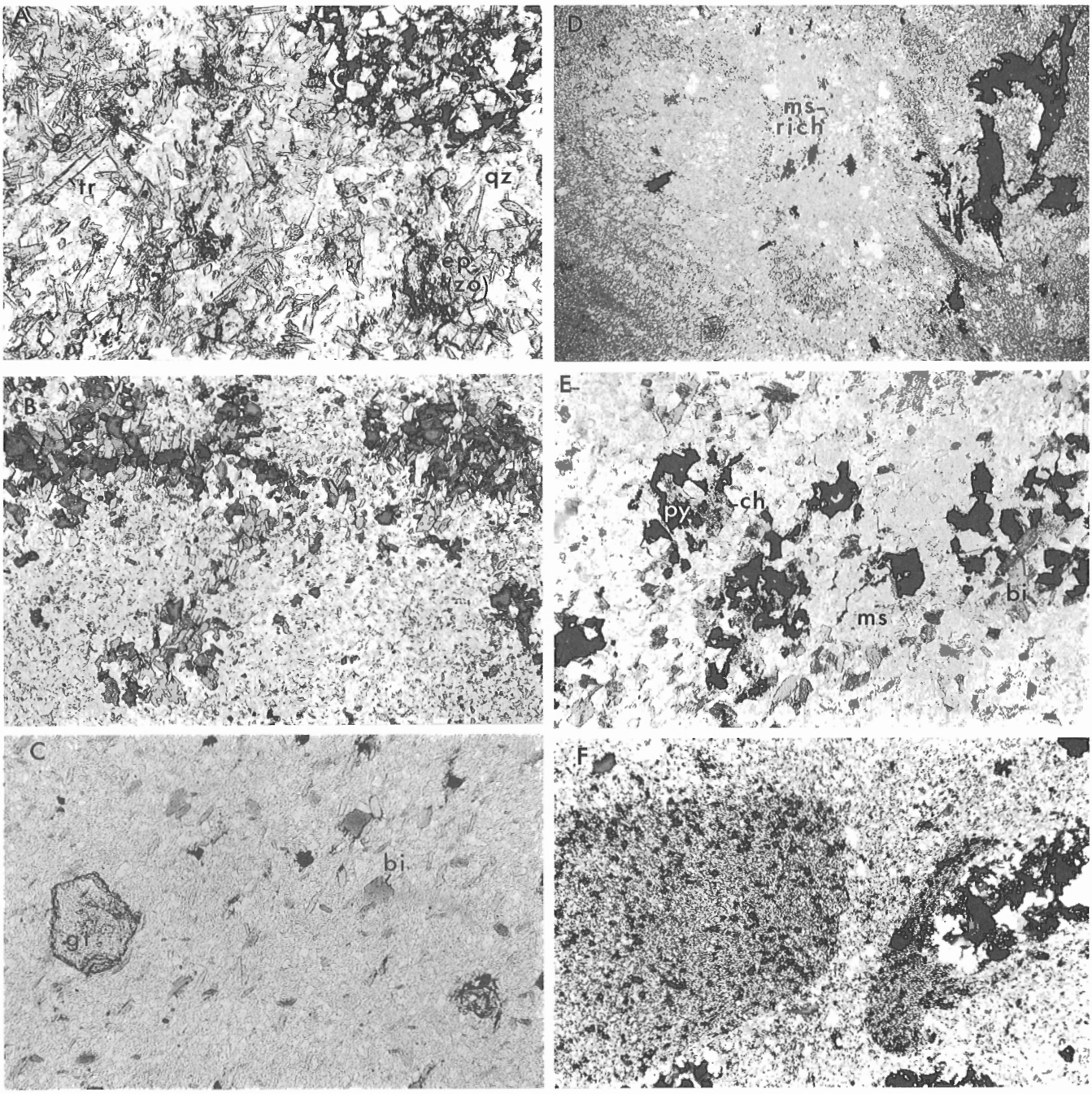

Figure 5. Photomicrographs of altered rocks (plane polarized light, width of view in mm; abbreviations in Table 1). **A)** Tremolite-zoisite-(quartz); carbon "spot", upper right (1.25 mm, K38-7b). **B)** Biotite-quartz in spots grading to lenses; dark colour caused by radiation haloes around monazite crystals (2.5 mm, 90NSH3B). **C)** Muscovite-rich rock, minor biotite; rim of garnet lightly altered to chlorite and epidote (1.25 mm, 90NSH2C). **D)** Muscovite, biotite, or pyrrhotite-rich heterogeneous clasts (5 mm, K38-37). **E)** Pyrite-muscovite-chlorite, relict biotite, euhedral tourmaline (1.25 mm, 90NSH2B). **F)** Chloritized clast (dark) in muscovite-rich matrix, clot of pyrite-pyrrhotite-epidote-sphene (5 mm, NSH4D).

(?)siderite. Calcite or rarely dolomite with a similar habit, is present in Sullivan ore, possibly due to late chlorite-pyrite-calcite alteration (Hamilton et al., 1983).

Metamorphosed hydrothermal component

In metamorphosed altered samples, chlorite in the "clots" or spots of alteration minerals is magnesian, forming coarse euhedral flakes up to 0.5 mm diameter similar to those seen in contact with the massive orebody at Sullivan (Leitch and Turner, 1991). Epidote abundance (1-3% in unaltered sediments) is clearly elevated in altered Lower Aldridge rocks, especially in tourmalinite (7-13%). Epidote occurs principally in the clots (Fig. 4D, F) of altered rocks, as subhedral grains up to 0.3 mm diameter lacking pleochroism, suggesting low Fe clinozoisite. Samples separated as "granophyre" in Figure 3 contain abundant zoisite (deep blue anomalous birefringence) and clinozoisite as subhedral crystals up to 0.5 mm, plus tremolite as bladed laths up to 1 mm long in a distinctive assemblage that has a more recrystallized texture than the majority of sediments studied (Fig. 5A). These samples lie well outside the Sullivan-North Star trend, but may be part of wet sediment alteration related to intrusion of nearby Moyie sills (cf. Höy, 1989).

Garnet is present in almost all altered Lower Aldridge samples from within the Sullivan-North Star trend but is absent from the samples studied from outside the trend. The absence of garnet in unaltered Aldridge metasediments is supported by regional work of Edmunds (1977) who noted garnets only in a few samples from the core of the Purcell anticlinorium south of the St. Eugene Mine. Garnet is also absent from samples close to or overlying the Sullivan orebody (samples K39-2 to 5b). Garnets occur as euhedral crystals up to 2 mm diameter with sieve texture due to inclusions of quartz (Fig. 4D), and less commonly as anhedral masses in bed-parallel veins. Garnets at the Sullivan Mine are manganiferous (to 28% MnO; J. Hamilton, pers. comm., 1991); four analyses of Edmunds (1977) indicate 5-10% MnO and 10-28% FeO.

Tourmaline has two distinct forms in the altered rocks: a) 1-5% coarse (up to 0.4 mm: Fig. 4D, E) euhedral prisms of greenish-brown to slate-blue Fe-rich schorl, or rarely yellow-brown Mg-rich dravite, and b) up to 25% extremely fine (5-15 μ m), felted pale greenish needles probably intermediate in composition between schorl and dravite (Ethier and Campbell, 1977). Fine grained tourmaline replaces feldspar grains interstitial to the detrital quartz as well as the margins and some centers of other minerals, including quartz, biotite, garnet, and epidote. The coarse tourmaline is similar to detrital schorl present in unaltered sediments. Fine grained tourmaline characterizes the tourmalinite samples, and reflects hydrothermal alteration.

Sulphide abundance increases progressively from unaltered rock to altered rock to tourmalinite to massive sulphide. The variety of base metal sulphides increases with sulphide abundance from sphalerite to galena, chalcopyrite, and finally arsenopyrite (and rare native Bi). Pyrite, as euhedral cubes to 0.5 mm across, is generally more abundant than pyrrhotite, except in tourmalinite, where pyrrhotite is dominant. Pyrrhotite forms subhedral aggregates of 0.25 mm grains (Fig. 4F); it is commonly oxidized to lamellar marcasite-pyrite. All Fe-sulphides in surface samples show some replacement by limonite. Red-brown sphalerite indicating moderate Fe content similar to that at Sullivan, and galena, form subhedral to anhedral grains up to 0.35 mm across. Chalcopyrite and arsenopyrite occur as minor anhedral blebs and euhedral rhombs respectively, up to 0.1 mm across, within the other sulfides; minute (25 μ m) rounded blebs of possible native Bi are rare.

Interpreted sedimentary protoliths

Altered bedded sedimentary rocks contain abundant detrital grains of quartz, remnants of finer K-feldspar and plagioclase, and tourmaline, sphene, apatite, zircon, organic carbon, and monazite; maximum grain size is 0.05-0.1 mm. Sediments probably originally consisted of laminae of (1) light-coloured muddy feldspathic quartz silt and (2) thin dark layers of sphene-, monazite- and organic carbon-rich silt. The 10-20% feldspar content probably reflects their immaturity: Huebschmann (1973) described the Middle Aldridge as "greywacke" that underwent little sorting or winnowing during sedimentation. Where these sediments are massive, bedding has been partly obscured by alteration.

Fragmental rocks (noted in Table 1; Fig. 5D, F) have either a fine grained or sand sized matrix. The former are typically polymict, matrix supported and poorly sorted, with fragments to 1 cm and shard-like quartz grains; the original matrix was likely muddy. Small sericite-chlorite altered fragments may represent altered volcanic or feldspar-rich rocks. Intense sericite-pyrite alteration is associated with these fragmental rocks. Fragmental rocks with sand sized matrix contain elongate oriented lithic clasts to 5 cm in a matrix (up to 15%) of quartz, muscovite, and tourmaline, possibly after feldspar. Some "felsic-looking" clasts might be from igneous rocks. These fragmentals may represent lithic clast-rich sandstone or sandy breccia/conglomerate, or the coarse matrix could be a hydrothermal quartz-muscovite-biotite cement between up to 40% fine grained lithic pyritic clasts to 5 mm diameter. Clasts within clasts are seen, implying multiple fragmentation and/or hydrothermal brecciation.

"Megacrystic" is a term applied to rocks, or certain layers, that contain euhedral 0.25 to 2.5 mm metacrysts of biotite, chlorite, or carbonate (Fig. 6A), or else similar sized areas of biotite-quartz-carbonate that have euhedral, generally rectangular, outlines (Fig. 6B). There are also rounded to oval patches (Fig. 6C), that resemble feldspar phenocrysts pseudomorphed by fine muscovite, but could be muscovite after biotite. The significance of these textures is not clear; they may suggest the presence of a tuffaceous or volcanic component in the Aldridge rocks, or they may simply be a metamorphic texture caused by recrystallization.

Biotite-garnet metamorphic assemblage

The euhedral and nonoriented nature of biotite, and poikilitic texture of garnet suggest these minerals are metamorphic; the key indicators of metamorphic grade are biotite, garnet,

albite, microcline, Mg-chlorite, and epidote. A biotite-garnet assemblage is generally indicative of greenschist grade. The absence of prograde Fe-chlorite and abundance of biotite indicates that the grade is above greenschist chlorite facies. If the garnet is Mn-rich spessartine rather than Fe-rich almandine as data suggest, it is stable at lower (chlorite) or middle (biotite) greenschist grade (Winkler, 1971). Although microcline, epidote, and Mg-chlorite are stable to lower amphibolite facies, the apparently ubiquitous albite (<An_8) rather than oligoclase (An_{14}: Edmunds, 1977) would rule out amphibolite facies. Metamorphic grade therefore appears to be about middle greenschist, indicating 400-450°C; pressure, estimated from a maximum 7.3 km depth of cover, is about 2 kbar (Edmunds, 1977).

Pre-biotite/garnet assemblage ("early alteration")

Muscovite± pyrite alteration (Fig. 5C, D) is characterized by abundant (up to 55%) fine grained muscovite greater than or subequal to biotite, and modest to high (5-20%) pyrite content (Fig. 5E). The absence of tourmaline needles distinguishes it from tourmalinite. The average muscovite content of altered Lower Aldridge rocks (26%) is well above the local average for unaltered rocks (10%: Fig. 3), although it is close to Edmunds (1977) average for "argillites" in all Aldridge rocks (Table 1). A spotted texture, sometimes present, is due to "clots" or porphyroblasts of biotite-quartz (Fig. 5B) or epidote-pyrite (Fig. 4F). The high muscovite contents occur as probable alteration of muddy beds, as matrix to fragmentals, and in clasts (Fig. 5D, F). This alteration type grades to tourmalinite with increasing tourmaline and pyrrhotite, and decreasing muscovite (e.g. 90NSH4A-F, 5A-C).

The evidence for an alteration, rather than metamorphic, origin of muscovite is as follows: 1) it is weakly to strongly oriented, unlike porphyroblastic metamorphic biotite; 2) abundant muscovite is associated with high pyrite ± trace pyrrhotite, sphalerite content or fragmental rocks; (3) abundant muscovite coincides with lower biotite and epidote, the metamorphic equivalents of clays and feldspar, whereas lower muscovite correlates with higher feldspar and epidote (e.g. 90NSH4A). We interpret the early alteration of clays and feldspar to a sericite-muscovite assemblage, whereas unaltered residual clay or feldspar changed to biotite and epidote respectively by metamorphism.

Tourmalinite samples contain 5-25% fine felted needles (Fig. 7A) of 10-20 micron tourmaline, distinct from the regionally extensive occurrence of about 1% 0.1 mm euhedral green schorl. Tourmalinite is a distinctive hard flinty black rock with conchoidal fracture, a high pyrrhotite/pyrite ratio and accessory chalcopyrite and arsenopyrite. It is transitional from muscovite-pyrite with increasing tourmaline. The tourmaline occurs as feathery replacements of plagioclase; clasts in fragmental rocks are variably tourmalinized (Fig. 7B). The association of tourmalinization with high sulphides and fragmental rocks indicates an early alteration

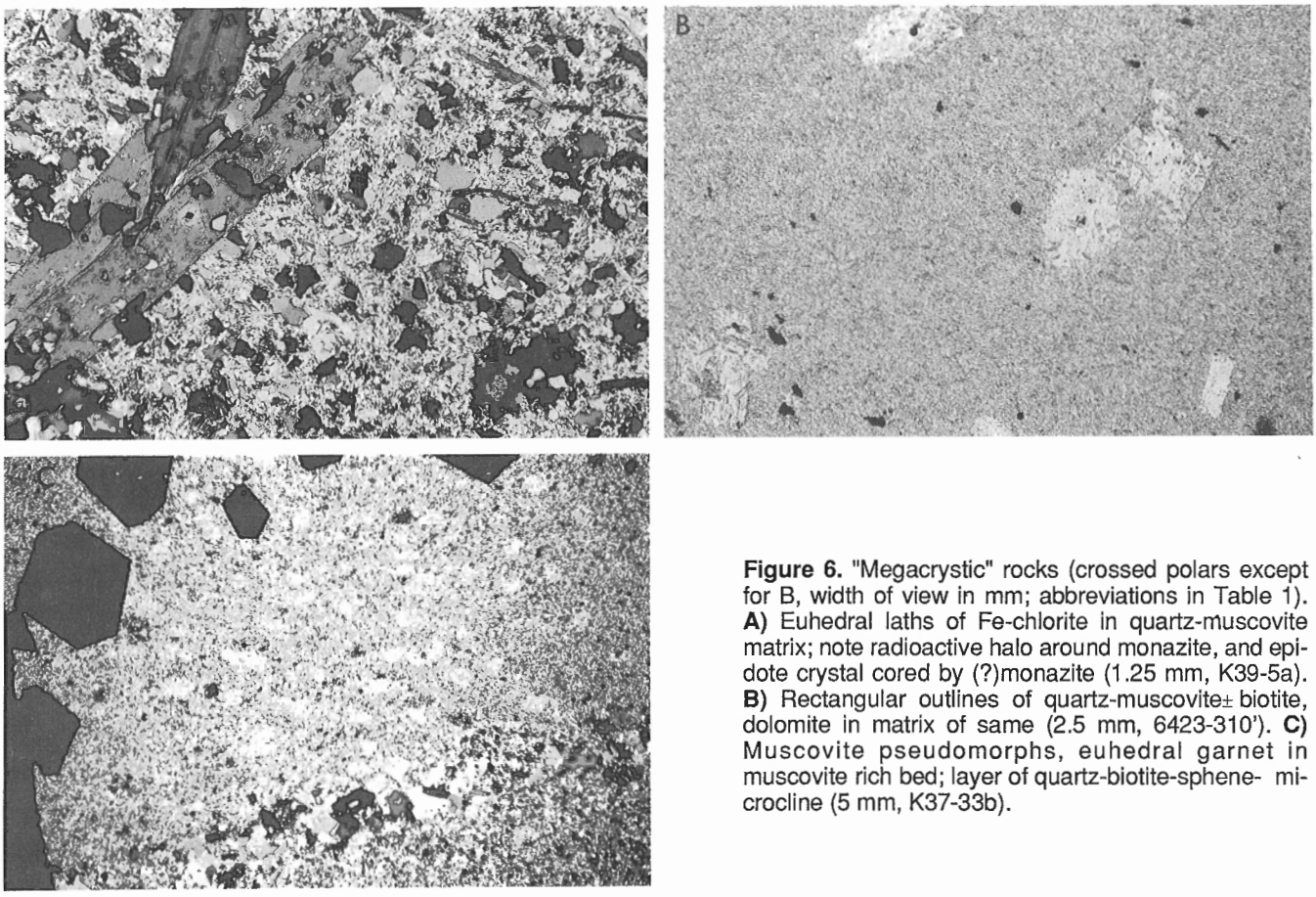

Figure 6. "Megacrystic" rocks (crossed polars except for B, width of view in mm; abbreviations in Table 1). **A)** Euhedral laths of Fe-chlorite in quartz-muscovite matrix; note radioactive halo around monazite, and epidote crystal cored by (?)monazite (1.25 mm, K39-5a). **B)** Rectangular outlines of quartz-muscovite± biotite, dolomite in matrix of same (2.5 mm, 6423-310'). **C)** Muscovite pseudomorphs, euhedral garnet in muscovite rich bed; layer of quartz-biotite-sphene- microcline (5 mm, K37-33b).

origin. However, fine tourmaline needles replacing metamorphic grains of biotite, epidote, quartz, and garnet suggest metamorphic recrystallization of originally fine tourmaline or other precursor boron mineral.

Post-biotite/garnet assemblage ("late alteration")

A common, but volumetrically minor late alteration consists of an Fe-chlorite, muscovite, pyrite, and possibly epidote. This alteration principally affects biotite, which is interleaved or replaced by muscovite, chlorite with a moderate Fe content, minor pyrite, and traces of epidote, apatite and sphene (Fig. 7C). Grain margins of garnet are locally replaced by chlorite and minor epidote; rarely, porphyroblasts are pseudomorphed (Fig. 7D). Thin veinlets of quartz-chlorite and quartz-pyrite are late, as are fracture envelopes of sericite after biotite. Intense chlorite alteration of biotite imparts a greenish caste to the rock in 90NSH3C, but chlorite alteration is generally only macroscopically visible along fractures. Chlorite mainly represents a retrograde phase of the metamorphic event, although substantial amounts (5%) of magnesian chlorite in strongly altered rocks, and Fe-chlorite metacrysts, are early. The timing of epidote is also equivocal: pre-biotite as diagenetic alteration of feldspar; with biotite during metamorphism; and to a lesser degree with chlorite as retrograde alteration of feldspar that survived peak metamorphism.

DISCUSSION

Sullivan-North Star "early" feldspar-destructive alteration

Two major types of early alteration are recognized in the Sullivan-North Star belt: muscovite-pyrite, and tourmalinite. Both assemblages are characterized by the absence or rarity of feldspar. Where present, feldspar is partly replaced by muscovite, tourmaline, and possibly epidote, suggesting large-scale destruction of detrital feldspar of the Lower Aldridge sediments within the alteration zone. A Proterozoic age for the muscovite-pyrite and tourmalinite alteration in the Sullivan-North Star zone is indicated by association with 1) early fragmentals and zones of massive fluidized sediments lacking bedding, of inferred Proterozoic age (Höy, 1984); and

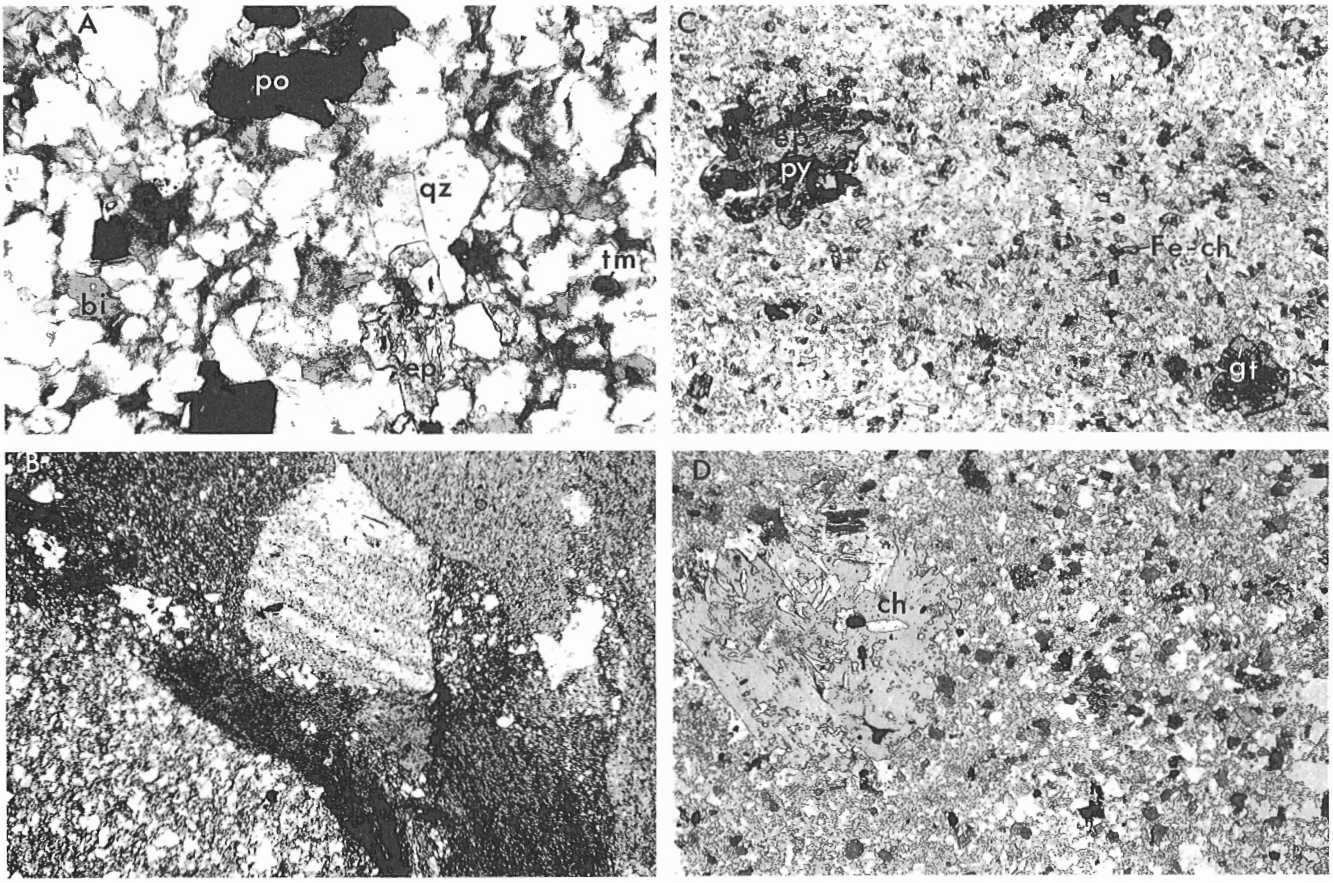

Figure 7. Tourmalinized and retrograde altered rocks (plane polarized light, width of view in mm; abbreviations in Table 1). **A)** Incipient tourmaline replacing former interstitial feldspar, margins of quartz and biotite; dark euhedral detrital schorl at extreme right (1.25, 90NSH4F). **B)** Variably tourmalinized fragments with original sedimentary texture, breccia pipe at base of North Star Hill (5 mm, 90NSH5C). **C)** Fe-chlorite pseudomorphs after biotite; euhedral garnet-epidote-pyrite clots (2.5 mm, 90NSH3C). **D)** Fe-chlorite pseudomorph after euhedral garnet; quartz-biotite-muscovite-epidote matrix (5 mm, 90NSH5A).

2) stratiform lead and zinc sulphides of the North Star, a Proterozoic seafloor deposit. Evidence for a pre-metamorphic age of the muscovite-pyrite alteration lies in the foliated nature of some muscovite that implies transposition during deformation, in contrast to metamorphic biotite which is randomly oriented.

Exploration significance

An important result of this study is that garnet appears to be absent from Lower Aldridge rocks outside the Sullivan-North Star trend and possibly also from Middle Aldridge rocks above the Sullivan. Since there is no evidence for a local increase in metamorphic grade within the trend, the presence of garnets is provisionally related to elevated Mn content of the sediments within the trend and below the Lower-Middle Aldridge time horizon. This seems reasonable in light of Mn haloes associated with some stratiform deposits, mainly Zn-Pb in reactive carbonate rocks (e.g. Meggen: Gwosdz and Krebs, 1977) but also Au in siliceous rocks (Thompson-Bousquet: Valliant and Barnett, 1982).

The feldspathic nature of the Lower Aldridge renders it sensitive to alteration. Plagioclase is rare or absent in altered rocks of the Sullivan-North Star trend, although K-feldspar appears to be more stable. Alteration associated with SEDEX deposits in the Aldridge Formation might be expected to be more developed than that associated with deposits hosted by less reactive rocks such as quartz siltstone and sandstone (e.g. MacMillan Pass district, Yukon; Gataga district, B.C.). Muscovite± pyrite is an important alteration type, but its recognition can be ambiguous due to the muscovite-rich nature of unaltered Aldridge argillites. Most chlorite is a post-metamorphic alteration of biotite, and therefore not related to chloritic alteration associated with mineralization (such as at Sullivan); simple petrographic inspection can discriminate between these chlorites.

Altered rocks are distinguished by minerals or textures that include disseminated garnet, fine tourmaline, epidote-pyrite/pyrrhotite ± garnet-biotite-muscovite-chlorite-quartz-microcline-albite "clots" that grade into bedding-parallel lenses and layers, sericite and/or chlorite after biotite, or destruction of bedding. Many of these alteration features can be recognized in the field: greenish tinge indicates retrograde chlorite after biotite; grey, muscovite rich rock; brown to black and flinty, tourmalinite; dark spots are porphyroblasts of biotite-quartz, epidote-pyrite, or pyrrhotite-chalcopyrite-epidote-chlorite-muscovite-garnet-quartz-biotite-tourmaline-apatite.

Questions for future research include probe analyses to confirm the Mn character of the garnet and the Ab content of the plagioclase, confirming the middle greenschist facies metamorphic grade, and the Mg content of the various tourmalines. The formation time of key minerals such as tourmaline, biotite, muscovite, and epidote, and of the "spots", needs further investigation. Silicification is not apparent in the rocks examined; it could be present but not recognizable in such a quartz-rich host. The modal composition of the host needs further refinement, principally by examination of more, well-distributed Lower Aldridge samples well removed from effects of hydrothermal alteration.

ACKNOWLEDGMENTS

We are grateful to Cominco staff at the Sullivan Mine for permission to sample the Sullivan-North Star zone, access to drawings and information at the mine site, and valuable discussions. John Hamilton and Ken Dawson are thanked for critical reading of the manuscript; Richard Lancaster prepared and photographed the polished slab used in this study.

REFERENCES

Abbott, J.G. and Turner, R.J.W.
1990: Paleotectonic setting of Devonian stratiform Zn-Pb-barite deposits, MacMillan Fold Belt, Yukon; Mineral Deposits of the Northern Canadian Cordillera: in I.A.G.O.D. Field Guide #14, (ed.) J.G. Abbott and R.J.W. Turner.

Beaty, D.W., Hahn, G.A., and Threlkeld, W.E.
1988: Field, isotopic, and chemical studies of tourmaline-bearing rocks in the Belt-Purcell Supergroup: genetic constraints and exploration significance of Sullivan type ore deposits; Canadian Journal of Earth Sciences, v. 25, p. 392-402.

Boles, J.R.
1982: Active albitization of plagioclase, Gulf Coast Tertiary; American Journal of Science, v. 292, p. 165-180.

Edmunds, F.R.
1977: The Aldridge Formation, B.C., Canada; Ph.D. thesis, Pennsylvania State University, University Park, Pennsylvania, 368 p.

Ethier, V.G. and Campbell, F.A.
1977: Tourmaline concentrations in Proterzoic sediments of the southern Cordillera of Canada and their economic significance; Canadian Journal of Earth Sciences, v. 14, p. 2348-2363.

Freeze, A.C.
1966: The origin of the Sullivan Orebody, Kimberley, B.C.; in Tectonic History and Mineral Deposits of the Canadian Cordillera, Canadian Institute of Mining and Metallurgy, Special Volume 8, p. 263-294.

Gwosdz, W. and Krebs, W.
1977: Manganese halo surrounding Meggen ore deposit, Germany; Transactions Institution of Mining and Metallurgy (Sect. B: Applied earth science), v. 86, p. 73-77.

Hamilton, J.M., Delaney, G.D., Hauser, R.L., and Ranson, P.W.
1983: Geology of the Sullivan deposit, Kimberley, British Columbia, Canada; in Sediment-hosted Stratiform Lead-Zinc Deposits, (ed.) D.F. Sangster; Mineralogical Association of Canada, Short Course notes, v. 8, p. 31-83.

Höy, T.
1983: Geology in the vicinity of the Sullivan Deposit, Kimberley, British Columbia (82F,G); in Geological Fieldwork, 1982, British Columbia Ministry of Energy, Mines and Petroleum Resources, Paper 1983-1, p. 9-17.
1984: Structural setting, mineral deposits, and associated alteration and magmatism, Sullivan camp, southeastern British Columbia (82 F,G); in Geological Fieldwork, 1982, British Columbia Ministry of Energy, Mines and Petroleum Resources, Paper 1983-1, p. 25-35.
1989: The age, chemistry, and tectonic setting of the Middle Proterozoic Moyie sills, Purcell Supergroup, southeastern British Columbia; Canadian Journal of Earth Sciences, v. 26, p. 2305-2317.

Huebschmann, R.P.
1973: Correlation of fine carbonaceous bands across a Precambrian stagnant basin; Journal of Sedimentary Petrology, v. 43, p. 688-699.

Leitch, C.H.B.
1991: Preliminary fluid inclusion and petrographic studies of the Sullivan sedimentary exhalitive Pb-Zn deposit, southeastern B.C.; in Current Research, Part A; Geological Survey of Canada, Paper 91-1A, p. 91-101.

Leitch, C.H.B. and Turner, R.J.W.
1991: The vent complex of the Sullivan stratiform sediment-hosted Zn-Pb deposit, B.C.: preliminary petrographic and fluid inclusion studies; in Current Research, Part E; Geological Survey of Canada, Paper 91-1E (this volume).

Nesbitt, B.E., Longstaffe, F.J., Shaw, D.R., and Muehlenbachs, K.
1984: Oxygen isotope geochemistry of the Sullivan massive sulfide deposit, Kimberley, British Columbia; Economic Geology, v. 79, p. 933-946.

Schofield, S.J.
1915: Geology of Cranbrook area, Geological Survey Canada, Memoir 76, 245 p.

Shaw, D.R. and Hodgson, C.J.
1986: Wall-rock alteration at the Sullivan mine, Kimberley, B.C., in The Genesis of Stratiform Sediment-Hosted Lead and Zinc Deposits: conference proceedings, (ed.) R.J.W. Turner and M.T. Einaudi; Stanford University Publications, School of Earth Sciences, v. XX, p. 13-21.

Valliant, R.I. and Barnett, R.L.
1982: Manganiferous garnet underlying the Bousquet gold orebody, Quebec: metamorphosed manganese sediment as a guide to ore; Canadian Journal of Earth Sciences, v. 19, p. 993-1010.

Winkler, H.G.F.
1971: Petrogenesis of Metamorphic Rocks: New York, Springer-Verlag, 3rd Edition, 237 p.

Re-evaluation of slope failure volume estimates involving 3D computer graphics for the Fraser River delta front, British Columbia

Rowland J. Atkins[1] and John L. Luternauer
Cordilleran Division, Vancouver

R.J. Atkins and Luternauer, J.L., 1991: Re-evaluation of slope failure volume estimates involving 3D computer graphics for the Fraser River delta front, British Columbia; in Current Research, Part E; Geological Survey of Canada, Paper 91-1E, p. 59-65.

Abstract

Three-dimensional computer images of the pre- and post-failure surfaces for the large June-July, 1985, slope failure, at the mouth of the Fraser River Main Channel, were generated using a computer aided design program. Comparison of the pre- and post-failure data resulted in the re-estimation of the slope failure minimum volume to 1.4x10^6 m^3. Extrapolation of the plotted data resulted in an estimate of 3.0x10^6 m^3 for the total volume of the slope failure.

Résumé

Des images informatiques tridimensionnelles des surfaces antérieures et postérieures de la grande rupture de pente de juin-juillet 1985, à l'embouchure du chenal principal du Fraser, ont été produites à l'aide d'un programme de conception assistée par ordinateur. La comparaison des données antérieures et postérieures à la rupture a mené à la réévaluation du volume minimal de rupture de pente à 1,4 x 10^6 m^3. L'extrapolation des données portées sur graphique a permis d'estimer à 3,0 x 10^6 m^3 le volume total de la rupture de pente.

[1] Home address: 2542 Cavendish Drive, Burlington, Ontario L7P 4E4

INTRODUCTION

In response to concerns for more accurate estimates of slope failure volumes to aid in the assessment of geohazards on the Fraser River delta front and slope (Fig. 1, 2) (McKenna and Luternauer, 1987; Luternauer et al., 1989), bathymetric data for the 1985 slope failure, documented by McKenna and Luternauer (1987), were computer plotted in 3-dimensional block diagrams to help define the area subject to failure. The 1985 failure was chosen because it was the largest event at the mouth of the Fraser River identified so far (McKenna and Luternauer, 1987). The images provided a sufficient base from which to extrapolate an estimate for the total failure volume. The data used to generate the computer images were manipulated by a small calculation formula to provide a minimum estimate for the failure volume.

COMPUTER DRAFTING

Methods

The Public Works Canada, Marine Survey Division, charts (1985a, b) were hand contoured at an interval of 1 m over the common sample area between the two surveys (Fig. 3). These hand contoured maps were created with the aid of a third survey chart (1985c) used as a supplemental reference for the gaps in the post-failure survey chart (1985b). An arbitrary grid, with a scale spacing of 10 m, was constructed over the common survey area and coordinates for each grid intersection were determined: consisting of the X,Y location on the grid with respect to an arbitrarily defined grid origin, and the water depth at that point (relative to mean low low water) as interpolated from the contoured sheets. The points were recorded in an array and entered directly into AutoCAD Release 10 by keyboard. The 3-dimensional drafting commands of AutoCAD were then used to generate block diagrams of the pre-failure (June 27) and post-failure (July 11) surveys.

All plotted images (Fig. 4, 5) were created with a vertical exaggeration of 10 times. This vertical exaggeration was chosen so that the images would be readily comparable to previously generated computer images based on the 1985 slope failure data (Luternauer et al., 1989).

All work involving computerization and plotting was done using an AST 286 computer. All images were plotted on an HP 7475A pen plotter using P.3 pens to get a fine-web-like appearance on the surface mesh. Each image was plotted from three different views in both perspective and isometric configurations.

Discussion

The images generated by the AutoCAD program took advantage of the hidden line command to present views of the surface with the laws of line-of-sight kept intact. The results (Fig. 4, 5) were comparable to those of Luternauer et al. (1989), but provided clearer resolution of the surface as a result of the hidden lines being hidden. These surfaces appeared realistic from all angles of view and could be viewed from any point in space desired.

The perspective and isometric plots differed significantly in their appearance. The perspective plots were plotted with the assumption that all parallel lines converge at infinity. Thus each plot had a vanishing point and appeared (in exaggerated form) as it would if viewed in situ minus the intervening water. The isometric plots were plotted with the assumption that parallel lines remain equidistant at infinity and, thus, have no vanishing point. These plots appeared warped as a result of the inherent optical illusion in the isometric representation, but provided a more stable basis for comparison between plots as a result of the uniform scale over the entire image. The perspective plots suffered in this manner as a result of changing scales over the entire image.

True vertical representations for the June 27 and July 11 data were not plotted using AutoCAD as these images had already been generated by Luternauer et al. (1989).

VOLUME ESTIMATES

Method A

The generation of computer images for the pre- and post-failure surfaces required the creation of 2 sets of gridded data matched to a common origin and area. This set of data provided opportunity to re-evaluate the size of the slope failure over the surveyed area. The gridded coordinates were run through a simple formula on a calculator to provide an estimate of the volume. The calculation formula took the form:

$$V = \sum_i \sum_j \left[(B_{i,j} + B_{i+1,j} + B_{i,j+1} + B_{i+1,j+1}) - (A_{i,j} + A_{i+1,j} + A_{i,j+1} + A_{i+1,j+1}) \right] / 4 \times G$$

where:

V = the volume change as a result of the failure,

i = 0 to M-1, where M is the "X-size" of the grid,

j = 0 to N-1, where N is the "Y-size" of the grid,

$B_{i,j}$ = the depth before failure at the grid intersection "i,j",

$A_{i,j}$ = the depth after failure at the grid intersection "i,j"

G = the areal scale of the grid spacing.

Depths for this calculation were taken relative to datum, where datum was set equal to mean low low water. The formula calculates the average depth of each grid square for both "before" and "after" surveys. The "after" depths are subtracted from the "before" depths for each grid square in turn resulting in a series of columns of known depth: columns representing the increase in depth (negative values) and the decrease in depth (positive values) for each grid square. The multiplication by the areal size of each column allows for the calculation of the loss or gain in material between each survey. Only negative (material loss) values were included

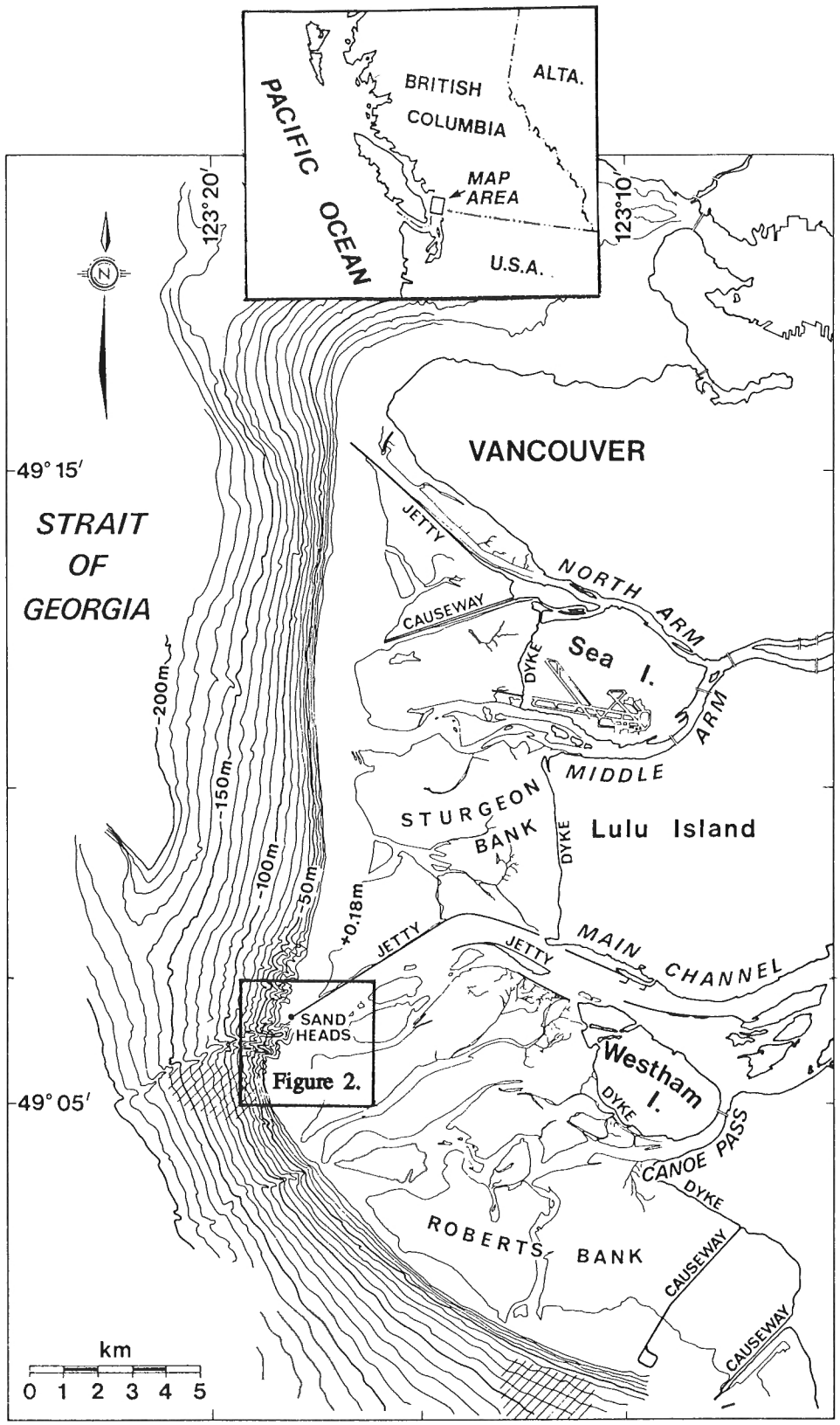

Figure 1. Detailed morphological setting of the Sand Heads Lighthouse at the mouth of the Main Channel of the Fraser River.

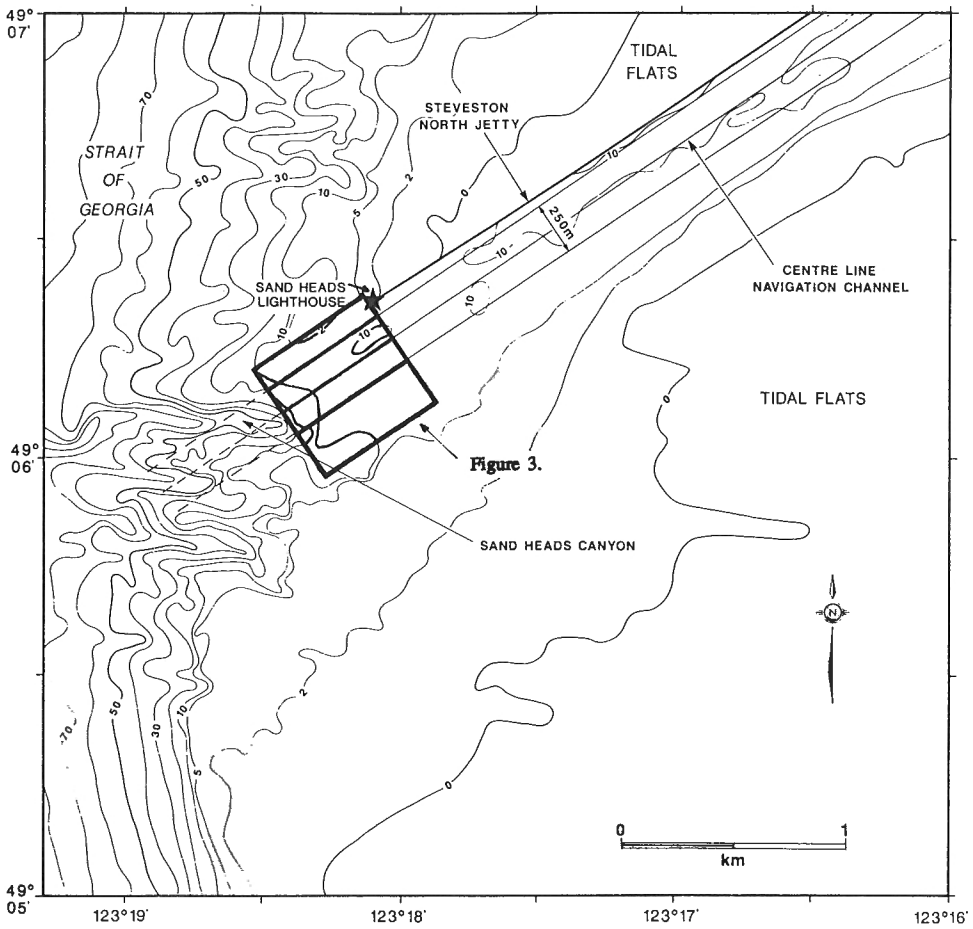

Figure 2. Morphology of the Fraser River delta foreslope off the Main Channel. Contours are in metres. Source: Canadian Hydrographic Service Chart 3490.

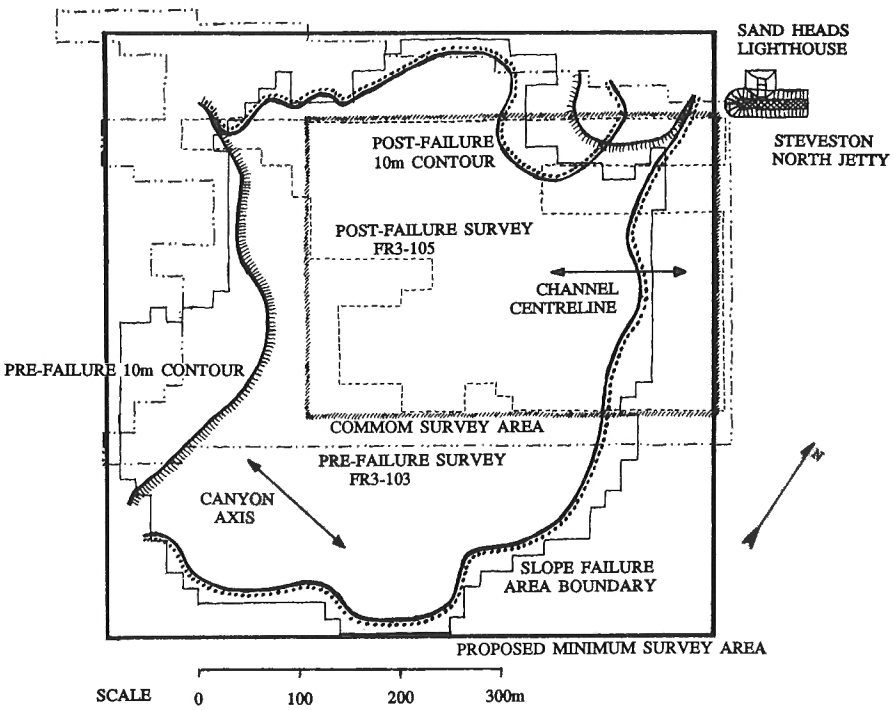

Figure 3. Comparison of surveyed areas, calculated slope failure area, and estimated total slump surface area with reference to the suggested minimum survey area.

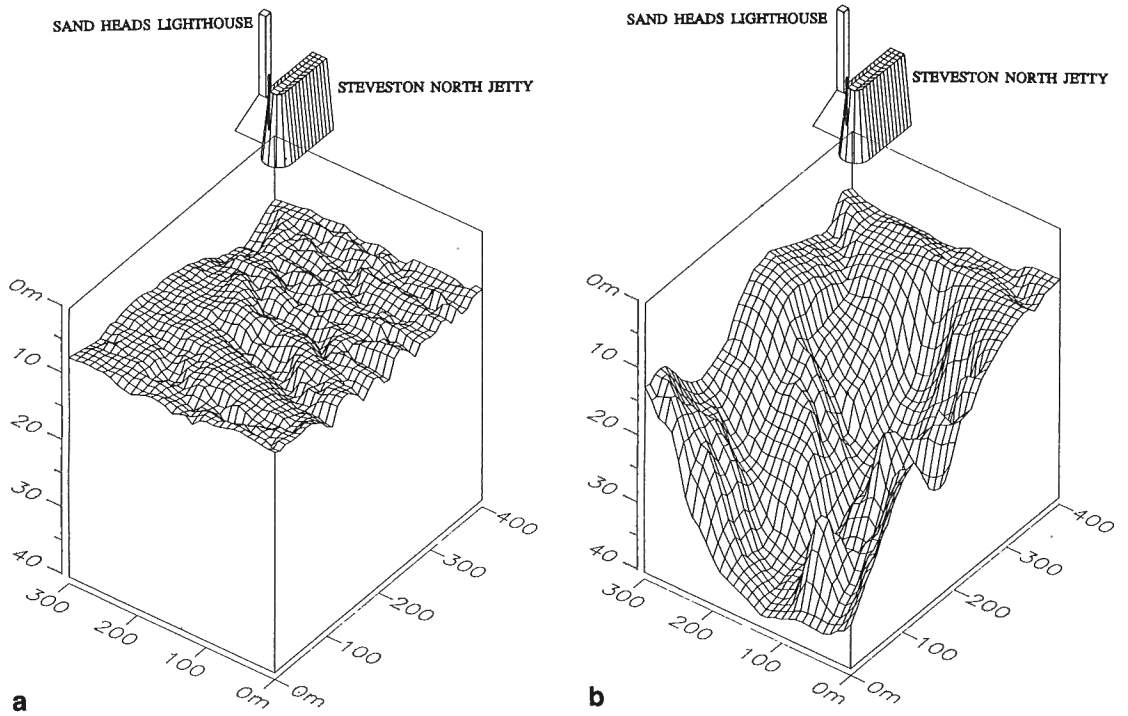

Figure 4. Isometric computer-generated images of the Fraser River Main Channel mouth for the common survey area between June and July, 1985. Vertical exaggeration 10x, 0 m depth = mean low low water. **a.** Pre-failure surface, June 27th, 1985. **b.** Post-failure surface, July 11th, 1985.

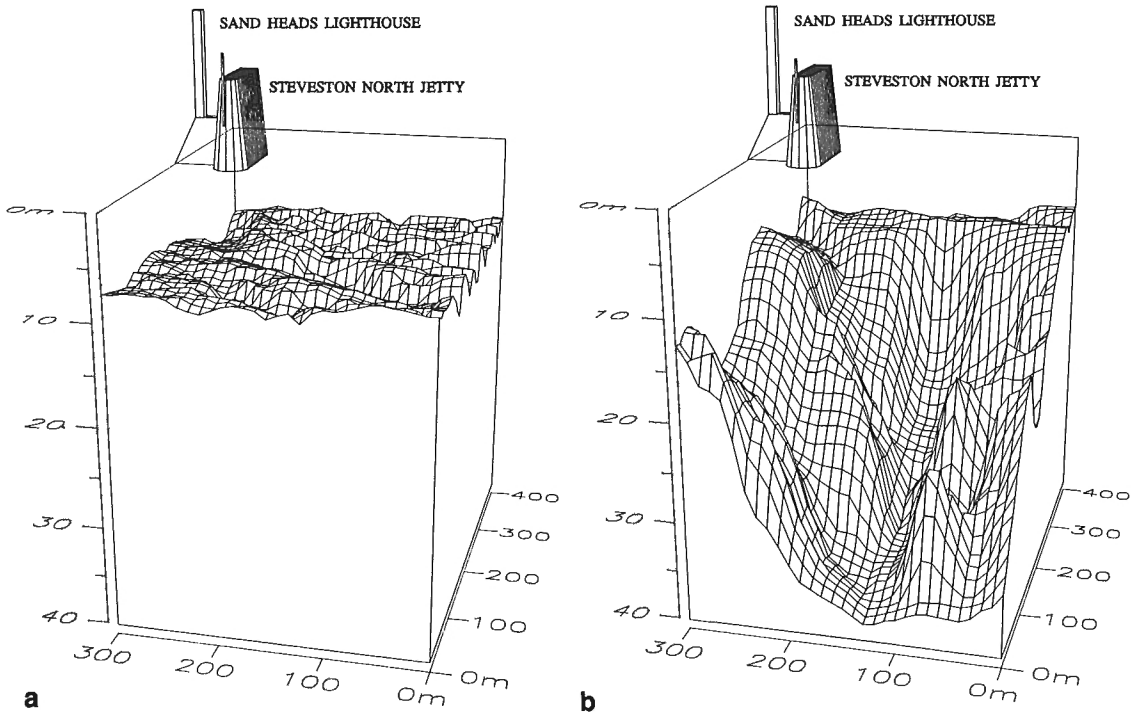

Figure 5. Perspective computer-generated images of the Fraser River Main Channel mouth for the common survey area between June and July, 1985. Vertical exaggeration 10x, 0 m depth = mean low low water. **a.** Pre-failure surface, June 27th, 1985. **b.** Post-failure surface, July 11th, 1985.

in the slope failure volume estimate under the assumption that all volume gain values were a result of continual deposition of sediment by the river. The volume of deposition occurring between surveys was assumed to be negligible compared to the volume of the failure event, although the application of this assumption leads to an underestimation of the minimum volume if the deposition volume was not negligible. McKenna and Luternauer (1987) estimated a minimum volume of 1.0×10^6 m^3 for the event. The minimum achieved by the above estimation method was 1.4×10^6 m^3, an increase of 40%.

Method B

Visual inspection of the slope failure images determined that the failure was not confined to the survey area (Fig. 2), but exceeded such boundaries and was, therefore, much larger in volume than the minimum estimate (Fig. 6). The pre-failure surface survey area (Public Works, 1985a), being larger than the post-failure survey area (Public Works, 1985b), was compared with the September 1985 survey area (Public Works, 1985c) to determine the extent of the slump area and to provide an estimate of the total slope failure volume. Several assumptions were made to facilitate this process:

1) the face of the pre-failure delta front had a linear slope from the pre-failure delta crest to where the extrapolated slope intercepted the September 1985 survey surface. This assumption erred on the side of too small an estimate of volume change.
2) where the September survey was shallower than the June survey, there was no change in volume due to slope failure; all decreases in depth were attributable to sedimentation by the river. This assumption erred on the side of too big an estimate of volume change.
3) the June surface, where no data had been gathered, was at an average depth of 8 m below datum (mean low low water) inshore of the delta crest. This depth was chosen as it was the dredge limit for the shipping channel (Masse and Hay Consultants, phone conversation) despite the unevenness of the delta surface, ranging from 7 to 10 m depth. This assumption erred on the side of too large an estimate of volume change.
4) the September surface was not significantly different from the July surface. The intervening 2 months of sedimentation was negligible compared to the magnitude of the slope failure volume. This assumption erred on the side of too small an estimate of volume change.

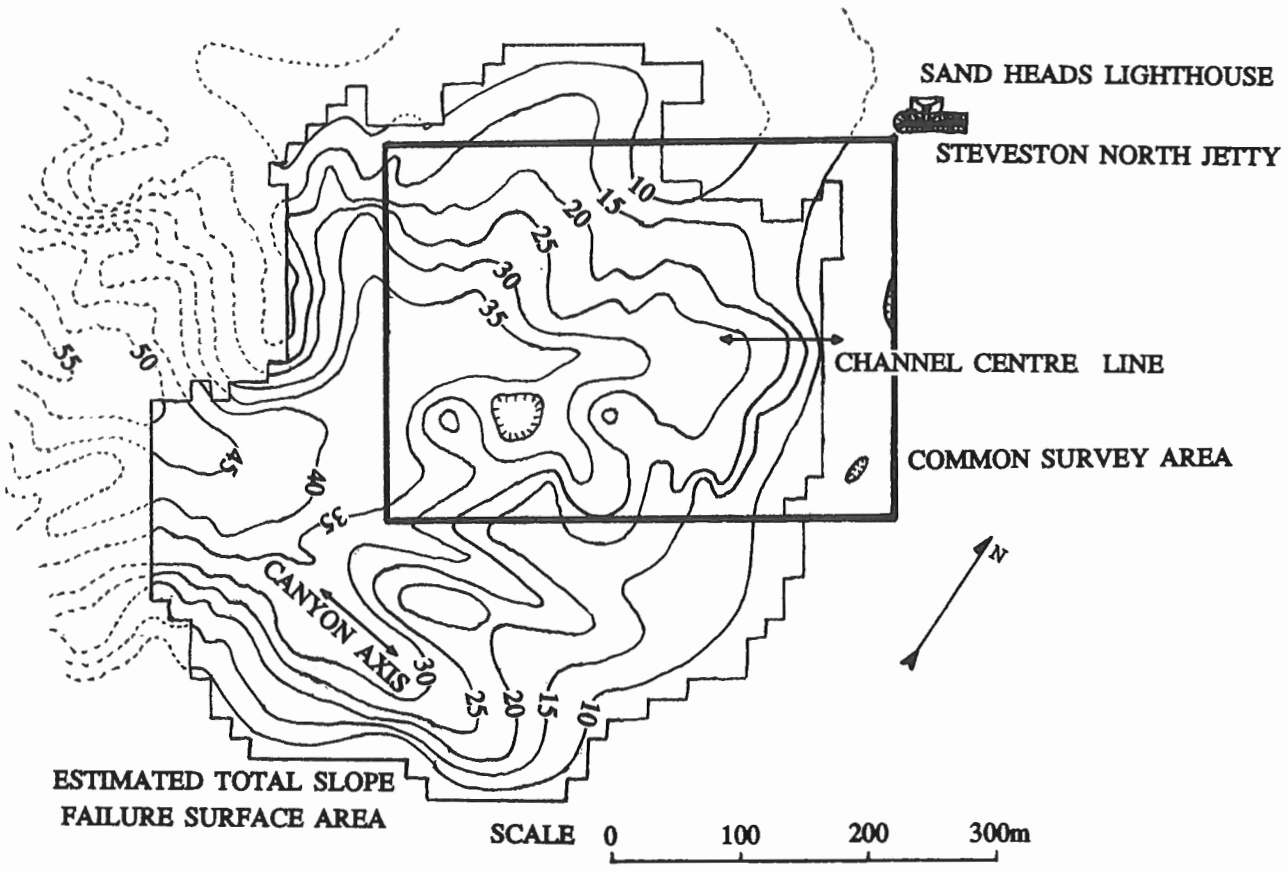

Figure 6. Coverage of the estimated slope failure area by the common survey area for the pre- and post-failure surveys. Contour interval: 5 m. Depth contours measured from mean low low water.

5) the errors induced by the above assumptions cancelled each other out when related to the scale of the volume change being estimated.

The slope area was gridded with squares approximately 250 m^2 in surface area (error in favour of too small an estimate). The average depth for the post-failure surface was calculated for each square by hand contouring the September chart and then estimating the depth for each square by interpolation. This depth value was subtracted from the determined pre-failure (June) depth for each square [8 m inshore of crest, linear decrease on delta front face from 10 to 50 m] and summed for all grid squares. The total volume for this estimate was $1.6x10^6$ m^3.

The summation of the surveyed area volume, measured with Method A, and the extrapolated area volume, measured with Method B, resulted in a slope failure volume estimate of $3.0x10^6$ m^3: a result 3 times as large as the original minimum estimate.

DISCUSSION

As can be noted from Figure 6, the estimates for volume come from a failure area much larger than the area commonly surveyed. The necessity for accurately estimating the risk of geohazards to the shipping beacons and lighthouse requires increased survey coverage of the delta front area at the mouth of the Fraser River Main Channel. An increase in coverage would create opportunity for a more in-depth assessment of the recurrence intervals of (and sediment dynamics of) failures at the river mouth. A common minimum survey area would allow for comparison between surveys and for an accurate calculation of volume changes at the delta crest.

The volume estimate of $1.4x10^6$ m^3 obtained in Method A should be considered as a re-evaluation of the minimum slope failure volume for the 1985 event. This value is 40% larger in size than the original estimate (McKenna and Luternauer, 1987) and should replace the smaller value. The second estimate can be considered as an estimate of the total volume of the 1985 event. This value should be considered when determining recurrence intervals for the failures at the delta front, and should replace the value quoted for this event by McKenna and Luternauer (1987).

CONCLUSION

Volume estimates of the common survey area for the 1985 slope failure at the Fraser River Main Channel delta front indicate a minimum volume estimate of $1.4x10^6$ m^3 revised from the original estimate (McKenna and Luternauer, 1987) of $1.0x10^6$ m^3. Extrapolation of the surveyed area with the help of an additional survey chart suggests the total volume estimate of the slope failure to be $3.0x10^6$ m^3. Identification of the area subject to slope failures indicates that the survey area needs to be enlarged to fully cover the area at risk. More precise estimates of slope failure events could be achieved by increasing the size of the minimum survey area to a square 600 m on a side (Fig. 3): 250 m north of the channel centreline, 350 m south of the channel centreline, 600 m west of the end of the Steveston North Jetty. The extension of the survey area to a minimum control area would enable a more accurate investigation of the hazard of slope failures at the delta front.

ACKNOWLEDGMENTS

This paper is the result of work undertaken during a COSEP summer position with the Geological Survey of Canada.

REFERENCES

Luternauer, J.L., Dunkley, D., Gunkel, R., and Kostaschuk, R.A.
1989: New base map and computer graphics to help identify failures off the mouth of the Fraser River, British Columbia; in Current Research, Part E; Geological Survey of Canada, Paper 89-1E, p. 213-220.

McKenna, G.T. and Luternauer, J.L.
1987: First documented large failure at the Fraser River delta front, British Columbia; in Current Research, Part A; Geological Survey of Canada, Paper 87-1A, p. 919-924.

Public Works Canada
1985a: Marine Survey Division chart soundings: FR3-103 June 27.
1985b: Marine Survey Division chart soundings: FR3-105 July 11.
1985c: Marine Survey Division chart soundings: FR3-107 September 18.

New biostratigraphic data for the northern Cache Creek Terrane, Teslin map area, southern Yukon

F. Cordey, S.P. Gordey, and M.J. Orchard
Cordilleran Division, Vancouver

Cordey, F., Gordey, S.P., and Orchard, M.J., 1991: New biostratigraphic data for the northern Cache Creek Terrane, Teslin map area, southern Yukon; in Current Research, Part E; Geological Survey of Canada, Paper 91-1E, p. 67-76.

Abstract

Identifiable radiolarian associations are found within northern Cache Creek strata of Teslin Plateau in: [1] thick, folded and faulted sequences of radiolarian ribbon chert (radiolarite), [2] isolated outcrops of radiolarite, [3] siliceous argillite interbedded with greywacke and (?)chert, [4] millimetre- and centimetre-size chert clasts in greywacke and conglomerate, and [5] as metre-sized radiolarite blocks in mélange.

We report here the results obtained from sampling along a ridge located north of Sterlin Lake and Mount Bryde, Teslin map area (105C), where nine chert localities from lithological associations [1] and [2], and one argillite locality from lithological association [3] range in age from Late Triassic to Early Jurassic. The first Early Jurassic age from true ribbon chert of the northern Cache Creek Terrane is reported from a structurally disrupted succession, which includes at a lower stratigraphic level the uppermost Norian conodont Misikella posthernsteini.

Résumé

Des associations de radiolaires identifiables sont découvertes dans les strates sédimentaires du Terrain Nord Cache Creek sur le plateau de Teslin au sein de: [1] épaisses séquences de jaspes rubannés à radiolaires (radiolarites) plissés et faillés, [2] affleurements isolés de radiolarites, [3] argilites siliceuses interstratifiées à des greywackes et (?) jaspes, [4] clastes millimétriques et centimétriques de jaspes au sein de greywackes et conglomérats, et [5] blocs métriques de radiolarites dans un mélange.

Nous reportons ici les résultats obtenus à partir de l'échantillonnage d'une crête située au Nord du Lac Sterlin et du Mont Bryde, feuille Teslin (105C), où neuf localités de radiolarites des types [1] et [2] et une localité d'argilite du type [3] ont un âge Trias supérieur à Jurassique inférieur. Des radiolarites d'âge Jurassique inférieur sont découvertes pour la première fois dans le Terrain Nord Cache Creek et sont issues d'une coupe tectonisée qui comprend, à un niveau stratigraphique inférieur, le conodonte Norien terminal Misikella posthernsteini.

INTRODUCTION

Radiolarian sampling undertaken during the summer 1991 in Teslin map area in southern Yukon (105C) (Fig. 1) is part of a five year project to remap the geology of this region at 1:250 000 and locally 1:50 000 scale (Gordey, 1991). A geological framework was established by Mulligan (1963), but little geological work has been done since. Many map units and their relationships remain poorly understood, largely because of poor age control. Major insights into the geology of this region can be gained through the use of modern micropaleontological techniques, particularly the identification of radiolaria in siliceous rocks, a method not available to Mulligan.

Teslin map area is underlain by several terranes of the Intermontane and Omineca belts that originated in continental margin, oceanic, and island arc settings (see Wheeler et al., 1988) and which underwent strikingly different structural and metamorphic modifications during the Mesozoic. The southwest part of the map area (Teslin Plateau) is underlain largely by the Cache Creek Terrane (Atlin Terrane of Monger, 1975), which consists of Mississippian to Permian greenstone, chert, and limestone, and overlying late Paleozoic and Triassic chert and clastic rocks (Cache Creek Group, Mulligan, 1963; units 4,5,7, Fig. 2). Radiolarians have been observed in five different lithologic associations within the Cache Creek: [1] thick, folded and faulted sequences of radiolarian ribbon chert (radiolarite), [2] isolated outcrops of radiolarite, [3] siliceous argillite interbedded with greywacke and (?)chert, [4] millimetre- and centimetre-size chert clasts in greywacke and conglomerate, and [5] as metre-sized radiolarite blocks in mélange. Laboratory work in progress shows that all of the above contain identifiable radiolarians with the potential to provide age-control.

The age (and character) of the Mesozoic chert/clastic succession, the focus of this report, is critical in providing constraints on terrane interactions in the northern Cordillera. Wheeler et al. (1988) identified the chert/clastic succession as part of the Lewes River overlap assemblage, a usage followed by Gordey (1991). However, in this paper, we assign the strata to the northern Cache Creek terrane (sensu lato; see discussion).

STRATIGRAPHIC AND STRUCTURAL FRAMEWORK

The chert/clastic succession sampled for the present work consists regionally of ribbon-bedded, radiolarian chert, argillite, sandstone, and greywacke. The chert generally weathers grey, white, black, or rusty, and is medium grey to black on fresh surfaces. Beds range from 3 to 10 cm thick, and are evenly bedded to lensoid. Interbedded shale ranges from partings, to beds usually less than 3 cm thick. The greywacke is light grey-green to locally orange-white weathering, and well indurated; fresh surfaces are medium grey. The sandstone is massive, and occurs in members as much as 200 m thick. Rare sedimentary structures include shale rip-up clasts, convolute bedding, planar lamination, and graded bedding. Grain size in the sandstone is typically fine- to

Figure 1. Location of northern Cache Creek Terrane with location of index map in Figure 2 shown in solid black. The square indicates the boundaries of Teslin map area (105C).

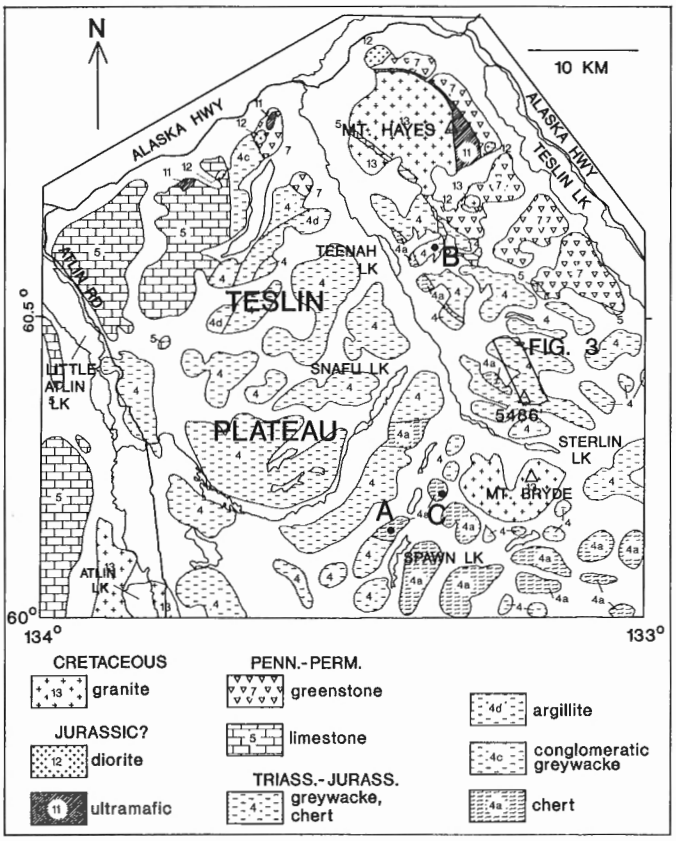

Figure 2. Geological sketch map of part of the Teslin Plateau, in southwestern part of Teslin map area (105C) (from Mulligan, 1963). Polygon outlines the location of Figure 3.

coarse-grained. Angular lithic clasts are locally abundant, range up to 5 cm in diameter, and are dominated by grey to white weathering chert, some radiolarian-bearing, and lesser argillite. Pebble conglomerate occurs locally. Cursory petrographic examination shows the greywacke comprises subequal proportions of quartz and plagioclase, hornblende, and minor orthoclase and lithic clasts. The greywacke and chert form alternating packets from 20 to 200 m thick, a geometry that may result from either thrust imbrication and folding, as well as original sedimentary interbedding (Gordey, 1991).

FOSSIL LOCALITIES

Previous work

Triassic conodonts and radiolarians from chert interbedded with argillite/greywacke were previously reported from three localities in Teslin Plateau. Samples of chert interbedded with greywacke collected by J.W.H. Monger and D.J. Tempelman-Kluit on a ridge-top south-southeast of Snafu Lake (locality A, Fig. 2) yielded Late Carnian and Early Norian conodonts (Orchard, 1986). More recently, M.J. Orchard has identified the uppermost Norian conodont *Misikella posthernsteini* Kozur and Mock from chert also interbedded with argillite and greywacke (Jackson et al., 1990) on a ridge east of Teenah Lake (locality B, Fig. 2); Triassic radiolarians were recovered from chert at the same locality. Farther west near Spawn Lake (locality C, Fig. 2), Middle (Ladinian) and Late (Late Carnian through Middle Norian) Triassic radiolarians were extracted from chert (reported in Cordey, 1990b); stratigraphic relations to nearby clastics at this locality are uncertain.

New data

Nine new radiolarian and one new conodont localities are reported from a five kilometre long ridge north of Mount Bryde and Sterlin Lake (Fig. 2, 3). The ridge consists of successive outcrops and isolated sections of radiolarite, greywacke, argillite/siltstone/greywacke, and conglomeratic greywacke. The fossil collections (Table 1, Fig. 3) come from the following three different lithological associations: [1] thick, folded and faulted sequences of radiolarite; [2] isolated outcrops of radiolarite; and [3] siliceous argillite interbedded with greywacke and (?)chert. Laboratory extraction of radiolaria from chert clasts within greywacke and conglomerate is in progress.

Chert of association [1] ranges in age from Late Triassic (Late Carnian to Middle Norian, pro parte) to Early Jurassic (post-Hettangian, possibly late Sinemurian), and includes the Late Norian conodont *Misikella posthernsteini* Kozur and Mock. Chert of association [2] yielded Late Triassic (Late Norian) radiolarians. Siliceous argillite [3] is Early Jurassic (Pliensbachian or early Toarcian) in age.

As in most Cordilleran siliceous radiolarian-bearing strata, radiolarian fauna of the Teslin Plateau are moderately well preserved. However, obtaining identifiable and diverse

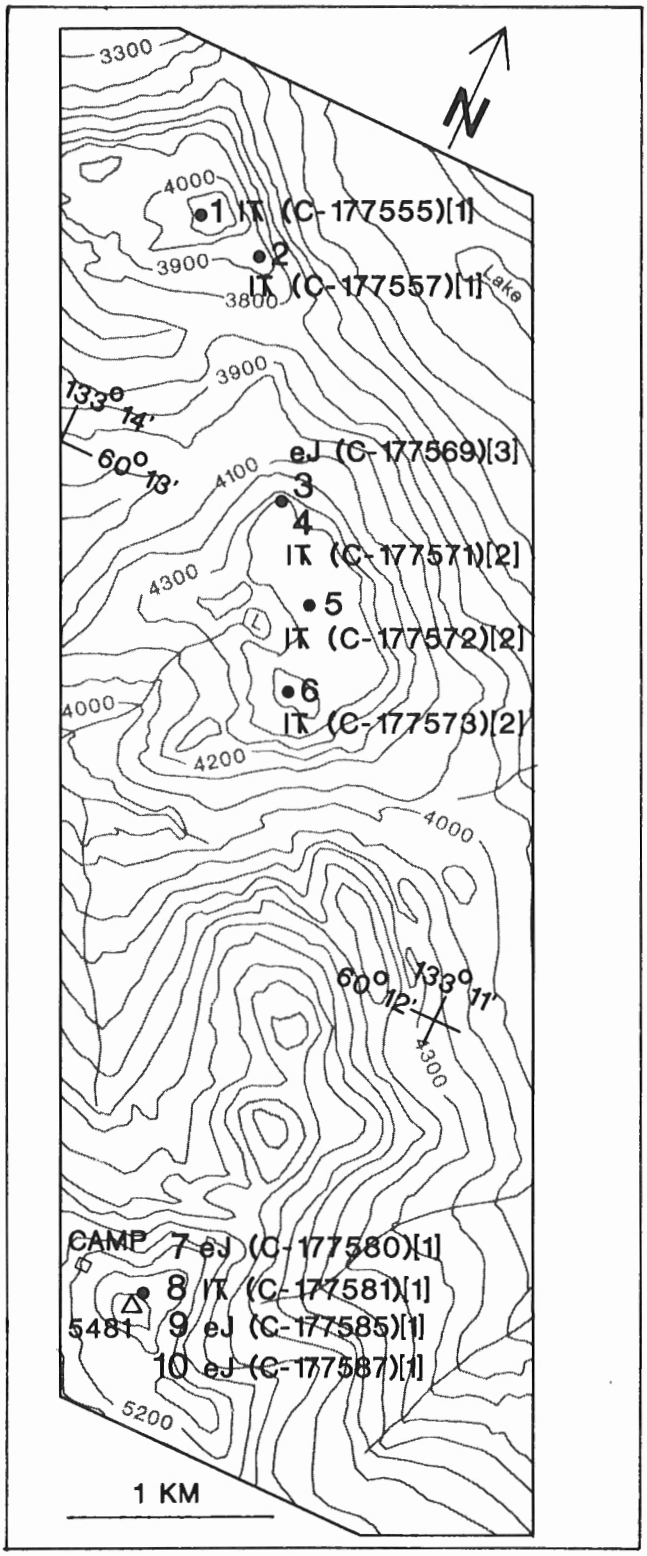

Figure 3. Location map of radiolarian and conodont localities. Annotations indicate Locality no., Age (lT = Late Triassic; eJ = Early Jurassic), GSC Locality no., and radiolarian-bearing rock type ([1] thick and disrupted section of massive and homogeneous radiolarian ribbon chert (radiolarite), [2] restricted radiolarite outcrop and [3] siliceous argillite or siltstone interbedded with greywacke). Topography from 1:50 000 NTS sheet 105C/3 (E1/2). Note that the peak at elevation 5481 feet is figured in Mulligan (1963), and therefore in Figure 2, as having an elevation of 5486 feet.

Table 1. Fossil determinations and age assignments for radiolarian and conodont collections - Ridge north of Sterlin Lake, southwestern Teslin map area (105C). Numbers 1 to 10 correspond to localities in Figure 3.

TEXT LOC.	GSC LOC.	SAMPLE NO.	UTM COORDINATES		LITHOLOGY AND TYPE	FAUNA AND AGE
			E.	N.		
1.	C-177555	90-FC-53-4	598075	6677940	grey-blue chert bed from radiolarite type [1]	*Capnodoce* sp. *Capnuchosphaera* sp. ?*Xiphotheca* sp. Late Triassic (late Carnian or pre-late Norian)
2.	C-177557	90-FC-54-2	598417	6677887	grey chert bed from radiolarite type [1]	-*Capnodoce* sp. -*Sarla* sp. *Triassocampe* sp. Late Triassic (late Carnian or pre-late Norian)
3.	C-177569	90-FC-56-6	599028	6676847	siliceous argillite interbedded with sandstone type [3]	*Bipedis* sp. ?*Broctus ruesti* Yeh *Canoptum* sp. aff. -*artum* (in Yeh, 1987) ?*Canutus giganteus* Pessagno and Whalen Gen. indet. X sp. (in Cordey, 1988) *Hagiastrum* sp. A (in Cordey, 1988) *Homoeoparonaella* sp. *Lantus* sp. *Napora cerromesaensis* Pessagno, Whalen and Yeh *Pantanellium* sp. cf. *cumshewaense* Pessagno and Blome *Paracanoptum anulatum* (Pessagno and Poisson) *Parahsuum* sp. *Pleesus* sp. *Praeconocaryomma* sp. aff. *P.* sp. B (in Yeh, 1987) -*Pseudocrucella* sp. *Wrangellium* sp. Early Jurassic (Pliensbachian or early Toarcian)
4.	C-177571	90-FC-57-2	599028	6676847	grey-black chert bed from radiolarite type [2]	*Conoptum*(?) sp. A (in Cordey, 1988) ?-*Ferresium* sp. *Livarella* sp. *Pantanellium fosteri* Pessagno and Blome *Paratriassoastrum* sp. *Squinabolella* sp. Late Triassic (late Norian)
5.	C-177572	90-FC-58-1	599410	6676371	grey chert bed from radiolarite type [2]	*Capnodoce* sp. Late Triassic (late Carnian or pre-late Norian)
6.	C-177573	90-FC-59-1	599445	6676013	grey chert bed from radiolarite type [2]	*Capnodoce* sp. Late Triassic (late Carnian or pre-late Norian)
7.	C-177580	90-FC-63-2	600094	6673025	black chert bed from radiolarite type [1]	*Canoptum* sp. *Praeconocaryomma* sp. cf. *immodica* Pessagno and Poisson ?*Wrangellium thurstonense* Pessagno and Whalen Early Jurassic (Sinemurian-Toarcian; possibly late Sinemurian)
8.	C-177581	90-FC-63-3	600094	6673025	grey-green chert bed from radiolarite type [1]	*Misikella posthernsteini* Kozur and Mock Late Triassic (late Norian)
9.	C-177585	90-FC-63-7	600094	6673025	grey-black chert bed from radiolarite type [1]	*Canoptum* sp. *Parahsuum* sp. *Praeconocaryomma* sp. Early Jurassic
10.	C-177587	90-FC-63-9	600094	6673025	grey-black chert bed from radiolarite type [1]	*Bipedis* sp. *Canoptum* sp. cf. *dixoni* Pessagno and Whalen *Gorgansium* sp. ?*Orbiculiforma* sp. A (in Carter et al., 1988) *Pantanellium* sp. *Parahsuum* sp. *Praeconocaryomma* sp. ?*Wrangellium* sp. Early Jurassic (Sinemurian-Toarcian, possibly late Sinemurian)

faunas depends on careful search and appraisal of the degree of recrystallization of radiolaria in the field using a high-powered hand-lens.

Late Triassic fauna

Details of fossil determinations and age assignments are in Table 1. Pre-Late Norian (loc. 1, 2, 5 and 6) diagnostic radiolarians include numerous specimens of *Capnodoce* sp., in place associated with *Sarla* sp. and *Triassocampe* sp.; all are widespread and well-known index taxa for the Late Triassic.

We report the first identifiable Late Norian radiolarian association of the northern Cache Creek Terrane (loc. 4). Diagnostic taxa includes radiolarians of the *Betraccium deweveri* Subzone of Blome (1984), for example *Pantanellium fosteri* Pessagno and Blome, and ?*Ferresium* sp. (Pl. 1, fig. 4), and also radiolarians reported from the Late Norian of Queen Charlotte Islands by Carter (1990) e.g. *Livarella* sp. (Pl. 1, fig. 2), *Paratriassoastrum* sp. (Pl. 1, fig. 3), and *Squinabolella* sp. Late Triassic assemblages do not show differences with previous collections from the Teslin Plateau (Cordey, 1990b), nor with those from the Cache Creek Terrane of southern British Columbia (Cordey, 1988).

Locality 8 also yielded the Late Norian conodont *Misikella posthernsteini* Kozur and Mock (Pl. 1, fig. 1). This distinctive species characterizes the youngest conodont zone of the Triassic in both Europe and North America (Orchard, 1991) where it is associated with the ammonoid *Choristoceras*, diagnostic for the Crickmayi Zone of Tozer (1980). In North America, *M. posthernsteini* has only been found in the Kunga Group of Queen Charlotte Islands, the Tyaughton Group of Cadwallader Terrane in south-central British Columbia, and in the Cache Creek cherts of Teslin map area (this report). Other records of the species from bedded chert are those described from the Mino-Tamba Belt in southwest Japan (Isozaki and Matsuda, 1982).

Early Jurassic fauna

Jurassic radiolarians from siliceous argillite (loc. 3) and radiolarite (loc. 7, 9 and 10) are of similar abundance and diversity, although preservation in the siliceous argillite is better. This latter observation confirms the biostratigraphical potential of radiolarians to date this lithology in the Canadian Cordillera (Cordey, 1990a).

At locality 3, diagnostic radiolarians (see Table 1) include post-Hettangian *Praeconocaryomma* sp. (Pl. 2, fig. 16), post-Sinemurian and pre-Aalenian *Paracanoptum anulatum* (Pessagno and Poisson) (Pl. 2, fig. 1) and taxa like *Lantus* sp. (Pl. 2, fig. 6-7), *Napora cerromesaensis* Pessagno, Whalen and Yeh (Pl. 2, fig. 12), *Pleesus* sp. (Pl. 2, fig. 8), *Wrangellium* sp. (Pl. 2, fig. 9-10), ?*Broctus ruesti* Yeh (Pl. 2, fig. 6), and ?*Canutus giganteus* Pessagno and Whalen (Pl. 2, fig. 5). These forms indicate a reliable Pliensbachian or early Toarcian age.

At localities 7 and 10 (see Table 1), the age is within the Sinemurian-Toarcian interval, as indicated by post-Hettangian *Praeconocaryomma* sp., and pre-Aalenian *Canoptum* sp. A possible late Sinemurian age is suggested by the occurrence of *Canoptum* sp. cf. *dixoni* Pessagno and Whalen (Pl. 1, fig. 7) and ?*Wrangellium thurstonense* Pessagno and Whalen (Pl. 2, fig. 12).

DISCUSSION AND INTERPRETATION

The radiolarian faunas indicate that sampled radiolarite ranges in age from Late Triassic (Late Carnian to Middle Norian; Late Norian) to Early Jurassic (post-Hettangian; possible late Sinemurian) (loc. 1-2, 4-10). In one locality (loc. 3, Fig. 3), siliceous argillite interbedded with sandstone is Early Jurassic (Pliensbachian or early Toarcian) in age. Localities 7-10 are located within the same succession, where there may be juxtaposition of Upper Triassic (Late Norian) and Lower Jurassic (post-Hettangian; possible upper Sinemurian) beds through folding and/or faulting. These results indicate that a stratigraphic succession in the sampled area probably comprises Late Triassic grey-blue, grey and grey-black radiolarite, Early Jurassic grey and black radiolarite and Early Jurassic argillite/sandstone. The relationship between the Jurassic chert and Jurassic argillite/sandstone is uncertain, but the latter may be younger. Previous dates (Cordey, 1990b) indicate that chert associated with greywacke/argillite west of Spawn Lake (loc. C, Fig. 2) is also as old as Middle Triassic (Ladinian) in age; the stratigraphic relationship between the dated chert and greywacke/argillite at that locality is uncertain.

The degree to which chert and greywacke are interbedded, rather than structurally imbricated on a fine scale, is a major problem that can only be resolved through careful field work and better age control (see Gordey (1991) for example). In particular, there is only one age so far reported from direct sampling of the clastic strata (loc. 3; Early Jurassic). At other previously reported localities the Late Triassic age of the clastics has been inferred from ages determined from associated chert.

Depositional intercalation of chert and greywacke is known from other areas of the northern Cache Creek Terrane. The French Range Subterrane of Monger and Berg (1984) consists of Permian volcanics and limestone (Teslin Formation) locally overlain by argillite, greywacke and Norian radiolarian chert (Kedahda Formation). West of the French Range near Dease Lake in northern British Columbia, Late Triassic radiolarian chert (Cordey, 1990a, b) interbedded with greywacke possibly overlies Permian(?) limestone (Monger, 1968; H. Gabrielse, pers. comm., 1989). Similar successions are known elsewhere in the southeast continuation of the Cache Creek Terrane in Dease Lake-Cry Lake map areas.

Intercalation of chert and greywacke is not common, but is observed in other orogens. In the Alps, for example, Mesozoic radiolarian chert is commonly intercalated with sequences of laminated shale and greywacke (Cressman, 1962; Schlager and Schlager, 1973). The chert/greywacke

sequence of Teslin Plateau resembles Japanese accretionary deposits in the Inuyama area of the Mino-Tamba terrane, where Early Triassic to Early Jurassic radiolarites change gradually to siliceous siltstone in Early Jurassic, and are capped by Middle Jurassic coarse-grained terrigenous clastics (Isozaki et al., 1990 and references therein). The record there is interpreted to reflect progressively coarser grained sedimentation above a subducting oceanic plate slab, i.e. successive pelagic, hemi-pelagic and trench-fill sedimentation, above the slab as it approached the arc margin. In reviewing North American radiolarian-bearing terranes, Murchey et al. (1983) defined a clastic/chert association characterized by the intercalation of chert deposits (1-30 m) and clastics, and interpreted it as a marine environment within the depositional influence of a continental margin.

As in the above examples, detrital input into the Mesozoic northern Cache Creek ocean likely occurred from flanking sources, including contiguous terranes like Stikinia (Monger and Berg, 1984; for opposing viewpoint see Jackson et al., 1990) or Quesnellia. In addition, detritus may have been contributed through cannibalization of older Cache Creek strata (through off-scraping and erosion of accretionary complex slices), as suggested by radiolarian chert clasts in the greywacke, sandstone, and conglomerate. Our results and previous ages from Teslin Plateau suggest a long time span (Late Triassic and Early Jurassic) of starved oceanic chert sedimentation broken by pulses of clastic input. It is also possible that chert deposition may have been more continuous and less frequently interrupted by clastic incursions in some areas than in others. The clastics may be an overlap succession (Lewes River assemblage of Wheeler et al., 1988), linking the Cache Creek to an adjacent terrane(s). In practice however, the long time span of intercalation and lateral facies changes make it impossible to delineate the boundary where the oceanic Cache Creek Terrane ends and the generally overlying Lewes River chert/greywacke overlap assemblage begins.

PLATE 1

Scanning electron micrographs of Late Triassic conodont (fig. 1) and Late Triassic and Early Jurassic radiolarians (fig. 2-16) from the Teslin Plateau, Teslin map area, southern Yukon. The following are indicated for each figure: identification, locality (cf. text-Fig. 3), GSC locality no., field sample no., GSC specimen no., and magnification.

fig. 1. *Misikella posthernsteini* Kozur and Mock, Loc. 8, GSC C- 177581, 90-FC-63-3, GSC 101398, x180.

fig. 2. *Livarella* sp., Loc. 4, GSC C-177571, 90-FC-57-2, GSC 101399, x200.

fig. 3. *Paratriassoastrum* sp., Loc. 4, GSC C-177571, 90-FC-57- 2, GSC 101400, x200.

fig. 4. ?*Ferresium* sp., Loc. 4, GSC C-177571, 90-FC-57-2, GSC 101401, x215.

fig. 5. ?*Xiphotheca* sp., Loc. 1, GSC C-177555, 90-FC-53-4, GSC 101402, x130.

fig. 6. *Canoptum*(?) sp. A (in Cordey, 1988), Loc. 4, GSC C- 177571, 90-FC-57-2, GSC 101403, x180.

fig. 7. *Canoptum* sp. cf. *dixoni* Pessagno and Whalen, Loc. 10, GSC C-177587, 90-FC-63-9, GSC 101404, x160.

fig. 8-11. Gen. indet. X sp. (in Cordey, 1988), Loc. 3, GSC C- 177569, 90-FC-56-6; 8 = GSC 101405, 9 = GSC 101406, 10 = GSC 101407, 11 = GSC 101408; 8,11 = x130, 9,10 = x150.

fig. 12. *Napora cerromesaensis* Pessagno, Whalen and Yeh, Loc. 3, GSC C-177569, 90-FC-56-6, GSC 101409, x190.

fig. 13. *Pantanellium* sp. cf. *cumshewaense* Pessagno and Blome, Loc. 3, GSC C-177569, 90-FC-56-6, GSC 101410, x200.

fig. 14. *Hagiastrum* sp. A (in Cordey, 1988), Loc. 3, GSC C- 177569, 90-FC-56-6, GSC 101411, x130.

fig. 15. *Homoeoparonaella* sp., Loc. 3, GSC C-177569, 90-FC-56- 6, GSC 101412, x160.

fig. 16. ?*Orbiculiforma* sp. A (in Carter et al., 1988), Loc. 10, GSC C-177587, 90-FC-63-9, GSC 101413, x190.

PLATE 1

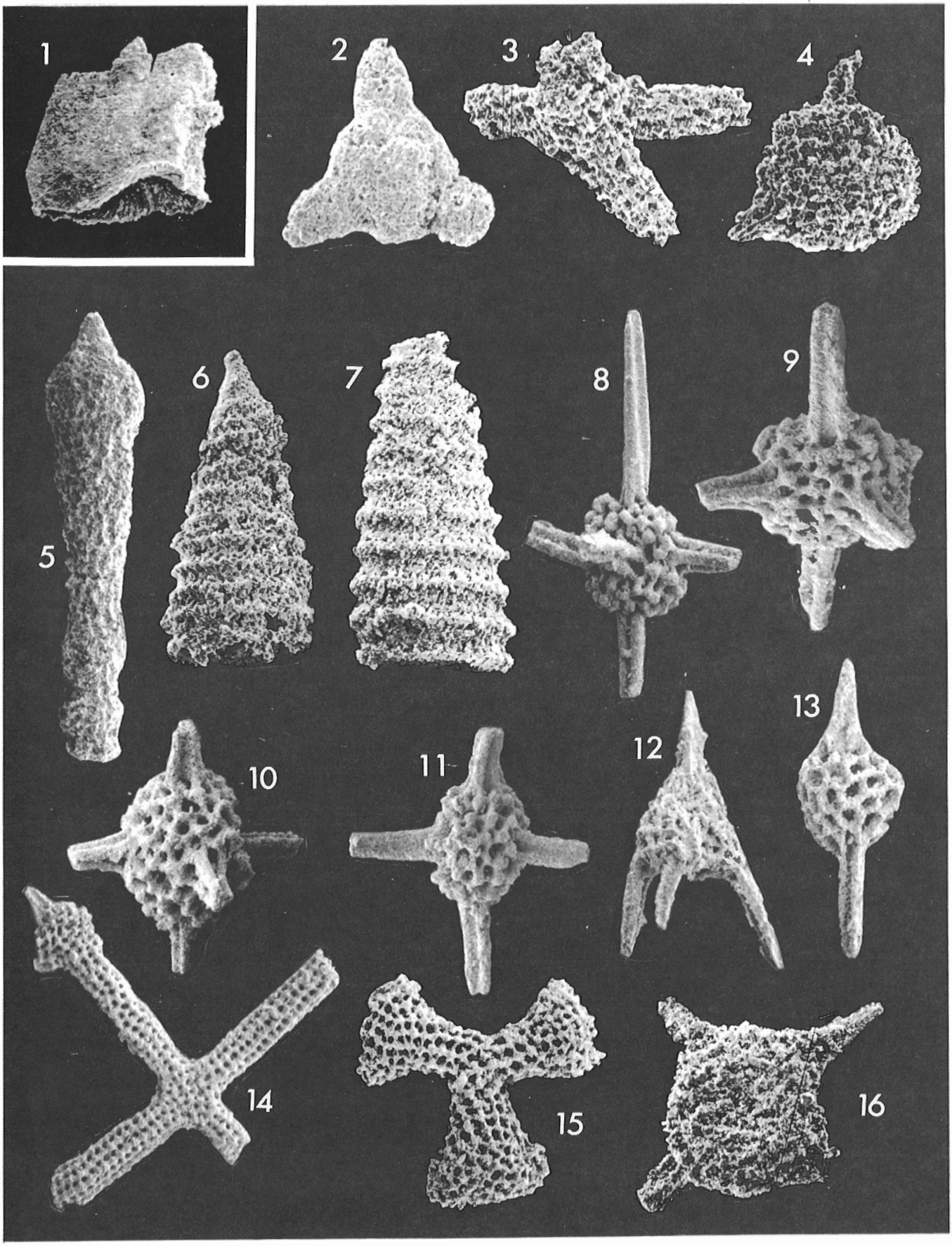

Previous indirect evidence that Cache Creek sedimentation persisted after the Triassic in northern Cache Creek Terrane was suggested through discovery of an Early Jurassic chert pebble (from a Cache Creek source(?)) recovered from conglomerate in the northern Bowser basin (Cordey, 1990b; Cordey and Evenchick, in prep.). The Jurassic chert ages reported here show the northern Cache Creek ocean persisted at least into the Sinemurian, and perhaps into the Pliensbachian or early Toarcian. They confirm previous suggestions of the upper age of the northern Cache Creek by Mortimer (1986) and Jackson et al. (1990). The Jurassic age is similar to the youngest ages in the Cache Creek Terrane of southern British Columbia where Early or Middle Jurassic (Pliensbachian to Bajocian) radiolarians have been extracted from tuffaceous argillite in the western belt (Cordey et al., 1987). Interbedded siliceous argillite and volcaniclastic sandstone are common in this belt and in Trettin's (1980) "Pavilion Beds" (Mortimer, 1987). The Jurassic radiolarite in the northern Cache Creek resembles that of the Bridge River Terrane of southern British Columbia. However, Jurassic Bridge River radiolarite sequences are more widespread and younger, and include several Middle Jurassic radiolarian localities (unpublished data). Also, interbedding of clastics with Bridge River radiolarite does not occur until Early or Middle Jurassic time.

The youngest ages of the northern Cache Creek (Sinemurian, perhaps Pliensbachian or early Toarcian) are also compatible with the previously suggested age for deformation and overthrusting of northern Cache Creek onto Stikinia along Nahlin and King Salmon faults, an event which is probably as young as Toarcian to Middle Bajocian (Thorstad and Gabrielse, 1986). The youngest ages are also compatible with the latest Toarcian or Aalenian initiation of Bowser Basin as a result of Cache Creek overthrusting (Ricketts and Evenchick, 1991).

ACKNOWLEDGMENTS

Research was funded by GSC project 900036. Helicopter support was provided by Capital helicopters (Atlin). We thank Peter Krauss and Tonia Oliveric for respective Scanning Electron Microscope and drafting contributions. Comments by Hu Gabrielse and Jim Monger are also appreciated.

PLATE 2

Scanning electron micrographs of Early Jurassic radiolarians from the Teslin Plateau, Teslin map area, southern Yukon. The following are indicated for each figure: identification, locality (cf. text-Fig. 3), GSC locality no., field sample no., GSC specimen no., and magnification.

fig. 1. *Paracanoptum anulatum* (Pessagno and Poisson), Loc. 3, GSC C-177569, 90-FC-56-6, GSC 101414, x160.

fig. 2-3. *Canoptum* sp. aff. *artum* Yeh (in Yeh, 1987), Loc. 3, GSC C-177569, 90-FC-56-6, GSC 101415 & 101416, 2-3 = x190.

fig. 4. ?*Broctus ruesti* Yeh, Loc. 3, GSC C-177569, 90-FC-56-6, GSC 101417, x200.

fig. 5. ?*Canutus giganteus* Pessagno and Whalen, Loc. 3, GSC C- 177569, 90-FC-56-6, GSC 101418, x150.

fig. 6-7. *Lantus* sp., Loc. 3, GSC C-177569, 90-FC-56-6, GSC 101419 & 101420, 6 = x180, 7 = x200.

fig. 8. *Pleesus* sp., Loc. 3, GSC C-177569, 90-FC-56-6, GSC 101421, x180.

fig. 9-10. *Wrangellium* sp., Loc. 3, GSC C-177569, 90-FC-56-6, GSC 101422 & 101423, 9-10 = x190.

fig. 11. ?*Wrangellium* sp. Loc. 10, GSC C-177587, 90-FC-63-9, GSC 101424, x170.

fig. 12. ?*Wrangellium thurstonense* Pessagno and Whalen, Loc. 7, GSC C-177580, 90-FC-63-2, GSC 101425, x165.

fig. 13-14. Gen. sp. indet., Loc. 10, GSC C-177587, 90-FC-63-9, GSC 101426 & 101427, 13 = x140, 14 = x170.

fig. 15. *Bipedis* sp., Loc. 3, GSC C-177569, 90-FC-56-6, GSC 101428, x180.

fig. 16. *Praeconocaryomma* sp. aff. *P.* sp. B (in Yeh, 1987), Loc. 3, GSC C-177569, 90-FC-56-6, GSC 101429, x155.

PLATE 2

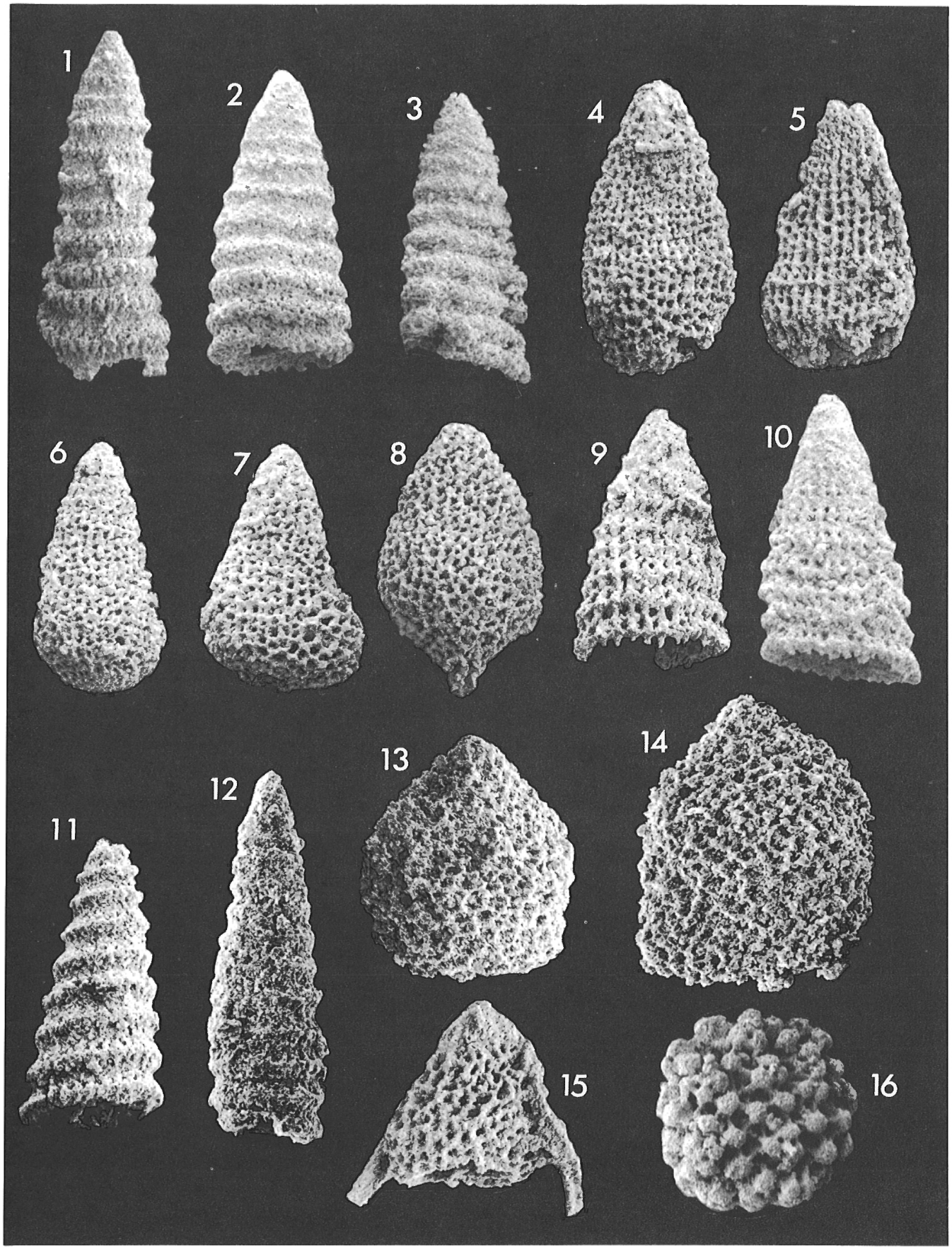

REFERENCES

Blome, C.D.
1984: Upper Triassic Radiolaria and radiolarian zonation from western North America; Bulletin of American Paleontology, v. 85, n. 318, 88 p.

Carter, E.S.
1990: New biostratigraphic elements for dating Upper Norian strata from the Sandilands Formation, Queen Charlotte Islands, British Columbia, Canada; Marine Micropaleontology, v. 15, p. 313-328.

Carter, E.S., Cameron, B.E.B., and Smith, P.L.
1988: Systematic paleontology in Lower and Middle Jurassic radiolarian biostratigraphy and systematic paleontology, Queen Charlotte Islands, British Columbia; Geological Survey of Canada, Bulletin 386, 109 p.

Cordey, F.
1988: Etude des radiolaires permiens, triasiques et jurassiques des complexes ophiolitiques de Cache Creek, Bridge River et Hozameen (Colombie-Britannique, Canada): implications paleogeographiques et structurales; Memoire des Sciences de la Terre, Universite Pierre et Marie Curie, Paris, 398 p.
1990a: Radiolarian age determinations from the Canadian Cordillera; in Current Research, Part E; Geological Survey of Canada, Paper 90-1E, p. 121-126.
1990b: Comparative study of radiolarian faunas from the sedimentary basins of the Insular, Coast, and Intermontane belts; unpublished manuscript, 57 p.

Cordey, F., Mortimer, N., DeWever, P., and Monger, J.W.H.
1987: Significance of Jurassic radiolarians from the Cache Creek terrane, British Columbia; Geology, p. 1151-1154.

Cressman, E.R.
1962: Data of geochemistry. Nondetrital siliceous sediments; United States Geological Survey, Professional Paper 440-T, p. 1-23.

Gordey, S.P.
1991: Teslin map area, a new geological mapping project in southern Yukon; in Current Research, Part A; Geological Survey of Canada, Paper 91-1A, p. 171-178.

Isozaki, Y. and Matsuda, T.
1982: Middle and Late Triassic conodonts from bedded chert sequences in the Mino-Tamba Belt, southwest Japan; Journal of Geosciences, Osaka City University, v. 25, p. 103-136.

Isozaki, Y., Maruyama, S., and Furuoka, F.
1990: Accreted oceanic materials in Japan; Tectonophysics, v. 181, p. 179-205.

Jackson, J.L., Gehrels, G.E., and Patchett, P.J.
1990: Geology and Nd isotope geochemistry of part of the northern Cache Creek terrane, Yukon: implications for tectonic relations between Cache Creek and Stikine; in Geological Association of Canada/Mineralogical Association of Canada, Joint Annual Meeting, Program with Abstracts, v. 15, p. A64.

Monger, J.W.H.
1968: Atlin Horst, British Columbia (104 J, K, N); in Report of Activities, Part A; Geological Survey of Canada, Paper 68-1A, p. 34-36.
1975: Upper Paleozoic rocks of the Atlin Terrane, northwestern British Columbia and south-central Yukon; Geological Survey of Canada, Paper 74-47.

Monger, J.W.H. and Berg, H.C.
1984: Part B - Lithotectonic map of western Canada and southeastern Alaska; in Lithotectonic Terrane Maps of the North American Cordillera, (ed.) N.J. Silberling and D.L. Jones; United States Geological Survey, Open File Report 84-523.

Mortimer, N.
1986: Late Triassic, arc-related, potassic igneous rocks in the North American Cordillera; Geology, v. 14, p. 1035-1038.
1987: Lithologic map of Pavilion (92I/13) map area, British Columbia; British Columbia Ministry of Energy, Mines and Petroleum Resources, Open-File 1987-18, scale 1:50 000.

Mulligan, R.
1963: Geology of Teslin map area, Yukon territory (105C); Geological Survey of Canada, Memoir 326, 96 p.

Murchey, B., Jones, D.L., and Holdsworth, B.K.
1983: Distribution, age, and depositional environments of radiolarian chert in western North America; in Siliceous Deposits in the Pacific Region, (ed.) A. Iijima, J.R. Hein and R. Siever; Developments in Sedimentology, v. 36, Elsevier, p. 109-126.

Orchard, M.J.
1986: Conodonts from western Canadian chert: their nature, distribution and stratigraphic application; in Investigative Techniques and Applications, Ellis Horwood Limited, p. 94-119.
1991: Late Triassic conodont biochronology and biostratigraphy of the Kunga Group, Queen Charlotte Islands, British Columbia; in Evolution and Hydrocarbon Potential of the Queen Charlotte Basin, British Columbia, (ed.) G.J. Woodsworth; Geological Survey of Canada, Paper 90-10, p. 173-193.

Ricketts, B.D. and Evenchick, C.A.
1991: Analysis of the Middle to Upper Jurassic Bowser Basin, northern British Columbia; in Current Research, Part A; Geological Survey of Canada, Paper 91-1A, p. 65-73.

Schlager, W. and Schlager, M.
1973: Clastic sediments associated with radiolarites (Tauglboden-Schchten, Upper Jurassic, Eastern Alps); Sedimentology, v. 20, p. 65-89.

Thorstad, L.E. and Gabrielse, H.
1986: The Upper Triassic Kutcho Formation, Cassiar Mountains, north-central British Columbia; Geological Survey of Canada, Paper 86-16, 53 p.

Tozer, E.T.
1980: Latest Triassic (Upper Norian) ammonoid and *Monotis* faunas and correlations; Rivista Italiana di Paleontologica e Stratigrafia, v. 85, p. 843-876.

Trettin, H.P.
1980: Permian rocks of the Cache Creek Group in the Marble Range, Clinton area, British Columbia; Geological Survey of Canada, Paper 79-17, 13 p.

Wheeler, J.O., Brookfield, A.J., Gabrielse, H., Monger, J.W.H., Tipper, H.W., and Woodsworth, G.J.
1988: Terrane map of the Canadian Cordillera; Geological Survey of Canada, Open-File 1894.

Yeh, K.Y.
1987: Taxonomic studies of Lower Jurassic Radiolaria from east-central Oregon; National Museum of Sciences, Taichung, Taiwan, Republic of China, Special Publication no. 2, 169 p.

A new assessment of the age of the basal Nanaimo Group, Gulf Islands, British Columbia

James W. Haggart
Cordilleran Division, Vancouver

Haggart, J.W., 1991: A new assessment of the age of the basal Nanaimo Group, Gulf Islands, British Columbia; in Current Research, Part E; Geological Survey of Canada, Paper 91-1E, p. 77-82.

Abstract

Strata preserved at Hamley Point, on Sidney Island in the southern Gulf Islands, contain ammonites of Early Turonian age. This is the first unequivocal demonstration of strata of this age in the Nanaimo Basin. The Hamley Point succession likely records the initiation of marine transgression in the southern Nanaimo Basin and this deposition may have been terminated in later Turonian time by sea level drop. Subsequent deposition in this region appears to have been locally of nonmarine nature and likely correlates with the initial phase of sedimentation in more northerly parts of the Nanaimo Basin.

Résumé

Les couches conservées à la pointe Hamley, sur l'île Sidney dans le sud des îles Gulf, renferment des ammonites du Turonien précoce. Il s'agit de la première preuve irréfutable de l'existence de couches de cette époque dans le bassin de Nanaimo. La succession de Hamley Point témoignerait du début de la transgression marine dans le sud du bassin de Nanaimo, et cette sédimentation aurait pris fin vers la fin du Turonien à cause d'une baisse du niveau de la mer. La sédimentation ultérieure dans cette région semble avoir été par endroits de nature non marine et être reliée à la phase initiale de sédimentation dans les parties plus septentrionales du bassin de Nanaimo.

INTRODUCTION

Based on its extensive and well-preserved mollusc fauna, the Cretaceous Nanaimo Group of Vancouver Island and adjacent Gulf and San Juan islands has long been considered to include marine rocks of mid-Santonian through Early Maastrichtian age (Usher, 1952; Jeletzky, 1970). In these earlier studies, the presence of unfossiliferous strata at the base of some sections of the Nanaimo Group suggested the possibility of older strata, although no fossil evidence for marine rocks older than Santonian age was known.

Several brief references in the more recent literature have proposed that older rocks may indeed be present in the Nanaimo Group succession, although this dating has all been considered tentative. Popenoe et al. (1987), in a study of Cretaceous gyrodiform gastropods of the North American Pacific coast, proposed that some rocks in the southern part of the Nanaimo basin were likely of Turonian age, based on the presence of *Gyrodes dowelli* White at one locality in the Gulf Islands. The exact age range of this gastropod species is not well constrained, however (L. Saul, pers. comm., 1991), and definitive evidence of Turonian age strata at this locality was thus lacking.

P.D. Ward (pers. comm., 1985, 1991; *in* Garver, 1988) also suggested that Upper Turonian strata might be present in the eastern San Juan Islands, where ammonite fragments possibly referable to the genus *Reesidites* had been collected from turbidite deposits.

More recently, the author identified molluscs in collections submitted to the Geological Survey for age determinations (Haggart, 1988a, b) which also suggested the likely presence of Turonian deposits in the southern part of the Nanaimo Basin. Again, however, unequivocal age-diagnostic fossils, such as ammonites, were lacking in the collections. These identifications have subsequently been cited in England's (1990) synthesis study on the geology of the Nanaimo Group and England and Calon's (1991) structural analysis of the basin.

Motivated by these suggestions of older rocks in the basin, the author initiated a study to directly address the age of the basal Nanaimo Group succession. This is part of a long-term project focusing on the age and faunal content of the poorly-known older and younger parts of the Nanaimo Group. In this paper I report the results of an investigation of basal Nanaimo Group exposures at one locality in the southern Gulf Islands.

STRATIGRAPHY

The studied section is exposed on the southeast side of Sidney Island at Hamley Point (Fig. 1). The succession of Nanaimo Group strata preserved at this locality dips moderately to the northeast and is separated by a cobble beach from outcrops of the Jurassic Saanich Batholith (Muller, 1983), several hundred metres to the southwest. The base of the section is not exposed and the upper limit is covered by water to the northeast. The uppermost beds of the section continue along strike to the northwest, forming the northeast shore of Sidney Island.

The contact of the Nanaimo Group strata with the granodiorite has been mapped as a nonconformable overlap (Muller, 1983; England, 1990; England and Calon, 1991). At Hamley Point the covered interval separating the Cretaceous and Jurassic outcrops precludes an objective interpretation of the relationship between the two units.

The Cretaceous succession at Hamley Point consists of sandstone with discontinuous conglomerate horizons at the base, which fines upward into fine- to medium-grained silty sandstone (Fig. 2). Muller (1983) assigned all these strata to the Comox Formation while England (1989) differentiated the conglomerate and sandstone beds as the Tzuhalem and Saanich members, respectively, of the Benson Formation. As discussed below, there are problems with both of these stratigraphic assignments.

A section 145 m in thickness was measured through the Hamley Point exposure using pace and compass. Four principal lithofacies units were identified in the section. The following discussion provides a brief summary of the rock types and sedimentary structures present within each of these lithofacies units.

Unit 1 (0-9 m): The lowest 9 m of the section consist of massive to plane-laminated, fine- to medium-grained sandstone, moderately well sorted. Most of these strata are lithic arenites but locally approach arenite compositions. Pebbles and small cobbles, well rounded and up to 8 cm in diameter, are found dispersed in the matrix of these lowermost beds.

No fossils were noted in the matrix of the sandstones but rounded calcareous concretions in the uppermost part of the unit, just beneath the conglomerate horizons of Unit 2, did yield some fossils, mostly inoceramid bivalves.

Unit 2 (9-13 m): Overlying the lower beds of Unit 1 are about 4 m of medium- to coarse-grained, massive sandstone with distinct conglomerate lenses. These lenses are about 1 m thick but thicken and thin dramatically; the maximum lateral extent observed is about 10 m. The conglomerates are locally channelled into the underlying sandstone beds, with up to 15 cm of relief noted locally. Conglomerate clasts are well rounded cobbles to 15 cm, composed of metavolcanic, sedimentary, and lesser plutonic lithologies, all in a coarse grained sandstone matrix. The conglomerates vary from clast to matrix supported.

Locally, extensive accumulations of thick shelled molluscs, mostly trigoniid bivalves and naticid and strombid gastropods, are found within the conglomerate lenses. Substantial numbers of trigoniid and gastropod fossils are also found singly in the coarser sandstone beds of the unit.

Unit 3 (13-28 m): The top beds of Unit 2 grade rapidly into an approximately 15 m-thick succession of muddy siltstone and minor, thin sandstones. Locally, these rocks contain soft-sediment deformation features indicative of slumping and they are rich in volutiform gastropods. The siltstones display no internal structures and are thus considered to have

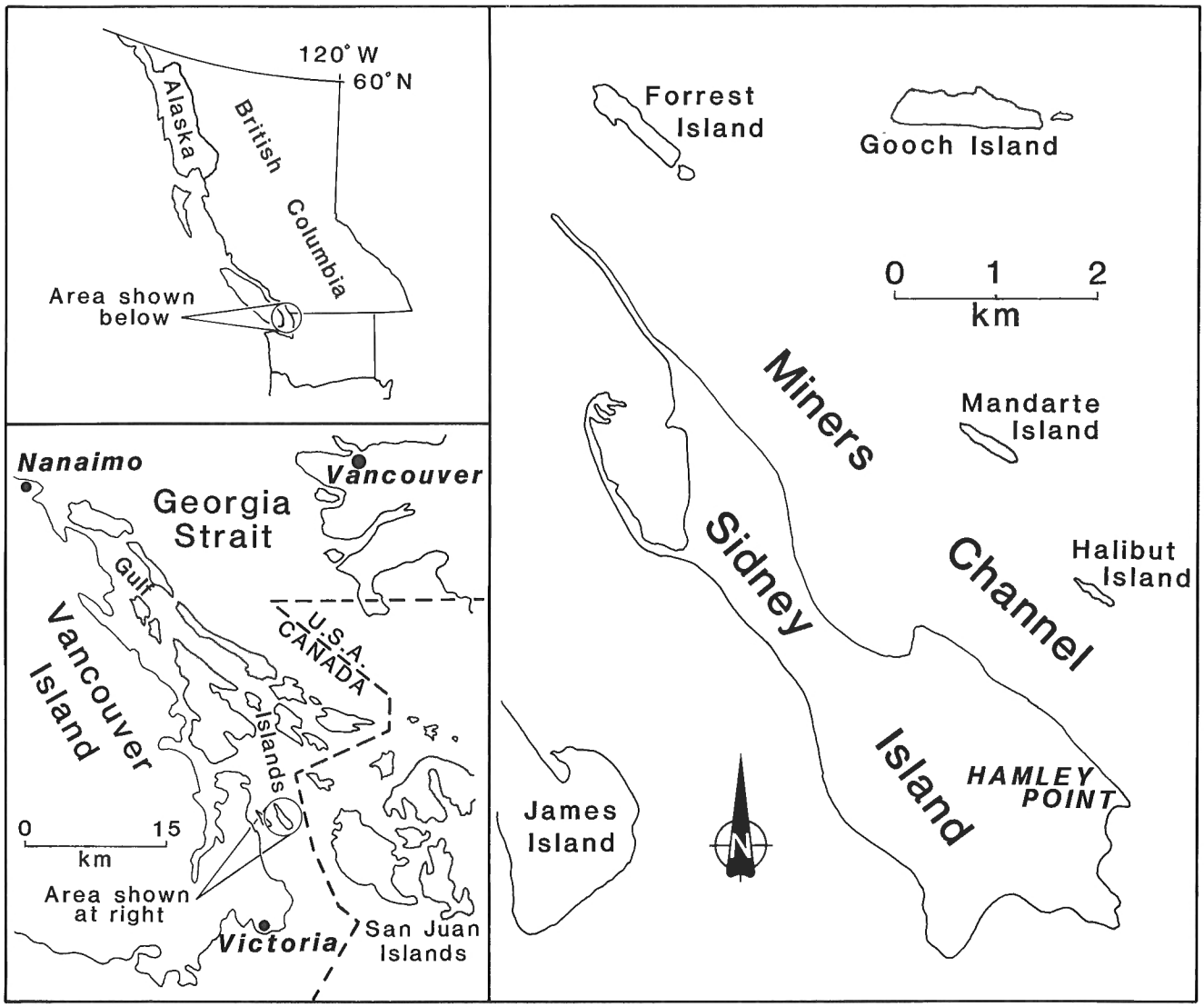

Figure 1. Location map showing principal study area.

been thoroughly bioturbated by the gastropod fauna. Spheroidal calcareous concretions to 6 cm diameter are common in the siltstone beds.

The siltstones are interstratified with laterally continuous, plane-laminated or graded sandstone beds, generally between 3 and 8 cm in thickness.

Unit 4 (28-143 m): The siltstones of Unit 3 are conformably but abruptly overlain by a succession of massive to cross-stratified, fine- to coarse-grained sandstones, similar to those in Unit 2. Approximately 115 m of strata are assigned to this unit which extends to the top of the measured section. The sandstone beds in the lower 48 m of the unit are more thickly bedded and coarse grained than the sandstones in the upper part (0.5 to 1.5 m thickness), and are amalgamated or separated by thin, siltstone interbeds. The lower sandstone beds are plane-laminated to planar cross-stratified and show dewatering features. Fossils are rare in these beds.

Sandstones in the upper part of the unit are more thinly bedded, generally finer-grained, and typically massive to hummocky cross-stratified. The thickness and proportion of siltstone interbeds is greater in the upper part of the unit as well. Fossils are uncommon, but typically found on bedding plane exposures or within the middle of individual massive sandstone beds.

FOSSIL COLLECTIONS

Molluscs were collected from several horizons within the Hamley Point section (Fig. 2). The lowest locality, GSC loc.**C-187545** (6.5 m), provided the following taxa:

Hyphantoceras? sp.

Mytiloides cf. *mytiloides* (Mantell)

gyrodiform gastropod, indet.

Slightly higher in the section, GSC loc.**C-184901** (9.5 m), in the thickest conglomerate lens, included many broken and abraded shells. Many specimens of thick-shelled molluscs are found in this conglomerate. The following were identified:

Mytiloides cf. *mytiloides* (Mantell)

Mytiloides duplicostatus (Anderson, 1958)

Pterotrigonia klamathonia (Anderson, 1902)

Litschkovitrigonia? fitchi (Packard, 1921)

Acteonella sp.

Gyrodes dowelli White

perissityid? gastropod

At 31 m in the section, at GSC loc.**C-184902**, the following was identified:

Inoceramus sp.

In the upper part of the section, in finer-grained sandstones, GSC loc.**C-184903** (76 m) provided the following:

Tragodesmoceras ashlandicum (Anderson, 1902)

Pachydesmoceras? sp.

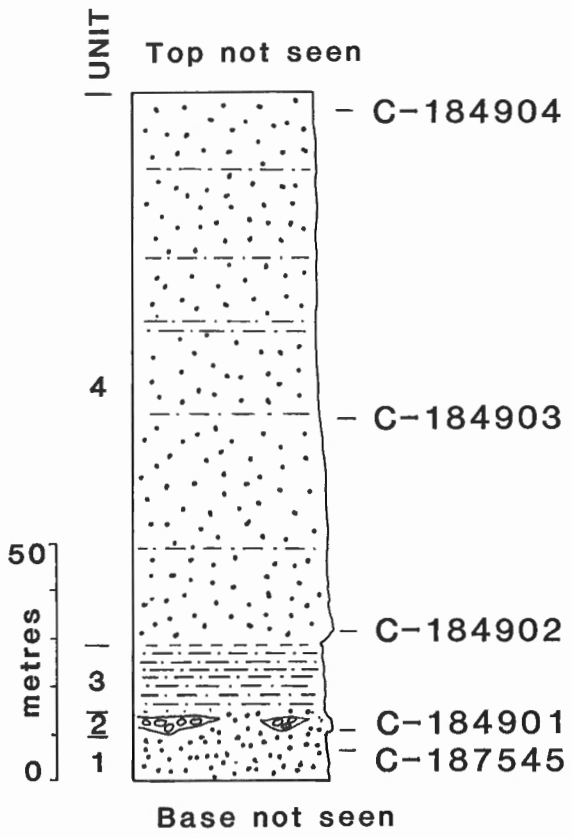

Figure 2. Generalized stratigraphic column of the Cretaceous succession at Hamley Point showing horizons of GSC fossil localities.

Mytiloides duplicostatus (Anderson, 1958)

Pterotrigonia klamathonia (Anderson, 1902)

Litschkovitrigonia? sp.

Anchura? sp.

Gyrodes? sp.

turritelliform gastropod, indet.

And finally, at the highest sampled locality, about 5 m below the top of the measured section, GSC loc.**C-184904** (140 m) provided:

Tragodesmoceras? sp., approximately 45 cm original diameter

solitary horn coral

DISCUSSION

Age

The Hamley Point section is critical for determining the age of the basal part of the Nanaimo Group in this part of the Nanaimo Basin. Most of the molluscan taxa found in this section have not previously been identified in British Columbia. The ammonite *Tragodesmoceras ashlandicum* and the inoceramid bivalve *Mytiloides duplicostatus* are known from the lower Turonian of California (Matsumoto, 1960; Anderson, 1958) and *Mytiloides mytiloides* is a cosmopolitan indicator of the lower Turonian as well (Kauffman and Powell, 1977). *Pterotrigonia klamathonia* ranges through the Turonian and possibly into lowermost Coniacian strata of the Pacific coast (Jones, 1960). Finally, *Litschkovitrigonia? fitchi* occurs in early to middle Turonian strata of southern Oregon and northern California (Saul, 1978). The molluscan assemblages thus indicate an early Turonian age for the Hamley Point section. This is significantly older than any previously known Nanaimo Group strata; indeed, no ammonites from the middle and upper Turonian nor the Coniacian have yet been identified in the Nanaimo Group succession (Usher, 1952; Jeletzky, 1970; Ward, 1978).

Depositional environment

The succession of rock types and sedimentary structures preserved in the Hamley Point section represents an overall transgressive marine sequence. The base of the transgressive sequence is not seen in the Hamley Point section, but the extensive accumulations of broken and abraded trigoniid bivalves and other molluscs found in the channelized conglomerates and surrounding coarse sandstones of the lower part of the section indicate that these strata were deposited in very shallow water, probably $\leq$30 m depth.

The presence of hummocky cross-stratification in the finer grained strata of the upper part of the section, as well as the associated fauna of ammonites and shelf molluscs, indicate that these strata were also deposited on the shelf, subject to extensive wave activity, but probably at greater depths than the basal strata in the section.

Although it is not possible to rule out significant earlier deposition at the Hamley Point locality, given that the base of the sequence is not preserved, it is considered likely that the section records the initiation of sedimentation in this part of the Nanaimo Basin.

Stratigraphy

The interpretation of the stratigraphy at Hamley Point proposed by Muller (1983) does not appear tenable. He correlated the Hamley Point strata with the Comox Formation but the thick siltstone sequence in the middle of the succession and the rather thin conglomerates and finer clastics in the lower and upper parts of the succession, respectively, do not compare well with typical descriptions of the Comox Formation as exposed on Vancouver Island and the more westerly of the Gulf Islands.

England (1989) correlated the Sidney Island succession with the Benson Formation, recognizing a basal unit, the Tzuhalem member, and the overlying Saanich member. Within the Saanich member England (1989) described a coaly siltstone lithofacies, developed at other localities than Sidney Island, which appears, from his lithological description, to be a shallower water facies than that seen at Hamley Point and likely of nonmarine origin.

According to England (1989), outcrops of this coaly siltstone lithofacies, with associated shallow-marine trigoniid beds, are present on Forrest Island, north of Sidney Island and separated from it by Miners Channel (Fig. 1). Strata of Forrest Island appear to strike into outcrops to the southeast on Mandarte and Halibut islands, also north of Sidney Island and separated from it by Miners Channel.

The strata preserved on Forrest, Mandarte, and Halibut islands may thus all be equivalents and may represent a separate stage of sedimentation, with a locallized nonmarine phase, from that represented by the Hamley Point succession. Thus, the beds on Forrest, Mandarte, and Halibut islands may include the younger Turonian and Coniacian strata which have not yet been conclusively identified in the Nanaimo Group.

Given the pronounced eustatic drop recognized in the later part of the Turonian (Hancock and Kauffman, 1979; Haq et al., 1987) it is quite possible that the Early Turonian phase of Nanaimo Group deposition recorded at Hamley Point was terminated due to sea level fall. Subsequent deposition in the area in later Turonian to Coniacian time may have produced the nonmarine/shallow-water facies recognized by England (1989) within the Saanich member of the Benson Formation on Forrest Island. This deposition would thus correspond with the initial phase of Nanaimo Group deposition in the more northerly parts of the basin (Muller and Jeletzky, 1970).

There does not seem to be sufficient evidence at this time to postulate an unconformity within the Late Cretaceous succession of the southern Nanaimo Basin. Rather, the preservation of strata of Early Turonian age in this part of the basin suggests that deposition in the Nanaimo Basin commenced in the south, was interrupted in later Turonian time by sea level fall, but was renewed and subsequently progressed northward in Coniacian to Santonian time.

CONCLUSIONS

1. Ammonites and other molluscs in strata preserved at Hamley Point on Sidney Island, in the southern part of the Nanaimo Basin, are of Early Turonian age. This is the first unequivocal determination of Nanaimo Group strata older than Santonian in age.
2. The Hamley Point succession may represent the initial phase of sedimentation in the Nanaimo Basin, this deposition possibly interrupted in later Turonian time by sea level fall.
3. The deposits at Hamley Point likely represent a separate phase of sedimentation from the typical Nanaimo Group sequence preserved in the more northerly parts of the Nanaimo Basin. Deposition in the Nanaimo Basin thus appears to have initiated first in the southern part of the basin and subsequently progressed northwards.

ACKNOWLEDGMENTS

The author thanks P. Mustard for review of the manuscript. T.D.J. England provided thoughtful comments and corrections.

REFERENCES

Anderson, F.M.
1958: Upper Cretaceous of the Pacific coast; Geological Society of America, Memoir 71, 378 p., 75 pls.

England, T.D.J.
1989: Lithostratigraphy of the Nanaimo Group, Georgia Basin, southwestern British Columbia; in Current Research, Part E; Geological Survey of Canada, Paper 89-1E, p. 197-206.
1990: Late Cretaceous to Paleogene evolution of the Georgia Basin, southwestern British Columbia; Ph.D. thesis, Memorial University of Newfoundland, St. John's, 481 p.

England, T.D.J. and Calon, T.J.
1991: The Cowichan fold and thrust system, Vancouver Island, southwestern British Columbia; Geological Society of America Bulletin, v. 103, p. 336-362.

Garver, J.
1988: Stratigraphy, depositional setting, and tectonic significance of the clastic cover to the Fidalgo Ophiolite, San Juan Islands, Washington; Canadian Journal of Earth Sciences, v. 25, p. 417-432.

Haggart, J.W.
1988a: Report on Upper Cretaceous fossils collected from the Nanaimo Group of Vancouver Island in the summer of 1987 by Chris Yorath of the Pacific Geoscience Centre, B.C., and submitted for identification in September, 1987 (51 lots); Geological Survey of Canada unpublished Fossil Report No. JWH-1988-04, 18 p.
1988b: Report on Upper Cretaceous fossils collected from various localities of the Nanaimo Group of southern Vancouver Island and the adjacent San Juan Islands, British Columbia, submitted for identification by C.J. Yorath of the Pacific Geoscience Centre and forwarded by ISPG, Calgary, on September 28, 1988 (9 lots); Geological Survey of Canada unpublished Fossil Report No. JWH-1988-12, 5 p.

Hancock, J.M. and Kauffman, E.G.
1979: The great transgressions of the Late Cretaceous; Journal of the Geological Society of London, v. 136, pt. 2, p. 175-186.

Haq, B.U., Hardenbol, J., and Vail, P.R.
1987: Chronology of fluctuating sea levels since the Triassic; Science, v. 235, p. 1156-1167.

Jeletzky, J.A.
1970: Biochronology; in Geology of the Upper Cretaceous Nanaimo Group, Vancouver Island and Gulf Islands, British Columbia, (ed.) J.E. Muller and J.A. Jeletzky; Geological Survey of Canada, Paper 69-25, p. 35-58.

Jones, D.L.
1960: Pelecypods of the genus *Pterotrigonia* from the west coast of North America; Journal of Paleontology, v. 34, no. 3, p. 433-439, pls. 59-60.

Kauffman, E.G. and Powell, J.D.
1977: Paleontology; in Stratigraphic, Paleontologic, and Paleoenvironmental Analysis of the Upper Cretaceous Rocks of Cimarron County, Northwestern Oklahoma, (ed.) E.G. Kauffman, D.E. Hattin, and J.D. Powell; Geological Society of America, Memoir 149, p. 47-114, pls. 1-12.

Matsumoto, T.
1960: Upper Cretaceous ammonites of California. Part II; Memoirs of the Faculty of Science, Kyushu University, Series D (Geology), Special Volume 1, 172 p., 41 pls.

Muller, J.E.
1983: Geology, Victoria, British Columbia; Geological Survey of Canada, Map 1553A, 1 sheet, scale 1:100 000.

Muller, J.E. and Jeletzky, J.A.
1970: Geology of the Upper Cretaceous Nanaimo Group, Vancouver Island and Gulf Islands, British Columbia; Geological Survey of Canada, Paper 69-25, 77 p.

Popenoe, W.P., Saul, L.E., and Susuki, T.
1987: Gyrodiform gastropods from the Pacific coast Cretaceous and Paleocene; Journal of Paleontology, v. 61, no. 1, p. 70-100.

Saul, L.R.
1978: The North Pacific Cretaceous trigoniid genus *Yaadia*; University of California Publications in Geological Sciences, v. 119, 65 p., 12 pls.

Usher, J.L.
1952: Ammonite faunas of the Upper Cretaceous rocks of Vancouver Island, British Columbia; Geological Survey of Canada, Bulletin 21, 182 p., 30 pls.

Ward, P.D.
1978: Revisions to the biostratigraphy and biochronology of the Upper Cretaceous Nanaimo Group, British Columbia and Washington State; Canadian Journal of Earth Sciences, v. 15, no. 3, p. 405-423.

Acoustic images of turbulent flow structures in Fraser River estuary, British Columbia

R.A. Kostaschuk[1], M.A. Church[2], and J.L. Luternauer
Cordilleran Division, Vancouver

Kostaschuk, R.A., Church, M.A., and Luternauer, J.L., 1991: Acoustic images of turbulent flow structures in Fraser River estuary, British Columbia; in Current Research, Part E; Geological Survey of Canada, Paper 91-1E, p. 83-90.

Abstract

A selectable frequency sounder was deployed in the Fraser River estuary, British Columbia, to provide first-ever acoustic images of large-scale turbulent vortices called kolks. Kolks occurred only during unstratified flow over falling and rising tides. They developed on the lower stoss face of large dunes and were then sheared away from the bed and carried downstream. Kolks were manifested at the river surface as boils. There are at least three possible causes of kolks: flow separation on the lee sides of dunes, pressure variations associated with flow acceleration on the stoss sides of dunes and microturbulent bursts. Our data are consistent with the second and third of these. Kolks are seen to be an important mechanism for entraining bed sediment into suspension.

Résumé

Un sondeur à fréquence réglable a été déployé dans l'estuaire du Fraser en Colombie-Britannique pour produire des images acoustiques inédites de grands tourbillons turbulents appelés kolks. Ces derniers n'ont été observés que lorsqu'un écoulement non stratifié s'est formé sur l'eau durant les marées montantes et descendantes. Ils se sont formés sur la face en pente douce inférieure de grandes dunes, puis ont été détachés du lit et transportés en aval. Des kolks ont été observés à la surface du fleuve sous forme de bouillonnements. Il y a au moins trois causes possibles de la formation de kolks: la séparation des écoulements du côté sous le vent des dunes, les variations de pression associées à l'accélération des écoulements du côté en pente douce des dunes et les explosions microturbulentes. Les présentes données corroborent les deuxième et troisième causes. Les kolks sont considérés comme un important mécanisme d'entraînement des sédiments de fond en suspension.

[1] Department of Geography, University of Guelph, Guelph, Ontario N1G 2W1
[2] Department of Geography, University of British Columbia, Vancouver, B.C. V6T 1Z2

INTRODUCTION

The Main Channel of the Fraser River in its delta (Fig. 1) is a salt-wedge estuary. In spite of extensive development occurring along the river, sedimentary processes remain poorly understood. To address this problem, a project was initiated in 1985 involving the University of Guelph, Geological Survey of Canada, University of British Columbia, Sediment Survey Section of the Inland Waters Directorate and Public Works Canada. Recently, the investigation has focused on interrelations between flow, bedforms and sediment transport (e.g. Kostaschuk et al., 1989, 1990). In 1990, this research was extended to examine the role of large turbulent structures in suspending sediment.

Turbulent "bursting" in open channel flows is assumed to play a major role in the transport of bed-material in suspension (e.g. Allen, 1985) although few data are available to test this assumption (Lapointe, 1990). Numerous flow-visualization studies in small laboratory flumes (e.g. Rao et al., 1971) have led to the description of a microturbulent "burst-sweep" cycle, in which relatively slow-moving bottom water is violently ejected (burst) toward the surface, being replaced by an inrush (sweep) of high-velocity water from higher in the flow. On the surfaces of rivers, macroscale turbulent fluctuations include "boils", circular features that project above the surface and are characterized by an upwelling of fluid (e.g. Jackson, 1976; Coleman, 1969; Rood and Hickin, 1989). Boils appear to be the surface manifestation of "kolks", slowly rotating, upward-tilting vortices (Jackson, 1976). Dyer (1986) believes that kolks result from intermittent flow separation effects in the lee of dunes. Jackson (1976) suggests that kolks are the product of microturbulent bursts, although this connection has not been properly demonstrated (Allen, 1985).

The purpose of the 1990 investigation was to examine the relations amongst kolks, boils and bedforms in the Fraser Estuary. The Fraser Estuary has a sandy bed with large dunes (Kostaschuk et al., 1989) and well-developed boils have been noted on many occasions (Fig. 2). This paper describes the methodology and presents some preliminary results and interpretation.

METHODS

Data were collected aboard CSL Jaeger in June 1990, over a variety of river discharge and tidal conditions. We used a Datasonics DFT selectable acoustic profiler, operated at 25 kHz, with an EPS 4800 19 inch graphic recorder. The acoustic record identifies small variations in water density, which may result from variations in suspended sediment content, or in water temperature and salinity. All of these effects are present in Fraser Estuary. Fluctuations in current speed were measured with a Marsh McBirney Model 527 electromagnetic current meter and suspended sediment concentration with a D&A Instruments Model OBS 3 optical backscatter turbidity probe.

Temporal variations in kolks and boils were assessed by anchoring the vessel at stations on either side of the navigation channel (Fig. 1). The sounder provided time series records of kolks propagating past the station. The current meter and turbidity probe were deployed simultaneously, at a variety of levels above the bed, to evaluate fluctuations in horizontal and vertical current speed and sediment concentration. Current and turbidity data were logged at 0.33 s intervals on a microcomputer. Spatial and temporal variations in kolks and potential sites of kolk generation were determined by operating the sounder as the vessel ran along a survey line in the centre of the channel (Fig. 1). The current meter and turbidity probe data are not yet completely analyzed and the following description of preliminary results focuses on the description of surface boils and on the acoustic imagery.

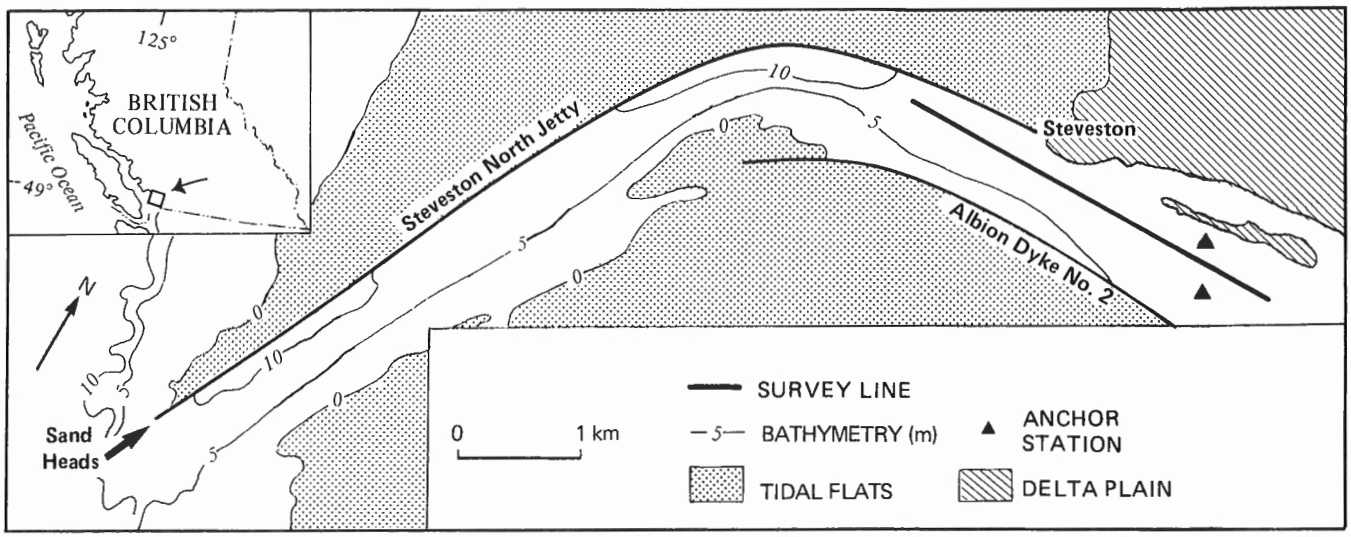

Figure 1. Study reach in lower Fraser Estuary.

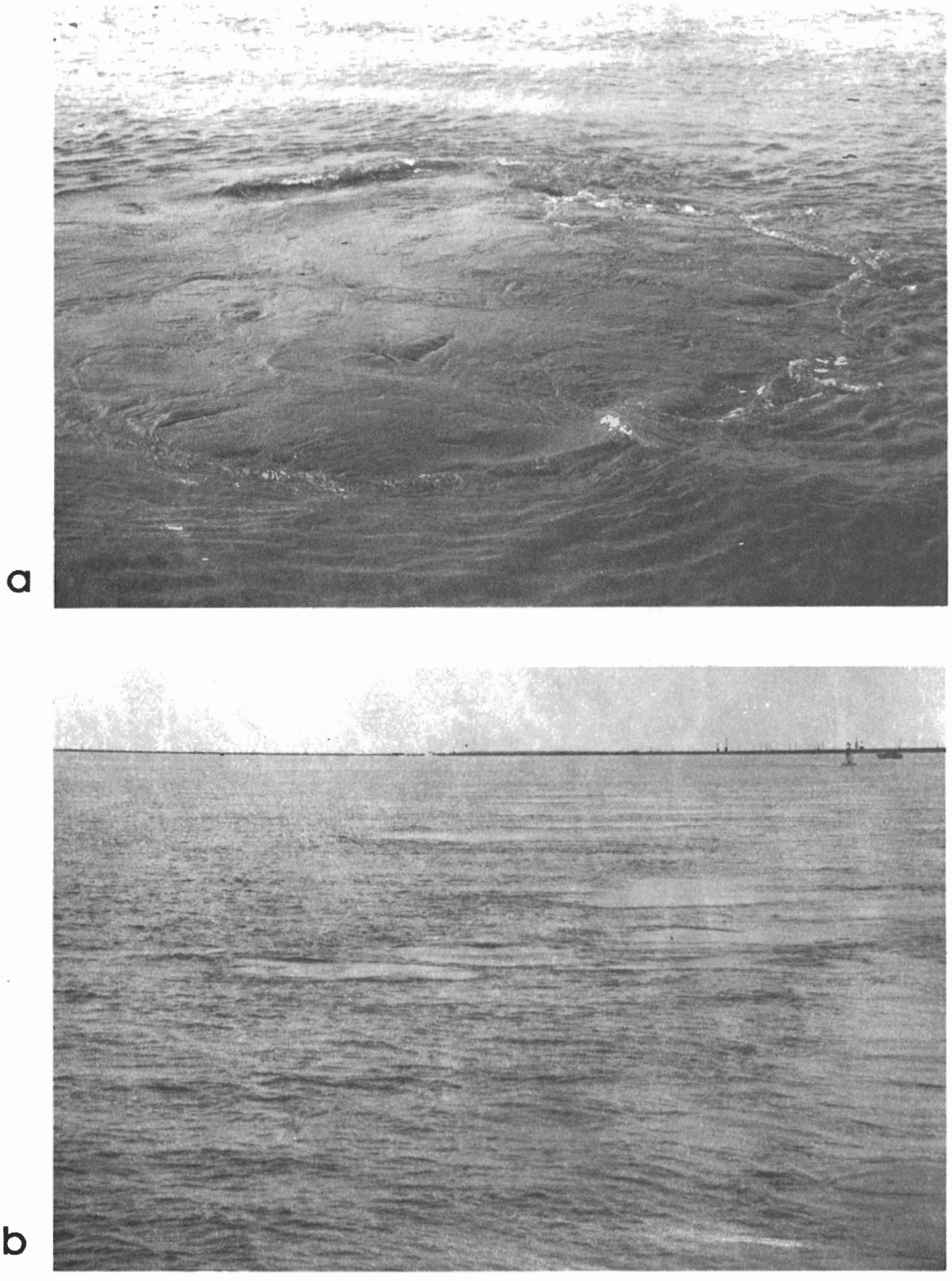

Figure 2. Boils at anchor station on north side of channel (Fig. 1): **a.** 1 m diameter boil surfacing beside boat. **b.** boils that had surfaced near the vessel propagating downstream. The closest boil is approximately 2 m in diameter.

RESULTS

We observed that the presence of boils in the Fraser was related to tidal conditions. At high tide, when the flow was stratified, fresh surface water flowed seaward over the salt-wedge and the water surface was smooth with no obvious boils. As the tide fell and the salt-wedge was flushed seaward, isolated boils appeared. Flow acceleration during the falling tide was associated with more frequent and energetic boils. Boils were also apparent during much of the rising tide, but disappeared as high tide approached, current velocity decreased and the salt-wedge intruded back into the channel.

On June 25, a series of boils surfaced beside the anchored vessel during a six minute period mid-way through a falling tide. They appeared at the surface in a similar position and had diameters of 1-2 m (Fig. 2a). There was a strong upward and outward component to the flow within boils and smaller vortices were apparent in the larger structure. Sand was visible in suspension in the boils but not in the ambient flow. Immediately after surfacing, boils propagated downstream and increased in diameter and became flatter. However, they maintained their shape and were clearly visible of order hundreds of metres downstream (Fig. 2b).

The acoustic images from anchor stations provided a record of temporal variations of strong perturbations in the water column which may be compared with the surface observations of boils. For descriptive purposes, we refer to these perturbations as kolks. We found that as the tide fell and the wedge was flushed from the channel, currents accelerated and kolks appeared. During periods of maximum sediment transport surrounding low tide the acoustic records were uniformly dark, because of high overall sediment concentrations, and it was impossible to identify individual kolks. Immediately before and after this period, however, kolks were usually visible (Fig. 3). The images from anchor stations showed that kolks maintained their integrity when separated from the bed and were propagated upward and seaward.

On June 25 when boils were surfacing near the boat, we were able to observe the passage of a series of them past the sounder. These records clearly showed that the features we interpreted as kolks were connected to the boils at the surface. On a few occasions we also observed boils passing the current meter and a rapid increase was noted in the magnitude and variability in the vertical velocity component of the flow, reflecting the passage of a kolk.

Soundings along the survey line provide data to further assess the conditions associated with temporal variations in kolk activity. We believe that these records revealed the locations of kolk generation. When flow was stratified at high tide the salt-wedge surface was apparent on the profile and there was evidence for salt water entrainment by the upper layer (Fig. 4). There was no indication of kolk activity during these conditions. During unstratified flow, kolks were

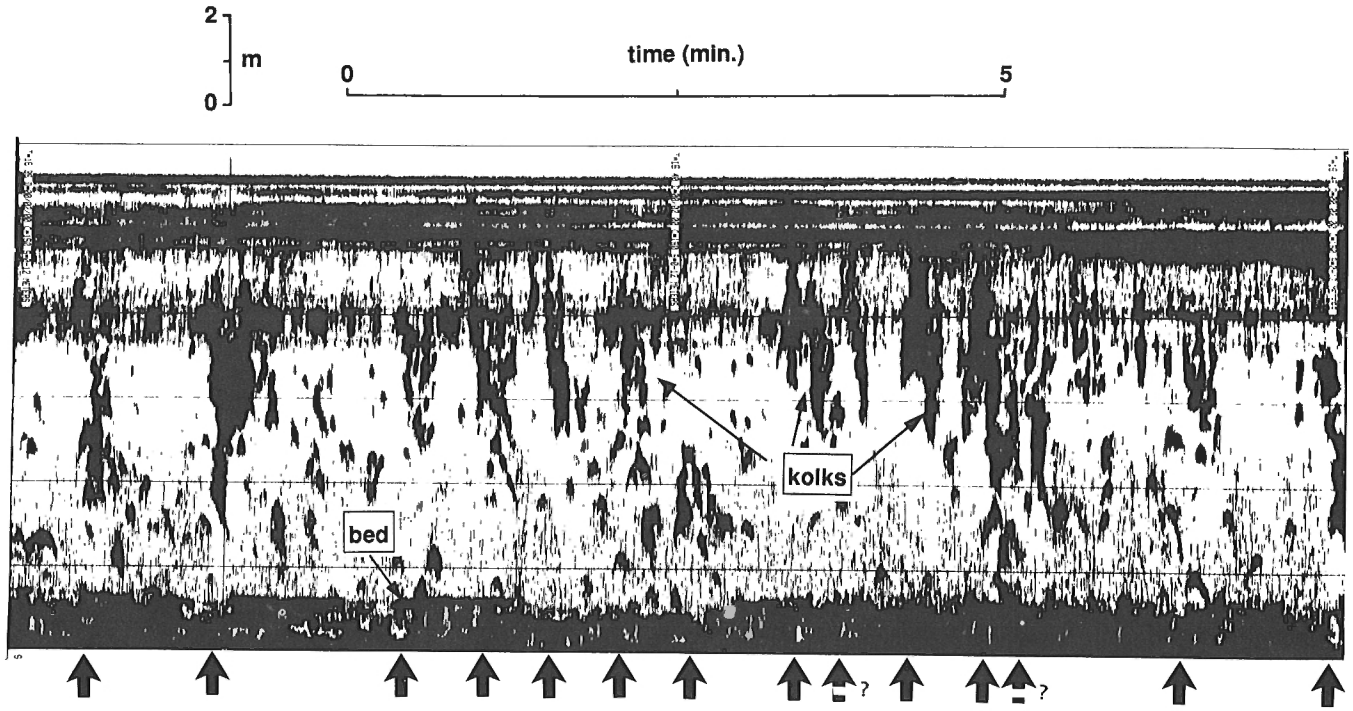

Figure 3. Time series acoustic record of kolks propagating past anchor station on south side of channel (Fig. 1), on June 18 during a rising tide. A low tide of 1.3 m occurred at 0840 and a high tide of 3.7 m at 1545. The dark zone approximately 7 m from the bed represents interference from the current meter and the dark record above that is noise. Major kolks are indicated by a solid arrow at the bottom of the record and possible kolks by a broken arrow. Features marked ? may not be independent of adjacent features. Dunes in the centre of the channel ranged from 1 to 3 m in height and 60 to 200 m in length.

present and seemed to originate over the distal lee side or proximal stoss side of dunes (Fig. 5, 6 and 7). Kolks were usually tilted downstream at angles of 5-8° from the horizontal, although secondary features were sometimes ramped off the lee sides of dunes at lower angles, of order 3° (Fig. 5). Interestingly, the sites of kolk generation, and presumably entrainment and suspension of bed sediment, showed considerable spatial variability in the dune field. Typically only a few bedforms displayed intense kolk activity during a survey period (Fig. 6) and these sites remained consistent during surveys. As the tide rose and flow decelerated, kolk generation was restricted to fewer bedforms and kolks extended only a few metres above the bed (Fig. 7). As high tide approached and the salt-wedge intruded into the study reach, kolk activity ceased.

DISCUSSION

We found that kolk generation and temporal variability in the Fraser Estuary depended primarily on tidal conditions. Kolks were not observed at high tide during stratified conditions because the strong, downstream flowing upper layer was not in contact with the bed. As the tide fell and the salt-wedge was flushed from the channel, kolk generation began. During unstratified flows over both falling and rising tides, kolks developed on a limited number of large bedforms and were then sheared away from the bed and carried downstream. Observations of surface boils indicated that kolks expanded and lost energy as they propagated down the channel. As high tide approached and currents decelerated, kolk activity decreased and was restricted to a zone close to the bed.

These data allow us to test several hypotheses about relations between kolks, boils and bedforms. The first hypothesis is that boils are the surface manifestations of kolks. Our data support this. The second hypothesis is that kolks are caused by flow separation effects of the lee side of dunes. Flow separation usually extends one third of the downstream distance between bedform crests (e.g. Allen, 1985). This is the position where most kolks are initiated on the Fraser dunes, lending support to this hypothesis. However, velocity profiles obtained by Kostaschuk et al. (1990) over dunes in the Fraser provided no evidence for lee side flow separation. In addition, Dyer (1986) reviewed the literature and found that dunes with height to length ratios (H/L) less than about 0.07 do not experience flow separation. Kostaschuk et al. (1989) report H/L values between 0.04 and 0.05 for Fraser dunes in 1986. Measured values of H/L for dunes with active kolk generation in this investigation (Fig. 5, 6 and 7) were

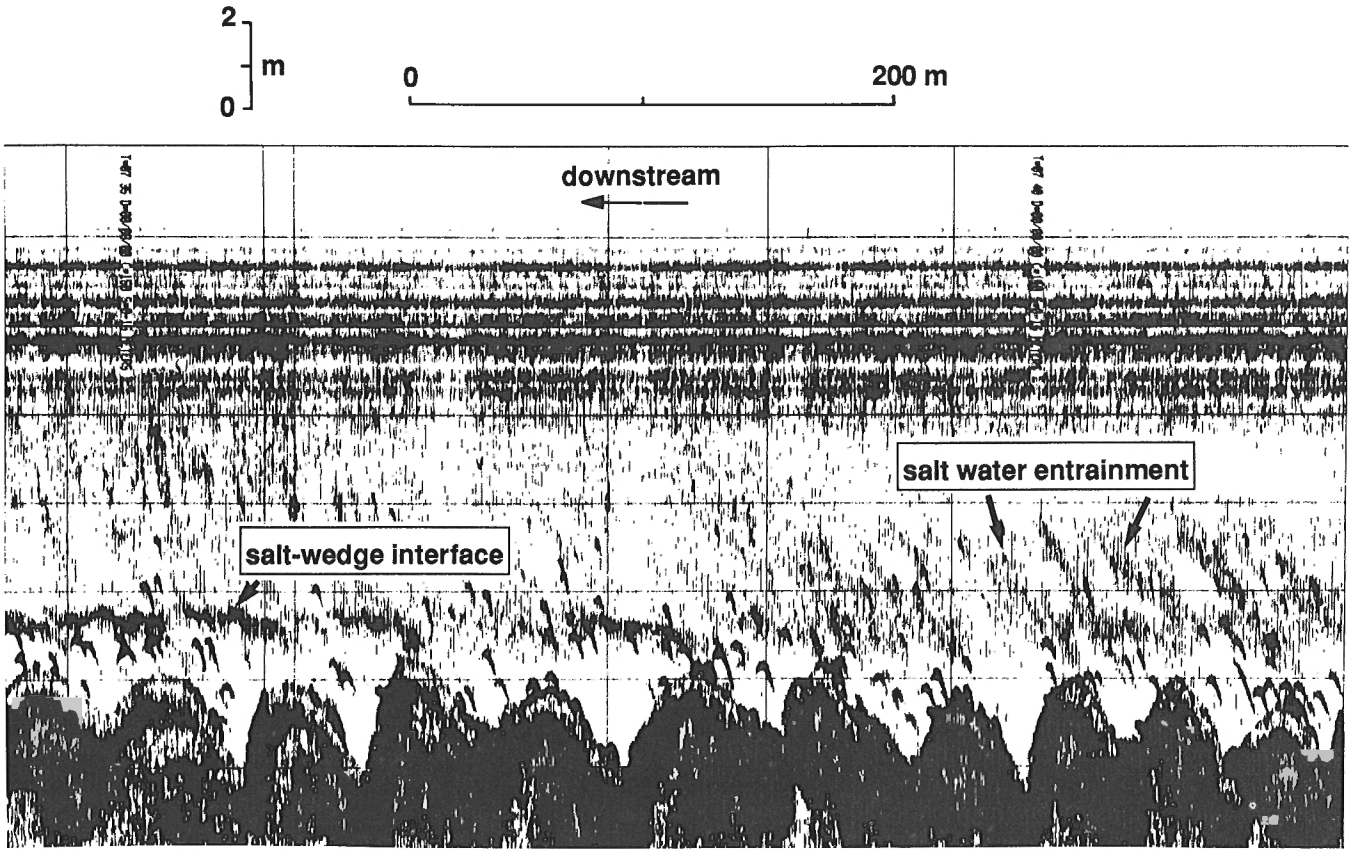

Figure 4. Acoustic record along the survey line (Fig. 1) between 0735 and 0740 during a falling tide on June 24. A high tide of 4.2 m occurred at 0555 and a low tide of 0.2 m at 1320. Note the absence of kolks, the position of the salinity interface and internal waves indicating entrainment of water from the salt wedge. The sharp 'hyperbolic' echoes within the salt wedge probably represent fish.

between 0.02 and 0.05. These results suggest flow separation is unlikely on Fraser dunes and this mechanism of kolk generation may not be operative. A possible alternative explanation for kolk generation in the Fraser is that it is not directly associated with the dunes. Jackson (1976) notes that kolks do form on flat beds. If this were the case in the Fraser, however, we might expect a more random distribution of the sites of kolk generation rather than the persistent position just downstream of the dune lee face. The visualizations over the dunes reflect substantial increases in suspended sediment associated with the kolks. The sediment is clearly derived from the stoss face of the dunes. Hence it is possible that kolks are the result of pressure variations associated with flow acceleration up the stoss sides of the dunes, which also induces major sediment entrainment. This issue requires further investigation.

Our data permit a preliminaty evaluation of the likelihood that the Fraser kolks are associated with burst-sweep processes, or with some macroturbulent equivalent. Several investigators (cf. Rao et al., 1971) have shown that burst periodicity (T_b) scales with boundary layer thickness (δ) and free-stream velocity (U_s) as

$$T_b = a\delta/U_s \qquad 3 \leq a \leq 7 \qquad (1)$$

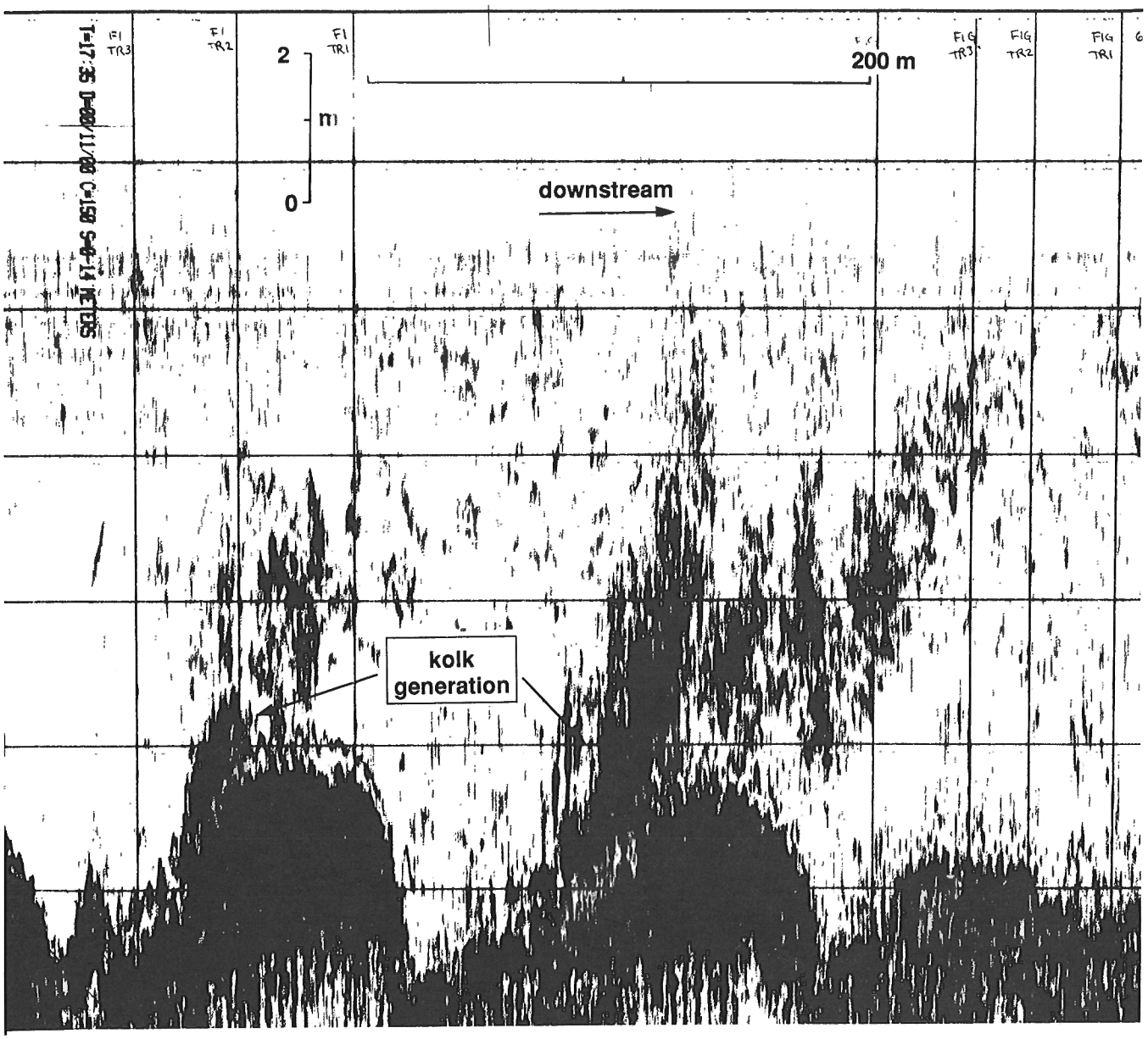

Figure 5. Acoustic record along the survey line (Fig. 1) between 1735 and 1737 during a rising tide on June 27. A low tide of 1.4 m occurred at 1530 and a high tide of 4.7 m at 2245. The "spiked" surface of the dunes reflects ship motion caused by wind waves. On the dune with two kolks, the upstream feature is inclined at 7.6° and the secondary feature at 2.9°. The secondary feature may represent a kolk originally inclined at a steeper angle that was tilted as it was sheared from the bed and propagated downstream.

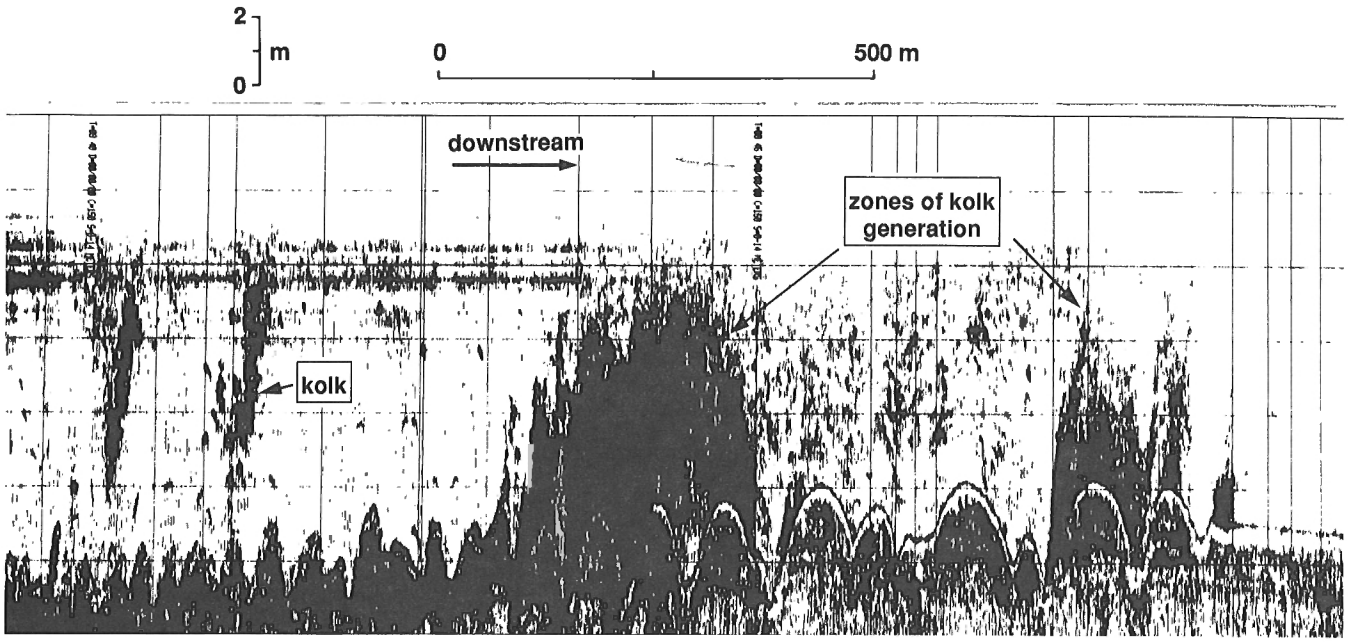

Figure 6. Acoustic record along the survey line (Fig. 1) during a falling tide on June 22. A high tide of 4.5 m occurred at 0400 and a low tide of -0.1 m at 1145. Note the localized nature of kolk generation and bed-material suspension. The two isolated kolks on the upstream record are probably features that were generated upstream but have sheared from the bed and propagated downstream.

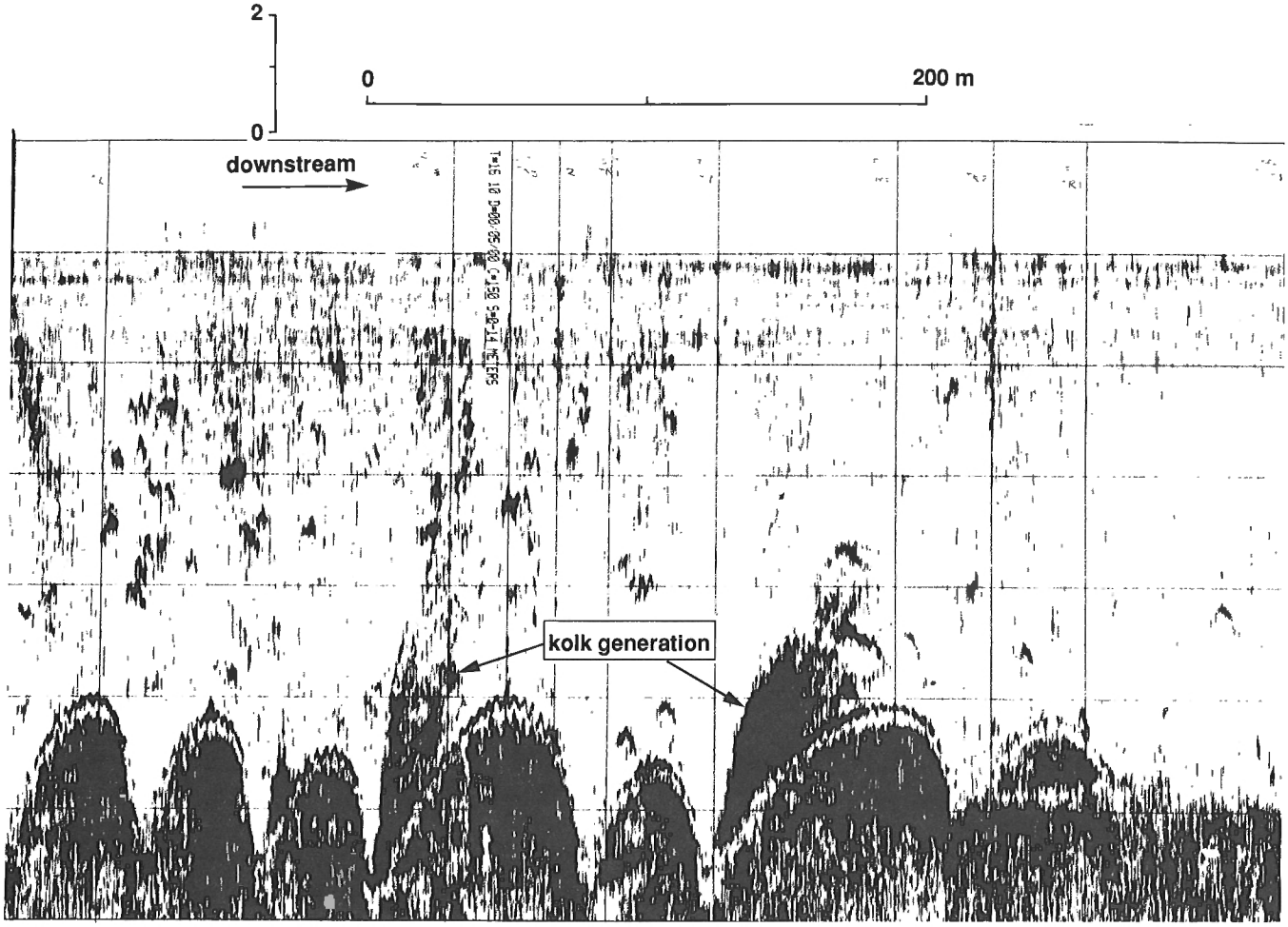

Figure 7. Acoustic record along the survey line (Fig. 1) during a rising tide on June 21. A low tide of 0.1 m occurred at 1100 and a high tide of 4.7 m at 1850. Of the two major kolks illustrated, the upstream one extends at least 10 m surfaceward while the other is limited to a zone within 5 m of the bed.

Taking $\delta = 11$ m (flow depth) and $U_s = 1.0$ m/s (surface velocity), we obtain from the scale equation $33 \leq T_b \leq 77$, with median value of 55 s. In Figure 3 there are between 12 and 14 major kolks evident in 607 s of record, for a periodicity between 43 and 51 s. This represents remarkable agreement with the scale equation. Microturbulent bursts are supposed to occur at random, whereas the Fraser features appear to be tied to dunes, although the record of Figure 3 indicates substantial irregularity in shedding frequency. Our result indicates that the analogy bears further study.

As far as we are aware, the acoustic images of macroturbulent kolks presented here are the first ever published. The images demonstrate unequivocally the movement of bed-material into suspension from the dunes. Some material is convected high into the water column and presumably travels many dune lengths downstream before it settles out. The technique has tremendous potential for the description of large-scale flow structures in rivers, estuaries and tidal environments. However, this potential, plus applications to sediment transport, will only be fully realized with digital data acquisition and analysis.

ACKNOWLEDGMENTS

Financial support was provided by Natural Sciences and Engineering Research Council Operating Grants to Kostaschuk and Church, and Luternauer's Geological Survey of Canada Project 790006. We wish to thank Randy Smith for piloting the CSL Jaeger, Wendy Hales for field assistance, and Warren Williams and Public Works Canada for their ongoing logistical support.

REFERENCES

Allen, J.R.L.
1985: Physical Sedimentology; George Allen & Unwin, London, 272 p.

Coleman, J.M.
1969: Brahmaputra River: channel processes and sedimentation; Sedimentary Geology, v. 3, p. 129-139.

Dyer, K.R.
1986: Coastal and Estuarine Sediment Dynamics; John Wiley & Sons, Toronto, 342 p.

Jackson, R.G.
1976: Sedimentological and fluid-dynamic implications of the turbulent bursting phenomena in geophysical flows; Journal of Fluid Mechanics, v. 77, p. 531-560.

Kostaschuk, R.A., Church, M.A., and Luternauer, J.L.
1989: Bedforms, bed-material and bedload transport in a salt-wedge estuary: Fraser River, British Columbia; Canadian Journal of Earth Sciences, v. 26, p. 1440-1452.

Kostaschuk, R.A., Ilersich, S.A., and Luternauer, J.L.
1990: Relationships between bed-material load and bedform migration, Fraser River estuary, British Columbia; in Current Research, Part E; Geological Survey of Canada, Paper 90-1E, p. 239-244.

Lapointe, M.F.
1990: Intermittent turbulent suspension events over sand dunes on the bed of the Fraser River near Mission, British Columbia; in Canadian Hydrology Symposium 1990: Abstract Proceedings; Canada Centre for Inland Waters, Burlington, Ontario, Session 3.

Rao, K.N., Narasimha, R., and Narayanan, M.A.B.
1971: The 'bursting' phenomenon in a turbulent boundary layer; Journal of Fluid Mechanics, v. 48, p. 339-352.

Rood, K.M. and Hickin, E.J.
1989: Suspended-sediment concentration and calibre in relation to surface flow structure in Squamish River estuary, southwestern British Columbia; Canadian Journal of Earth Sciences, v. 26, p. 2172-2176.

Porosity and permeability of ocean floor sediments from the Middle Valley Zone in the northeast Pacific: Borehole PAR90-1

T.J. Katsube, K. Wires[1], B.I. Cameron, and J.M. Franklin
Mineral Resources Division

Katsube, T.J., Wires, K., Cameron, B.I., and Franklin, J.M., 1991: Porosity and permeability of ocean floor sediments from the Middle Valley zone in the northeast Pacific: Borehole PAR90-1; in Current Research, Part E; Geological Survey of Canada, Paper 91-1E, p. 91-97.

Abstract

Porosity and fluid permeability have been measured for 10 core samples of sediments, obtained from a depth range of 0 to 7.7 metres below the ocean floor at the Middle Valley area of the northeast Pacific. The purpose of this study is to establish the porosity and permeability of ocean floor sediments that play an important role in the formation of large sulphide deposits. Middle Valley is an area with such significance.

The porosities are 72 to 80%, surprisingly high values, resembling those of unconsolidated clays. The permeabilities in the range of 10^{-15} to 10^{-11} m^2 are also high values, similar to those of unconsolidated silt to silty sand. The lower permeability values resemble those of unweathered marine clays, and may be due to both precipitation from heated seawater and cooled hydrothermal fluids.

Résumé

La porosité et la perméabilité aux fluides de dix carottes de sédiments prélevés à des profondeurs de 0 à 7,7 mètres sous le fond marin dans la vallée médiane dans le nord-est du Pacifique, ont été mesurées. Le but de la présente étude est d'établir la porosité et la perméabilité des sédiments de fond océanique qui jouent un rôle important dans la formation des grands gisements de sulfures. La vallée médiane est une région d'une telle importance.

Les porosités sont de 72 à 80 %, valeurs étonnamment élevées qui sont voisines de celles des argiles non consolidées. Les perméabilités dans la gamme de 10^{-15} à 10^{-11} m^2 sont aussi élevées, de l'ordre de celles du limon non consolidé au sable limoneux. Les valeurs plus faibles sont de l'ordre de celles des argiles marines non altérées, et elles pourraient être dues à la précipitation de matières en suspension dans l'eau de mer chauffée ou dans les fluides hydrothermiques refroidis.

[1] Agriculture Canada, Land Resource Research Centre, Ottawa, Canada K1A 0C6

INTRODUCTION

Porosity and fluid permeability have been measured for 10 core samples of ocean floor sediments, obtained from depth ranging from 0 to 7.7 m below the ocean floor surface, at the Middle Valley area of the northeast Pacific. The ocean depth at the core site is about 2440 m. The purpose of this study is to establish the porosity and permeability of ocean floor sediments that play an important role in the formation of large sulphide deposits. Middle Valley is an area of such significance (Kappel and Franklin, 1989).

High temperature fluids at Middle Valley are probably generated in the volcanic "basement" (Franklin et al., 1989) and rise up along a fault or fracture through the overlying 300-400m of hemipelagic and turbiditic sediment. As fluids rise through the sediment, they seem to have diffused outward from their main conduit, causing zones of alteration (Goodfellow and Blaise, 1988) and hydrothermal precipitation in the immediate sub-seafloor, over areas several hundred metres in diameter. Preliminary studies of the pore water data (Lydon, et al., 1990) indicates that fluids are moving upwards in a plume shaped zone within the sediments. Cooling of these fluids, possibly by advectively driven convection or else by conduction, causes precipitation of sulphides. Mixing of hydrothermal fluid with seawater causes barite precipitation.

Thermally-driven advection of cold seawater through the sediment, a probable mechanism for heat transfer away from the hydrothermal "plume", also has a mineralogical effect on the sediments. Heated seawater interacts with clays to form Mg-smectite (see Turner et al., 1991). Anhydrite also precipitates from seawater as a result of heating.

The net result of precipitation from either hydrothermal fluid or heated seawater is to potentially reduce the porosity and permeability of the sediment, causing it to become more indurated. Quantitative measurement of these physical properties has not been undertaken in areas of hydrothermal upwelling. In order to constrain models of fluid flow through the sediments, these measurements are needed. This paper reports the results of measurements of absolute porosity and permeability on a suite of sediment samples from a core taken from the Middle Valley area, northeast Pacific ocean.

METHOD OF INVESTIGATION

Samples

Some of the geological attributes of the Middle Valley area have been described by Davis et al. (1987), Goodfellow and Blaise (1988) and Kappel and Franklin (1989). The "High Heat Flow " area (also described as the "Area of Active Venting") is an area of seafloor, about 900 m long and 250 m wide, where twelve active vents were examined during an ALVIN dive program in 1990. Core PAR90-1 was obtained by W. Goodfellow and B. Cameron from near the northern edge of this area (Fig. 1). The graphic strip log in Figure 2 shows the vertical distribution of sedimentological units, structures, alteration facies, and authigenic minerals. Ten core samples, each 6.5 cm in diameter and 15 cm in length, were obtained from this core. These samples were sealed and refrigerated in core tube containers for transportation to the laboratories for petrophysical measurements. The depth range of the samples are listed in Table 1 and shown in Figure 2. Comments on the character of the samples, based on sedimentological descriptions of the upper and lower sections adjacent to the samples, are also included in the table. Preliminary scanning electron microscopic examination revealed the presence of sulphide precipitate from the hydrothermal fluid (Fig. 3a) and smectite precipitate through reaction of seawater with heated sediment (Fig. 3b).

Experimental procedures

The petrophysical measurements carried out on these samples consist of permeability, k, or hydraulic conductivity, $K_{\S}$ porosity, 0, volumetric water content, Θ_v, and bulk density, δ.

Hydraulic conductivity is defined as the flux of water per unit gradient of the hydraulic potential. Using the hydraulic conductivity ($K_{\S}$) measuring procedure described by Elrick et al. (1987), each sample was resaturated with a 3% saline solution to simulate the seawater at the core site. This was accomplished by immersing the sample and container in a tank with the bottom and top of each container open. The water level was raised to a position slightly above the top of the sample container so that the sample would be resaturated from the bottom up. $K_{\S}$ was determined using the equation

$$K_{\S} = (Q\ )/(At\Delta h)$$

where

Q = volumetric flow rate with time (mL/s),

1 = length of sample (cm),

t = time in seconds (s),

A = cross section area of the core (cm^2)

Δh= hydraulic head (cm/cm).

A constant hydraulic head (Δh) was established and Q was measured when steady state was achieved. The permeability (k) is determined by converting $K_{\S}$ into k (Freeze and Cherry, 1979):

$$1\ m/s\ (K_{\S}) = 10^{-7}\ m^2\ (k).$$

Volumetric water content (Θ_v), bulk density (δ) and porosity (-) were determined using the method described in Sheldrick (1984). The length of some of the samples was slightly less than the container length of 15 cm. In order to maintain a constant length of 15 cm, the missing volume of each core was corrected by using 30 μm diameter glass beads to fill any cavities. Porosity was calculated from Θ_v and δ assuming a particle density of 2.65 g/mL.

EXPERIMENTAL RESULTS

The experimental results for bulk density (δ), volumetric water content (Θ_v), porosity (0) and permeability (k) for the 10 samples are listed in Table 2. The effect of sample mineralogy and chemistry on the petrophysical properties of the

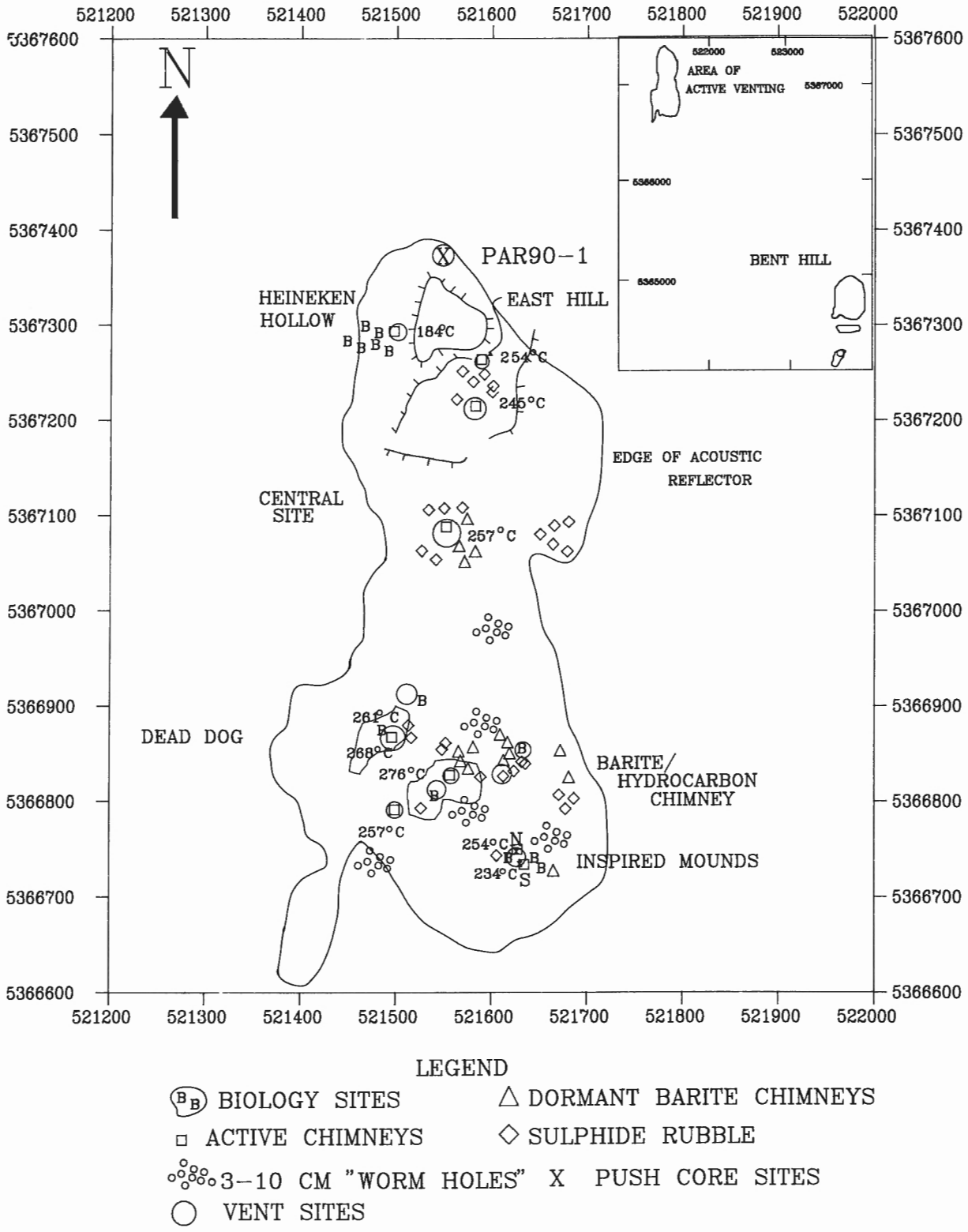

Figure 1. Location of piston core PAR90-1 at the nothern edge of the Area of Active Venting. The area outlined as an acoustic reflector represents indurated sediments. The inset shows the two known areas of active hydrothermal venting within Middle Valley. UTM grid coordinates are in metres.

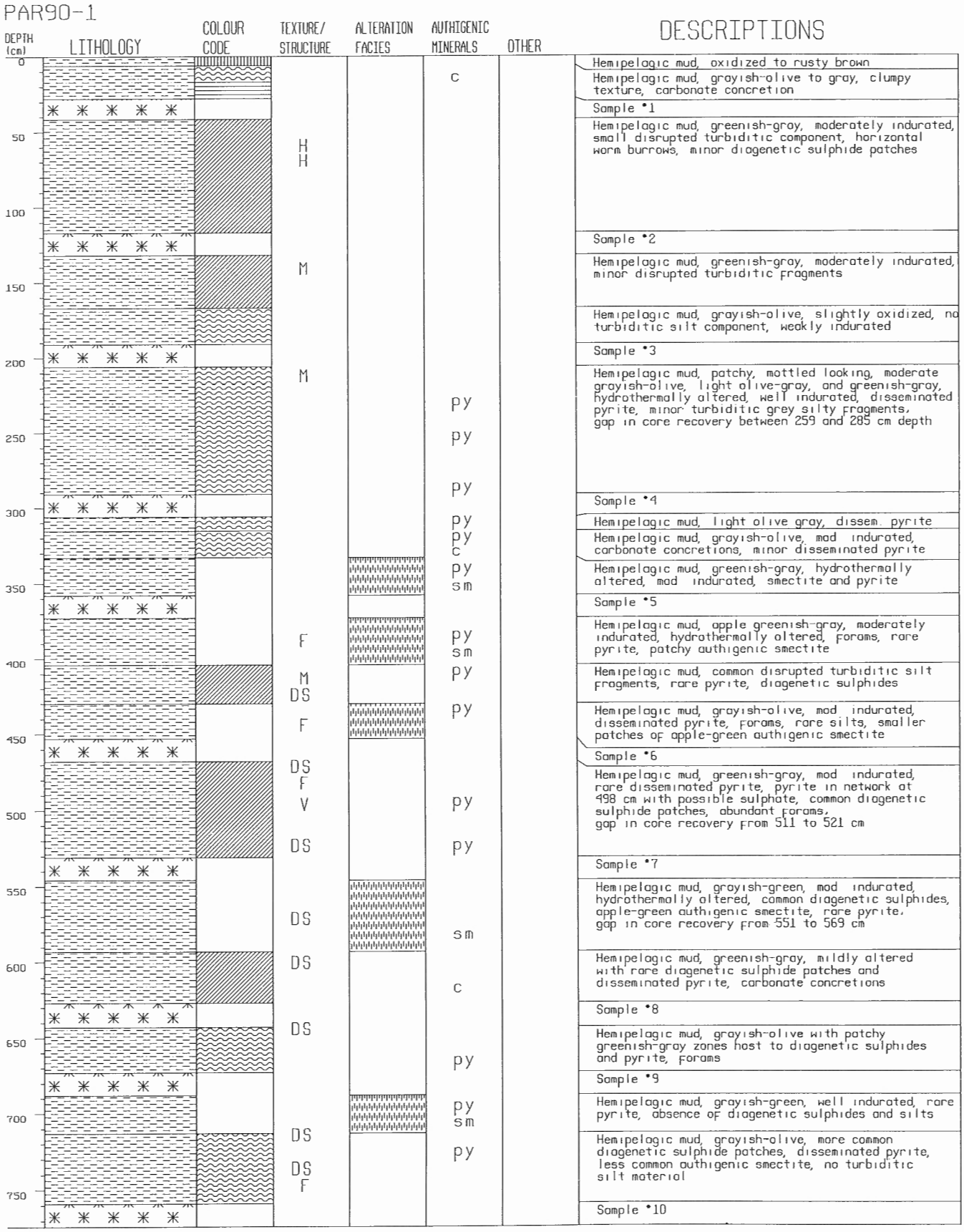

Figure 2. Graphic strip log of PAR90-1 showing sample locations with respect to unaltered and altered ocean floor sediments.

samples have not been investigated. Evidence of gas bubble eruption during decompression was observed for some of the samples, causing concern that flow channels having an increasing effect on K_s might develop. There were also sulphurous gas odours emitted from some of the core samples when they were disassembled. Gas bubbles reduce the water content and can impede the flow of water through sediments, therefore reducing K_s. However, there has been no evidence of these effects on our measurements.

DISCUSSIONS AND CONCLUSIONS

The porosity range of 72 to 80 per cent is surprisingly high. The porosity values are in the upper range of published data for unconsolidated clays (Freeze and Cherry, 1979, p.37). The permeabilities of 10^{-15} to 10^{-11} m^2 are also high, values similar to those of unconsolidated silt to silty sand (Freeze and Cherry, 1979, p.26), and the lower end of our permeability values resemble those of unweathered marine clays. The values for porosity, bulk density and permeability are plotted against depth in Figure 4.

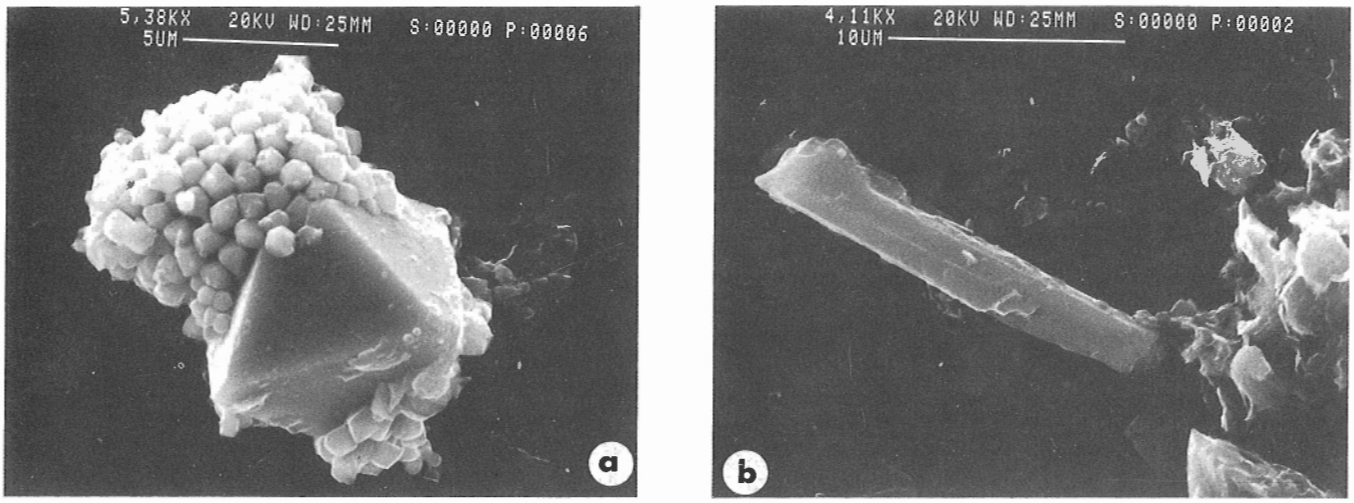

Figure 3. SEM photomicrographs of alteration minerals from processed bulk sediment samples. Operating conditions and scales are recorded on the upper margin of the photographs.

(**a**) Authigenic pyrite octahedron with smaller cubes of pyrite on its surface. The host sediment is from Core PAR90-1, Sample 02S, Section 04, 140-142 cm (4.98-5.00 m).

(**b**) Bladed smectite grain approximately 15 μm in length, a Ca-Fe-Mg silicate filling the pore space. The host sediment is from Core PAR90-1, sample 01S, Section 04, 64-68 cm (4.22-4.26 m).

Figure 2. Legend (opposite)

LEGEND

Sedimentary Units	Colour Code	Alteration
Hemipelagic mud	Brown	Apple-green
	Olive-gray	
Sample Location	Light-gray	
	Green-gray	

H = Horizontal worm burrow
M = Mottled
F = Forams
DS = Diagenetic Sulphides
V = Vein

c = carbonate concretion
py = cubic pyrite
sm = smectite

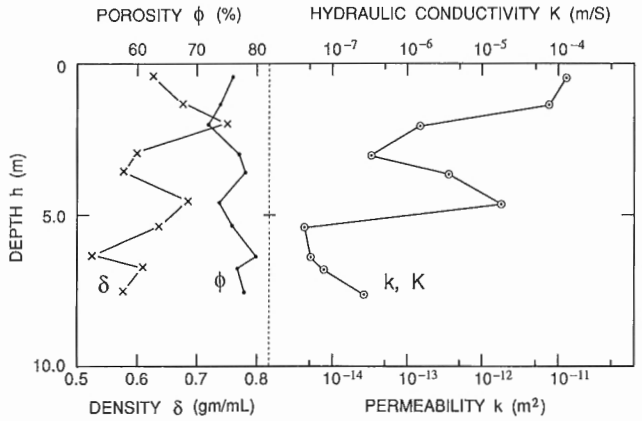

Figure 4. Permeability (k) or hydraulic conductivity (K_s), porosity (ϕ) and bulk density (δ) versus depth for the 10 ocean floor samples.

Table 1. Description of core samples from PAR90-1

Sample /Section		location (cm)	Depth Range (m)	Comments on Sediments
# 1	01	30- 45	0.30-0.45	greenish-grey MIH
# 2.	02	20- 35	1.19-1.34	greenish-grey MIH
# 3.	02	94-109	1.93-2.08	greyish-olive HM HT MIH mud, Dis-Py
# 4.	03	85-100	2.91-3.06	greenish-grey MIH Dis-Py
# 5.	04	0- 15	3.58-3.73	greenish-grey HT MIH, smectite,Dis-Py,Py-cubes
# 6.	04	95-110	4.53-4.68	greenish-grey HT MIH Dia-S, abundant Dis-Py, Py-cubes
# 7.	05	20- 35	5.31-5.46	greenish-grey HT MIH Dia-S, Dis-Py
# 8.	05	116-132	6.27-6.43	greyish-olive MIH smectite
# 9.	06	30- 45	6.73-6.88	greyish-green HT WIH greyish-olive HM
#10.	06	116-131	7.59-7.74	altered-HM, Dis-Py

MIH = moderately indurated hemipelagic mud
WIH = well indurated hemipelagic mud
HM = hemipelagic mud
HT = hydrothermally altered
Dis = disseminated
Py = pyrite
Dia = diagenetic
S = sulphide

The permeability (k) varies over three orders of magnitude, from just over 10^{-11} m^2 to under 10^{-14} m^2, within a depth range of 0 to 8 m from the ocean floor. This is a large variation. However, the porosity (-) is almost constant, showing a slight increase with depth over the same distance. This suggests that either the pore throats between the pore spaces decrease in size with depth, or the grain size of the matrix material decreases with depth.

Further analysis of the petrophysical (bulk density, volumetric water content, porosity, and permeability) and sedimetological data is being carried out in order to explain the reason for the large variation in permeability. The results to date indicate that filling of the pore throats by precipitation is likely the main cause of the permeability variation.

Table 2. Petrophysical properties (including porosity and permeability of sub-ocean floor samples

Sample Number	Depth Range (m)	δ (g/mL)	Θ_v	ϕ (%)	k* (m^2)	K_s (m/s)
1	0.30-0.45	0.626	0.510	76	1.1×10^{-11}	1.1×10^{-4}
2	1.19-1.34	0.675	0.488	74	7.2×10^{-12}	7.2×10^{-5}
3	1.93-2.08	0.750	0.517	72	1.5×10^{-13}	1.5×10^{-6}
4	2.91-3.06	0.600	0.490	77	3.1×10^{-14}	3.1×10^{-7}
5	3.58-3.73	0.577	0.513	78	3.3×10^{-13}	3.3×10^{-6}
6	4.52-4.67	0.685	0.412	74	1.8×10^{-12}	1.8×10^{-5}
7	5.31-5.46	0.640	0.449	76	4.3×10^{-15}	4.3×10^{-8}
8	6.27-6.42	0.527	0.555	80	5.5×10^{-15}	5.5×10^{-8}
9	6.73-6.88	0.611	0.514	77	8.0×10^{-15}	8.0×10^{-8}
10	7.59-7.74	0.580	0.528	78	2.8×10^{-14}	2.8×10^{-7}

δ = bulk density
Θ_v = volumetric water content
ϕ = porosity
k = permeability
K_s = hydraulic conductivity
* : 1 m^2 (permeability) = 10^7 m/s (hydraulic conductivity).

Sedimentological characteristics of the samples (Table 1) indicate that both hydrothermal precipitate (sulphide) and precipitates from seawater (Mg-smectite) are present. If the permeability values for the two samples which contain pyrite cubes (Table 1) in the depth range of 3.5-4.7 m are not considered, the permeability versus depth curve in Figure 1 can be interpreted to be showing a permeability decrease down to about 5 m followed by a permeability increase with depth. These decreasing and increasing trends with depth could be due to precipitation from heating of seawater at the top, and from cooling of hydrothermal fluids at the bottom end of the permeability curve. The conspicuous absence of grey, horizontal turbiditic silt laminae in PAR90-1 suggests that the primary sedimentary layering has been disrupted by precipitation of authigenic sulphides and smectite.

ACKNOWLEDGMENTS

The authors are grateful to W.D. Goodfellow (Geological Survey of Canada) for supervising the coring operation and for obtaining the samples. The authors acknowledge the assistance of L. Radburn (Geological Survey of Canada) for the SEM work. The authors are also grateful to G.C. Topp (Agriculture Canada) for providing the laboratory facilities and making it possible for these measurements to be made, and to K.A. Richardson (Geological Survey of Canada) for critically reviewing this paper.

REFERENCES

Davis, E.E., Goodfellow, W.D., Bornhold, B.D., Adshed, J., Blaise, B., Villinger, H., and Le Cheminant, B.
1987: Massive sulphides in a sediment rift valley, northern Juan de Fuca Ridge; Earth and Planetary Science Letters, v. 82, p. 49-61.

Elrick, D.E., Sheard, R.W., and Baumgartner, N.
1981: A simple procedure for determining the hydraulic conductivity and water retention of putting green soil mixtures; Proceedings, IV International Turfgrass Research Conference, Guelph, p. 189-200.

Franklin, J.M., Goodfellow, W.D., Blaise, B., Anglin, C.D., Harvey-Kelly, F.L., Macdonald, R., and Kappel, E.
1987: Geological map and distribution of sulfide deposits in Middle Valley, northern Juan de Fuca Ridge; EOS, v. 68, p. 1545.

Freeze, R.A. and Cherry, J.A.
1979: Groundwater; Prentice Hall, New Jersey, 604 p.

Goodfellow, W.D. and Blaise, B.
1988: Sulfide formation and hydrothermal alteration of hemipelagic sediment in Middle Valley, northern Juan de Fuca Ridge; Canadian Mineralogist, v. 26, p. 675-696.

Kappel, E.S. and Franklin, J.M.
1989: Relationships between geologic development of ridge crests and sulfide deposits in the Northeast Pacific ocean; Economic Geology, v. 84, p. 485-505.

Lydon, J.W., Goodfellow, W.D., and Franklin, J.M.
1990: Chemistry of sediment pore waters around active hydrothermal vents, Middle Valley poster; EOS, v. 71, no. 43, p. 1569.

Turner, R.J.W., Leitch, C.H.B., Ames, D.E., Höy, T., Franklin, J.M., and Goodfellow, W.D.
1991: Character of hydrothermal mounds and adjacent altered sediments, active hydrothermal areas, Middle Valley sediment rift, nothern Juan de Fuca Ridge: evidence from ALVIN push cores; in Current Research, Part E; Geological Survey of Canada, Paper 91-1E.

Sheldrick, B.N. (ed.)
1984: Analytical Methods Manual: Agriculture Canada, Land Resource Research Institute, Ottawa, Ontario.

Character of hydrothermal mounds and adjacent altered sediments, active hydrothermal areas, Middle Valley sedimented rift, northern Juan de Fuca Ridge, northeastern Pacific: evidence from ALVIN push cores

R.J.W. Turner[1], C.H.B. Leitch[1], D.E. Ames, T. Höy[2], J.M. Franklin, and W.D. Goodfellow
Mineral Resources Division

Turner, R.J.W., Leitch, C.H.B., Ames, D.E., Höy, T., Franklin, J.M., and Goodfellow W.D., 1991: Character of hydrothermal mounds and adjacent altered sediments, active hydrothermal areas, Middle Valley sedimented rift, northern Juan de Fuca Ridge, northeastern Pacific: evidence from ALVIN push cores; in Current Research, Part E; Geological Survey of Canada, Paper 91-1E, p. 99-108.

Abstract

The youngest sediments on hydrothermal mounds are altered fragments of presently active sulphide-poor anhydrite chimneys. Underlying sulphide-rich clastic layers indicate that higher temperature black smoker discharge (>300° C) occurred in the recent past. The predominance of clastic material suggests chimney collapse has an important role in mound formation. In situ growth of saponite, talc, chalcopyrite, isocubanite, sphalerite, and galena, and replacement of pyrrhotite by pyrite and marcasite indicate in situ alteration within the mound. Subhorizontal talc-saponite fractures suggest inflation as a process contributing to mound growth. Authigenic silicates are zoned from talc-saponite in mounds to illite-smectite in proximal sediments. Detrital chlorite, mica, and illite occur in distal sediments.

Résumé

Les sédiments les plus jeunes sur les buttes hydrothermales sont des fragments altérés de cheminées d'anhydrite pauvre en sulfure actuellement actives. Les couches détritiques sous-jacentes, riches en sulfure, indiquent qu'il y a eu dans le passé récent rejet de panaches noirs à température élevée (> 300 ° C). La dominance des matériaux détritiques indique que l'effondrement des cheminées a un rôle important à jouer dans la formation des buttes. La croissance sur place de saponite, de talc, de chalcopyrite, d'isocubanite, de sphalérite et de galène, et le remplacement de la pyrrhotite par la pyrite et la marcasite témoignent d'une altération sur place au sein de la butte. Des fractures subhorizontales de talc-saponite peuvent indiquer qu'une tumescence aurait contribué à la croissance de la butte. Les silicates authigéniques sont zonés, allant de talc-saponite dans les buttes à de l'illite-smectite dans les sédiments proximaux. La chlorite, le mica et l'illite détritiques se manifestent dans des sédiments distaux.

[1] Mineral Resources Division, 100 West Pender St., Vancouver, B.C.
[2] B.C. Ministry of Energy, Mines and Petroleum Resources, Geological Survey Branch, 756 Fort St., Victoria, B.C. V8V 1X4

INTRODUCTION

Middle Valley, only 300 km west of the continental margin of British Columbia and Washington, is a sediment-filled failed rift on the east flank of the Endeavour segment of the Juan de Fuca spreading ridge system (Davis et al., 1987; Fig. 1). In the area of present hydrothermal activity at water depths of about 2450 m, over 350 m of turbidite sediment has flooded the rift valley. At least two areas of hydrothermal activity are known in Middle Valley (Fig. 2). The largest is a flat, north-trending area 700 m by 250 m referred to as the "Area of Active Venting" (Goodfellow and Blaise, 1988) or "High Heat Flow area" (Franklin et al., 1991). Dives by the submersible ALVIN during the summer of 1990 discovered high temperature discharge (maximum 276° C) from chimneys on mound structures typically 25 m across and 7 m high (Franklin et al., 1991: Fig. 2 and 3). Primary inclusions in anhydrite (previously incorrectly identified as barite) from active chimneys have seawater salinity and a pressure-corrected trapping temperature of 265° C (Leitch, 1991). Barite from a hydrocarbon-bearing, clay-rich dormant chimney contain primary inclusions with homogenization temperatures (Th) of 170° C and hydrocarbon-bearing secondary inclusions with a Th of 110° C (Leitch, 1991).

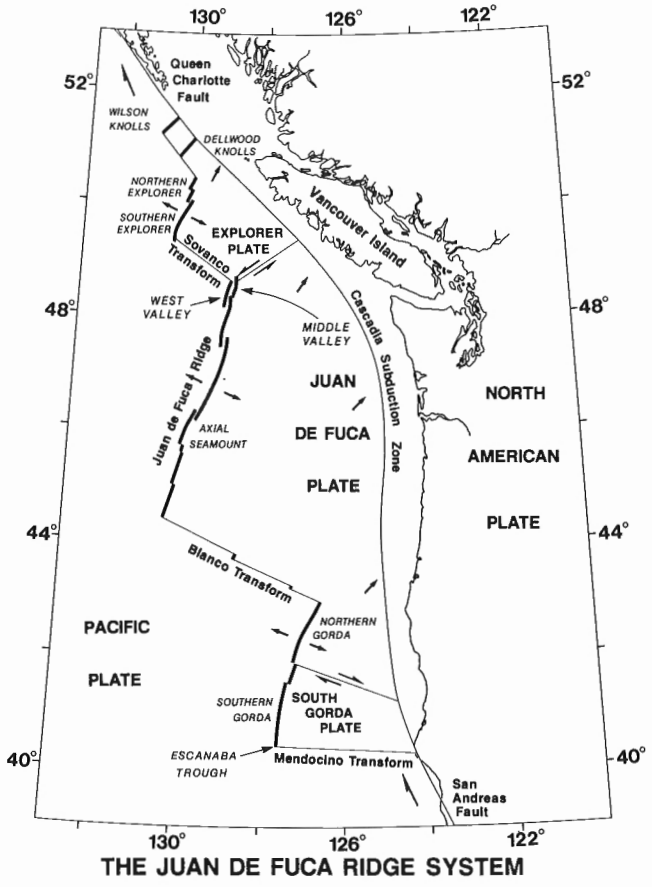

Figure 1. Map of the Juan de Fuca ocean ridge system showing the location of the Middle Valley hydrothermal area.

Two kilometres southeast of the Area of Active Venting is Bent Hill, a subcircular uplifted block of sediment approximately 400 m in diameter and 50 m high (Davis et al., 1987; Goodfellow and Blaise, 1988; Franklin et al., 1991; Fig. 2). Sulphide material is exposed over an area 200 m by 50 m along the southern flank of Bent Hill (Fig. 2; Franklin et al., 1991). A single mound with an active vent was discovered 400 m south of Bent Hill during the ALVIN dives (Franklin et al., 1991).

1990 Push core program

During investigations of the Middle Valley hydrothermal areas with the ALVIN submersible during August 1990 (Franklin et al., 1991), 10 push cores of shallow sediment on and near mound structures were collected (Fig. 3). Push cores can be inserted into unlithified or partially lithified sediment to a depth of 30 cm by the mechanical arm of the ALVIN. Specific seafloor features can be cored with this technique, making push core data a valuable complement to data from much longer piston cores (up to 12 m long).

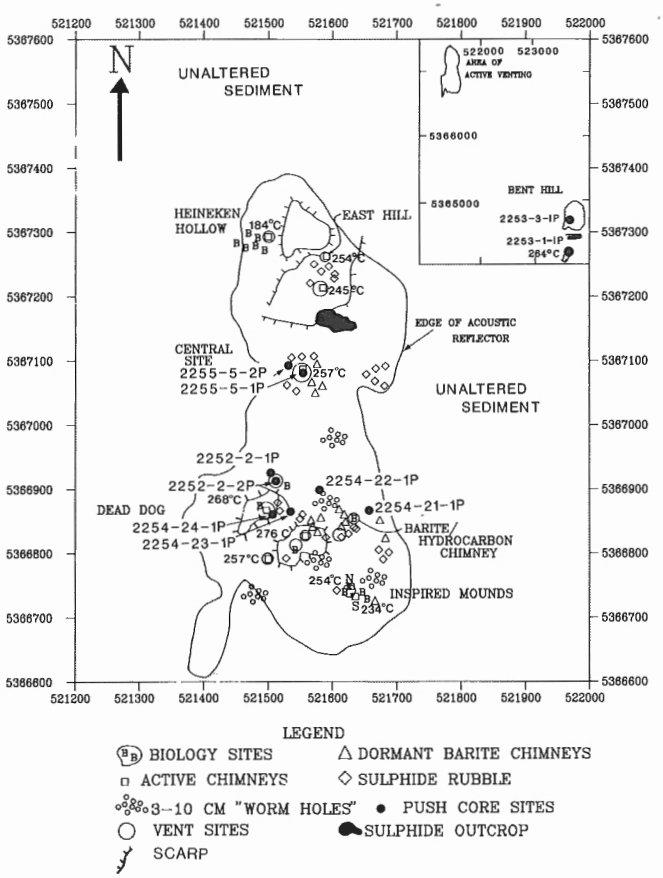

Figure 2. Preliminary map of the seafloor in the Area of Active Venting (Franklin et al., 1991).* Inset map shows location of Area of Active Venting with respect to the Bent Hill sediment uplift and nearby hydrothermal vent. The locations of push core samples are noted on the two maps.
* the acoustic reflector, not visibly distinguishable from the submersible represents indurated sediment.

Push cores described in this paper were collected on ALVIN dives 2252 to 2255 (Fig. 2). Observing scientists on these dives were: R. McDuff and E. Southward (2252); W. Goodfellow and R. Zierenberg (2253); P. Johnson (2254); and J.M. Franklin and B. Taylor (2255). Push core mineralogy is in Figure 4 and Table 1; textures are illustrated by photomicrographs (Fig. 5) and grain size distributions are in Figure 6.

HYDROTHERMAL MOUNDS

Core 2253-1-1

Core 2253-1-1P was collected from a clastic sediment-filled depression near an active vent on a small hydrothermal mound 400 m south of Bent Hill (Fig. 2). The clastic infilling is covered by a white anhydritic sediment as described below. The core is composed of 3 discrete layers (Fig. 3). The upper massive anhydrite layer is composed of fine grained (150-500 μ m) lath-like crystals of anhydrite and 1-2% pyrite grains (<500 μ m). Anhydrite is partially cemented by yellowish silica (?) creating 'pebble'-like forms. Pyrite content increases to 10% near the sharp contact with underlying massive sulphide. Flame structures of massive sulphide penetrate the overlying massive anhydrite. Sulphides are oxidized to Fe-oxides at this contact.

The black massive sulphide layer is composed of fine grained clay, pyrrhotite, pyrite, marcasite, chalcopyrite, and sphalerite. Pyrrhotite occurs as fragments of radiating crystals; pyrrhotite laths are partly replaced by pyrite and marcasite (Fig. 5A). The basal centimetre of this layer is coarser and contains 1-3% ?talc and saponite.

The lower dark grey sulphide-rich saponite-clay unit is composed of saponite (cf. Adshead, 1988), talc, mixed-layer clay with expandable component (illite-smectite), muscovite, clay, pyrite, pyrrhotite, marcasite and isocubanite. Sulphide increases from 20% near the top to 50% at depth. Pyrrhotite

Table 1. Summarized mineralogy of the push cores as estimated from X-ray diffraction and petrography

2255-5-1		2253-1-1		2254-24-1		2254-23-1		2255-5-2		2254-22-1		2254-21-1		2253-3-1	
XRD	PTS	XRD	PTS	XRD	PTS	XRD	PTS	XRD	PTS	XRD	PTS	XRD	PTS	XRD	PTS
0-9	2-5	5-9	3-5	1-11	0-16	0-5		0-5		0-5	1-5	0-6		0-8	
	gp 40		cl 40	cl	cl 70	cl		ch			ch 30	ch		ch	
	an 15		po 15	py	?an 15	ch		ms			ox 25	ms		ms	
	cl 15		py 15	po	fs 5	qz		cl			cl 10	cl		cl	
	cp 13		?an 10	fs	py 3	fs		ca			ms 10	qz		qz	
	sa 10		?sa 5	?ca	ox 2	ca		qz			or 10	fs		fs	
	py 5		mc 5		cp 2	5-10	6-10	fs			ca 5	am		am	
	sl 2		cp 5		or 2		*sm 45	5-12			qz 5	6-13		ca	
	gn <1		sl 5		sl 1		cl 20	ch			fs 5	ch		8-23	
	9-13	9-14		11-16			ox 18	ms			py <1	ms		ch	
	cl 60	sa		cl			fs 5	cl		5-8		cl		ms	
	sa 35	py		?ca			qz 5	qz		ch		qz		cl	
	ba 2	po					py 5	fs		cl		fs		qz	
	cp 2	cp					ca 2	12-13		qz		am		fs	
	sl 1	ta					sl <1	ch		ms		13-16		am	
	gn <1	cl				10-20		ms		fs		ch		ca	
		14-17				*sm		cl		8-13		ms			
		sa				ch		?*sm		ch		cl			
		cl				qz		qz		ms		qz			
		py				fs		fs		cl		fs			
		mc				20-23		13-30	23-26	qz		16-26	23-26		
		cp				cl			ch 25	fs			ch 15		
		po				ch			ms 15	am			ms 15		
		ta				qz			?*sm 10	13-18	14-19		ca 15		
		17-30	16-20			fs			cl 10		ms 30		cl 10		
			cl 35			sa			qz 13		ch 15		fs 10		
			ta 15						ox 8		cl 10		am 10		
			sa 15						am 7		qz 10		ox 10		
			py 10						fs 5		ca 10		qz 5		
			po 10						ca 5		or 10		py 5		
			cp 5						py 2		am 5		or 5		
			ox 5								fs 5				
			fs 5								ox 3				
			sl <1								py 2				
										18-23					
										ch					
										ms					
										cl					
										qz					
										fs					
										am					

Abbreviations: am=amphibole; an=anhydrite; ba=barite; ca=calcite; ch=chlorite; cl=clay; cp=chalcopyrite; fs=feldspar; gn=galena; gp=gypsum; mc=marcasite; ms=mica; or=organic; ox=Fe-Ti oxides, hydroxides; po=pyrrhotite; py=pyrite; qz=quartz; sa=saponite; sl=sphalerite; *sm=illite-smectite; ta=talc. Question marks indicate identification uncertain. Underlined numbers give depths in core (cm) for each sample, analysed by X-ray diffraction (XRD), which is qualitative, or petrography and X-ray diffraction (PTS), which is semi-quantitative (visually estimated modes).

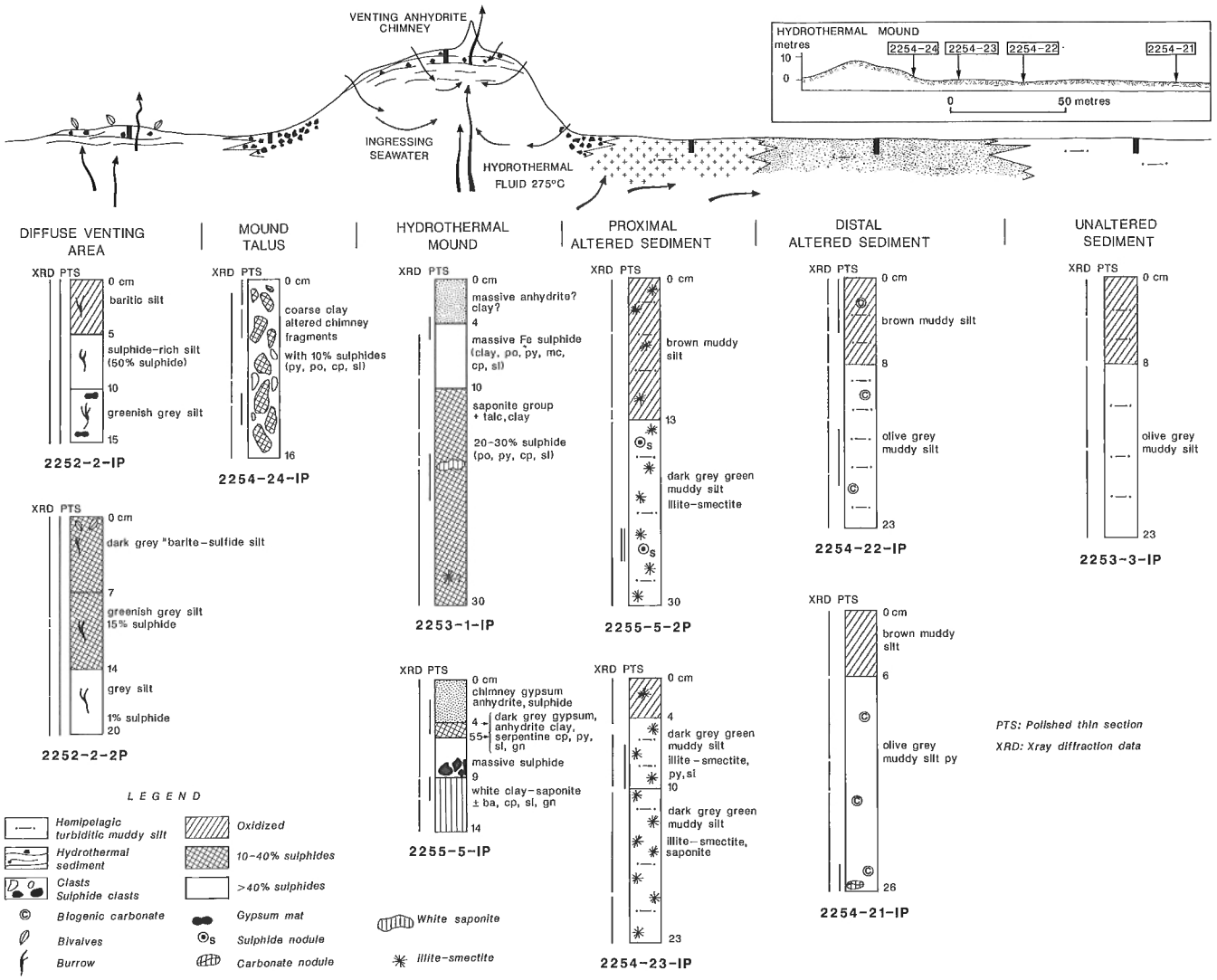

Figure 3. Graphic logs of push cores showing approximate position with respect to schematic profile of a hydrothermal mound and adjacent sediment. Based on core logging by Turner and Höy, petrographic study by Leitch, and XRD analysis by Ames. Inset: true-scale profile of Dead Dog mound and adjacent seabottom with push core sample sites noted. See Fig. 2 for location.

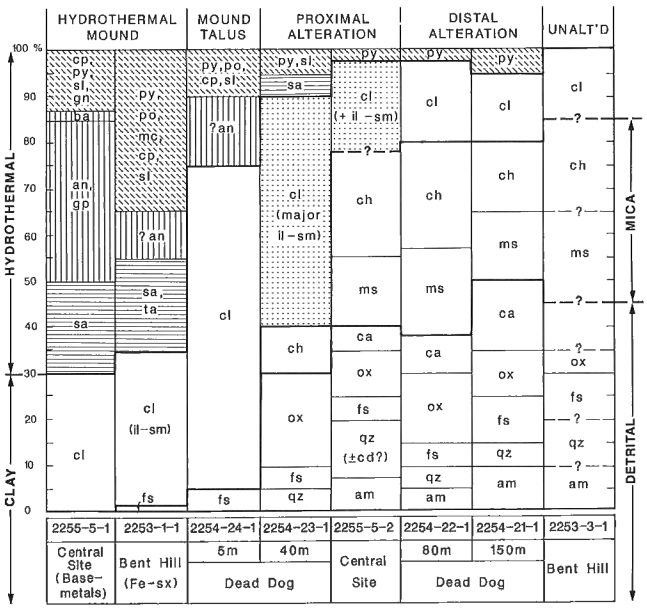

Figure 4. Average mineral abundance for each push core based on petrographic study by Leitch and X-ray diffraction determinations by Ames.

occurs as fragments of radiating crystals. Irregular grey patches of fine grained saponite and talc up to 1 cm across, and white nodules of very fine grained talc with minor disseminated pyrite grains (<50 μ m) occur within the sulphide-rich sediment.

Core 2255-5-1P

Core 2255-5-1P was taken adjacent to an active anhydrite chimney on the top of a mound at the Central site, Active Venting Area (Fig. 2). The core penetrated anhydrite chimney fragments that the ALVIN toppled onto a white sediment surrounding the chimney base. The core contains four beds (Fig. 3, 6). The upper fragmental bed of grey chimney material is a coarse sand of anhydrite crystals (up to 2 mm) with 2-3% pyrite and sphalerite grains (up to 0.5 mm). Anhydrite-sulphide fragments up to 10 mm across constitute 10% of the bed. Within the anhydrite sand are several disc-shaped mats (up to 4 cm) composed of interlocking 1-2 mm gypsum crystals.

The underlying unit is composed predominantly of gypsum (125-250 μ m) with lesser anhydrite laths, clay, chalcopyrite and saponite, and minor pyrite, sphalerite, and galena. Within the unit are clasts of a white talc/saponite. Chalcopyrite grains have rims of covellite suggesting seafloor oxidation. Both upper and lower contacts are gradational.

The brownish-black massive sulphide bed is composed of very fine grained (<50 μ m) sulphide, mostly pyrrhotite, pyrite, and (?)chalcopyrite that contains sulphide clasts to 1.5 cm diameter along the sharp basal contact. Clasts are composed of very fine grained black sulphide (≈ 40%) intergrown with grey 50-100 μ m anhydrite grains (Fig. 5B). Minor white grains (gypsum?) up to 200 μ m across increase to 2% near the top of the unit.

The milky white unit at the bottom of the core is composed of clay and saponite with minor barite crystals (200 μ m), chalcopyrite, sphalerite and galena (Fig. 5C). Sulphides are unusual in that the high proportion of base metal to iron sulphides is high and the grain size of sulphides is relatively coarse (up to 150 μ m?). Some composite sulphide grains appear to be fragments because clast margins truncate sulphide grain boundaries. Subhorizontal, locally bifurcating milky saponite(?) veins make up about 20% of this unit.

AREA OF DIFFUSE HYDROTHERMAL DISCHARGE

Core 2252-2-1

Two cores are from a 2 m by 4 m clam-rich area northeast of Dead Dog mound (Fig. 2). All sediment in the core is highly colonized by polychaete worms, is rich in organic matter, and the core releases a strong odour of H_2S. The 2252-2-1P core contains 3 distinct layers (Fig. 3, 6). The upper grey-brown bioclastic sandy silt contains fragments of creamy white barite and anhydrite(?) up to 250 μ m long (5%), coarser barite or anhydrite grains up to 2 mm (≈ 1%), and shell fragments including Cryptogena (≈ 3%). Siliceous casts of polychaete worm borrows (M. Black, pers. comm., 1990) up to 5 mm diameter are common, as they are throughout the core. Worm casts are encrusted with sulphides. Clasts or clots up to 250 μ m in diameter of very fine grained sulphide comprise 5% of the silty matrix.

The middle dark grey to black sulphidic sandy silt unit is composed of about 50% very fine grained sulphide (<50 μ m), 30% fine grey gypsum grains (50-100 μ m), and 5% coarser creamy barite grains (100-200 μ m). Large branching indurated worm tube casts up to 5 mm diameter are common. The upper unit may be the oxidized equivalent of this middle sulphide-rich silt. The contact between the two units is sharp but irregular.

A sharp but irregular colour break separates the lower unit of yellowish green anhydrite(?) silt (<50 μ m) from the overlying dark sulphide unit. Within this unit are minor dark grey clots up to 1 mm in diameter of very fine grained sulphide, and 20% branching subhorizontal "mats" of interlocking gypsum crystals up to 2mm long. Similar gypsum "mats" were noted in anhydrite chimney material composing the upper unit of core 2255-1-1P. Worm tube casts are common.

Core 2252-2-2P

The second core at the 2252-2 site was also characterized by a strong H_2S odour, sulphide-rich composition and abundant fauna. The upper 7 cm is a dark grey, organic-rich, pebbly sulphide-rich baritic material with 5-10% white granular barite clasts to 1 mm, 3-5% black sulphide grains to 250 μ m, and 5% cream barite grains to 100 μ m. Life forms include brown 5-7 mm methanotrophic(?) mussels (M. Black, pers. comm.) near the surface, abundant worm casts, minor siliceous microspheres, and black spines or crystals (to 500 μ m). Worm casts protruded above the sediment surface suggesting loss of the uppermost sediment layer.

Below a gradational contact is a greenish-grey pebbly unit (7-14 cm depth) with a distinctly paler colour, lower sulphide content (15%), and abundant disseminated cubic pyrite (to 50 μ m). This unit contains a 4 cm fragment containing 500 μ m anhydrite? crystals radiating from a central orifice, possibly a hydrothermal chimney. A lower silt unit contains 5-7% rounded white fine grained angular fragments up to 1 mm in diameter with disseminated sulphides that are similar in texture to samples collected from surface chimney structures. Several knobby calcite concretions, each a few centimetres in diameter, occur near the base of the core.

SEAFLOOR ADJACENT TO HYDROTHERMAL MOUNDS

Talus apron flanking mound

A coarse grained porous grey-green gravel composed of clay-altered fragments up to 5 cm across with only minor muddy sand matrix was collected at the base of Dead Dog mound in core 2254-24-1P (Fig. 2 and 3). Fragments include black-coated tube-shaped chimneys (up to 4 cm) composed of clay pseudomorphs of crystals radial about a central

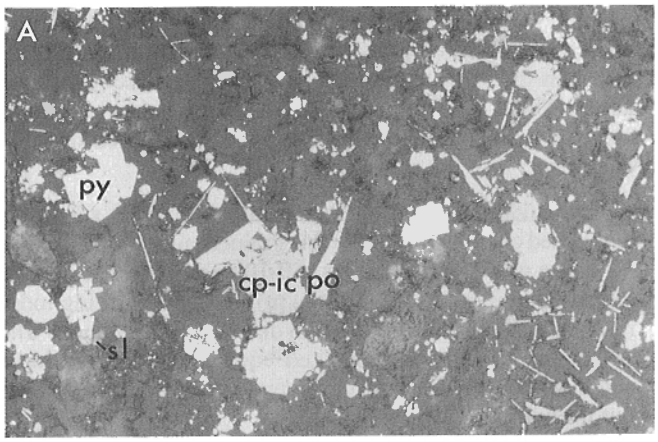
A
py
cp-ic
po
sl


E

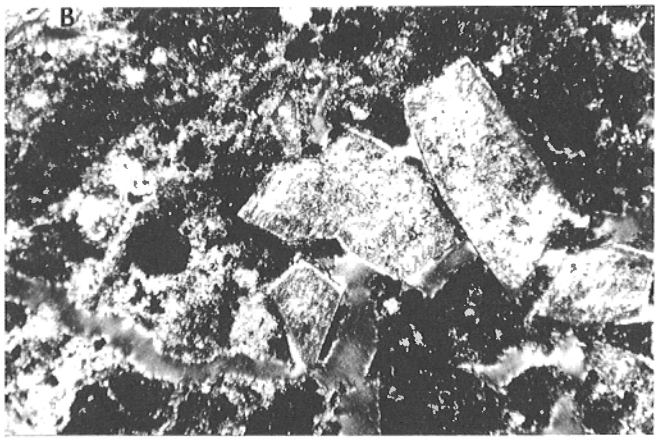
B

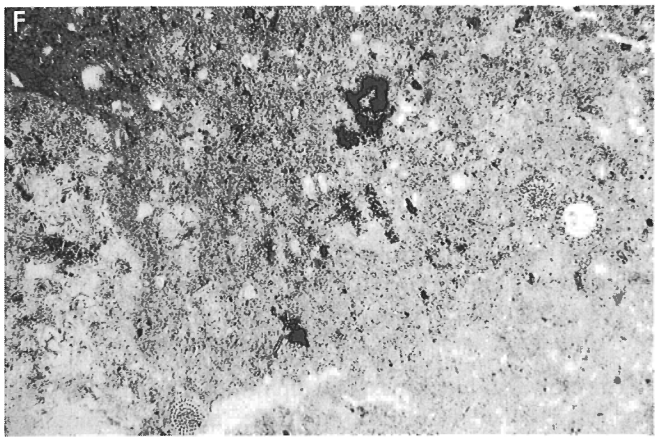
F

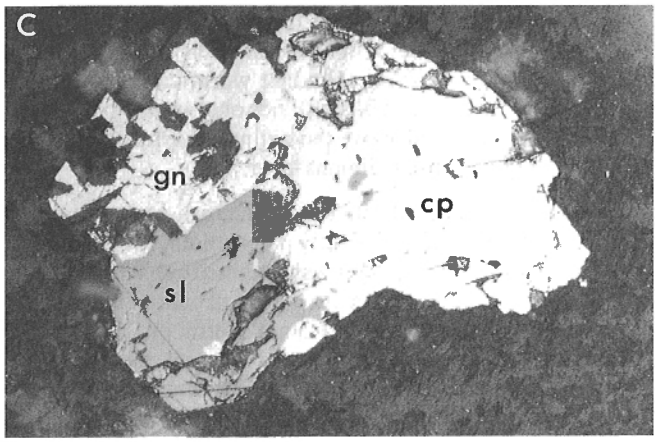
C
gn
cp
sl

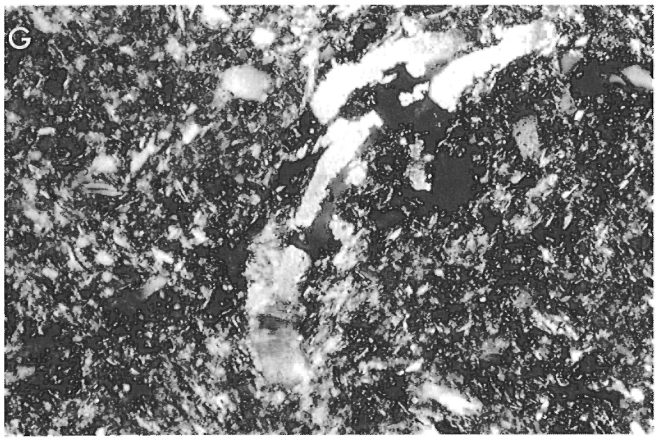
G

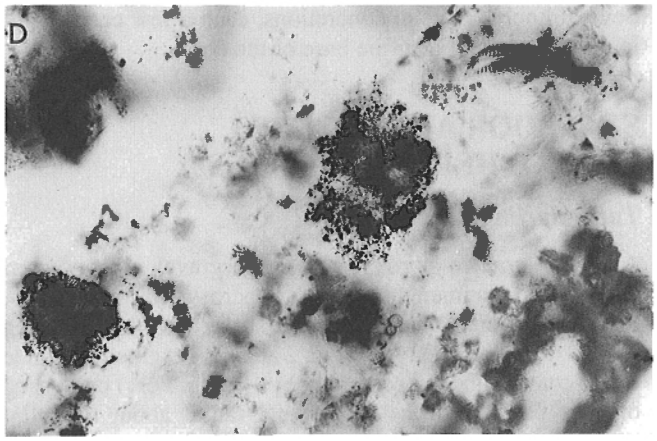
D

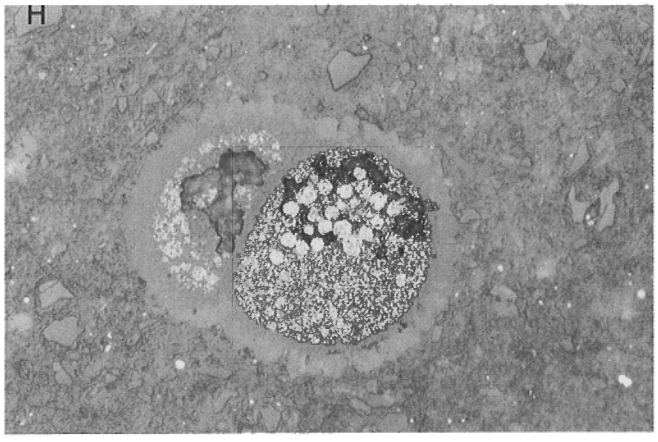
H

orifice, clay pseudomorphs of crystal aggregates, and sulphide-coated platelets (2-5 mm) of Mg-smectite (Fig. 5D). The coarse nature of fragments (Fig. 6), and hydrothermal composition of fragments, some of which are chimney-like, suggests a talus sediment derived from mound-top material.

Illite-smectite altered terrigenous and hemipelagic sediments adjacent to mounds

Core 2254-23-1

A 23 cm core was taken from a flat sediment surface near an inactive vent complex with barite chimneys, rubble, and dead tubeworms, 40 m from the summit of Dead Dog mound (Fig. 2, 3, 6). Several attempts to collect a push core were required due to the hard, indurated nature of much of the sediment. The uppermost 4 cm consists of grey-brown muddy silt with knobby nodules up to 3 cm along bedding of grey acicular calcite or anhydrite crystals (to 5 mm). The silt fraction is composed of quartz, feldspar, chlorite, and radiolaria. Below an irregular contact with the oxidized cap is a grey-green muddy siltstone consisting mainly of 10-15 μ m illite-smectite and illitic clay (locally with a fragmental collomorphic texture (Fig. 5E)), minor saponite, chlorite, and framboidal pyrite. Above 10 cm depth minor very fine black disseminated pyrite is present; below 10 cm are irregular black patches up to 2 cm in diameter of intermixed fine grained sulphide and saponite (Fig. 3).

Core 2255-5-2P

The 2255-5-2P core was taken near the base of the mound at the Central site (Fig. 2). It comprises a dark grey-green muddy silt with the upper 12 cm oxidized to a brown colour (Fig. 3, 6). The silt is composed of detrital quartz, plagioclase, dark green amphibole, chlorite, illite, biogenic carbonate, radiolaria, and diatoms (Fig. 5F). Elongate green illite-smectite grains (50-100 μ m) give the core a green colour. The core contains about 2% sulphide as disseminated pyrite framboids, and as pyrite and chalcopyrite within diffuse fine grained patches to 1 cm in diameter. Chalcopyrite is noted locally replacing microfossils. Chlorite, clay, and muscovite may be detrital or authigenic.

SEAFLOOR DISTAL TO MOUNDS

Weakly altered sediment

Core 2254-22-1P

This core was taken on a flat mud plain with no evidence of nearby chimney structures or sulphide rubble, 80 m from the summit of Dead Dog mound (Fig. 2). Here as well, several attempts to collect a push core were necessary due to the indurated nature of the sediment. The upper 8 cm of the core is an orange-brown oxidized zone with an irregular basal contact with olive-grey muddy siltstone (Fig. 3, 6). The siltstone is composed of chlorite, clay, and sericite, with scattered silt-size grains of foraminifera tests (Fig. 5G), quartz, feldspar and amphibole, and coarser lithic grains. Minor pyrite occurs as cubic grains and very fine clots (50-150 μ m). Lithic fragments up to 1.5 mm across of similar composition to the matrix suggest resedimentation of turbidite/hemipelagic sediment.

Core 2254-21-1P

Core 2254-21-1P was collected on a flat sediment plain 150 m east of the summit of Dead Dog Mound and just north of a north-trending cluster of dormant barite chimneys (Fig. 2). It is simiar to core 2254-22-1P, with 6 cm of brown oxidized silt overlying olive-grey muddy silt composed of chlorite, clay, and muscovite, with scattered silt-size grains of biogenic carbonate, quartz, plagioclase and amphibole. About 5% pyrite occurs as framboidal grains, locally within (?)foraminifera tests (Fig. 5H). This core is more indurated (breaks easily along fractures) than core 2254-22-1P. Hard, irregular-shaped nodules of very fine grained grey calcite are present near the base of the core.

"Unaltered" sediment

Core 2253-3-1P was taken to sample fauna growing on Bent Hill, several hundred metres north of the closest known sulphides. Below an upper reddish-brown oxidized layer 8 cm thick (Fig. 3, 6), massive olive-grey muddy silt is cohesive, plastic, and composed of chlorite, illitic clay and muscovite, with scattered silt-size grains of foraminifera, quartz, feldspar and amphibole, and 1-2% pyrite (Fig. 3). Two horizontal burrows approximately a centimetre in diameter, one open and the other sediment-filled, occur at depths of 10 and 22 cm.

Figure 5. (opposite) Microphotographs from push core samples. **A)** Bladed pyrrhotite (po), euhedral pyrite (py), rounded mass of chalcopyrite-isocubanite (cp-ic), rare sphalerite (sl) in matrix of clay and minor saponite (2253-1-1P, 4 cm; reflected plane polarized light, field of view 300 μ m). **B)** Euhedral pseudomorphs up to 2 mm long, possibly gypsum or bassanite after anhydrite, in sulphide-gypsum matrix (2255-5-1, 3 cm; transmitted light, crossed polars). **C)** Coarse chalcopyrite (cp), sphalerite (sl) and galena (gn) in 200 μ m (?)chimney fragment (2255-5-1P, 11 cm; reflected plane polarized light). **D)** Very fine (10-20 μ m) grains of pyrite and chalcopyrite rimming 0.5 mm diameter rosettes of clay mineral; note nearby diatom (2254-24-1, 5 cm; transmitted plane polarized light). **E)** Fine fragments of collomorphic (?)illite-smectite, clay and Fe-oxides/hydroxides (2254-23-1, 8 cm; transmitted plane polarized light, field of view 2.5 mm). **F)** Lithic fragments and microfossils (radiolaria, diatoms) in matrix of detrital chlorite, quartz, amphibole, feldspar, mica and clay. Minor ?illite-smectite reflects some hydrothermal alteration (2255-5-2, 25 cm; transmitted plane polarized light). **G)** Foraminifera fragments (to 100 μ m) in matrix of detrital chlorite, mica, clay, quartz, feldspar, amphibole (2254-22-1, 17 cm; transmitted light, crossed polars). **H)** Pyrite framboids within foraminifera test (150 μ m) contained in detrital matrix similar to photo G (2254-21-1, 24 cm; reflected plane light polarized light).

DISCUSSION

Chimney collapse as a process of mound growth

Discrete beds of hydrothermal fragmental material typifies material recovered from the top 30 cm of two hydrothermal mounds. The upper clay-rich and sulphide-rich units have sharp contacts and abundant fragments indicating a sedimentary origin. Such fragmental sediments may reflect mass flow deposition from the collapse of nearby chimneys, or the decomposition of fallen chimneys due to anhydrite dissolution resulting in a fragmental residue. The lack of oxidation of hydrothermal sediments suggests rapid sedimentation on the mounds.

Existing chimneys are dominantly anhydrite, but also contain clay, pyrite, pyrrhotite, barite, and sphalerite (Franklin et al., 1991). Anhydrite in inactive or collapsed chimneys dissolves rapidly (Johnson and Tunnicliffe, 1985); this may account for the minor anhydrite noted in the push core material. The upper clay-rich beds may have been derived from the collapse of clay-altered chimneys; a clay-altered chimney cut by anhydrite veins was recovered by one of the ALVIN dives from the Area of Active Venting.

Massive sulphide beds: evidence for recent higher temperature discharge

The massive sulphide beds cored on the two mounds are interpreted as sedimentary deposits because of the sharp contacts with overlying and underlying units, and the presence in one sulphide bed of large sulphide clasts near the base (2255-5-1P). The collapse of a sulphide-bearing anhydrite chimney followed by dissolution of the anhydrite could result in the residual sulphide-rich sediment. A sulphide-rich layer was tentatively correlated in two cores about 20 m apart in the diffuse venting area north of Dead Dog mound (2252-2-2P/1P). Sulphide-rich chimneys that might act as a source for such sulphide beds were not observed in 1990

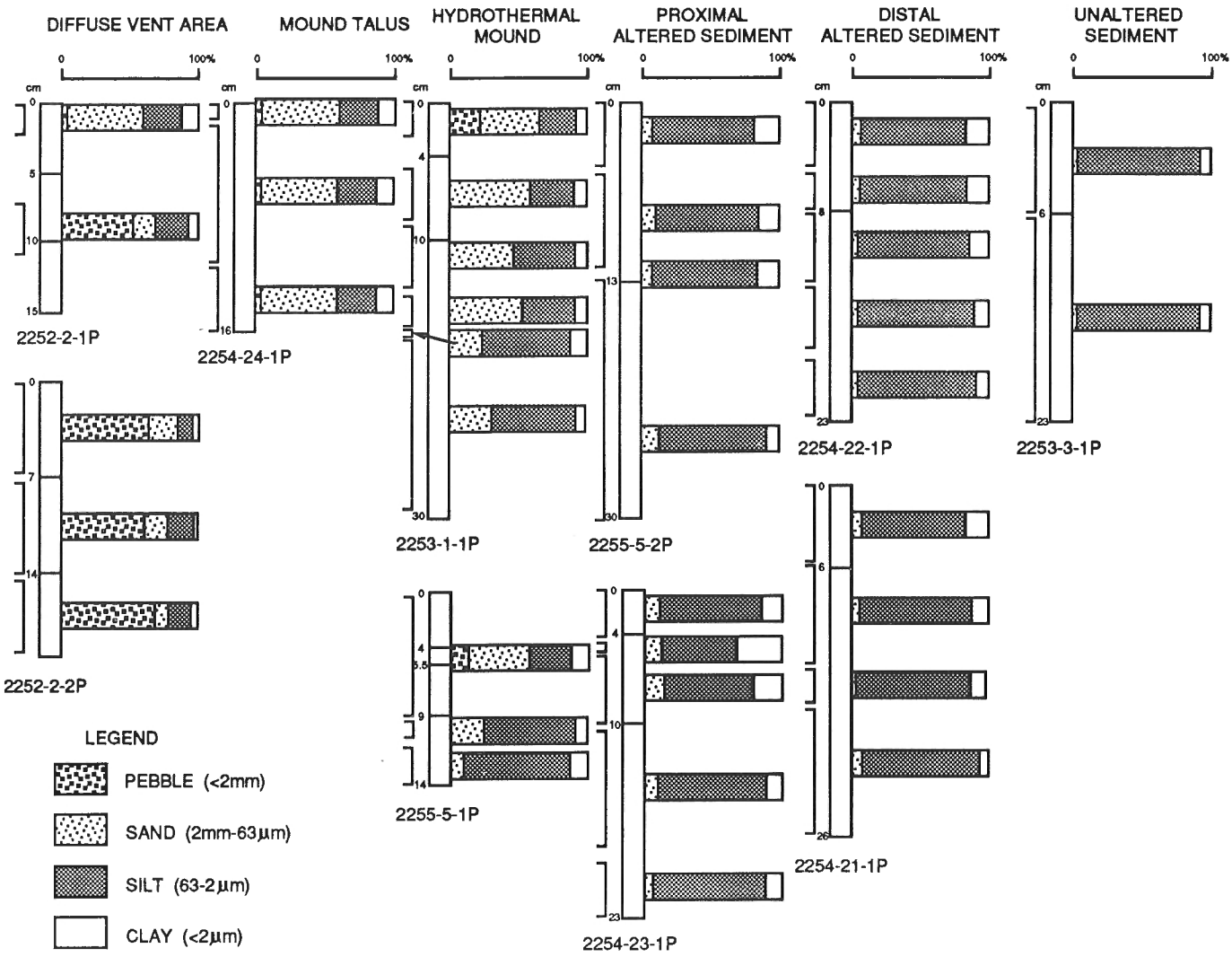

Figure 6. Variation in grain size within core samples; see Fig. 3 for relation to schematic profile of hydrothermal mound.

(Franklin et al., 1991) though a black smoker was noted in deep-towed camera work in 1987 and a chimney fragment with a high-temperature pyrrhotite-wurtzite-isocubanite assemblage was dredged from the area in 1986.

It is interesting to speculate on the significance of a widespread occurrence of an older sulphide-rich layer in both the Area of Active Venting and Bent Hill hydrothermal area. This sulphide layer suggests the current hydrothermal regime discharging 275° C, sulphide-deficient fluids was preceded by a period of sulphide-rich, black smoker chimneys likely related to higher-temperature (>300° C) discharge. Given the thin clay cover on this sulphide sediment, this high temperature discharge likely ceased very recently. This hypothesis suggests that temperature and volume of hydrothermal discharge throughout the Middle Valley hydrothermal field fluctuate over time. Such periodic or cyclical changes in seafloor hydrothermal systems was predicted by Cann et al. (1985) and corroborated by observation of a recent high volume of discharge or megaplume over Juan de Fuca Ridge (Baker et al., 1987).

Alteration and mineral growth within hydrothermal mounds

The abundance of nodules, concretions, clot-like mineral distribution, and veins indicate active alteration and mineral precipitation within the shallow hydrothermal sediments of the mounds. Gypsum "mats" within toppled chimney anhydrite (2255-5-1P) indicate gypsum growth within active chimneys. The diffuse patches, nodules, and subhorizontal veins of talc and saponite indicate in situ deposition and crystallization of Mg-silicates. Some pyrrhotite in the mounds occurs as fragments of radiating crystal aggregates possibly suggestive of derivation from chimney structures. Pyrrhotite is commonly pseudomorphed by pyrite and marcasite reflecting in situ sulphidation. Coarser grained chalcopyrite, sphalerite and galena occur within a large talc nodule (2255-5-1P), suggesting in situ precipitation of the base metal sulphides with talc. However, some of these base metals occur within polymineral clast-like aggregates that may be detrital fragments. Such in situ mineral growth is supported by evidence of elevated pore water temperatures within the hydrothermal mounds (P. Johnston, pers. comm., 1990).

Subhorizontal talc-filled fractures within the saponite-talc unit could suggest volume expansion and a mechanism of nodule growth or mound growth by inflation. Alternatively, these veins could represent shrinkage cracks related to the dehydration of the saponites.

The abundance of Mg-silicates within hydrothermal mounds is likely caused by heating of inflowing Mg-bearing seawater by conductive heating or mixing with hydrothermal fluids as suggested by Goodfellow and Blaise (1988). Seawater reflux appears limited to the mounds as Mg-silicates are absent in adjacent sediments.

Diffuse venting areas

The presence of fragments of barite, gypsum, and sulphide throughout core 2252-2-2P, including one large chimney-like fragment, suggests this core from the diffuse venting area is largely derived from collapsed chimney material. The sharp boundaries of units, defined by sharp changes in sulphide content, may reflect separate chimney collapse events. Sulphide-rich beds occur at the top of 2252-2-2P core (with evidence of some loss of the uppermost sediment) and at 5 cm depth in core 2252-2-1P. These sulphide-rich beds of the diffuse venting area may correlate with shallowly buried sulphide-rich beds within the hydrothermal mounds. In situ sulphide precipitation is also important as indicated by sulphide-encrusted worm tubes, local clot-like distribution of fine sulphides, and the H_2S-rich nature of pore fluids. The increase of coarser pyrite relative to fine grained sulphide with depth suggests recrystallization or replacement of pyrrhotite or biogenic material.

The high H_2S content of the pore fluids probably indicates diffuse upward flow of sulphide-rich hydrothermal fluids. The abundance of biological activity such as clams, mussels, and worms is clearly linked to these H_2S-rich hydrothermal fluids.

Zoned silicate-sulphide alteration associated with mounds

Cores of turbiditic/hemipelagic sediment up to 40 m distant from actively venting mounds (2254-23-1P, 2255-5-2P) are sulphide-rich and have a distinctive green colour due to an abundance of iron bearing illite-smectite. In situ growth of illite-smectite and sulphide is indicated by a radiating rosette habit and coarse grained nature of some smectite, and the patch-like distribution of much of the sulphide. The scarcity of illite-smectite in mound samples argues against dispersal by fallout from the hydrothermal plume. This iron metasomatism of sediments suggests alteration from rising and spreading Fe-bearing hydrothermal fluids, and is distinct from the Mg-metasomatism of mound material related to the ingress and heating of seawater. Authigenic silicates are zoned with respect to the hydrothermal mounds; Mg-silicates (talc, saponite) are abundant within mounds and minor in immediately adjacent sediments, whereas illite-smectites are abundant in proximal sediments but lacking in distal sediments.

Pyrrhotite, commonly replaced by pyrite and marcasite, occurs in the mounds and proximal sediments but is absent in distal sediments. Pyrite occurs in all environments including distal sediments though it is rare in "unaltered" sediment. Framboidal pyrite is limited to turbidite-hemipelagic sediment, and is absent within the hydrothermal mounds.

The 2253-3-1P core from Bent Hill does not lie within a high reflectivity area, lacks Fe smectite, carbonate nodules, and pyrite, and is less indurated than the distal altered sediments.

ACKNOWLEDGMENTS

We would like to thank Paul Johnson, Russ McDuff, Bruce Taylor, and Rob Zierenberg for many helpful discussions, for sharing their seabottom observations and for their involvement in the collection of the push cores. We thank E. Koopman and M. Tivey for assistance with navigation, the crew of the Atlantis II for their help and hospitality, and the ALVIN pilots for collection of the push cores. We thank Vee Ann Atnipp for instruction with the core squeezing apparatus, Mike Black for his help identifying the animal life, R. Delabio for assistance with XRD analyses, and Murray Journeay and Bev Vanlier for their critical reading of the manuscript.

REFERENCES

Adshead, J.D.
1988: Magnesium distribution and the nature of magnesian silicates in hydrothermally-altered Juan de Fuca sediments; EOS, Transactions of American Geophysical Union, v. 69, p. 266-267.

Baker, E.T., Massoth, G.J., and Feely, R.A.
1987: Cataclysmic hydrothermal venting on the Juan de Fuca Ridge; Nature, v. 329, p. 149-151.

Cann, J.R., Strens, M.R., and Rice, A.
1985: A simple magma-driven thermal balance model for the formation of volcanogenic massive sulphides; Earth Planetary Science Letters, v. 76, p. 123-134.

Davis, E.E., Goodfellow, W.D., Bornhold, B.D., Adshead, J., Blaise, B., Villinger, H., and Le Cheminant, G.
1987: Massive sulphides in a sedimented rift valley, Northern Juan de Fuca Ridge, Earth Planetary Science Letters, v. 82, p. 49-61.

Franklin, J.M., Goodfellow, W.D., Ames, D.E., Lydon, J.W., Jonasson, I.R., and Davis, E.E.
1991: Middle Valley, a major centre of hydrothermal activity in a sedimented ridge crest, northern Juan de Fuca Ridge; Program with Abstracts, Geological Survey of Canada, Current Activities Forum, Ottawa, p. 20.

Goodfellow, W.D. and Blaise, B.
1988: Sulphide formation and hydrothermal alteration of hemipelagic sediment in Middle Valley, northern Juan de Fuca Ridge; Canadian Mineralogist, v. 26, p. 675-696.

Johnson, H.P. and Tunnicliffe, V.
1985: Time-series measurements of hydrothermal activity on northern Juan de Fuca Ridge, Geophysical Research Letters, v. 12, p. 685-688.

Leitch, C.H.B.
1991: Preliminary studies of fluid inclusions in barite from the Middle Valley sulphide mounds, northern Juan de Fuca Ridge; in Current Research, Part A; Geological Survey of Canada, Paper 91-1A, p. 27-30.

Diatom assemblage analysis and sea level change, Serpentine River, British Columbia

Andrew J.M. Palmer[1] and John J. Clague
Terrain Sciences Division, Vancouver

Palmer, A.J.M. and Clague, J.J., 1991: Diatom assemblage analysis and sea level change, Serpentine River, British Columbia; in Current Research, Part E; Geological Survey of Canada, Paper 91-1E, p. 109-116.

Abstract

Late Holocene sediments in the Serpentine River area south of Vancouver have been studied to provide information on recent sea level change in south-coastal British Columbia. Fifteen sediment samples from a 1.8 m-deep backhoe trench on the Serpentine River flats were analyzed for diatoms. Of the 98 taxa recognized in the eight lowest samples, 95 were assigned taxonomic names. Statistical analysis of the diatom assemblages and assignment of taxa to various salt-sensitivity groups indicate that there was a relative rise in sea level in the lower part of the sequence, with a salinity maximum recorded at a depth of 105 cm (estimated age = 3500-4000 BP). The diatom assemblage at this level suggests that deposition occurred in a middle-to-upper intertidal marsh environment. This implies that the sea was near its present position (± 1 m) about 3500-4000 BP. Sea level changes since that time probably have been relatively minor (<1 m).

Résumé

Des sédiments de la fin de l'Holocène de la région de la rivière Serpentine au sud de Vancouver ont été étudiés dans le but de fournir de l'information sur les variations récentes du niveau de la mer le long du littoral méridional de la Colombie-Britannique. Le contenu en diatomées de quinze échantillons de sédiments prélevés dans une tranchée de 1,8 m creusée à la rétrocaveuse dans la plaine de la rivière Serpentine a été établi. Des 98 taxons répertoriés dans les huit échantillons inférieurs, 95 ont reçus des appellations taxonomique. L'analyse statistique des assemblages de diatomées et le rattachement de taxons à divers groupes selon leur sensibilité au sel indique une élévation relative du niveau de la mer dans la partie inférieure de la séquence, avec une salinité maximale enregistrée à une profondeur de 105 cm (âge estimé = de 3 500 à 4 000 ans BP). L'assemblage de diatomées à ce niveau révèle que la sédimentation s'est produite dans un milieu marécageux correspondant à une zone intertidale moyenne à supérieure. Cela suppose que le niveau de la mer était voisin de celui d'aujourd'hui (±1 m) il y a de 3 500 à 4 000 ans. Les variations du niveau de la mer depuis ce temps ont probablement été relativement négligeables (<1 m).

[1] 55 Robarts Crescent, Kanata, Ontario K2L 4A5

INTRODUCTION

As part of its program of geological studies aimed at determining the character and extent of Quaternary crustal movements in the Canadian Cordillera, the Geological Survey of Canada is studying the pattern and chronology of Holocene sea level change at several places on the British Columbia coast (Clague, 1989; Clague and Bobrowsky, 1990; Clague et al., 1991). This work may provide information on the frequency and magnitude of large earthquakes in this region during the Holocene.

The modern sea surface provides a datum for determining vertical crustal movements. Regional uplift and subsidence during large earthquakes cause sudden shifts in the level of the land relative to the sea. These shifts commonly are recorded by raised beaches and other littoral landforms in uplifted areas and by submerged marshes and soils in areas of subsidence. Former sea level positions are reconstructed through airphoto interpretation, stratigraphic and sedimentological logging of natural and artificial exposures and cores, paleoecological analysis, and radiocarbon dating of organic material contained within the sediments.

Plant and animal fossils are sensitive paleoenvironmental indicators, and changes in certain taxa within a sedimentary sequence may record past changes in sea level. In the sea level investigations that have been conducted to date in south-coastal British Columbia, a variety of types of fossils have been analyzed, including pollen, plant macrofossils, diatoms, foraminifera, and arcellaceans (Clague and Bobrowsky, 1990; Clague et al., 1991). Of these, diatoms are perhaps the most useful because many taxa have narrow salinity preferences (Kolbe, 1927; Simonsen, 1962; applied in Palmer and Abbott, 1986), and their value in studies of this sort has already been demonstrated in other areas, for example Atlantic Canada (Palmer, 1974, 1978).

In this paper, we report on diatoms recovered from a sequence of mud and peat exposed in a backhoe trench near Serpentine River, 30 km southeast of Vancouver (Fig. 1). We attempt to demonstrate the value and power of diatom analysis in sea level studies, and also present an objective statistical methodology for assessing paleoenvironmental change from fossil data.

STUDY AREA AND SITE STRATIGRAPHY

The study site is located on a low-elevation plain, bordered on the south, north, and east by Pleistocene uplands and on the west by Mud Bay, part of the Strait of Georgia. The plain itself is underlain by thick marine sediments which commonly are capped by thin peat. Until recently, this low area was an embayment of the Strait of Georgia (Clague et al., 1983); much of it is still below high tide level and has been dyked to prevent flooding by the sea and Serpentine and Nicomekl rivers.

Samples were collected from the wall of a backhoe trench located approximately 200 m east of Serpentine River and 4 km east of Mud Bay (49°05.5'N, 122°48.1'W). The surface elevation at this site is +0.9 m (Geodetic Datum). The following

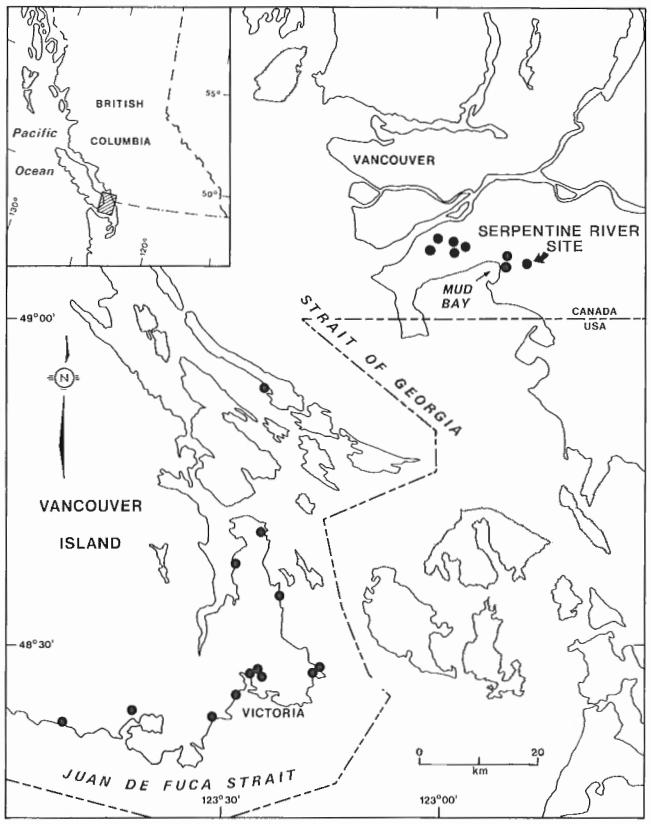

Figure 1. Location map showing the Serpentine River study site and other similar sites in southwestern British Columbia that have been investigated since 1988 for their record of Holocene sea level change.

stratigraphy (Fig. 2), from top to bottom, was recorded in the trench beneath 30 cm of surface fill (top of fill = 0 cm): peat (30-61 cm); muddy peat (61-63 cm); peat (63-76 cm); peat and muddy peat (76-111 cm); peaty mud with laminae and thin lenses of mud which increase in abundance downward (111-136 cm); sandy mud (136-141 cm); sandy silt (141-141.5 cm); and sandy mud and mud (141.5-178 cm). Fifteen samples were collected for diatom analysis (Fig. 2). In addition, a piece of wood at 30 cm and samples of peat at 61-63 cm and 114-119 cm (datum = top of fill) were collected and submitted to Saskatchewan Research Council for radiocarbon dating.

METHODS

Each diatom sample was gently dispersed in dilute hydrogen peroxide (3%) and passed through window-screen fabric (1.25 mm mesh) to remove coarse organic matter. Floating organic debris and sub-micron mineral grains were removed by a procedure involving, successively, resuspension in bottled spring water (pH 6.5-7.0), timed settling (for >1 micron separations), and supernatant removal with an aspirator siphon (3 mm tubing) (Fenner, 1984). This cyclical washing was continued until the supernatant appeared clear and colourless against window light. Diatomaceous residues were mounted in Hyrax on coverslips for microscopic examination

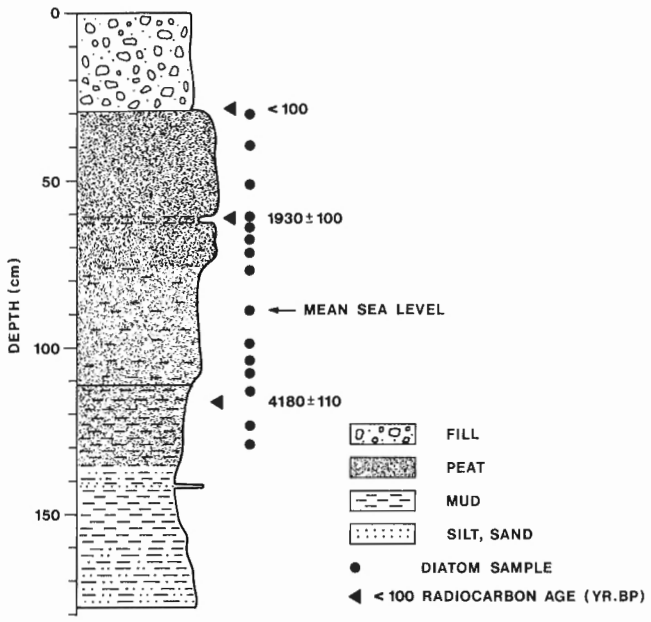

Figure 2. Stratigraphy of sediments exposed in the Serpentine River backhoe trench. Radiocarbon age determinations and diatom samples are also shown. Mean and large tidal ranges in this area are 3.3 m and 4.9 m, respectively.

(1000X oil, Nomarski) and photomicrography. A photographic atlas was prepared of most of the taxa with Polaroid film, and names were provisionally assigned to these taxa before counting began (taxonomic references: Hustedt, 1930-1966; van der Werff and Huls, 1957-1974; Hendey, 1964; Patrick and Reimer, 1966-1975).

Approximately 300 specimens were counted in each sample. After final identifications and data tabulation and analysis, the actual numbers ranged from 260 to 360.

To facilitate the interpretation of variations in abundances of specific taxa, the raw counts were converted to percentages. Probable error ranges (in per cent, at 95% confidence level) then were computed to provide a measure of the reliability of the data (see Fig. 3 for examples). These values were calculated using the equation $PE_{95} = 1.96[P(100-P)/N]^{0.5}$ (Galehouse, 1971), where PE_{95} is the probable error in per cent, P is the percentage of a species, and N is the total number of specimens counted.

In order to evaluate changes in the composition of diatom assemblages through time, all assemblages were analyzed for statistical correlations in pair-wise fashion. Missing taxa in sample pairs (i.e., those that were not recorded) were omitted from the analyses rather than being recorded as zero values. Spearman Rank Correlation coefficients (SRC) and related parameters were computed from the raw data and presented in tabular form. The results for each sample pair are: SRC; the 'z' value derived from the normal curve; the 'p', or probability, value; and 'n', the number of taxa appearing in common in a sample pair.

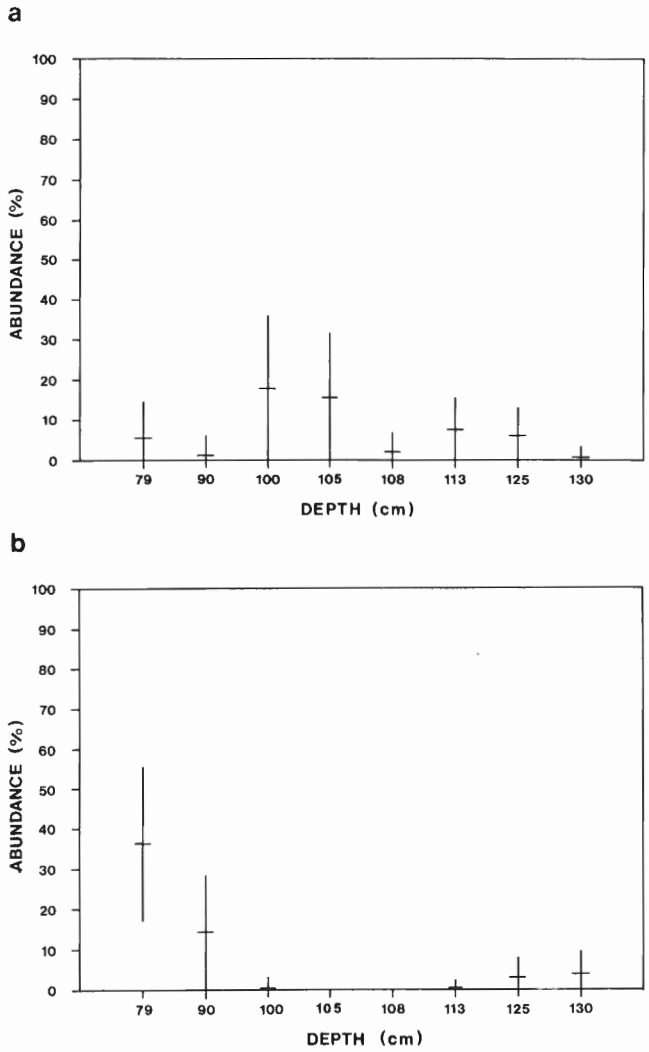

Figure 3. Variations in abundance of (**a**) *Diploneis smithii* (de Brébisson *ex* Wm. Smith) Cleve v. *smithii* (marine diatom) and (**b**) *Fragilaria construens* v. *venter* (Ehrenberg) Grunow (freshwater diatom) with depth in the Serpentine River trench. Vertical bars indicate probable error ranges at 95% confidence level (Galehouse, 1971).

Lastly, as an aid to paleoenvironmental interpretation, the diatom taxa were assigned to four salt-sensitivity groups in the Halobian Spectrum (Kolbe, 1927; Hustedt, 1957; Simonsen, 1962; Schrader and Schuette, 1981). For simplicity, these groups are referred to here as freshwater, fresh-brackish, brackish, and marine. Unidentified specimens and taxa of poorly known habitat preference were placed in a separate category ('unassigned'); these do not exceed 6% of the total specimens in any sample. The taxonomic and halobian assignments are considered to be relatively firm, although some minor revisions may yet be made. The possibility of taxonomic uncertainty is greatest for very rare specimens.

Table 1. Spearman Rank Correlation matrix, Serpentine River diatom assemblages

	Sample							
	79 cm	90 cm	100 cm	105 cm	108 cm	113 cm	125 cm	130 cm
79 cm								
SRC	1.0000	0.4053	0.2068	0.6648	0.4091	-0.2061	0.5583	-0.3714
Z	4.8990	1.7194	0.6540	2.3031	1.2937	0.6182	1.5792	0.8305
p	0.0002	0.0815	0.5203	0.0200	0.1926	0.5437	0.1101	0.4113
n	25	19	11	13	11	10	9	6
90 cm								
SRC		1.0000	0.3848	0.2969	0.1488	-0.3095	0.8375	0.2000
Z		4.6904	1.1545	0.8909	0.3937	0.8189	2.3688	0.4000
p		0.0003	0.2466	0.3766	0.6953	0.4181	0.0169	0.6910
n		23	10	10	8	8	9	5
100 cm								
SRC			1.0000	0.7409	0.6731	0.6042	0.4750	-0.0066
Z			4.0000	2.3429	2.3316	1.7088	1.3435	0.1732
p			0.0002	0.0180	0.0186	0.0834	0.1756	0.8388
n			17	11	13	9	9	8
105 cm								
SRC				1.0000	0.5755	0.2750	0.2091	-0.2767
Z				4.2426	1.9938	0.8696	0.6273	0.6779
p				0.0010	0.0433	0.3886	0.5377	0.5050
n				19	13	11	10	7
108 cm								
SRC					1.0000	-0.0079	0.2517	0.2527
Z					5.0990	0.2973	0.9073	0.9454
p					0.0001	0.7596	0.3674	0.3467
n					27	15	14	15
113 cm								
SRC						1.0000	0.4963	0.1667
Z						6.2350	2.3802	0.7046
p						0.0000	0.0164	0.4882
n						40	24	20
125 cm								
SRC							1.0000	0.6344
Z							6.7082	3.3567
p							0.0006	0.0011
n							46	29
130 cm								
SRC								1.0000
Z								6.7082
p								0.0006
n								46

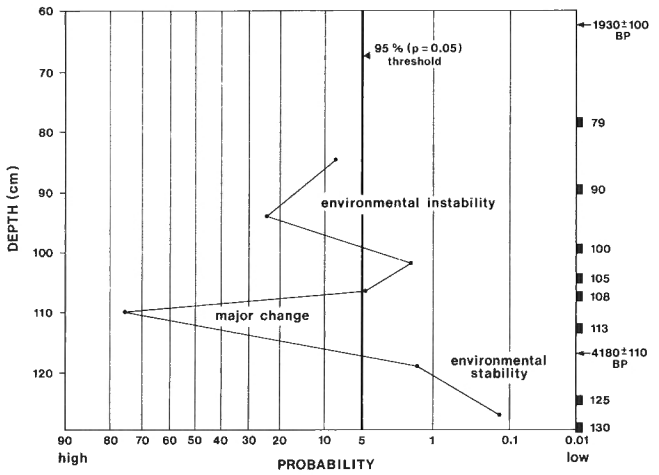

Figure 4. Probability of mutual independence, or 'no correlation', between samples evaluated in pairs up the Serpentine River section. Low probabilities indicate that samples are closely related, and high probabilities indicate that they are different. A major environmental change, indicated by a significant change in diatom assemblages, occurs between 113 and 108 cm.

RESULTS

Peat samples at 114-119 cm and 61-63 cm depth gave ages of 4180 ± 110 BP and 1930 ± 100 BP, respectively (S-3186 and S-3185). A piece of wood at the top of the peat sequence (30 cm depth) yielded a radiocarbon age of <100 BP (S-3184).

Of the 15 samples prepared for analysis, only the lowermost eight (79-130 cm depth) contained diatoms. Ninety-eight diatom taxa were recognized during counting, 95 of which were given taxonomic assignments (see Appendix for a list of taxa which have overall abundances of 2% or more).

Diatoms are generally well preserved in the lowest samples, whereas those in the middle samples (especially 108 cm and 105 cm) are severely fragmented. This fragmentation coincides with an observed increase in silt content in the samples, and may have been caused by physical abrasion during or after deposition. Preservation improves in the uppermost diatom-bearing samples (90 cm and 79 cm).

The two lowest samples (130 cm and 125 cm) each have diverse assemblages comprising 46 diatom taxa. There is a general decline in diversity above 125 cm, with a minimum at 100 cm (17 taxa). Approximately 25 taxa are present in samples between 100 and 79 cm.

Rank-correlation analyses on assemblages from adjacent samples illustrate the changing relationships up the section (Table 1, Fig. 4). To evaluate the significance of the calculated Spearman Rank Correlation coefficients, we look to see if 'z' is less or greater than 1.96 and if 'p' is less or greater than 0.05 (corresponding to the 95% confidence threshold; these values can be approximated by computing the comparable t-distribution values when the number of pairs exceeds 10; Edwards, 1967). If the statistics suggest that the Null Hypothesis of mutual independence (or 'no correlation') be rejected, then the assemblage pair is accepted as being correlated (i.e., the result cannot be attributed to chance alone).

The results of the pair-wise analysis of diatom assemblages is summarized as follows:

1) The lowest sample pair (130/125 cm) has the largest number of taxa in common (n = 29). The Spearman Rank Correlation coefficient is 0.63, quite high considering the large number of taxa that were considered. The z value of 3.36 greatly exceeds the normal curve value of 1.96 for the 95% level of confidence, and the Null Hypothesis of no correlation thus is rejected. Indeed, the p value of 0.001 indicates an exceptionally strong rank-correlation.

2) The next sample pair (125/113 cm), with 24 taxa in common, also has a high rank-correlation (SRC = 0.50, z = 2.38, p = 0.02). Again, the critical value of z = 1.96 is exceeded and p is less than 0.05; the Null Hypothesis is rejected and the pair is accepted as being correlated.

3) A marked departure is evident in the third sample pair (113/108 cm). It has the lowest SRC (-0.01) and z (0.30) in the sequence, suggesting that the two samples cannot be correlated. The p value is 0.76, thus the Null Hypothesis is not rejected. The samples have 15 taxa in common, but the proportions are very different. The discord is caused by changes in the assemblage composition at 108 cm.

4) The fourth sample pair (108/105 cm), with 13 common taxa, yielded SRC = 0.58, z = 1.99, and p = 0.04. The Null Hypothesis is rejected, and a close relationship is inferred.

5) The fifth sample pair (105/100 cm) also has relatively few common taxa (11), but the highest SRC of the sequence (0.74). The z value of 2.34 exceeds the critical 1.96 value and p = 0.018. Again, the Null Hypothesis is rejected, and a close relationship is inferred.

6) The sixth sample pair (100/90 cm; n = 10) records a second discordance, with SRC = 0.38, z = 1.15, and p = 0.25. The Null Hypothesis is not rejected, thus it is concluded that the two samples are very different, i.e., there is a significant change in the diatom assemblage at 90 cm.

The final sample pair (90/79 cm; n = 19) yielded SRC = 0.41, z = 1.72, and p = 0.08. Again, the Null Hypothesis is not rejected, and it is concluded that there is a substantial difference between the two samples.

In summary, the lower samples are highly rank-correlated, the middle samples also are highly correlated but have a different character from those below them, and the upper samples are not well rank-correlated because of compositional differences.

Sample differences are also indicated by the relative proportions of freshwater versus brackish and marine taxa (Table 2). Saline (brackish + marine) forms constitute 68% of the total in the basal sample, decline to 55% at 113 cm, and peak at 95% at 105 cm. This peak is followed by a decline to 47% in the uppermost diatom-bearing samples. The best indicators of the maximum saltwater influence at 105 cm are *Navicula peregrina* (Ehrenberg) Kützing v. *peregrina* and v.

Table 2. Salinity distribution of diatoms (%)

Category	Sample							
	79 cm	90 cm	100 cm	105 cm	108 cm	113 cm	125 cm	130 cm
Fresh	46.4	18.3	5.6	2.6	3.1	26.3	24.4	15.4
Fresh-brackish	1.9	4.4	0.0	1.0	10.7	16.0	9.2	12.1
Brackish	24.2	18.3	37.7	63.3	75.2	38.6	41.2	51.1
Marine	22.8	54.3	53.0	31.2	6.9	16.0	19.1	16.4
Unassigned	4.7	4.7	3.7	1.9	4.1	3.1	6.1	5.0
Brackish + marine	47.0	72.6	90.7	94.5	82.1	54.6	60.3	67.5

minor Kolbe, *Stauroneis amphioxys* Gregory v. *obtusa* Hendey, *Diploneis smithii* (de Brébisson *ex* Wm. Smith) Cleve v. *smithii*, and *Fragilaria oceanica* Cleve (Appendix).

INTERPRETATION

Our interpretations are based collectively on stratigraphic relationships, diatom assemblage composition and preservation, statistical correlations, proportions of halobian categories in the samples, and miscellaneous laboratory observations. We recognize that diatomaceous reference material from modern environments would have been useful in calibrating the fossil assemblages and improving interpretations.

The three lowest samples (130, 125, and 113 cm) record a progressive decline in brackish diatom taxa. Successive pairs (130/125 cm and 125/113 cm) are highly correlated statistically, suggesting that this change occurred gradually through time. The mix of freshwater, brackish, and marine taxa is indicative of an uppermost intertidal marsh, influenced to some extent by river discharge. Comparable modern environments are 1-3 m higher in elevation, thus shorelines were lower during the period encompassed by this part of the sequence (ca. 4500-4000 BP) than they are today.

The sample at 108 cm (interpolated age = 3800 BP) differs markedly in composition from that at 113 cm; this is indicated by an abrupt increase in saline (= brackish + marine) diatoms from 55% to 82%. The assemblage at 108 cm is thought to record a middle-to-upper intertidal marsh environment, with sea level near its present position (± 1 m).

Saline diatoms continue to increase upward to 105 cm (95% brackish + marine taxa). We attribute this increase to a comparatively rapid marine transgression. The change from a relatively low salinity assemblage (55% saline diatoms) to the most saline assemblage in the sequence (95% saline diatoms) occurs within a vertical distance of 8 cm, estimated to represent about 300 years.

The decline in saline diatoms above 105 cm indicates a decrease in salinity through time. This could be due to a marine regression, to sediment accretion, or to geomorphic changes at or near the site.

The muddy peat layer at 61-63 cm (1930 ± 100 BP) records an influx of silt and clay, probably the result of either local river flooding or sea level rise. A choice between these two possibilities cannot be made at this time because diatoms were not found in this bed, or for that matter in any sample above 79 cm. Evidence for a minor transgression about 2000 BP has been found, however, at other sites in this region (Clague, 1989).

The sea level changes recorded in the Serpentine River sediment sequence, although small in magnitude (<1 m), appear to have been relatively sudden and may provide evidence for crustal subsidence during moderate to large earthquakes. Other explanations, however, are possible, and additional evidence is required to demonstrate a link between local sea level change and seismicity.

These paleoenvironmental interpretations are consistent with interpretations that have been made from Holocene sediments at nearby Burns Bog on the Fraser River delta (Clague et al., 1991) and at sites on southern Vancouver Island near Victoria (Clague, 1989; Clague and Bobrowksy, 1990). At all of these sites, there is evidence for lower sea levels and one or more transgressions during the late Holocene.

REFERENCES

Clague, J.J.
1989: Late Quaternary sea level change and crustal deformation, southwestern British Columbia; in Current Research, Part E, Geological Survey of Canada, Paper 89-1E, p. 233-236.

Clague, J.J. and Bobrowsky, P.T.
1990: Holocene sea level change and crustal deformation, southwestern British Columbia; in Current Research, Part E, Geological Survey of Canada, Paper 90-1E, p. 245-250.

Clague, J.J., Luternauer, J.L., and Hebda, R.J.
1983: Sedimentary environments and postglacial history of the Fraser Delta and lower Fraser Valley, British Columbia; Canadian Journal of Earth Sciences, v. 20, p. 1314-1326.

Clague, J.J., Lichti-Federovich, S., Guilbault, J.-P., and Mathewes, R.W.
1991: Holocene sea level change, south-coastal British Columbia; in Current Research, Part A, Geological Survey of Canada, Paper 91-1A, p. 15-21.
Edwards, A.L.
1967: Statistic methods; Holt, Rinehart and Winston, New York, 462 p.
Fenner, J.
1984: Middle Eocene to Oligocene planktonic diatom stratigraphy from deep sea drilling sites in the South Atlantic, Equatorial Pacific, and Indian Oceans; Initial Reports of the Deep Sea Drilling Project, v. 75, p. 1245-1271.
Galehouse, J.S.
1971: Point counting; in Procedures in Sedimentary Petrology, (ed.) R.E. Carver; Wiley-Interscience, New York, p. 385-407.
Hendey, N.E.
1964: An introductory account of the small algae of British coastal waters, Part V, Bacillariophyceae; Her Majesty's Stationery Office, London, 317 p.
Hustedt, F.
1930-1966: Die Kieselalgen Deutschland, Österreichs und der Schweiz; Akademische Gesellschaft, Leipzig, v. I (1930), 920 p., v. II (1957), 845 p., v III (1961-1966), 816 p.
1957: Die Diatomeen Flora des Fluss-Systems der Weser im Gebiet der Hansestadt Bremen; Abhandlungen Naturwissenschafflichen Verein, Bremen, v. 34, p. 181-440.
1985: The pennate diatoms [translation of Hustedt's "Die Kieselalgen, 2. Teil", with supplement by N.G. Jensen]; Koeltz Scientific Books, Koenigstein.
Kolbe, R.W.
1927: Zur Ökologie, Morphologie, und Systematik der Brackwasser-Diatommen. Die Kieselalgen des Sperenberger Saltzgebeits; Pflanzenforschung, v. 7, p. 1-146.
Palmer, A.J.M.
1974: Diatom stratigraphy and post-glacial history of Basin Head Harbour, Prince Edward Island; MSc thesis, Dalhousie University, Halifax, Nova Scotia, 143 p.
1978: Diatom stratigraphy of Basin Head Harbour, Prince Edward Island; Proceedings, Nova Scotian Institute of Science, v. 28, p. 201-215.
Palmer, A.J.M. and Abbott, W.H.
1986: Diatoms as indicators of sea-level change; in Sea-Level Research: A Manual for the Collection and Evaluation of Data, (ed.) O. van de Plassche; Geo Books, Norwich, p. 457-487.
Patrick, R. and Reimer, C.W.
1966-1975: The diatoms of the United States; Monographs of the Academy of Natural Sciences of Philadelphia, v. I (1966), 688 p., v. II (1975), 213 p.
Schrader, H.-J. and Schuette, G.
1981: Marine diatoms; in The Sea, Volume 7, The Oceanic Lithosphere, (ed.) C. Emiliani; John Wiley & Sons, New York, p. 1179-1232.
Simonsen, R.
1962: Untersuchungen zur Systematik und Ökologie der Bodendiatomeen dur westlichen Ostee; Internationale Revue der Gesamten Hydrobiologie, Systematische Beihefte I, 143 p.
van der Werff, A. and Huls, H.
1957-1974: Diatomeenflora van Nederland; Abcoude, Den Haag.

Appendix 1. Diatom taxa in the Serpentine River sequence with overall relative frequencies of at least 2%

Taxon	Salinity category[1]	Overall %[2]	79 cm	90 cm	100 cm	105 cm	108 cm	113 cm	125 cm	130 cm
Fragilaria construens v. *venter* (Ehrenberg) Grunow[3]	F	8.1	36.3	14.2	0.3	0.0	0.0	0.3	3.1	3.9
Pinnularia borealis Ehrenberg v. *brevicostata* Hustedt[4]	F	2.3	0.0	0.0	1.2	0.0	0.6	6.8	5.7	5.4
Navicula cincta (Ehrenberg) Van Heurck[5]	F-B	2.7	0.3	0.0	0.0	0.3	3.5	4.8	6.1	8.2
Navicula elegans Wm. Smith[5]	B	6.3	4.7	0.0	4.7	15.6	23.0	0.7	0.0	0.0
Navicula mutica Kützing v. *cohnii* (Hilse) Grunow[6]	B	3.3	0.0	0.0	0.0	0.0	0.3	5.8	4.2	18.2
Navicula peregrina (Ehrenberg) Kützing v. *peregrina*[3]	B	8.5	13.5	3.8	6.9	9.4	13.8	5.1	7.3	6.8
Navicula peregrina (Ehrenberg) Kützing v. *minor* Kolbe[6]	B	9.0	1.4	0.9	14.0	29.5	14.5	4.8	1.1	4.6
Navicula pygmaea Kützing[7]	B	2.4	0.0	0.0	5.6	0.0	6.6	2.7	3.1	1.1
Stauroneis amphioxys Gregory v. *obtusa* Hendey[5]	B	5.7	2.5	2.5	6.2	7.1	16.0	4.8	3.4	2.1
Diploneis smithii (de Brébisson *ex* Wm. Smith) Cleve v. *smithii*[8]	M	7.1	5.5	1.3	17.8	15.6	1.9	7.5	6.1	0.7
Fragilaria oceanica Cleve[7]	M	11.3	5.8	38.8	32.4	7.5	1.6	0.0	0.0	0.0
Not assigned[8]		4.2	4.7	4.7	3.7	1.9	4.1	3.1	6.1	5.0

[1]F = freshwater; B = brackish; M = marine.
[2]This value equals the total number of specimens of the given diatom taxon divided by the total number of specimens of all taxa.
[3]Taxonomic source: Patrick and Reimer (1966-1975).
[4]Taxonomic source: Hustedt-Jensen (1985).
[5]Taxonomic source: Hendey (1964).
[6]Taxonomic source: van der Werff and Huls (1957-1974).
[7]Taxonomic source: Hustedt (1930-1966).
[8]Includes the sum of three taxa that have not yet been identified and specimens that are truly unidentifiable (dirty, broken, tilted, or lacking diagnostic features).

Upper Nanaimo Group and younger strata, outer Gulf Islands, southwestern British Columbia

T.D.J. England[1,2] and R.N. Hiscott[2]
Cordilleran Division, Vancouver

England, T.D.J. and Hiscott, R.N., 1991: Upper Nanaimo Group and younger strata, outer Gulf Islands, southwestern British Columbia; in Current Research, Part E; Geological Survey of Canada, Paper 91-1E, p. 117-125.

Abstract

In the outer Gulf Islands, the upper Nanaimo Group comprises up to 2600 m of upper Campanian to Maastrichtian marine sandstone, conglomerate and shale. The complex geometry and lithofacies distribution of these deposits reflect sedimentation in an outer neritic to mid-bathyal, sand-rich turbidite system. Many sandstone and conglomerate bodies are lenticular, with erosional basal contacts; one deposit occupies a scour about 550 m deep and 7 km wide. The major coarse grained units are interpreted to have been deposited in channels carrying density currents principally to the west and northwest. The fine grained units are interpreted as interchannel levee deposits. The Nanaimo Group is overlain by about 400 m of sandstone and pebble conglomerate, interpreted as fluvial deposits. The contact is probably an unconformity, traceable for over 40 km at the base of a prominent submarine ridge and which cuts out about 1850 m of upper Nanaimo Group in the area.

Résumé

Dans les îles Gulf tournées vers le large, le groupe supérieur de Nanaimo comprend jusqu'à 2 600 m de grès, de conglomérat et de shale marins couvrant l'intervalle s'étendant du Campanien supérieur au Maastrichtien. La géométrie et la distribution de lithofaciès complexes de ces dépôts tiennent à une sédimentation dans un système extérieur de turbidites riches en sable correspondant à un milieu néritique à médio-bathyal. Plusieurs masses de grès et de conglomérat sont lenticulaires, et présentent des contacts basaux d'érosion; un dépôt occupe un affouillement d'environ 550 m de profond et de 7 km de large. Les grandes unités à grain grossier auraient été mises en place dans des chenaux de courants de densité se dirigeant principalement vers l'ouest et le nord-ouest. Les unités à grain fin seraient des dépôts de levée qui se seraient accumulés entre les chenaux. Le Groupe de Nanaimo est recouvert d'environ 400 m de grès et de conglomérat à galets qui seraient des dépôts fluviatiles. Le contact est probablement une discordance, retraçable sur plus de 40 km à la base d'une dorsale sous-marine proéminente, qui retranche environ 1 850 m du groupe supérieur de Nanaimo dans la région.

[1] BP Exploration Inc., 5151 San Felipe, P.O. Box 4587, Houston, Texas, 77210 U.S.A.
[2] Department of Earth Sciences, Memorial University of Newfoundland, St. John's, Newfoundland A1B 3X7

INTRODUCTION

The Upper Cretaceous Nanaimo Group is widely exposed in the Gulf Islands and on eastern Vancouver Island (Fig. 1) along the exhumed western margin of Georgia Basin. Ancestral Georgia Basin was a major forearc basin situated between Vancouver Island and the mainland of British Columbia, comparable in many respects to the Great Valley of California (England, 1990; Ingersoll, 1978; Dickinson, 1976). During the Paleogene, the focus of sedimentation in Georgia Basin shifted from linear subbasins adjacent to eastern Vancouver Island to depocentres in the southeast (Fig. 1). The Tertiary deposits overlap or unconformably overlie the Nanaimo Group.

The upper part of the Nanaimo Group was mapped in detail in the summer of 1990 in the southern Gulf Islands (Fig. 2) where there are extensive coastal exposures. In the field area, both onland topography and submarine bathymetry accurately reflect the bedrock geology: resistant sandstone and conglomerate bodies form mappable hills, headlands, and offshore ridges, and fine grained units form prominent valleys, coves, and submarine depressions (Fig. 3). The 1:50 000 scale map (NTS 92B/14) of England (1990) and the bathymetric charts of the surrounding waterways, on which resistant bedrock ridges can be traced, and faults can be recognized by ridge offset, were used as base maps.

In this report we briefly describe the structure and stratigraphic succession in the field area, and then discuss the origin of the succession and some regional aspects of its development in this part of Georgia Basin. Field localities (Fig. 3) are referred to by superscripted numbers.

STRUCTURE

The succession of strata in the field area is well exposed as the northeastern limb of a major anticline, the axis of which runs along the southwestern side of Trincomali Channel, through Navy Channel, and across the central part of Saturna Island (Fig. 3). The strata are interrupted by generally north-trending high-angle faults with minor offset, and the larger Active fault that cuts across the eastern end of Galiano Island, offsetting both onshore and offshore ridges[91]. Except for the

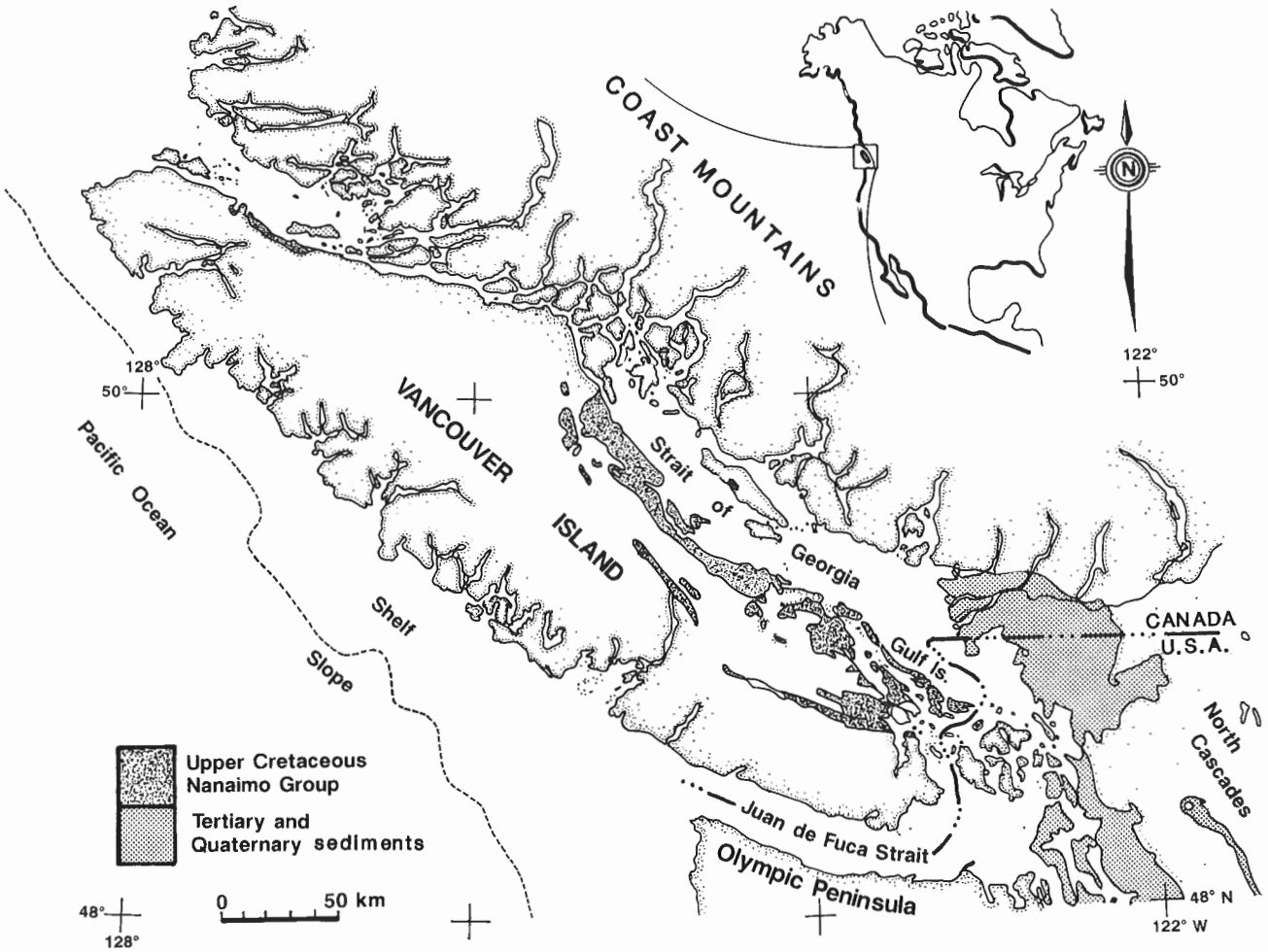

Figure 1. Outcrop areas of Upper Cretaceous Nanaimo Group and Tertiary strata of Georgia Basin. The area of study is in the Gulf Islands.

large syncline on southern Saturna Island, the remainder of the folds in the field area are minor. The trace of a major normal fault interpreted from seismic data (Machacek, 1971, as cited by England, 1990) is shown in the Strait of Georgia. To the southwest of the field area, a series of thrust faults emerge, such as the inferred Ganges-Pender thrust which cuts across North Pender Island. These thrusts are interpreted to have caused the folding observed in the field area (England, 1990), and are part of the Eocene Cowichan fold and thrust system (England and Calon, 1991). The strata in the field area lie in the highest and least-deformed thrust sheet of this system.

STRATIGRAPHY

Nanaimo Group

The upper Nanaimo Group comprises up to 2600 m of sandstone, conglomerate, and shale in the field area, assigned to the Northumberland, Galiano, Mayne, and Gabriola formations (Fig. 3). At map scale, many of the sandstone and conglomerate bodies are lenticular with basal contacts that erode variably into underlying strata. For example, the conglomerate unit that outcrops on Mt. Galiano[26] (Galiano Island) and Mt. Parke[37] (Mayne Island), has an erosional base which cuts through two shale units, one sandstone unit, and into the top of the sandstone unit that underlies Parker Island[5]; the total stratigraphic thickness removed by erosion is about 350 m. The conglomerate pinches out completely into shales near Montague Harbour[10], and is laterally replaced by sandstone on eastern Mayne Island. Elsewhere, map relationships suggest about 550 m of erosion beneath the sandstone and conglomerate sequence that extends from Edith Point[47] (Mayne Island) to the north side of Georgeson Bay[25] (Galiano Island), removing one shale unit, one sandstone unit, and the top of a second shale unit that to the east underlies Miners Bay[39] (Mayne Island).

At individual outcrops, the bases of coarse grained units are abrupt and locally erosional (Fig. 4A). Scours a few metres to over 10 m deep are locally present. Deep scours can be seen on the cliff face below Mt. Parke[37]. Typical facies include poorly sorted, disorganized pebble and cobble conglomerates; graded or graded-stratified pebble conglomerates and pebbly sandstones; medium to very thick, graded beds of coarse- to medium-grained sandstone with some examples containing large rip-up clasts (Fig. 4B), fluid-escape pillars, dish structures, local parallel lamination and rare cross-stratification. Paleocurrents from rare sole markings, pebble imbrication, and plentiful ripple lamination generally indicate flow toward the west or northwest. Some sections contain little or no mudrock, whereas others have horizons as thick as about 10 m of thinly bedded shales and fine- to very fine-grained graded sandstone beds. The finer-grained horizons and associated coarser-grained sandstone beds are locally rich in trace fossils, pelecypods, ammonites, and gastropods (Table 1). Foraminifers occur in many of the associated fine grained beds indicating marine paleodepths of 100-600 m (Table 1; B.E.B. Cameron, pers. comm., 1988).

Figure 2. Oblique aerial photograph of the field area, looking northwest, with northwestern Saturna Island in the foreground, Mayne Island in the middle, Galiano Island in the distance, and the Strait of Georgia on the right.

Fine grained units are poorly exposed inland, but commonly outcrop beneath beach deposits in the wave-swept coastal areas. In the Mayne Island area, a lower shaly unit, the Northumberland Formation, outcrops at Village Bay[32], where it is about 200 m thick. An upper shaly unit, the Mayne Formation, is exposed in Miners Bay[39] and in the vicinity of Bennett Bay[50], where it is 255-330 m thick.

The Northumberland Formation consists of grey silty shales interbedded with thin- to medium-graded beds of very fine grained sandstone and siltstone (Fig. 5A). Sideritic and calcitic concretions are common. The sandstones and siltstones are structureless or parallel laminated, and their upper surfaces are commonly marked by burrows and grazing trails (Table 1). Large fragmented shells of pelecypods and ammonites, as well as coalified plant litter, are locally present. The shales contain abundant and diverse foraminifers indicating marine paleodepths of 150-1200 m (Table 1; B.E.B. Cameron, pers. comm., 1988).

The Mayne Formation in Miners Bay[39] and Bennett Bay[50] consists mainly of grey silty shales and very thin- to medium-graded interbeds of fine grained sandstone and siltstone that contain T_{bcd} or T_{cd} Bouma sequences and burrowed tops (Fig. 5B-G). Organic remains include coalified vegetation, pelecypods, brachiopods, and ammonites. The shales contain abundant and diverse foraminifers indicating marine paleodepths of 200-600 m (Table 1; B.E.B. Cameron, pers. comm., 1988). Paleocurrent data from ripple-lamination in thin-bedded turbidites define a bimodal distribution to the east and northwest.

The upper contact of the Mayne Formation is erosional beneath sandstones and local conglomerates of the Galiano Formation on Galiano and Mayne islands. Extrapolation of strike lines across Active Pass indicates that a significant part of the top of the upper shale unit must be eroded beneath the conglomerate and sandstone of the Galiano Formation at Bluffs Park[24] (Galiano Island).

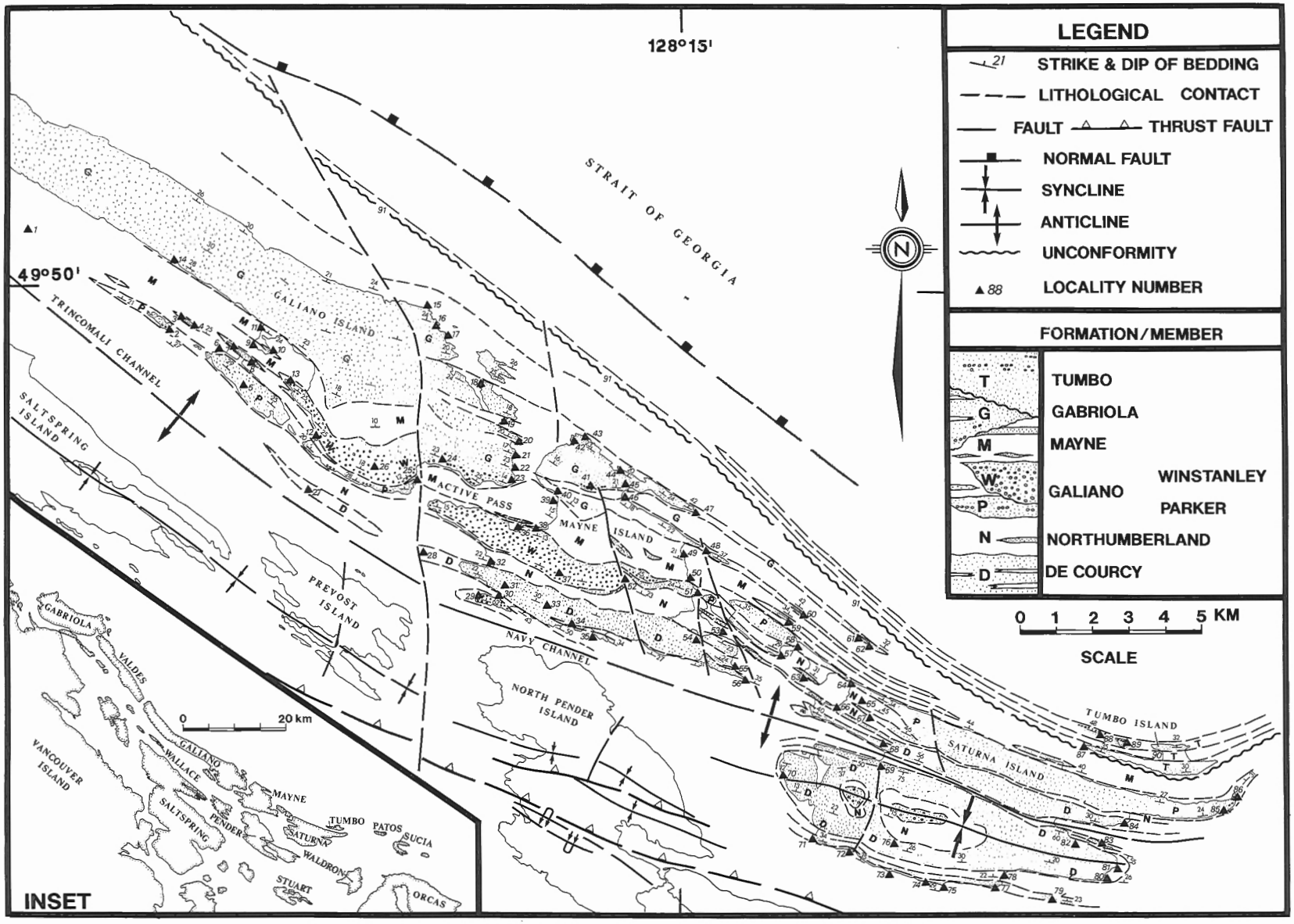

Figure 3. Summary geological map of the study area, based in part on England (1990), Carter (1976), Stickney (1976), Sturdavant (1975), and Muller and Jeletzky (1970). Onshore coarse grained units are stippled, fine grained units are unpatterned (Saltspring, Prevost, and Pender islands excluded). Offshore units are mapped on the basis of seafloor bathymetry.

Succession on Tumbo Island

The succession on Tumbo[87] and Cabbage[89] islands comprises: 1) a lower sandstone member which forms the southern main backbone of the island; 2) an intermediate, unexposed, fine grained member inferred by the shape of the islands and the local bathymetry; and 3) an upper coarse grained member of lower sandstone and upper conglomerate which forms Cabbage Island and the northern part of Tumbo Island.

The lower sandstone member on Tumbo Island is characterized by trough crossbedded, medium- to coarse-grained sandstones (Fig. 4C). Maximum crossbed set height is about 3 m, and gravel-filled scours occur locally. Crossbedding is unidirectional, with no evidence of foreset bundling (Allen, 1980), reactivation surfaces, or flow reversals. The lower sandstone of the upper coarse grained member, which is well exposed on Cabbage Island[89], is trough crossbedded as well, but contains significantly more dispersed pebbles, and maximum crossbed set thickness is 4.7 m. The conglomerate of the upper coarse grained member is predominantly clast-supported, crudely stratified, imbricated, and contains polymictic fine to coarse pebbles. It rests sharply on the underlying sandstone. There are local scour-and-fill structures within the lower part of the conglomerate, with scours as deep as 3 m. Above this lower interval, the conglomerate contains lenses and interbeds of crossbedded or parallel laminated, medium- to coarse-grained sandstone. Paleocurrent directions vary considerably throughout the succession: east for the lower sandstone member, from northeast to southwest for the upper sandstone unit, and from south to west for the conglomerate unit (England and Hiscott, in prep.).

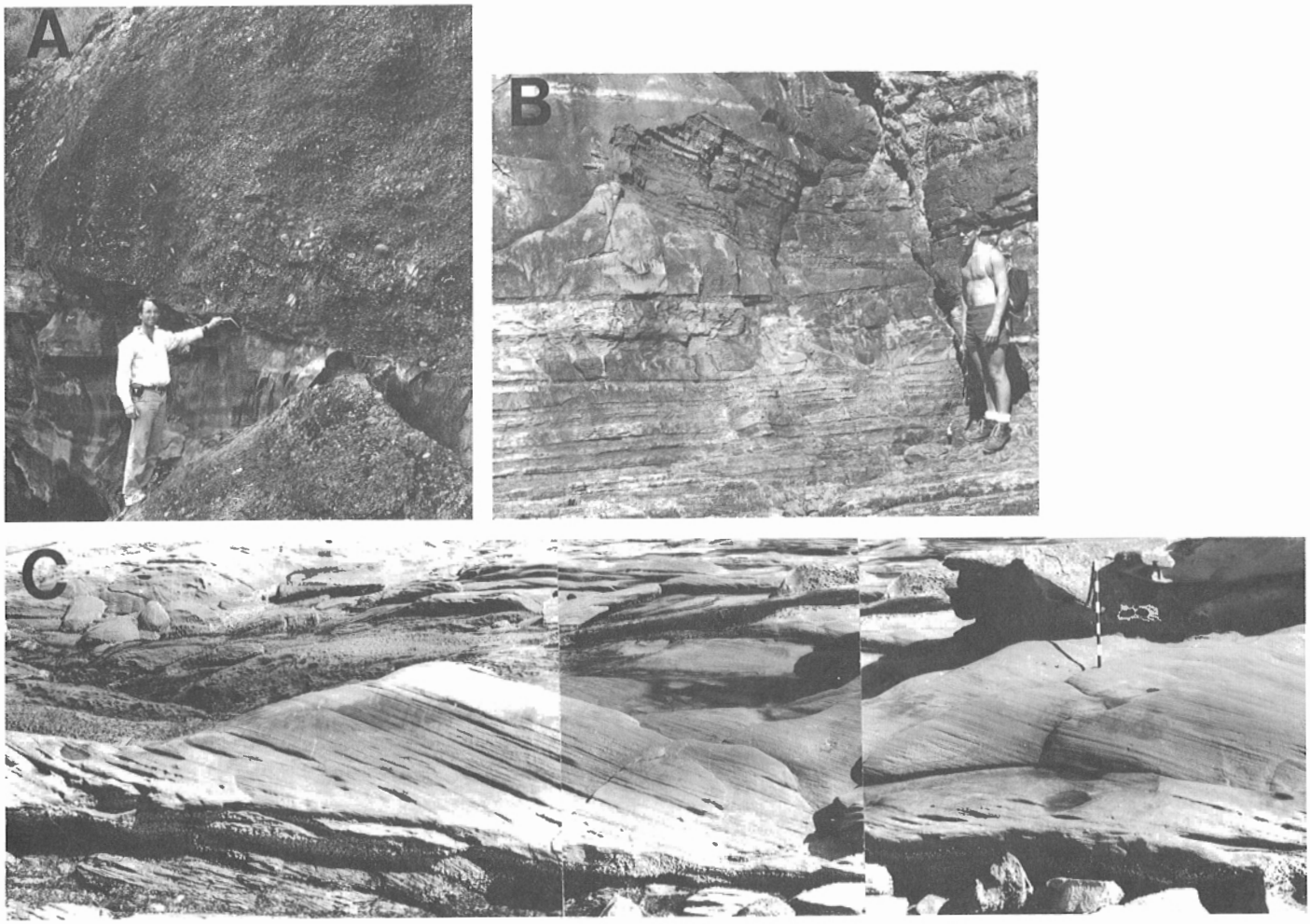

Figure 4A. Heterogeneous pebble to cobble conglomerate filling in a deep erosional surface in planar stratified sandstone, Galiano formation at Georgeson Bay[25], Galiano Island. The person is standing on a fallen block of the conglomerate, and indicating the dip of the in-place conglomerate. **4B.** Large planar stratified rip-up clast within a massive, thick sandstone bed of the Galiano formation, East Point[85], Saturna Island. **4C.** Large trough crossbedded, medium grained sandstone of the lower sandstone member on Tumbo Island[87] (metre stick has 10 cm scale divisions).

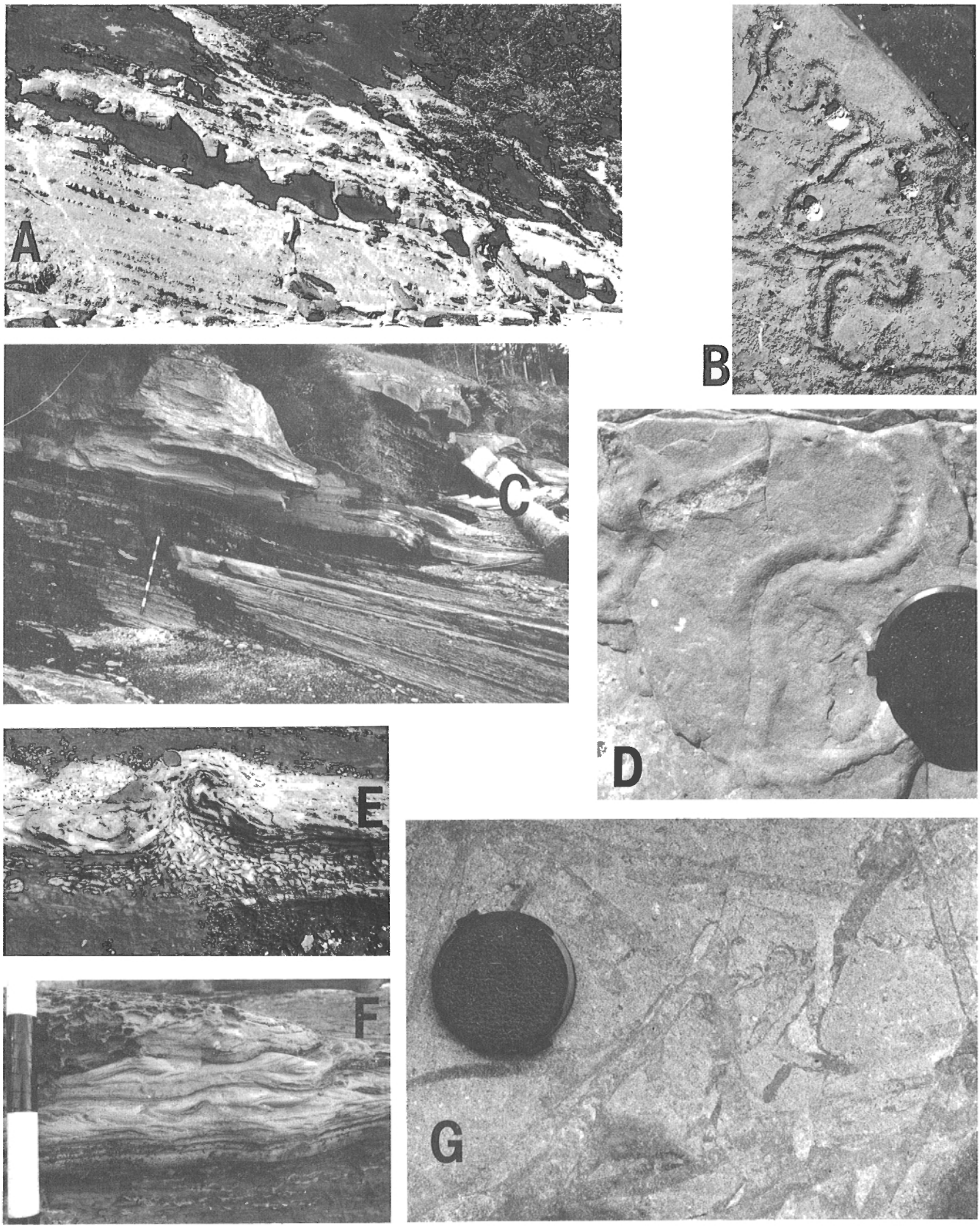
A
B
C
D
E
F
G

DISCUSSION

Nanaimo Group

Facies in the upper Nanaimo Group resemble those described from ancient deep-sea settings (Pickering et al., 1989). The lenticular geometry of sandstone and conglomerate bodies, and their erosional bases, indicate that the major coarse grained units were deposited in large channels. The deeper channels cut into and through underlying shale and sandstone bodies. The channels funnelled density currents to the west or northwest into the basin. Discordant paleoflow directions between coarse grained channel facies and thick, fine grained units suggest that the latter may represent levee deposits. The dilute tops of turbidity currents that overtopped the levees would have spilled down the backslopes of the levees at right angles to the channel.

Channels in deep-sea fan systems are important conduits for sediment gravity flows that disperse across distal aprons and the adjacent basin floor. It is probable that the amount of sediment that is eventually deposited within a feeder channel is greatly exceeded by the amount of sediment that passes through the channel on its way to more basinward sites. If true, then the substantial sandstones of the upper part of the Nanaimo Group imply an enormous volume of contemporaneous sand bodies that must have accumulated in deep water to the northwest.

The widespread fine grained units in the Nanaimo Group may be levee deposits, but they may also be partly attributable to regional rises in relative sealevel (Mutti, 1985). Regionally in the Nanaimo Group, marine paleodepths provided by benthic foraminifers (B.E.B. Cameron, pers. comm., 1988) suggest deeper water during deposition of the sandstone-dominated formations (Table 1), consistent with a partial sealevel control. Also, the impressive downcutting that preceded deposition of the Galiano and Gabriola formations can be attributed to erosion during relative sea-level fall.

Even with the relatively good ammonite biostratigraphy of the Nanaimo Group, dating is not sufficiently precise to decide if the times of inferred high and low stands of relative sea level in the basin correspond to the global scheme of Haq et al. (1987). Within the latitude of the age control, the coarse grained formations of the Nanaimo Group compare well with low-stand positions of the global scheme (England, 1990). Our preference, however, is that the relative sealevel changes that are reflected in the stratigraphy were induced by regional tectonics, not solely by eustasy, because the tectonic setting is an active forearc setting (England, 1990).

Tumbo Island deposits

The lack of macrofossils and trace fossils, unidirectional crossbedding in individual parts of the section, and lack of any sedimentary structures formed by tidal currents or waves, suggest that the sandstone and conglomerates on Tumbo and Cabbage islands are fluvial deposits. Major switches in paleoflow are interpreted as responses to channel switching and tectonically induced change in the source area. The paleocurrents and facies of the succession on Tumbo and Cabbage islands are distinctly different from those that characterize sandstones and conglomerates elsewhere in the field area.

England (1990) described the strata on Tumbo and Cabbage islands as part of the Nanaimo Group. The lower sandstone member on Tumbo Island, however, can be traced directly into a continuous offshore ridge[91] that persists at least as far west as 123.5°W longitude, just outside of the field area (see Canadian Hydrographic Service chart 3462). Across the field area, the stratigraphic thickness from the top of the De Courcy Formation to the base of the offshore ridge of Tumbo Island sandstone varies smoothly from about 2600 m in the west to about 750 m in the east as a result of progressive loss of the sandstone unit that forms the central spine of Galiano Island. This observation and the orientation of bedding in the vicinity of Salamanca Point[15] (Galiano Island), which strikes toward the ridge, suggests the presence of an unconformity just below the Tumbo Island sandstone.

The Tumbo Island deposits, which can be traced as the prominent offshore ridge, extend about 40 km to the northwest of Tumbo Island and about 5 km to the east of the island, perhaps surfacing again on Patos Island (Fig. 3, inset). Both the age of the formation and its regional correlatives are uncertain. It strikingly resembles the sandstones which overlie the Campanian-Maastrichtian Fossil Bay shale (England, 1990; Muller and Jeletzky, 1970; Usher, 1952) on the Sucia Islands. These sandstones have been assigned both to the Nanaimo Group (Pacht, 1984) and the Paleogene Chuckanut Formation based on fission-track data (Johnson, 1984). If the sandstones on Tumbo and Sucia islands are correlative, then the Tumbo Island deposits may be latest Paleocene-early Eocene in age. Furthermore, if the Fossil Bay shale is equivalent to the Cedar District Formation of the Nanaimo Group (which underlies the De Courcy Formation), then the sub-Tumbo unconformity may cut out the rest of the upper Nanaimo Group (ca. 1.5 km of section) between Tumbo and Sucia islands. Alternatively, these "missing" units may never have been deposited there.

Figure 5A. (opposite) Thin-bedded shale with graded interbeds of fine- to medium-grained sandstone, Northumberland Formation, Curlew Island[53]. **5B.** Grazing trail (*Helminthopsis*?) on the top surface of a calcareous sandstone interbed, lower Mayne Formation, Miners Bay[38]. Scale divisions are 10 cm. **5C.** Thin-bedded siltstone and shale (Bouma T_{cde} cycles) with two thick, medium grained sandstone interbeds, lower Mayne Formation, Bennett Bay[50], Mayne Island. Metre stick for scale. **5D.** Sinuous bilobate crawling trace *Scolicia*, upper Mayne Formation, Bennett Bay[49], Mayne Island. Lens cap is about 6 cm in diameter. **5E.** Large flame structure and contorted fine grained sandstone bed, Mayne Formation, Bennett Bay[49], Mayne Island. **5F.** Common ripple cross-laminated fine grained sandstone bed, Mayne Formation, Bennett Bay[49], Mayne Island. **5G.** Top surface of sandstone bed mainly showing the annelid burrow *Ancorichnus*, Mayne Formation, Bennett Bay[49], Mayne Island.

Table 1. Summary of extant paleontological data for the upper Nanaimo Group in the study area (England, 1990; J.W. Haggart, pers. comm., 1988, 1991; Muller and Jeletzky, 1970; Carter, 1976; Stickney, 1976; Sturdavant, 1975; Usher, 1952; and Ward, 1976). Paleo-water depths are based on foraminiferal assemblages (B.E.B. Cameron, pers. comm., 1988). The numbers in brackets refer to field stations (Fig. 3). Complete locality descriptions are available in England (1990).

FORMATION	MACROFOSSILS	PALEOWATER-DEPTH (m)	TRACE FOSSILS
GABRIOLA	*Pachydiscus suciaensis(46)* gastropods, pelecypods	200(19)	*Teichichnus* *Skolithos?* *Ophiomorpha?*
MAYNE	*Diplomoceras? sp.(49)* *Pseudophyllites indra (39,50)* *Pachydiscus suciaensis(50)* *Pachydiscus cf. hidakaensis (49)* *Pachydiscus sp. (9)* *Inoceramus sp. cf. pilvoensis (38)* *Pterotrigonia sp. (39)*	200-600(39) 400-600(49)	*Thalassinoides* *Paleophycus* *Scolicia* *Ancorichnus* *Zoophycus?* *Cladichnus?* *Taenidium?*
GALIANO	*Inoceramus sp. (63)*		*Rutichnus* *Planolites* *Thalassinoides* *Helminthopsis* *Helminthoidea?* *Cladichnus?*
NORTHUMBERLAND	*Pachydiscus suciaensis(66)* ammonites, brachiopods inoceramids, Mytilus	600-1200(32) 200-600 (57,65) 200-400(53) 150-200(52)	*Taenidium* *Scolicia* *Thalassinoides* *Planolites* *Helminthoidea?*
DE COURCY	*Pachydiscus sp. (55)* *Inoceramus sp.*	200-300(68) 100-200(55)	burrows
CEDAR DISTRICT	*Inoceramus ex. gr. I. balticus(72)* *Inoceramus sp. cf. vancouverensis (74)* *Phylloceras sp. (75)* *Baculites rex(75), Baculites sp.* *Schluteria selwyniana(74)* *Glycymeris veatchii (74)* *Veniella crassa (74)* *Cymbophora sp. (74)* inoceramids, pelecypods gastropods, brachiopods	200-600 (34,72) 150-300 (73)	*Diplocraterion* *Thalassinoides* *Helminthoidea?*

ACKNOWLEDGMENTS

This study would not have been possible without the support of C.J. Yorath of the Pacific Geoscience Centre, BP Canada Resources Limited, and the Natural Sciences and Engineering Research Council, during thesis studies by the senior author. Support for fieldwork during 1990 was from EMR Research Agreement #127-04-90. Able field assistance was provided by S. Phillips and G. Linden (University of British Columbia), and L.A. England. Ship charter out of Fulford Harbour, Saltspring Island, was arranged by S. Phillips. Thanks are also due to the critical reader who diligently reviewed and commented on the manuscript.

REFERENCES

Allen, J.R.L.
1980: Sand waves: a model of origin and internal structure; Marine Geology, v. 26, p. 281-328.

Carter, J.M.
1976: The stratigraphy and sedimentology of the Cretaceous Nanaimo Group, Galiano Island, British Columbia; MSc. thesis, Oregon State University, Corvallis, 203 p.

Dickinson, W.R.
1976: Sedimentary basins developed during evolution of Mesozoic-Cenozoic arc-trench system in western North America; Canadian Journal of Earth Sciences, v. 13, p. 1268-1287.

England, T.D.J.
1990: Late Cretaceous to Paleogene evolution of the Georgia Basin, southwestern British Columbia; Ph.D. thesis, Memorial University of Newfoundland, St. John's, 481 p.

England, T.D.J. and Calon, T.J.
1991: The Cowichan fold and thrust system, Vancouver Island, southwestern British Columbia; Geological Society of America Bulletin, v. 103, p. 336-362.
Haq, B.U., Hardenbol, J., and Vail, P.R.
1987: Chronology of fluctuating sea levels since the Triassic; Science, v. 235, p. 1156-1167.
Ingersoll, R.V.
1978: Submarine fan facies of the Upper Cretaceous Great Valley Sequence, northern and central California; Sedimentary Geology, v. 21, p. 205-230.
Johnson, S.Y.
1984: Stratigraphy, age and paleogeography of the Eocene Chuckanut Formation, northwest Washington; Canadian Journal of Earth Sciences, v. 21, p. 92-106.
Muller, J.E. and Jeletzky, J.A.
1970: Geology of the Upper Cretaceous Nanaimo Group, Vancouver Island and Gulf Islands, British Columbia; Geological Survey of Canada, Paper 69-25, 77 p.
Mutti, E.
1985: Turbidite systems and their relations to depositional sequences; in Provenance of Arenites, (ed.) G.G. Zuffa; NATO Advanced Scientific Institute, D. Reidel, Dordrecht, Holland, p. 63-93.
Pacht, J.A.
1984: Petrologic evolution and paleogeography of the Late Cretaceous Nanaimo Basin, Washington and British Columbia: implications for Cretaceous tectonics; Geological Society of America Bulletin, v. 95, p. 766-778.
Pickering, K.T., Hiscott, R.N., and Hein, F.J.
1989: Deep marine environments, clastic sedimentation and tectonics; Unwin Hyman, London, 416 p.
Stickney, R.B.
1976: Sedimentology, stratigraphy, and structure of the Late Cretaceous rocks of Mayne and Samuel Islands, British Columbia; M.S. thesis, Oregon State University, Corvallis, 226 p.
Sturdavant, C.D.
1975: Sedimentary environments and structure of the Cretaceous rocks of Saturna and Tumbo islands, British Columbia; MSc. thesis, Oregon State University, Corvallis, 195 p.
Usher, J.L.
1952: Ammonite faunas of the Upper Cretaceous rocks of Vancouver Island, British Columbia; Geological Survey of Canada, Bulletin 21, 182 p.
Ward, P.D.
1976: Stratigraphy, paleoecology and functional morphology of heteromorph ammonites of the Upper Cretaceous Nanaimo Group, British Columbia and Washington; Ph.D. thesis, McMaster University, Hamilton, Ontario.

A 367 m core from southwestern Fraser River delta, British Columbia

John L. Luternauer, John J. Clague, and Tracey D. Feeney
Cordilleran Division, Vancouver

Luternauer, J.L., Clague, J.J., and Feeney, T.D., 1991: A 367 m core from southwestern Fraser River delta, British Columbia; in Current Research, Part E; Geological Survey of Canada, Paper 91-1E, p. 127-134.

Abstract

A detailed descriptive log of a 367 m drillhole provides a record of the Quaternary deposits underlying the southwestern Fraser River delta. The lower half of the cored sequence is Pleistocene in age and comprises diamicton, gravel, sand, and mud deposited, in large part, in glaciomarine environments. Nonglacial muds deposited in ancestral Strait of Georgia at the close of the Pleistocene and during the early Holocene overlie the uppermost diamicton at 185 m. These muds, in turn, are overlain by dominantly sandy foreset beds deposited on the Fraser delta slope and by a thin cap of clayey and silty topset beds.

Résumé

Une diagraphie descriptive détaillée d'un sondage de 367 m constitue un enregistrement des dépôts du Quaternaire reposant sous la partie sud-ouest du delta du Fraser. La moitié inférieure de la séquence carottée date du Pléistocène et comprend du diamicton, du gravier, du sable et de la boue accumulés en grande partie dans des milieux glaciomarins. Les boues non glaciaires déposées dans le détroit ancestral de Georgie à la fin du Pléistocène et au début de l'Holocène recouvrent le diamicton supérieur à 185 m. Ces boues sont à leur tour recouvertes de lits frontaux essentiellement sableux qui se sont accumulés sur la pente du delta du fleuve Fraser et par un mince chapeau de lits sommitaux argileux et limoneux.

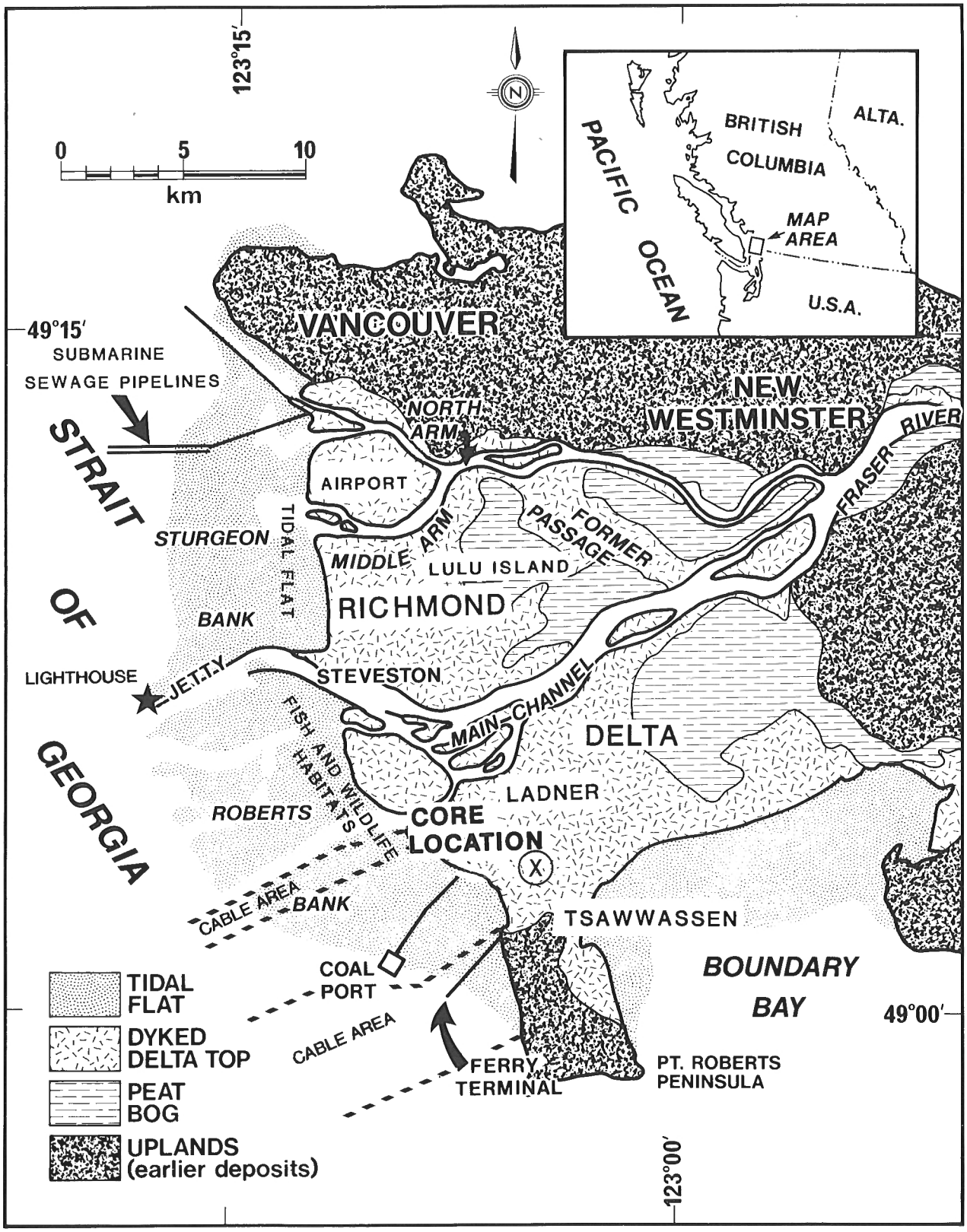

Figure 1. Location map of the study area.

INTRODUCTION

Coring is an integral part of a co-operative Geological Survey of Canada (GSC)/university/private sector program initiated by the GSC Cordilleran Division in 1985 to better define the potential earthquake response, and seismic and sea-level history of the highly populated and industrialized Fraser River delta (Luternauer, 1988, 1990, 1991; Finn et al., 1989; Williams and Roberts, 1989, 1990; Clague et al., 1991). A 367 m hole (FD87-1), the deepest to date in this study, was drilled on the southwestern part of the delta in the Municipality of Delta near the intersection of 28th Avenue and 56th Street (49°3.2′N, 123°4.0′W) (Fig. 1).

The purpose of this report is to make available, in response to public demand, a detailed log of this drillhole, which includes information on sedimentary structures, inclusions, lithology, and radiocarbon ages of wood and shells recovered from the sediments. A brief interpretation of paleoenvironments is drawn, in part, from Clague et al. (1991). A more detailed summary and discussion of the geology, paleontology, geophysical characteristics, and stratigraphy of the subsurface sediments of the southwestern Fraser delta will be presented in a forthcoming GSC Bulletin.

METHODS

FD87-1 was drilled by Foundex Exploration Ltd. from March 13 to April 2, 1987. Tri-cone rotary drilling was done from the surface to a depth of 137 m; Standard Penetration Test split tube samples were collected every 3 m to 46 m depth and then every 6 m from 46 m to 137 m. Drill cuttings were sampled intermittently throughout this part of the sequence. Carbide bit, wire-line, continuous coring was done from 137 m to 303 m, followed by tri-cone rotary drilling with no sampling from 303 m to 313 m. This, in turn, was followed by carbide bit, wire-line, continuous coring from 313 m to 318 m, tri-cone rotary drilling from 318 m to 340 m, and finally continuous coring to 367 m, the bottom of the hole. Tri-cone rotary drilling had to be used wherever there were significant thicknesses of noncohesive sands. Core was logged by JJC and JLL shortly after the drilling program was completed, and is presently archived at Simon Fraser University.

The grain-size sand, silt, and clay distributions of representative samples were determined at the Geological Survey of Canada (Sidney, B.C.) using a 2 m long settling tube for sand and a Sedigraph 5000D for silt and clay. Detailed size distributions are available, but only the weight percent proportions of the main textural categories are shown on the logs presented in this paper (Fig. 2, 3a-h). The textural profiles shown in Figure 3 are based on grain-size analyses of core samples and drill cuttings, and visual inspection of the core.

Shell and wood recovered from the core were dated by the accelerator mass spectrometry method (AMS) at the IsoTrace Laboratory of the University of Toronto.

Drillhole logs were prepared on the CorelDRAW system (Corel System Corporation, 1990) by TDF. We used CorelDRAW to easily create and edit symbols. All symbols in the left column were created individually and then imported into the section where appropriate. The program was set up for 81/2 x 11 inch paper, which made it easy to create a suitable scale for the diagrams and accurately plot the grain sizes of analyzed samples in the centre column. The right column was created using a 20% black fill placed in the entire length of the column, to indicate where sand was present in the core. A white-filled box was placed above the 20% black fill to represent silt and clay.

Although using the computer to draft the sections allowed us to readily make revisions, the method has some drawbacks. Because CorelDRAW is limited to the number of fills it can print at any one time, all silt and clay symbols had to be drawn individually and then copied rather than treated as a fill. Another problem involved the size and complexity of the diagrams. When the three columns for a 50 m section were complete, the section was saved as a separate file. Calling up these files on a 386SX computer became increasingly time consuming as more and more objects were added. Saving and

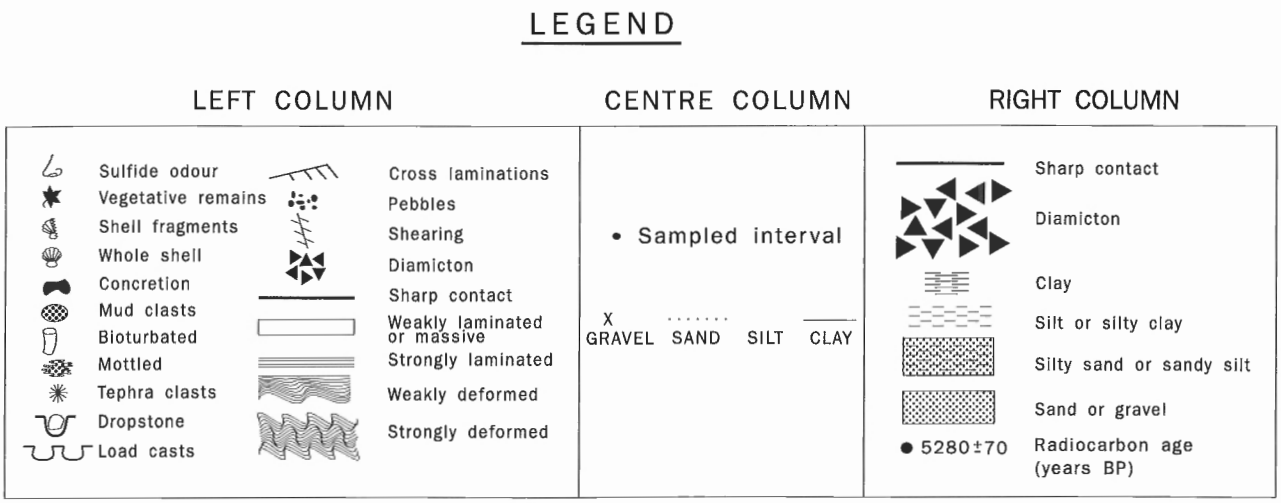

Figure 2. Legend for drillhole logs in Figures 3a-h.

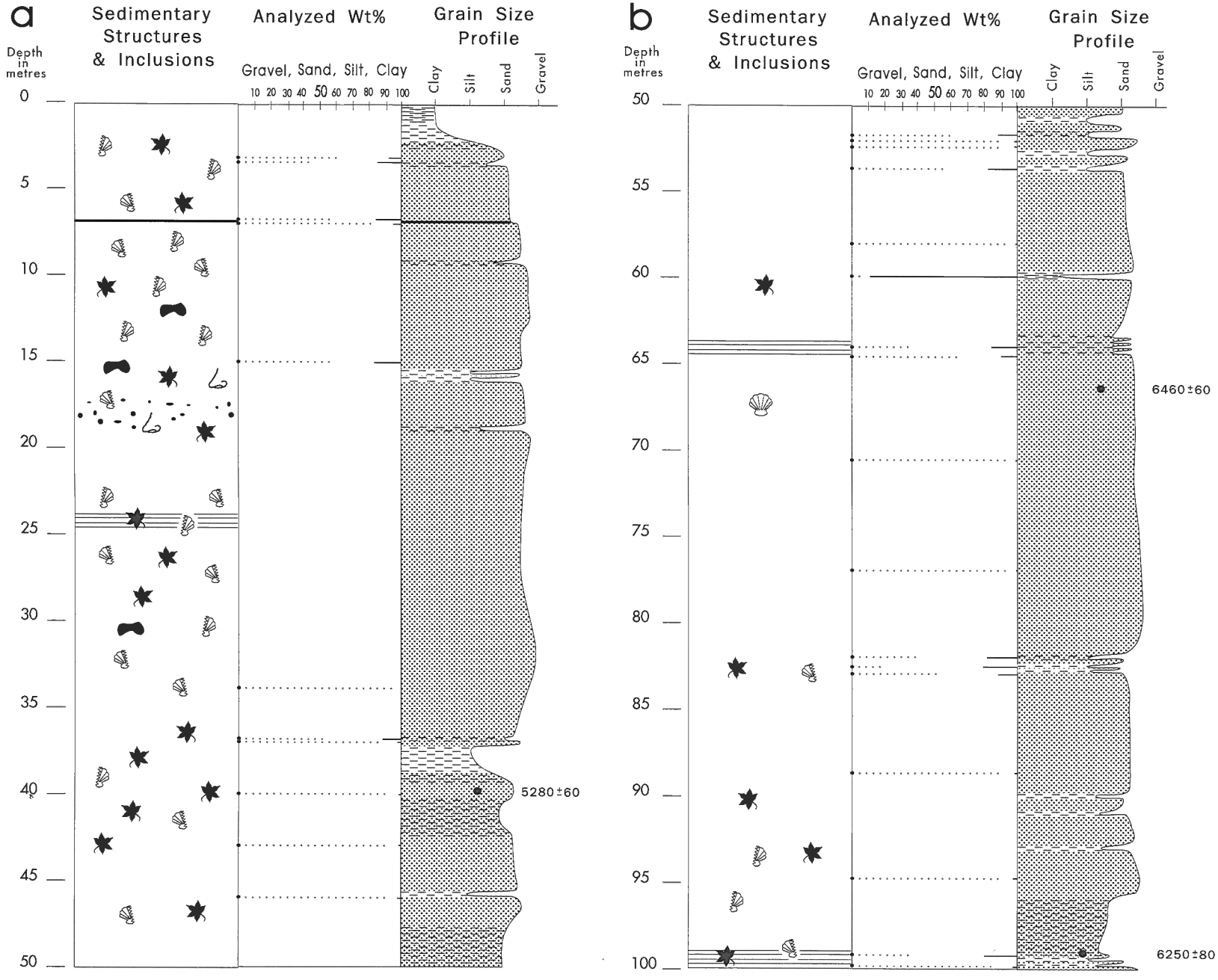
a
Sedimentary Structures & Inclusions
Analyzed Wt%
Gravel, Sand, Silt, Clay
10 20 30 40 50 60 70 80 90 100
Grain Size Profile
Clay
Silt
Sand
Gravel
Depth in metres
0
5
10
15
20
25
30
35
40
45
50
5280±60
b
Sedimentary Structures & Inclusions
Analyzed Wt%
Gravel, Sand, Silt, Clay
10 20 30 40 50 60 70 80 90 100
Grain Size Profile
Clay
Silt
Sand
Gravel
Depth in metres
50
55
60
65
70
75
80
85
90
95
100
6460±60
6250±80

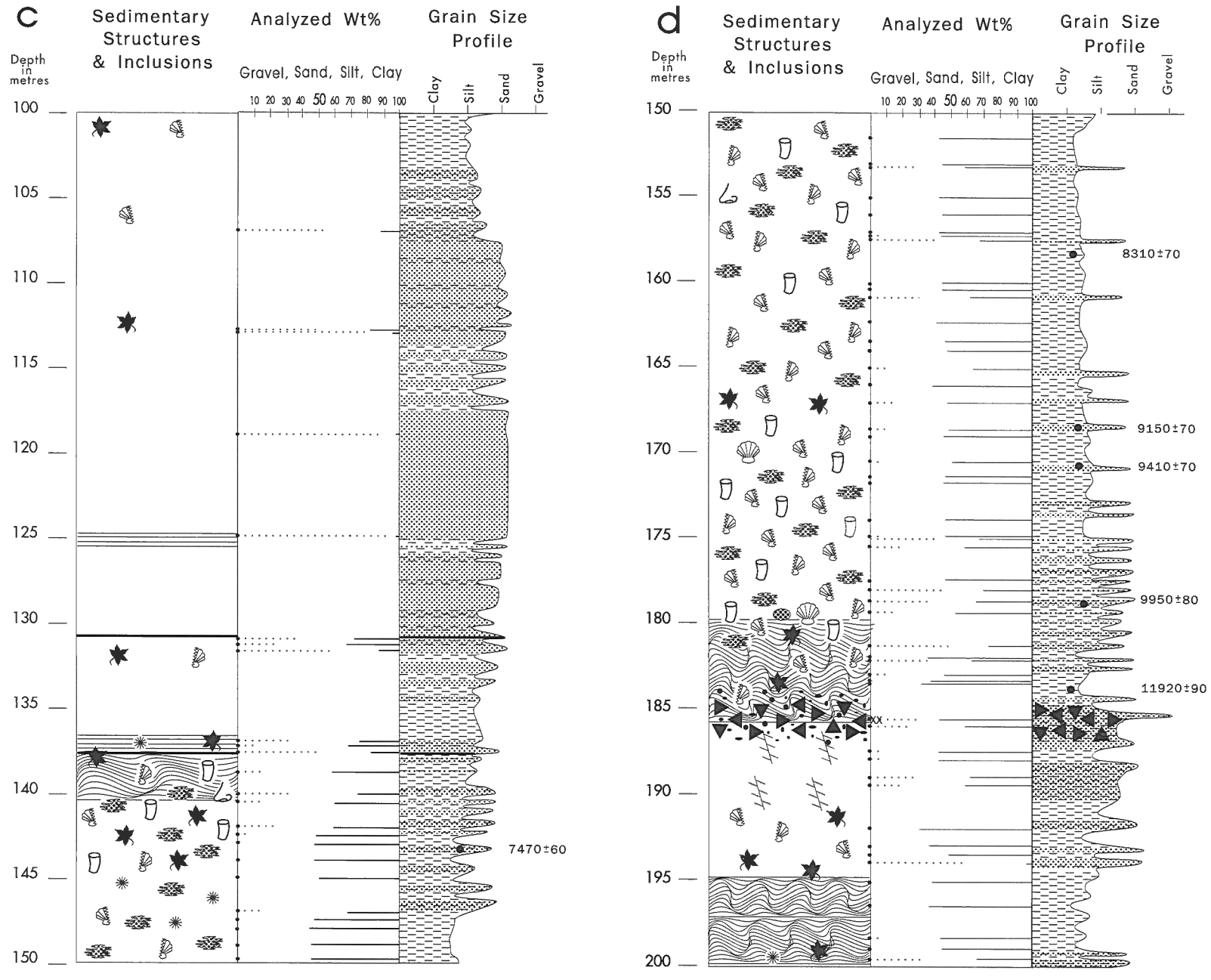

Figure 3a-h. Drillhole logs.

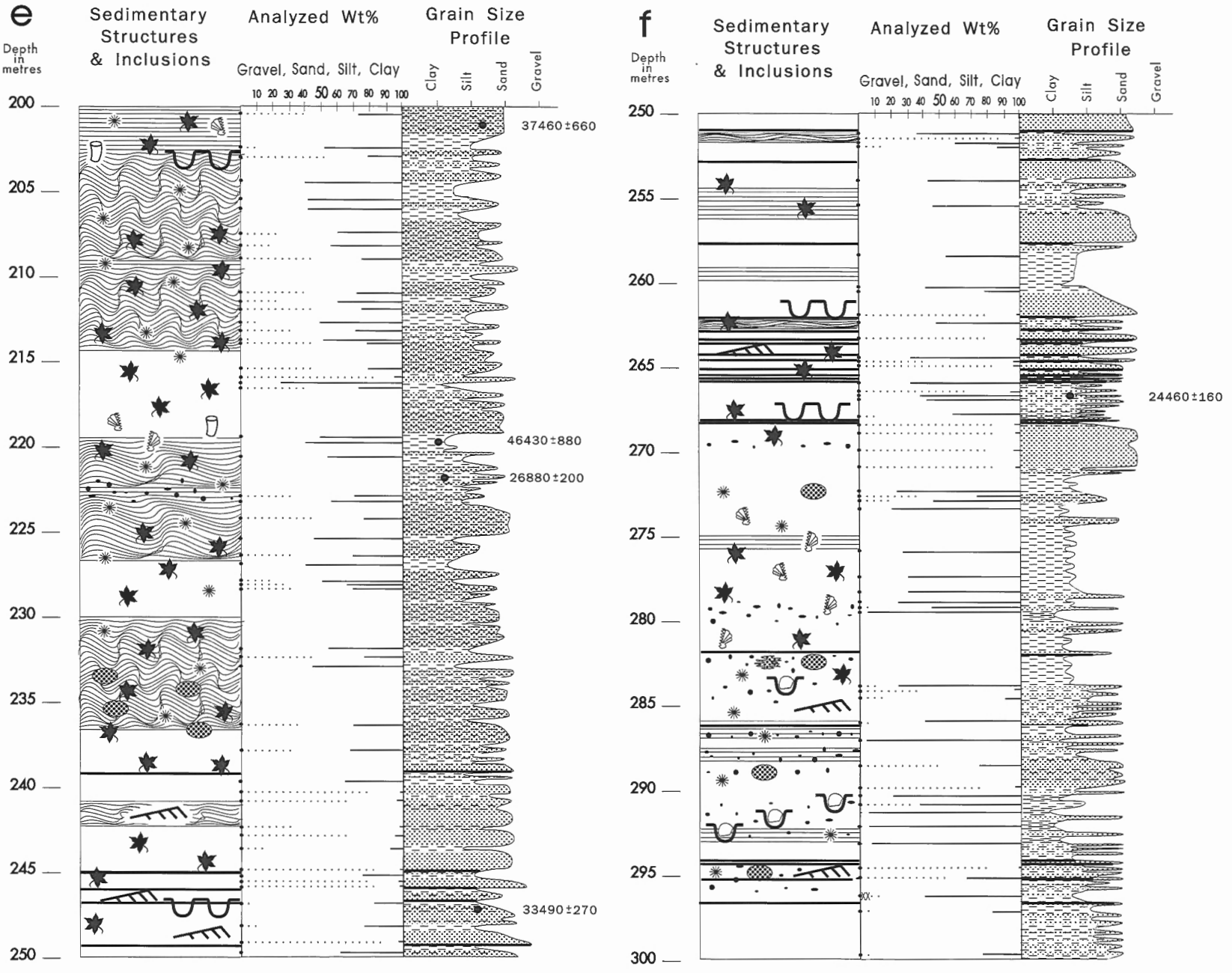
e
Depth in metres
Sedimentary Structures & Inclusions
Analyzed Wt%
Gravel, Sand, Silt, Clay
10 20 30 40 50 60 70 80 90 100
Grain Size Profile
Clay
Silt
Sand
Gravel
200
205
210
215
220
225
230
235
240
245
250
37460±660
46430±880
26880±200
33490±270
f
Depth in metres
Sedimentary Structures & Inclusions
Analyzed Wt%
Gravel, Sand, Silt, Clay
10 20 30 40 50 60 70 80 90 100
Grain Size Profile
Clay
Silt
Sand
Gravel
250
255
260
265
270
275
280
285
290
295
300
24460±160

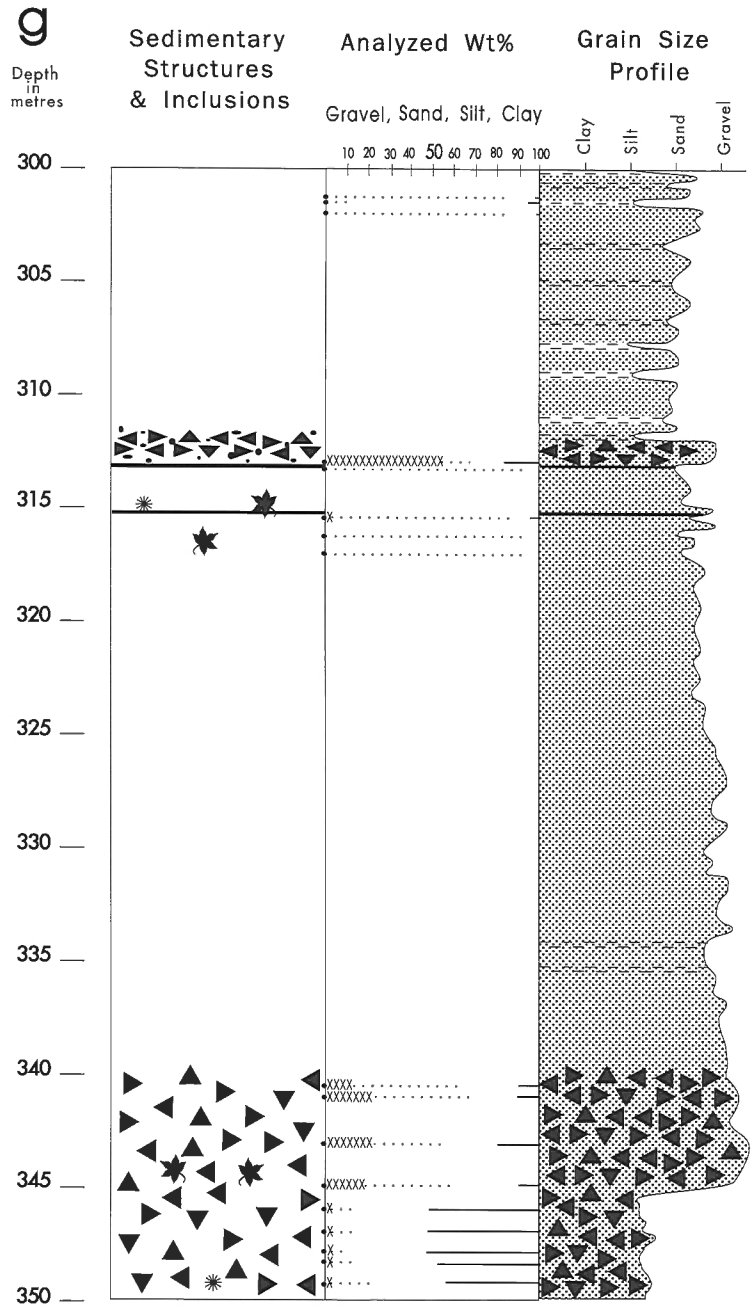

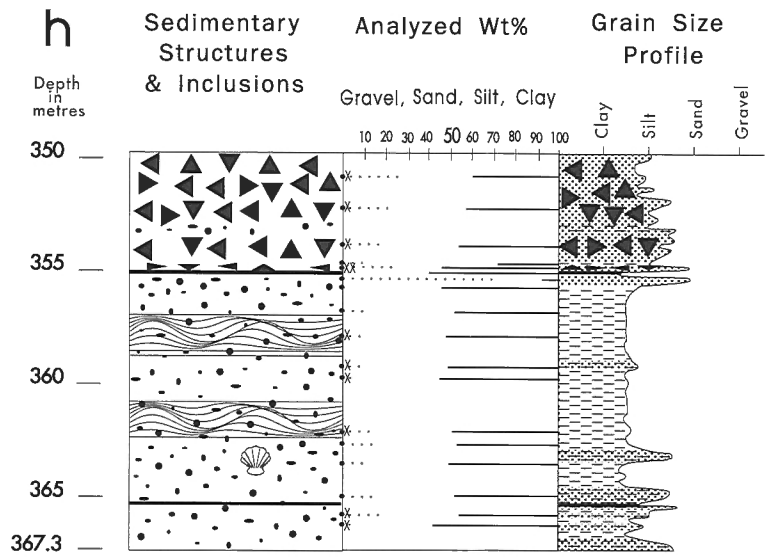

Figure 3a-h. (cont.)

printing each diagram added even more time to the project. The largest diagram (485K, 1900 objects) took up to 40 minutes to retrieve, save, and print when even the smallest changes were made. Despite these deficiencies, a complex diagram capable of accurately illustrating many aspects of the 367 m core was created using the CorelDRAW program.

GENERAL LITHOLOGY AND PALEOENVIRONMENTS

Interlayered diamicton, gravel, sand, and mud in the lower part of the sequence (312-367 m) probably are glacial and glaciomarine deposits (Patterson and Cameron, 1990). Between this and the uppermost diamicton at 185 m depth is a thick sequence of interbedded mud and sand with load casts, dropstones, cross laminae, deformed laminae, and mud and tephra clasts. These sediments may be glaciomarine in origin and probably date, at least in part, to the early part of the last (Fraser) glaciation. Sediments immediately below the uppermost diamicton are sheared, perhaps due to glacier overriding during the Fraser Glaciation.

The mottled and bioturbated muds lying above the uppermost diamicton were deposited in the ancestral Strait of Georgia between 12 000 and 7500 years ago (Clague et al., 1991). The dominantly sandy sediments overlying the muds represent a thick succession of foreset beds that record active progradation of the Fraser delta from an apex south of New Westminster between 7500 and 5000 years ago (Clague et al., 1991). The thin sequence of capping muds at the top of the drillhole was deposited in intertidal and fluvial channel and overbank environments during the last half of the Holocene (Clague et al., 1991).

ACKNOWLEDGMENTS

Assistance in logging core was provided by A. Bentley, G. Brierley, G.R. Brooks, V. Cameron, K.W. Conway, C.D. Frew, E.A. Fuller, T.S. Hamilton, L.E. Jackson, Jr., H.M. Jol, G. McKenna, M.C. Roberts, J. Robinson, G. Thomson, R.J. van Ryswyk, R. Von Sacken, H.F.L. Williams, and J. Wood. L.E. Jackson, Jr. critically read the manuscript.

REFERENCES

Clague, J.J., Luternauer, J.L., Pullan, S.E., and Hunter, J.A.
1991: Postglacial deltaic sediments, southern Fraser River delta, B.C.; Canadian Journal of Earth Sciences, in press.

Corel Systems Corporation
1990: CorelDRAW (Version 2.0); Corel Systems Corporation, Ottawa, Ontario.

Finn, W.D.L., Woeller, D.J., Davies, M.P., Luternauer, J.L., Hunter, J.A., and Pullan, S.E.
1989: New approaches for assessing liquefaction potential of the Fraser River delta, British Columbia; in Current Research, Part E; Geological Survey of Canada, Paper 89-1E, p. 221-231.

Luternauer, J.L.
1988: Geoarchitecture, evolution and seismic risk assessment of the southern Fraser River delta, B.C.: status of investigations; in Current Research, Part E; Geological Survey of Canada, Paper 88-1E, p. 105-109.
1990: 1989 field activities and accomplishments of geophysical and geotechnical land-based operations and marine/fluvial surveys, Fraser River delta, British Columbia; in Current Research, Part E; Geological Survey of Canada, Paper 90-1E, p. 235-237.
1991: 1990 field activities and accomplishments, Fraser River delta, British Columbia; in Current Research, Part A; Geological Survey of Canada, Paper 91-1A, p. 43-47.

Patterson, R.T. and Cameron, B.E.B.
1990: Depositional environments of two late Quaternary cores bearing foraminifera and ostracodes from the Fraser Delta, British Columbia (abstract); Geological Association of Canada/Mineralogical Association of Canada, Program with Abstracts, v. 15, p. A102.

Williams, H.F.L. and Roberts, M.C.
1989: Holocene sea-level change and delta growth: Fraser River delta, British Columbia; Canadian Journal of Earth Sciences, v. 26, p. 1657-1666.
1990: Two middle Holocene marker beds in vertically accreted floodplain deposits, Lower Fraser River, British Columbia; Géographie physique et Quaternaire, v. 44, p. 27-32.

Summary of the results of a reconnaissance study of late Quaternary benthic foraminifera from the central continental shelf of western Canada

R. Timothy Patterson[1]
Cordilleran Division, Vancouver

Patterson, R.T., 1991: Summary of the results of a reconnaissance study of late Quaternary benthic foraminifera from the central continental shelf of western Canada; in Current Research, Part E; Geological Survey of Canada, Paper 91-1E, p. 135-140.

Abstract

Seven foraminiferal biofacies were identified in samples from five Quaternary cores collected from the Queen Charlotte Sound-Hecate Strait area of western Canada. These biofacies include: two relict lower to middle bathyal biofacies introduced to shallow depths during a colder interval; four biofacies representative of various neritic depth environments; and a biofacies characteristic of shallow banks. Species such as Buliminella elegantissima have proven useful in tracking the migration of the Fraser Glaciation forebulge across the region, while high concentrations of Cassidulina reniforme at certain core intervals, indicative of glacial or near glacial conditions, signals a return to cooler conditions between about 10 000 and 12 000 years B.P. This cool interval approximately corresponds to the Younger Dryas event of Europe and eastern North America.

Résumé

Sept biofaciès à foraminifères ont été identifiés dans des échantillons provenant de cinq carottes du Quaternaire prélevées dans la région des détroits de la Reine-Charlotte et d'Hécate dans l'Ouest canadien. Ces biofaciès comprennent: deux biofaciès résiduels correspondant à un milieu bathal inférieur à moyen, mis en place à de faibles profondeurs pendant un intervalle plus froid; quatre biofaciès représentatifs de divers milieux abyssaux néritiques; et un biofaciès caractéristique des bancs peu profonds. Des espèces telles que Buliminella elegantissima se sont avérées utiles pour retracer la migration du front de la glaciation de Fraser dans la région, tandis que des concentrations élevées de Cassidulina reniforme dans certains intervalles de carotte, dénotant des conditions glaciaires ou presque glaciaires, indiquent un retour à des conditions plus froides entre il y a 10 000 et 12 000 ans environ. Cet intervalle de froid correspond approximativement au Dryas récent de l'Europe et de l'est de l'Amérique du Nord.

[1] Ottawa-Carleton Geoscience Centre and Department of Earth Sciences, Carleton University, Ottawa, Ontario K1S 5B6

INTRODUCTION

The Quaternary sedimentary record of the Queen Charlotte Sound-Hecate Strait region of the Georgia-Hecate Depression of coastal British Columbia is important because of the clues that these sediments provide about the paleoceanographic history of Canada's west coast (Fig. 1). In addition, renewed oil industry interest in the depression has sparked a major research impetus in an effort to better understand the Neogene depositional history of the basin and potential hazards to hydrocarbon exploration. As part of this effort Patterson (1989) made a biostratigraphic and paleoecological examination of benthic and planktonic foraminifera from the southern part of the basin.

The purpose of the present research was to analyze the foraminiferal faunas found in Quaternary core samples from Queen Charlotte Sound. Foraminiferal assemblages have been shown to be very useful in recognizing temperature and salinity changes expected in water masses during glaciation and deglaciation. The resulting foraminiferal distributional data coupled with the sedimentological and geochronological results (Luternauer et al., 1989a, b) are used to determine paleoenvironmental conditions during Quaternary deposition at these sites. A good understanding of the sea-level history is essential to the rigorous interpretation of offshore geohazards to hydrocarbon exploration. Qualitative and quantitative analysis of benthic foraminifera at closely spaced sampling intervals should provide supporting evidence for suspected rapid water depth changes accompanying a regression *ca.* 13-10 ka and a subsequent (*ca.* 10-9 ka) transgression, as indicated by sedimentological results. Finally, as there has never been a thorough examination of Quaternary foraminifera from this area, this research will provide a valuable base line on foraminiferal distribution and ecology for future researchers (see Patterson (1990) for a complete discussion of previous work).

METHODS AND MATERIALS

Forty-six samples were obtained from five Geological Survey of Canada vibracores collected from Queen Charlotte Sound off the coast of British Columbia (Fig. 1). Core END 87A-023 was collected from Cook Bank off the northwestern tip of Vancouver Island, core END 84B-04 and END 84B-07 from the margin of Moresby Trough off the southeastern tip of Queen Charlotte Island, and cores END 84B-08 and END 84B-10 were collected from Goose Island Trough southwest of Calvert Island (Fig. 2). Locations of cores are as follows:

Core END 87A-23, Latitude 50°59.94′; Longitude 128°26.55′

Core END 84B-04, Latitude 52°14.72′; Longitude 130°09.05′

Core END 84B-07, Latitude 52°16.70′; Longitude 130°12.27′

Core END 84B-08, Latitude 51°31.07′; Longitude 128°23.11′

Core END 84B-10, Latitude 51°28.14′; Longitude 128°25.14′

All samples were boiled with soda ash to cleanse the tests of the foraminifera contained in the sample. Samples were then rinsed using 63 m screens to retain the foraminifera. Samples containing excessive amounts of sand were dried, and the foraminifera separated from the sand by floatation in sodium polytungstate (s.g. 2.28). These samples yielded a fauna of 95 species. Forty-three of the 46 samples were found to contain at least some foraminifera, and 40 of these samples contained populations large enough for statistical analysis (Patterson and Fishbein, 1989).

DISCUSSION

Analysis of Late Quaternary benthic foraminifera in cores from Queen Charlotte Sound and Hecate Strait has yielded new information on the paleoceanographic history of the region. These results are discussed in much greater detail and all foraminiferal taxa are fully illustrating in Patterson (in press). Q-mode cluster analysis separated samples into seven groups distinguished by seven benthic foraminiferal biofacies: the *Gyroidina-Bolivina* Biofacies and *Gyroidina-Seabrookia* Biofacies are relict lower to middle bathyal faunas introduced to shallower depths when cooler water masses influenced the area; the *Cribroelphidium* Biofacies, *Islandiella* Biofacies, *Epistominella* Biofacies, and *Buccella* Biofacies are all similar in faunal makeup and characterize varying depositional conditions at neritic depths; and the *Lobatula-Gavelinopsis* Biofacies characterizes shallow banks.

The upper part of the B_1 unit, the entire B_2 unit of cores END 84B-08 and END 84B-10, and the B_2 unit of the deeper water Core END 84B-04 are characterized by relatively high proportions of *Buliminella elegantissima*, indicating an environment enriched in nutrients (Snyder, 1989; Fig. 3). In a study centred around the mouth of the Columbia River, Harmon (1972) identified abundant vascular plant debris and large populations of diatoms in association with the maximum abundance zone of *Buliminella elegantissima*. The terrestrial plant debris that sustained *Buliminella elegantissima* may have been flushed into Goose Island Trough from

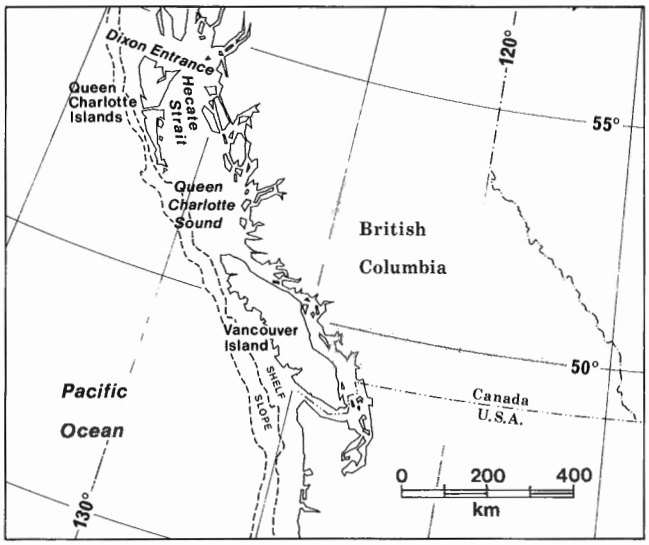

Figure 1. Continental shelf of western Canada showing location of Queen Charlotte Sound and Hecate Strait.

subaerial exposures of Goose Island Bank or Sea Otter Shoals and/or from an area adjacent to a much larger ancestral Calvert Island. Sedimentological evidence that relative sealevels in this area were at least 95 m lower has been provided by several marine and land-based studies in the area (Howes, 1981; Clague et al., 1982; Luternauer et al., 1989a; Barrie and Bornhold, 1989). Changes in the proportion of *Buliminella elegantissima* throughout the cores provides evidence of the degree of relative sea-level change in the area at the time. The increase in the proportion of *Buliminella elegantissima* in the cores through the B_1 and B_2 lithological units suggests an increasing supply of terrigenous debris accompanying marine regression. It is interesting to note that the maximum abundance spike of *Buliminella elegantissima* in these cores occurs in the B_2 lithological unit. Luternauer et al. (1989b) suggested that the winnowed and lagged sediments of this unit, observed in cores throughout the region, were deposited during the period of lowest sealevel. The lagged B_2 deposits of cores END 84B-08 and END 84-10 were deposited between 11 000 and 12 000 years B.P. The gradational nature of the lower contact of the B_2 unit provides sedimentological evidence of a gradual regressive event (Luternauer et al., 1989b). Although lagging has undoubtedly caused some reworking of *Buliminella elegantissima* specimens, the present-day preference of this species for shallow, nearshore habitats along the west coast indicates a probable minimal difference between thanatocoenosis (death assemblage) and the time-average taphocoenosis (generated by lagging) in the B_2 units at these sites (Fürsich and Aberhan, 1990). Immediately following deposition of the B_2 unit, the proportion of *Buliminella elegantissima* inhabiting the area dropped precipitously. A very rapid transgression of the terrestrial source of this debris best explains the sudden collapse of this population. The sharp contact of the upper

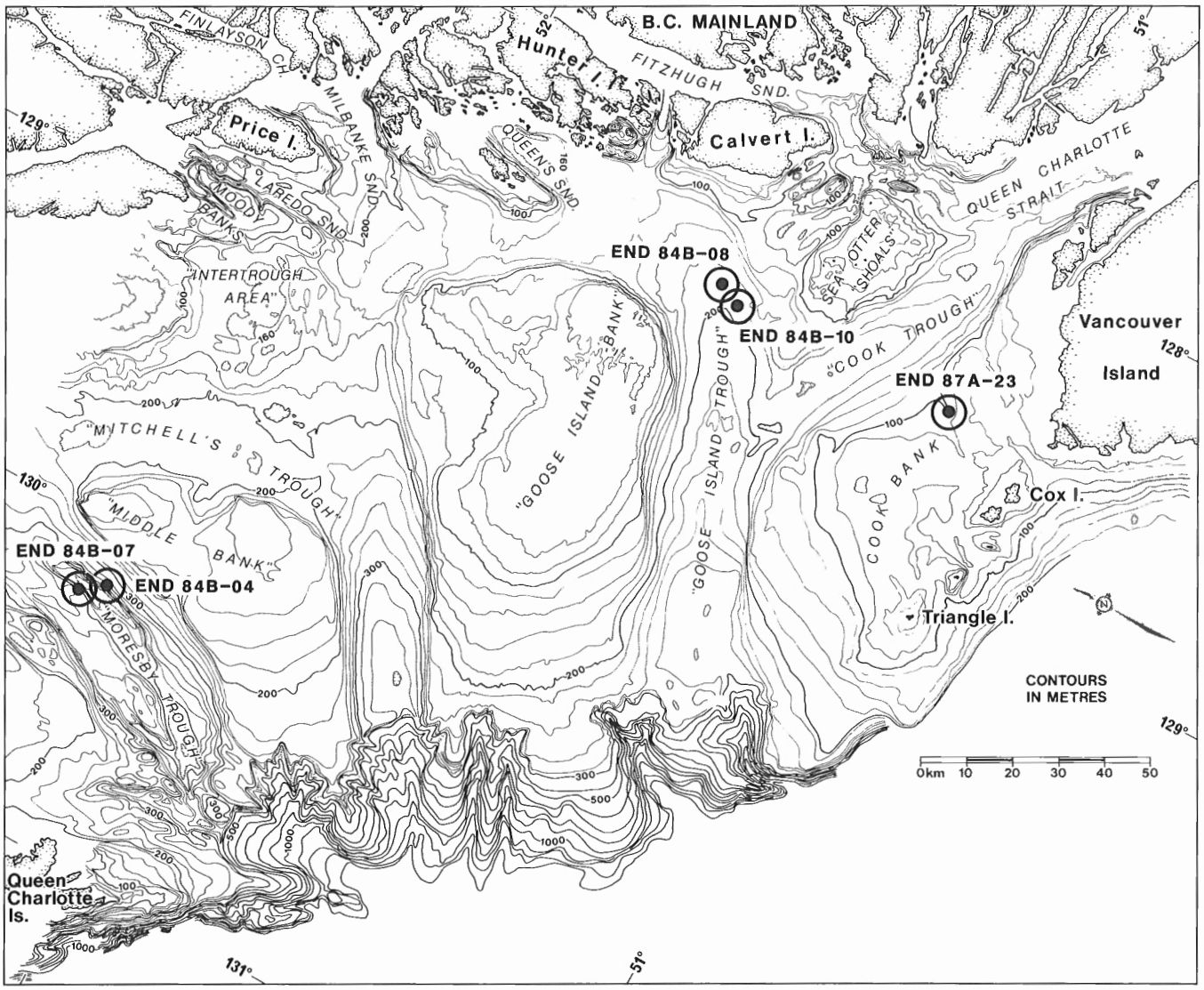

Figure 2. Bathymetric map of Queen Charlotte Sound and southern Hecate Strait (after Luternauer and Murray, 1983) showing location of cores (encircled solid dots) from which Late Quaternary benthic foraminifera were examined.

margin of the B_2 unit with B_3 sediments also supports the hypothesis of rapid subsidence (Luternauer et al., 1989b). Clague (1983) and Luternauer et al. (1989a) suggest that rapid migration and collapse of the forebulge during deglaciation would result in this scenario.

High proportions of *Cassidulina reniforme* characterize the upper part of the B_1 unit through the lower part of the B_3 lithological unit, indicating that water temperatures were generally quite cool during deposition of this interval (Fig. 3). The presence of high proportions of this species in all cores (spanning an interval between approximately 12 000

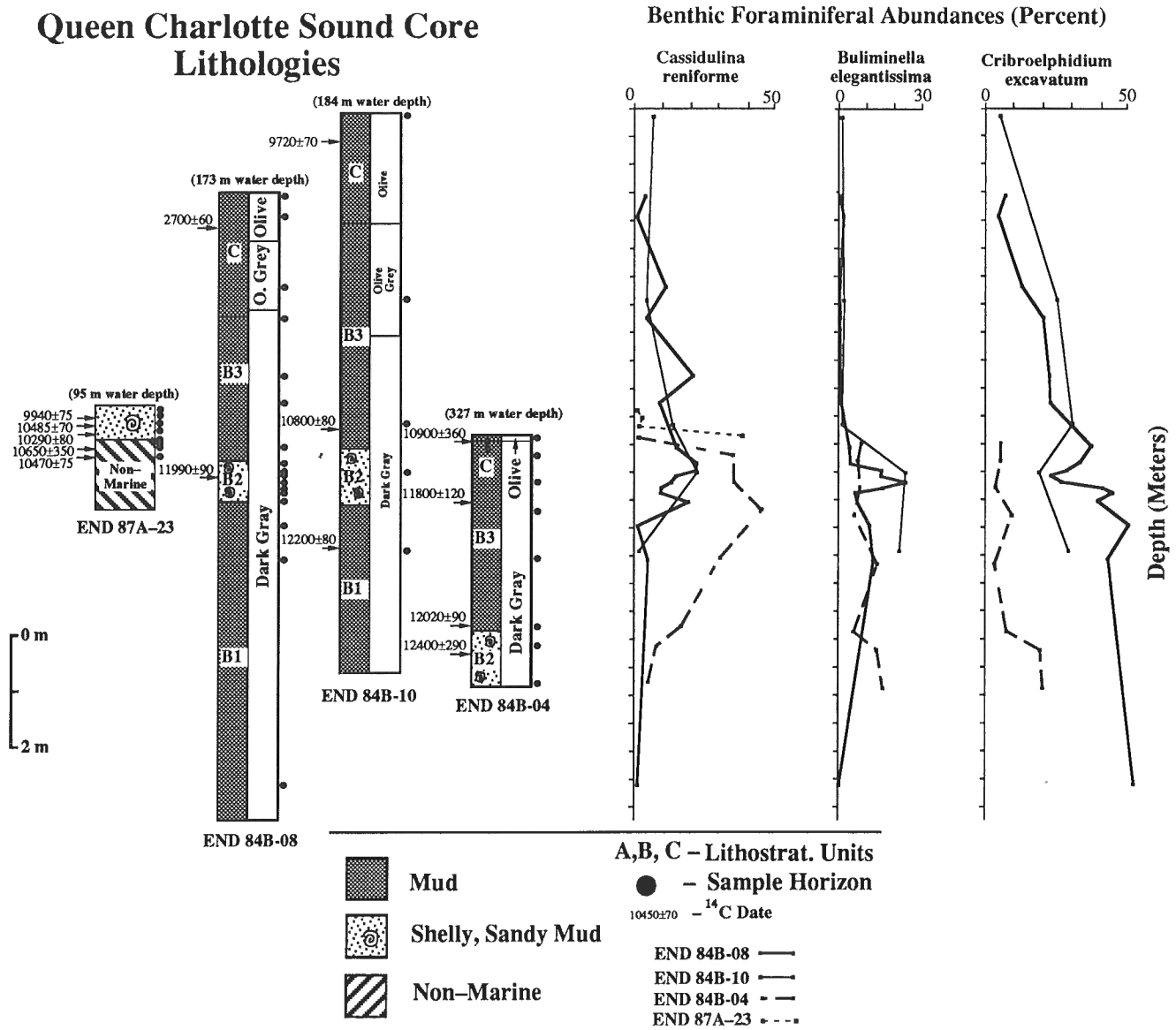

Figure 3. Correlation between cores END 84B-04, END 84B-08, END 84B-10, and END 87A-23 showing lithology, ^{14}C radiocarbon dates given in years B.P., foraminiferal biofacies, and distribution of key indicator species through the cores interval. Correlation of cores is based on best alignment of ^{14}C dates. Faunal distribution patterns show a substantial increase in the proportion of the near-glacial indicator species *Cassidulina reniforme* about 12 000 years B.P. and a tailing off in numbers of the same species about 10 000 years B.P. The proportion of the high organic content indicator species *Buliminella elegantissima* increases dramatically in intervals characterized by diachronous lag deposits indicating a shallow, coast proximal position. *Cribroelphidium excavatum* decreases in relative abundance through the cores in response to habitat reduction following the cessation of glacial conditions.

and 10 000 years B.P.) indicates a major cooling of marine waters off the coast of British Columbia. The presence of high proportions of this species, long associated with very cold water (glacial or near-glacial) regimes (Sejrup and Guilbault, 1980), indicates a brief return to cooler conditions during deglaciation, at roughly the same time as the Younger Dryas event of Europe and eastern North America. Based on a shift in the coiling of the planktonic foraminifera *Neogloboquadrina pachyderma*, in turbidites from the central California continental margin, Brunner and Ledbetter (1989) also identified a cooling event about 11 000 years B.P. Evidence of terrestrial cooling has also been found in the Pacific Northwest. Subalpine pollen spectra have been recorded in the BC-2 Zone -- dated at 11 000 to 9200 years B.P. -- at Bear Cove near Port Hardy on Vancouver Island (Hebda, 1983). Pollen of similar age from the terrestrial part of core END 87A-23 is also subalpine in nature, indicating a cooler climatic interval. This interval correlates very well with the similarly dated Younger Dryas cooling event recorded from marine and terrestrial sediments from Europe (Mörner, 1970, 1976) and eastern North America (Mott et al., 1986; Broecker et al., 1988), indicating that they may be related. However, evidence of previous warmer terrestrial conditions at either the Bear Cove site or from the nonmarine portion of Core END 87A-23 are lacking. Earlier pollen profiles from the Bear Cove site are primarily pioneering in nature and older sediments from Core END 87A-23 have not been examined for their pollen content. However, Heusser (1960) in an analysis of Late Pleistocene pollen profiles from the east side of Vancouver Island and Mathewes (1973) in a similar analysis of sediments from the Fraser Valley both reported an increase in the proportion of *Tsuga mertensiana* between 11 000 and 10 000 years B.P., isochronous with the Younger Dryas cooling event. Heusser (1973) suggested that this species became more abundant because of a climatic cooling, although Hebda (1983) suggests that an increase in moisture levels would have had a similar effect.

The B_1 sediments of the lower part of cores END 84B-08 and END 84B-10 were deposited shortly after deglaciation, as evidenced by the presence of large proportions of *Cribroelphidium excavatum* in this interval (Fig. 3). *Cribroelphidium excavatum* is an important component of modern foraminiferal faunas on the shelves surrounding North America and Europe, particularly at higher latitudes, where it commonly composes more than 30% of the fauna (Cockbain, 1963; Vilks et al., 1979; and Miller et al., 1982). In Pleistocene sediments, this species has long been associated with glacial conditions, particularly in Wisconsin-aged occurrences where it often constitutes 60-80% of the foraminiferal fauna (Feyling-Hanssen, 1976; Knudsen, 1976; Osterman, 1984; Hald and Vorren, 1987; Rodriguez and Richard, 1986). However, Hald and Vorren (1987) pointed out that this species also lives today in lower latitude areas of the North Atlantic, albeit in much lower numbers. These workers suggested that this species is as much a salinity indicator as a temperature indicator, because these areas are subject to shifting salinities. Furthermore, the low abundance of the cold-water indicator *Cassidulina reniforme* at this horizon suggests that depressed salinities rather than very cold water conditions explain the high proportion of *Cribroelphidium excavatum*. The proportion of *Cribroelphidium excavatum* declines gradually toward the surface through both cores. Osterman (1984) suggested that the reduction in the proportion of *Cribroelphidium excavatum* in modern oceans is related to habitat reduction precipitated by the retreat of glaciers and associated reduction in suitable environments for this species. If this hypothesis is correct the distribution of this species in these cores suggests a gradual response to loss of ecospace.

ACKNOWLEDGMENTS

This research was partly supported by Natural Sciences and Engineering Research Council of Canada Operating Grant OGPOO41665 and Department of Supply and Services Contract 23254-9-05-2/01-XSB. I would like to thank John Luternauer of the Geological Survey of Canada, Vancouver, British Columbia, for providing the core samples examined for this report. I also wish to thank J. Luternauer for providing use of the scanning electron microscope at the Geological Survey of Canada, Vancouver, and to Peter Krauss for assistance in its operation. I also thank J. Luternauer for critically reviewing the manuscript.

REFERENCES

Barrie, J.V. and Bornhold, B.D.
1989: Surficial geology of Hecate Strait, British Columbia continental shelf; Canadian Journal of Earth Sciences, v. 26, p. 1241-1254.

Broecker, W.S., Andree, M., Wolfli, W., Oeschger, H., Bonani, G., Kennett, J., and Peteet, D.
1988: The chronology of the last deglaciation: implications to the cause of the Younger Dryas Event; Paleoceanography, v. 3, p. 1-19.

Brunner, C.A. and Ledbetter, M.T.
1989: Late Quaternary quantitative planktonic foraminiferal biostratigraphy in turbidite sequences of the central California continental margin; Micropaleontology, v. 35, p. 321-336.

Clague, J.J.
1983: Glacio-isostatic effects of the Cordilleran Ice Sheet, British Columbia, Canada; in Shorelines and Isostasy, (ed.) D.E. Smith and A.G. Dawson; Academic Press, London, p. 321-343.

Clague, J.J., Harper, J.R., Hebda, R.J., and Howes, D.E.
1982: Late Quaternary sea levels and crustal movements, coastal British Columbia; Canadian Journal of Earth Sciences, v. 19, p. 597-618.

Cockbain, A.E.
1963: Distribution of foraminifera in Juan de Fuca and Georgia straits, British Columbia, Canada; Contributions from the Cushman Foundation for Foraminiferal Research, v. 14, p. 37-57.

Feyling-Hanssen, R.W.
1976: A mid-Wisconsinian Interstadial on Broughton Island, Arctic Canada, and its foraminifera; Arctic and Alpine Research, v. 8, p. 161-182.

Fürsich, F.T. and Aberhan, M.
1990: Significance of time-averaging for palaeocommunity analysis; Lethaia, v. 23, p. 117-224.

Hald, M. and Vorren, T.O.
1987: Foraminifera stratigraphy and environment of Late Weichselian deposits on the continental shelf off Troms, Northern Norway; Marine Micropaleontology, v. 12, p. 129-160.

Harmon, R.A.
1972: The distribution of microbiogenic sediment near the mouth of the Columbia River; in The Columbia River Estuary and Adjacent Ocean Waters, (ed.) A.T. Pruter and D.L. Alverson; University of Washington Press, Seattle, p. 265-277.

Hebda, R.J.
1983: Late-glacial and postglacial vegetation history at Bear Cove Bog, northeast Vancouver Island, British Columbia; Canadian Journal of Botany, v. 61, p. 3172-3192.

Heusser, C.J.
1960: Late-Pleistocene environments of North Pacific North America; American Geographical Society, Special Publication 35.
1973: Environmental sequence following the Fraser advance of the Juan de Fuca Lobe, Washington; Quaternary Research, v. 3, p. 284-306.

Howes, D.E.
1981: Terrain inventory and geological hazards: northern Vancouver Island; Assessment and Planning Division, Terrestrial Studies Branch, British Columbia Ministry of Environment, Bulletin 5.

Knudsen, K.L.
1976: Foraminifera faunas in Weichselian stadial and interstadial deposits of the Skaerumhede boring, Jutland Denmark; in First International Symposium on Bethonic Foraminifera of Continental Margins, Halifax, 1975, Part B: Paleoecology and Biostratigraphy, (ed.) C. Schafer and B.R. Pelletier; Maritime Sediments, Special Publication 1, p. 131-151.

Luternauer, J.L. and Murray, J.W.
1983: Late Quaternary morphologic development and sedimentation, central British Columbia continental shelf; Geological Survey of Canada, Paper 83-21, 38 p.

Luternauer, J.L., Clague, J.J., Conway, K.W., Barrie, J.V., Blaise, B., and Mathewes, R.W.
1989a: Late Pleistocene terrestrial deposits on the continental shelf of western Canada: evidence for rapid sea-level change at the end of the last glaciation; Geology, v. 17, p. 357-360.

Luternauer, J.L., Conway, K.W., Clague, J.L., and Blaise, B.
1989b: Late Quaternary geology and geochronology of the central continental shelf of western Canada; Marine Geology, v. 89, p. 57-68.

Mathewes, R.W.
1973: A palynological study of postglacial vegetation in the University Research Forest, southwestern British Columbia; Canadian Journal of Botany, v. 51, p. 2085-2103.

Miller, A.A.L., Scott, D.B., and Medioli, F.S.
1982: *Elphidium excavatum* (Terquem); Ecophenotypic versus subspecific variation; Journal of Foraminiferal Research, v. 12, p. 116-144.

Mörner, N.-A.
1970: The Younger Dryas Stadial. Geologiska Föreningens i Stockholm; Förhandlingar, v. 92, p. 5-20.
1976: The Pleistocene/Holocene boundary in southern Sweden; in The Pleistocene/Holocene Boundary: A Proposed Boundary-Stratotype in Gothenburg, Sweden, (ed.) N.-A. Mörner; Boreas, v. 5, p. 197-204.

Mott, R.J., Grant, D.R., Stea, R., and Occhietti, S.
1986: Late-glacial climatic oscillation in Atlantic Canada equivalent to the Allerød/Younger Dryas event; Nature, v. 232, p. 247-250.

Osterman, L.
1984: Benthic foraminifera zonation of a glacial/interglacial transition from Frobisher Bay, Baffin Island, North West Territories, Canada; in Benthos '83, Second International Symposium on Benthic Foraminifera (Pau, 1983), (ed.) H.J. Oertli; Elf Aquitane, Esso REP, TOTAL, CFP, Bordeaux, France, p. 471-476.

Patterson, R.T.
1989: Neogene foraminiferal biostratigraphy of the southern Queen Charlotte Basin; Contributions to Paleontology, (ed.) L. Reynolds; Geological Survey of Canada, Bulletin 396, p. 229-265.
1990: Analysis and interpretation of Quaternary and Holocene benthic foraminifera from the Queen Charlotte-Hecate Strait area; in Current Research, Part F; Geological Survey of Canada, Paper 90-1F, p. 83-86.
in press: Benthic foraminiferal biofacies in Queen Charlotte Sound and Southern Hecate Strait, British Columbia: Late Quaternary distribution and paleoecological importance; Geological Survey of Canada, Paper.

Patterson, R.T. and Fishbein, E.
1989: Re-examination of the statistical methods used to determine the number of point counts needed for micropaleontological quantitative research; Journal of Paleontology, v. 63, p. 245-248.

Rodriguez, C.G. and Richard, S.H.
1986: An ecostratigraphic study of Late Pleistocene sediments of the western Champlain Sea Basin, Ontario and Quebec; Geological Survey of Canada, Paper 85-22, 33 p.

Sejrup, H.P. and Guilbault, J.-P.
1980: *Cassidulina reniforme* and *C. obtusa* (foraminifera), taxonomy, distribution and ecology; SARSIA, v. 65, p. 79-85.

Snyder, S.W.
1989: Relationship between benthic foraminiferal assemblages and Neogene phosphatic sediments, North Carolina coastal plain and continental shelf; in Phosphates of the World, III, (ed.) S.R. Riggs and W. Burnett; Cambridge University Press, Cambridge, U.K., p. 445-465.

Vilks, G., Wagner, F.J.E., and Pelletier, B.R.
1979: The Holocene marine environment of the Beaufort Shelf; Geological Survey of Canada, Bulletin 303, 43 p.

Patterns and rates of sedimentation on the Fraser River delta slope, British Columbia

T.F. Moslow[1], J.L. Luternauer, and R.A. Kostaschuk[2]
Cordilleran Division, Vancouver

Moslow, T.F., Luternauer, J.L., and Kostaschuk, R.A., 1991: Patterns and rates of sedimentation on the Fraser River delta slope, British Columbia; in Current Research, Part E; Geological Survey of Canada, Paper 91-1E, p. 141-145.

Abstract

A process sedimentological description of 17 piston cores up to 5.2 m in length has provided the basis for identifying Late Holocene sedimentation events on the Fraser delta slope. Evidence of seafloor instability is inferred by the high degree of soft sediment deformation. Turbidity current generated deposits are contained within cores adjacent to the Sand Heads submarine channel system and seaward of an abandoned distributary channel on northern Roberts Bank. Preliminary results from Cesium-137 radiometric analyses indicate sedimentation rates of 2.0 cm/a from 1953 to 1963, and 2.2 cm/a for 1963 to 1989.

Résumé

Une description sédimentologique de 17 échantillons de carotteuse à piston de longueur atteignant 5,2 m a permis d'identifier des phénomènes de sédimentation de l'Holocène récent sur la pente du delta du Fraser. La preuve de l'instabilité du fond marin découle du degré élevé de déformation des sédiments mous. Des dépôts produits par les courants de turbidité se retrouvent dans des carottes prélevées près du réseau de chenaux sous-marins de Sand Heads et du côté faisant face à la mer d'un chenal d'effluent abandonné sur la partie nord du banc Roberts. Les résultats préliminaires des analyses radiométriques au césium 137 indiquent des vitesses de sédimentation de 2,0 cm/a de 1953 à 1963 et de 2,2 cm/a de 1963 à 1989.

[1] Department of Geology, University of Alberta, Edmonton, Alberta T6G 2E3
[2] Department of Geography, University of Guelph, Guelph, Ontario N1G 2W1

INTRODUCTION

This study provides an analysis and synthesis of lithological characteristics of piston cores collected by the Geological Survey of Canada to meet objectives of the GSC's environmental and geohazards assessment of the Fraser River delta. Specific objectives include: 1) an investigation of the patterns and rates of sedimentation on the Fraser River delta slope through use of radiometric dating of core samples, and 2) an analysis of instability processes and deposits on the Fraser River delta slope.

The first objective will be achieved through interpretation of Cesium-137 radiometric analyses of samples from piston cores from the Fraser delta slope. A determination will be made of sedimentation rates and recurrence interval of sedimentary processes at various core locations seaward of Sturgeon and Roberts Bank.

The second objective will involve compilation and analysis of geological and geophysical data collected during the July 24 to August 4, 1989 research cruise on the Fraser delta slope. Emphasis has been placed on the sedimentological description of piston cores in order to examine the sedimentary record of any instability events and document the internal sedimentologic fabric of associated deposits.

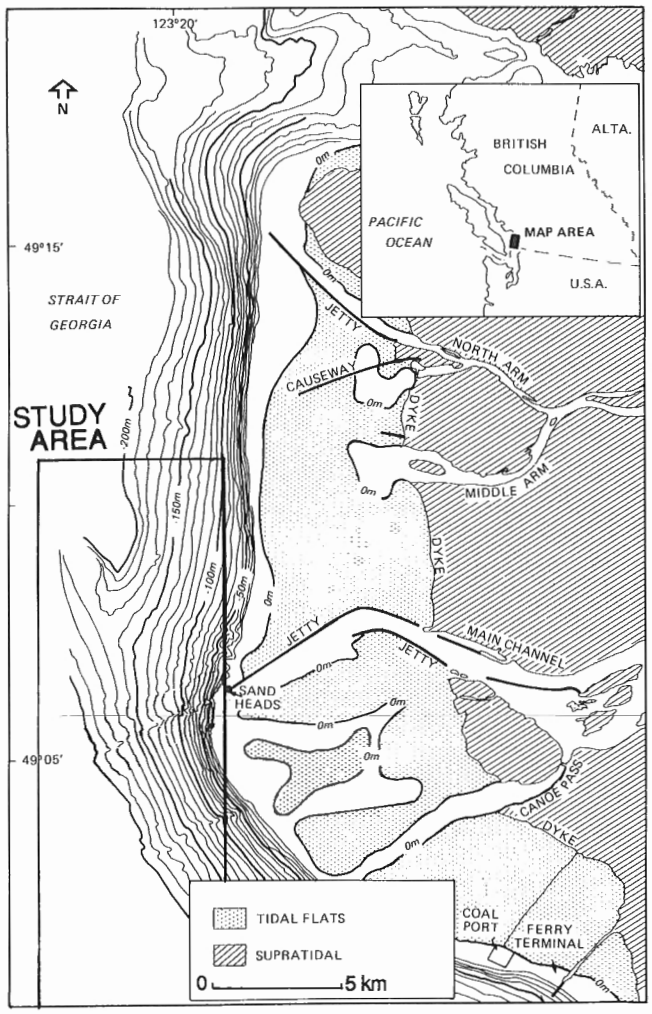

Figure 1. Location map of study area within the Fraser River delta slope. Area enclosed within the rectangular box is shown in greater detail in Figure 2 (from Kostaschuk et al., in press).

METHODS

Piston cores taken on the Fraser River delta slope during the CSS Vector-1989 cruise have been described using a process-sedimentological approach to identify sedimentary facies and genetic stratigraphic units. For Cesium-137 analysis, subsamples were taken from three cores, at 5 or 10 cm intervals from the tops of the cores to depths of approximately 2 m. Sample preference is given to the silt and clay units, as opposed to sand deposits, as the finer grained sediment fraction is associated with higher concentrations of Cesium-137. With subsequent interpretation of results, the sampling technique can be modified to a different resolution or to a different depth in the core, but minimally to the 1953 fallout horizon. Cesium-137 activity in each section was determined using the methods of Delaune et al. (1982), De Jong (1982) and Kiss et al. (1988). Results were plotted graphically to display temporal and spatial variability in sedimentation rates.

GEOLOGICAL SETTING

The Fraser River delta is located south of Vancouver, British Columbia, and is the largest, most important delta on the west coast of Canada. The Fraser delta shoreline bordering Georgia Strait is 40 km long. This seaward margin consists of a series of tidal flats up to 9.0 km in width with an average slope of <0.1° (Fig. 1) (Clague et al., in press).

The study area for this research project is an approximately 20 km long, 7.5 km wide portion of the subaqueous platform of the Fraser delta (Fig. 1), commonly referred to as the delta slope. Water depths in this part of the slope increase from -50 m to -200 m over approximately 3.0 km distance at an average gradient exceeding 3°. The relative steepness of this slope compared to many other delta slope environments, probably contributes to the unstable nature of the subaqueous portion of the Fraser River delta. The concern over the stability of the subaerial and subaqueous portions of the Fraser delta in response to earthquakes has provided the impetus for geological investigations of the nature reported here.

RESULTS

Locations of piston cores described and analyzed for this study are shown in Figure 2. All but three of the 17 core sites are located between the 50 m and 200 m isobath on the delta slope. Core sites were chosen in an attempt to develop along-slope and cross-slope transects that would best display shallow subsurface facies relationships. The cross-slope transects are oblique or perpendicular to the incised channels or "seavalleys" (Kostaschuk et al., in press) that cut across the delta slope. Transects A-A' and C-C' are designed to examine distal-proximal facies relationships across the slope for Roberts and Sturgeon banks respectively (Fig. 2).

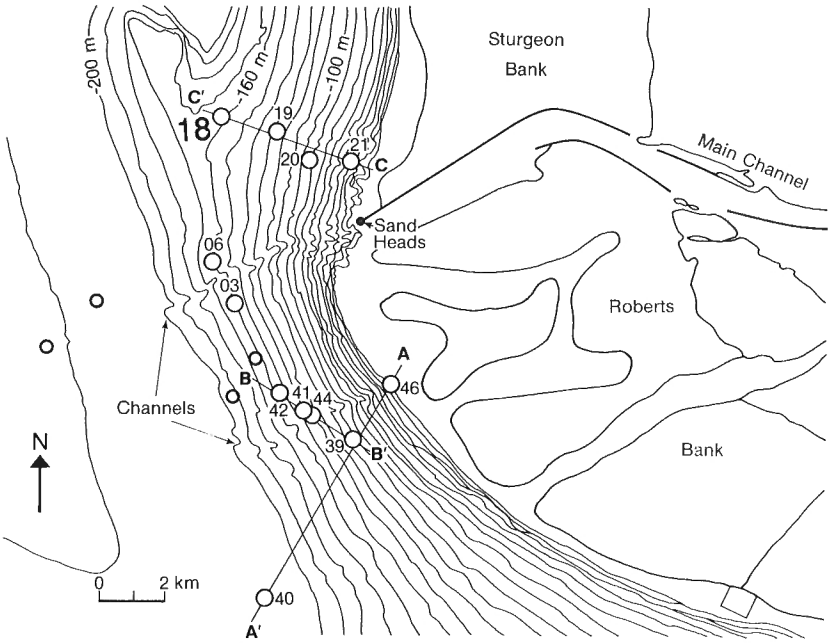

Figure 2. Map displaying bathymetric contours at a 5 and 10 m contour interval for the portion of the Fraser delta slope examined in this study. All but one of 17 piston core sites are indicated by open circles and identified by numbers. A sedimentological description for core VEC 89A-18 at the downslope end of transect C-C' is shown in Figure 3.

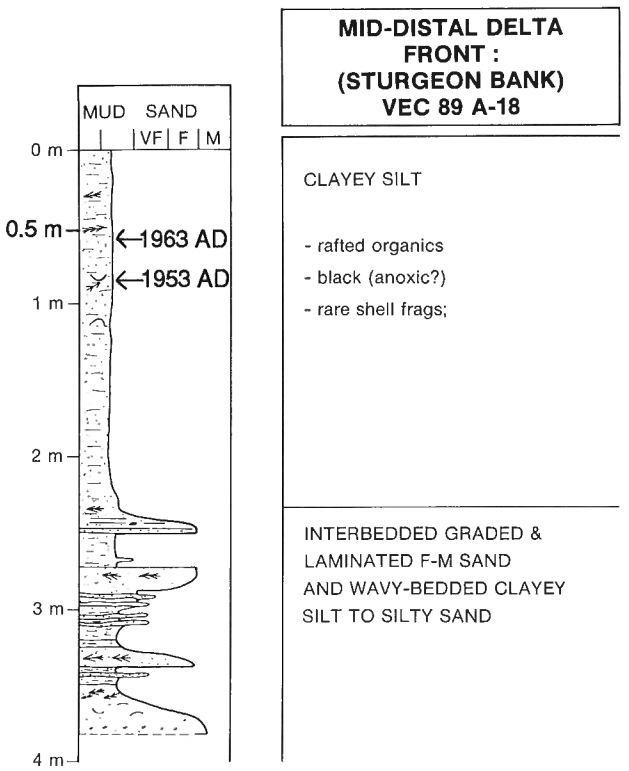

Figure 3. Sedimentological description and graphic log of sedimentary facies for VEC 89A-18. Core location is shown in Figure 2.

A graphic representation of core VEC 89A-18 is shown in Figure 3. This core site is located on the Sturgeon Bank slope at the distal end of transect C-C' in approximately 160 m water depth (Fig. 2). Core VEC 89A-18 is 3.75 m long and consists of two sedimentary facies. The lower 1.5 m of the core is an interbedded fine- to medium-grained sand and clayey silt to silty clay, referred to as the interbedded sand and silt facies. Sand beds are 20 cm to 50 cm thick with abrupt basal contacts. Resedimented organic detritus, comprised mostly of plant material, commonly occurs on bedding planes and within laminations. Sand beds are normally graded and display parallel subhorizontal to horizontal laminations and are interpreted as a product of sediment gravity flows, probably turbidity currents. The clayey silt to silty sand beds average 5 cm to 15 cm thick, are graded at their base and display parallel laminations and wavy bedding. These finer grained interbeds are inferred to be a product of a combination of suspension sedimentation and current transport under tranquil or waning flow. Based in large part on the observations of cored sequences observed from sites immediately adjacent to the Sand Heads seavalley, the interbedded sand and silt facies is interpreted to be either: 1) an abandoned, or relict, delta slope channel deposit; or 2) non-channelized sediment gravity flow deposits produced by upslope failures.

The overlying 2.25 m of VEC 89A-18 is a massive-appearing or faintly laminated clayey-silt. This clayey silt facies contains rafted organics, mostly as resedimented plant material and some shell fragments (Fig. 3). Examination of X-ray radiographs of this facies in several cores revealed two identifiable *Skolithos* burrow traces less than 1.0 cm in length, and several examples of convoluted to deformed silty laminations. This facies is inferred to be a product of suspension deposition occurring primarily in association with sediment

Table 1. Sedimentation rates for VEC 89-A-18, Fraser Delta Slope

Time Period (years AD)	Average Rate of Sedimentation
1953-1963	2.00 cm/a
1963-1989	2.22 cm/a
1953-1989	2.16 cm/a

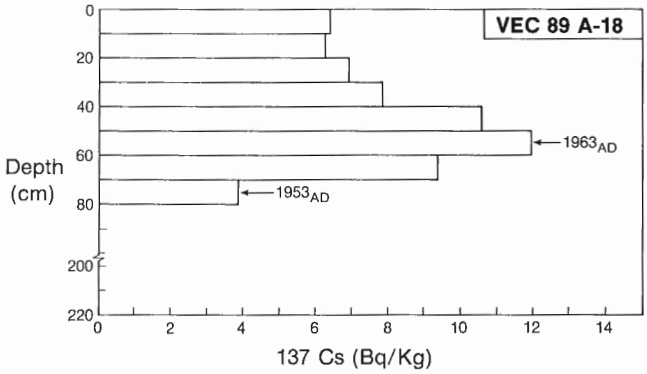

Figure 4. Plot of Cesium -137 concentration versus depth in core VEC 89A-18. The inferred 1953 AD and 1963 AD time horizons are labelled.

discharge from the mouth of the Main Channel distributary. Soft-sediment deformation features observed in cores suggest post-depositional alteration due to instability on the delta slope.

Cesium-137 concentrations were determined from subsamples taken every 10 cm from the top of the core to the first sand layer at -2.25 m in VEC 89A-18. The results are displayed graphically in Figure 4 for the sampled section in VEC 89A-18. Measurable concentrations of Cesium-137 were detected at a depth of -80 cm in the core and are interpreted as the 1953 AD horizon, marking the initiation of Cesium-137 dispersion into the atmosphere through nuclear weapons tests (Delaune et al., 1982). Cesium-137 concentrations in VEC 89A-18 peak at -50 cm. This interval is interpreted to represent the 1963 AD horizon that reflects the proliferation of hydrogen bomb detonations preceding the Nuclear Weapons Test Ban Treaty (Fig. 4).

Assuming that the top of the cored interval reflects the 1989 sampling date, three time horizons exist within the core. These rates are summarized in Table 1. The time horizons determined from Cesium-137 concentrations are labelled on the graphic log of VEC 89A-18 (Fig. 3). An average sedimentation rate of 2.0 cm/year was calculated for the interval between the 1953 AD and 1963 AD time horizons, and 2.22 cm/year for the 1963-1989 interval (Table 1). The average sedimentation rate for the entire period of record, 1953 to 1989, is 2.16 cm/year. Assuming a constant rate of sedimentation for the upper fine grained unit, an extrapolation of these values yields 2.16 m/century or 21.6 m/millennium of fine grained sediment accumulation on the Fraser delta slope. While these values are relatively high for many marine or deltaic environments of deposition in 160 m water depth, it has been suggested that sedimentation rates on the Fraser delta slope and plain were much higher just 3000 to 5000 years ago (Clague et al., in press).

STATUS OF INVESTIGATIONS AND PRELIMINARY CONCLUSIONS

Preliminary results from sedimentological analyses of 17 piston cores taken on the Fraser delta slope (only one of which is described in detail here) indicate that instability processes have played an important role in the recent depositional history of the subaqueous portion of the Fraser delta. Soft-sediment deformation features, especially convoluted laminations, are found in fine- and coarse-grained deposits and are likely a product of sediment dewatering due to differential loading or mass wasting. Evidence for turbidity current generated deposition is contained within cores on the delta slope adjacent to the Sand Heads submarine channel system. Several 25 cm thick, normally graded beds of medium grained sand to coarse silt are found in all cores from this area between 2.5 m and 4.2 m beneath the seafloor. Sedimentary and textural characteristics of these beds display Bouma sequences. Similar deposits are found seaward of an abandoned distributary channel on northern Roberts Bank, and in the lower half of core VEC 89A-18 in 160 m water depth near southern Sturgeon Bank (Fig. 2, 3). Chaotically bedded deposits consisting of 75% resedimented plant material and 25% poorly sorted lithic sand may have up to 7.0 km of lateral continuity across the slope off of southern Roberts Bank. These deposits are interpreted to be a product of debris flows.

Preliminary results from Cesium-137 radiometric analyses indicate a sedimentation rate of 2.16 cm/year averaged over the period of record from 1953 AD to 1989 AD. These results are derived from Cesium-137 concentrations within the uppermost 80 cm of core VEC 89A-18 from a clayey silt sedimentary facies. This overlies an interbedded sand and silt facies interpreted as either a buried slope channel sediment or gravity flow deposit produced by upslope failures (Fig. 3). If the preliminary radiometric results and sedimentological interpretations are accurate, then it may be concluded that delta slope channel deposits are readily preserved beneath the sea floor and rapidly covered with fine-grained sediments.

Further Cesium-137 radiometric analyses are being conducted to determine the temporal and spatial variability of sedimentation rates on the Fraser delta slope.

ACKNOWLEDGMENTS

B. Hart and G. McKenna kindly offered many helpful suggestions for improving the first draft of this manuscript.

REFERENCES

Clague, J.L., Luternauer, J.L., Pullan, S.E., and Hunter, J.A.
in press: Postglacial deltaic sediments, southern Fraser River delta, British Columbia; Canadian Journal of Earth Sciences.

DeLaune, R.D., Baumann, R.H., and Gosselink, J.G.
1982: Relationships among vertical accretion, coastal submergence, and erosion in a Louisiana gulf coast marsh; Journal of Sedimentary Petrology, v. 53, p. 147-157.

De Jong, E., Villar, H., and Bettany, J.R.
1982: Preliminary investigations on the use of Cesium-137 to estimate erosion in Saskatchewan; Canadian Journal of Soil Science, v. 62, p. 673-683.

Kiss, J.J., De Jong, E., and Bettany, J.R.
1988: The distribution of natural radionuclides in native soils of southern Saskatchewan, Canada; Journal of Environmental Quality, v. 17, p. 437-445.

Kostaschuk, R.A., Luternauer, J.L., McKenna, G.T., and Moslow, T.F.
in press: Sediment transport in a submarine channel system: Fraser River delta, Canada; Journal of Sedimentary Petrology.

Phanerozoic time scale, biochronology, geochronometry, and some mineral deposits in the Canadian Cordillera and adjacent parts of Alaska

R.G. Anderson (compiler)
Cordilleran Division, Vancouver

Anderson, R.G., (comp.), 1991: Phanerozoic time scale, biochronology, geochronometry, and some mineral deposits in the Canadian Cordillera and adjacent parts of Alaska; in Current Research, Part E; Geological Survey of Canada, Paper 91-1E, p. 147-153.

Abstract

The time scale compilation presented here has three objectives: to illustrate the diversity of Canadian Cordilleran fossil biotas and underscore their importance in precise age dating; to indicate the correlation of a numerical time scale based on isotopic ages to the "relative" but more precise biochronology; and to list well dated and well known mineral deposits typical of some Cordilleran metallogenic environments and episodes.

Résumé

La compilation de l'échelle chronologique présentée ici vise trois objectifs: illustrer la diversité des biotes de fossiles de la Cordillère canadienne et souligner leur importance au regard d'une datation précise; indiquer la corrélation qui existe entre l'échelle chronologique numérique basée sur les âges isotopiques et la biochronologie qui est "relative" mais plus précise; et énumérer les gisements minéraux bien datés et bien connus qui sont typiques de certains phénomènes et épisodes métallogéniques de la Cordillère.

INTRODUCTION

Time is geology's fourth dimension. The breadth of geological time makes geology not only special among physical sciences but provides a long-ranging perspective with which to interpret crustal processes including mineral deposition.

For well over a century, paleontologists with the Geological Survey of Canada (GSC), universities and industry have provided age determinations which have been instrumental in developing a stratigraphy and correlation of the Phanerozoic rocks of the western Canadian Cordillera and have contributed to a time scale of worldwide application. The time scale compilation (Fig. 1) purports to: illustrate the diversity of Canadian Cordilleran fossil biotas and underscore their importance in precise age dating; indicate the correlation of a numerical time scale based on isotopic ages to the "relative" but more precise biochronology; and list well dated and well known mineral deposits typical of some Cordilleran metallogenic environments and episodes. This note supersedes a compilation provided as a hand-out for the Cordilleran Roundup session "Time-the Fourth Dimension in Understanding Cordillera Geology and Mineral Deposits" held in Vancouver, B.C., January 29, 1991.

BIOCHRONOLOGY

The first, best known, and probably most important role of fossils is their use as geological chronometers. The time scale comprises successively finer divisions of time: periods (e.g. Triassic), epochs (e.g. Late Triassic), and ages (e.g. Norian). Development of the time scale was based on the observation that certain rock horizons were endowed with distinct and characteristic fossil assemblages recognizable over broad regions. These rock units represent geological stages, the basic building blocks of the geological time scale. Each stage can potentially be subdivided into fossil zones, provided that sufficient stratigraphic and taxonomic work has defined more than one stratigraphically unique fossil association within the stage. The succession of fossil zones represents biochronological divisions of very short time span — at some levels, less than 1 million years. For some biota (e.g. early Paleozoic and late Mesozoic radiolaria), precise zonations have been developed elsewhere but have yet to be confirmed or refined in the Canadian Cordillera.

Through the efforts of GSC, university and industry paleontologists, the Canadian Cordilleran biochronological scheme was developed and continues to be refined. Geological mapping and mineral and hydrocarbon exploration are the principal beneficiaries. The following paleontologists have provided published and unpublished data incorporated into the time scale: Wayne Bamber (GSC), Joanna Beyers (University of B.C.), Bruce Cameron (GSC), Beth Carter (Consultant), Fabrice Cordey (PDF, GSC), Peter Forster (University of B.C.), Bill Fritz (GSC), Jim Haggart (GSC), Russell Hall (University of Calgary), Charles Henderson (University of Calgary), Steve Irwin (University of B.C.), Sandy McCracken (GSC), Colin McGregor (GSC), Dave McNeil (GSC), Bernard Mamet (Université de Montréal), Walter Nassichuk (GSC), Brian Norford (GSC), Willy Norris (GSC), Godfrey Nowlan (GSC), Mike Orchard (GSC), Tim Patterson (Carleton University), Alan Pedder (GSC), Terry Poulton (GSC), Paul Smith (University of B.C.), Art Sweet (GSC), Ray Thorsteinsson (GSC), Howard Tipper (GSC), Tim Tozer (GSC), John Utting (GSC), Tom Uyeno (GSC), John Wall (GSC), and James White (GSC).

NUMERICAL TIME SCALE

Calibration of paleontologically well-dated intervals by isotopic dating provides numerical estimates for durations of stages, yields dates for geological events and is the basis for the numerical time scale. However, the precision limitations of isotopic dating and the rarity of biostratigraphically well controlled sequences suitable for dating prohibit the same precision achievable with biochronology. The Decade of North American Geology (DNAG) time scale (Palmer, 1983) was used as the standard for the DNAG Geology of the Cordilleran Orogen in Canada volume (Gabrielse and Yorath, 1989; in press) and as a framework for plotting dated mineral deposits in Figure 1.

Alternatively, the newer and more precise time scale of Harland et al. (1990) could have been used (Fig. 2). The greatest divergence between the two scales concerns the Early Cretaceous, Middle and Early Jurassic, Middle Triassic, Permian, Late Carboniferous, Early Devonian and Early Silurian, and Late Cambrian calibrations. Compared with the DNAG time scale, the Harland time scale has smaller uncertainties. The uncertainties in stage boundaries picks are important when trying to correlate isotopically dated events with the biochronological time scale. For example, uncertainties in Early Jurassic stage boundary ages in the DNAG scale are about one-half the duration of the Jurassic period; they are equally significant but only on the order of one or two stage durations according to the Harland et al. (1990) scale.

MINERAL DEPOSIT AGE AND CORDILLERAN METALLOGENY

Fossil-rich strata which host mineral deposits provide a maximum age for the mineralizing event. When mineral deposition occurred simultaneously with deposition of the dated horizon, e.g. sedimentary exhalative (SEDEX) and volcanogenic massive sulphide (VMS) deposits, biochronology provides a precise age estimate of the age of mineralization. Examples of Silurian, Devonian, and Early Carboniferous (Mississippian) mineral deposits whose ages are well constrained by the conodont ages of their bounding strata include: the SEDEX Llandoverian Howards Pass and Vulcan base metal deposits; Eifelian-Givetian Walt/Cathy barite deposit; Frasnian Macmillan Pass base metal deposit; Famennian Driftpile, Cirque, and Fluke base metal deposits; and Mississippian Tea barite deposit. A Late Triassic example is the Windy-Craggy VMS deposit. Radiolarian biochronology holds great potential for delimiting the age of Jurassic stratabound VMS deposits such as at Eskay Creek.

K-Ar, $^{40}Ar/^{39}Ar$, and zircon U-Pb geochronometry play a comparable role to fossils for plutons and nonfossiliferous volcanic strata hosting base and precious metal veins. Ages of mineralization based on isotopic dates may be more interpretative than ages of SEDEX deposits based on biochronology, however, because commonly it is difficult to date the mineralization directly. The geochronologist must rely on dates of host and crosscutting igneous units to bracket the age of mineralization. Examples abound: Triassic-Jurassic Highland Valley porphyry Cu-Mo; Early Jurassic Iskut "Golden Triangle" mesothermal and epithermal precious metal; Early Cretaceous Britannia base metal VMS; Late Cretaceous Bralorne-Pioneer mesothermal precious metal; Eocene Grew Creek Au; and Late Miocene Salal Creek porphyry Mo deposits are a few of the well known and well dated deposits.

The mineral deposits listing was based on Chapter 19 ("Metallogeny") in the DNAG Canadian Cordilleran Orogen volume (Dawson et al., in press). GSC Cordilleran Division regional mappers as well as mineral deposit experts and/or geochronologists Grant Abbott (Geological Services, INAC), Georges Beaudoin (University of Ottawa), Ken Dawson (GSC), Phillipe Erdmer (University of Alberta), Tryg Höy (B.C. Geological Survey Branch [BCGSBr]), Rod Kirkham (GSC), Dave Lefebure (BCGSBr), Craig Leitch (GSC), Bill McMillan (BCGSBr), Jim Mortensen (GSC), Randy Parrish (GSC), Chris Roddick (GSC), Don Sangster (GSC), Dave Sinclair (GSC), and Bob Turner (GSC) provided discussion, many useful comments, and unpublished data to supplement or revise the DNAG mineral deposit lists.

ACKNOWLEDGMENTS

Editing assistance on the AutoCAD graphic files by Bud Patel and on an earlier version of the manuscript by Bev Vanlier is appreciated.

REFERENCES

Dawson, K.M., Panteleyev, A., Sutherland Brown, A., and Woodsworth, G.J.
in press: Chapter 19, Metallogeny; in Geology of the Cordilleran Orogen in Canada; (ed.) H. Gabrielse and C.J. Yorath; Geological Survey of Canada, Geology of Canada, no. 4 (also Geological Society of America, The Geology of North America, v. G2).

Gabrielse, H. and Yorath, C.J.
1989: DNAG #4. The Cordilleran Orogen in Canada. Geoscience Canada, v. 16, no. 2, p. 67-83.

_____ (editors).
in press: Geology of the Cordilleran Orogen in Canada; Geological Survey of Canada, Geology of Canada, no. 4 (also Geological Society of America, The Geology of North America, v. G2).

Harland, W.B., Armstrong, R.L., Cox, A.V., Craig, L.E., Smith, A.G., and Smith, D.G.
1990: A Geological Time Scale 1989; Cambridge University Press, 279 p.

Palmer, A.R.
1983: The Decade of North American Geology 1983 geologic time scale; Geology, v. 11, p. 503-504.

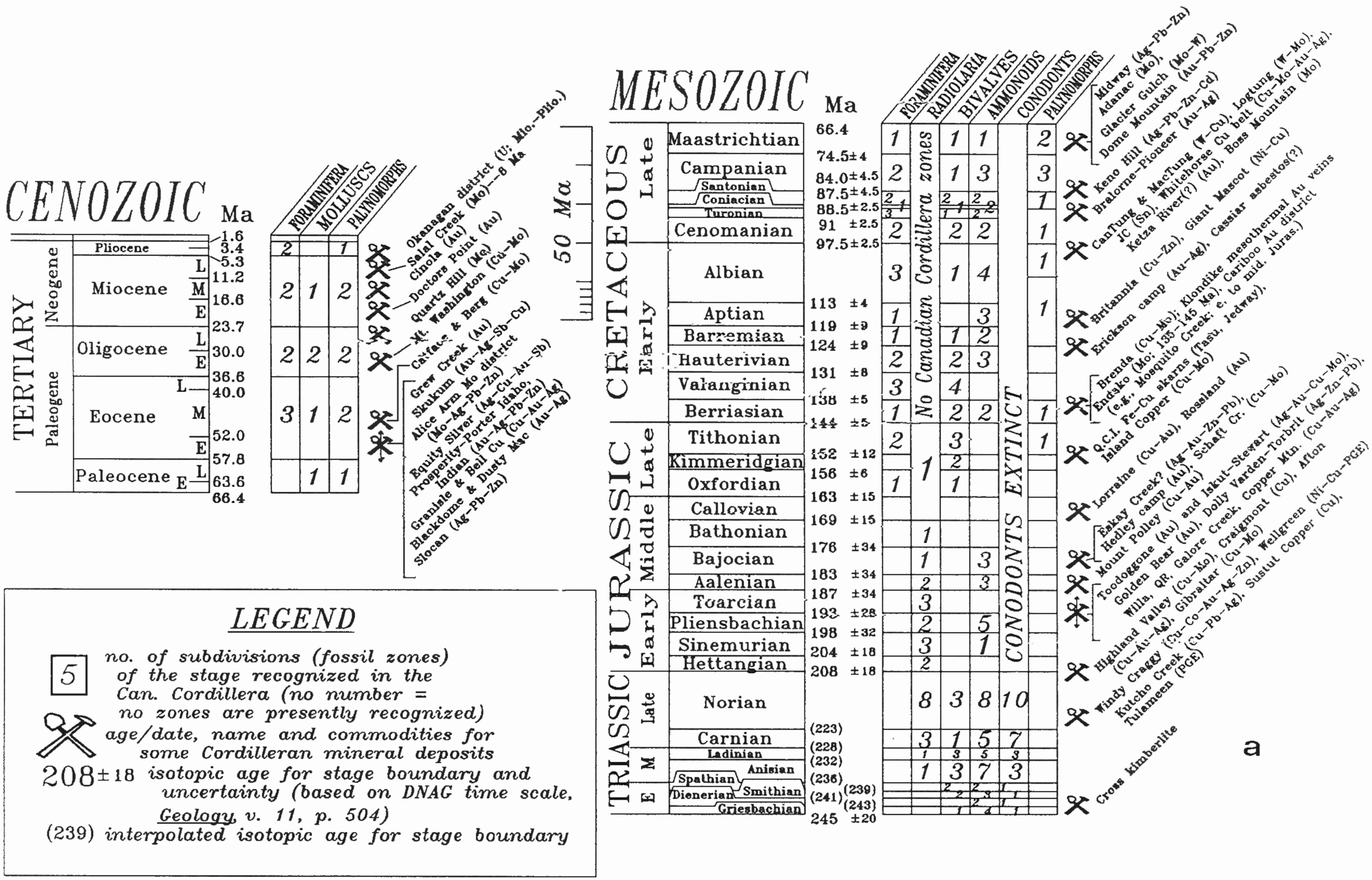
CENOZOIC
Ma
TERTIARY
Neogene
Paleogene
Pliocene
Miocene
Oligocene
Eocene
Paleocene
1.6
3.4
5.3
11.2
16.6
23.7
30.0
36.6
40.0
52.0
57.8
63.6
66.4
FORAMINIFERA
MOLLUSCS
PALYNOMORPHS
Okanagan district (U; Mio.-Plio.)
Salal Creek (Mo)—8 Ma
Cinola (Au)
Doctors Point (Au)
Quartz Hill (Mo)
Mt. Washington (Cu-Mo)
Catface & Berg (Cu-Mo)
Grew Creek (Au)
Skukum (Au-Ag-Sb-Cu)
Alice Arm Mo district
(Mo-Ag-Pb-Zn)
Equity Silver (Ag-Cu-Au-Sb)
Prosperity-Porter Idaho (Au-Ag-Pb-Zn)
Indian & Bell Cu (Cu-Au-Ag)
Granisle & Dusty Mac (Au-Ag)
Blackdome
Slocan (Ag-Pb-Zn)
50 Ma
MESOZOIC
Ma
CRETACEOUS
JURASSIC
TRIASSIC
Late
Early
Middle
M
E
Maastrichtian
Campanian
Santonian
Coniacian
Turonian
Cenomanian
Albian
Aptian
Barremian
Hauterivian
Valanginian
Berriasian
Tithonian
Kimmeridgian
Oxfordian
Callovian
Bathonian
Bajocian
Aalenian
Toarcian
Pliensbachian
Sinemurian
Hettangian
Norian
Carnian
Ladinian
Anisian
Spathian
Smithian
Dienerian
Griesbachian
66.4
74.5±4
84.0±4.5
87.5±4.5
88.5±2.5
91 ±2.5
97.5±2.5
113 ±4
119 ±9
124 ±9
131 ±8
138 ±5
144 ±5
152 ±12
156 ±6
163 ±15
169 ±15
176 ±34
183 ±34
187 ±34
193 ±28
198 ±32
204 ±18
208 ±18
(223)
(228)
(232)
(236)
(239)
(241)
(243)
245 ±20
FORAMINIFERA
RADIOLARIA
BIVALVES
AMMONOIDS
CONODONTS
PALYNOMORPHS
No Canadian Cordillera zones
CONODONTS EXTINCT
Midway (Ag-Pb-Zn)
Adanac (Mo)
Glacier Gulch (Mo-W)
Dome Mountain (Au-Pb-Zn)
Keno Hill (Ag-Pb-Zn-Cd)
Bralorne-Pioneer (Au-Ag)
CanTung & MacTung (W-Cu), Logtung (W-Mo),
JC (Sn), Whitehorse Cu belt (Cu-Mo-Au-Ag),
Ketza River(?) (Au), Boss Mountain (Mo)
Britannia (Cu-Zn), Giant Mascot (Ni-Cu)
Erickson camp (Au-Ag), Cassiar asbestos(?)
Brenda (Cu-Mo); Klondike mesothermal Au veins
Endako (Mo; 135-145 Ma), Cariboo Au district
(e.g., Mosquito Creek; e. to mid. Juras.)
Fe-Cu skarns (Tasu, Jedway),
Q.C.I. Island Copper (Cu-Mo)
Lorraine (Cu-Au), Rossland (Au)
Eskay Creek? (Ag-Au-Zn-Pb), Schaft Cr. (Cu-Mo)
Hedley camp (Au)
Mount Polley (Cu-Au)
Toodoggone (Au) and Iskut-Stewart (Ag-Au-Cu-Mo),
Golden Bear (Au), Dolly Varden-Torbrit (Ag-Zn-Pb),
Willa, QR, Galore Creek, Copper Mtn. (Cu-Au-Ag)
Highland Valley (Cu-Mo), Craigmont (Cu), Afton
(Cu-Au-Ag), Gibraltar (Cu-Mo)
Windy Craggy (Cu-Co-Au-Ag-Zn), Wellgreen (Ni-Cu-PGE),
Kutcho Creek (Cu-Pb-Ag), Sustut Copper (Cu),
Tulameen (PGE)
Cross kimberlite
a
LEGEND
5 no. of subdivisions (fossil zones) of the stage recognized in the Can. Cordillera (no number = no zones are presently recognized)
age/date, name and commodities for some Cordilleran mineral deposits
208±18 isotopic age for stage boundary and uncertainty (based on DNAG time scale, Geology, v. 11, p. 504)
(239) interpolated isotopic age for stage boundary

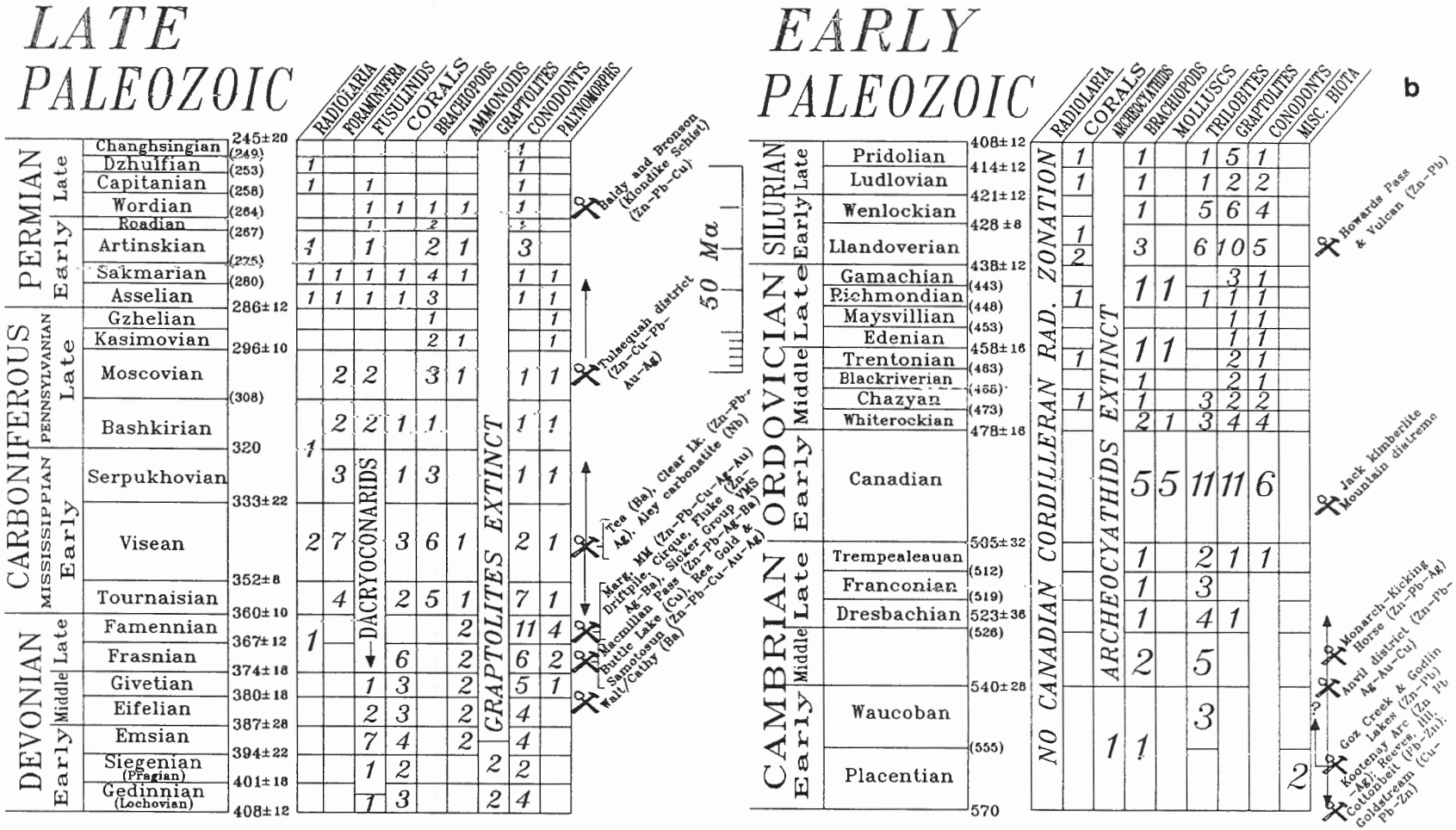

Figure 1. DNAG Phanerozoic time scale, biochronology, geochronometry, and some mineral deposits in the Canadian and Alaskan Cordillera. Estimates for numerical values of boundaries of stages not included in the DNAG time scale are shown in parentheses and interpolated between known stage boundary picks of Palmer (1983).

CENOZOIC AND MESOZOIC

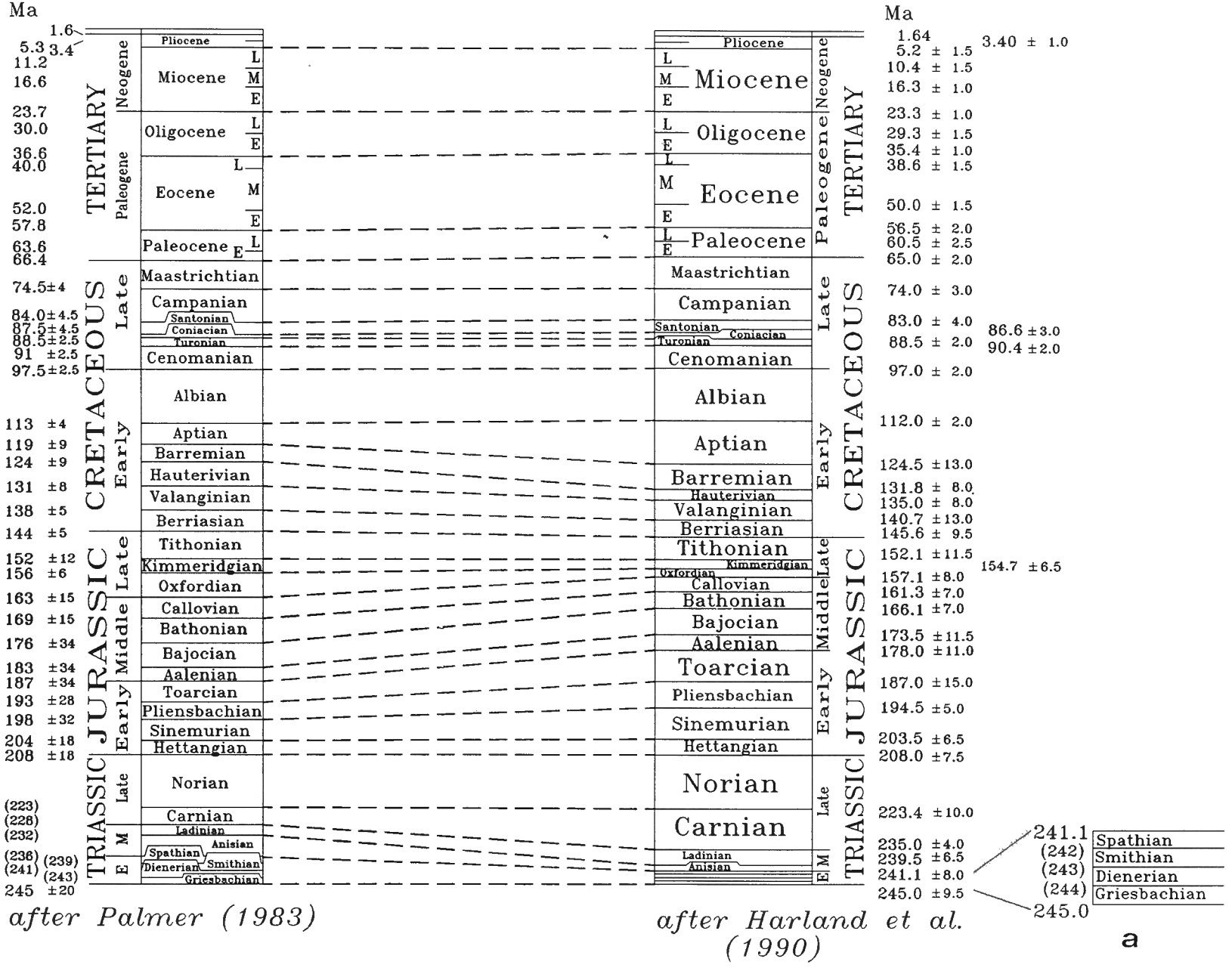

Figure 2. Comparison between time scales of Palmer (1983, left columns) and Harland et al. (1990; right columns), both drawn to scale. As in Figure 1, parenthesized values for boundaries of stages not included in these scales are interpolated between known stage boundary picks. The base of the Cambrian period is the datum for the Paleozoic part of the scale, the base of the Triassic period the datum for the Mesozoic and Cenozoic part of the scale.

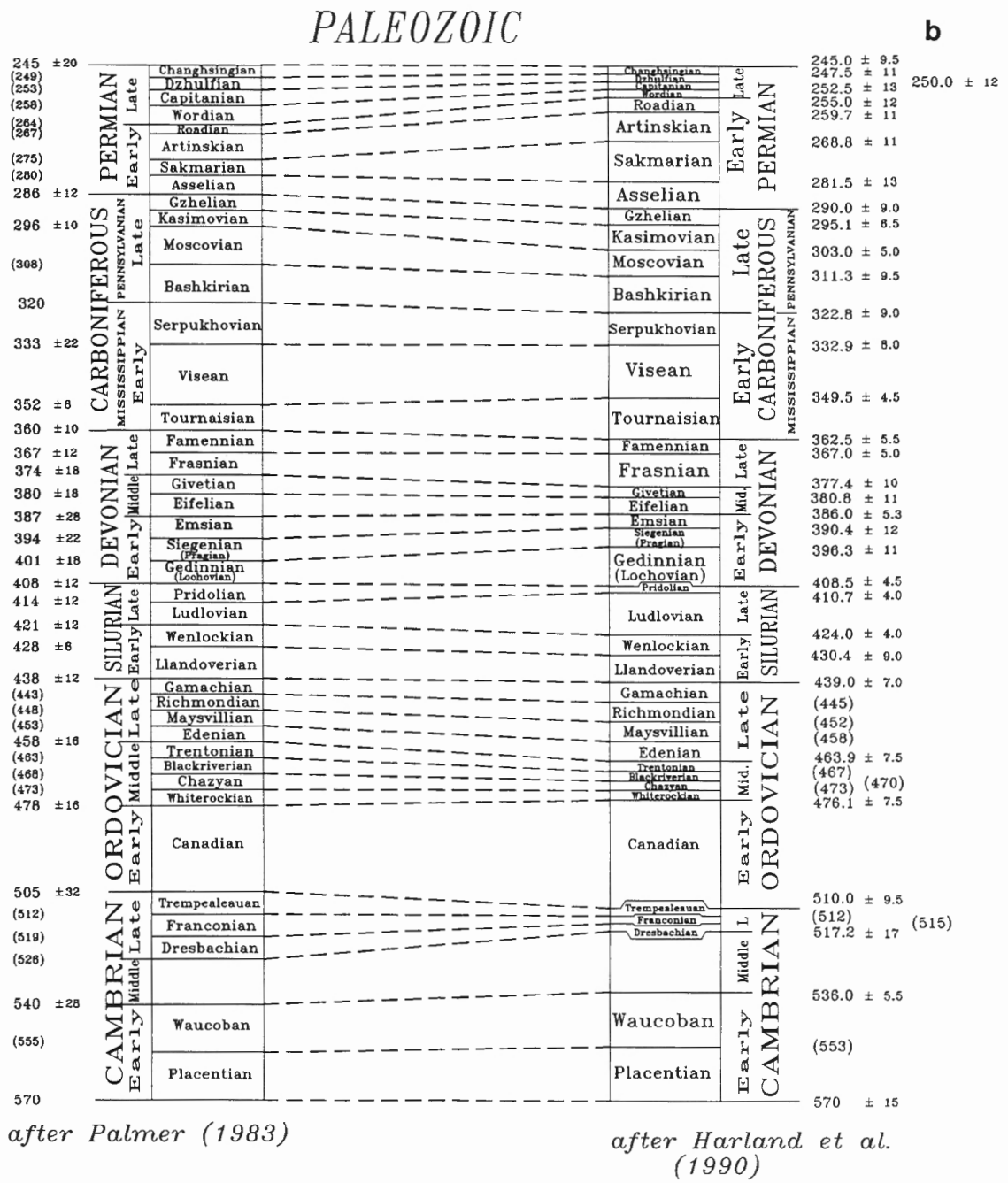

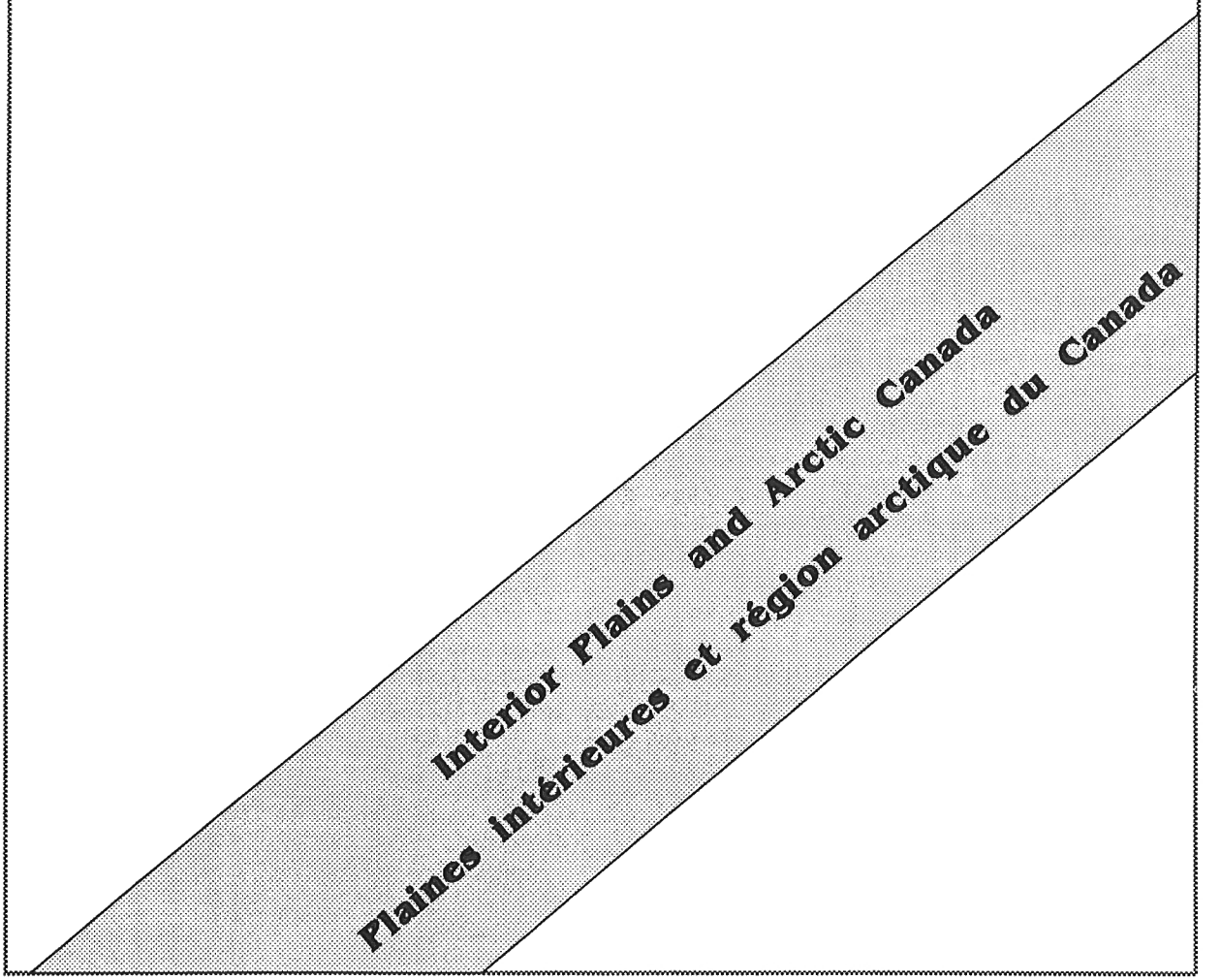
Interior Plains and Arctic Canada
Plaines intérieures et région arctique du Canada

Surficial materials of Hot Weather Creek basin, Ellesmere Island, Northwest Territories

D.A. Hodgson, D.A. St-Onge, and S.A. Edlund
Terrain Sciences Division

Hodgson, D.A, St-Onge, D.A., and Edlund, S.A., 1991: Surficial materials of Hot Weather Creek basin, Ellesmere Island, Northwest Territories; in Current Research, Part E; Geological Survey of Canada, Paper 91-1E, p. 157-163.

Abstract

The 140 km^2 lowland basin, which contains no glaciers, drains south via an incised creek into Slidre River. The dominant surface material is weathered and colluviated bedrock composed of silty sand and clasts derived from poorly consolidated clastics of the upper Cretaceous-lower Tertiary Eureka Sound Group. High terraces of Neogene fluvial sands have been partially recycled into lower deposits, possibly in the Quaternary. The gravelly till veneer over the terrace remnants is reduced to scattered clasts on adjacent materials. The central and southern basin below 145 m elevation was inundated by the early Holocene (and possibly older) sea into which thick fine grained sediments were deposited; locally, massive ground ice in these marine deposits triggers failures. Holocene emergence approximates a glacioisostatic pattern, despite the lack of clear evidence of a preceding ice cover over western Fosheim Peninsula. Peat deposits to several metres thick in wetlands have yielded middle Holocene ages.

Résumé

Le bassin de basses terres de 140 km^2, qui ne contient aucun glacier, se draine au sud par un ruisseau encaissé dans la rivière Slidre. Le matériau de surface dominant est de la roche en place altérée et colluviée, composée de sable silteux et de fragments de roche provenant de roches clastiques faiblement consolidées du Crétacé et du Tertiaire inférieur du groupe d'Eureka Sound. Des terrasses élevées de sable fluviatile du Néogène ont été partiellement remaniées en dépôts inférieurs, peut-être durant le Quaternaire. La pellicule de till graveleux couvrant les vestiges de la terrasse est dispersée en fragments sur les matériaux adjacents. Le bassin du centre-sud d'altitude inférieur à 145 m a été inondée par la mer de l'Holocène inférieur (voire d'une époque plus ancienne) dans laquelle d'épais sédiments à grains fins se sont déposés; par endroits dans ces dépôts marins, des pingos massifs déclenchent des ruptures. L'émergence de l'Holocène a un caractère glacioisostatique, malgré le manque de preuve évidente de la précédence d'une couverture de glace sur la partie ouest de la péninsule de Fosheim. Les dépôts de tourbes de plusieurs mètres d'épaisseur dans les marais remonteraient à l'Holocène moyen.

INTRODUCTION

The lower drainage basin of Hot Weather Creek (HWCk) is the focus of a number of continuing studies of climate, vegetation, soil hydrology, and past and present geomorphic processes (Edlund et al., 1989; Woo et al., 1990; Egginton and Hodgson, 1990; Lewkowicz, 1990). Some of these parameters (materials, vegetation, processes) were mapped and described for all the Fosheim Peninsula (Fig. 1) by Hodgson and Edlund (1977); both the open file map and Figure 2, in this report, were compiled largely from 1:60 000 scale airphotos taken in 1959. Materials, especially ground ice, also were observed throughout western Fosheim Peninsula in cores recovered from more than 100 holes of less than 3 m depth drilled with powered hand-held CRREL barrels. A further 35 holes were drilled to depths of 3-8 m by M. Nixon and J.J. Veillette using Winkie GW-15 and JKS 300 drills (cf. Veillette and Nixon, 1980). This summary of surficial materials and introduction to Quaternary history draws on those earlier data, collected in 1972-74, and reinterprets them using more recent though sporadic observations.

The basin

Hot Weather Creek is a south-flowing tributary of Slidre River, contained in a narrow strike valley. HWCk basin has an area of about 140 km^2 and an elevation range of 20-300 m above present sea level. The basin contains no permanent ice and has a nival hydrological regime which is subject to modification by ground ice thaw in warm summers (Edlund et al., 1989). Slidre River drains much (1300 km^2) of the interior of central Fosheim Peninsula to Slidre Fiord (Fig 1); its basin includes about 100 km^2 of glaciers in the Sawtooth Range which strongly influence river flow in summer.

The sector of the rolling landscape containing HWCk basin is underlain by generally west dipping poorly consolidated sandstone and subordinate shale and coal of the upper Cretaceous-lower Tertiary Eureka Sound Group. Weathered and colluviated bedrock is the dominant surface material; elsewhere there are remnants of a cover of Neogene and younger sandy fluvial deposits, a discontinuous veneer of Quaternary till, thick early and middle Holocene fine grained marine and deltaic deposits, isolated Holocene peat deposits, and recent silt to gravel fluvial sediments.

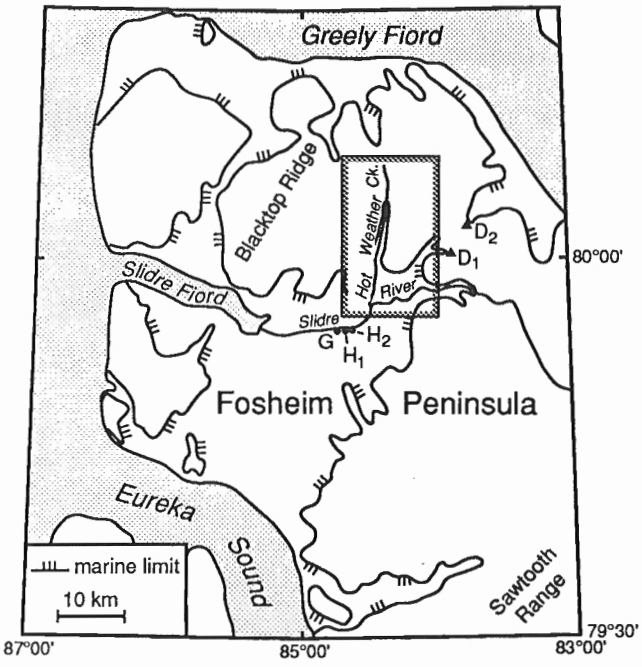

Figure 1. Location of Hot Weather Creek map area and early Holocene marine limit (140-145 m) on western Fosheim Peninsula. D1 and D2 are deltas, H1 and H2 are ^{14}C sites.

LITHOSTRATIGRAPHY

Bedrock (Eureka Sound Group)

The Eureka Sound deposits were described by Troelsen (1950), examined at Hot Weather Creek by McMillan (1963), defined as a formation by Tozer (1963), broadly mapped for western Fosheim Peninsula by Thorsteinsson (1971a, b), and raised to a group of four basic lithostratigraphic units by Ricketts (1986) following Miall (1984). The lower three units have been identified at Hot Weather Creek, but have not been mapped on Fosheim Peninsula. The oldest is the Expedition Formation, more than 600 m thick where measured south of HWCk. It is composed of quartz-rich white sandstone (barrier island deposition), overlain by alternating sandstone, shale, and coal beds (wave dominated deltas). The latter show a distinctive striped weathering pattern both in stream cuts and surface outcrop. Overlying is the Strand Bay Formation, less than 200 m thick at HWCk. This is composed of thick sandstone and thin coal seams, and thick dark grey shale, representing beach, delta, prodelta, and shelf deposits. The Iceberg Bay Formation is the uppermost unit at HWCk, and by far the thickest with possibly 2000 m of sediment. At HWCk the formation almost entirely consists of fining-upward sandstone-coal cycles, deposited as barrier islands and delta plains, as well as lagoon deposits. Carbonaceous beds (i.e. "coal") can be 6 m thick and are composed mostly of lignite (including petrified logs and stumps; McMillan, 1963). Deformation of these rocks during the Eurekan Orogeny resulted in north-south to northeast-southwest structural trends in HWCk basin. Unweathered outcrop is found only in incised meanders of HWCk, mainly in the lower reaches.

High terrace sediments

Unconsolidated sand lies under gravel veneeered terraces rising up to 600 m above sea level in west-central Ellesmere Island (Fyles, 1989). This material is better drained and more resistant to mass wasting than underlying finer grained rock, and thus commonly forms buttes and mesas. The horizontally stratified fluvial sediments include organic material that Fyles deduced is of Neogene age. Thus deposition occurred after the Paleogene Eurekan Orogeny but before modern rivers (and probably marine channels) were entrenched. The deposits may be polycylic, that is, highest and most extensive areas may be Neogene whereas the lowest remnants may be

composed of material recycled by fluvial or even fluvioglacial processes in the Neogene or Quaternary. Certainly, meltwater channels are incised into some deposits.

A deposit of 0.25 km^2 in the northeast sector of HWCk basin lying 280 m a.s.l. was investigated (A in Fig. 2). The veneer of bouldery gravel overruns and armours the bordering scarp. This material includes clasts of quartzitic sandstone more resistant than that found in Eureka Sound Formation, carbonate and diabase blocks commonly to 1 m diameter, and in places forms knolls to 6 m high; it is likely till (see below). Unusually, a gully exposed underlying sediment to a depth of 27 m. This was composed of generally planar bedded, in places crossbedded, fine sand, subordinate sandy silt, granule beds, and coal fragments. Fragments of unaltered wood, to 30 cm long and 10 cm diameter, lay in colluvial deposits at the base of the section.

The flat-lying summits of apparently similar deposits in and adjacent to the upper HWCk basin vary from 180 m to 340 m a.s.l. The plateau capped by gravelly sand on the southeast margin of the basin (B in Fig. 2) lies as low as 150 m a.s.l., just above marine limit. No natural exposures of ground ice were observed, and no holes were drilled in these materials.

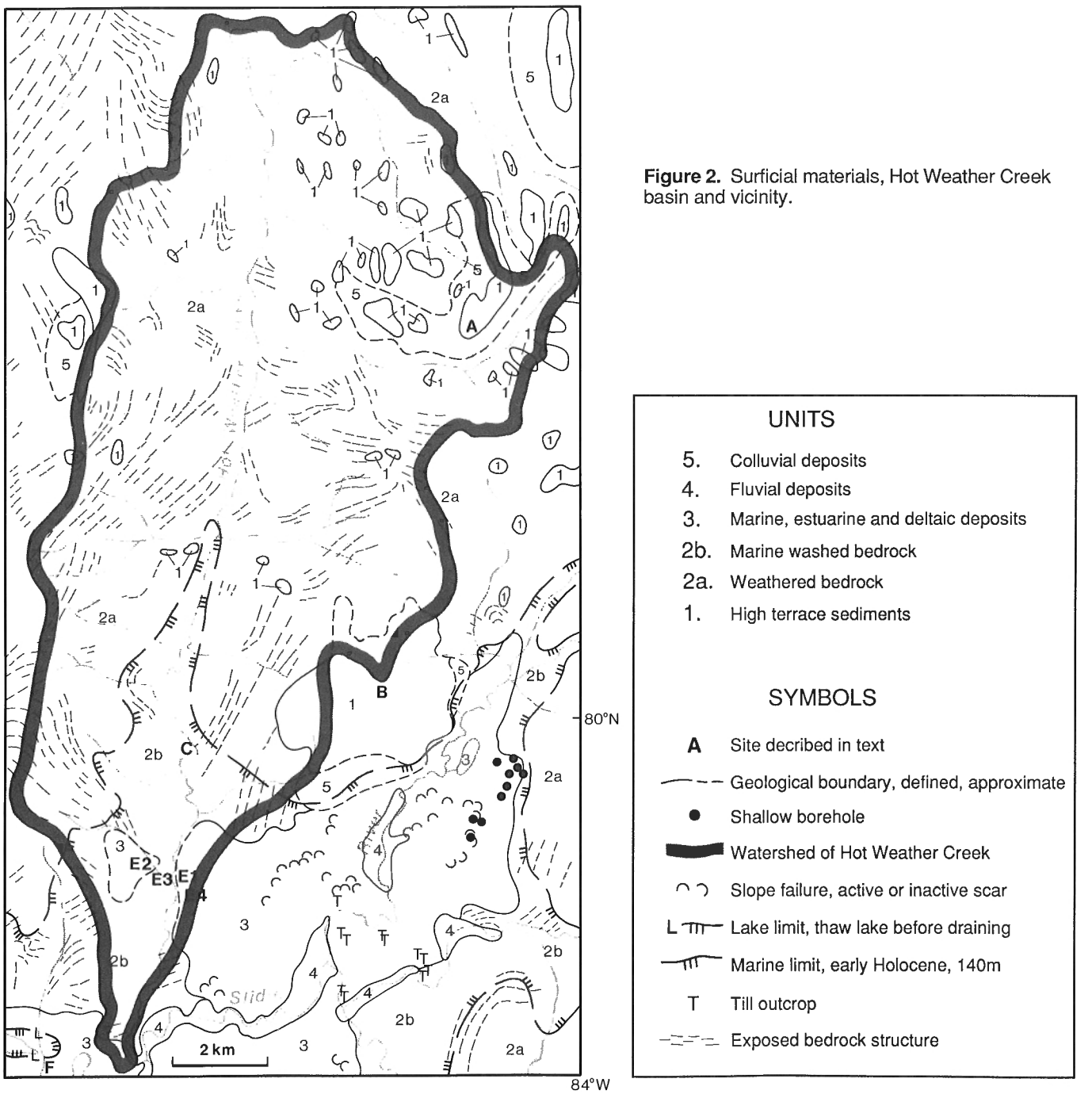

Figure 2. Surficial materials, Hot Weather Creek basin and vicinity.

Weathered bedrock

Strike-aligned patterns showing folded and faulted sandstone and shale are conspicuous on airphotos over large areas of the basin, particularly on drainage divides. The surface of such areas is greyish brown sandy loam containing clasts of sandstone, siltstone, shale or coal, in places arranged in strike-aligned bands. Drilling, mainly outside the basin, commonly penetrated 1 to 1.5 m of disaggregated rock above undisturbed bedrock (which ranges from unconsolidated to consolidated). In this weathered rock, below the maximum depth of seasonal thawing (50 cm), segregated ice in the form of lenses represents 5% to 50% of volume (except 100% in ice wedges, see below). Ice volumes in apparently otherwise undisturbed rock are generally much lower; commonly no ice is visible in sandstone or clayey shale. Shallow runs and, locally, thin solifluction lobes occur on slopes.

Till

Glaciation of lowland Fosheim Peninsula in the Quaternary is indicated by flights of marginal meltwater channels cut in the north end of Blacktop Ridge to 600 m a.s.l., 10 km west of the head of HWCk basin (Hodgson, 1985). Evidence of former glacial ice within the basin is provided by scattered granule to boulder (up to 4 m diameter) clasts of lithologies not found in Eureka Sound Group. These include resistant quartzitic sandstone, dolomite, limestone, and diabase, all lithologies that outcrop within 50 km of HWCk. Coarse grained crystalline erratics were not observed within the basin, but granites were reported immediately south of Slidre River by T. Bell (personal communication, 1989); the northernmost Canadian Shield lies 120 km southeast. No striated bedrock and few striated clasts were observed. Erratics are largely confined to flat-lying high terrace deposits where mass wasting processes are least active, and to river channels where colluviated coarse material accumulates. No observed exposures show whether the silty sand matrix in which erratics are found is glacial or a lag deposit of high terrace sediments. No glacial landforms were identified.

Discrete areas of more readily identifiable till occur just outside the basin, both 5 km northeast (Fig. 2) and southwest of the junction of Hot Weather Creek and Slidre River, below maximum Holocene sea levels. Deposits of stony till, in places stratified, and several metres thick, are exposed through flanking marine and estuarine deposits. Carbonate and basic clasts are commonly striated. Till ridges south of Slidre River are being studied by T. Bell (personal communication, 1989). Neither the discontinuous veneer nor the till exposed in section forms a mappable unit.

The last major expansion of ice sheets on Ellesmere Island occurred in the Late Pleistocene or earliest Holocene; however, at that time ice may not have covered western Fosheim Peninsula, including HWCk basin (Hodgson, 1989; England, 1990). Meltwater or ice from this or an earlier event likely cut the col that links HWCk with drainage flowing north to Greely Fiord. The limit of marine submergence, apparently associated with glacioisostatic unloading, is approximately 140-145 m a.s.l.; recession from this level started about 9000 years ago (Hodgson, 1985).

Marine washed bedrock

Below an elevation of about 145 m, weathered rock has been washed by Holocene and probably Pleistocene marine inundations, leaving discontinuous marine deposits (see below). If the considerable recent stream incision is excluded, topography below this level is more subdued than above.

Marine, estuarine, and deltaic deposits

Slidre Fiord was double its present 23 km length during the high sea level of the early Holocene and at that time included lower HWCk basin (Fig. 2). Marine and fluvial sediments, in places 30 m or more thick, were deposited into the inlet possibly burying older Quaternary deposits (McMillan, 1963, p. 406). These were dissected and reworked by lower Slidre River and tributaries during the subsequent fall in base level. Distribution of this sediment within existing valleys indicates that most drainage follows pre-Holocene valleys, though lowermost Hot Weather Creek is entirely cut through bedrock, possibly bypassing a buried valley to the east. The northernmost marine sediments in the basin were found 96 m a.s.l. (C, Fig. 2), though marine shells occur to 120 m a.s.l. a few kilometres to the south. Degraded deltas of unknown age east of HWCk basin record a water plane 143 m a.s.l. (D1 and D2, Fig 1).

Marine, estuarine, and deltaic deposits are composed of medium or fine grained sand, silt, and minor clayey silt, sandstone granules, coal fragments, detrital plant material, or molluscs. These materials commonly are interbedded 1 mm to 10 cm thick. Beds are commonly subhorizontal, in places inclined up to 15° (Slidre River pro-deltaic sediments), generally planar, may show climbing ripples, and are rarely crossbedded or convoluted (apart from convolutions induced by ice wedge growth). A white crust up to several millimetres thick, probably of calcium/magnesium sulphate, remains on some unvegetated silt or finer deposits after evaporation from the snowmelt saturated active layer (McMillan, 1963; Christie, 1967).

Segregated ground ice in addition to wedge ice is present in marine and estuarine sediments. Massive ice at least 4 m thick was exposed by a failure in HWCk basin at site E1 (Fig. 2). The marine (?) sediment at this site may be either undisturbed or colluvially reworked. To the east, where many square kilometres are scarred by active layer and deeper failures (Fig. 2), borehole records showed apparently undisturbed stratified marine or estuarine deposits containing locally massive tabular ice. In addition to slope failures, these deposits are locally dissected by concentrations of closely spaced gullies where slopes have been steepened by incision of main drainage lines. Flat-lying vegetated terrain has been locally stripped by deflation, exposing strata deformed by ice wedge growth.

The approximate rate of emergence of western Fosheim Peninsula during the Holocene was illustrated by Hodgson (1985, Fig. 8). Figure 3 shows an emergence curve, following points representing shell samples collected on the shores of Slidre Fiord, Eureka Sound, and Greely Fiord (the terrestrial organic samples are described below). The curve is at

best approximate because the contemporary sea level (i.e. related sea level) is not known for any of the shell samples. Sea level is assumed to lie at or above the elevation of each sample, though there is a slight possibility that a few of the shells could have been raised a few metres above sea level by sea ice thrusting. Furthermore, in the absence of data, interpolation is required between 8 ka and 4 ka, and from 2 ka to the present. The curve shows a typical pattern of uplift in a glaciated area, notwithstanding the absence of evidence of late Quaternary glaciers in western Fosheim Peninsula. Hodgson (1985, p. 363) questioned the validity of the 9550 ± 250 BP date obtained for shells plotted as L-647B (Fig. 3); they appeared too old and too low relative to the rest of the data. Since then, however, 36 g of shells collected from one site in HWCk basin yielded an age of 10 500 ± 90 BP (GSC-4784 at E2 in Fig. 2; Fig. 3; Table 1b). Possibly a high sea level was maintained from the latest Pleistocene into the Holocene (cf. the full glacial sea of England, 1983) or a transgression preceded Holocene regression forming a cusp in the emergence curve around 9 ka.

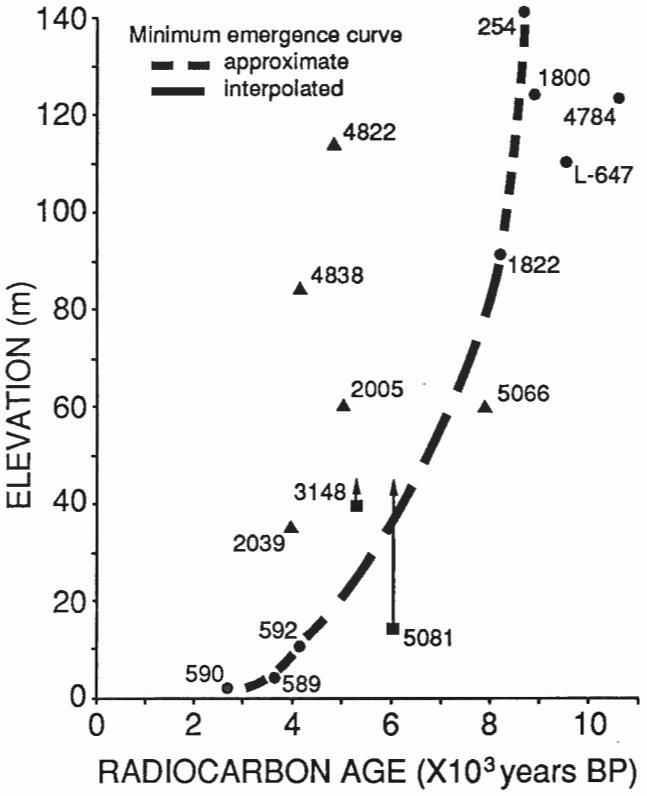

Figure 3. Age-elevation data from western Fosheim Peninsula. Samples identified by GSC radiocarbon laboratory numbers, except L-647.

- ▲ Terrestrial peat, *in situ*; described in Table 1a
- ■ Terrestrial plant material, redeposited below contemporary sea level (at arrowhead); described in Table 1a
- ● Marine shell sample, *in situ* or redeposited below contemporary sea level (described in Hodgson, 1985, Table 1, except GSC-4784 in this report, Table 1b)

Fluvial deposits

Hot Weather Creek and its larger tributaries are relatively deeply incised, leaving terraces and floodplains too narrow to be shown in Figure 2. Deposits emphasize the coarse fraction of surficial materials in the basin, especially in HWCk, where in some upper reaches quartzitic sandstone boulders reworked from till veneer dominate, and in lower reaches sandstone clasts are derived directly from Eureka Sound Group. Deposits along Slidre River and other tributaries (Fig. 2) are composed of sand and gravel, with boulders adjacent to till outcrop.

Colluvial deposits

Most surficial materials deposits in HWCk basin are undergoing mass wasting to some degree. Notwithstanding the efficacy of slope processes in this area, colluvium is mapped only where materials from several units are so intermixed that they differ markedly in composition from a subjacent unit. This occurs chiefly on flanks of high terrace outliers where gravel and sand overrun finer grained weathered rock.

Terrestrial organic deposits

Peat composed of mosses and vascular plants (including shrubs) is accumulating in numerous depressions (Edlund et al. 1989, p. 128). Thickness generally does not appear to exceed a few centimetres; however thicker deposits are sporadically exposed where nick points have worked back into wetlands and gullies eroded ice along frost fissures. Samples from two such deposits, adjacent to lower HWCk, provided middle Holocene ages (GSC-4822 at E3 and GSC-4838 at E4 in Fig. 2; Table 1a, Fig. 3).

Peat deposits several metres thick have been exposed by incision of other tributaries of Slidre River in the vicinity of Hot Weather Creek. Two of the samples (GSC-2005 at F, Fig. 2; and GSC-2039 at G, Fig. 1; see also Table 1a) are also middle Holocene, and lie above the interpolated contemporary marine limit (Fig. 3), as expected of terrestrial in situ peat. A third sample (GSC-5066, Table 1a) collected at the base of the same deposit that yielded GSC-2005, is older (7950 ± 120 BP) and lies in an aberrant position below the interpolated emergence curve. Further samples from this exposure will be dated. Reworked plant material was recovered from sediments deposited at the front of the prograding Slidre River delta of the middle Holocene, when the delta lay 10 to 15 km east of its present position. Willow twigs extracted from these samples (GSC-3148 at H1 and GSC-5081 at H2 in Fig 2; Table 1a) yielded ages that are slightly too young relative to the position of the contemporary sea level (top of section?) on the interpolated emergence curve (Fig. 3).

Radiocarbon ages are all middle Holocene; but this does not necessarily indicate a more favourable paleoclimate at that time (cf. Ovenden, 1988, p. 2). The concentration of dates may result from the best exposures being in the thick marine-deltaic sediments of central Slidre Valley, where both stream incision is greatest and peat accumulation commenced

Table 1a. Radiocarbon ages, terrestrial organic material, Hot Weather Creek vicinity

^{14}C age (years BP)[1] $\delta^{13}C$	Laboratory No. Field No.	Material	Location # Site on Fig. 1 ## Site on Fig. 2	Elevation of sample (m)	Related sea level (m)	Site description	Geological environment	Collector	References
7950 ± 120 **7910 ± 120** -27.3‰	**GSC-5066** - SV 90-1	Peat	2 km W of mouth HWCk 79°56.0'N, 84°35'W (49G/16) ## F	60	>80	Sample from base of 2.85 m peat, exposed >100 m horizontally by reincision of stream (see GSC-2005)	Drained, dissected wetland in pre–existing valley	D.A. St-Onge 1990	This report
6040 ± 170	**GSC-5081** PL-90.34[2] HCA-90-8.8.1	*Salix* sp. twigs	S bank Slidre River, 4.5 km SW of HWCk 79°54.4'N, 84°38'W (49G/16) # H2	15	>44?	Plant debris and clayey silt; interbedded sand, silt; 7 m above base of 36 m exposure	Prodelta deposits	D.A. Hodgson, 1990	This report
5300 ± 60 **5280 ± 60** -26.7‰	**GSC-3148** PL-80.41[2] HCA-78-8.7.3c	*Salix* sp. twig [4]	S bank Slidre River, 5 km SW of HWCk; 0.5 km W of GSC-5081 79°54.4'N, 84°41'W (49G/16) # H1	40	>44?	Plant debris, sand, lignite; under *Portlandia arctica* fragments (reworked?); 26 m above base of 30 m exposure	Delta-front deposits	D.A. Hodgson, 1978	This report
4950 ± 60	**GSC-2005** 268[3] HCA-72-11.7.3a	Rhizome-moss peat	2 km W of mouth HWCk 79°56.0'N, 84°35'W (49G/16) ## F	60	>20	6 cm thick sample from 30 cm below top of 2.2 m peat, in same exposure as GSC-5066	Drained, dissected wetland in pre–existing valley	D.A. Hodgson, 1972	Table 2 in Ovenden, 1988
4870 ± 70 **4820 ± 70** -27.9‰	**GSC-4822** - EJ-88-128A	Peat	0.4 km W of HWCk, 4.5 km N of mouth 79°58.6'N, 84°28.0'W (49G/16) ## E3	114	>20	Sample from 1.5 m exposed by erosion along frost fissures	Drained wetland	S.A. Edlund 1988	This report
4120 ± 60 **4050 ± 60** -29.5‰	**GSC-4838** - EJ-88-127C	Peat	0.25 km E of HWCk, 3.5 km N of mouth 79°57.9'N, 84°25.5'W (49G/16) ## E4	84	>10	Sample near base of 2 m peat (over rock) exposed by erosion along frost fissures	Drained wetland	S.A. Edlund 1988	This report
3970 ± 80	**GSC-2039** 277[3] HCA-72-3.8.2c	Rhizome-moss peat	S bank Slidre River, 6 km SW of HWCk; 1 km W of GSC-3148 79°54.5'N, 84°44'W (49G/16) # G	35?	>10	Sample at top of 1.8 m peat; over 1.4 m sand and plant debris; over 28 m interbedded sand and silt	Delta wetland over delta-front deposit over prodelta deposit	D.A. Hodgson, 1972	Table 2 in Ovenden, 1988

1 Uncorrected age shown over age corrected for isotopic fractionation where known; standard value for terrestrial materials is $\delta^{13}C$=-25‰. Error represents 95% probability
2 Material identified by R.J. Mott (Unpublished GSC *Wood Identification Report No.*)
3 Material identified M. Kuc (Unpublished GSC *Bryological Report No.*)
4 Other plant material, including abundant *Dryas integrifolia*, identified by A. Telka (Unpublished GSC *Plant Microfossil Report No. 91-03*)

Table 1b. Radiocarbon age, marine shells, Hot Weather Creek

^{14}C age (years BP)[1] $\delta^{13}C$	Laboratory No. Field No.	Material	Location ## Site on Fig. 2	Elevation of sample (m)	Related sea level (m)	Site description	Geological environment	Collector	References
10 500 ± 90 **10 600 ± 90** +1.0‰	**GSC-4784** EJ-88-92 S	Marine shells and fragments (*Hiatella arctica?*)	W side HWCk, 4 km N of mouth 79°58.2'N, 84°29'W (49G/16) ## E2	122-123	>123	Silt strata with abundant shells exposed on surface by deflation	Paralic sediments?	S.A. Edlund 1989	This report

1 Uncorrected age shown over age corrected for isotopic fractionation; standard value for marine shells is $\delta^{13}C$=0.0‰. Error represents 95% probability

in the middle Holocene when the area emerged. Older deposits inland from the marine limit, and younger deposits closer to modern shorelines are less likely to be exposed.

Ground ice

It has been shown above that segregated ground ice has been observed on western Fosheim Peninsula in many of the types of surficial deposit found in HWCk basin (note that most holes were drilled below marine limit). The tabular ice bodies within Holocene raised marine and deltaic deposits are assumed to be epigenetic because of their accordance with the enclosing waterlaid silt and sand. Tabular ice also was recorded in marine washed weathered Eureka Sound Group sediments. Massive ground ice was rarely observed above the 140-145 m early Holocene marine limit; however reticulate ice in places forms 50% by volume of the 1 to 2 m weathered bedrock, and 3 m of ice was cored in fine grained till (not a material found at HWCk) below a wetland site. Palsas 1 m high were observed in peat in HWCk headwaters, but ice was not observed in bedrock exposed along the lower creek. High ice content is expected at any elevation in slopes subject to seepage. Ice wedges occur in all materials; they have been recorded to widths of 5 m and depths exceeding 8 m.

ACKNOWLEDGMENTS

Surface and subsurface data was enthusiastically collected by R.J. Richardson (1972), D. Feldbruegge and L.R. Stevenson (1973), W.G. Green and A.C. Liard (1974), and N. Giroux (1990). Valuable discussions have been held with Trevor Bell, University of Alberta, who is completing a Ph.D. dissertation on Quaternary geology of western Fosheim Peninsula. Dr. J.G. Fyles kindly improved the clarity of the text.

REFERENCES

Christie, R.L.
1967: Reconnaissance of the surficial geology of northeastern Ellesmere Island, Arctic Archipelago; Geological Survey of Canada, Bulletin 138, 50 p.

Edlund, S.A., Alt, B.T., and Young, K.L.
1989: Interaction of climate, vegetation, and soil hydrology at Hot Weather Creek, Fosheim Peninsula, Ellesmere Island, Northwest Territories; in Current Research, Part D, Geological Survey of Canada, Paper 89-1D, p. 125-133.

Egginton, P.A. and Hodgson, D.A.
1990: Preliminary asessment of selected drainage basins in western Fosheim Peninsula, Ellesmere Island, as sites for global change studies; in Current Research, Part D, Geological Survey of Canada, Paper 90-1D, p. 71-77.

England, J.
1983: Isostatic adjustments in a full glacial sea; Canadian Journal of Earth Sciences, v. 20, p. 895-917.

1990: The late Quaternary history of Greely Fiord and its tributaries, west-central Ellesmere Island; Canadian Journal of Earth Sciences, v. 27, p. 255-270.

Fyles, J.G.
1989: High terrace sediments, probably of Neogene age, west-central Ellesmere Island, Northwest Territories; in Current Research, Part D, Geological Survey of Canada, Paper 89-1D, p. 101-104.

Hodgson, D.A.
1985: The last glaciation of west-central Ellesmere Island, Arctic Archipelago, Canada; Canadian Journal of Earth Sciences, v. 22, p. 347-368.
1989: Quaternary geology of the Queen Elizabeth Islands; Chapter 6 in Quaternary Geology of Canada and Greenland, (ed.) R.J. Fulton; Geological Survey of Canada, Geology of Canada, no. 1 (also Geological Society of America, The Geology of North America, v. K-1).

Hodgson, D.A. and Edlund, S.A.
1977: Biophysical regions, western Fosheim Peninsula and eastern Axel Heiberg Island; Geological Survey of Canada, Open File 501.

Lewkowicz, A.G.
1990: Frequency and magnitude of active layer detachment on the Fosheim Peninsula, Ellesmere Island: past present and future (abstract); in Program and Abstracts, 19th Arctic Workshop, March 8-10, 1990, INSTAAR, University of Colorado, p. 46.

McMillan, N. J.
1963: Slidre River; in Geology of the North-central part of the Arctic Archipelago, Northwest Territories (Operation Franklin), (ed.) Y. O. Fortier; Geological Survey of Canada, Memoir 320, p. 400-407.

Miall, A.D.
1984: Sedimentation and tectonics of a diffuse plate boundary: The Canadian Arctic Islands from 80 Ma B.P. to the present; Tectonophysics, v. 107, p. 261-277.

Ovenden, L.
1988: Holocene proxy-climate data from the Canadian Arctic; Geological Survey of Canada, Paper 88-22, 11 p.

Ricketts, B.D.
1986: New formations in the Eureka Sound Group, Canadian Arctic Islands; in Current Research, Part D; Geological Survey of Canada, Paper 86-1B, p. 363-374.

Thorsteinsson, R.
1971a: Geology, Eureka Sound north, District of Franklin; Geological Survey of Canada, Map 1302A, scale 1:250 000.
1971b: Geology, Greely Fiord west, District of Franklin; Geological Survey of Canada, Map 1311A, scale 1:250 000.

Tozer, E.T.
1963: Mesozoic and Tertiary stratigraphy; in Geology of the north-central part of the Arctic Archpelago, Northwest Territories (Operation Franklin), (ed.) Y.O. Fortier; Geological Survey of Canada, Memoir 320, p. 74-95.

Troelsen, J.
1950: Contributions to the geology of northwest Greenland, Ellesmere Island and Axel Heiberg Island; Meddelelser om Grønland, v. 49, no. 7.

Veillette, J.J. and Nixon, F.M.
1980: Portable drilling equipment for shallow permafrost sampling; Geological Survey of Canada, Paper 79-21, 35 p.

Woo, M.K., Young, K.L., and Edlund S.A.
1990: Effects of soil, vegetation, and microclimate on slope hydrology, Hot Weather Creek basin, Ellesmere Island, Northwest Territories; in Current Research, Part D, Geological Survey of Canada, Paper 90-1D, p. 85-93.

Organic maturity/time-temperature models of the Ellesmerian (Paleozoic) Orogeny, Melville Island, Northwest Territories

D.N. Skibo, C. Harrison, T. Gentzis[1], and F. Goodarzi
Institute of Sedimentary and Petroleum Geology

Skibo, D.N., Harrison, C., Gentzis, T., and Goodarzi, F., 1991: Organic maturity/time-temperature models of the Ellesmerian (Paleozoic) Orogeny, Melville Island, Northwest Territories; in Current Research, Part E; Geological Survey of Canada, Paper 91-1E, p. 165-175.

Abstract

Melville Island, located at the southwestern corner of Sverdrup Basin in the Queen Elizabeth Islands, is a part of the Innuitian Orogen and lies mainly in the Franklinian Mobile Belt of the Canadian Arctic Archipelago. More than fifty exploration drillholes have been completed on Melville Island, leading to the discovery of over 9 Tcf (250 billion cubic metres) of gas in the Drake, East Drake, and Hecla fields. Details of the geological history are combined with organic petrographic studies to calculate thermal/subsidence models for two exploration drillholes in central and southwestern Melville Island. Kinetic models of hydrocarbon generation indicate that organic maturation of Upper Ordovician/Lower Devonian source rocks commenced in Late Devonian time and was essentially completed by the Early Carboniferous.

Résumé

L'île Melville, située à l'angle sud-ouest du bassin de Sverdrup dans les îles de la Reine-Élisabeth, fait partie de l'orogénèse innuitienne et repose principalement dans la zone mobile franklinienne de l'archipel de l'Arctique canadien. Plus de cinquantes sondages d'exploration ont été faits dans l'île, menant à la découverte de plus de 250 milliards de mètres cubes de gaz répartis dans les champs Drake, East Drake et Hecla. Des détails de l'histoire géologique combinés à des études de pétrographie organique permettent d'établir des modèles de subsidence thermique pour deux sondages d'exploration dans le centre et le sud-ouest de l'île Melville. Des modèles cinétiques de production d'hydrocarbures indiquent que la maturation organique des roches mères de l'Ordovicien supérieur au Dévonien inférieur a commencé à la fin du Dévonien et s'est essentiellement terminée au début du Carbonifère.

[1] Alberta Research Council, Coal Research Centre Devon, 1 Oil Patch Drive, Devon, Alberta T0C 1E0

INTRODUCTION

Gentzis and Goodarzi (in press) and Gentzis (1991) have studied the regional thermal maturity and source-rock potential of hydrocarbons from the Paleozoic sedimentary succession on Melville Island. Their studies were based on samples of whole rock cuttings and core from drillholes, and they combined vitrinite reflectance measurements on phytoclasts with reflectance measurements on natural bitumens, extending the assessment of thermal maturity to sedimentary strata devoid of vitrinites. (This includes formations of pre-Early Devonian age.) Organic maturation data from two of the wells studied, Panarctic Apollo C73 and Panarctic Dome Dundas C80, together with chronostratigraphic relationships and lithological data, mainly from the work of Harrison (1991), are used to calculate models of time-temperature history, organic maturation, and hydrocarbon generation.

The objectives of the present study are: 1) to provide calculated vitrinite reflectance profiles for extrapolation to sub-Lower Devonian formations for comparison with bitumen reflectance observations; 2) to provide calculated time-temperature histories for each of the two wells studied, in order to 3) assess conditions of bitumen reflectance evolution (which will be given in more detail in a future publication), and 4) conduct a test of mathematical model simulations of organic maturation under the diverse conditions of geological history determined for each of the wells; and 5) to establish constraints on the timing and extent of hydrocarbon generation within local source rocks.

In order to achieve these objectives, several numerical modelling methods are available in the literature as well as several commercially available software packages that include MATOIL (IFP/BEICIP, Rueil Malmaison, France) and BASINMOD (Platte River Associates, Denver, CO, U.S.A.). This study will present results obtained using the MATOIL (version 2) package.

GEOLOGICAL HISTORY

Melville Island straddles three major geological provinces: the Cambrian through Devonian Arctic Platform in the south; correlative rocks of the Franklinian Mobile Belt, and unconformable Carboniferous through Tertiary cover of the Sverdrup Basin in the north (Fig.1). Studies of Trettin (1989) and Ziegler (1988) detail the tectonic framework of the Canadian Arctic Islands. Previous work is reviewed and Cambrian to Early Devonian history is given in Trettin et al., 1989. Structural history since Precambrian time was summarized in an earlier work by Thorsteinsson and Tozer (1960) and geology and evolution of the arctic archipelago by Thorsteinsson and Tozer (1970) and Kerr (1981). The Carboniferous and Permian geology of the Sverdrup Basin is discussed in Davies and Nassichuk (in press). Upper Paleozoic stratigraphy and basin analysis is given in Beauchamp et al. (1989a, b); Middle-Upper Devonian sedimentation related to the Ellesmerian Orogeny is discussed in Embry (1987) and Devonian shelf systems on Melville Island by Goodbody (1988). Stratigraphic and structural studies of Melville and adjacent islands are reported in Balkwill and Fox (1982), Fox (1985), Harrison and Bally (1988), Harrison and Brent (in press), Harrison et al. (1989) and Harrison (1991). Stephenson et al., 1987 gave thermo-mechanical model calculations for the Late Carboniferous Early Permian (Muscovian-Sakmarian) crustal attenuation and rifting (and post-Early Permian thermo-isostatic subsidence of the Sverdrup Basin).

Refraction surveys (Overton, 1970, 1982) and gravity modelling (Sobczak et al., 1986; Sweeney et al., 1986) are interpreted to indicate (?)Middle and (?)Late Proterozoic extension with 50% thinning of the Precambrian crust over a distance of 300 km (from the Arctic Platform south of Viscount Melville Sound extending to central Melville Island). The two drillholes presented in this study, Panarctic APOLLO C-73 and Panarctic Dome DUNDAS C-80 (Fig. 2), are positioned towards the northern edge of this region of crustal thinning.

The following summary of the development of the Franklinian Miogeocline from 640 through 360 Ma and younger is taken from Harrison (1991). Stratigraphic units of central and western Melville Island in the vicinity of the two studied wells are illustrated on the simplified correlation chart (Fig. 3). These units include: a seismically-imaged (?)Lower Cambrian through pre-Arenig Lower Ordovician outer shelf sedimentary prism (3.8-7.5 km thick) above an extensive angular unconformity imaged at 10-14 km below surface; generally unmetamorphosed shelf carbonates of variable Arenig through Ashgill ages intersected by drilling at 2.8 to 5.0 km below surface (Eleanor River, upper Bay Fiord, Thumb Mountain and Irene Bay formations); Arenig to Llanvirn evaporites (lower Bay Fiord Formation) deposited within an extensive intra-shelf basin, and; a younger unit comprised of Ashgill through lower Eifelian basin-facies graptolitic mudrocks, chert and argillaceous carbonates (Cape Phillips Formation) deposited in an equally extensive intra-shelf embayment that in the lower part is age equivalent to several embayment-fringing shallow marine carbonate formations (Allen Bay and Cape Storm formations and the Read Bay Group) and that in the upper part passes laterally into platform cover of condensed Lochkovian through lower Eifelian mudrocks (Kitson Formation).

In the far northwestern part of the island, strata age-equivalent to the Eleanor River Formation are exposed at surface and, in these areas, exist as slope-facies carbonates and debris flows (Canrobert Formation). Likewise, the entire upper Arenig through upper Emsian or lower Eifelian succession was deposited in condensed and periodically-starved deep-water realms (Ibbett Bay Formation).

Six syn-orogenic siliciclastic formations of Middle and Late Devonian ages are much more widely exposed at surface and are also preserved to depths locally in excess of 4.5 km. These strata are the depositional evidence of ancestral phases of the Ellesmerian Orogeny and are derived from pre-existing orogenic terrains once located over the site of the deep-water basin in the north and northwest. From the base, these formations include: (?)Emsian-lower Eifelian cyclical siliciclastic sediment gravity flows of the Blackley Formation; Eifelian clinoformed basin-rise, basin-slope, and basin-fill mudrocks (Cape De Bray Formation); Eifelian-Givetian cyclical

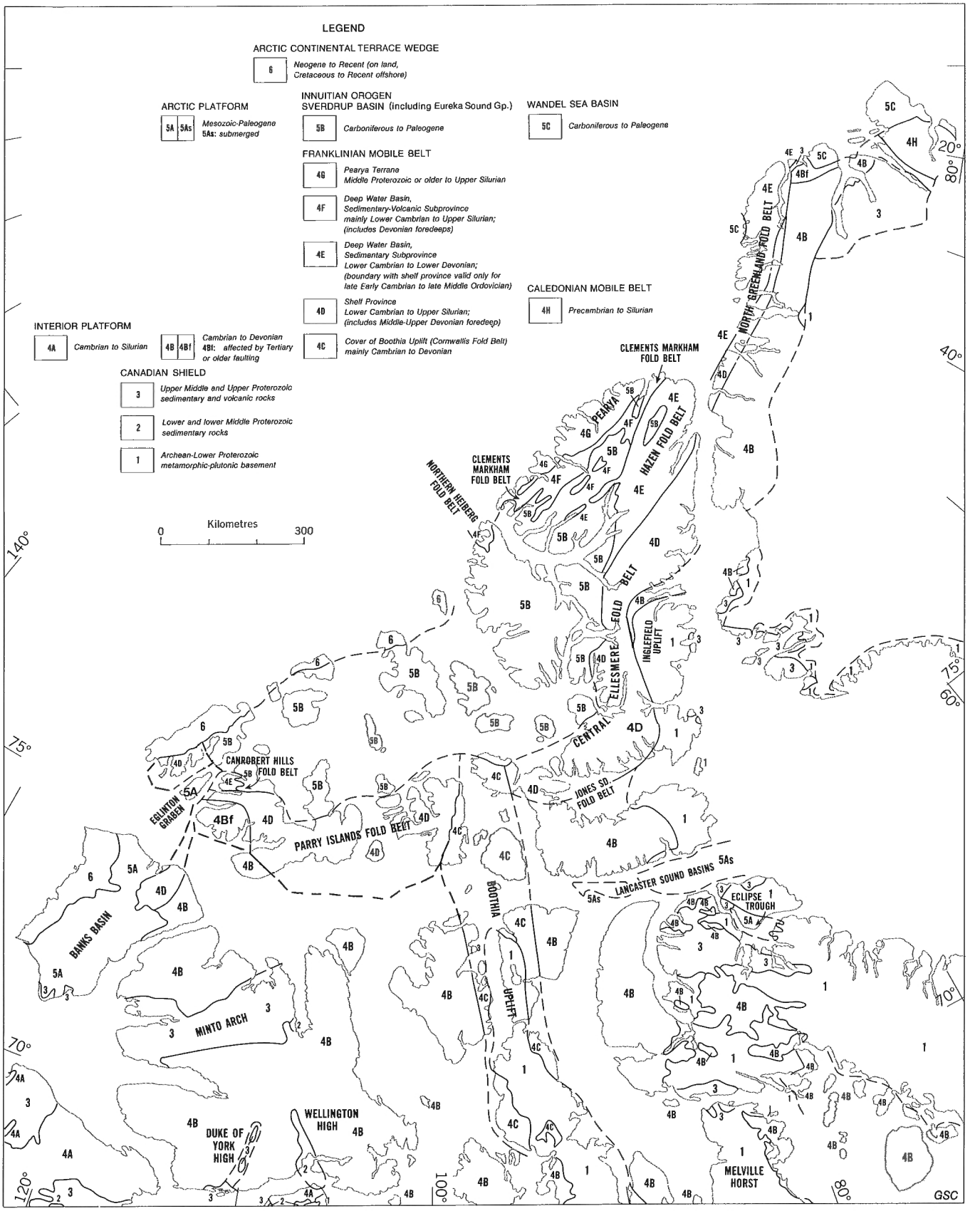

Figure 1. Geological provinces of the Canadian Arctic Archipelago. (After Trettin, 1989; Harrison, 1991.)

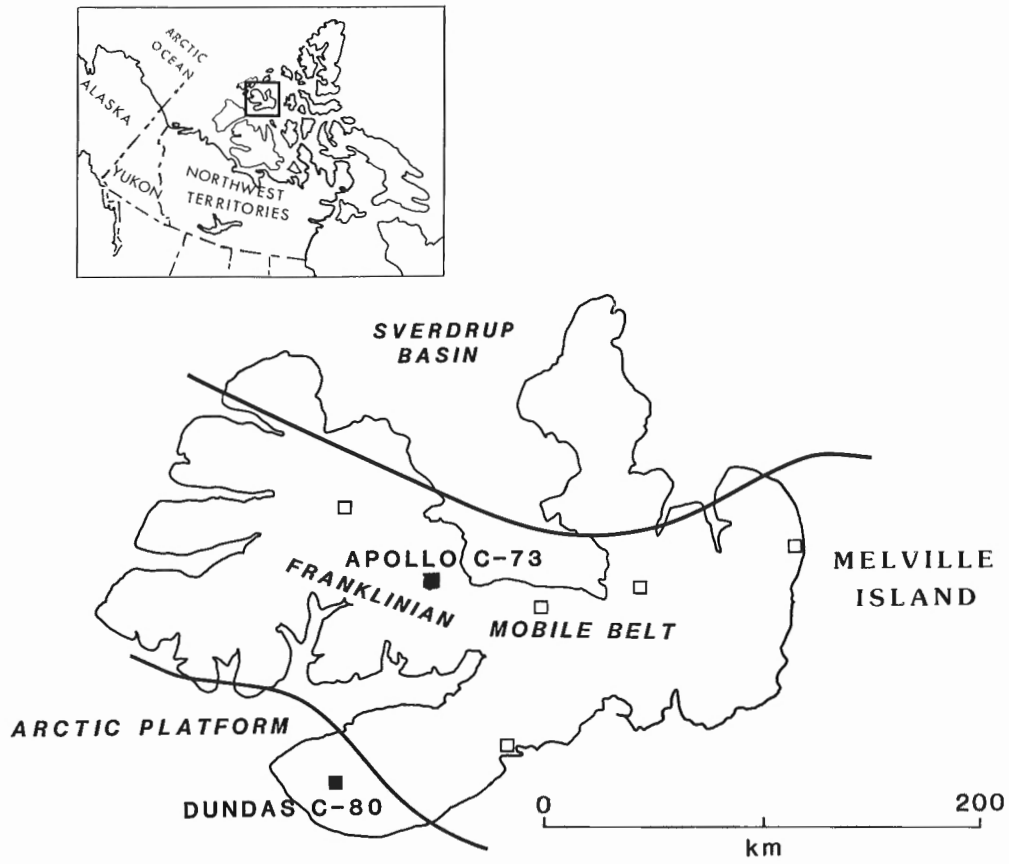

Figure 2. Location map of drillholes modelled in this paper (Apollo C--73 and Dundas C--80), and additional drillholes studied by Gentzis and Goodarzi (in press).

shallow marine shelf-deltaic sediments (Weatherall Formation); Givetian delta-front and delta-plain sandstones (Hecla Bay Formation) and; in the Frasnian and Famennian, two unconformity-bound fluvial-deltaic and marginal marine formations (Beverley Inlet and Parry Islands formations).

Lower Paleozoic sedimentation was terminated by the culminating phases of the Ellesmerian Orogeny at the end of the Famennian or in the Tournaisian-Viséan. Structural styles in the vicinity of the studied wells include harmonic upright open and close folds affecting the Devonian clastic wedge, ductile flow of Cape De Bray mudrocks and Bay Fiord evaporites, thin-skinned subsurface thrusts of the Ordovican through Devonian carbonates and basin-facies mudrocks, and related salt-based décollement tectonics. This older of the two culminating phases of the Ellesmerian Orogeny was modified by a partly coeval and partly superimposed phase of deep-seated long-wavelength folding and uplift.

Subsequent geologic events, (including upper Paleozoic rifting and inversion within the Carboniferous through Tertiary Sverdrup Basin, Mesozoic diapirism and mafic igneous activity, and cessation of Sverdrup Basin sedimentation by the mid-Tertiary Eurekan Orogeny), generally occurred beyond the region of interest considered by the present report.

ORGANIC PETROGRAPHY

Samples of whole-rock cuttings and a small number of cores were taken from shaly/silty and carbonate units in the two drillholes discussed here. Gentzis (1991) and Gentzis and Goodarzi (in press) examined polished samples for their organic matter content, using a Zeiss MPM II reflected light microscope, equipped with both incident white and fluorescent light sources. Random reflectance was measured for vitrinite and maximum reflectance for bitumens. Based on organic matter type and optical properties, these workers identified three different sections with progressively increasing thermal maturity with depth (Figs. 4, 5):

A. An upper section containing higher land plant remains with very little bitumen and a vitrinite reflectance ranging from about 0.72 to 0.90% at the top in the Apollo C73 and Dundas C80 drillholes (averaging about 0.80% for all drillholes studied in the area; Gentzis and Goodarzi, in press), up to values of about 1.5% (in Apollo C73, base of Weatherall Formation, Middle Devonian) and 1.1% (Dundas C80, Lower Weatherall).

B. A middle section, Middle Devonian and older, containing very little vitrinite suitable for determining thermal maturation, but commonly containing bitumen that may be categorized into low, high, and very high reflecting populations.

C. A lower section, in the Dundas C80 drillhole (Fig. 4), below about 2400 m (Cape De Bray Formation, lower Middle Devonian), in which bitumen occurs as coatings and fillings among carbonate grains. The reflectance of the bitumen in section C revealed the highest level of thermal maturity. These bitumens are not soluble in oil immersion and have no fluorescence under UV excitation.

Textural and optical properties and matrix association were used as relative criteria for classifying bitumen populations. In general, low reflecting bitumen has an irregular morphology, a "pitted" surface, and a reflectance range from 1.5 to 3.0% R_o max (epi- to meso-impsonite maturity stage; Jacob, 1985). High reflecting bitumen has a reflectance ranging from 2.6 to 3.2% R_o max (Apollo C73) and 3.0 to 4.1% R_o

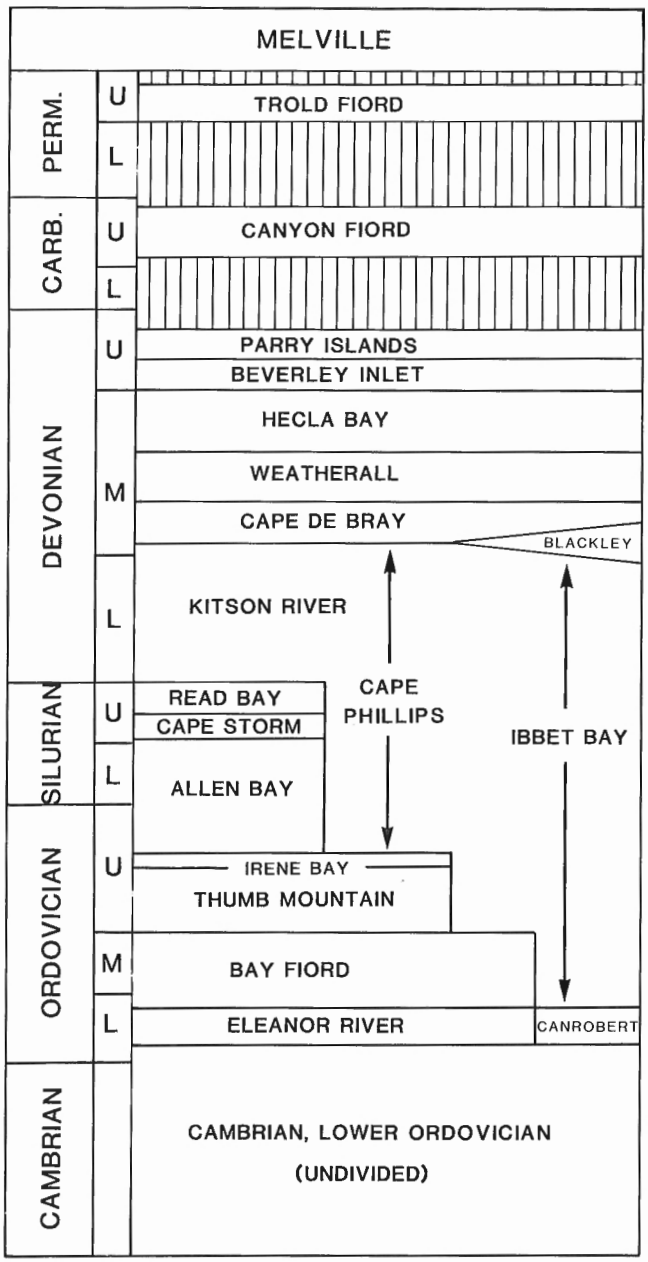

Figure 3. Stratigraphic column of Paleozoic formations on Melville Island.

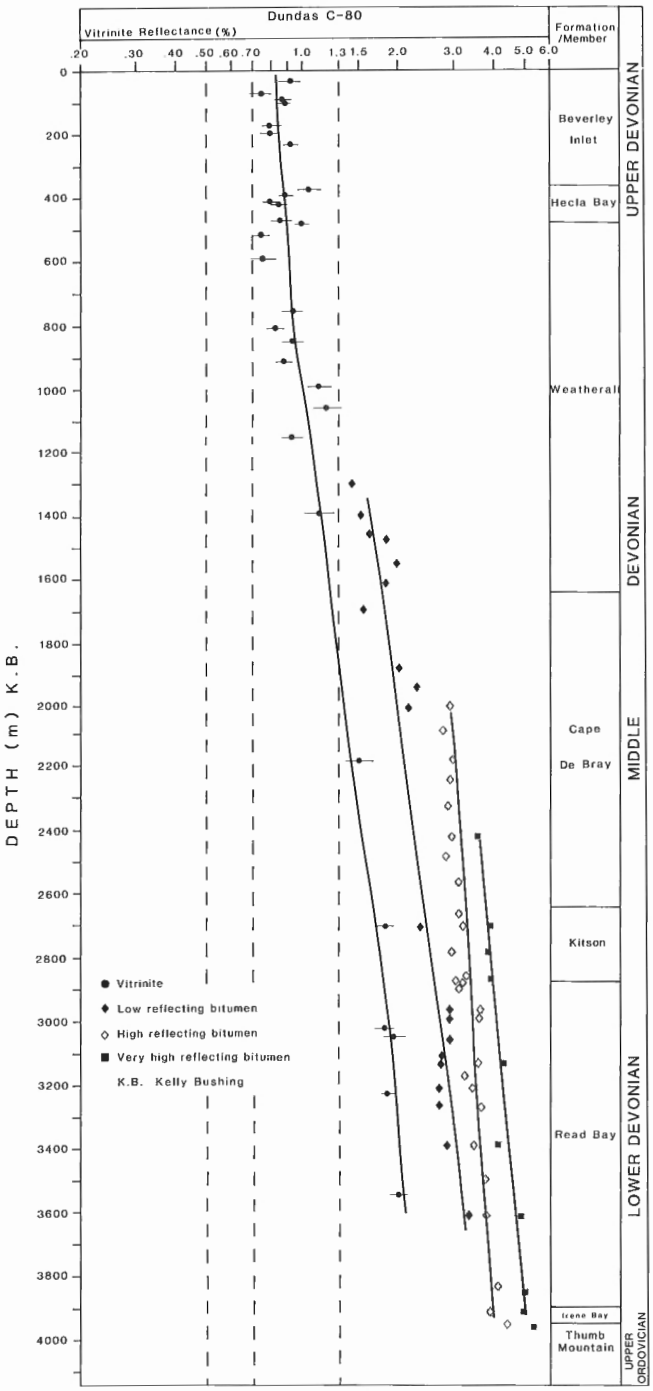

Figure 4. Reflectance measurements for vitrinite and bitumen populations, Dundas C--80 well. (From Gentzis, 1991.)

max (Dundas C80) with increasing depth, is angular, granular under crossed polars, is associated with carbonate grains, and closely resembles metabituminite.

In the Dundas C80 well, the strongly reflecting bitumen in section C (Middle Devonian to Ordovician) has granular anisotropy and is in the meso- to cata-impsonite stage (Khavari-Khorasani, 1975; Jacob, 1975, 1983; Goodarzi and Macqueen, 1990). Microbrecciation, pores, and vesicles, ranging in diameter from a few to 50 microns, have developed in some of the strongly reflecting bitumens, perhaps indicative of de-asphalting. Reflectance increases from 3.5 to 5.1% R_0 max between about 2400 m and total depth (3939 m).

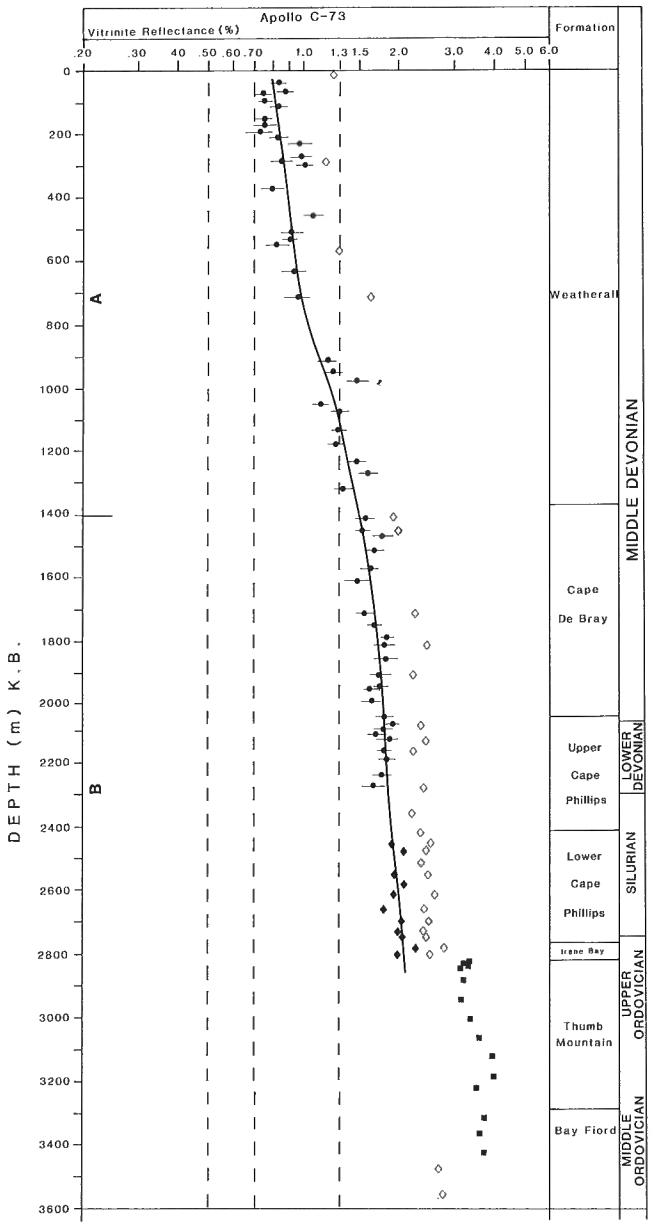

Figure 5. Reflectance measurements for vitrinite and bitumen populations, Apollo C--73 well. Symbols as in Figure 4. (From Gentzis, 1991.)

In the Apollo C73 well, in carbonate rocks of the Thumb Mountain Formation and mixed carbonates and anhydrites of the Bay Fiord Formation (about 2800 to 3400 m), the strongly reflecting bitumen is in the cata-impsonite range (Jacob, 1985). This bitumen shows microbrecciation, and its reflectance ranges from 3.1 to 4.0% R_0 max. It occurs as massive, subangular fragments, is anisotropic, and has a bireflectance of almost 2.0%. The bitumen is angular, non-granular to slightly granular, and resembles metabituminite.

In the Dundas C80 drillhole, vitrinite was identified in all formations with the exception of the two deepest (Irene Bay and Thumb Mountain, Upper Ordovician). It can be seen from Figure 4 that reflectance of vitrinite and of all three bitumen types increases with depth following almost subparallel trends. In the Apollo C73 drillhole, vitrinite was identified in all formations down to the Lower Devonian. A subparallel trend similar to that in Dundas C80, is seen in the data for the Apollo C73 drillhole (Fig. 5).

ORGANIC MATURATION/SUBSIDENCE HISTORY MODELS

For the Dundas C80 well (Fig. 4), vitrinite reflectance data from the upper 1200 m has a logarithmic coalification gradient of 0.114 (+/- 0.034) log $\%R_0$/km. Based on assumed surface R_0 of 0.2%, this gradient gives an erosion estimate of 5.23 km (+2.58 / -2.60 km). A least squares fit to vitrinite reflectance measurements for the entire section sampled gives 4.15 +/- 2.22 km. Similarly, for the Apollo C73 well, for the upper 800 m, a gradient of 0.108 (+/- 0.027) yields an estimate of eroded section thickness of 5.84 km (+2.5/-1.6 km) because of the non-linear character of the data for this well (Fig. 5), no calculation was attempted for the entire drilled section. (Further details of the methodology and comparison to other wells in the Melville Island area will be given in a separate paper.)

These estimates are likely to be upper limits. Vitrinite reflectance gradients in the missing, eroded sections may have been higher than those observed in the present section (near-surface sections generally have steeper gradients in both temperature and log vitrinite reflectance than more deeply buried strata).

Model Input

Formation ages, depths and erosional histories for the Apollo C73 and Dundas C80 drillholes were obtained from studies by Harrison (1991). These are given in Tables 1 and 2. The Dundas C80 well is located just outside the foreland edge of the Franklinian Mobile Belt, where the probable thickness of mid-Frasnian to mid-Famennian sediment is estimated to have been 1800 m. This value was taken as a minimum estimate of erosion at the well location. The Apollo C73 well lies on a periclinal culmination within a major Devonian depocentre. The known local thickness of mid-Eifelian through lower Givetian sediment is 4200 m (Harrison, 1991). This in turn furnished the estimate of erosion amount for the Apollo C73 location. Erosionally removed thicknesses of

Table 1. Panarctic Dome Dundas C-80 well (model D6) - sedimentation history

STRATA Number	Name	Period Ma	DEPOSITION RATE Depth m	Uncompacted m/m.y.	Solid m/m.y.
1	QUATERNARY	0 – 5.0	0 – 1	0.20	0.14
2	BEVERLEY INLET	372.5 – 375.0	1 – 365	155.83	107.13
3	HECLA BAY	375.0 – 376.0	365 – 498	151.90	104.43
4	WEATHERALL	376.0 – 380.0	498 – 1711	375.52	258.17
5	CAPE DE BRAY	380.0 – 382.0	1711 – 2649	617.16	424.29
6	KITSON	382.0 – 410.0	2649 – 2883	11.19	7.69
7	READ BAY GROUP	410.0 – 418.0	2883 – 3563	114.85	78.96
8	CAPE STORM/ALLEN BAY	418.0 – 444.0	3563 – 3899	17.61	12.11
9	IRENE BAY	444.0 – 445.0	3899 – 3950	69.68	47.90
10	THUMB MOUNTAIN	445.0 – 446.0	3950 – 4000	67.81	46.62

EROSION EPISODE Number	Name	Period Ma	EROSION RATE Amount eroded m	Uncompacted m/m.y.	Solid m/m.y.
1	EUREKAN OROGENY	5.0 – 30.0	230	13.36	9.19
2	UPPER CRETACEOUS	30.0 – 100.0	40	-.83	-.57
3	END UPLIFT (ELL)	100.0 – 280.0	15	1.21	.83
4	LATER PHASE (ELL)	280.0 – 315.0	450	18.70	12.86
5	LATER PHASE (ELL)	315.0 – 340.0	750	43.64	30.00
6	ELLESMERIAN OROGENY	340.0 – 350.0	235	34.18	23.50
7	PARRY ISLANDS	350.0 – 370.0	1390	-101.09	-69.50
8	BEVERLEY INLET	370.0 – 372.5	385	-223.82	-153.88

Table 2. Panarctic Apollo C-73 well (model B3) - sedimentation history

STRATA Number	Name	Period Ma	DEPOSITION RATE Depth m	Uncompacted m/m.y.	Solid m/m.y.
1	QUATERNARY	0.0 – 5.0	0 – 1	.20	
2	WEATHERALL	379.0 – 382.0	1 – 1134	387.82	322.27
3	CAPE DE BRAY	382.0 – 383.0	1134 – 2055	978.65	813.25
4	UPPER CAPE PHILLIPS	383.0 – 410.0	2055 – 2415	14.38	11.95
5	LOWER CAPE PHILLIPS	410.0 – 444.0	2415 – 2770	11.34	9.42
6	IRENE BAY	444.0 – 445.5	2770 – 2825	39.95	33.20
7	THUMB MOUNTAIN	445.5 – 457.0	2825 – 3285	43.76	36.36
8	BAY FIORD	457.0 – 465.0	3285 – 3555	37.11	30.84

EROSION EPISODE Number	Name	Period Ma	EROSION RATE Amount eroded m	Uncompacted m/m.y.	Solid m/m.y.
1	EUREKAN OROGENY	5.0 – 30.0	389	18.73	15.56
2	UPPER CRETACEOUS	30.0 – 100.0	289	-4.97	-4.13
3	END UPLIFT (ELL)	100.0 – 280.0	100	-0.67	-0.55
4	LATER PHASE (ELL)	280.0 – 325.0	1145	30.61	25.44
5	LATER PHASE (ELL)	325.0 – 340.0	2000	160.45	133.33
6	ELLESMERIAN OROGENY	340.0 – 350.0	1090	131.17	109.00
7	POST PARRY ISLANDS	350.0 – 360.0	640	-77.02	-64.00
8	PARRY ISLANDS	360.0 – 370.0	1250	-150.42	-125.00
9	BEVERLEY INLET	370.0 – 375.0	750	-180.51	-150.00
10	HECLA BAY	375.0 – 378.0	1335	-535.50	-445.00
11	WEATHERALL	378.0 – 379.0	260	-312.68	-259.83

1815 m for Dundas C80, and 4235 m for the Apollo C73 drillhole location are used in Tables 1 and 2, respectively (these two erosion thickness estimates are the sum of the "Amount eroded" column for either the positive or the negative erosion rate items – negative values in the erosion rate columns signify deposition of a formation that was subsequently eroded). The difference between values in the two columns labelled "Uncompacted" and "Solid" indicates average porosity of the formation during deposition or erosion. The vitrinite-reflectance based estimates of erosion are seen to be substantially higher than those deduced from stratigraphic, sedimentological, and seismic evidence. Possible reasons for the discrepancies have been discussed in the preceding section. Similar behaviour was also noted in a well from the Mesozoic of Sverdrup Basin with a discrepancy factor of at least three (Skibo et al., 1990).

The lithology of each formation (taken from Harrison, 1991, and Canstrat logs and well history reports) was entered as input. However, the corresponding porosities, as calculated by the MATOIL program, were generally larger than those actually observed (e.g., in Figure 7a, the curve labelled "Paleoporosity" is seen to have significantly larger values at all depths than the observed "Present Porosity" values). Consequently, an alternative program input option was tried. Visually estimated values of porosity (Canstrat logs) and values inferred from sonic velocity logs (Harrison, 1991) were entered, and thermal conductivity and heat capacity were then recalculated according to the given lithology. This approach was rejected for the following reasons. Present porosities represent results of a long history of mechanical compaction, burial metamorphism, and other diagenetic processes. When calculating a subsidence history for cases such as these, it is, therefore, incorrect to use present porosity variation with depth as a model for (numerical) decompaction of sedimentary strata. Such a procedure gives paleoporosities that are too small (and therefore calculated thermal conductivities that are too high).

In addition, heat transport toward the surface by advection of hydrothermal pore fluids expelled during mechanical compaction is underestimated, although this may have had only a minor effect on the thermal history of the sediments. However, paleo-overpressures may have had a more significant influence on thermal history. These may have developed at the time of maximum subsidence rates just prior to the Ellesmerian Orogeny. Tables 1 and 2 show subsidence rates approaching 1000 m/m.y. at that time. The empirical procedure of Mann and Mackenzie (1990) for predicting pore fluid pressures in sedimentary basins, indicates the likelihood of overpressuring at these high deposition rates. These authors present several examples from various sedimentary basins, showing the onset of overpressuring at about 2000 m depth. Overpressuring, with its consequent maintenance of higher porosity and water content and, therefore, relatively low thermal conductivity, causes an increased thermal gradient and temperatures. Temperature history models, showing this increase in temperature just prior to and during the Ellesmerian Orogeny, are shown in Figure 6.

The temperature history of the Apollo C73 well was calculated using the porosity distribution ("paleoporosity") given in Figure 7a. This was found to be a valid procedure for this well since negligible thermal maturation occurred after about 330 Ma. Consequently, details of subsequent sediment dewatering and compaction are of negligible concern in modelling organic maturation. However, for strata in the Dundas C80 well, because of less profound burial and a less intense uplift and erosion history, it was found that post-Ellesmerian Orogeny thermal activity exerted some influence on calculated organic maturity. Consequently, the porosity model (Fig. 7b) was modified to give higher porosity for shallow depths, but with a rapid decrease to very low values of porosity below about 2000 m depth.

RESULTS

Calculated vitrinite reflectance, plotted in Figure 8 on a linear scale vs. depth, is compared to representative measured values for the two wells. (For both wells, the value at total depth, indicated as 'measured', actually represents an extrapolation from the entire set of measurements given on Figures 4 and 5.) Standard, twelve component, kinetic parameters were used to calculate the Type IV kerogen transformation ratio from which vitrinite reflectance grade was calculated (e.g., Espitalié, 1986; Ungerer and Pelet, 1987). These kinetic

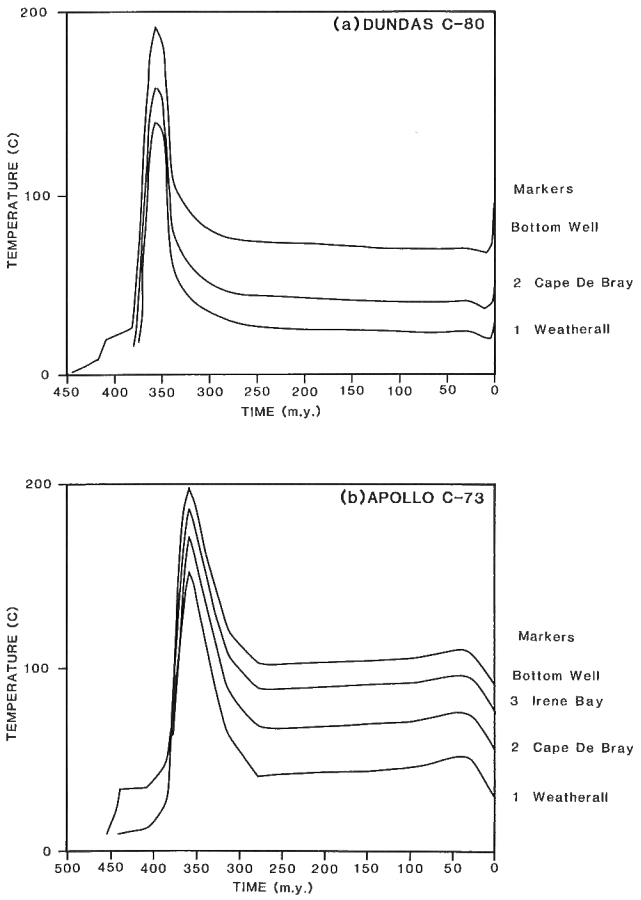

Figure 6. Calculated temperature histories of selected horizons. **a** - Dundas C--80 well. **b** - Apollo C--73 well.

parameters (vitrinite, Lower Jurassic, North Sea) were also used for computation of the oil, condensate and gas generation "windows" given on the subsidence history plots (Figs. 9, 10).

These subsidence history plots for the Dundas C80 and Apollo C73 wells both show an extremely rapid burial, beginning at about 380 Ma and continuing until about the end of Devonian time (360-350 Ma). At this time, the deepest formation in Apollo C--73 (Bay Fiord) was buried at a depth of more than 8 500 m and experienced temperatures of nearly 200°C. The deepest formation in Dundas C80 (Thumb Mountain) was buried more than 5 800 m and experienced temperatures exceeding 190°C. Uplift and erosion due to the Ellesmerian Orogeny commenced in the latest Devonian. Ellesmerian and post-Ellesmerian uplift is believed to have continued with diminishing intensity into the Early Permian. Little evidence has been found of any subsequent deposition in the area (Harrison, 1991), so that only minimal further

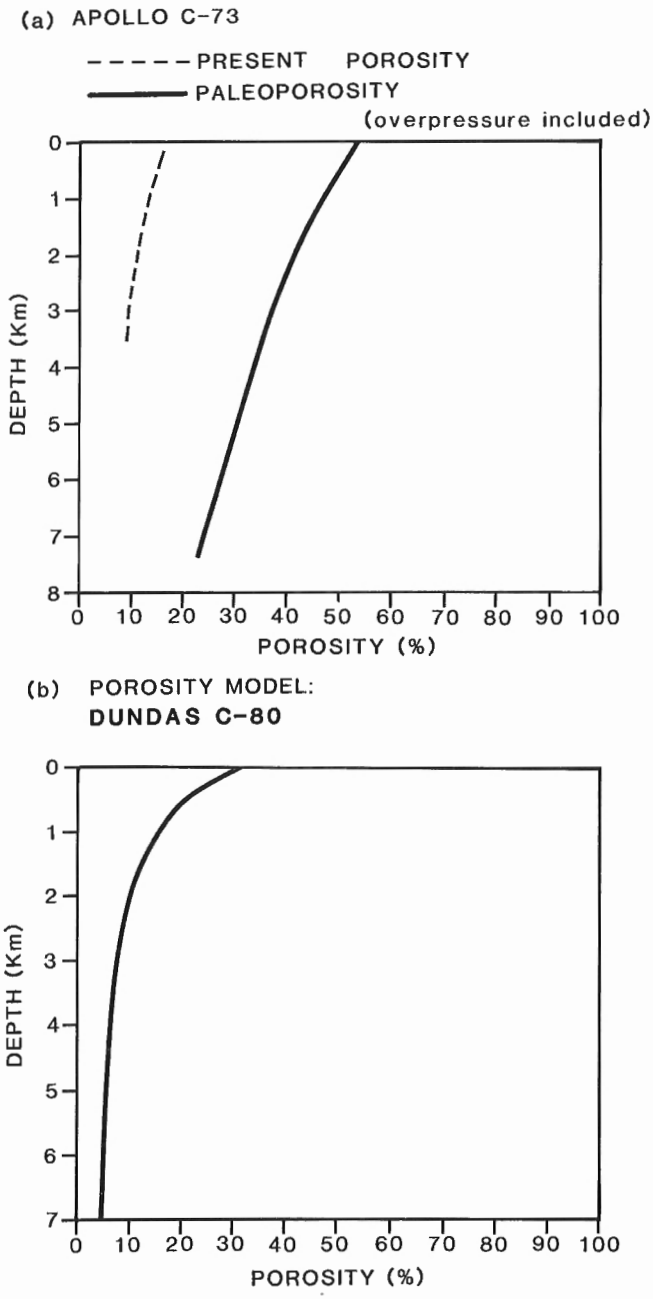

Figure 7. Porosity vs. depth models. **a** - Differences between initial (paleoporosity) and present values for the Apollo C--73 well. **b** - Porosity distribution used in the calculation of a subsidence history model for the Dundas C–80 well.

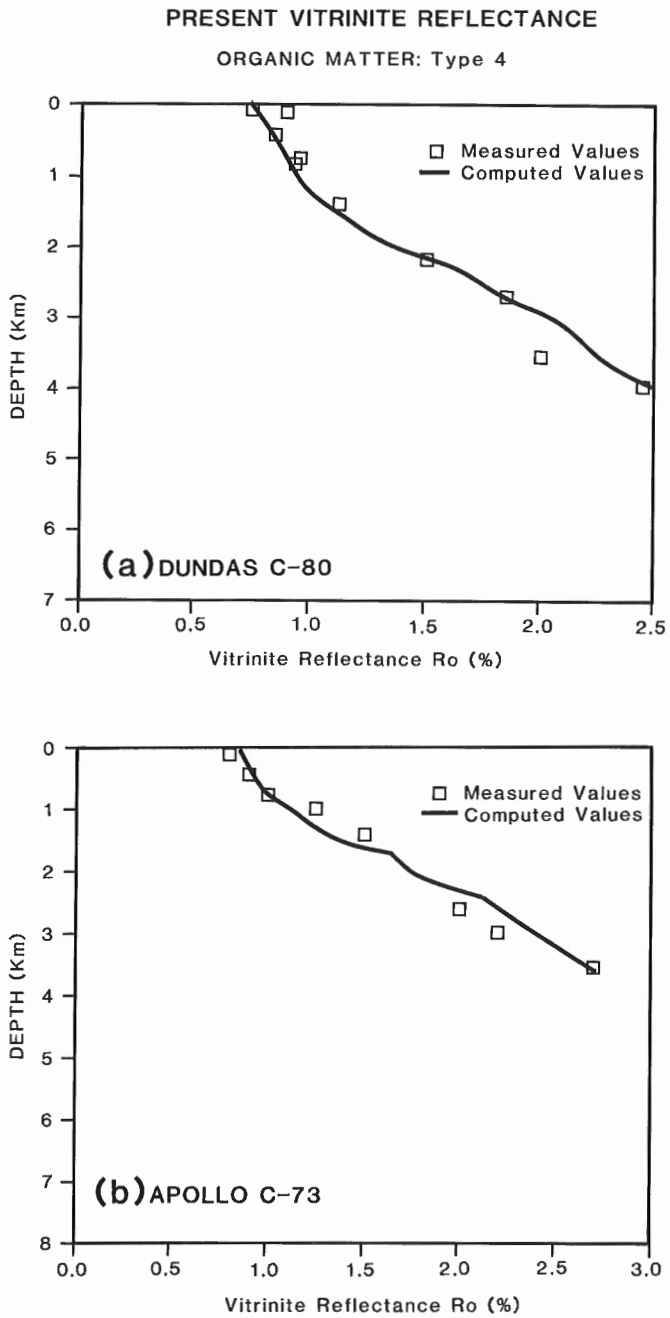

Figure 8. Comparison between calculated vitrinite reflectance and selected representative measurements vs. depth. **a** - Dundas C–80 well. **b** - Apollo C--73 well.

change is given in the plots, apart from uplifts in the order of a few hundred metres at the time of the Eurekan Orogeny (about 35 Ma).

The subsidence histories imply that organic-rich source horizons, such as the Cape Phillips, traversed the oil window extremely rapidly, perhaps within 10 m.y., during the latest Devonian. Such a scenario unfortunately reduces local hydrocarbon potential. Such a short timespan may well have been inadequate for the development of suitable hydrocarbon reservoirs and migration of hydrocarbons to appropriate trapping configurations. Any trapping configurations established, may have been subsequently eroded or breached. In addition, large, potential hydrocarbon accumulations that might have developed during the Late Devonian may have been converted to bitumen as uplift and a consequent reduction in pressure caused deasphalting during the Ellesmerian Orogeny (Hamilton and Varney, 1982).

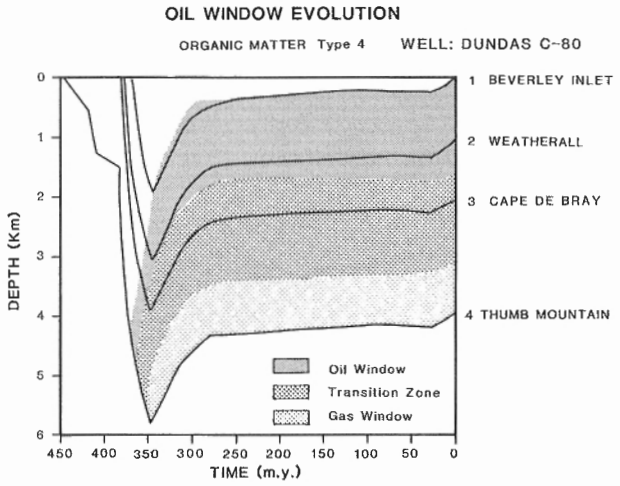

Figure 9. Burial history and oil window evolution: Dundas C–80 well.

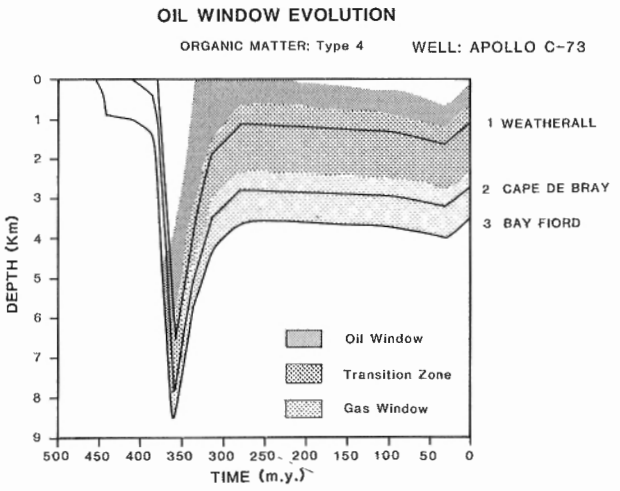

Figure 10. Burial history and oil window evolution: Apollo C–73 well.

DISCUSSION

The stratigraphic position of the deepest formations drilled in the two wells studied differed by about 500 m (see the "Formations" columns in Figures 4 and 5). Similarly, the calculated temperature histories have nearly identical maximum temperatures for both bottom-hole formations (nearly 200°C for both the Apollo C73 and Dundas C80 wells, Fig. 6a, b). However, comparison of the two subsidence models (Figs. 9, 10) shows a difference of almost 3 km in maximum burial depth. If a regional temperature gradient of about 20 $mK.m^{-1}$ existed at the time, then a difference of almost 60°C between the maximum temperatures in the two wells would be expected. Therefore, further studies of regional paleotemperature gradients, or a reconsideration of estimates of thickness of eroded section, thermal conductivity, or the assumed basal heat flow are called for. However, such reconsiderations will not markedly affect the time/temperature histories already calculated, since these are reasonably satisfactory in accounting for the observed vitrinite reflectance maturity data (Fig. 8a, b). Revised model input parameters (estimated heat flow, surface temperature, and thermal conductivity histories) would still give time/temperature histories and, therefore, calculated vitrinite reflectance profiles very nearly the same as those already presented. Revisions or refinements of these input parameters or of estimates of erosion are subject to the constraints of geophysical and geological evidence. Alternatively, the differences in thermal conductivity variation between the two wells need to be more fully and systematically studied. In addition, no systematic analysis of the sensitivity of model calculations to assumed thermal histories has been presented. However, of the wide variety of models calculated (over 25 for each well), the two presented here were clearly the most satisfactory in accounting for observed data.

In summary, the subsidence models presented here:

1. Place additional constraints on geological and organic petrographic estimates of the amounts of eroded section
2. Provide a calculated temperature history, which will be used in further studies of maturation rates of bitumens
3. Provide estimates of the extent of hydrocarbon generation that are generally in accord with previous studies indicating the gas-prone nature of hydrocarbon source rocks in the Melville Island area (Powell, 1978)
4. Provide quantified estimates of the timing and duration of hydrocarbon generation in hydrocarbon source rocks within the Melville Island area.

ACKNOWLEDGMENTS

Constructive, insightful and valuable reviews provided by A.R. Cameron and D.R. Issler are gratefully acknowledged. Pertinent comments by K.R. Stewart, Arctic Geochem Consultants, Calgary, were most helpful. Work on the figures by D.C. McGeachy and staff of the Cartographic and Photomechanical sections at ISPG is acknowledged with pleasure.

REFERENCES

Beauchamp, B., Harrison, J.C., and Henderson, C.M.

1989a: Upper Paleozoic stratigraphy and basin analysis of the Sverdrup Basin, Canadian Arctic Archipelago: Part 1, time frame and tectonic evolution. Geological Survey of Canada, Paper 89-1G, p. 105-113.

1989b: Upper Paleozoic stratigrapy and basin analysis of the Sverdrup Basin, Canadian Arctic Archipelago: Part 2, transgressive--regressive sequences. Geological Survey of Canada, Paper 89-1G, p. 115-124.

Davies, G.R. and Nassichuk, W.W.

in press: Carboniferous to Permian geology of the Sverdrup Basin, Canadian Arctic Archipelago; in Innuitian Orogen and Arctic Platform: Canada and Greenland, H.P. Trettin (ed.); Geological Survey of Canada, Geology of Canada, No. 3. (Also, The Geology of North America, Geological Society of America, v. E.)

Embry, A.F.

1987: MiddleUpper Devonian sedimentation in the Canadian Arctic Islands and the Ellesmerian Orogeny; in Proceedings of the Second International Symposium on the Devonian, N.J. McMillan, A.F. Embry, and D. Glass (eds.); Canadian Society of Petroleum Geologists, Memoir 14, p. 15-28.

Espitalié, J.

1986: Use of Tmax as a maturation index for different types of organic matter. Comparison with vitrinite reflectance; in Thermal Modelling in Sedimentary Basins, J.Burrus (ed.); Éditions Technip, p. 475-496.

Fox, F.G.

1985: Structural geology of the Parry Islands Fold Belt. Bulletin of Canadian Petroleum Geology, v. 33, no. 3, p. 306-340.

Gentzis, T.

1991: Regional maturity and source-rock potential of Paleozoic and Mesozoic strata, Melville Island, Arctic Canada. Unpublished Ph.D. thesis, University of Newcastle-upon-Tyne, U.K.

Gentzis, T. and Goodarzi, F.

in press: Regional thermal maturity and source-rock potential of sedimentary rocks from the Franklinian Geosyncline, Melville Island, Arctic Canada. Marine and Petroleum Geology.

Goodarzi, F. and Macqueen, R.W.

1990: Optical/compositional character of six bitumen species from Middle Devonian rocks of the Pine Point Pb-Zn property, Northwest Territories. Canadian Bulletin of Petroleum Geology, v. 14, no. 3, p. 197-216.

Goodbody, Q.H.

1988: Devonian shelf systems on Melville Island, Canadian High Arctic; in Proceedings of the Second International Symposium on the Devonian, N.J. McMillan, A.F. Embry, and D. Glass (eds.); Canadian Society of Petroleum Geologists, Memoir 14, v. 2, p. 29-52.

Hamilton, J.K. and Varney, G.R.

1982: Cores from the Canadian Arctic Archipelago, geology and hydrocarbon occurrences. American Association of Petroleum Geologists/CSPG Core Conference Manual, 21 p.

Harrison, J.C.

1991: Melville Island's salt based fold belt (Arctic Canada). Unpublished Ph.D. thesis, Rice University, 703 p.

Harrison, J.C. and Bally, A.W.

1988: Cross-sections of the Parry Islands Fold Belt on Melville Island. Bulletin of Canadian Petroleum Geology, v. 36, p. 311-332.

Harrison, J.C. and Brent, T.

in press: Late DevonianEarly Carboniferous deformation, Prince Patrick and Banks islands and adjacent areas, Canadian Arctic Islands. Chapter 12H, in Innuitian Orogen and Arctic Platform: Canada and Greenland, H.P. Trettin (ed.); Geological Survey of Canada, Geology of Canada, No. 3. (Also, The Geology of North America, Geological Society of America, v. E.)

Harrison, J.C., Embry, A.F., and Poulton, T.P.

1988: Field observations of the structural and depositional history of Prince Patrick and adjacent areas, Canadian Arctic Islands; in Current Research, Part D, Geological Survey of Canada, Paper 88-1D, p. 41-50.

Harrison, J.C., Fox, F.G., and Okulitch, A.V.

in press: Late DevonianEarly Carboniferous deformation of the Parry Islands and Canrobert fold belts. Chapter 12G, in Innuitian Orogen and Arctic Platform: Canada and Greenland, H.P. Trettin (ed.); Geological Survey of Canada, No. 3. (Also, The Geology of North America, Geological Society of America, v. E.)

Jacob, H.

1975: Mikroskopphotometrische Analyse natürlicher fester Erdölbitumina; in Pétrographie de la matière organique des sédimentes, relations avec la paléotemperature et le potentiel pétrolier, Alpern, B. (ed.); CNRS, Paris, p. 103-113.

1983: Report on bitumens. International Committee for Coal Petrology; Meeting, Oviedo, Spain.

1985: Dispersed solid bitumens as an indicator for migration and maturity in prospecting for oil and gas. Erdöl und Kohle-Erdgas-Petrochemie, 38, p. 365.

Kerr, J.W.

1981: Evolution of the Canadian Arctic Islands: a transition between the Atlantic and Arctic Oceans; in The Ocean Basins and Margins, A.E.M. Nairn, M. Churkin, and F.G. Stehli (eds.); Plenum Press, New York, v. 5, p. 105-199.

Khavari-Khorasani, G.

1975: The properties and structural ordering of some fossil bitumen. Unpublished Ph.D. thesis, University of Newcastle-upon-Tyne, U.K., 350 p.

Mann, D.M. and Mackenzie, A.S.

1990: Prediction of pore fluid pressures in sedimentary basins. Marine and Petroleum Geology, v .7, p. 54-65.

Overton, A.

1970: Seismic refraction surveys, western Queen Elizabeth Islands and polar continental margin. Canadian Journal of Earth Sciences, v. 7, p. 346-365.

1982: Seismic reconnaissance profiles across the Sverdrup Basin, Canadian Arctic Islands; in Current Research, Part B; Geological Survey of Canada, Paper 82-1B, p. 139-145.

Powell, T.G.

1978: An assessment of the hydrocarbon source rock potential of the Canadian Arctic Islands. Geological Survey of Canada, Paper 78-12, 82 p.

Skibo, D.N., Osadetz, K.G., and Goodarzi, F.

1990: Models of maturation and hydrocarbon potential: application to Lougheed Island drillholes, Sverdrup Basin, Canadian Arctic Islands; in Current Research, Part D, Geological Survey of Canada, Paper 90-1D, p. 201-211.

Sobczak, L.W., Mayr, U., and Sweeney, J.F.

1986: Crustal section across the polar continentocean transition in Canada. Canadian Journal of Earth Sciences, v. 23, p. 608-621.

Stephenson, R.A., Embry, A.F., Nakiboglu, S.M., and Hasticoglu, M.A.

1987: Rift-initiated Permian to Early Cretaceous subsidence of the Sverdrup Basin; in Sedimentary Basins and Basin-forming Mechanisms, C. Beaumont and A.J. Tankard (eds.); Canadian Society of Petroleum Geologists, Memoir 12.

Sweeney, J.F., Balkwill, H.R., Franklin, R., Mayr, U., McGrath, P., Snow, E., Sobczak, L.W., Wetmiller, R.J., and Panarctic Oils Ltd.

1986: G. Somerset Island to Canada Basin. Centennial Continent/Ocean Transect # 11; Geological Society of America.

Thorsteinsson, R. and Tozer, E.T.

1960: Summary account of structural history of the Canadian Arctic Archipelago. Geological Survey of Canada, Paper 67-64, 16 p.

1970: Geology of the Arctic Archipelago; in Geology and Economic Minerals of Canada, R.J.W. Douglas (ed.); Geological Survey of Canada, Economic Geology Report No. 1, p. 547-590.

Trettin, H.P.

1989: The Arctic Islands; in The Geology of North America An Overview, A.W. Bally and A.R. Palmer (eds.); The Geology of North America, Geological Society of America, v. A, p. 349-370.

Trettin, H.P., Mayr, U., Long, G.D.F., and Packard, J.J.

in press: Cambrian to Early Devonian deposition, Arctic Islands; in Innuitian Orogen and Arctic Platform: Canada and Greenland, H.P. Trettin (ed.); Geological Survey of Canada, Geology of Canada, No. 3. (Also, The Geology of North America, Geological Society of America, v. E.)

Ungerer, P. and Pelet, R.

1987: Extrapolation of the kinetics of oil and gas formation from laboratory experiments to sedimentary basins. Nature, v. 327, no. 6117, p. 52-54.

Ziegler, P.A.

1988: Evolution of the ArcticNorth Atlantic and the western Tethys. American Association of Petroleum Geologists, Memoir 43, 198 p.

Size population and cyclicity of combined flow bedforms: a study from the Jurassic-Cretaceous, Fernie-Kootenay transition beds in the southern Alberta Foothills

Indranil Banerjee and Marcel Labonté
Institute of Sedimentary and Petroleum Geology, Calgary

Banerjee, I. and Labonté, M., 1991: Size population and cyclicity of combined flow bedforms: a study from the Jurassic-Cretaceous, Fernie-Kootenay transition beds in the southern Alberta Foothills; in Current Research, Part E, Geological Survey of Canada, Paper 91-1E, p. 177-185.

Abstract

The wavelengths (WL) and ripple heights (RH) of 182 combined-flow bedforms with a wide range of sizes (WL = 0.1-2.8 m) were measured in an upward sequence in sandstones in the upper part of the Middle to Upper Jurassic Fernie Formation in the southern Alberta Foothills. These sandstones exhibit hummocky cross-stratification (HCS), and the section represents a shallowing-upward, storm-dominated shoreline sequence.

Statistical analysis of the WL values demonstrates a 16-bed periodicity in the lower part of the sequence (bed numbers 1 to 105), superimposed on a strong linear trend (increasing upward). Statistical tests also show that 3-D bedforms belong to a single log-normal population that is distinct from the 2-D bedform population.

The linear trend has been explained as a "proximality trend" normally found in storm beds in shallowing-upward shoreline sequences. The 16-bed cycle, representing 64 000 to 200 000 years, may probably be attributed to a fourth- or fifth-order eustatic cycle falling within the Milankovitch band of frequencies.

Résumé

Les longueurs d'ondes et les hauteurs des ondulations de 182 modelés de couches d'écoulement combiné de tailles très variées (de 0,1 à 2,8 m de longueurs d'ondes) ont été mesurées dans une séquence ascendante dans des grès de la partie supérieure de la formation de Fernie du Jurassique moyen à supérieur dans le piémont de l'Alberta méridionale. Ces grès présentent une stratification entrecroisée mamelonnée, et le profil est une séquence de ligne de rivage, de profondeur décroissante vers le haut, dominée par des tempêtes.

L'analyse statistique des valeurs des longueurs d'ondes révèle une périodicité de 16 couches dans la partie inférieure de la séquence (numéros de couche 1 à 105), qui se superpose à une forte tendance linéaire (croissante vers le haut). Les tests statistiques montrent aussi que le modelé tridimensionnel des couches appartient à une même population de couches log-normale qui est distincte de la population de couches de modelé bidimensionnel.

La tendance linéaire a été expliquée par une "tendance de proximalité" normalement présente dans les couches de tempête des séquences de ligne de rivage de profondeur décroissante vers le haut. Le cycle de 16 couches, correspondant à une période de 64 000 à 200 000 ans, est probablement attribuable à un cycle eustatique de quatrième ou de cinquième ordre se situant dans la bande de fréquences de Milankovitch.

INTRODUCTION

In geological records of storm-dominated siliciclastic shorelines, a diagnostic sedimentary structure commonly encountered is hummocky cross-stratification (HCS). Most authors believe (Swift et al., 1983; Greenwood and Sherman, 1986; Nøttvedt and Kreisa, 1987) that HCS is produced by combined flow with an oscillatory and a unidirectional component. Experimental data also support this interpretation (Arnott and Southard, 1990).

The size range of bedforms producing HCS have never been well defined. Craft and Bridge (1987) compiled data from the literature to show the variable terminology and wide range of dimensions applied to hummocky bedforms by various authors. Their table (Craft and Bridge, 1987; Table 1) shows a range from 0.1 m to 10 m in the wavelengths (WL) of these bedforms. Some authors prefer to name the smaller ones (with wavelengths in centimetres) micro-hummocky lenses and their stratification micro-HCS (Dott and Bourgeois, 1982).

In this study, wavelengths of the bedforms range from 0.1 to 2.8 m and have been divided into the following two groups: 1) two-dimensional (2-D) bedforms with a continuous crest line; and 2) three-dimensional (3-D) bedforms with an elliptical plan view and a scarcely discernible crest area. The 3-D bedforms are interpreted as being of combined flow origin, and the 2-D bedforms could have been produced by either combined flow or pure oscillatory flow.

Two questions regarding these combined flow bedforms were considered in this study:

1. Is there a continuous size-population in 3-D bedforms, ranging from decimetre-scale forms to metre-scale ones?
2. In shallowing-upward records of storm-dominated shorelines, is there a detectable trend and cyclicity in the size parameters (wavelength) of 3-D bedforms?

These two questions have been addressed with the help of an empirical study involving 182 field measurements of wavelengths and ripple heights of inferred combined flow bedforms from a cliff section located in the abandoned Adanac Mine in the Crowsnest Pass area of the southern Alberta Foothills (Fig. 1). The section straddles the boundary (Fig. 2) between the Morrissey Formation of the Kootenay Group (Jura-Cretaceous) and the Fernie Formation (Middle to Upper Jurassic). The sedimentary record studied here represents a shallowing-upward sequence of offshore marine shales, grading upward into shoreface deposits which in turn pass into foreshore sandstones with backshore coal swamp sediments on top (Hamblin and Walker, 1979). The wavelengths of bedforms increase upward in this sequence and, in addition to this upward increasing "trend", there are fluctuations in size which seem to be periodic. Both the periodic nature of upward size variation (in a time series) and the bimodal versus unimodal nature of the size population of the bedforms have been tested statistically. These results have been interpreted in terms of a geological process-response model.

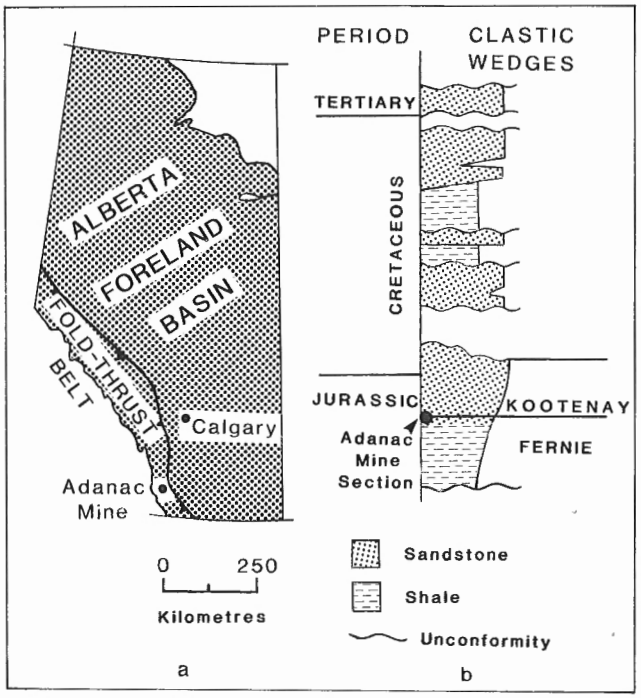

Figure 1. (**a**) Location map showing the position of the Adanac Mine within the fold/thrust belt of the Alberta Foreland Basin. (**b**) Stratigraphic section of the Alberta Foreland Basin, showing the location of the Adanac Mine section at the Fernie-Kootenay contact. (After Cant, 1990.)

GEOLOGICAL FRAMEWORK

The Adanac Mine section is located within the fold/thrust belt in the lowermost clastic wedge in the Alberta Foreland Basin (Fig. 1). The detailed sedimentology of this part of the stratigraphic column has been described by Hamblin and Walker (1979) and Gibson (1985).

Figure 2 illustrates the detailed stratigraphy as well as the paleoenvironmental interpretation of the 40 m thick section measured by one of the authors (IB). This is part of a 100 m thick section exposed in the Adanac Mine. The section consists of black marine shales with very thin silty beds at the bottom grading upward into thicker sandstones with fewer shale interbeds with a 5 m thick coal seam at the top. In the middle of this section, 182 beds were selected for detailed bedform measurements.

DESCRIPTION OF THE BEDFORMS

Internal stratification found within the sandstone beds that range in thickness from centimetres to metres is invariably low- to high-angle cross-stratification. Ripple forms are clearly seen in many cases (Fig. 3a, b, c) and the three-dimensional shape of ripples can be viewed by digging out the indurated sandstone slabs (see Fig. 3d). Smaller sized bedforms are mostly two-dimensional (2-D), becoming more elliptical in plan (3-D) as they grow bigger. Ripple spacings or wavelengths and ripple heights were measured in each bedform in sections normal to the ripple crest line. As the

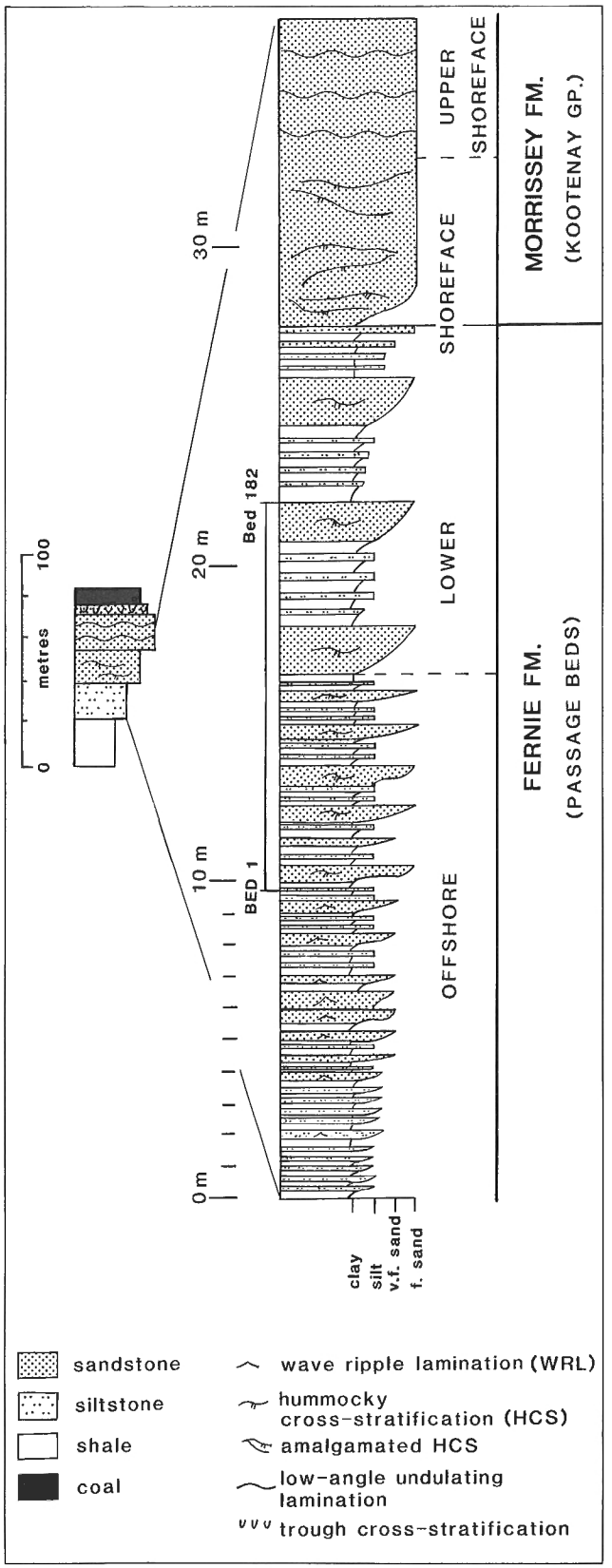

ripples get bigger they are more difficult to dig out and, because they are more likely to be amalgamated, the ripple forms become difficult to discern. The data become less reliable, therefore, in the larger 3-D forms.

Although the 182 measurements have been plotted as a continuous time series (Fig. 4), it must be mentioned that, in some cases, especially in the thicker top part of the series, successive beds could not always be measured and at least 10 per cent of the data for the series is missing.

All internal laminae of the bedforms are low-angle (<20°) and they have the following characteristics:

1. Bundles of laminae are separated by low-angle (<15°) truncation planes
2. Laminae converge toward "hummocks" and diverge toward "swales"
3. Scour-and-drape features are common.

These features broadly characterize the HCS and micro-HCS, and suggest that the whole group of bedforms, from the largest to the smallest, are genetically similar. All beds studied consist of indurated, well sorted, fine to very fine grained sandstone. Lower and upper contacts with adjoining black shales are always very sharp.

ORIGIN OF THE BEDFORMS

A combined flow origin for the bedforms associated with HCS studied here has been assumed, based on:

1. A discernible 3-D elliptical shape of all bedforms larger than a certain size (wavelength >0.75m) in the study area;
2. Unidirectionally dipping laminae within some bedforms;
3. A measurable unidirectional paleocurrent direction, found earlier in the same outcrop by Hamblin and Walker (1979).

Theoretical support for a combined flow origin of HCS comes from:

1. Evidence gathered from modern examples of HCS (Swift et al., 1983; Greenwood and Sherman, 1986);
2. Evidence gathered from geometry and paleocurrent data of ancient HCS bedforms Nøttvedt and Kreisa, 1987);

Figure 2 (opposite). Measured section at the Adanac Mine. The left hand column shows the entire section exposed (after Hamblin and Walker, 1979). The right hand column shows the part measured in this study. The measured bedform series lies between beds 1 and 182 as shown. "Offshore" and "shoreface" refer to inferred paleoenvironments.

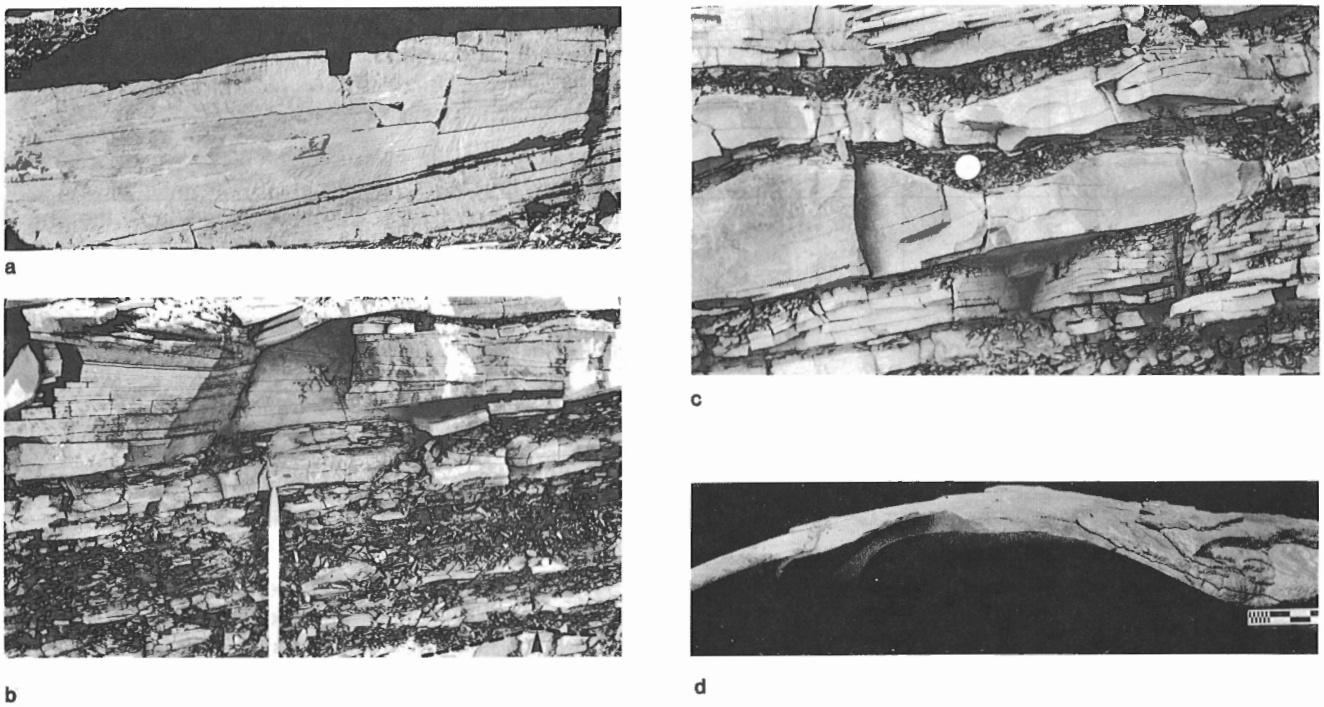

Figure 3. Photographs of the bedforms measured in this study. (**a**) Partly exhumed larger scale bedform (3-D) with HCS. Note convergence of laminae, low-angle truncations, and hummock near the top. Pen is 15 cm long. (**b**) Vertically stacked beds showing the increasing size of the bedforms, from small ripples (arrow) at the bottom to larger ones (with HCS) at the top. This is one individual cycle of the series which, on the whole, has a linear trend of increasing size (both WL and RH). Pen is 15 cm long. (**c**) Exhumed top of a mini-HCS 3-D bedform. Note the convergence of laminae and low-angle truncations. Also note the uniformly dipping laminae within the ripple to the left of the coin. Coin is 2.3 cm in diameter. (**d**) A 3-D bedform dug out from the shale. Note the convergence of laminae at the crest and the 3-D shape of the bedform. Scale is in centimetres.

3. Experimental data in which combined flow was able to produce 3-D bedforms that, in turn, produced HCS and micro-HCS (Arnott and Southard, 1990).

FIELD MEASUREMENT OF BEDFORMS

The following steps constituted the measurement procedure:

1. Bedforms were dug out or dug around by removing the adjacent splintery shale;
2. The shape of the bedform (2-D or 3-D) was noted;
3. In a section perpendicular to the crest line, the crest to crest length (wavelength or WL) and the crest to trough height (ripple height or RH) were measured;
4. The measurements were continued upward in successive beds.

Shortcomings of the data are as follows:

1. Both very small bedforms (<5 cm WL) and very large bedforms (>1 m) are difficult to measure because of difficulty in recognizing the very small ripple forms, and the amalgamation problem in the larger bedforms. The population studied here, therefore, is truncated at both ends.
2. In larger bedforms (>0.6 m WL) many wavelengths measured were apparent wavelengths (Craft and Bridge, 1987) rather than true wavelengths.
3. The vertical sequence is not continuous. There are gaps in the series because of non-preservation of good bedforms.

A log-log plot of the WL vs. RH data (Fig. 5) shows a good correlation between WL and RH (r=0.892). It also shows that although there is a large overlap in size between 2-D and 3-D bedforms, all bedforms with WL greater than 75 cm are 3-D.

SIZE POPULATION

Introduction

Because the two parameters measured on individual bedforms, wavelength and ripple heights, are so well correlated, only the wavelength data are presented here; it is assumed that the statistical behaviour of the ripple height would be similar.

The frequency distribution of the wavelengths of the bedforms is shown in Figure 6. The total data show a highly skewed distribution (Fig. 6a), probably suggesting a log-normal distribution. When separated into 2-D

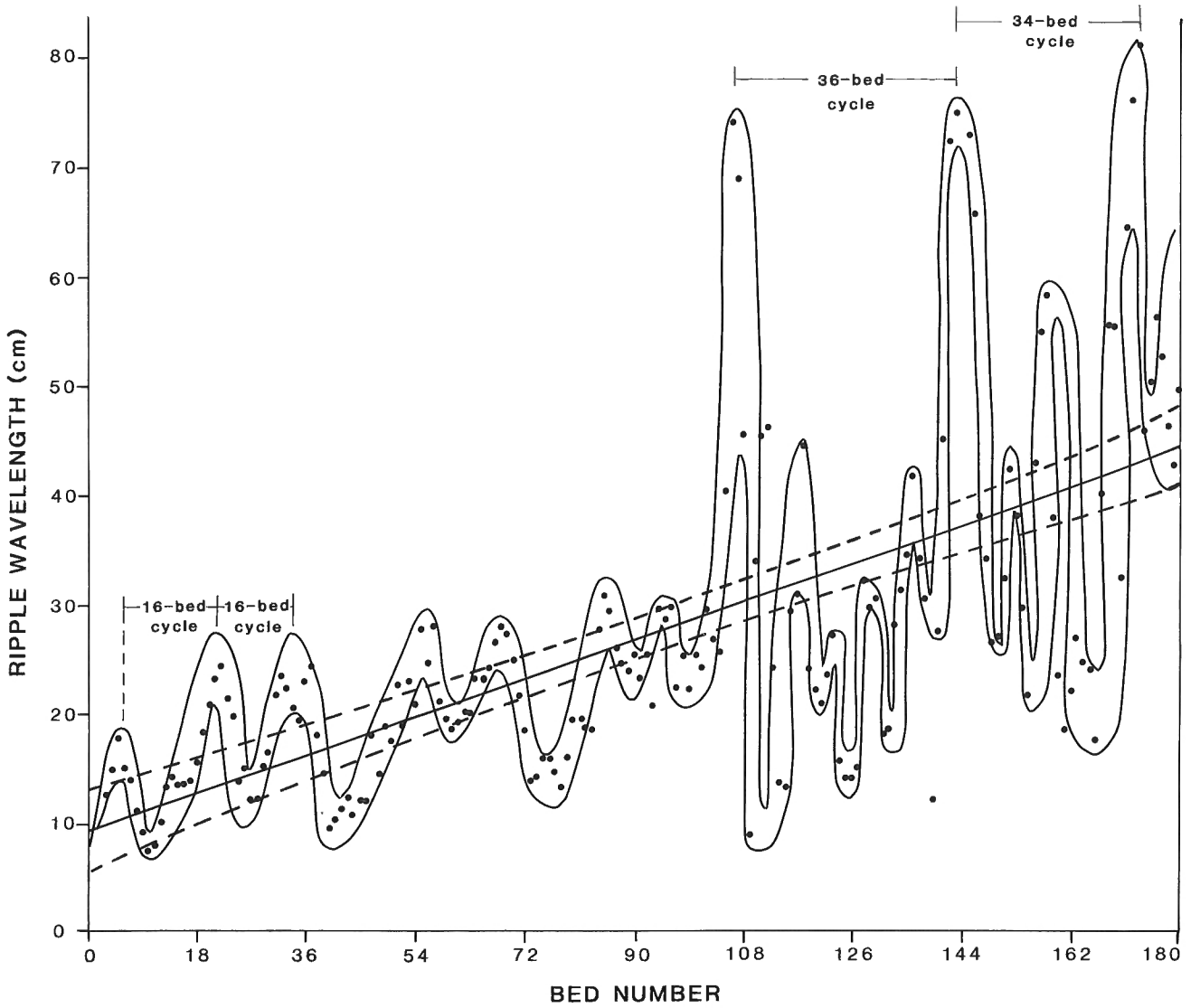

Figure 4. A 5-point moving average plot of ripple wavelengths against the upward sequence of beds (bed number). The lines enveloping the points show the 16-bed cyclicity in the lower part of the series (bed numbers 1 to 105). The upper part of the series is too noisy due to measurement difficulties, but a high-amplitude 32-bed cycle might be present (see Fig. 7). The linear trend is indicated by the regression line (solid) in the middle and the confidence interval is shown by the two dashed lines.

and 3-D subpopulations, the former shows a highly truncated population (Fig. 6b) with a narrow range, while the 3-D subpopulation (Fig. 6c) again shows a skewed distribution, which suggests a log-normal population. This is confirmed by a plot of the same data on logarithmic probability paper (Fig. 7) – the points fall on a straight line, signifying that all 3-D bedforms ranging in wavelength from 0.1 to 2 m belong to a single population.

3-D bedforms

The wavelengths of 3-D bedforms measured here range from 10 to 280 cm, spanning the entire field of both "ripples" and "dunes" for bedforms produced by unidirectional currents. A gap between the ripple and dune populations normally occurs at a wavelength value of approximately 0.5 m (Ashley et al., 1990). The genetic reason for these two distinct bedform populations in unidirectional currents was given by Yalin (1977). The two populations are the results of two distinct processes. Ripples are produced by deformation of the unstable bed surface and their wavelengths are functions of grain size only (Yalin, 1977, p. 235). In contrast, dunes are produced by a different process, namely, the propagation of a disturbance of the structure of macroturbulence which is related only to the depth. Thus, a genetic difference controls the existence of the two size populations. In the combined-flow regime, presumably, this distinction does not hold true, and the single population of wavelengths, from 10 cm to 2 m, shown by the data of 3-D beforms (Fig. 7) indicates a single

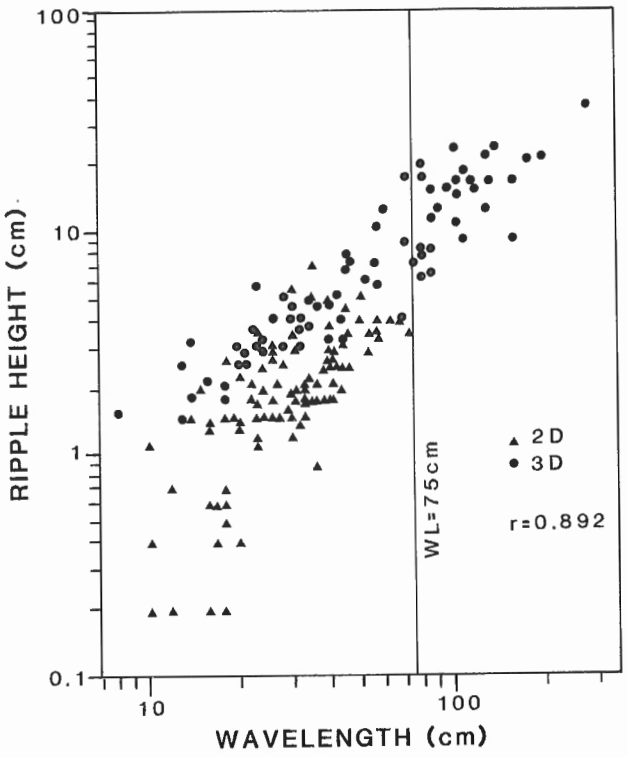

Figure 5. Log-log plot of wavelength (WL) vs. ripple heights (RH) showing a good linear relationship, confirmed by a correlation coefficient value of 0.892. Note that all bedforms larger than WL = 75 cm are 3-D.

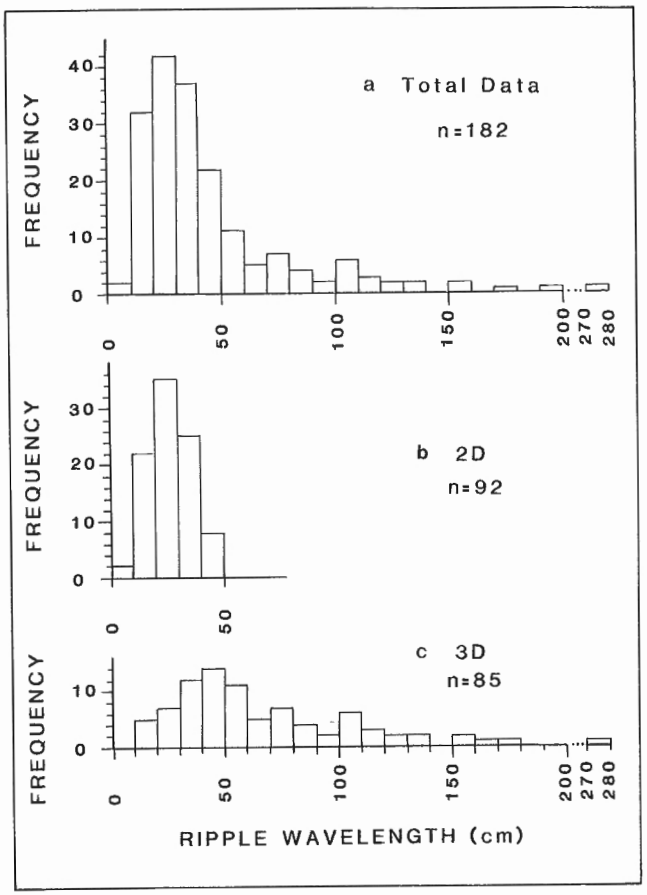

Figure 6. Histograms showing the size population of the bedforms in terms of their measured wavelengths (WL). (**a**) Total data, showing a highly skewed distribution probably suggesting a log-normal population. (**b**) Data for the 2-D bedforms. Most data fall within four classes. The right hand side of the histogram (larger size) is truncated. (**c**) Data for 3-D bedforms showing a large range. Skewed distribution suggests a log-normal population (see Fig. 7).

underlying process of bedform generation. The exact nature of this process is not known for certain at this stage, although maximum excursion length of water particles (Allen, 1985) and propagation of macroturbulence disturbances must both have played their part.

2-D bedforms

The distinction between wavelength size-distributions for 2-D and 3-D bedforms was statistically tested by comparing the two sample means with the "t" test, according to the method outlined in Till (1974). The test shows that the means are different, suggesting a genetic difference between the two bedforms. Although no definite explanation for this can be presented at this stage, experimental data (Arnott and Southard, 1990) showed that 2-D combined flow bedforms are produced only at very small oscillatory and unidirectional velocities, indicating very sluggish conditions.

CYCLICITY

In Figure 4, filtered data (using a 5-point moving average) of the wavelengths of all bedforms have been plotted against the bed number; based on the vertical upward sequence of beds. As mentioned above, there is a gap of at least 10 per cent in data points. The plot on the whole shows a broad linear trend rising to the right, illustrating an increase in the size of bedforms at stratigraphically higher positions. This trend is also apparent from the measured section (Fig. 2). A regression line with confidence intervals brings out this trend (Fig. 4). Superimposed on this trend a cyclic pattern is also detectable. In the lower part of the series (bed numbers 1 to 105) a 16-bed cycle can be identified visually. At the upper end of the series the data become too "noisy" and there are wide fluctuations. This phenomenon occurs because of measurement difficulties caused by problems related to digging out large bedforms and the amalgamation of individual bedforms. However, a 34- to 32-bed cycle can be reconstructed with some effort. The validity of these cycles has also been tested statistically, as detailed below.

STATISTICAL TESTING FOR A TREND AND CYCLICITY

Introduction

The data values representing the wavelength of bedforms were tested to establish whether a statistically significant trend exists, constituting a departure from random variations

in wavelengths. For this purpose, a set of programs performing various implements of moving averages and statistical testing, as per the article of Waldron (1987), were coded to process the numbers. The trend is shown by a regression line and a confidence interval (Fig. 4).

Statistical filtering

The moving average filter was the only method of pre-filtering utilized, a decision based on the graphical appearance of the resulting sequence of numbers when plotted against a monotonically increasing sequence of bed numbers. Various sizes of filter were tried, and the one retained, the one with 12 points each assigned an equal weight, provides a suitable appearance while containing a minimum number of points to be averaged. The moving median filter of equal size was also tested but not retained, owing to the difficulty in interpreting the filtered sequences. The sequences resulting from the moving average filtering were submitted to an autocorrelation procedure, in order to detect the periods more effectively, and to test them against the various autocorrelation models for sequences, as proposed by Chestnut (1966). The data for

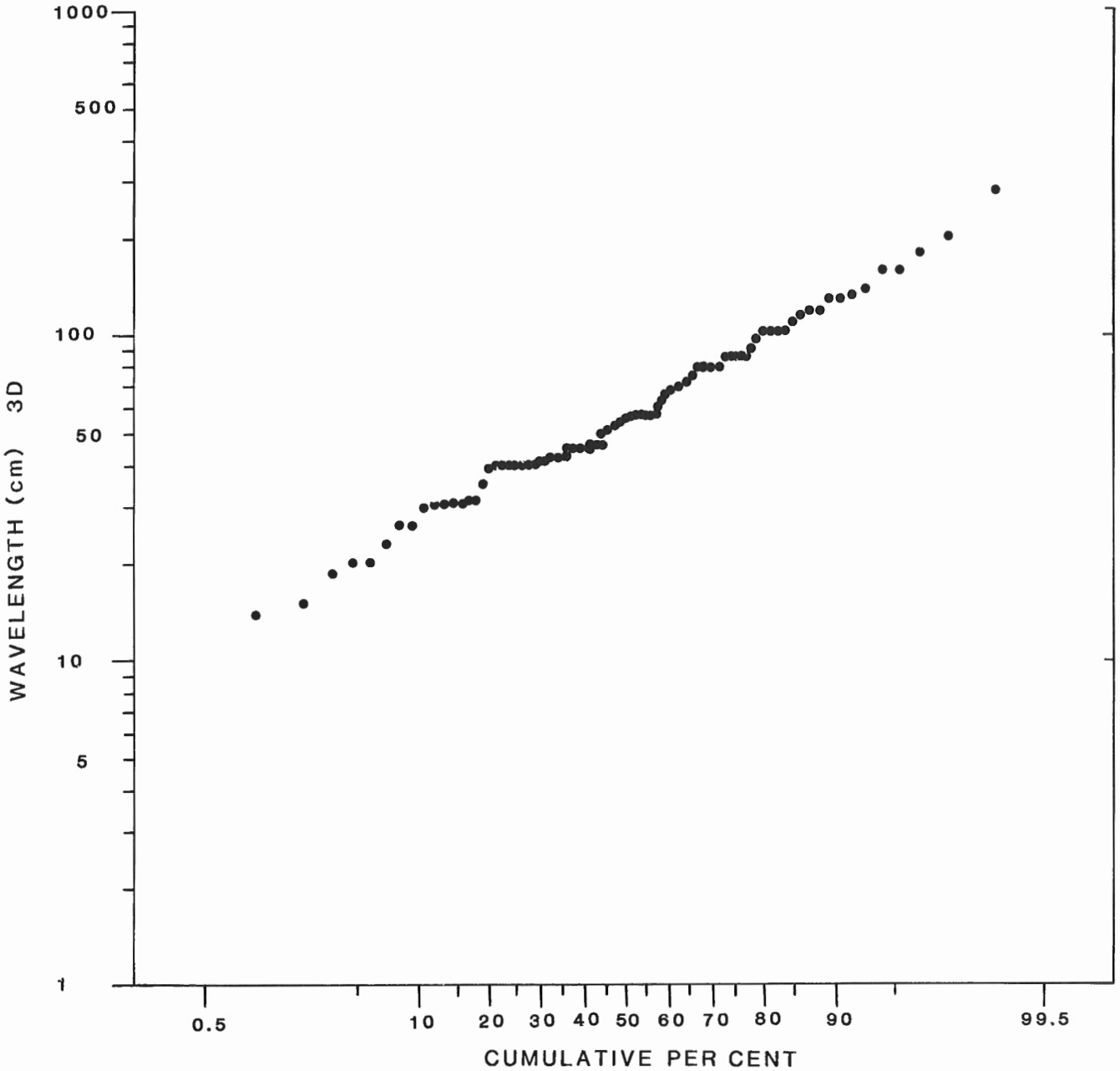

Figure 7. Wavelengths of 3-D (combined-flow) bedforms plotted on 3-cycle logarithmic probability paper. Data points (the same as in Fig. 6c) fall along a straight line, suggesting a unimodal log-normal distribution. There is no break between ripples and dunes, as is the case for unidirectional current bedforms.

WL and RH were equally submitted to a Fast Fourier Transform procedure, as implemented in the software package MathCad (Mathsoft Inc., 1989), and a periodogram was produced. However, the results of Fast Fourier Transform analysis were not incorporated in the analysis as we preferred to rely on autocorrelation only. According to Southworth (1967), a sequence of numbers must be stationary in order to use the Power spectrum for frequency analysis. The autocorrelation procedure (Correlogram) was used directly for frequency analysis in terms of the lag. As Waldron (1989) has indicated, information concerning the asymmetry of the cycles is contained in the phase angles associated with the periodic component. Thus autocorrelation alone is utilized in the "older approach", where the autocorrelogram is first computed (Davis, 1986), and the periodicity can be observed broadly in terms of the lags on the correlogram. The Fourier transform is not performed as a follow up to the "older approach", owing to the possible phase instabilities in the signal.

Statistical testing

The filtered sequences, as obtained by the moving average filtering process, were also submitted to a sign test proposed by Waldron (1987). The object of the test was to decide if a significant trend of increasing thickness existed to corroborate the relevant geological model. Graphically, both of the filtered sequences appear to have two parts; the first part (105 points – beds 1 to 105) seemed to have a better appearance after filtering, while the second part appeared to be impervious to filtering. No detectable (or smooth) signal appeared to emerge in the "noisy part" (beds 105-182) from any of the various filter sizes tried.

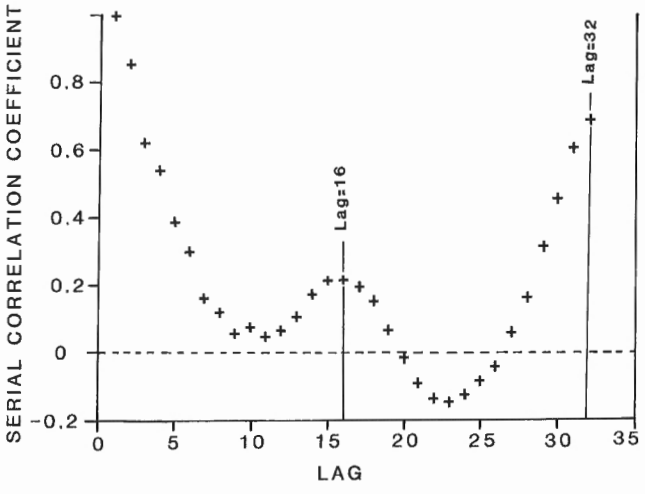

Figure 8. Correlogram for wavelength values. The 16-bed cycle is clearly marked by the peak at lag = 16. The other peak at lag = 32 is not well defined because of truncation at that point, and might disappear with a better filtering device.

Results

The first portion of the sequence presented a score slightly under 1.96, which is a requirement under the "z" test at 95% of significance (a value of 1.74 was obtained for the WL sequence), whereas the inclusion of the second portion made the sequences too noisy to filter properly and the sign test did not indicate a deviation from randomness. Thus, only the first portion of the WL sequence (bed numbers 1 to 105) appears to differ significantly from randomness, if an error of type II threshold of 90% is acceptable. It must be indicated, however, that since the sign test is non-parametric in nature, this method of testing is somewhat rigorous and the weakness of this test is probably due to the erratic behaviour of the phase for a signal that is geological in nature (Walanus, 1990).

The statistical and mathematical methods utilized in the evaluation of the periodicity of the data were as follows:

1. Calculation of the autocorrelation function and Fast Fourier Transform. The autocorrelation function for the data was computed using the method outlined by Chestnut (1966). The autocorrelation function value has no units and varies from 1 to -1 on the ordinate. The correlogram (Fig. 8), shows two peaks at Lag=16 and Lag=32, thus confirming the 16-bed and 32-bed cycles detected visually (Fig. 4).
2. The analysis of cycles in natural data sequences. The work of Walanus (1990) was utilized to analyze the data, which shows a rather consistent sequence in the first 105 points (beds), but then becomes more noisy for the last points – where missing data are involved and a modification of the phase of the geological signal is also possible.
3. The decision that the appearance of a Probability Distribution Function (PDF) is indicative of log-normal distribution. The work of Sinclair (1971) showed that if a PDF is plotted on a log-probability plot, and if the appearance is that of a straight line, then the probability distribution function (PDF) is that of a log-normal distribution – as in the case of 3-D bedforms shown in Figure 7. A normal PDF would appear as a curved line.

CAUSES OF TREND AND CYCLICITY

The trend, as shown by the wavelength data, reflecting an upward increase in the size of bedforms, is a common feature of storm beds in a shallowing-upward, prograding shoreline sequence. This trend has been interpreted as a proximality "trend", based on the fact that more proximal ends of storm beds, with thicker and larger bedforms, are encountered as shallower depths are reached toward the top of a sequence (Aigner and Reineck, 1982).

The cycles superimposed on the "trend" have to be explained in terms of a periodic process in time. A rough calculation for the duration of the 16-bed cycle can be made from the estimates made by Hamblin and Walker (1979) regarding the recurrence interval of storm event beds in this part of the stratigraphic section. Their estimated values for the recurrence interval of storm beds, vary from 4033 to 12 000 years. A 16-bed cycle of such beds should, therefore,

represent a cycle of anywhere between 64 000 and 192 000 years. Probable geological cycles within that order of magnitude could be: i) the 100 000 year Milankovitch cycle of eccentricity of the earth's orbit (Hays et al., 1976), or ii) a fourth- to fifth-order (100 000 to 300 000 years) eustatic sea-level change, or iii) a regional sedimentary cycle caused by local variations in sediment supply, current activity, and subsidence (Fulthorpe, 1991). Unless we obtain more reliable data on the recurrence interval of storm beds, such conclusions remain highly speculative. Because of the high noise in the upper part of the series (beds 106 to 182) the 32-bed cyclicity detected in that part may not be real, and therefore has not been taken into account.

CONCLUSIONS

1. Field measurements of wavelengths and ripple heights of 182 combined flow bedforms (both 2-D and 3-D), in a series of vertically stacked storm beds in a shallowing-upward shoreline sequence in the passage beds of the Fernie Formation in the southern Alberta Foothills, have been statistically analyzed to determine: i) the nature of the size populations; ii) to detect any linear trend; and iii) to detect any cyclicity in the wavelength values.

2. Because the wavelengths and ripple heights are strongly correlated (r = 0.892) only the wavelength values were used in the study, on the assumption that the ripple heights would show a similar relationship.

3. The 2-D and 3-D bedforms show two distinct means that are statistically different, as determined by the "t" test.

4. The wavelength values of the 3-D bedforms belong to a single log-normal population, indicating that a ripple vs. dune distinction is not valid for combined flow bedforms.

5. A statistically significant linear trend of increasing upward values is present in the wavelength values. This can be explained in terms of a proximality trend of storm beds on a shallowing-upward shoreline.

6. A 16-bed cycle has been detected in the filtered values of wavelengths in the first part (beds 1 to 105) of the 182-bed series. This represents a periodicity of 64 000 to 200 000 years and may probably be attributed to a fourth- to fifth-order eustatic cycle falling within the Milankovitch band of frequencies.

REFERENCES

Aigner, T. and Reineck, H.-E.
1982: Proximality trends in modern storm sands from the Heligoland Bight (North Sea) and their implications for basin analysis; Senckenbergiana maritima, v. 14, p. 183-215.

Allen, P.A.
1985: Hummocky cross-stratification is not produced purely under progressive gravity waves; Nature, v. 313, p. 562-564.

Arnott, R.W. and Southard, J.B.
1990: Exploratory flow-duct experiments on combined-flow bed configurations, and some implications for interpreting storm-event stratification; Journal of Sedimentary Petrology, v. 60, p. 211-219.

Ashley, G.M. (Chairperson) et al.
1990: Classification of large-scale subaqueous bedforms: a new look at an old problem; Journal of Sedimentary Petrology, v. 60, p. 160-172.

Cant, D.J.
1990: Zuni Sequence: the Foreland basin. Lower Zuni Sequence: Middle Jurassic to Middle Cretaceous; in Western Canada Sedimentary Basin – a case study, (ed.) B.D. Ricketts; Canadian Society of Petroleum Geology, p. 251-286.

Chestnut, H.
1966: Systems Engineering Tools; John Wiley & Sons, New York, 646 p.

Craft, J.H. and Bridge, J.S.
1987: Shallow-marine sedimentary processes in the Late Devonian Catskill Sea, New York State; Geological Society of America, Bulletin, v. 98, p. 338-355.

Davis, J.C.
1986: Statistics and Data Analysis in Geology. (Second edition.); John Wiley and Sons, New York, 646 p.

Dott, R.H. Jr. and Bourgeois, J.
1982: Hummocky stratification: significance of its variable bedding sequences; Geological Society of America, Bulletin, v. 93, p. 663-680.

Fulthorpe, C.S.
1991: Geologic controls on seismic sequence resolution; Geology, v. 19, p. 61-65.

Gibson, D.W.
1985: Stratigraphy, sedimentology and depositional environments of the coal-bearing Jurassic-Cretaceous Kootenay Group, Alberta and British Columbia; Geological Survey of Canada, Bulletin 357, 108 p.

Greenwood, B. and Sherman, D.J.
1986: Hummocky cross-stratification in the surf zone: flow parameters and bedding genesis; Sedimentology, v. 33, p. 33-45.

Hamblin, A.P. and Walker, R.G.
1979: Storm-dominated shallow marine deposits: the Fernie-Kootenay (Jurassic) transition, southern Rocky Mountains; Canadian Journal of Earth Sciences, v. 16, no. 9, p. 1673-1690.

Hays, J.D., Imbrie, J., and Shackleton, N.J.
1976: Variations in the Earth's orbit: pacemaker of the ice ages; Science, v. 194, no. 4270, p. 1121-1132.

Mathsoft Inc.
1989: MathCad version 2.5, User's Guide; Mathsoft Inc., 1 Kendal square, Cambridge, MA, U.S.A.

Nøttvedt, A. and Kreisa, R.D.
1987: Model for the combined-flow origin of hummocky cross-stratification; Geology, v. 15, p. 357-361.

Sinclair, A.J.
1981: Applications of probability graphs; Association of Exploration Geochemists; Richmond, B.C., Canada, v. 4., 95 p.

Southworth, R.W.
1967: Autocorrelation and spectral analysis; in Mathematical Methods for Digital Computers, (ed.) A. Ralston and H.S. Wilf; John Wiley and Sons, New York, 293 p.

Swift, D.J.P., Figueiredo, A.G. Jr., Freeland, G.L., and Oertel, G.F.
1983: Hummocky cross-stratification and megaripples: a geological double standard?; Journal of Sedimentary Petrology, v. 53, p. 1295-1317.

Till, R.
1974: Statistical Methods for the Earth Scientist; John Wiley and Sons, New York, 154 p.

Walanus, A.
1990: Running phase analysis – a method for cycle searching in long series; Computers and Geosciences, v. 16, no. 3, p. 367-370.

Waldron, J.W.F.
1987: A statistical test for significance of thinning- and thickening-upward cycles in turbidites; Sedimentary Geology, v. 54 p. 137-146.

Yalin, M.S.
1977: Mechanics of Sediment Transport. (Second edition.); Pergamon Press, Oxford, 298 p.

Structural evolution of the Kulutingwak zone, northwestern Ellesmere Island, Northwest Territories: the northern edge of Paleozoic North America?

M.G. Bjornerud[1]
Institute of Sedimentary and Petroleum Geology, Calgary

Bjornerud, M.G., 1991: Structural evolution of the Kulutingwak zone, northwestern Ellesmere Island, Northwest Territories: the northern edge of Paleozoic North America?; in Current Research, Part E; Geological Survey of Canada, Paper 91-1E, p. 187-195.

Abstract

The Kulutingwak structural zone of northwestern Ellesmere Island records a sequence of deformational events associated with the Late Silurian(?) collision between North America and a terrane to the north. The rocks incorporated into this zone of south-verging folds and thrusts include a thick Lower Silurian turbidite sequence, the Imina Formation, and a probable arc complex of carbonate and volcanic rocks. Deformation apparently began during or shortly after the deposition of the Imina Formation in Llandovery time. Many mesoscale structures in the turbidites formed in response to expulsion of fluids from the sediments before they were lithified. Superimposed structures, including chevron folds and imbricate thrusts, reflect progressive strengthening of the rocks. The early structural evolution of the Kulutingwak zone corresponds closely with that of modern accretionary wedges in subduction settings. The later stages of deformation apparently record telescoping of the wedge and arc complex southward onto the continental margin.

Résumé

La zone structurale de Kulutingwak du nord-ouest de l'île Ellesmere renferme une séquence d'événements de déformation associés à la collision du Silurien supérieur (?) entre l'Amérique du Nord et un terrane au nord. Les roches incorporées dans cette zone de plis et de chevauchements de direction sud comprennent une épaisse séquence de turbidites du Silurien inférieur, la formation d'Imina, et un complexe en arcs probable de carbonates et de roches volcaniques. La déformation aurait commencé pendant ou peu après le dépôt de la formation d'Imina à l'époque de Llandovery. Nombre de mésostructures se sont formées dans les turbidites en remplacement des fluides expulsés des sédiments avant qu'ils ne soient lithifiés. Des structures superposées, comprenant des plis en chevrons et des chevauchements imbriqués, témoignent du renforcement progressif des roches. L'évolution structurale ancienne de la zone de Kulutingwak correspond étroitement à celle des coins d'accrétion récents dans les zones de subduction. Les phases ultérieures de déformation semblent témoigner du téléscopage du complexe en coins et en arcs vers le sud sur la marge continentale.

[1] Geology Department, Miami University, Oxford, Ohio 45056 U.S.A.

INTRODUCTION

This report summarizes results of structural investigations of lower Paleozoic rocks between Phillips Inlet and Yelverton Bay, northwestern Ellesmere Island (Fig. 1). The area lies at the junction between the early Paleozoic margin of North America and a postulated terrane, "Pearya", accreted during or after Late Silurian time (Trettin, 1987). The principal goal of the present study was to constrain the interpretation of this accretionary event by characterizing the architecture of the terrane boundary zone.

Pearya is a polydeformed composite terrane whose pre-accretion history has not been resolved in detail. However, several features clearly distinguish Pearya from the rest of Ellesmere Island and Arctic Canada:

1. "Grenvillian" basement-complex metamorphic ages (1.0 to 1.1 Ga), which stand in contrast to Archean and Early Proterozoic ages elsewhere in the Arctic Archipelago (Sinha and Frisch, 1975; Trettin et al., 1987).
2. Lower Ordovician mafic/ultramafic suites without equivalents in adjacent areas (Trettin, 1987, 1989).
3. Evidence of a mid-Ordovician orogeny recorded by an angular unconformity between Lower and Upper Ordovician strata, a variety of granitic intrusions, and regional metamorphism up to amphibolite grade within Pearya but not elsewhere on Ellesmere Island or the surrounding islands (Trettin, 1987, 1989).

These characteristics suggest a possible link with the Scandinavian Caledonides, and Svalbard in particular (Trettin, 1987; Bjornerud 1989). The age of the accretionary event is inferred from stratigraphic comparisons between the lower Paleozoic successions in Pearya and those of the adjacent Clements Markham Fold Belt (Fig. 1), which consists of rocks deposited in a deep-water basin that may have lain outboard of the continental shelf of North America (Trettin, 1987). Pearyan rocks as old as Late Ordovician show some affinities with those derived from the continent, but substantive differences in composition persist into Lower Silurian strata. Middle Ludlow rocks are the first that are demonstrably continuous from Pearya into the Clements Markham Fold Belt, though stratigraphic links between Ludlow rocks in Pearya and the Hazen and central Ellesmere fold belts (Fig. 1) are less clear. The available evidence suggests that Pearya was joined to the rest of Ellesmere Island by Late Silurian time (Trettin, 1987).

STRATIGRAPHY OF THE KULUTINGWAK ZONE

The inferred terrane boundary between Pearya and the Clements Markham Fold Belt is a zone of tremendous structural complexity. In northwestern Ellesmere Island, it is best exposed in an 8 km wide, 55 km long swath from the east arm of Kulutingwak Fiord westward to Phillips Inlet (Fig. 2), an area informally referred to as the Kulutingwak zone.

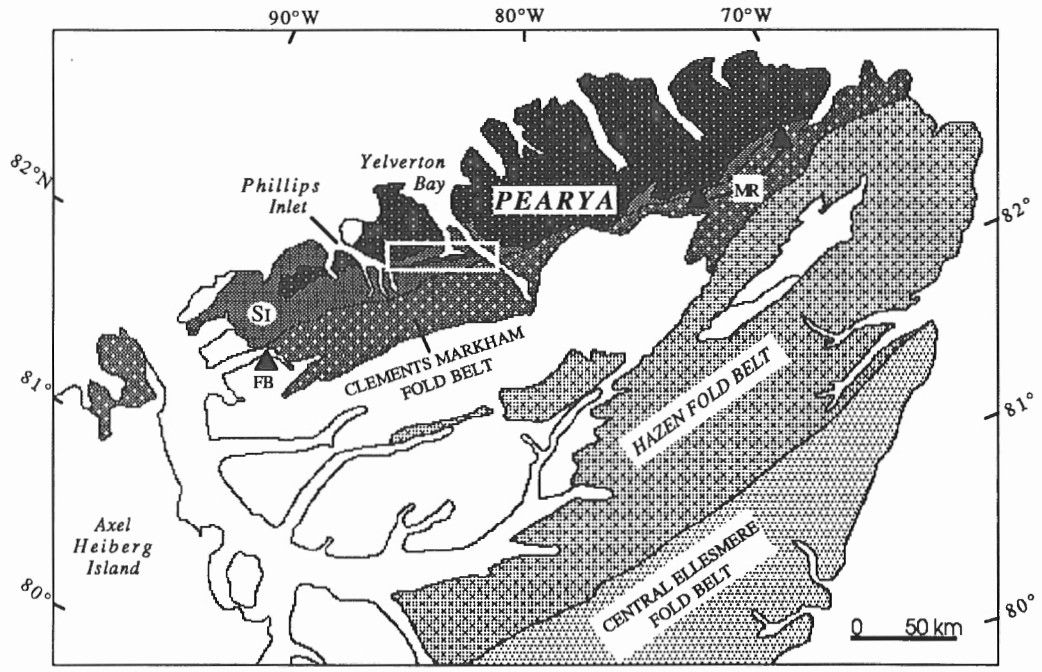

Figure 1. Simplified geological map of northern Ellesmere Island, showing the location of Pearya and the principal Paleozoic fold belts. Unshaded areas are underlain by post-Devonian rocks. Triangles mark the locations of volcanic/carbonate complexes, which may be correlative with rocks in the Kulutingwak zone. FB = Fire Bay; MR = Mount Rawlinson; S_I = Silurian Imina Formation. White rectangle outlines the area shown in Figure 2.

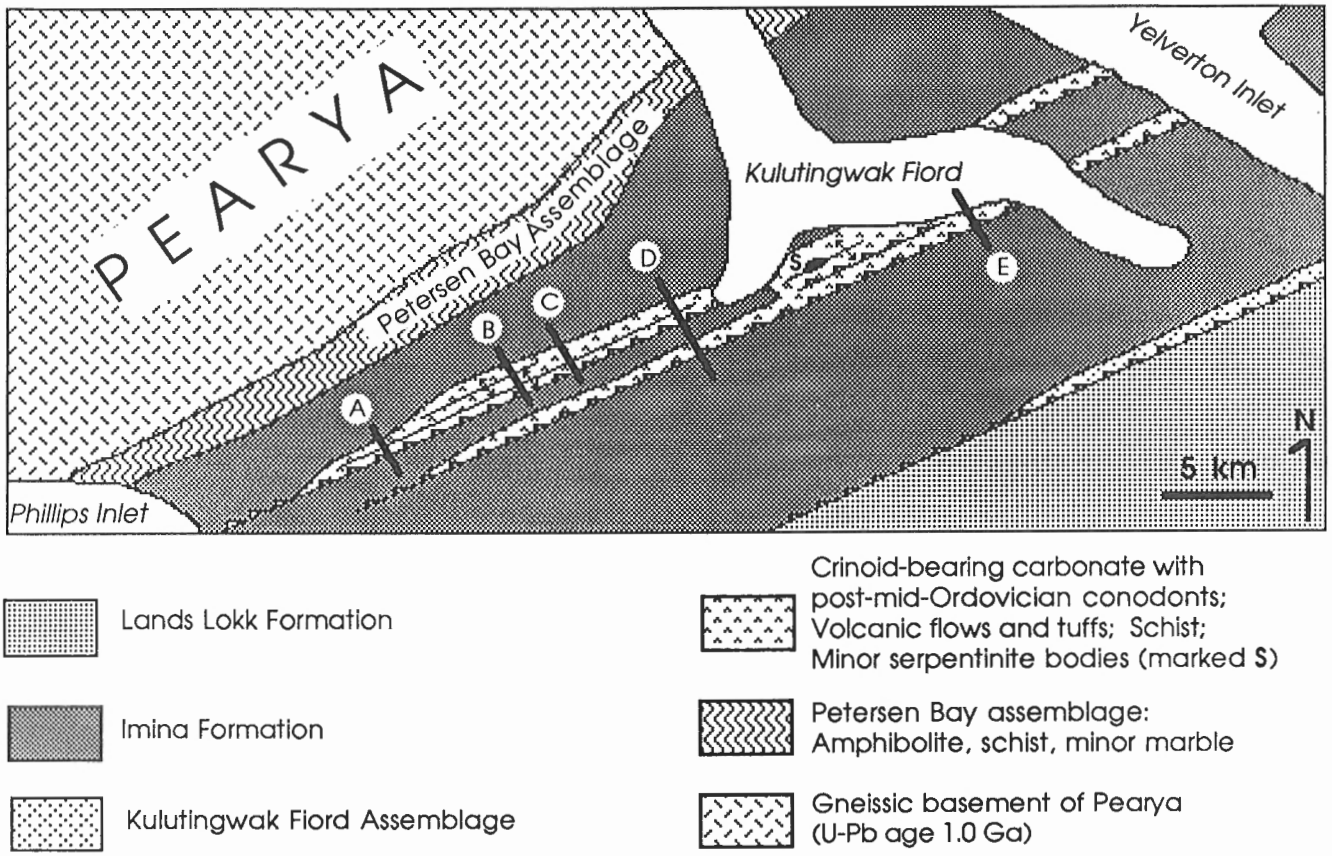

Figure 2. Simplified geological map of the Kulutingwak zone and adjacent areas. A-E = cross-sections shown in Figure 4. Location shown in Figure 1.

Three main rock types are incorporated into south-verging folds and thrust sheets within this zone: 1) a calcareous turbidite sequence, the Imina Formation, whose upper strata contain late Llandovery graptolites (Trettin, 1979; Trettin and Frisch, 1987); 2) a massive, locally crinoidal limestone/dolomite unit that has yielded post-mid-Ordovician conodonts; and 3) a volcanic/sedimentary complex that includes andesitic flows, shallow intrusives, and argillaceous schists that appear to be meta-tuffs. The units within the Kulutingwak zone have experienced only low grade metamorphism. Local occurrences of chlorite plus muscovite in the Imina Formation and the volcanic unit suggest peak metamorphic conditions within the lower greenschist facies. North of the zone, however, the metamorphic grade of the Imina Formation increases; this is discussed below.

Contacts between the three rock types commonly coincide with layer-parallel faults or shear zones, and stratigraphic relationships among the units were not clear until 1990 field investigations. It now appears that they belong to a single depositional sequence, in which the volcanic rocks are generally lowest and strata of the Imina Formation highest. Commonly, however, tuffs and flows occur within the massive limestone/dolomite unit (and have locally marbleized it). At some of these sites, the carbonate unit also contains crystalline volcanic clasts, centimetres to metres in diameter, probably deposited by episodic debris slurries (Fig. 3). At another locality, a crinoid stem fragment was found within a layer of micaceous tuff. These relationships indicate that the volcanic and carbonate sequences are largely coeval and that the carbonate bank was proximal to the volcanic source.

Similar relationships link the lowermost Imina Formation with the other two rock types. Apparent gradational contacts occur between the Imina Formation and both the carbonate and volcanic units. The transition from the carbonate unit into the Imina Formation is typically marked by a layer of either gritty dolomite or flat-pebble carbonate conglomerate with a sandy matrix. No volcanic flows have been observed within the Imina Formation, but in several places the formation interfingers with apparent meta-tuffs and contains substantial fractions of euhedral feldspar that is probably volcanogenic. Further evidence of nearby volcanic activity is a layer of cobble- to boulder-sized andesite clasts within the Imina Formation at the east end of the Kulutingwak zone. The Imina Formation also contains apparently olistostromal bodies of brecciated carbonate as large as 15 m in length. These observations suggest that the basin in which the Imina Formation accumulated received periodic influxes of material from the volcanic/carbonate complex.

Designation of the volcanic rocks as andesites is based on petrographic observations; chemical analyses are forthcoming. It seems likely, however, that the volcanic complex is correlative with flows and tuffs exposed southeast of Kulut-

ingwak Fiord, in apparent fault contact with the Imina Formation. Stable trace element analyses of these rocks, which are also associated with crinoidal limestones, place them in the trachyandesite field (Trettin and Frisch, 1987, their Figure 4). A chemically similar suite of volcanic rocks, the Mount Rawlinson assemblage, occurs some 150 km eastward along strike from the Kulutingwak zone (Fig. 1). A Mount Rawlinson dacite has yielded a U-Pb zircon age of 454.7 +9.7/-4.5 Ma (Caradoc) (Trettin et al., 1987). Like its Kulutingwak-area counterparts, the Mount Rawlinson volcanic complex occurs in juxtaposition with carbonate rocks and the Imina Formation. Trettin and Nowlan (1990) have suggested that the Mount Rawlinson assemblage is also correlative with felsic volcanic flows, carbonate rocks, and chert exposed at Fire Bay, Emma Fiord (Fig. 1). It seems plausible that these various volcanic/carbonate assemblages, exposed discontinuously along the Pearya/North America junction, represent parts of a single Middle Ordovician/Early Silurian arc system between the two land masses.

A fourth rock type, serpentinite, occurs in the area immediately south of Kulutingwak Fiord, which may be the deepest structural level of the zone. Lenticular bodies of serpentinite, 50 to 500 m in length, are exposed along the axis of the zone, commonly coinciding with the traces of thrust faults. In most places, the serpentinite is either massive or fibrous, and no original textures are preserved. In at least two localities, however, it has a fragmental texture in which sedimentary layering and even graded beds are discernible. By analogy with sedimentary serpentinites observed elsewhere (Stigh, 1980), the apparently detrital serpentinite may represent ocean floor slide deposits (Trettin, in prep.). Because the age of the serpentinite in the Kulutingwak zone is unknown, however, its relationship to other rock types is not yet clear.

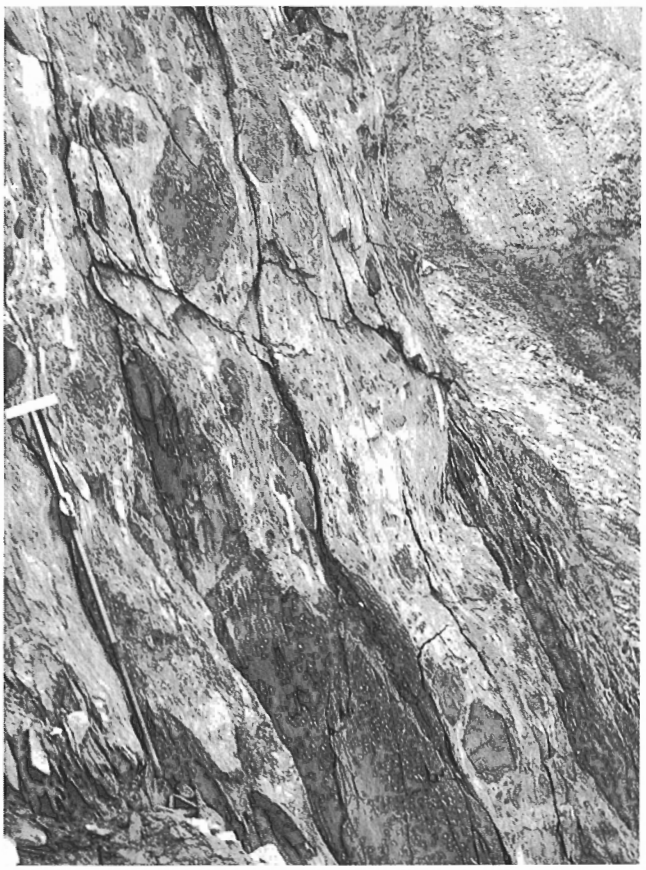

Figure 3. Olistostromal volcanic blocks in carbonate matrix, central Kulutingwak zone. Jacob's staff for scale.

STRUCTURAL CHARACTER OF THE KULUTINGWAK ZONE

Macroscopic structures

The first-order structures of the Kulutingwak zone are kilometre-scale, south-verging thrusts and folds whose displacements and amplitudes decay eastward and westward from a central area on the western arm of Kulutingwak Fiord (Fig. 2). These structures are most recognizable where they involve the carbonate and volcanic unit, but the absence of stratigraphic markers within the Imina Formation makes it difficult to determine the extent of structural repetition within the turbidite, the original thickness of which is unknown.

In the central part of the Kulutingwak zone (cross-section DD′, Fig. 4), the carbonate/volcanic sequence is exposed in two major culminations: an overturned, faulted antiform in the north and a thrust zone to the south. The southern thrust can be traced for at least 5 km both eastward and westward (Fig. 2). The northern antiform, however, shows considerable variations along strike. In the centre of the Kulutingwak zone, it is a nearly recumbent, south-verging fold with a strongly attenuated lower limb. Both limbs of the fold are transected by smaller, apparently late, south-directed thrust faults, and the hinge zone defined by the carbonate unit is back-rotated toward the north. Similar overturning of the upper part of the structure is seen along strike to the west, but fold and fault geometries vary in successive transects (cross-sections A-C, Fig. 4). In this area, the fold plunges westward, and the visible hinge zone in the carbonate unit disappears about 10 km east of Phillips Inlet (Fig. 2). The eastern extremity of the Kulutingwak zone, in contrast, comprises a stack of south-directed imbricate thrust sheets in which the base of the carbonate unit has acted as the surface of detachment (Fig. 2; cross-section E, Fig. 4). The eastern continuation of the zone is concealed by Yelverton Inlet and a tributary glacier.

Meso- and microscopic structures

Small-scale structures in the rocks of the Kulutingwak zone record a polyphase deformation history which, at least partly, predates development of the largest-scale structures and which may have begun shortly after the rocks were deposited.

Pre-lithification structures in the Imina Formation

The Imina Formation, a classical flysch, is exposed over a wide region of northern Ellesmere Island (Trettin, 1979, his Figure 1) and is probably correlative with the turbiditic Danish River Formation of the Hazen and Central Ellesmere fold belts (Trettin, 1989) and the Merqujôq Formation of North

Greenland (Hurst and Surlyk, 1982). Both the Imina and Merqujôq formations have a considerable amount of fine grained detrital and diagenetic carbonate (Trettin, 1979; Hurst and Surlyk, 1982). The Imina Formation is overlain (?)conformably by another turbidite unit, the Lands Lokk Formation, which lacks any significant carbonate component (Trettin and Frisch, 1987). In the Kulutingwak Fiord area, the Imina Formation is characterized mainly by the lower divisions of the archetypal Bouma (1962) sequence: the coarsely sandy, structureless A division; the sandy, laminated B division; and the sandy to silty, finely laminated C division in which convolute layering is common. Division D, very finely layered siltstone, is observed locally but is less typical. Division E, a massive, commonly bioturbated, pelitic layer, has not been recognized in the Kulutingwak Fiord area. Within the present study area, the formation has the coarsest and thickest beds in the north-central part of the Kulutingwak zone.

The Imina Formation contains many primary structures that are typical of rapidly deposited, fluid-rich sediments: graded bedding, centimetre-scale crossbedding, climbing ripples, convolute bedding and flame structures are all typical features. Equally common are other structures that apparently formed before lithification yet are tectonic in the sense that they reflect a deviatoric stress field with a subhorizontal maximum principal stress. These pre-lithification tectonic

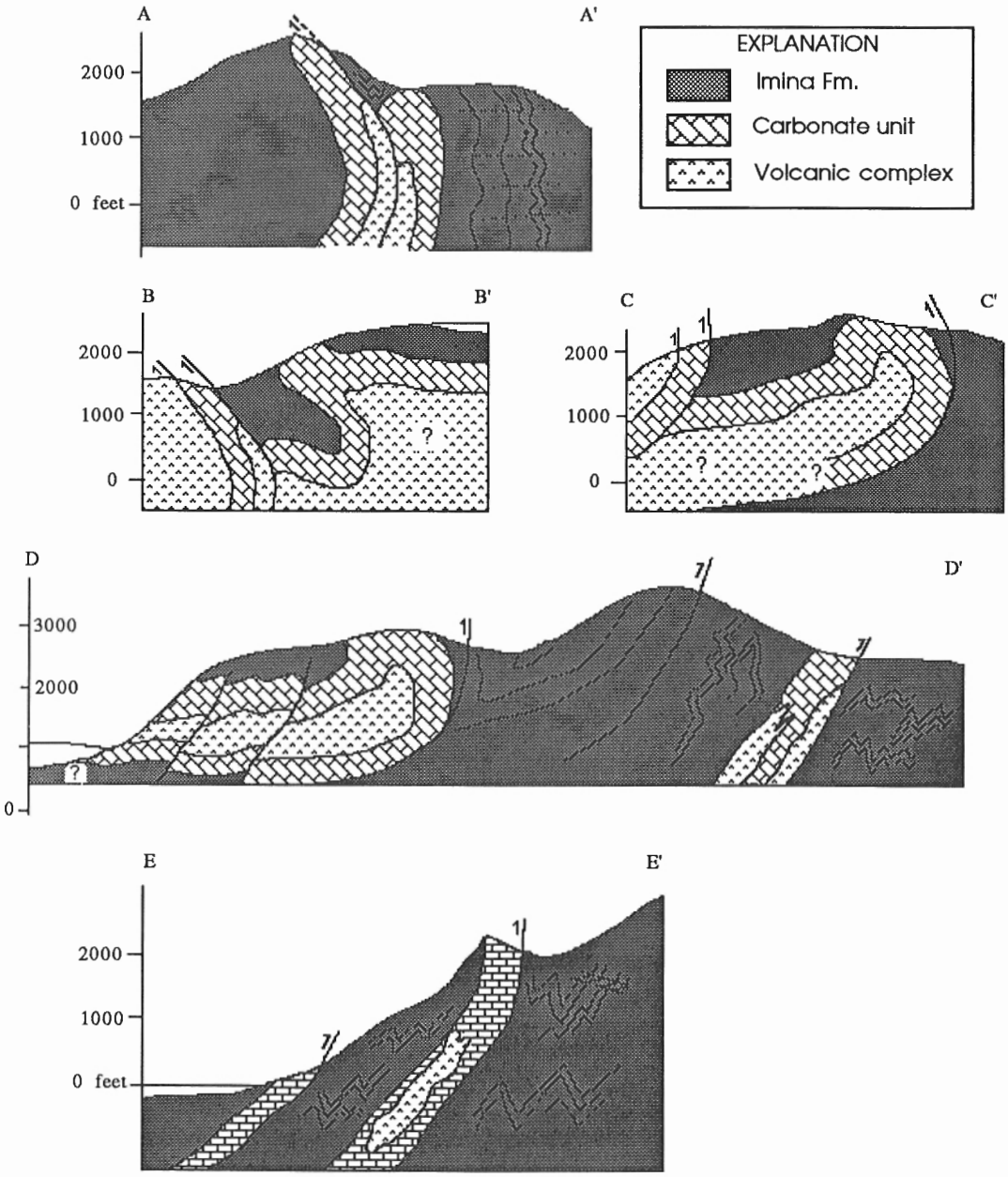

Figure 4. North-south cross-sections through the Kulutingwak zone. (No vertical exaggeration.) See Figure 2 for the locations of the transects.

a - Apparent fluid escape conduits and associated fissility. In this view, bedding dips gently toward the left, and the conduits dip steeply toward the right.
b - Conjugate conduits. Conduit pairs are symmetrically oriented with respect to bedding (marked "BDD").

Figure 5. Fluid expulsion conduits in the Imina Formation, north-central Kulutingwak zone.

structures including cleavages, folds, clastic dykes, and faults seem to lie in a continuum between simple depositional features and solid state deformational structures. The structures resemble features observed in Deep Sea Drilling Project and Ocean Drilling Project cores from forearc and trench settings (Lundberg and Moore, 1986), and attest to the role of pore fluids in the deformation of unlithified sediments.

A swarm of sedimentary dykes was observed in a relatively sandy interval of the Imina Formation in the central part of the Kulutingwak zone. The metre-scale dykes are consistently oriented and show 2 to 5 cm dilational offsets of bedding planes. This suggests that they developed as tensile hydrofractures under a regional deviatoric stress regime. When bedding is restored to horizontal, the dykes dip at an angle of 33° toward the southwest, implying a gently plunging maximum principal stress.

At many localities, penetrative cleavages in the Imina Formation seem to be linked with expulsion of fluids from unconsolidated sediments. (Other cleavages were clearly formed by solid state deformational processes; these will be discussed in the next section.) Northwest of Kulutingwak Fiord, the Imina Formation has a pervasive fissility, parallel to apparent water-expulsion conduits which are defined by sedimentary laminae oblique to bedding (Fig. 5a). Bedding planes seem to have acted as feeders into these conduits. At one site, the conduits parallel the axial plane of a metre-scale isoclinal similar fold, suggesting that the fold is also a pre-lithification structure and essentially coeval with the fluid-escape channels. The conduits locally occur as conjugate sets, suggesting that they originated as shear fractures in sediment made brittle by high pore pressures (Fig. 5b). The orientations of these fractures after bedding is restored to horizontal indicate that they formed under a subhorizontal maximum principal stress with a N32°WS32°E trend. Once formed, the fractures would have provided convenient escape routes for the pore fluids.

Apparent pre-lithification cleavages also are associated with extreme "ductile" distortion of layering, which is inconsistent with the low metamorphic grade of the Imina Formation. Along these cleavage surfaces, bedding is commonly transposed, thinned, or swept into small, cuspate similar folds with sharp anticlinal crests (Fig. 6). In spite of the large mesoscopic strains recorded in some layers, microscopic examination shows a complete absence of associated intragranular deformation. This implies that the deformation was accomplished by disaggregated particulate flow of incompletely consolidated, fluid-rich sediment (Knipe, 1989). In addition, the sharp crests of cuspate folds like those in Figure 6 all point in the same direction (stratigraphic "up"), unlike cuspate buckle folds formed at interfaces between different rock types during solid state deformation, which point toward the more competent layer. This suggests that the folds formed as fluids were forcefully expelled along spaced pathways at high angles to bedding. Finally, cleavage planes associated with the distorted bedding are not refracted as they pass from coarse to fine grained beds. This is consistent with

the idea that the cleavage orientation reflects an ambient hydraulic gradient and not the relative mechanical competence of beds deforming in the solid state.

In summary, the pre-lithification structures in the Imina Formation are more than superficial, gravity-induced, "soft sediment" features. Most can be considered tectonic in the sense that they developed under a deviatoric stress regime that was probably a direct consequence of the convergent tectonic setting. Pickering (1987), who observed similar features in a Caradoc-Llandovery turbidite in the Dunnage zone of Newfoundland, advocated the term "wet sediment" structures because it carries no depth connotation. Studies of deep sea drill cores from modern accretionary prisms indicate that such structures form in sediments at burial depths of 1 to 2 km (Lundberg and Moore, 1986), and the deformational style recorded by seismic imaging of these prisms suggests that fluid-rich, unlithified material persists to depths of at least 4 to 5 km (Moore and Lundberg, 1986). The existence of these structures poses intriguing questions. For example: What is the significance of their regional spatial distribution? Are certain types of structures diagnostic of particular depths or hydrologic regimes? How quickly do such structures form? Could seismic activity and concomitant fluid pressure effects be important in controlling their development? Perhaps the most fundamental question is: How did these generally fragile structures survive subsequent deformation associated with the final accretion of Pearya?

Post-lithification structures in the Imina Formation and other units

The "hard rock" structures of the Kulutingwak zone chronicle a complex and protracted deformational history, but generally it is not possible to recognize distinct orogenic phases at the regional scale. Although local event chronologies can be resolved, these do not seem applicable across the entire zone. An overall temporal trend toward more brittle behaviour can be recognized, however, and this presumably reflects increasing rock strength with dewatering and burial. The absolute age of the post-lithification structures is not yet known, but the lack of structural fabrics in Cretaceous mafic dykes indicates that the structures in the Paleozoic rocks are not relicts of Eurekan (Tertiary) deformation.

Figure 6. Cuspate folds probably formed by fluid expulsion.

Poles to bedding in the Imina Formation and carbonate and volcanic units (Fig. 7a, b) define a statistical fold axis that plunges gently toward N75°E. Steeply dipping to subvertical, eastwest striking beds are most common. Bedding/cleavage intersection lineations also reflect a regional east-northeast trending fold axis (Fig. 7c). These structural summaries, however, do not reveal the mesoscale complexity of the rocks, in which there is clear evidence of superimposed episodes of folding and cleavage formation.

The earliest folds in the Imina Formation are typically similar folds, with strongly thinned limbs and a variably developed axial planar cleavage. Their morphology indicates that they developed passively, with little mechanical contrast between layers of different composition. Some of these folds, as discussed above, may represent pre-lithification structures. Later folds, in contrast, are generally parallel folds with features that reflect more brittle folding mechanisms and mechanically active layering. These later folds have chevron hinge zones in which much of the strain has been accommodated by local brittle failure and dissolution. Extensive development of bedding plane slickenfibres on the limbs of these folds indicates that flexural slip was the dominant folding mechanism. Neither the early similar folds nor the later parallel folds are uniformly developed throughout the area.

The occurrence of multiple cleavage surfaces within the Imina Formation indicates an even more complex structural history than suggested by the two recognizable fold generations. In many places, as many as three cleavage or parting surfaces can be recognized: an early, apparently pre-lithification fissility and one or two solid state foliations defined by flattened grains and/or pressure solution seams. In most cases, none of the cleavages are obviously related to mesoscopic folds. Figure 7d shows the measured orientations of post-lithification, spaced cleavages where two distinct generations could be discerned. Figure 7e depicts cleavage orientations at sites where only one generation was observed. The range of orientations suggests that the cleavages, like bedding, have been folded about an east-northeast trending axis.

Two other distinct and relatively late foliation types can be recognized in the Kulutingwak zone. One is a mylonitic, generally bedding-parallel foliation best developed in the proximity of major thrust faults, and its average orientation reflects the steep northerly dip of most of these faults (Fig. 7f). This is the only foliation consistently observed in the carbonate and volcanic/sedimentary units. Where it is recognizable in the Imina Formation, it crosscuts earlier foliations. Where the massive carbonate unit defines the bases of major thrust sheets, the mylonitic fabric has been disrupted by meso- and microscale cataclasis. These observations suggest that the main phase of thrusting followed the formation of most cleavages and folds, and that the mylonitic fabric was related to the thrusting but developed before the final stages of thrust emplacement.

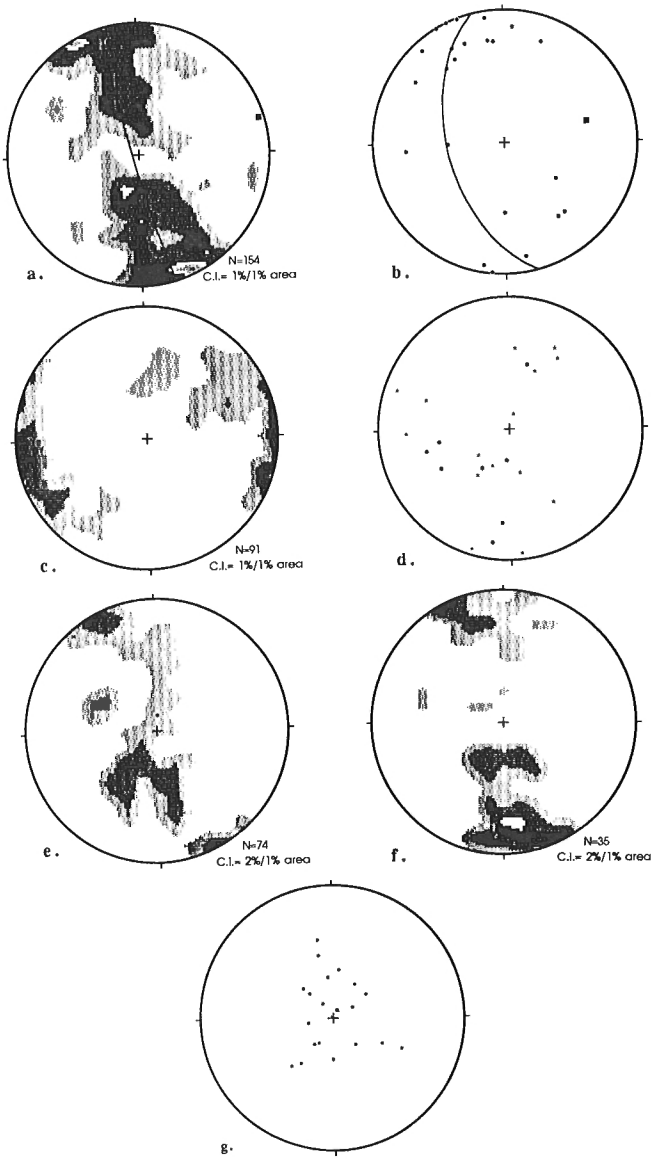

a - Poles to bedding in the Imina Formation. The square symbol marks the fold axis defined by the best-fit great circle.
b - Poles to bedding in the carbonate and volcanic units.
c - Intersections of bedding and post-lithification cleavage surfaces in the Imina Formation.
d - Poles to first cleavage (dots) and second cleavage (stars) for sites where two post-lithification cleavages were observed.
e - Poles to post-lithification cleavage, where only one was observed.
f - Poles to mylonitic foliation in the Imina Formation and the carbonate and volcanic units.
g - Poles to late, flat-lying crenulation cleavage in the Imina Formation.

Figure 7. Stereonet plots (lower hemisphere, equal area) of the principal structural elements in the Kulutingwak zone. In the contoured diagrams, the number of observations and contour interval are indicated below the plots.

The other late-stage foliation is a kink-like crenulation cleavage that overprints other foliations and is notable for its consistently shallow dip (typically <30°; Fig. 7g). The foliation is best developed at the eastern and western extremities of the Kulutingwak zone, where bedding planes are steep to vertical. The crenulation cleavage occurs locally as flat-lying conjugate kink bands whose orientation suggests a subvertical maximum principal stress. If this interpretation is correct, the crenulations may reflect gravitational collapse of the thickened thrust belt, in the manner predicted by critical taper theory (Davis et al., 1983).

DISCUSSION AND CONCLUSIONS

Summary of structural evolution

The rocks of the Kulutingwak zone chronicle a deformational history which defies conventional structural interpretations on several counts. First, the earliest structures appear to record deformation that was accompanied and influenced by expulsion of fluids from the not-yet-lithified Imina Formation. This stage of deformation must have occurred during or shortly after the deposition of the Imina Formation, mainly in Llandovery time. The regional geological setting of the Kulutingwak zone, together with the widespread occurrence of "wet sediment" structures like those observed in turbidites in modern subduction settings, suggest that early structures in the Kulutingwak zone may have developed in an accretionary prism.

Such an interpretation could also account for the lack of regionally identifiable orogenic phases (D_1, D_2, etc.) in the Imina Formation. Studies of Cenozoic accretionary prisms (e.g., DiTullio and Byrne, 1990) illustrate the spatial and temporal heterogeneity of deformation typical of these settings, where domains with different structural styles occur in juxtaposition and deformation fronts migrate with time. In the Kulutingwak zone, a general period of post-lithification cleavage development and chevron folding can be recognized in the Imina Formation, but particular cleavage and fold phases are not readily correlated at the regional scale. The major thrust faults, which involve the volcanic and carbonate units and define the large-scale geometry of the zone, appear to have developed relatively late. These probably record the eventual emplacement of the sedimentary prism and arc complex onto the North American continental margin. The latest structures, flat-lying crenulations and kink bands, may reflect extensional collapse of the thickened thrust wedge during the final stages of collision.

Regional context of events in the Kulutingwak zone

The next step in understanding the significance of the Kulutingwak zone is to place the structural history of the zone into a regional framework. A principal question is the relationship between the Kulutingwak zone and a narrow belt of undated amphibolite facies rocks, the Petersen Bay Assemblage (PBA), exposed just to the north (Fig. 2). The Petersen Bay Assemblage consists of interlayered hornblende, biotite, and biotite-garnet schists in association with tremolitic marble in which fragmental crinoid stems have been identified (Trettin

and Frisch, 1987). The occurrence of crinoidal carbonate within the assemblage suggests a possible link with the rocks of the Kulutingwak zone. The intercalation of hornblende and biotite schists could reflect a tuff/pelite protolith (Y. Ohta, pers. comm., 1988), but this interpretation awaits the results of chemical analyses. The Petersen Bay Assemblage is in fault contact with Middle Proterozoic gneiss to the north, but there is no distinct boundary between the assemblage and the Imina Formation to the south. In fact, the Imina Formation passes from chlorite- to biotite- and locally to garnet-grade over a distance of about 15 km as the Petersen Bay Assemblage is approached from the south (Trettin, 1979). Understanding the significance of this steep metamorphic gradient north of the Kulutingwak zone is critical to interpretations of regional tectonics. Porphyroblasts in the Imina Formation overprint cleavages and crenulations, indicating that the rocks experienced a major thermal pulse that postdated deformation. The only estimate of the age of this thermal event is a newly determined, preliminary, hornblende $^{40}Ar/^{39}Ar$ plateau age of 428.4 ± 4.6 Ma from a Petersen Bay Assemblage amphibolite (J.C. Roddick, pers. comm., 8th January 1991). This suggests that all of the major events in the Kulutingwak zone, from deposition of the Imina Formation through the post-kinematic growth of porphyroblasts, took place during Llandovery, Wenlock and possibly early Ludlow time that is, within a period of about 15 Ma.

The evolution of the Kulutingwak zone must also be linked with the development of the mid-Paleozoic fold belts of northern and central Ellesmere Island, but this will require better constraints on the absolute timing of Kulutingwak deformation. Klaper (1990) has shown that diachronous "Ellesmerian" events in the Hazen and Central Ellesmere fold belts reflect migration of the deformation front toward the foreland during Early Devonian through Early Carboniferous time. Deformation in the Kulutingwak zone, which apparently began as the Imina Formation was deposited in Early Silurian time, could represent the beginning of that sequence of orogenic events.

ACKNOWLEDGMENTS

This project was made possible by American Chemical Society Petroleum Research Fund grant #22998-G2 and by the logistical support of the Polar Continental Shelf Project. I thank Hans Trettin for giving me the opportunity to work on Ellesmere Island.

REFERENCES

Bjornerud, M.
1989: Structural transects in northwestern Ellesmere Island, Canadian Arctic Archipelago; in Current Research, Part G; Geological Survey of Canada, Paper 89-1G, p. 125-131.

Bouma, A.H.
1962: Sedimentology of Some Flysch Deposits; a Graphic Approach to Facies Interpretation; Elsevier, New York, 168p.

Davis, D., Suppe, J., and Dahlen, F.
1983: Mechanics of fold-and-thrust belts and accretionary wedges; Journal of Geophysical Research; v. 88, p. 1153-1172.

DiTullio, L. and Byrne, T.
1990: Deformation paths in the shallow levels of an accretionary prism: the Eocene Shimanto belt of southwest Japan; Geological Society of America, Bulletin, v. 102, p. 1420-1438.

Hurst, J. and Surlyk, F.
1982: Stratigraphy of the Silurian turbidite sequence of North Greenland; Grønlands Geologiske Undersøgelse, Bulletin 145, 121 p.

Klaper, E.M.
1990: The mid-Paleozoic deformation in the Hazen Fold Belt, Ellesmere Island, Arctic Canada; Canadian Journal of Earth Sciences, v. 27, no. 10, p. 1359-1370.

Knipe, R.J.
1989: Deformation mechanisms recognition from natural tectonites; Journal of Structural Geology, v. 11, p. 127-146.

Lundberg, N. and Moore, J. Casey
1986: Macroscopic structural features in Deep Sea Drilling Project cores from forearc regions; in Structural Fabric in Deep Sea Drilling Project Cores from Forearcs, (ed.) J.C. Moore; Geological Society of America, Memoir 166, p. 13-44.

Moore, J. Casey and Lundberg, N.
1986: Tectonic overview of Deep Sea Drilling Project transects of forearcs; in Structural Fabric in Deep Sea Drilling Project Cores from Forearcs, (ed.) J.C. Moore; Geological Society of America, Memoir 166, p. 1-12.

Pickering, K.T.
1987: Wet-sediment deformation in the Upper Ordovician Point Learington Formation; an active thrust-imbricate system during sedimentation, Notre Dame Bay, north-central Newfoundland; in Deformation of Sediments and Sedimentary Rocks, (ed.) M.E. Jones et al.; Geological Society of London, Special Publication 29, p. 213-240.

Sinha, A.K. and Frisch, T.
1975: Whole-rock Rb/Sr ages of metamorphic rocks from northern Ellesmere Island, Canadian Arctic Archipelago. I. The gneiss terrain between Ayles Fiord and Yelverton Inlet; Canadian Journal of Earth Sciences, v. 12, p. 90-94.

Stigh, J.
1980: Detrital serpentinites of the Caledonian allochthon in Scandinavia; in The Caledonides in the USA, IGCP Project 27; Virginia Polytechnic Institute, Memoir 2, p. 149-155.

Trettin, H.P.
1971: Reconnaissance of lower Paleozoic geology, Phillips Inlet region, north coast of Ellesmere Island, District of Franklin; Geological Survey of Canada, Paper 71-12.
1979: Middle Ordovician to Lower Devonian deep-water succession at southeastern margin of Hazen Trough, Canon Fiord, Ellesmere Island; Geological Survey of Canada, Bulletin 272, 84 p.
1987: Pearya: a composite terrane with Caledonian affinities in northern Ellesmere Island; Canadian Journal of Earth Sciences, v. 24, p. 224-245.
1989: The Arctic Islands; in The Geology of North America; an Overview, (ed.) A.W. Bally et al.; Geological Society of America, The Geology of North America. v. A, p. 349-370.

Trettin, H.P. and Frisch, T.
1987: Bedrock geology, Yelverton Inlet map area, northern Ellesmere Island, interim report and map (340 F, 560 D); Geological Survey of Canada, Open File 1651.

Trettin, H.P. and Nowlan, G.S.
1990: Middle Ordovician sedimentary and volcanic rocks at Fire Bay, Emma Fiord, northwestern Ellesmere Island; in Current Research, Part D, Geological Survey of Canada, Paper 90-1D, p. 147-151.

Trettin, H.P., Parrish, R., and Loveridge, W.D.
1987: U-Pb age determinations on Proterozoic to Devonian rocks from northern Ellesmere Island, Arctic Canada; Canadian Journal of Earth Sciences, v. 24, p. 246-256.

Correlation of thermal maturity indicators for the Tenlen A-73, Crossley Lake South K-60, and Kugaluk N-02 wells in the northern District of Mackenzie, Northwest Territories

B.J. Dougherty, H.J. Abercrombie, A. Achab[1], R. Bertrand[1], F. Goodarzi, L.R. Snowdon, and J. Utting
Institute of Sedimentary and Petroleum Geology, Calgary

Dougherty, B.J., Abercrombie, H.J., Achab, A., Bertrand, R., Goodarzi, F., Snowdon, L.R., and Utting, J., 1991: Correlation of thermal maturity indicators for the Tenlen A-73, Crossley Lake South K-60, and Kugaluk N-02 wells in the northern District of Mackenzie, Northwest Territories; in Current Research, Part E, Geological Survey of Canada, Paper 91-1E, p. 197-202.

Abstract

In an attempt to correlate a variety of thermal maturity indices, reflectance (R_o) of dispersed organic matter, palynomorph Thermal Alteration Index (TAI), conodont Colour Alteration Index (CAI), geochemical composition of the organic material (Rock-Eval Tmax, S2, TOC), and clay mineralogy were determined for the Tenlen A-73 (lat. 67°52'7.5"N; long. 130°43'21.6"W), Crossley Lake South K-60 (68°29'39"N; 129°29'14"W), and Kugaluk N-02 (68°31'55"N; 131°31'19"W) wells.

All indices show that the wells are overmature with respect to oil generation. R_o, CAI and TAI showed a progressive increase with depth, while trends are not readily apparent in the Rock-Eval results, as the organic material has been altered beyond the limits of reliable interpretation. Further work is needed to develop clay mineralogy into a useful thermal maturity index for the study area.

Résumé

Dans un effort pour corréler divers indices de maturité thermique, la réflectance de la matière organique dispersée, l'indice d'altération thermique palynomorphe, l'indice d'altération des couleurs des conodontes, la composition chimique de la matière organique (Rock-Eval Tmax, S2, TOC) et la minéralogie des argiles ont été établis pour les puits Tenlen A-73 (lat. 67°52'7,5"N; long. 130°43'21,6"W), Crossley Lake South K-60 (68°29'39"N; 129°29'14"W) et Kugaluk N-02 (68°31'55"N; 131°31'19").

Tous les indices montrent que les puits ont dépassé le stage de la maturité quant à la production de pétrole. La réflectance, l'indice d'altération des couleurs des conodontes et l'indice d'altération thermique palynomorphe ont progressivement augmenté avec la profondeur, tandis que les tendances ne sont pas apparentes dans les résultats de la composition chimique de la matière organique (Rock-Eval), car la matière organique a été altérée au-delà des limites d'une interprétation fiable. D'autres travaux s'imposent pour établir un indice de maturité thermique utile pour la région à l'étude à partir de la minéralogie des argiles.

[1] Quebec Geoscience Centre, Institue National de la Recherche Scientifique-Géoressources, 2700 rue Einstein, C.P. 7500, Ste. Foy, Québec, P.Q. G1V 4C7

INTRODUCTION

The Geological Survey of Canada has initiated a program to compile and coordinate thermal maturity information. The Mackenzie Corridor and Beaufort Sea area was selected for the initial, detailed study, because levels of thermal maturity vary across the area (Feinstein et al., 1988; Dougherty and Uyeno, 1989; Link and Bustin, 1989; Utting, et al., 1989), and the geology is reasonably well known (Pugh, 1983; Norris, A.W., 1985; Norris, D.K., 1985). In order to correlate thermal maturity indices within the study area, three wells from which continuous cores are available were selected. This correlation will allow the integrated, regional interpretation of maturity using whatever index or indices are available or appropriate in a given geological setting.

In this paper, we present the results from the analysis of reflectance of dispersed organic matter (R_o for humic material, zooclasts and solid bitumens), palynomorph Thermal Alteration Index (TAI), conodont Colour Alteration Index (CAI), geochemistry of the organic material (Rock-Eval Tmax, S2, TOC), and clay mineralogy for the Tenlen A-73 (lat. 67°52'7.5"N; long. 130°43'21.6"W), Crossley Lake South K-60 (68°29'39"N; 129°29'14"W), and Kugaluk N-02 (68°31'55"N; 131°31'19"W) wells (Fig. 1).

The age of the uppermost rocks sampled in all three wells is Devonian. Most of the samples analyzed were collected from the Imperial, Canol, Hare Indian, Hume, Gossage and Tatsieta formations, and from the Ordovician/Silurian rocks in the Ronning Group, which consists of the Peel, Mount Kindle and Franklin Mountain formations.

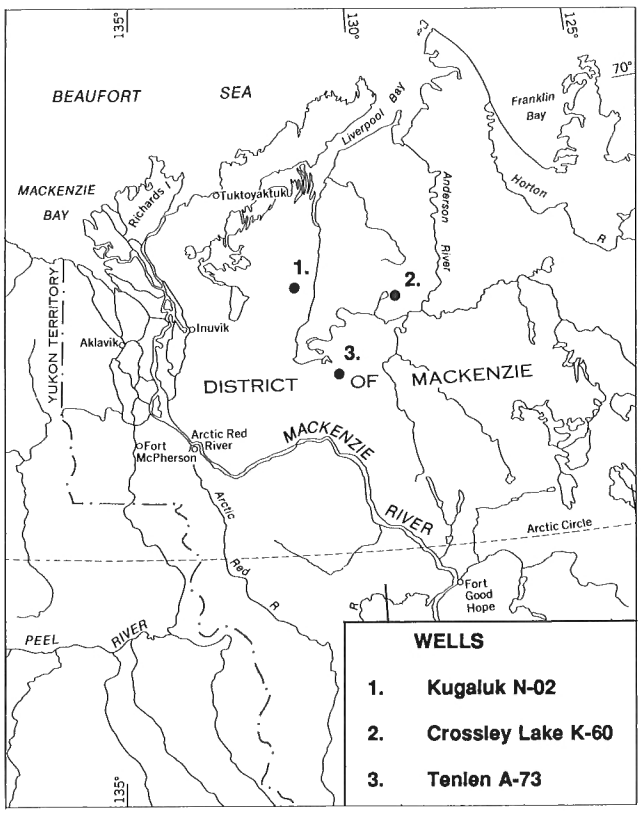

Figure 1. Locations of the Tenlen A-73, Crossley Lake South K-60, and Kugaluk N-02 wells in the northern District of Mackenzie.

The Imperial Formation consists of fine grained siltstone and shale. It is absent in the Crossley Lake South K-60 well, and ranges from 143 m in thickness in Tenlen A-73, to 814 m in thickness in Kugaluk N-02. This formation was analyzed for clay mineralogy, TAI, geochemistry Rock-Eval, and R_o.

The mudstones and shales of the Canol and Hare Indian formations, which range in thickness from 81 to 349 m, were sampled for all indices. The remainder of the Devonian units are primarily muddy carbonates and again were analyzed for all indices.

The rocks of the lower Paleozoic Ronning Group are massive dolostone and limestone units and were analyzed primarily for CAI.

METHODS AND RESULTS

The TAI and CAI assessments were made by applying the techniques outlined in the paper by Utting et al. (1989). The palynology and organic petrology slides were prepared and interpreted by the Institue National de la Recherche ScientifiqueGéoressources. Extraction, mounting and reflectance measurements of organic matter were made using the techniques of Bertrand et al. (1985). Rock-Eval analysis followed the procedure outlined in Snowdon et al. (1987). Clay mineralogy was determined by X-ray diffraction.

Table 1 shows the relationship between the various thermal maturity indices. The data from which this table was derived are included in Appendix A. Results indicate that, with the exception of the uppermost part of the Tenlen A-73 well, the area is overmature with respect to oil generation throughout the sampled intervals. Tenlen A-73 shows the lowest maturity levels at the surface and does give some indication of how the geochemical data relate to the other indices. Rock-Eval data become unreliable once Tmax values exceed 470°C. This is reflected in the wide variation in Tmax values and low S2 peaks. The R_o, TAI and CAI show good correlation without anomalous values in any of the indices. This is indicative of the relatively constant, gradual heating that would be expected from heating due to sedimentary overburden rather than rapid heating by a thermal hot spot.

Mixed layer clays essentially are absent from the samples, so that the smectite-to-illite reaction cannot be used to estimate thermal maturity. Illite and chlorite abundances appear to vary more or less systematically with depth and, with caution, and keeping in mind possible lithological controls on their distributions, might be used as indicators of thermal maturation. With the limited data available it is not possible to use the apparent variations in clay abundances to establish a maturity index. Absence of mixed layer clays suggests that temperatures exceeded 100°C throughout the section. Further work, with tighter lithological control on sampling, would be necessary to integrate the clay data with the other thermal maturity indicators.

Table 1. Comparison of thermal maturity indices based on alteration of organic material in continuous core from the Tenlen A-73, Crossley Lake South K-60 and Kugaluk N-02 wells

$\%R_o$	Thermal Alteration Index (TAI)	Conodont Colour Alteration Index (CAI)	Tmax (°C)
1.20	3-\3		450
1.30			
1.40	3+	3.5	
1.50			
1.60			475
1.70			
1.80	4-		500
1.90			
2.00			
2.10		4.0	
2.20			550
2.30	4		
2.40			
2.50			
2.60			
2.70	4+		
2.80	4+,5	4.5	

DISCUSSION AND CONCLUSIONS

Analytical data from various thermal maturity indicators for the reference wells in the study area have been presented. CAI, TAI, and R_0 show consistent increase with depth (Table 1). No trends are readily apparent in the Rock-Eval results because the organic material has been altered beyond the limits of reliable interpretation. Further work is needed to develop clay mineralogy as a useful thermal maturity index in the study area.

An expansion of the thermal maturity program is now underway. The design of a computerized database has been initiated to facilitate the generation of maps showing the distribution of thermal maturity data over a given geographic area. Outputs will also include tables illustrating the relationship between indices, and diagrams showing thermal variation with depth and time.

ACKNOWLEDGMENTS

The authors wish to thank Hans Wielens for his effort in sampling and organizing all the material used in this study.

REFERENCES

Bertrand, R., Bérubé, J.-C., Héroux, Y., and Achab, A.
1985: Pétrographie du kérogène dans la Paléozoïque inférieur: méthode de préparation et exemple d'application; Revue de l'Institut français du Pétrole, v. 40, p. 155-167.

Dougherty, B.J. and Uyeno, T.T.
1989: A conodont-based thermal maturation study of some Lower and Middle Devonian rocks, northwestern District of Mackenzie and Yukon Territory; in Current Research, Part G, Geological Survey of Canada, Paper 89-1G, p. 37-42.

Feinstein, S., Brooks, P.W., Gentzis, T., Goodarzi, F., Snowdon, L.R., and Williams, G.K.
1988: Thermal maturity in the Mackenzie Corridor, Northwest and Yukon Territories, Canada; Geological Survey of Canada, Open File 1944.

Link, C.M. and Bustin, R.M.
1989: Organic maturation and thermal history of Phanerozoic strata in Northern Yukon and northwestern District of Mackenzie; Bulletin of Canadian Petroleum Geology, v. 37, p. 266-292.

Norris, A.W.
1985: Stratigraphy of Devonian outcrop belts in Northern Yukon Territory and northwestern District of Mackenzie (Operation Porçupine area); Geological Survey of Canada, Memoir 410, 81 p.

Norris, D.K.
1985: Eastern Cordilleran foldbelt of northern Canada: its structural geometry and hydrocarbon potential; American Association of Petroleum Geologists, Bulletin, v. 69, p. 788-808.

Pugh, D.C.
1983: Pre-Mesozoic geology in the subsurface of Peel River map area, Yukon Territory and District of Mackenzie; Geological Survey of Canada, Memoir 401, 61 p.

Snowdon, L.R., Brooks, P.W., Williams, G.K., and Goodarzi, F.
1987: Correlation of the Canol Formation source rock with oil from Norman Wells; Organic Geochemistry, v. 11, p. 529-548.

Utting, J., Goodarzi, F., Dougherty, B.J., and Henderson, C.M.
1989: Thermal maturity of Carboniferous and Permian rocks of the Sverdrup Basin, Canadian Arctic Archipelago; Geological Survey of Canada, Paper 89-19.

Appendix A

Well: Tenlen A-73; Lat. 67° 52'07.5"N, Long. 130° 43'22"W; TD: 8510'/2593.8 m

Depth (Ft/m)	Fm (top)	%R_o est. telinite	Tmax	S2	TOC	TAI	Kaolinite <.2µm	Chlorite <.2µm	Illite <.2µm	CAI
200/61.0	Imperial	1.19	436.5	0.515	1.715	3-/3	0.00	2.59	97.41	
250/76.2	(surface)		442.5	0.85	1.71					
300/91.4		1.20	433.5	0.83	1.085					
350/106.7			369	0.68	1.085	3-/3	4.00	1.38	94.63	
400/121.9		1.09	446	0.885	1.05	3-/3	0.00	2.60	97.40	
450/137.2	Canol	1.32	430.5	1.34	3.015	3-/3	0.00	2.39	97.61	
500/152.4	(470/143.3)	1.27	451	3.445	2.335	I	0.00	1.77	98.23	
550/167.6			450	4.185	3.16					
600/182.9		1.28	449.5	4.21	3.135	I				
650/198.1			453	4.0	2.925					
700/213.4			439	6.145	6.485	I				
750/228.6		1.49	452	9.945	6.455	I				
850/259.1		1.28	449	8.3	5.95	I				
900/274.3		1.31	451	10.395	6.03	I	5.85	0.00	94.15	
950/289.6	Hare Indian		451	7.69	4.295					
1000/304.8	(986/300.5)	1.43	449.5	3.845	2.30	3	13.68	0.00	85.35	
1050/320.0			427	0.25	0.235					
1100/335.3			444	1.84	1.20	3+	10.74	0.00	87.34	
1150/350.5		1.40	451	3.885	3.06	4	5.38	0.00	92.63	
1200/365.8	Hume		444.5	17.22	9.96	I	0.00	0.00	100.00	3.0-4.0pp
1250/381.0	(1203/366.7)		445.5	0.48	0.67					
1300/396.2			455	1.13	1.795	4	9.80	0.00	90.20	3.0-3.5*
1350/411.5		1.51	434	0.90	1.10	4-	5.19	0.00	94.81	
1400/426.7	Gossage									3.0*-3.5
1450/442.0	(1402/427.3)		399.5	0.31	0.55					
1500/457.2										I
1650/502.9			356	0.46	0.225					
1700/518.2										3.0-3.5*
1900/579.1										3.5*-4.0
2100/640.1										B
2300/701.0										3.0-3.5*
2500/762.0										
2700/823.0	Tatsieta									3.0-3.5*
2900/883.9	(2800/853.4)									B
3100/944.9	Ronning Gp									3.0-3.5*
3150/960.1	Peel									
3200/975.4	(3072/936.3)									2pp
3250/990.1										3.0*-3.5
3300/1005.8										3.0-3.5*
3500/1066.8										3.0-3.5*
3550/1082.0			459.5	0.16	0.88					
3700/1127.8										3.0-3.5*
3750/1143.0										3.5*-4.0
3800/1158.2	Mt. Kindle	3850/1173.5	(3238/986.9)							
3900/1188.7										I
3950/1204.0										3.5-4.0*
4100/1249.7										3.5
4150/1264.9										2.5-3.0*pp
4350/1325.9										I
4500/1371.6										4.0pp
4600/1402.1	Franklin Mtn									B
4650/1417.3	(4616/1407)									B
4900/1493.5										4.0*-4.5
5100/1554.5										4.0pp
5300/1615.4										B
5500/1676.4										B
5700/1737.4										I
5900/1798.3										B
6100/1859.3										B
6300/1920.2										B
6500/1981.2										B
6700/2042.2										I
6900/2103.1										B
7100/2164.1			350.5	0.015	0.505					B
7300/2225.0	Macdougal Gp									B
7500/2286.0	(7344/2238.5)		437	0.07	0.355	I	0.00	0.00	100.00	
7600/2316.5		3.10	449	0.08	0.535	I	0.00	0.00	100.00	

B — barren sample
I — colour indeterminate
* — this is the CAI value of the majority of the specimens
pp — poor state of preservation

Appendix A (cont'd.)

Well: Kugaluk N-02; Lat. 68° 31'55"N, Long. 131° 31'19"W; TD: 8045'/2464.3 m

Depth (Ft/m)	Fm (top)	%R_o est. telenite	Tmax	S2	TOC	TAI	Kaolinite <.2µm	Chlorite <.2µm	Illite <.2µm	CAI
800/243.8	Imperial	1.85	512.5	0.23	1.295	4-	0.00	3.04	96.96	
850/259.1	(surface)		488.5	0.465	1.02					
900/274.3		1.93	531.5	0.21	0.975	4-	0.00	4.46	95.54	
950/289.6			526.5	0.195	0.925					
1000/304.8		1.90	477	0.455	0.705	4-	0.00	2.89	97.11	
1050/320.0			520.5	0.18	0.71					
1100/335.3		1.97	528	0.17	0.635	4-	3.85	3.21	92.94	
1150/350.5			530	0.29	0.805					
1200/365.8		2.01	534	0.275	0.615	4	0.00	2.73	97.27	
1250/381.0			508	0.21	0.80					
1300/396.2		2.06	486.5	0.245	0.755	4	0.00	2.13	97.87	
1350/411.5			535	0.21	0.82					
1400/426.7		2.16	529.5	0.38	0.86	4	1.43	1.82	96.75	
1450/442.0			505.5	0.4	0.99					
1500/457.2		2.12	519.5	0.485	0.94	4	0.00	2.53	97.47	
1550/472.4			500	0.585	2.435					
1600/487.7		2.01	536	0.285	0.805	4	0.00	2.70	97.30	
1650/502.9			507.5	0.39	2.44					
1700/518.2		2.30	463.5	0.155	0.985	4	1.37	2.18	96.44	
1750/533.4			524	0.165	1.005					
1800/548.6		2.38	427	0.475	0.85	4	0.00	1.91	98.09	
1850/563.9			440.5	0.105	0.58					
1900/579.1		2.38	528.5	0.155	0.805	4	0.00	2.03	97.97	
1950/594.4			514	0.145	0.705					
2000/609.6		2.44	460	0.22	0.985	4	0.00	1.42	98.58	
2050/624.8			516	0.155	0.965					
2100/640.1		2.52	487.5	0.175	1.35	4	0.00	1.69	98.31	
2150/655.3			483	0.235	2.665					
2200/670.6		2.52	449	0.08	0.715	4	4.96	0.65	94.39	
2250/685.8			427.5	0.185	0.80					
2300/701.0		2.62	446.5	0.085	0.90	4	0.00	0.96	99.04	
2350/716.3			428.5	0.09	1.225					
2400/731.5		2.58	434.5	0.155	0.675	4+	0.00	1.60	98.40	
2450/746.8			376.5	0.08	0.745					
2500/762.0		2.54	500.5	0.205	1.40	4+	0.00	0.00	100.00	
2550/777.2			399.5	0.245	3.14					
2600/792.5		2.52	497	0.19	3.075	I	2.70	0.00	97.30	
2650/807.7	Canol/Hare Indian	2.59	465	0.095	5.40	I	1.59	0.00	98.41	
2700/823.0	(2672/814.4)	2.52	379.5	0.15	5.83	I	0.00	0.00	100.00	
2750/838.2		2.47	488	0.14	5.64					
2800/853.4		2.69	354.5	0.325	3.455	I	0.00	0.00	100.00	
2850/868.7			441.5	0.21	4.86					
2900/883.9	Hume	3.04	540	0.7	5.89	4+,5	0.00	0.00	100.00	
2950/899.2	(2938/895.5)	2.81	483	0.145	2.515	I	0.00	0.00	100.00	
3000/914.4		2.84	372.5	0.095	1.015	I	2.79	0.00	97.21	4.0*-4.5
3050/929.6			440.5	0.25	0.65	4	0.00	0.52	99.48	
3100/944.9	Gossage	3.34								B
3200/975.4	(3120/951)		342.5	0.05	0.62					3.5*-4.0
3250/990.6			333	0.045	0.435					
3300/1005.8		3.04	332.5	0.065	0.805	I				4.0
3350/1021.1			316.5	0.035	1.675					
3400/1036.3			338.5	0.05	1.16					
3700/1127.8			386	0.005	0.425					3.5
3900/1188.7										3.5*-4.0pp
4100/1249.7										B
4200/1280.2										3.5pp
4400/1341.1	Tatsieta									3.5*-4.0pp
4600/1402.1	(4505/1373.1)									B
4800/1463.0	Ronning Gp									3.5-4.0*pp
5000/1524.0	Peel									4.0*-4.5
5200/1585.0	(4798/1462.4)		499.5	0.145	2.65					4.0
5400/1645.9	Mt. Kindle		500.5	0.145	2.59					3.5-4.0*
5600/1706.9	(5522/1683.1)									4.0-4.5*
5800/1767.8										4.0
6000/1828.8										B
6200/1889.8	Franklin Mtn									B
6400/1950.7	(6344/1933.7)									B
6600/2011.7										B
6800/2072.6			503	0.10	0.37					B
7000/2133.6										B
7200/2194.6										4.0-4.5*
7400/2255.5										B
7600/2316.5			534	0.235	0.195					B
7800/2377.4			531	0.27	0.77					B
8000/2438.4			417.5	0.30	0.735					B

B — barren sample
I — colour indeterminate
* — this is the CAI value of the majority of the specimens
pp — poor state of preservation

Appendix A (cont'd.)

Well: Crossley Lake South K-60; Lat. 68° 29'39"N, Long. 129° 29'14"W; TD: 5529'/1685.2 m

Depth (Ft/m)	Fm (top)	%R_o est. telinite	Tmax	S2	TOC	TAI	Kaolinite <.2µm	Chlorite <.2µm	Illite <.2µm	CAI
450/137.2	Hare Indian		439.5	1.05	3.09					
500/152.4	(460/140.2)		438	0.83	3.18					
700/213.4		1.45				3+	16.38	1.94	81.68	
750/228.6			335	0.075	0.18					
800/243.8		1.49	427.5	0.455	0.33	3+	8.89	2.98	88.13	
850/259.1			400	0.16	0.185					
900/274.3		1.60	438.5	0.465	0.22	3+	11.52	2.47	86.00	
950/289.6			396.5	0.695	0.32					
1000/304.8		1.59	386	0.36	0.28	3+	12.50	2.39	85.12	
1050/320.0			515	0.4	0.26					
1100/335.3		1.66	433	0.47	0.375	4-	12.91	0.00	85.60	
1150/350.5			469	0.79	0.505					
1200/365.8		1.73	437.5	1.095	1.50	4	10.67	0.00	87.40	
1250/381.0		1.86	443	3.29	5.185	I	0.00	0.00	100.00	
1300/396.2	Hume	1.98	476	1.94	3.985	I				
1350/411.5	(1312/399.9)	1.96	515.5	5.26	8.655	4	6.14	0.00	93.86	3.5-4.0*
1400/426.7		1.72	503.5	0.525	0.27	4-	2.44	0.00	97.56	4.0
1450/442.0	Gossage		466	0.36	1.17					
1500/457.2	(1460/445)		407	0.305	0.82					3.5
1550/472.4			478.5	0.47	1.57					
1600/487.7			487.5	2.04	5.59					3.5*-4.0
1650/502.9			439.5	0.20	0.665					
1700/518.2										3.0-3.5*
1800/548.6										3.0-3.5*
1900/579.1			387.5	0.575	2.0					4.0
2100/640.1										3.5*-4.0
2300/701.0										3.5
2500/762.0										B
2700/823.0										3.5-4.0*
2800/853.4	Tatsieta									
2900/883.9	(2888/880.3)		389.5	0.695	0.945					B
3000/914.4	Ronning Gp									
3100/944.9	Peel									3.5-4.0*
3200/975.4	(3069/935.4)									
3300/1005.8			536	0.57	0.575					3.5-4.0*
3500/1066.8										3.5-4.0*
3700/1127.8										3.5-4.0*pp
3900/1188.7	Mt.Kindle									3.5-4.0*
4000/1219.2	(3918/1194.2)									
4100/1249.7										3.5-4.0*
4300/1310.6										3.5
4500/1371.6	Franklin Mtn									4.0
4600/1402.1	(4516/1376.5)									
4700/1432.6										B
4900/1493.5										3.5*-4.0pp
5200/1585.0										3.5pp
5400/1645.9										3.5pp
5600/1706.9										3.5

B — barren sample
I — colour indeterminate
* — this is the CAI value of the majority of the specimens
pp — poor state of preservation

La zone frontale des glaciers Thompson et White dans l'île Axel Heiberg du Haut Arctique canadien: quelques observations préliminaires

Michel Parent
Centre géoscientifique de Québec, Sainte-Foy

Parent, M., 1991: La zone frontale des glaciers Thompson et White dans l'île Axel Heiberg du Haut Arctique canadien: quelques observations préliminaires; dans Recherches en cours, Partie E; Commission géologique du Canada, Étude 91-1E, p. 203-210.

Résumé

La zone frontale des glaciers Thompson et White dans la région du fjord Expedition est l'une des rares régions du Haut Arctique où sont juxtaposés un glacier en progression et un autre en retrait. La zone frontale du Thompson est caractérisée par un écoulement trés compressif et par une énorme moraine de poussée formée de graviers fluvioglaciaires gelés. La moraine de poussée, déformée par écaillage glaciotectonique, s'est avancée d'environ 500 m au cours des derniers 30 ans. Par contre, la zone frontale du glacier White est caractérisée par un profil en long elliptique caractéristique, une maigre charge supra- et intraglaciaire et un retrait frontal de 100 m en 30 ans. Les moraines latérales et frontales en bordure du White sont des moraines à noyau de glace formées peu après 180 ± 60 BP, soit vers le milieu du Petit âge glaciaire. Ainsi, ce dernier a donc atteint son maximum néoglaciaire vers 1800 AD alors que le glacier Thompson ne l'a pas encore atteint. Comme le Thompson est trois fois plus long, son temps de réponse est considérablement plus long, d'où le diachronisme des avancées de ces glaciers adjacents.

Abstract

The frontal zone of Thompson and White glaciers in the Expedition Fiord region is one of the rare juxtapositions in the High Arctic of an advancing glacier and a retreating glacier. The frontal zone of Thompson Glacier is characterized by highly compressive flow and by a large push moraine made up of frozen glaciofluvial gravel. The push moraine, deformed by glaciotectonic imbrication, has advanced about 500 m over the last 30 years. On the other hand, the frontal zone of White Glacier is characterized by a typically elliptical longitudinal profile, a sparse supraglacial and intraglacial debris load, and a frontal retreat of 100 m in 30 years. The lateral and end moraines of White Glacier are ice cored moraines formed shortly after 180 ± 60 BP, approximately during the middle of the Little Ice Age. This glacier thus reached its Neoglacial maximum around 1800 AD, whereas Thompson Glacier has not yet reached its maximum. Since the Thompson Glacier is three times longer than White Glacier, its response time is considerably longer, which explains the diachronism in the advances of these adjacent glaciers.

INTRODUCTION

Les glaciers de la région du fjord Expedition dans l'ouest de l'île Axel Heiberg du Haut Arctique canadien, ont fait l'objet d'études glaciologiques approfondies par les chercheurs associés aux missions de la McGill-Jacobsen Axel Heiberg Research Expedition sous la direction de F. Müller (Adams, 1987). Bien que la majorité des travaux publiés depuis une trentaine d'années sur cette région aient porté sur le glacier White, quelques-uns ont aussi traité de la géomorphologie des marges glaciaires actuelles (Robitaille et Greffard, 1962; Maag, 1969; Kälin, 1971) dans la région du camp de base du lac Colour (fig. 1).

Les zones frontales des glaciers Thompson et White ont été choisies aux fins d'une étude sur les processus de transport et de sédimentation glaciaire en raison des aspects glaciologiques et morphologiques contrastés que présentent ces deux glaciers adjacents et aussi, en raison de leur relative accessibilité. Le but de cet article est de présenter brièvement les principaux aspects de la dynamique actuelle de cette zone frontale. L'obtention d'une série de photographies aériennes à l'été 1990 a permis la mise à jour de plusieurs des phénomènes géomorphologiques et glaciologiques survenus dans cette zone frontale depuis les survols photographiques antérieurs.

RÉGION ÉTUDIÉE

Le fjord Expedition et la vallée qui le prolonge vers le nord-est s'encaissent dans une région montagneuse de la chaîne innuitienne. Dans cette partie de la chaîne où le relief atteint communément 1000 m, le substratum rocheux, d'âge mésozoïque, est constitué principalement de roches sédimentaires détritiques, surtout des grès et des shales en alternance plus ou moins répétitive (Fricker, 1963; Thorsteinsson, 1971). Toutefois, ces roches sédimentaires du Bassin de Sverdrup sont recoupées par un important réseau de dykes et de sills mafiques d'âge crétacé. Ces roches mafiques forment d'ailleurs une part importante du cortège lithologique des sédiments quaternaires de cette région de l'île Axel Heiberg; de plus, les levés détaillés de Fricker (1963) montrent que ces roches constituent un bon nombre des arêtes qui percent cette partie de la calotte de Müller. Enfin, la série mésozoïque plissée est recoupée par plusieurs corps diapiriques formés surtout d'anhydrite et de gypse (Thorsteinsson, 1971).

L'examen des cartes et des photographies aériennes de la région révèle que la moitié orientale de la calotte de Müller forme un véritable dôme glaciaire, dont la ligne de partage atteint une altitude d'environ 1800 m, et forme d'ailleurs la principale ligne de faîte dans cette partie de l'île Axel Heiberg. Par contre, la moitié ouest de l'île présente un tout autre style d'englacement: le recouvrement et l'écoulement glaciaires y sont largement commandés par le relief. Les secteurs d'altitude plus basse, sous 800 m environ, n'y sont généralement pas englacés sauf évidemment dans le cas où les vallées sont occupées par des langues glaciaires (Crusoe, White et Thompson par exemple). À plus haute altitude, les champs de glace discontinus n'arrivent pas à masquer le modelé glaciaire alpin sous-jacent. Les cirques, arêtes et autres formes glaciaires alpines qui sont désormais recouverts de glaces minces et discontinues n'ont pu évidemment se former que lorsque le recouvrement glaciaire était moins important, concentré dans les parties basses du relief. La mise en évidence de ce recouvrement glaciaire moindre porte à croire que la région a connu un climat plus chaud ou plus sec qu'actuellement, présumément durant l'Hypsithermique ou durant un interglaciaire pré-wisconsinien.

La présence de morceaux de bois flotté et de débris organiques, datés entre 6,2 et 5,3 ka (Müller, 1963), dans la moraine de poussée et les débris sous-glaciaires actuels du glacier Thompson, semble indiquer d'ailleurs que la région connaît ou vient de connaître un modeste maximum glaciaire. Cette interprétation s'appuie aussi sur le fait que les moraines actuelles ou subactuelles sont les seules moraines post-wisconsiniennes observées dans la région. Ce maximum récent est toutefois bien moindre que celui du Wisconsinien auquel sont attribués de beaux affleurements de till observés au moins jusqu'à 400 m d'altitude sur le versant ouest de la vallée du glacier White. Les chenaux juxtaglaciaires et les moraines latérales identifiés par Lemmen et al. (1991) en aval, le long du fjord Expedition, sont présumément corrélatifs de cette nappe de till. S'il peut sembler évident que ces dépôts et formes glaciaires sont d'âge wisconsinien, il reste à établir s'ils sont attribuables au Wisconsinien supérieur, moyen ou inférieur. De plus, comme l'ont signalé Hodgson (1989) et Lemmen et al. (1991), le problème de l'extension et du style de la dernière avancée glaciaire régionale n'est pas encore résolu.

Bien que les zones frontales actuelles des glaciers White et Thompson soient juxtaposées, il s'agit de glaciers dont la nature et la taille diffèrent sensiblement. Le glacier White est un glacier alpin typique qui possède sa propre aire d'accumulation et dont la longueur est d'environ 13 km. Le glacier Thompson est essentiellement un glacier émissaire de la partie sud de la calotte de Müller. Ce dernier reçoit bien quelques glaciers affluents, le principal étant le glacier Piper, mais il est surtout alimenté à partir de la ligne de partage glaciaire principale passant à une vingtaine de kilomètres au nord de la région illustrée à la figure 1. Depuis la ligne de partage glaciaire vers 1800 m d'altitude jusqu'au front, à quelque 30 m d'altitude, le glacier Thompson s'étend sur une longueur d'environ 40 km.

LA ZONE FRONTALE DU GLACIER THOMPSON

Dans sa zone frontale, le glacier Thompson a une largeur d'environ 3 km (fig. 2); à la hauteur du lac Between, soit environ 3 km à l'amont du front actuel, la surface du glacier atteint une altitude de 350 m, ce qui n'y représente qu'une épaisseur minimale puisque, selon les travaux de Kälin (1971), la base du glacier est située sous le niveau de la mer. Le front du glacier Thompson peut être subdivisé en trois segments larges d'environ 1 km chacun. Le segment ouest est caractérisé par une falaise haute d'une soixantaine de mètres, surplombant l'actuel épandage proglaciaire (fig. 2). Étant donné le vêlage à sec qui s'y exerce ainsi que les chutes fréquentes de blocs et galets supraglaciaires, les zones de

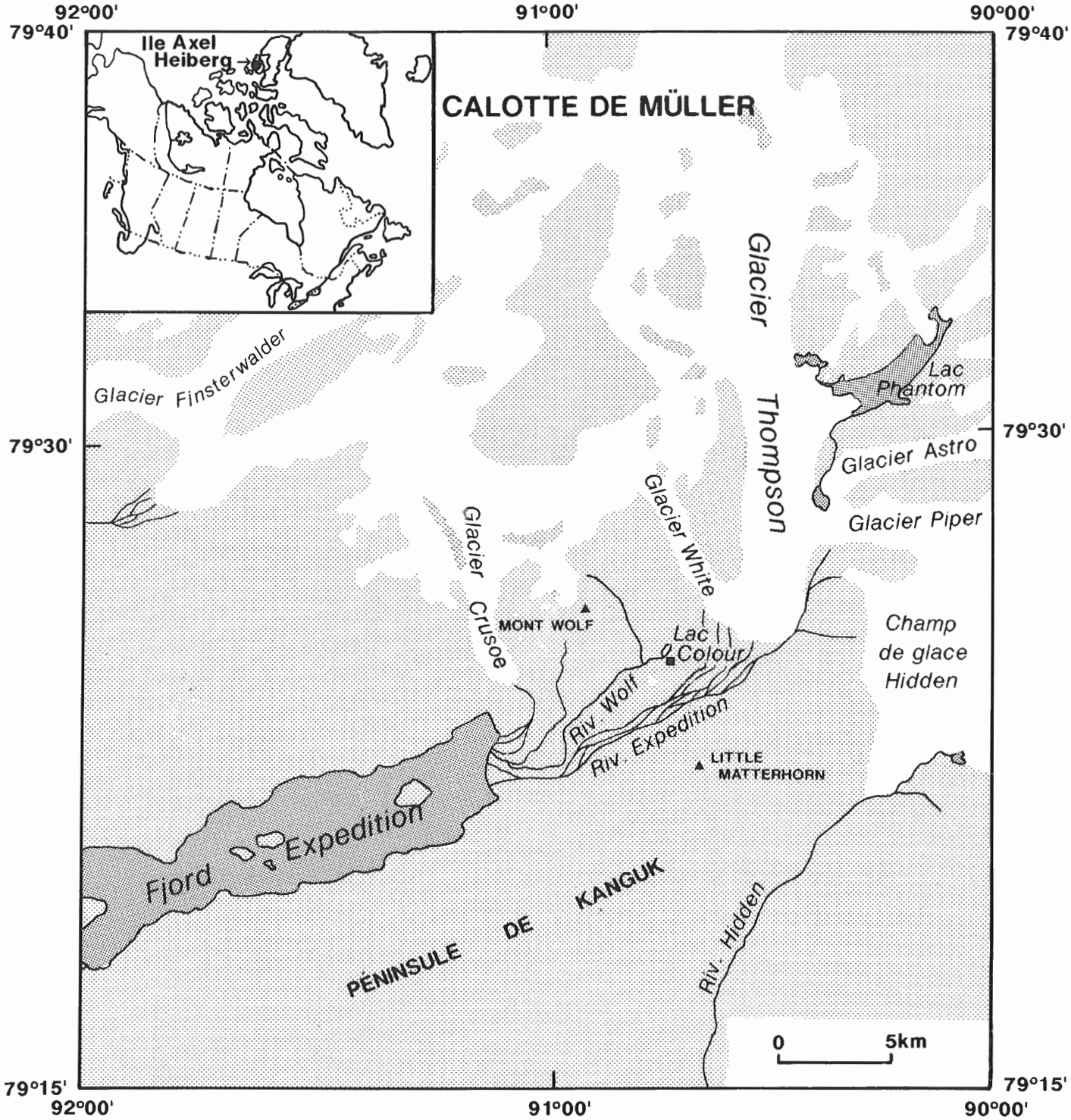

Figure 1. Région du fjord Expedition. Les glaciers et champs de glace sont en blanc, les zones extraglaciaires sont tramées en gris pâle et les nappes d'eau sont tramées en gris foncé. Le camp de base McGill-Jacobsen (■) est situé à proximité du lac Colour.

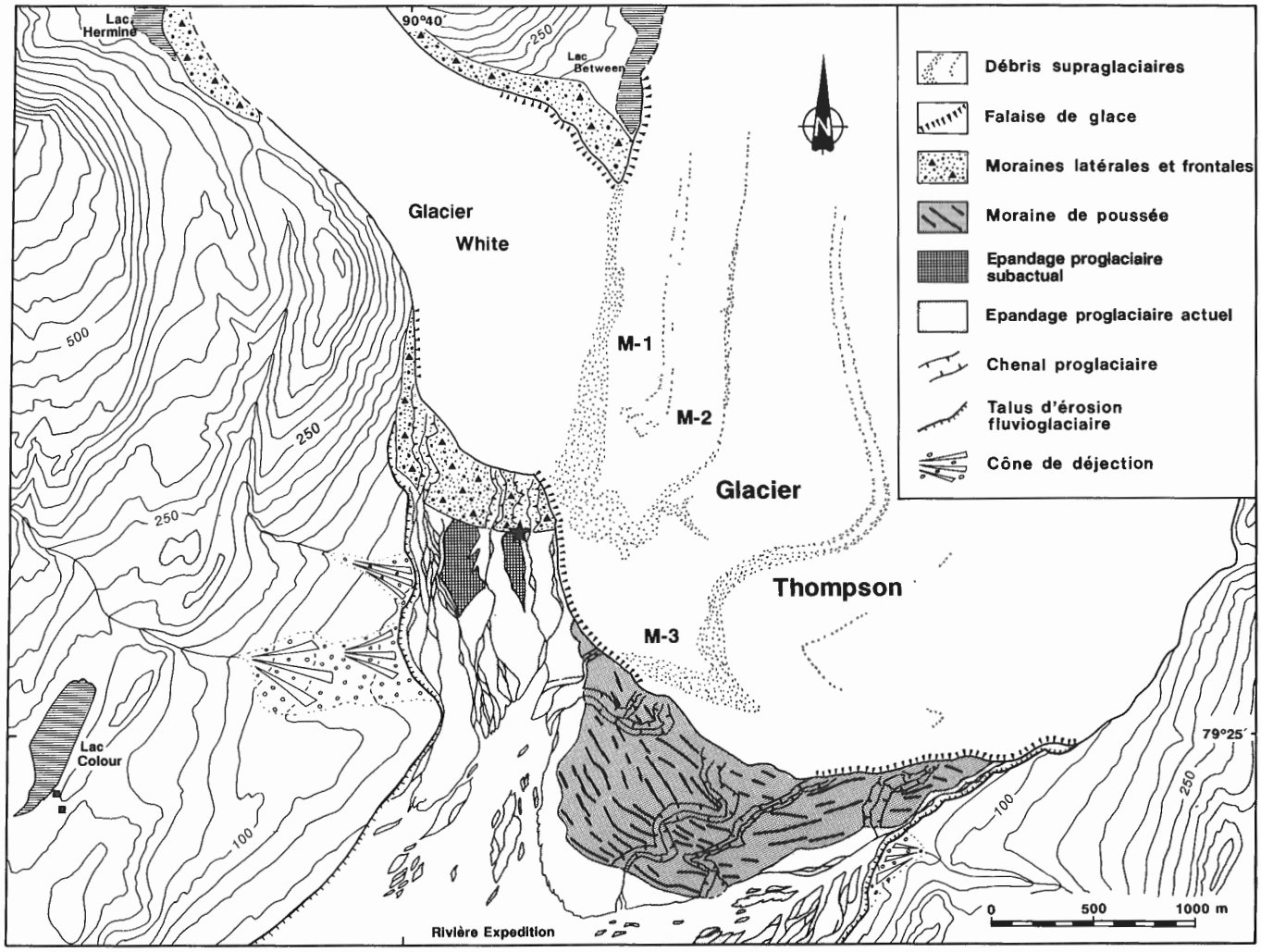

Figure 2. Croquis géomorphologique de la zone frontale des glaciers Thompson et White, établi d'après les photographies aériennes de 1990. Le glacier Thompson est bordé d'une moraine de poussée dont la formation se poursuit encore actuellement, tandis que le glacier White est bordé d'une moraine à noyau de glace dont la mise en place a débuté vers la fin du Petit âge glaciaire. L'astérisque indique la localisation de la datation ^{14}C mentionnée dans le texte.

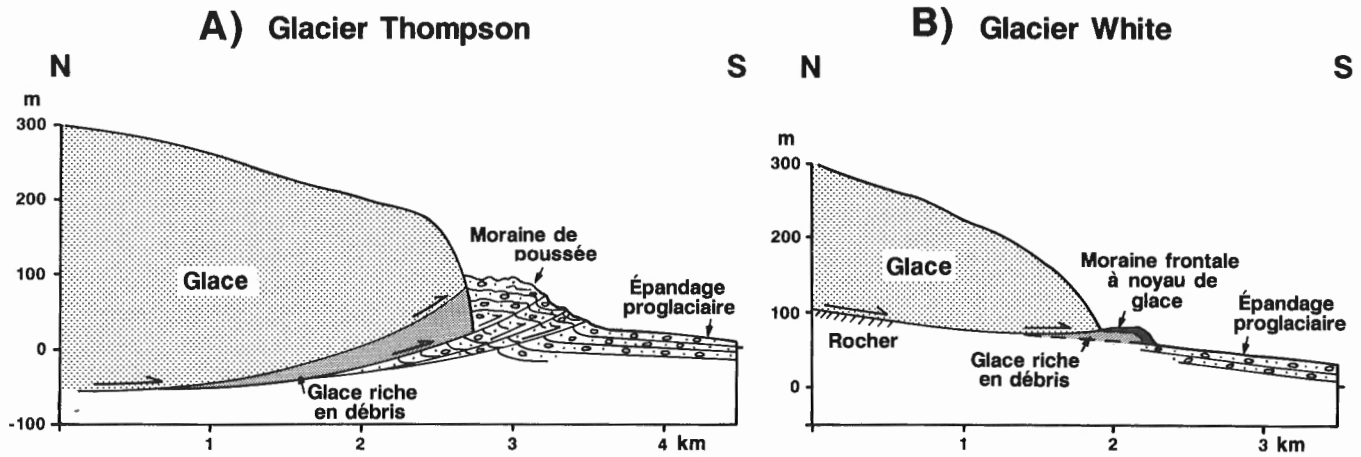

Figure 3. Coupes longitudinales schématiques de la zone frontale des glaciers Thompson (**A**) et White (**B**). Ces coupes illustrent les principaux contrastes de la dynamique d'un front glaciaire en progression (A) et d'un front glaciaire en retrait (B) dans une région pergélisolée.

débris infraglaciaires ainsi que les tabliers d'éboulis frontaux sont, pour la plupart, inaccessibles. Quant au segment est, son accessibilité est meilleure étant donné l'absence d'une charge intraglaciaire significative, mais la base de la falaise frontale ne laisse pratiquement pas voir la zone de débris infraglaciaires. Le segment central est caractérisé par une pente frontale plutôt typique (fig. 3A), mais la majeure partie de celle-ci est masquée par la moraine de poussée, de sorte que la zone de débris infraglaciaires n'a pu être observée qu'à quelques endroits, là où l'incision des chenaux proglaciaires l'avait dégagé. Cette zone de débris infraglaciaires est constituée soit de glace riche en débris façonnés par l'abrasion glaciaire, soit d'écailles de matériel sous-glaciaire plus ou moins déformé (silts stratifiés, par exemple) et entraîné jusqu'au front, soit d'un mélange plus ou moins complexe des deux. La présence de ces cailloux et galets striés ou façonnés dans la charge infraglaciaire indique qu'il y a glissement basal et donc, que la température basale du glacier oscille autour du point de fusion sous pression.

Dans sa moitié ouest, la langue glaciaire contient d'abondants débris intraglaciaires, certains disséminés, d'autres concentrés en bandes et donnant lieu à des moraines supraglaciaires médianes (M-1, M-2 et M-3 sur la fig. 2). La moraine M-3 est très mince, masquant à peine la glace sous-jacente, et elle se compose de débris anguleux ne présentant à peu près pas de marques de façonnement glaciaire. Par contre, les moraines M-2 et M-3 sont plus épaisses, atteignant parfois 1 m, et se composent d'un matériel mixte: certains cailloux sont anguleux, non usés, comme ceux de la moraine M-3, alors que d'autres sont plutôt subarrondis, sont souvent striés ou encore comportent des facettes d'abrasion glaciaire. Ainsi, une bonne partie du matériel de ces deux moraines supraglaciaires porte les traces caractéristiques d'un transport basal, antérieur à leur transport en zone intraglaciaire puis supraglaciaire. Il faut toutefois signaler que la moraine M-1, quoiqu'elle représente la moraine médiane Thompson-White, ne contient que des débris provenant du glacier Thompson. En fait, la suture entre les glaciers Thompson et White est facilement repérable sur le terrain et se situe à quelques décamètres tout au plus à l'ouest de la moraine M-1. La moitié est de la langue glaciaire est beaucoup plus propre; la seule bande importante de débris intraglaciaires et supraglaciaires y est celle associée au glacier Piper (fig. 1) qui d'ailleurs se referme à la hauteur du lac Between. Enfin, il est à remarquer que toute l'eau de fonte du glacier Thompson est évacuée par des bédières; en effet, aucun cours d'eau intra- ou sous-glaciaire n'a été observé dans la zone frontale du glacier, ce qui est normal puisqu'il s'agit d'un glacier subpolaire, caractérisé par des températures de surface bien inférieures à zéro (Blatter, 1985). Malgré la présence de glace basale dont la température est voisine du point de fusion sous pression, il semble que le volume des eaux de fonte produites soit nettement insuffisant pour donner naissance à d'éventuels cours d'eau sous-glaciaires.

Moraine de poussée et écailles glaciotectoniques

L'aspect le plus remarquable de la zone frontale du glacier Thompson est évidemment son énorme moraine de poussée (fig. 2). Cette moraine, dont la largeur atteint près de 800 m et dont l'altitude atteint 100 m et plus, est composée essentiellement de graviers fluvio-glaciaires gelés. Elle est formée d'une série de crêtes parallèles et arquées dont l'altitude décroît en s'éloignant du front glaciaire. Les sommets de la plupart des crêtes externes sont soulignés par des charnières anticlinales, bien visibles sur le terrain et sur les photographies aériennes. La présence de nombreuses cassures fraîches le long de ces charnières et celle de fractures de décrochement perpendiculaires au front indiquent que l'activité glaciotectonique est concentrée dans la zone externe de la moraine de poussée (fig. 3A). En effet, autant l'examen des photographies aériennes que les levés de terrain mettent en évidence ce contraste entre les zones externe et interne de la moraine de poussée: la dissection à partir des chenaux fluvio-glaciaires est le trait dominant de la zone interne, alors que la fracturation glaciotectonique caractérise la zone externe. Grâce aux nombreuses coupes pratiquées par les chenaux proglaciaires, on peut affirmer que la moraine de poussée ne contient pas de noyau de glace; sauf quelques minces plaques de glace d'origine incertaine, la moraine ne contient que la glace interstitielle des graviers fluvio-glaciaires. Le modèle glaciotectonique préconisé pour la genèse de la moraine de poussée est celui d'un prisme frontal d'accrétion, formé d'écailles chevauchantes sur lesquelles reposent passivement une masse de sédiments déformés antérieurement.

Figure 4. Moraine de poussée active au front du glacier Thompson. Juste derrière le grand naled, d'anciennes surfaces gauchies et soulevées de l'épandage fluvioglaciaire forment des rampes glaciotectoniques inclinées vers le front glaciaire. Ces rampes sont l'expression superficielle du déplacement des écailles glaciotectoniques sous-jacentes. La falaise frontale du Thompson est haute d'environ 50 m.

L'intense déblayage pratiqué par les cours d'eau fluvio-glaciaires médians a favorisé l'érosion de la partie supérieure du prisme d'accrétion dans la partie ouest de la moraine de poussée. Ceci permet d'observer le gauchissement et le soulèvement caractérisant le déplacement de l'écaille de chevauchement qui sous-tend cette partie de la plaine d'épandage fluvio-glaciaire (fig. 4). Ainsi, la surface soulevée de la plaine d'épandage forme une rampe légèrement inclinée vers le front glaciaire. Cette rampe, formée par le déplacement de l'écaille sous-jacente, ressemble beaucoup aux "glaciotectonic thrust plates" décrites par Klassen (1982) au front de certains glaciers de l'île Bylot.

LA ZONE FRONTALE DU GLACIER WHITE

La zone frontale du glacier White est poussée et transpressée vers l'ouest à cause des contraintes qu'y exerce la langue du glacier Thompson. À l'encontre de ce dernier, le profil de surface du glacier White est très proche du profil d'équilibre et les pentes inférieures du front oscillent autour de 30° (fig. 3B). Un forage dans le glacier, environ 2 km à l'amont du front, a révélé que la glace y a une épaisseur de 200 m et que sa température décroît depuis environ -15°C en surface jusqu'à 0°C à la base (Blatter, 1985; Koerner, 1989). Étant donné ces basses températures de surface, les eaux de fonte s'écoulent essentiellement dans des bédières et dans des chenaux juxtaglaciaires latéraux, comme dans le cas du glacier Thompson. Le chenal de vidange du lac Between fait toutefois exception à cette règle; ce lac, dont l'important trop-plein annuel avait l'habitude de s'écouler lors d'une crue soudaine (jokulhlaup) via un chenal supraglaciaire (Maag, 1969), se vidange désormais via un chenal sous-glaciaire (ou intraglaciaire) dont le tracé suit approximativement la marge ouest de la moraine médiane M-1. Ce cours d'eau surgit d'un tunnel sous-glaciaire et entaille profondément la moraine frontale du glacier White.

En net contraste avec le glacier Thompson, le glacier White ne présente que très peu de débris supraglaciaires ou intraglaciaires, d'où son nom d'ailleurs. Outre l'habituelle boue fine des trous à cryoconite, seules quelques minces bandes de débris intraglaciaires font surface dans la moitié ouest du glacier, jusqu'à environ 200 m à l'amont du front. Ces bandes donnent naissance à de petites moraines supraglaciaires à noyau de glace et dont le matériel est entièrement remanié par le fluage. Enfin, du côté est, près de la moraine M-1, la surface du glacier est couverte de quelques minces placages de graviers triés, dont quelques-uns forment de petits cônes supraglaciaires; ces placages représentent probablement des dépôts laissés dans les mouilles du paléo-chenal supraglaciaire du lac Between.

La zone frontale du glacier White est bordée d'une moraine frontale dont le relief d'environ 10 m et la largeur d'environ 300 m sont beaucoup plus modestes que ceux de la moraine de poussée du glacier Thompson. La moraine frontale du glacier White, tout comme ses moraines latérales d'ailleurs, est formée d'un ou deux mètres de till supraglaciaire flué reposant sur plusieurs mètres de glace morte riche en débris (fig. 3B). L'incision pratiquée par le chenal sous-glaciaire issu du lac Between permet d'observer que ce prisme de glace riche en débris se prolonge sous le front du glacier où il est surmonté directement par de la glace relativement propre. À cause d'une intense érosion thermique le long des chenaux proglaciaires, la moraine frontale est en voie de démantèlement rapide. Au droit de la bordure externe de la moraine, dans la berge d'un chenal proglaciaire, le till repose directement sur un paléosol développé sur une nappe de graviers fluvio-glaciaires (fig. 5). Les débris organiques du paléosol ont été datés à 180 ± 60 BP (GSC-5160), un âge très récent que l'on pouvait anticiper puisque la nappe fluvio-glaciaire associée au paléosol se prolonge directement à l'aval de la moraine frontale où elle est légèrement surélevée par rapport à l'épandage fluvio-glaciaire actuel. Ce contexte stratigraphique semble analogue à celui décrit par Müller (1963) et où un âge relativement imprécis de 240 ± 100 BP (B-464) avait été obtenu sur des racines de *Salix arctica*. La moraine frontale du glacier White s'est donc formée vers la fin du Petit âge glaciaire. Il semble qu'il s'agisse là des deux seules datations ^{14}C portant directement sur cet épisode de refroidissement marqué dans le Haut Arctique canadien.

Figure 5. Paléosol (ligne tiretée) développé à la surface de graviers fluvioglaciaires et enfoui sous la bordure externe de la moraine frontale du glacier White. Des débris organiques provenant de ce paléosol ont été datés à 180 ± 60 BP. La moraine frontale s'est formée lors du Petit âge glaciaire.

DISCUSSION

La comparaison d'un croquis géomorphologique de la zone frontale réalisé à l'aide des photographies aériennes de 1990 avec un croquis semblable réalisé avec les photographies aériennes de 1960 permet d'évaluer l'ampleur des changements survenus en 30 ans (fig. 6). L'aspect le plus remarquable est certes le fait que le front du glacier Thompson s'est avancé de quelque 500 m en 30 ans pendant que le front du glacier White a reculé d'environ 120 m au cours de la même période. L'examen d'autres séries de photographies aériennes prises durant cet intervalle de 30 ans permet d'établir que ces changements se sont produits graduellement et non pas lors de brefs épisodes marqués par des changements brusques. Ainsi le croquis multidate (fig. 6) permet d'estimer que le taux de progression du glacier Thompson a été de l'ordre de 16 $m \cdot a^{-1}$ durant les derniers 30 ans alors que le taux de retrait du glacier White a été d'environ 4 $m \cdot a^{-1}$. Le croquis révèle aussi que la suture entre les glaciers White et Thompson s'est déplacée d'environ 200 m vers l'ouest, reflétant l'empiétement progressif du glacier Thompson sur la zone frontale du glacier White. Enfin, la comparaison des photographies aériennes de 1960 et de 1990 indique que la moraine de poussée s'est avancée au même rythme que le front glaciaire du glacier Thompson, tout en maintenant sensiblement la même largeur et la même forme durant ces 30 ans. Toutefois, l'altitude des crêtes morainiques dans la partie plus passive du prisme d'accrétion frontal s'est rehaussée de quelque 15 à 20 m.

La vallée de la rivière Expedition est probablement l'une des rares régions où co-existent aussi étroitement un front glaciaire en récession et un autre en progression. Le fait que le glacier White était aussi en progression il y a environ 1800 ans indique que cet asynchronisme apparent est plutôt un diachronisme relié à un temps de réponse plus long pour le glacier Thompson. Ce temps de réponse plus long, qui résulte principalement du fait que le glacier Thompson est trois fois plus long que le glacier White, fait en sorte que le premier n'a pas encore atteint sa position maximale du Petit âge glaciaire.

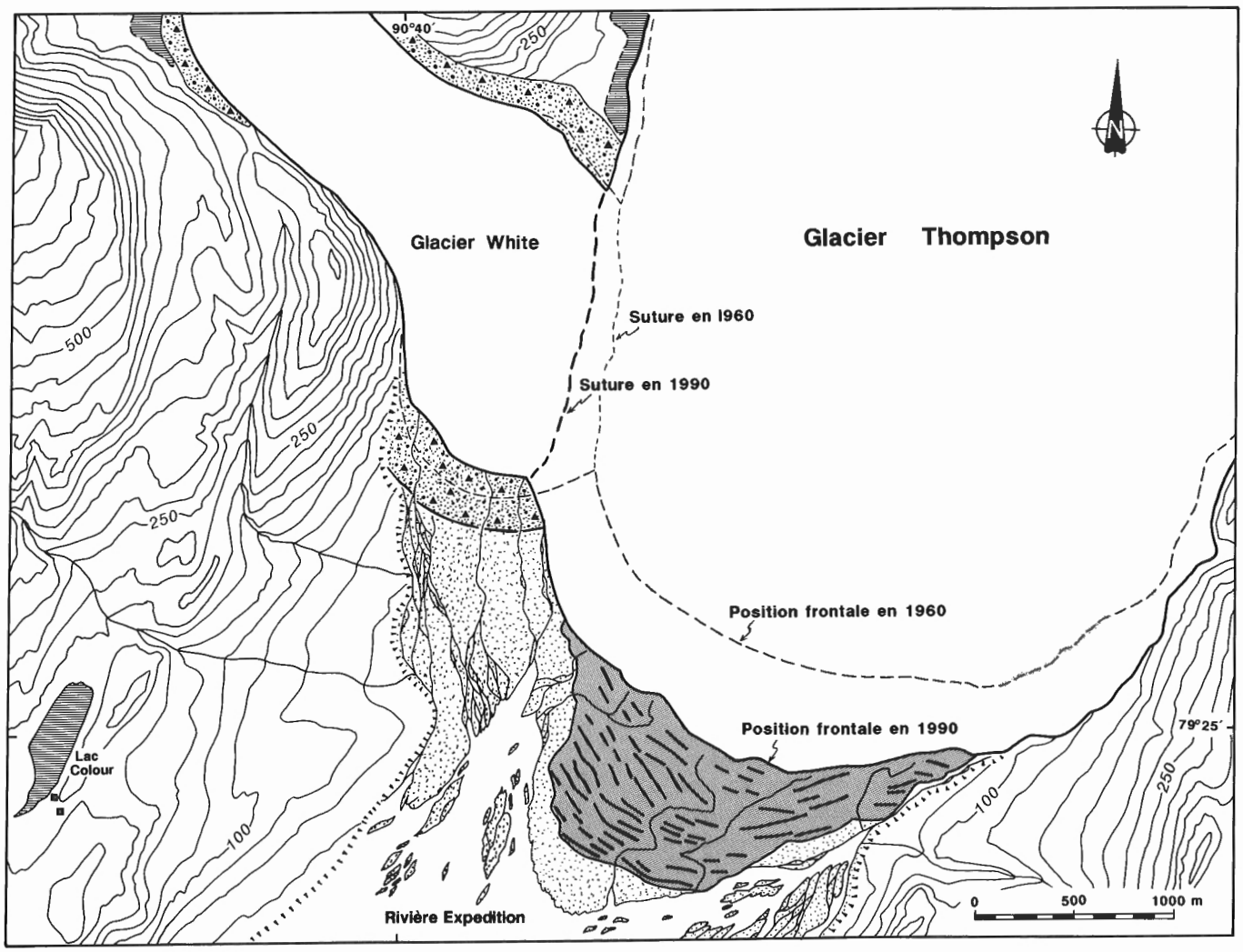

Figure 6. Comparaison de la position des marges des glaciers Thompson et White à l'été 1990 et à l'été 1960. Les faits dominants sont certes l'importante avancée du front du glacier Thompson et le léger recul du front du glacier White, de même que le déplacement de la suture entre les glaciers Thompson et White.

De tels décalages chronologiques mettant en relation le temps de réponse de glaciers et leur taille ont été abondamment documentés dans le cas d'une série de glaciers du massif du Mont Blanc dans les Alpes européennes (Reynaud, 1988). D'autre part, la possibilité que le glacier Thompson soit en crue rapide (surge) et que le décalage chronologique Thompson-White soit un phénomène aléatoire doit être rejetée. En effet, les multiples séries de photographies aériennes obtenues depuis 1960 indiquent que la progression du glacier Thompson a été régulière et continue, tout comme l'a été le retrait du front du glacier White. Les taux de progression du front du glacier Thompson étaient de l'ordre de 25 $m \cdot a^{-1}$ entre 1959 et 1969 (Müller, 1969) alors que le taux moyen a été de 16 $m \cdot a^{-1}$ entre 1960 et 1990, preuve que la progression du front a ralenti sensiblement au cours des derniers dix ou vingt ans. Il est d'ailleurs possible que le glacier Thompson soit sur le point d'atteindre sa position d'avancée maximale. D'autre part, l'étude de Kälin (1971) avait identifié, sur l'île Axel Heiberg, des moraines de poussée au front de plusieurs autres glaciers de taille comparable à celle du glacier Thompson, signe que l'actuelle avancée de ce dernier n'est pas un cas isolé ou aléatoire. Cette avancée semble donc revêtir une signification régionale puisqu'il y a tout lieu de croire qu'elle représente une réponse tardive au refroidissement du Petit âge glaciaire.

Enfin, l'important diachronisme observé ici, causé par les temps de réponse différents de deux glaciers voisins, laisse entrevoir la probabilité de diachronismes bien plus grands lors des avancées et retraits glaciaires majeurs qui ont caractérisé le Quaternaire de toutes les régions canadiennes. D'autre part, le diachronisme entre les glaciers White et Thompson indique que l'utilisation des fluctuations des marges glaciaires dans le but d'évaluer les changements climatiques récents exige au moins que l'on tienne compte des temps de réponse des différents glaciers. De plus, les temps de réponse relativement longs qui caractérisent ces glaciers polaires portent à croire que les fluctuations des marges glaciaires dans le Haut Arctique canadien sont probablement des indicateurs peu sensibles dans le cas de fluctuations climatiques de faible amplitude ou de courte période, ce qui n'exclut évidemment pas la possibilité que d'autres paramètres glaciologiques puissent constituer d'excellents indicateurs de fluctuations climatiques récentes.

REMERCIEMENTS

L'Étude du Plateau continental polaire est remerciée pour son indispensable soutien logistique. L'auteur remercie également M. Wayne Pollard (Université McGill) qui a permis et facilité l'accès de l'équipe de terrain au camp de base de Colour Lake. Il tient à remercier aussi Y. Moisan, G. Gosselin et S. Ziff avec lesquels la mission de l'été 1990 à l'île Axel Heiberg a été partagée avec enthousiasme. Des remerciements particuliers s'adressent à J. Godden, B. Hough et P. Roy dont la collaboration a permis la réalisation des clichés aériens de 1990. Enfin, il remercie Y. Michaud et J.C. Bourgeois pour leurs commentaires avisés lors de la lecture critique du manuscrit.

RÉFÉRENCES

Adams, P. (éd.)
1987: Field research on Axel Heiberg Island, N.W.T., Canada; McGill University, Axel Heiberg Island Research Report, Miscellaneous Papers no. 2, 207 p.

Blatter, H.
1985: On the thermal regime of Arctic glaciers; Zurcher Geographische Schriften, v. 22, Geographisches Institut, eidgenossische Technische Hoschule Zurich, 107 p.

Fricker, P.E.
1963: Geology of the Expedition area, western central Axel Heiberg Island, Canadian Arctic Archipelago; Axel Heiberg Island Research Reports, Geology no. 1, McGill University, Montreal, 156 p.

Hodgson, D.A. (coord.)
1989: Le Quaternaire des îles de la Reine-Elizabeth; dans Le Quaternaire du Canada et du Groënland, chapitre 6, sous la direction de R.J. Fulton, Commission géologique du Canada, Géologie du Canada, v. 1, p. 477-514.

Kälin, M.
1971: The active push moraine of the Thompson Glacier, Axel Heiberg Island, Canadian Arctic Archipelago; McGill University, Axel Heiberg Island Research Report, 68 p.

Klassen, R.A.
1982: Glaciotectonic thrust plates, Bylot Island, District of Franklin; Current Research, Part A, Geological Survey of Canada, Paper 82-1A, p. 369-373.

Koerner, R.M.
1989: Glaciers des îles de la Reine-Elizabeth; dans Le Quaternaire du Canada et du Groënland, chap. 6, sous la direction de R.J. Fulton, Commission géologique du Canada, Géologie du Canada, v. 1, p. 500-509.

Lemmen, D.S., Gilbert, R. and Aitken, A.E.
1991: Quaternary investigations in the Expedition Fiord area, west-central Axel Heiberg Island, Northwest Territories; in Current Research, Part B, Geological Survey of Canada, Paper 91-1B, p. 1-7.

Maag, H.
1969: Ice dammed lakes and marginal glacial drainage on Axel Heiberg Island, Canadian Arctic Archipelago; McGill University, Axel Heiberg Island Research Report, 147 p.

Müller, F.
1963: Radiocarbon dates and notes on the climatic and morphological history; in F. Müller et al., Preliminary Report 1961-1962; Axel Heiberg Island Research Reports, McGill University, Montreal, p. 169-172.
1969: Was the Good Friday Glacier on Axel Heiberg Island surging? Canadian Journal of Earth Sciences, v. 6, p. 891-894.

Reynaud, L.
1988: Le glacier d'Argentière, massif du Mont Blanc, France; Publications des Réserves Naturelles de Haute-Savoie, Sallanches (France), 19 p.

Robitaille, B. et Greffard, C.
1962: Notes sur les matériaux terminaux du glacier Thompson, Canada arctique; Geographical Bulletin, no. 17, p. 85-94.

Thorsteinsson, R.
1971: Geology of Strand Fiord, District of Franklin; Geological Survey of Canada, Map 1301A, 1:250 000.

Results of a rock and stream sediment geochemical sampling program in a proposed national park, Bluenose Lake area, District of Mackenzie, N.W.T.[1]

T.A. Jones[2] and C.W. Jefferson
Mineral Resources Division

Jones, T.A. and Jefferson, C.W., 1991: Results of a rock and stream sediment geochemical sampling program in a proposed national park, Bluenose Lake area, District of Mackenzie, N.W.T.; in Current Research, Part E; Geological Survey of Canada, Paper 91-1E, p. 211-221.

Abstract

Rocks and bulk stream sediments were sampled for geochemical analysis in the first stage of a mineral and energy resource assessment (MERA) of a proposed national park in the Bluenose Lake area. Heavy mineral concentrate (HMC) and standard silt fractions were separated from the bulk stream sediment samples for analysis. One diabase sample contained slightly elevated Au and Pd values. Base metal anomalies were found in Proterozoic, Cambrian and Cretaceous shales and sandstones. One 2-3 cm lower Cambrian green shale in friable sandstone reported 831 ppm copper. The lack of strongly anomalous results from stream sediment samples does not preclude the presence of economic mineral deposits because most samples were taken from large, diluted, first-order drainages. Rare-earth and uranium abundances in neutron activation analyses of HMCs are correlated with bulk sample grain size. Studies will continue for summer and fall of 1991.

Résumé

Des roches et des sédiments fluviatiles en vrac ont été échantillonnés à des fins d'analyses géochimiques lors de la première étape d'une évaluation des ressources minérales et énergétiques d'un projet de parc national dans la région du lac Bluenose. Les concentrés de minéraux lourds et les fractions standard de silt ont été séparés des échantillons de sédiments fluviatiles en vrac pour fin d'analyse séparée. Plusieurs anomalies de métaux communs ont été relevées dans des échantillons de schiste argileux et de grès des époques protérozoïque, cambrienne et crétacée. Un schiste vert du Cambrien inférieur de 2 à 3 cm logé dans du grès friable titrait à 831 ppm de cuivre. Aucun résultat anormal n'a été obtenu dans les analyses des silts et des concentrés de minéraux lourds. Les résultats pour le silt n'interdisent pas la présence de concentrations de métaux, parce que la plupart des échantillons ont été prélevés dans de grands bassins de drainage de premier ordre. Les recherches en laboratoire sur les cocentrés de minéraux lourds se poursuivent parce que la préparation des échantillons a posé des difficultés et qu'il faut plus de données minéralogiques pour leur interprétation. D'autres travaux d'échantillonnage de sédiments fluviatiles en vrac et de mise au jour de schistes argileux et de diabases sont prévus pour l'été 1991.

---

[1] Contribution to assessment of various resources of the Bluenose Lake area by Canadian Parks Service. Project carried by the Geological Survey of Canada (GSC), and contracted to the first author.

[2] Cambrian College, Sudbury, Ontario P3E 3V8

INTRODUCTION

The work outlined in this report was performed as part of a two-year MERA of the Bluenose Lake area, N.W.T., for government planning. The area has been proposed by Paulatuk as an addition to the national parks system (Fig. 1). It is the policy of Indian and Northern Affairs Canada to ensure that MERAs of areas in the Yukon and the Northwest Territories be compiled prior to their formal establishment as new national parks. The GSC has traditionally conducted the MERAs at the request of Canadian Parks Service (Jefferson et al., 1988, p.7). The information acquired may be used to modify the boundaries of the proposed park or, in areas of particularly high mineral potential, may suggest that establishment of a park is inappropriate if development of suspected mineral resources is desired.

This MERA follows the format outlined in Jefferson et al. (1988). A description of the 1990 fieldwork and a geological summary is given by Jones et al. (1991). The geological history of the area is summarized in Table 1 and Figures 2 and 3.

DESCRIPTION OF SAMPLING PROGRAM

One or more rock samples were collected at 55 outcrops investigated during the three-week field program (Tables 2,3; Fig. 2). Outcrops were selected in order to provide at least one example of each of the geological formations underlying the area of interest. Sample preparation for rock samples consisted of crushing, milling, and extraction by aqua regia, followed by multi-element inductively coupled plasma analysis. In addition, specific samples considered prospective for gold, platinum group elements, or uranium were analyzed by neutron activation and/or fire assay followed by direct current plasma emission spectroscopy.

A set of bulk stream sediment samples was also collected in the Bluenose area. The area of interest was divided into 25 watersheds, ranging in size from approximately 300 to 3000 km^2. One 5-9 kg sample of <1 cm stream sediment was collected at the downstream apex of each watershed (Table 4, Fig. 3). All sediment samples were taken from active or recently active bars, avoiding bank slump material. Considerable difficulty was experienced in locating sufficient fine (<1 cm) material in many of the streams. No panning or sieving of the samples was performed in the field in the interests of efficient helicopter usage and minimizing operator bias, hence the large sample sizes (for a discussion of possible field preparation stages for heavy mineral concentrates (HMCs), see Spirito et al., 1988, p. 122).

From each bulk sample a silt split and HMC were produced, using the following procedure. All samples were wet-sieved, and divided into +850 μm, 850-180 μm, and -180 μm fractions. A one-third split (ranging from 0.70 to 4.60 g) of the -180 μm fraction was submitted as a standard stream silt sample for geochemical analysis; analysis technique consisted of extraction by aqua regia, and multi-element inductively coupled plasma emission spectroscopy.

For HMCs, preliminary analysis of the Bluenose material indicated that heavy minerals were sparse. The size range processed was therefore made as large as possible to increase the yield of heavy minerals. The 180 to 850 μm fraction was processed on a black-deck concentrating table to remove the light minerals; the table operator purposely included a cut of heavier light minerals to increase HMC size for analytical purposes. This process was followed by magnetic separation of the heavy mineral fraction. A uniform 9 to 10 g split of the non-magnetic HMC was subsequently analyzed for gold plus a standard multi-element package by direct neutron activation.

The sampling and processing procedure outlined above resulted in final HMCs weighing between 15.3 and 63.4 g, derived from original samples of 5.6 to 9.1 kg (see Table 4 for other splits, and selected geochemical results). Assuming that about 70% of the table HMC consists of light minerals, the contained heavy minerals range from 4.6 to 19.0 g; the lower end of this range is marginal for analysis using neutron activation. The amount of -180 μm material present is very small in all samples, and the weight of the 180 to 850 μm fraction is highly variable (Table 4).

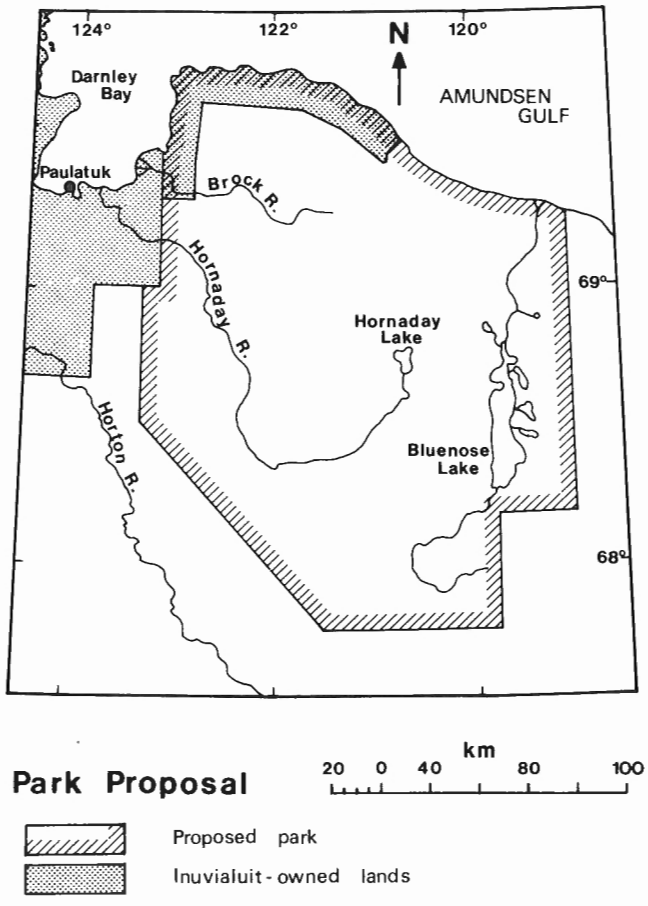

Figure 1. Area of proposed Bluenose Lake national park. Proposed park boundaries may be modified, subject to the results of this MERA, related studies for the Canadian Parks Service, and governmental and public consultations.

Three extra HMCs were produced from small samples (90-JP-49, 95, 101) which were originally collected as stream silts only, from several smaller streams, during geological investigations. These samples were processed using the same techniques as for the bulk stream sediment samples, and produced HMCs suitable for analysis.

RESULTS - ROCK SAMPLES

The rock sample analytical results are difficult to interpret for several reasons. There are too few samples, from too great a diversity of rock types, for statistical analysis to be a useful tool. All samples were analyzed for at least 23 and as many as 27 elements. Finally, we are looking for geochemical indications, possibly quite subtle, of a significant number of possible mineral deposit models (for a listing of models considered, see Jones et al (1991, p.66). For those samples which showed little or no evidence of mineralization, and which did not consist of vein-derived material, the following procedure was followed. As a filtering tool, we have relied largely on a detailed table of the range of mean values for common trace elements as found in 8 major igneous and sedimentary rock types compiled from the geochemical literature by J.H. Reedman (1979, p.99-101). We have taken

Table 1. Table of formations, after Okulitch (1991), and Baragar and Donaldson (1973)

EON	ERA	PERIOD	FORMATION		* SYMBOL	DESCRIPTION
PHANEROZOIC	CENOZOIC	QUATERNARY	[Quaternary alluvium]		TQ s	sand, gravel
			[Quaternary moraine]			
		NEOGENE (TERTIARY)	BEAUFORT FM.		mTN B	sand, gravel
	MESOZOIC	CRETACEOUS	HORTON RIVER FM.		K HR	shale, iron formation
			LANGTON BAY FM.		K LB	sandstone, limestone, shale
	PALEOZOIC	DEVONIAN	HUME FM.		D H	argillaceous limestone, calcareous shale
			BEAR ROCK FM.		D BR	dolomite, carbonate breccia
		ORDOVICIAN	FRANKLIN MOUNTAIN FM. (upper member)		O FM	stromolitic dolomite, chert
			FRANKLIN MOUNTAIN FM. (middle member)		CO FM m	laminated dolomite
		CAMBRIAN	FRANKLIN MOUNTAIN FM. (lower member)		C FM	cyclic laminated dolomite
			SALINE RIVER FM.		C SR	shale, evaporite, siltstone, dolomite
			MOUNT CAP FM.		mC MC	shale, glauconitic sandstone, siltstone
			MOUNT CLARK FM. OLD FORT ISLAND FM.		lC MC, C OFI	conglomerate, quartzite
PROTEROZOIC	HADRYNIAN	NEO-HADRYNIAN	SHALER GROUP	gabbro dykes, sills	H b	gabbro dykes, sills
		PALEO-HADRYNIAN		carbonate, evaporite	H ce	dolomite, limestone, shale, quartzite, chert, gypsum
				carbonate	H c	dolomite, shale, stromolitic limestone
				quartzite	H q	quartzite, sandstone
				carbonate, chert	H ct	dolomite, cherty dolomite
				pelite	H p	shale, siltstone, mudstone
	HELIKIAN	NEO-HELIKIAN	COPPER-MINE RIVER GROUP	COPPER CREEK FM.		plateau basalts, associated dykes and sills

* in the SYMBOL column, the types of contacts are indicated as follows:

———— conformable contact

– – – – – – angular unconformity

..... disconformity

▬▬▬ igneous intrusive contact

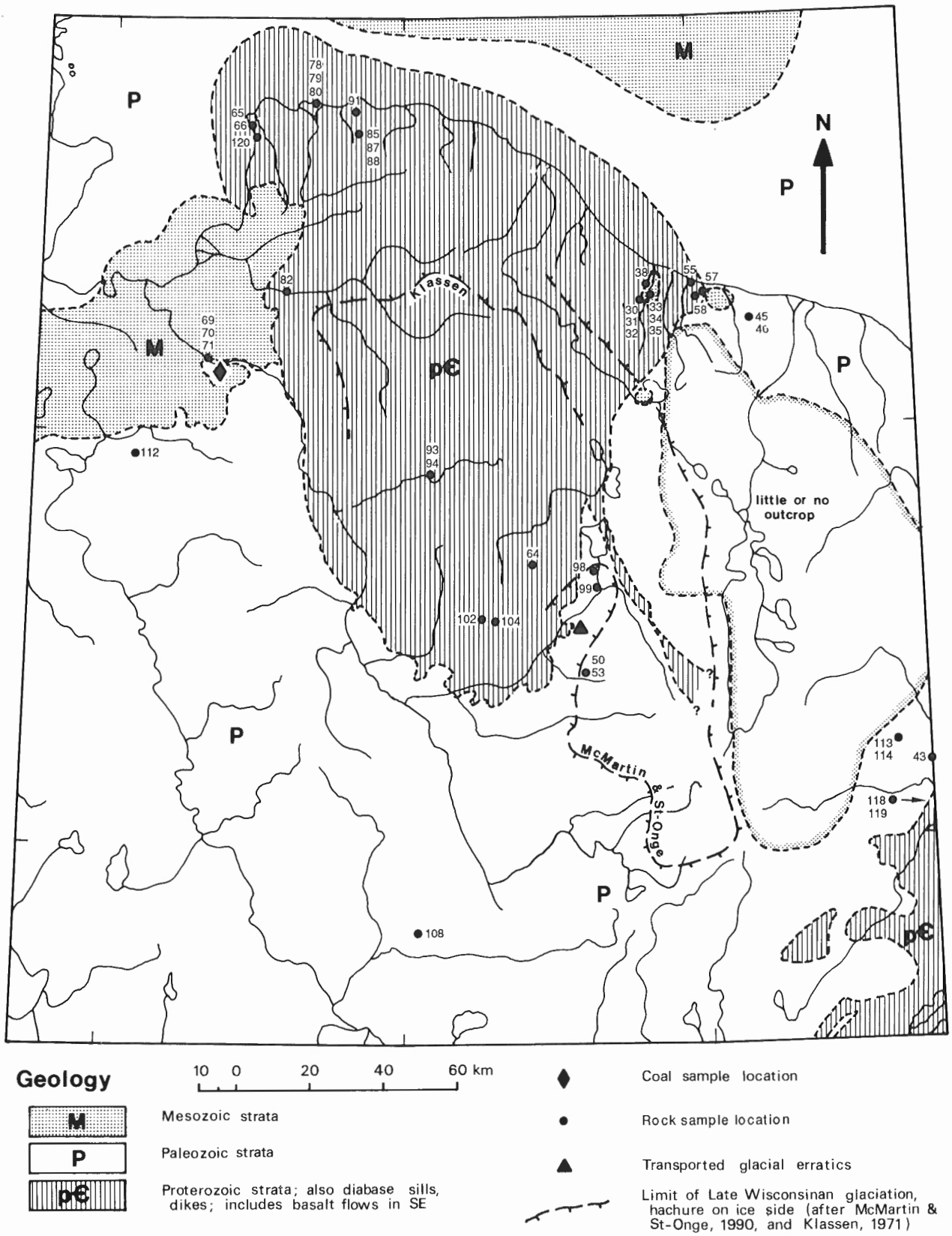

Figure 2. Locations of rock samples, Bluenose Lake resource assessment area. Bedrock geological contacts are after Okulitch (1991) and Fraser et al. (1960). All numbers are part of the sequence 90-JP-33-R to 90-JP-120-R. Elevated results are listed in Tables 2 and 3. The glacial erratics rest on Paleozoic limestone and include Proterozoic diabase and Cambrian conglomerate boulders.

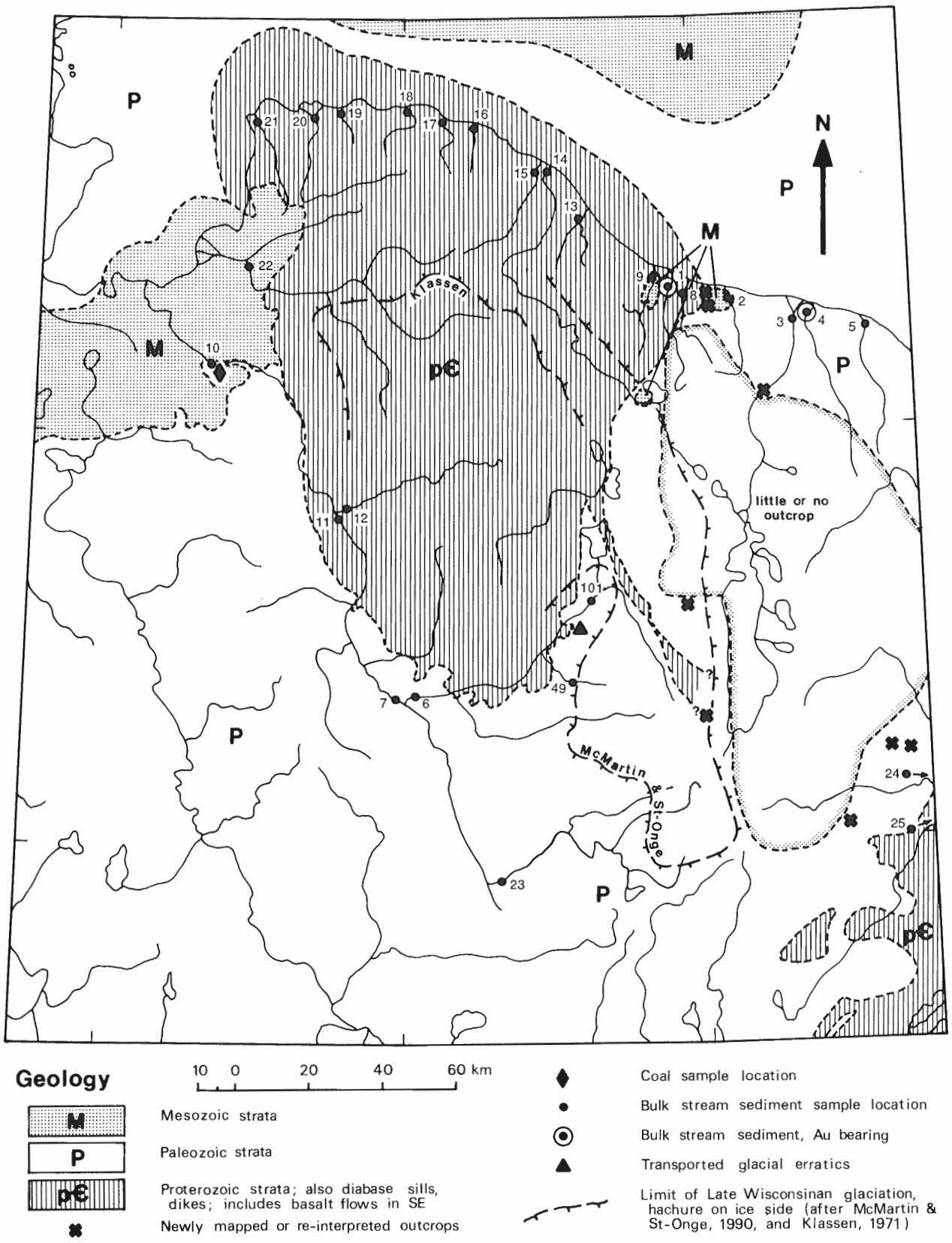

Figure 3. Locations of stream sediment samples, Bluenose Lake resource assessment area. Geology as in Figure 2. All numbers are part of the sequence 90-JP-001-H/S to 90-JP-101-H/S. Selected geochemical analyses of HMCs are shown in Table 4; selected silt analyses are listed in text.

the measured value for selected elements in each sample and compared them with the range of the mean of that element in the appropriate rock type as listed by Reedman. Most samples wherein the measured amount of at least one listed element exceed the mean value or range of mean values for the appropriate rock type are listed in Table 2, along with a description of their geological environment. The elements considered in this simple screening are: Ag, As, Be, Ba, Cr, Co, Cd, Li, Mo, Ni, Pb, Sb, U, V and Zn. Reedman did not report means for Au, Pd, or Pt. Our reported results for these elements are generally quite low, but the highest results are included in Table 2 for information. All diabase samples returned values of 14-25 ppb palladium, 1-10 ppb platinum and 100-200 ppm copper, which we do not consider anomalous.

Some of the samples are listed in Table 2 because the reported values, e.g. arsenic, are slightly above the filter threshold. Those samples in Table 2 which are considered to be anomalous using the above procedure are marked by asterisk and explained as follows.

The moderately elevated Ag-Au-Cu-Li-Pd suite in sample 33 is apparently of magmatic origin, possibly modified by the hydrothermal alteration recorded by pervasive quartz veins transecting the sill. Samples 34 (Pb 181 ppm), 38 (polymetallic), and 48 (Cu 831 ppm) are thought to record transport and precipitation of metals in local reducing environments during diagenesis. Sample 34 is a loose block taken at the foot of a 15-20 m Proterozoic diabase cliff, overlain by about 3 m of shale. Sample 38 is of a limonite-cemented concretion in Cretaceous sandstone. Sample 48 is of a 2-3 cm shale layer in friable Cambrian sandstone which returned background geochemical results.

Sample 69 was taken from a gossanous, friable, Cretaceous sandstone unit about 9-12 m thick and extending hundreds of metres laterally. This unit is exposed in a steep river bank close to an unconformity between the sandstone and underlying Devonian carbonates. This is also within a few metres of overlying coal measures and may represent (1) a burned-out coal bed, or (2) diagenetic concentration of metals in a local reducing environment, related to the unconformity. This is the same site as samples 71R and 72R (Table 3B).

Samples 99 and 112 record weakly elevated Cu and Mo in carbonate hosts; their significance is not understood.

Only rock analyses which belong to one of Reedman's reported lithology types have been evaluated using the above method. Complete results for the remaining samples (mostly vein material, or samples containing abnormal amounts of sulfide) are given in Table 3A. Anomalous values of vein samples are summarized in Table 3B.

RESULTS - STREAM SEDIMENT SAMPLES

The only HMC anomalies are one 300 x 300 μm flake of gold in each of samples 1H and 4H, and samples 7H and 12H which report 140 and 61 ppb gold respectively (Table 4). No pathfinder elements (e.g. arsenic and antimony) are elevated, the bedrock geology is not typical of gold districts, and significant moraines, drumlins and glacial outwash deposits mark the limits of Late Wisconsinan glaciation in the region (Figures 2, 3; McMartin and St-Onge, 1990). The gold is therefore interpreted as glacially transported, its presence in surficial deposits of this area being tentatively explained as caused by the concentrating effects of sustained ice flow to a particular site where glacial moraines and related deposits were built (after personal observations of the first author in the area of Sudbury Ontario, similar observations of auriferous outwash at the Wisconsinan terminal moraine in Ohio by W. Shilts, pers. comm. 1991, and discussions with D. Paré, pers. comm., 1991). Gold anomalies up to 77 000 ppb which were obtained in HMCs from the lower South Nahanni River region might also have a glacial origin (Jefferson and Paré, 1991).

A strong inverse correlation is evident between the proportion (<40%) of the +850 μm fraction of the bulk samples, and elevated neutron activation results for elements such as Zr, La, Ce, Sm, Hf, W, Th and U in HMCs. Table 4 compares the bulk grain-size distributions to analytical results represented by three elements of this suite. Most of the gold analyses are also inversely correlated with the size of the +850 μm fraction, although sample 4H which yielded a gold flake had a large +850 μm fraction.

Two possible explanations for the correlation consider the paucity of heavy minerals in the samples collected (as reported by Consorminex Inc. during sample preparation), and the sensitivity of the neutron activation analytical method to the above suite of elements which characterizes a mature heavy mineral suite, dominated by zircon.

One explanation is that the heavy mineral suites in finer grained fluvial deposits (silt + fine sand) of the Bluenose Lake area may be dominated by mature heavy minerals such as zircon which report high values of rare earths and uranium. Heavy mineral suites in coarser grained fluvial deposits would conversely contain a smaller proportion of mature heavy minerals. The variation in proportion of the coarse fraction (+850 μm) of the bulk sample is logically related to the energy level of the stream. This explanation predicts that zircons would be finer grained, hence their prevalence in lower energy environments (finest grained fractions) whereas orthopyroxenes, garnets and iron oxides would be coarser grained, hence their prevalence in higher energy environments (coarsest grained fractions).

Limited mineralogical data are compatible with the above explanation. Heavy minerals were identified and counted in splits of four HMCs (1H, 4H, 10H and 22H) by the method outlined in Jefferson and Paré (1991). The first two were selected because they yielded one gold flake each; the latter two were selected as representative samples from large, composite drainages. All four HMCs are dominated by orthopyroxene > hematite+goethite > garnet. The orthopyroxenes are thought to be derived from local diabase sills, the garnet represents distal metamorphic shield provenance, and the iron oxides and pyrite represent local gossans and sulphidic rocks. HMC sample 10H contains 43.7 % pyrite. Zircon abundances in the four samples are 0.3%, 0.3%, 7% and 3%

Table 2. Summary of elevated and anomalous geochemical results, representative rock samples

SAMPLE #	FORMATION SYMBOL	MATERIAL SAMPLED	VISIBLE MINERALIZATION	ELEVATED RESULTS (* = considered anomalous)		COMMENTS
90-JP-33-R	H b	diabase dyke + vein	red coating	Ag 0.4 ppm, Au 6 ppb, Cu 273 ppm, Li 17 ppm, Pd 25 ppb[b]		quartz veining with bright red stain
90-JP-34-R	H ce	green mudstone	--	Pb 181 ppm	*	loose block from above dyke 33-R
90-JP-38-R	K LB	sandstone	limonite concretion	Ag 0.5 ppm, As 4.0 ppm, Co 106 ppm, Ni 82 ppm, Zn 56 ppm	*	reduction zone in sandstone ?
90-JP-48-R	lC MC	green shale	--	Cu 831 ppm, U 6.3 ppm	*	2-3 cm shale interlayer in friable ss.
90-JP-53-R	C SR ?	brown carbonate	--	As 5.0 ppm, Be 2.3 ppm[a]		ripple marks
90-JP-54-R	und. Mes.	conglomerate	--	As 8.0 ppm[a]		chert pebble congl., carbonate matrix
90-JP-64-R	H b	olivine diabase	--	Cu 158 ppm, Li 17 ppm, Sb 5.0 ppm[c]		no sulphides; typical diabase
90-JP-65-R	H p	chert nodule	--	Ag 0.6 ppm		nodule in laminated shale, siltstone
90-JP-69-R	unconf. Dev.\Cret.	friable sandstone	large gossan	Ag 0.9 ppm, Ba 498 ppm, Be 1.4 ppm, Pb 48 ppm, Sb 13 ppm, Zn 76.5 ppm	*	altered mat'l, probably Cret. sandstone near unconformable contact, Dev. carb.
90-JP-80-R	H ct	carb. granule congl.	--	Be 2.7 ppm, Co 5.0 ppm		stratigraphically adjacent 79-R
90-JP-82-R	H q	siltstone	biological green	U 10 ppm		adjacent contact units H q and H ct
90-JP-85-R	H b	diabase sill	--	Cu 146 ppm[c]		samples from top to bottom of a single sill
90-JP-87-R	H b	"	--	Cu 176 ppm, Li 15 ppm[b]		
90-JP-88-R	H b	"	--	Au 6 ppb, Cu 175 ppm[b]		
90-JP-89-R	H b	"	--	Li 18 ppm[b]		
90-JP-91-R	H b	diabase dyke	--	Cu 184 ppm, Li 22 ppm[c]		est. 20 m wide
90-JP-93-R	H c	carbonate	--	As 3.0 ppm, Be 2.7 ppm[a]		stromatolitic
90-JP-94-R	H q	quartz arenite	--	As 7.0 ppm		found below carbonate unit
90-JP-98-R	C FM	dolomite	Cu stain ?	As 4.0 ppm, Be 3.3 ppm[a]		finely laminated, re-crystallized
90-JP-99-R	C FM	carbonate	--	Be 2.6 ppm, Cr 12 ppm, Cu 108 ppm	*	mud-cracked, adjacent green shale
90-JP-104-R	mC MC	hematized sandstone	Fe stain	As 5.0 ppm		basal congl. immed. above unconformity
90-JP-108-R	C FM	laminated dolomite	--	As 3.0[a]		inter-layered with green shale
90-JP-112-R	D BR	carbonate	bituminous	As 6.0 ppm, Be 4.1 ppm, Mo 5.0 ppm[a]	*	re'xtallized, oily smell, paleo-Karst ?
90-JP-118-R	?	meta-limestone	--	Be 2.3 ppm, Pb 55 ppm, Pd 3 ppb, Pt <10 ppb, Sb 6.0 ppm		immed. adjacent v. thick diabase sill
90-JP-119-R	?	meta-limestone	--	Be 2.9 ppm, Pd 10 ppb[a]		15 m stratigraphically below 119-R
90-JP-120-R	H b	diabase dyke	--	Cu 198 ppm[b]		coarse grained

[a] range of mean ppm for As, Be reported in Reedman (1979, p.99) for limestone appears to be low (As 2.5 ppm, Be <1-1 ppm)

[b] range of mean ppm for Cu (100 - 150 ppm) reported in Reedman (1979, p.100) for basic igneous rocks is low for Bluenose area diabases

Table 3A. Geochemical analyses of vein and sulphidic rock samples

ELEMENT	METHOD OF ANALYSIS	SAMPLE NUMBER								
		90-JP-030-R	90-JP-031-R	90-JP-032-R	90-JP-035-R	90-JP-043-R	90-JP-046-R	90-JP-066-R	90-JP-071-R	90-JP-072-R
Au (ppb)	FA/DCP	- -	- -	< 1.00	- -	- -	- -	- -	< 1.00	< 1.00
Au (ppb)	DNA	< 5.00	< 5.00	- -	< 5.00	< 5.00	< 5.00	< 5.00	- -	- -
Li (ppm)	ICP	21.00	16.00	22.00	6.00	< 1.00	< 1.00	< 1.00	< 1.00	< 1.00
Be (ppm)	ICP	3.50	3.10	1.40	2.10	3.00	1.60	2.50	< 0.50	< 0.50
B (ppm)	ICP	14.00	21.00	4.00	< 2.00	< 2.00	2.00	< 2.00	6.00	< 2.00
Sc (ppm)	ICP	2.60	3.40	2.40	1.30	< 0.10	< 0.10	1.70	< 0.10	< 0.10
V (ppm)	ICP	35.60	20.90	20.40	15.10	4.00	1.90	< 0.50	< 0.50	< 0.50
Cr (ppm)	ICP	15.00	16.00	12.00	9.00	6.00	7.00	7.00	7.00	6.00
Co (ppm)	ICP	5.00	19.00	14.00	6.00	< 1.00	< 1.00	17.00	2.00	3.00
Ni (ppm)	ICP	13.00	16.00	25.00	5.00	< 1.00	< 1.00	6.00	11.00	6.00
Cu (ppm)	ICP	11.00	82.80	60.10	7.00	4.60	3.20	14.60	4.70	0.70
Zn (ppm)	ICP	22.60	27.10	21.50	17.60	2.00	1.60	27.30	19.50	13.60
As (ppm)	DNA	4.00	18.00	- -	2.00	2.00	< 2.00	7.00	- -	- -
As (ppm)	ICP	< 3.00	10.00	< 3.00	5.00	4.00	< 3.00	9.00	47.00	3.00
Se (ppm)	ICP	< 20.00	< 20.00	< 20.00	< 20.00	< 20.00	< 20.00	< 20.00	< 20.00	< 20.00
Sr (ppm)	ICP	203.00	154.00	106.00	69.40	57.60	26.60	159.00	5.30	17.40
Y (ppm)	ICP	8.40	8.10	25.50	4.80	0.30	< 0.10	20.60	< 0.10	0.10
Zr (ppm)	ICP	13.30	10.70	1.70	6.70	< 0.50	< 0.50	3.50	6.70	2.80
Mo (ppm)	ICP	< 1.00	< 1.00	< 1.00	< 1.00	< 1.00	< 1.00	< 1.00	59.00	3.00
Pd (ppb)	FA/DCPIC	- -	- -	5.00	- -	- -	- -	- -	< 1.00	< 1.00
Ag (ppm)	P	0.20	< 0.10	0.20	< 0.10	< 0.10	< 0.10	0.70	0.40	0.10
Cd (ppm)	ICP	< 1.00	< 1.00	< 1.00	< 1.00	< 1.00	< 1.00	< 1.00	2.00	< 1.00
Sn (ppm)	ICP	< 10.00	10.00	< 10.00	< 10.00	< 10.00	< 10.00	< 10.00	< 10.00	< 10.00
Sb (ppm)	DNA	< 0.50	26.00	- -	< 0.50	< 0.50	< 0.50	1.20	- -	- -
Sb (ppm)	ICP	< 5.00	13.00	< 5.00	< 5.00	< 5.00	< 5.00	< 5.00	7.00	< 5.00
Ba (ppm)	ICP	48.00	25.00	29.00	19.00	4.00	5.00	28.00	27.00	16.00
W (ppm)	DNA	< 2.00	< 2.00	- -	< 2.00	< 2.00	< 2.00	< 2.00	- -	- -
W (ppm)	ICP	< 10.00	< 10.00	< 10.00	< 10.00	< 10.00	< 10.00	< 10.00	< 10.00	< 10.00
Pt (ppb)	FA/DCP	- -	- -	< 10.00	- -	- -	- -	- -	10.00	< 10.00
Pb (ppm)	ICP	< 2.00	84.00	< 2.00	6.00	< 2.00	< 2.00	75.00	28.00	8.00
U (ppm)	DNC	- -	- -	- -	- -	- -	- -	- -	- -	- -

Table 3B. Anomalous vein and sulphidic rock samples

SAMPLE #	HOST FORMATION	MATERIAL SAMPLED	VISIBLE MINERALIZATION	SELECTED ANOMALOUS RESULTS
90-JP-31-R	H ce	fault breccia	--	As 18.0 ppm, Cu 82.8 ppm, Sb 26 ppm, Sn 10 ppm, Sr 154 ppm
90-JP-32-R	H b	quartz vein in diabase	blood red coating	Sr 106.0 ppm, Pd 5.0 ppb, Y 25.5 ppm (see sample 33, Table 2)
90-JP-66-R	H p	fault with secondary carbonate	pyrite ?	Pb 75 ppm, Sr 159 ppm
90-JP-71-R	K LB	marcasite nodule	marcasite	As 47 ppm, Mo 59 ppm, Pt 10 ppb, Sb 7 ppm

Table 4. Comparison of weights of size fractions from bulk stream sediment samples with selected neutron activation analyses of HMCs

SAMPLE NUMBER	BULK STREAM SEDIMENT SAMPLE SPLITS					SELECTED GEOCHEMICAL ANALYSES			
	<180 µm fraction (g)	**>180, <850 µm fraction** (g)	**>850 µm fraction** (g)	**gross weight** (g)	**>850 µm / gross weight** (as %) [<40% = **bold**]	**Au** (ppb) [>5 = **bold**]	**Hf** (ppm) [>200 = **bold**]	**U** (ppm) [>13 = **bold**]	**W** (ppm) [>2 = **bold**]
90-JP-001-H	14.75	7,980.25	505	8500	**5.94**	<5**	14	2.7	<2
90-JP-002-H	4.2	1,370.80	7025	8400	83.63	<5	3	1.0	<2
90-JP-003-H	18.3	4,506.70	4175	8700	47.99	<5	35	4.0	2
90-JP-004-H	4.9	2,445.10	6650	9100	73.08	<5**	4	1.4	<2
90-JP-005-H	14.55	7,460.45	350	7825	**4.47**	<5	170	**14.0**	**5**
90-JP-006-H	6.15	3,243.85	4350	7600	57.24	<5	150	12.0	<2
90-JP-007-H	6.2	4,618.80	2300	6925	**33.21**	**140**	**1530**	**104.0**	**6**
90-JP-008-H	3.2	1,596.80	5200	6800	76.47	<5	<2	0.7	<2
90-JP-009-H	11.7	2,838.30	3975	6825	58.24	<5	44	4.7	<2
90-JP-010-H	12.3	29,887.70	1200	31100	**3.86**	**8**	**237**	**20.0**	<2
90-JP-011-H	10.4	6,614.60	975	7600	**12.83**	**7**	**541**	**37.0**	**3**
90-JP-012-H	13.1	6,986.90	75	7075	**1.06**	**61**	**2010**	**152.0**	**10**
90-JP-013-H	4.5	3,370.50	4800	8175	58.72	<5	7	1.2	<2
90-JP-014-H	8.1	3,391.90	4500	7900	56.96	<5	89	7.8	2
90-JP-015-H	5.55	5,819.45	1250	7075	**17.67**	<5	39	3.9	<2
90-JP-016-H	12.45	7,437.55	25	7475	**0.33**	<5	**457**	**37.0**	**7**
90-JP-017-H	7.5	7,367.50	50	7425	**0.67**	<5	**496**	**35.0**	**3**
90-JP-018-H	10.6	6,939.40	75	7025	**1.07**	<5	**254**	**16.0**	<2
90-JP-019-H	1.8	2,448.20	4700	7150	65.73	<5	8	1.1	<2
90-JP-020-H	8.45	7,866.55	700	8575	**8.16**	**18**	**462**	**46.0**	**<8**
90-JP-021-H	5.1	3,194.90	2475	5675	43.61	<5	10	1.8	**3**
90-JP-022-H	.85	6,074.15	1975	8050	**24.53**	<5	<2	0.9	<2
90-JP-023-H	6.65	1,643.35	6775	8425	80.42	<5	<2	0.6	<2
90-JP-024-H	15.1	2,834.90	5600	8450	66.27	<5	23	3.1	**<6**
90-JP-025-H	6.0	744.00	4900	5650	86.73	<5	3	0.9	<2
90-JP-049-H	3.35	771.65	25	800	**3.13**	<5	<2	0.5	<2
90-JP-095-H	15.4	609.60	275	900	**30.56**	<5	4	2.3	<2
90-JP-101-H	6.45	143.55	650	800	81.25	<5	<2	0.7	<2

** - Single flakes of gold (300 x 300 µ) were removed on the concentrating table before neutron activation analysis.

respectively. The 7% zircon in 10H suggests why it is the only HMC of the four which reported appreciable rare earths and uranium in the neutron activation analyses.

An alternative, or additional explanation for the inverse correlation of the +850 μm fraction with uranium, rare-earths (Hf, etc.) and tungsten is that HMCs made from the coarser samples are systematically diluted by lower density minerals (silicates, carbonates), which mask the geochemical signature of the mature heavy minerals. Some dilution was deliberately introduced during sample preparation, in order to attain uniform HMC size for neutron activation analysis and to ensure that no heavy minerals were lost. This dilution is documented by the methylene iodide separation performed on the four HMCs listed above; the percentage of minerals present with a specific gravity of less than 3.3 is both high and variable (68-85%). We do not have enough data, however, to document any systematic differences in dilution. In order to explain the inverse correlation noted above, this model requires that the degree of dilution would be positively correlated with the percentage of coarse material (+850 μm) present in the original sample, and thus positively correlated with the energy level of the fluvial environments which were sampled.

The hydraulic implications of the dilution model for the sample preparation method used here, and for the stream environments, require further investigation. According to this model, higher energy stream environments would yield lower proportions of heavy minerals from the 180 to 850 μm fraction. Laboratory preparation of the HMCs, using only the concentrating table method, might then systematically dilute the HMCs with light minerals to a greater extent for coarse samples in order to attain uniformity in size of the HMCs.

Further methyl iodide separations, heavy mineral counts, size analysis and neutron activation analyses are planned to investigate this correlation. We are aware that the method of preparing HMCs by sole use of a concentrating table is difficult to apply to regions which yield a small proportion of heavy minerals. The table operator deliberately attempted to incorporate a uniform proportion of light minerals in the HMCs, yet systematic variations in the proportions of heavy versus light minerals in the bulk samples may not have been removed on the table.

We consider that the above correlation is not likely to affect the lack of anomalous values in any other elements; the lack of anomalies in our standard silt samples supports this consideration. Regionally consistent results from HMCs prepared from more than 500 stream-sediment samples, by using only a concentrating table, are reported by Spirito et al. (1988) and Jefferson and Paré (1991).

Silt sample geochemical results for most elements are also uniformly low, supporting the tentative results of the HMC study. Although there were only 28 results available for each element, the Cu, Pb, and Zn values were statistically analysed. All values greater than their respective means (15.3, 7.9, 21.5 ppm) + one standard deviation (21.1, 10.5, 30.2) are listed as follows:

90-JP-001-S	12 ppm Pb
90-JP-002-S	33 ppm Cu (>3 s.d.), 12 ppm Pb
90-JP-004-S	22 ppm Cu
90-JP-013-S	25 ppm Cu, 34 ppm Zn
90-JP-014-S	11 ppm Pb
90-JP-021-S	22 ppm Cu, 11 ppm Pb, 37 ppm Zn
90-JP-024-S	47 ppm Zn (>2 s.d.)
90-JP-025-S	22 ppm Cu
90-JP-095-S	13 ppm Pb.

Only two of the above results exceed 2 standard deviations (26.9, 13.1, 38.8 ppm). The last four also contain greater than 1 standard deviation Fe and Mn, therefore the elevated Cu and Zn abundances may be a result of absorption. Pb, which is commonly transported as galena, may not be tied to Fe and Mn.

The silt results do not indicate the presence of mineral deposits, but neither do they negate the possibility of mineralization for the following reason. The bulk stream-sediment sample sites are too widely separated to fulfil the requirements of even a reconnaissance silt geochemical survey. Undetected anomalies in second- and third-order drainages could readily be diluted to near-uniformity in the first-order drainages sampled. The resources available for this MERA do not permit a comprehensive stream-silt survey over the entire MERA area, however we may sample second- and third-order drainage systems selected on the basis of geological models and available geochemistry in the 1991 field season.

SUMMARY OF RESULTS, PLANNED ADDITIONAL WORK

Slightly elevated Au and Pd values recorded in diabase sample 33-R are interpreted to be a result of igneous processes. Various anomalous base metal abundances in rock samples 34-R, 38-R, 48-R (831 ppm copper), and 69-R appear to represent diagenetic concentrations in local reducing environments, mostly in shales.

Neither silt nor HMC analyses revealed any anomalies. Heavy minerals are sparse in the surficial environment. Correlation between the size of the +850 μm fraction and the abundances of rare-earth elements + uranium + thorium + zirconium +/- gold has two possible explanations. Both explanations could apply; both ultimately relate to the hydraulic conditions of the sample sites:

(1) systematic variations, within the heavy mineral suites, in the proportion of zircon with respect to orthopyroxene + garnet + iron oxides + pyrite;

(2) systematic variations in the proportion of heavy minerals with respect to light minerals incorporated in the HMCs during sample preparation.

Possibility (1) would be a result of hydraulic separation of finer grained mature heavy minerals such as zircon into lower energy environments, and coarser grained pyroxenes, garnets, iron oxides and sulphides into higher energy environments. Possibility (2) would ultimately reflect an inverse correlation between the energy level of the stream environments and the proportion of heavy minerals versus light minerals in the 180 - 850 μm size fraction.

We plan further point counting and neutron activation analysis of HMCs which have been purified in methyl iodide to resolve these possibilities.

For the summer of 1991, we propose limited sampling of diabase dykes and contact zones for gold and precious metals, as well as detailed sampling of Proterozoic, Cambrian and Cretaceous stratigraphic sections of green shale for copper. Selected second- and third-order drainages may be bulk sampled for combined silt and HMC analyses.

ACKNOWLEDGMENTS

Funding was provided by on-going programs (A-base) of Canadian Parks Service and the GSC. Polar Continental Shelf Project provided a helicopter on a cost-recovery basis. The authors benefitted from discussions with F.M. Nixon, D.A. St-Onge, and R.W. Klassen prior to going into the field. A. Insinna provided field assistance, and collected most of the stream samples. Tracy Tindall (Canadian Helicopters pilot) was not averse to getting his feet wet during sample collection. P. Belanger coordinated analysis of all samples. Rock samples were analyzed by X-Ray Assay Laboratories, stream silts and HMCs by Bondar-Clegg. Consorminex Inc. prepared silt splits and HMCs; they also provided methyl iodide separations and mineralogical descriptions of 4 HMCs. W. Shilts and D. Paré critically evaluated the manuscript.

REFERENCES

Baragar, W.R.A. and Donaldson, J.A.
1973: Coppermine and Dismal Lakes map areas; Geological Survey of Canada, Paper 71-39, 20p.+ maps

Fraser, J.A., Craig, B.G., Davison, W.L., Fulton, R.J., Heywood, W.W., and Irvine, T.N.
1960: North Central District of Mackenzie; Geological Survey of Canada, Map 18-1960.

Jefferson, C.W., Scoates, R.F.J., and Smith, D.R.
1988: Evaluation of the regional non-renewable resource potential of Banks and northwestern Victoria Islands, arctic Canada; Geological Survey of Canada, Open File 1695, 63 p.

Jefferson, C.W. and Paré, D.
1991: New placer gold anomalies in the northern Liard Range - southern Ram Plateau area, South Nahanni River region, District of Mackenzie, N.W.T.; in Current Research, Part E; Geological Survey of Canada, Paper 91-1E.

Jones, T.A., Insinna, A., and Jefferson, C.W.
1991: Preliminary report on mineral resource assessment of a proposed national park, Bluenose Lake area, District of Mackenzie; in Current Research, Part C; Geological Survey of Canada, Paper 91-1C, p. 65-70

McMartin, I. and St-Onge, D.A.
1990: Late Wisconsinan deglaciation of the area south of Dolphin and Union Strait, northern District of Mackenzie; in Current Research, Part D; Geological Survey of Canada, Paper 90-1D, p. 55-66.

Okulitch, A.V.
1991: Geology, Horton River, Northwest Territories; Geological Survey of Canada, Geological Atlas, Map NR-9/10/11/12-G, scale 1:1 000 000.

Reedman, J.H.
1979: Techniques in mineral exploration; Applied Science Publishers, London, 533 p.

Spirito, W.A., Jefferson, C.W., and Paré, D.
1988: Comparison of gold, tungsten and zinc in stream silts and heavy mineral concentrates, South Nahanni resource assessment area, District of Mackenzie; in Current Research, Part E; Geological Survey of Canada, Paper 88-1E, p.117-126.

Stewart, R.A.
1986: Routine heavy mineral analysis using a concentrating table; Journal of Sedimentary Petrology, v. 56, p. 555-556.

Observations on massive ground ice on Fosheim Peninsula, Ellesmere Island, Northwest Territories

Wayne H. Pollard[1]
Terrain Sciences Division

Pollard, W.H., 1991: Observations on massive ground ice on Fosheim Peninsula, Ellesmere Island, Northwest Territories; in Current Research, Part E; Geological Survey of Canada, Paper 91-1E, p. 223-231.

Abstract

This report presents preliminary observations on ground ice at three locations on Fosheim Peninsula, Ellesmere Island. Cryostratigraphic characteristics, including ice contents and cryogenic textures, are described for sites located at Eureka, near Blue Man Cape, and at Hot Weather Creek. Exposed sections at all three sites contain icy to ice-rich fine grained sediments overlying massive ice. Gradation in cryogenic texture from fused sediments, to laminated or reticulate ice to massive ice, and the prevalence of gradational contacts between massive ice bodies and overlying sediments suggest that ice segregation during permafrost aggradation could be the primary process in ground ice formation.

Résumé

Le présent rapport contient des observations préliminaires sur des hydrolaccolithes en trois endroits de la péninsule Fosheim dans l'île Ellesmere. Il présente les caractéristiques cryostratigraphiques, notamment les teneurs en glace et les textures cryogéniques, d'endroits situés à Eureka près du cap Blue Man et au ruisseau Hot Weather. Les sections exposées aux trois endroits contiennent des sédiments à grain fin, glacés à riches en glace, reposant sur de la glace massive. La gradation de la texture cryogénique, soit de sédiments fondus à de la glace feuilletée ou réticulée et à de la glace massive, et la dominance des contacts progressifs entre les corps de glace massive et les sédiments sus-jacents indiquent que la ségrégation de la glace pendant l'extension de la zone de pergélisol pourrait être l'agent principal de formation des hydrolaccolithes.

[1] Department of Geography, McGill University, 805 Sherbrooke Street West, Montréal, Quebec H3A 2K6

INTRODUCTION

Ground ice constitutes a significant component of perennially frozen ground. Processes associated with it's aggradation and degradation contribute to the unique geomorphic nature and evolution of periglacial ecosystems. The term ground ice refers to all forms of frozen water beneath the surface of the ground. It is of particular significance in areas underlain by continuous permafrost. Massive ground ice, a large mass of ground ice having a gravimetric ice content >250% (Mackay, 1989, p. 6), is highly thaw sensitive due to the presence of excess ice. In view of recent predictions of warming and increased precipitation for arctic environments in response to global climate change (Schlesinger and Mitchel, 1987; Houghton et al., 1990) and potential terrain instability associated with thawing of massive ground ice and ice-rich permafrost, there is an immediate need for information on the nature and distribution of ground ice for the high Arctic.

Ground ice has been reported in unconsolidated sediments in many parts of the Canadian Arctic (e.g., Lamonthe and St-Onge, 1961; Mackay, 1966, 1971, 1973; French et al., 1982, 1986; Edlund et al., 1989; Egginton and Hodgson, 1990; Pollard, 1990). The main body of detailed research on ground ice origin and physical characteristics, however, has focused on occurrences in the Mackenzie Delta and northern Yukon Territory (e.g., Mackay, 1963, 1973; Pollard and French, 1980; Dallimore and Wolfe, 1988; Pollard and Dallimore, 1988; Harry et al., 1988;). Except for studies by French et al. (1986) and Lorrain and Demeur (1985), there has been little investigation of ice-rich permafrost or massive ground ice in the Canadian High Arctic. Knowledge about the distribution, origin, and nature of massive ground ice and ice-rich sediments is necessary to assess potential impacts of thermokarst in response to natural and anthropogenic disturbance of permafrost. Ground ice studies also provide useful proxy information on arctic paleoclimates and paleogeomorphology and thus may play a valuable role in environmental reconstruction.

This report describes preliminary observations on ground ice at three locations on Fosheim Peninsula, Ellesmere Island (Fig. 1). It is based on fieldwork undertaken in 1990 at the Global Change high arctic observatory established at Hot Weather Creek by Terrain Sciences Division (GSC) in 1988. These observations form the first part of a research program that will be conducted over the next 3 years. This program will systematically investigate ground ice characteristics, assess some of the geomorphic implications of climate warming for terrestrial ecosystems, and compliment other studies focusing on global change in arctic environments (e.g., Woo et al., 1990).

STUDY AREA

Based on field reconnaissance in 1990 and discussions with Dr. D.G. Harry and Dr. S.A. Edlund (Geological Survey of Canada), 7 sites were identified for detailed cryostratigraphic investigation (Fig. 2). All sites have exposures of massive ground ice outcropping in natural sections. In some instances the presence of multiple retrogressive thaw slumps and slump

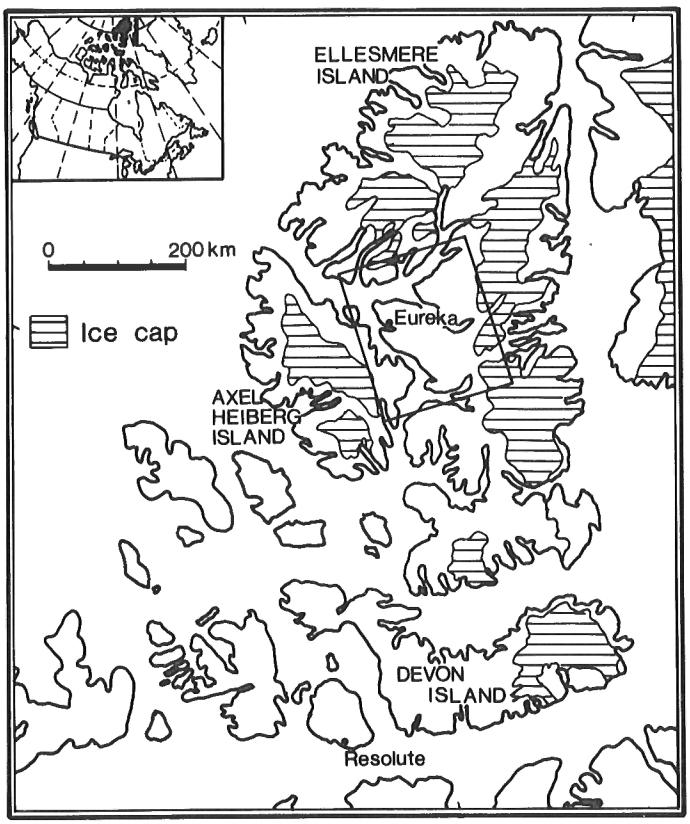

Figure 1. Location Map.

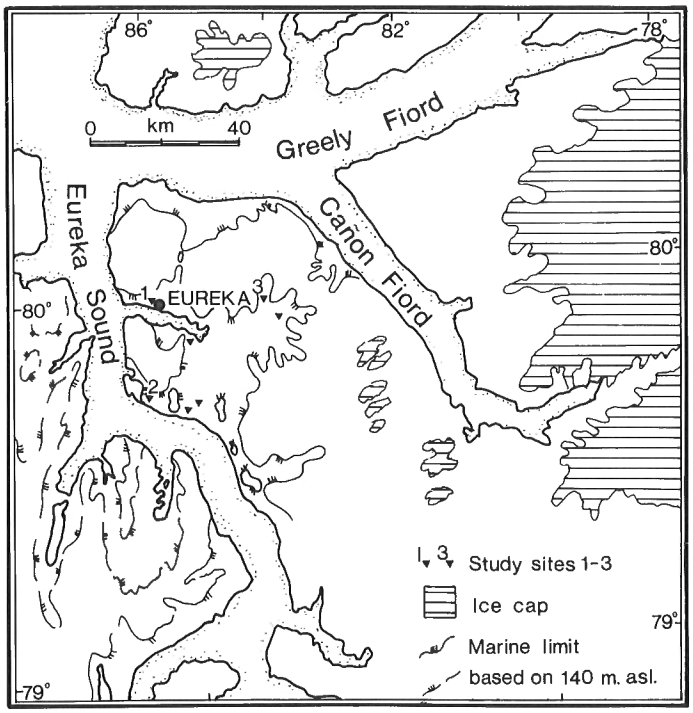

Figure 2. Location of study sites, numbered 1-3 (see text), marine limit after Egginton and Hodgson (1990), and inferred marine limit based upon the 140 m contour. The unnumbered study sites are locations identified for future investigation.

scars suggests that ground ice bodies may be of considerable size or that several ice bodies may exist. The three sites described here lie within a 80-90 km radius of Eureka, which is located on the north side of Slidre Fiord at 79° 59′ N, 85° 55′ W (Fig. 1, 2).

The current focus of this study is the west-central portion of Fosheim Peninsula, western Ellesmere Island and the Gibbs/Mokka Fiords area of western Axel Heiberg Island. This area forms a large rolling lowland surrounded by glacierized mountains rising to elevations of more than 500 m a.s.l. The surface is incised by numerous short river channels. Ice wedge polygons are ubiquitous in areas of sediment cover and active layer detachment scars are also common. The area is underlain by poorly lithified Mesozoic and Cenozoic clastic rocks of the Eureka Sound Group. Outcrops of weathered bedrock are widespread at elevations above marine limit. Fosheim Peninsula lies east of (thus beyond) a glacial drift belt that marks the Late Pleistocene glacial limit (Hodgson, 1985). The Holocene marine limit is placed at an elevation of approximately 140 m a.s.l. (Hodgson 1985; Egginton and Hodgson, 1990). Below this elevation a blanket of fine sediment (containing sandy silt and silty clay) of variable thickness covers much of the surface. These sediments contain whole shells (some valves are articulated) and shell fragments and are thus initially interpreted as marine in origin. Coarse sand and gravel occur in isolated layers as well as raised beach and surface lag deposits. Scattered cobbles and boulders also occur on most surfaces. A fine grained till and diamicton overlying bedrock are described by Hodgson (1985, p. 361) in the northern part of Fosheim Peninsula. The Quaternary history and the extent of Pleistocene glaciation in this area are still poorly understood (Hodgson, 1985) and could have a strong bearing on the interpretation of ground ice origin, in particular its age and the possible preservation of buried ice deposits. Thus, a particular concern of field mapping and section description is the identification of fine till or diamicton units and their association with massive ice.

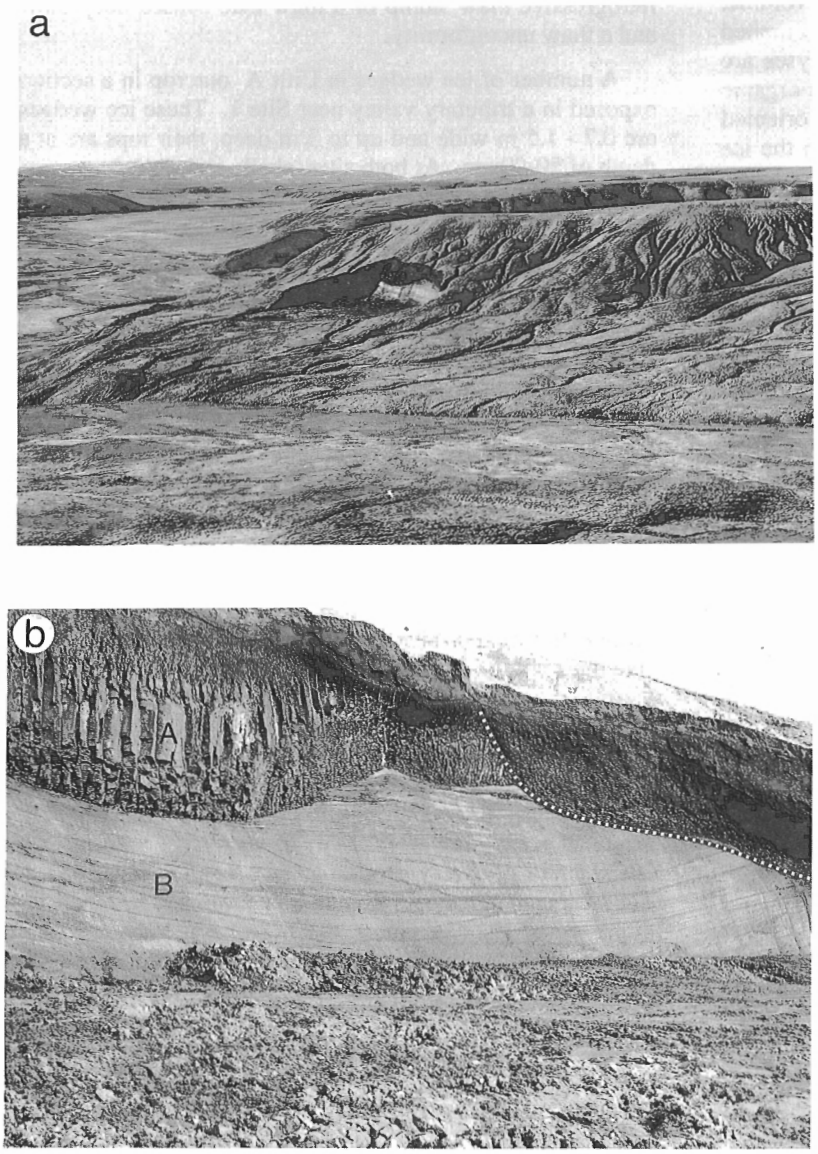

Figure 3. Site 1 at Station Creek: (a) low angle oblique view and (b) the main ground ice section defining Units A and B. The massive ice body is 3 m high. Note the reticulate cryogenic texture and thaw unconformity (dashed line).

The sites described in this report are Site 1, Station Creek near Eureka at 80° 00′ N, 85° 57′ W; Site 2, the north shore of Eureka Sound 8 km east of Blue Man Cape at 79° 44′ N, 85° 57′ W; and Site 3, Hot Weather Creek at 79° 58′ N, 84° 28′ W (Fig. 2, 3, 4, 5). Massive ground ice and ice-rich sediments also occur at the other four locations identified in Figure 2 (79° 42′ N, 83° 30′ W; 79° 43′ N, 85° 22W; 79° 54′ N, 85° 37′ W; and 79° 54′ N, 84° 15′ W).

METHODS

Stratigraphic descriptions are based on 2 or 3 measured sections for each site, in some cases steep unstable exposures limited access to upper parts of the section. Wherever possible the contact relationships between units were documented in detail and particularly between the massive ice and enclosing sediments. In this study only upper contacts of the massive ground ice units are described, bottom contacts are rarely seen in retrogressive thaw slumps. A number of grab samples were taken from each unit for grain size, moisture content, and hydrochemical analyses. In this report ice contents are expressed as a percentage of total sample volume. Measurement of the conductivity, salinity, and pH of melted ice samples was performed on site; all other analyses are being carried out at McGill University. Shell and organic materials were sampled for future analysis. Large oriented block samples of massive ice were excavated from the ice face to document gas and sediment inclusion characteristics. Exposure to direct solar radiation induces intercrystalline melting and the formation of Tyndall figures which allow preliminary observations on crystal texture.

GROUND ICE CHARACTERISTICS

Cryostratigraphy

The ground ice observed in 1990 occurs primarily in marine sandy silt and silty clay deposits and thus far has not been documented in the Eureka Sound Formation or in till. The elevations of the study sites range from 10 to approximately 80 m a.s.l., thus all are below the Holocene marine limit. At Site 2 articulated shells, including *Mya truncata* and *Hiatella arctica* were found in situ within the sediments directly overlying the massive ice.

Massive ground ice bodies exposed at Sites 1 and 2, Station Creek and Blue Man Cape, respectively (Fig. 3b, 4b, c), are similar in appearance and stratigraphic position, but ice at Site 3, Hot weather Creek (Fig. 5b), is distinctly different. At Sites 1 and 2, a layer of fine sediment (Unit A) ranging from 3 to >7 m in thickness overlies massive ice (Unit B) containing horizontally layered white and dark ice interbedded with laminae of icy sediment. In both cases, ice bodies are exposed near the base of steep-sided stream valleys and sediment thickness is estimated from a composite of several sections. Unit A consists of dark brown sandy silt with silty clay and clay layers grading into massive grey clay. The upper 1-1.5 m of this unit (below a 40 cm thick active layer) displays relatively low ice contents, with ice films, pore ice, and thin discontinuous horizontal ice lenses making up less than 15% of the total volume. From roughly 1.5-2.0 m below the ground surface to the top of the ice unit, a distinct reticulate texture is dominant. As illustrated in Figures 3b and 4b, variations in the size and spacing of vertical and horizontal ice veins produces 2-3 textural variations (cryofacies).

In general, the clay-rich sediment blocks between ice veins are free of visible ice and are highly consolidated when thawed. Ice contents within this part of Unit A were roughly 20-22%. The contact between Units A and B is generally abrupt and in most places appears gradational. The latter is inferred from the inclusion of clay fragments from Unit A in the upper 10 cm of the massive ice, the manner in which folia in the massive ice more or less parallel the upper contact, and the absence of fine particles from Unit A in gas inclusions or along intercrystalline boundaries in massive ice immediately below the contact. At both Sites 1 and 2, however, part of the contact that is clearly unconformable (Fig. 3a, 4c): the presence of mudflow deposits lacking a reticulate texture, together with truncation of the primary structures in the massive ice, suggests that a previous thermokarst event, possibly a retrogressive thaw slump or a thaw lake caused deep thaw and a thaw unconformity.

A number of ice wedges in Unit A outcrop in a section exposed in a tributary valley near Site 1. These ice wedges are 0.7 - 1.5 m wide and up to 3 m deep, their tops are at a depth of 80-90 cm. At both sites, shells and shell fragments litter the ground surface and occur in the upper part of Unit A.

Unit B at Sites 1 and 2 is composed of deformed horizontally foliated massive ice. At Site 1 the foliated appearance is produced by alternating layers of dark (clear) and white (bubble-rich) ice together with thin discontinuous clay laminae. The volumetric ice content of Unit B ranges from 98% for samples from the white ice bands to 79% for samples containing dark ice and clay laminae. At Site 2 thicker sediment layers and higher concentrations of suspended sediment result in an ice content drop to 65%. Part of the section at Site 2 displays a complex sequence including a series of faults and a thaw unconformity.

At Site 3, Hot Weather Creek, massive ground ice and icy sediments are exposed in the headwall of a bimodal retrogressive thaw slump, described by Edlund et al. (1989), and in a thermal erosional niche at the base of the stream bank (Fig 5). Both occur on the outside of a large meander loop of Hot Weather Creek which is cutting back into either a former tundra pond or a stabilized retrogressive thaw slump. In June 1990, the east bowl of the slump displayed a 2.8-3.1 m high headwall containing 90-100 cm of sandy silt grading into 20-30 cm of grey clay overlying 1.6-1.9+ m of massive ice. The silty sand unit varies from massive to finely bedded with thin clay bands. In places the bedding is contorted and faulted. Visible pore ice and thin ice lenses occur below the base of the active layer and yield low ice contents (<20-25% by volume). Larger ice lenses are associated with clay bands. The grey clay unit is icy (ice contents ranging from 25-35%), including pore ice, thin discontinuous horizontal ice layers (laminated texture), and zones of reticulate ice veins. The

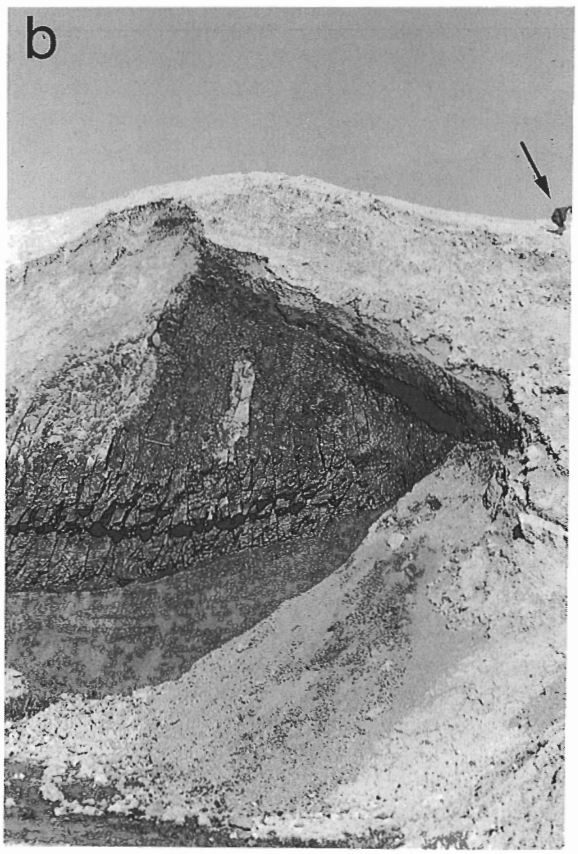

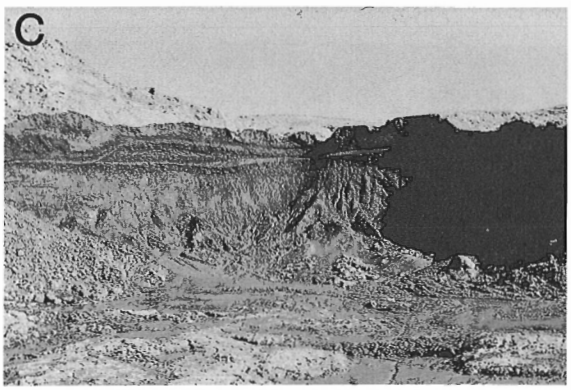

Figure 4. Site 2 east of Blue Man Cape: (a) high level oblique view showing 3 exposures, (b) massive ice body marked "b" in Figure 4a, note person (marked by arrow) for scale, and (c) the headwall of the section marked "c" in Figure 4a.

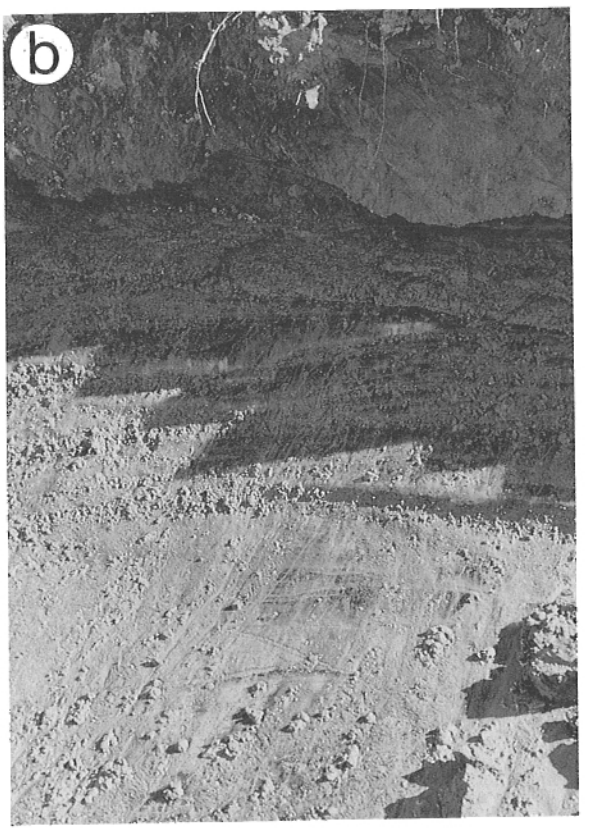

Figure 5. Site 3 at Hot Weather Creek: (a) low level oblique view of the retrogressive thaw slump, note the outline of a former structure marked by a dashed line, (b) massive ice unit exposed in the main bowl of the slump, location marked "b" in Figure 5a, and (c) an oblique section of an ice wedge exposed in stream bank.

massive ice unit consists of horizontal to gently dipping layers of clear ice, 15-30 cm thick, and thin irregular undulating sediment bands. The contact between the massive ice and overlying clay is abrupt and unconformable; it truncates ice/sediment bands and elongated gas bubbles which have a cloudy appearance.

Cryogenic textures

The aggradation or inclusion of ground ice in a stratigraphic sequence results in distinct textures being superimposed on the primary sedimentary structure. The resultant textures reflect (1) the process of permafrost aggradation and moisture redistribution associated with an advancing freezing plane, (2) burial and preservation of surface ice, or (3) various combinations of freezing and thawing of ice-rich sediments. The terms cryotexture or cryogenic texture are used to describe these phenomena (Demek, 1978; Permafrost Subcommittee, 1988). An integrated classification of terms exists in the Soviet literature to describe cryogenic textures; however, in North America the closest equivalent is a descriptive field classification proposed by Pihlainen and Johnston (1963). The following description combines Soviet cryogenic terminology (e.g., Demek, 1978, p. 145) with genetic and descriptive North American ground ice terminology (e.g., Pihlainen and Johnston, 1963; Mackay, 1989; Pollard, 1990). A more complete cryogenic classification which attempts to categorize a wide range of sediment-ice relationships ranging from pure ice with no sediment to an ice-bonded sediment mass with no visible ice is currently in preparation.

At least four distinct cryogenic textures occur in sections on the Fosheim Peninsula: (1) massive ice (including foliated segregated ice and wedge ice), (2) reticulate ice (rectangular and irregular), (3) laminated ice and (4) ice bonded or fused sediment. Massive ice, as defined by the Permafrost Subcommittee (1988), essentially includes all ice bodies with gravimetric ice contents >250% whether regular or irregular in shape. Clearly there are several types of massive ice (e.g., Mackay, 1989; Pollard 1990) and its recognition as a cryogenic texture requires further clarification. Two types of massive ice, foliated segregated and ice wedge ice, were documented. The massive ice bodies at Sites 1 and 2 consist of extensive bodies (vertical exposures up to 4 m high and horizontally continuous for >24 m) of horizontally foliated segregated ice with thin bands and laminae of fine sediment. Bands of white ice contained oval to vertically elongated gas inclusions up to 11 mm long. The layers of white ice are highly variable in thickness and are wavy in appearance. The dark ice contains small randomly spaced gas and sediment inclusions. Gas content is much lower than in the white ice and gas inclusions occur as small circular bubbles. Thin discontinuous sediment laminae and bands up to 25 mm thick contribute to the foliated appearance.

Ice wedges form discrete bodies of massive ice and, depending on wedge orientation and perspective, may generate different textural patterns. Large ice wedges are exposed near Site 1 and Site 3. Ice wedges in normal section are vertically foliated, wedge-shaped bodies of clear (dark) and dirty ice. Ice wedges ranging from 0.7-1.5 m in width and penetrating to depths of 4 m were documented.

Complex patterns of ice veins occur in fine sediments immediately overlying the massive ice bodies, producing a reticulate cryogenic texture. Reticulate ice veins can be subdivided into a hierarchy of primary and secondary veins depending on whether they continue or terminate at points of intersection (Mackay, 1974). As illustrated in Figures 3b and 4b, variations in the size and spacing of vertical and horizontal ice veins produces 2-3 subzones (cryofacies). Vertical and horizontal ice veins up to 3.5 cm wide and 45 cm long occur at Sites 1 and 2 where up to 7 m of silty clay overlies massive ice. Two reticulate textural variations are differentiated: (1) a rectangular reticulate texture with a well developed network of straight primary and secondary ice veins oriented normal and parallel (respectively) to the top of the massive ice and (2) a network of irregular secondary ice veins without an obvious preferred orientation. Initially the texture is poorly developed and is characterized by a primary network of thin straight unevenly spaced vertical ice veins and a weak secondary network of horizontal ice veins. With increasing depth the pattern becomes rectangular where large vertical primary ice veins up to 3.0 cm thick are spaced 14-16 cm apart and smaller horizontal secondary ice veins are up to 50 cm apart. Immediately above the massive ice the pattern of ice veins is irregular and more closely spaced; the distinction between primary and secondary ice veins is not as clear. The rectangular pattern also forms larger cells. As ice veins become progressively larger and sediment blocks occupy lower volumes, reticulate cryogenic textures give way to an ice-sediment breccia, termed a brecciated cryogenic texture. This occurs to a limited extent at Site 1.

Laminated cryogenic textures consist of thin discontinuous to semicontinuous parallel horizontal concordant ice lenses and layers. Variation in freezing rate, material, and soil water conditions will produce several textural variations or cryofacies; for example a gradation from fine ice lenses to larger more closely spaced lenses (lenticular) to rhythmic ice banding may simply reflect subtle fluctuations in this dynamic balance. At Site 3, a lenticular laminated cryogenic texture containing small (1-2 mm thick and 10-12 mm long) wavy ice lenses characterize the 30 cm grey clay layer unconformably overlying massive ice.

Ice bonded or fused textures include Pihlainen and Johnston's (1963) Nb, Nbn, Nbe, Vx, Vc ice types and consist primarily of ice coatings, pore ice, and matrix ice which is commonly so fine that its not readily visible. As a result, ice bonded or fused textures do not have a distinct pattern and often require close examination to identify. Ice bonded textures exist in the upper part of sections at Sites 1 and 2 immediately below the active layer.

DISCUSSION

Ground ice is an important component of unconsolidated materials below marine limit on Fosheim Peninsula. Preliminary observations in 1990 indicate it may have a much wider

distribution than previously documented. Cryostratigraphic analyses suggest that massive segregated ice forms large tabular bodies beneath a thick sequence of marine sediments. The vertical pattern and distribution of cryogenic textures, together with petrographic and inclusion characteristics of ground ice, suggest the following aggradational model. Shortly after emergence, a period of rapid permafrost aggradation froze relatively dry surficial sediments producing a fused or ice bonded cryogenic texture. With increasing depth, freezing proceeded either at a progressively slower rate or continued at the same rate into finer sediments with slightly higher water contents causing shrinkage cracks and formation of primary and secondary ice veins in a reticulate cryogenic texture. The latter implies colder surface temperatures. With greater depth, the rate of advance of the freezing plane slowed allowing moisture to be drawn toward it at a rate that effectively created a balance between water supply and freezing, resulting in the formation of massive segregated ice. Based on data from the Mackenzie Delta-Tuktoyaktuk Peninsula area, it seems highly probable that the massive ice bodies at Fosheim Peninsula are underlain by coarse grained sediments with hydraulic conductivities higher than the fine grained materials overlying the ice. Following permafrost formation, local thaw events associated with retrogressive thaw slumps or tundra pond formation disrupted primary cryogenic textures and in places induced reworking of materials. Ice wedge polygons are common in unconsolidated sediments. Ice wedge formation has also been superimposed on primary cryogenic textures. Clearly this model forms only a working hypothesis and more research is required to either confirm or reject it.

Although massive ground ice was not observed within the Eureka Sound Formation, the tentative identification of retrogressive thaw slumps in weathered bedrock based on airphoto analyses suggests that it should not be ruled out.

Future research

A systematic program of ground ice research will be carried out in this area over the next three years. In year one a detailed reconnaissance of the Fosheim Peninsula and eastern Axel Heiberg Island will map the distribution of natural exposures of ground ice (this will involve airphoto analysis and terrain mapping prior to fieldwork). In each field season detailed cryostratigraphic investigations will be carried out at 3 or 4 different sites. Site investigations involving a series of measured sections and sampling of sediment, ice, and organic materials will be undertaken. General observations on topographic setting, elevation, and surficial geology will be made to add detail to airphoto-based terrain maps. Cryogenic texture, ground ice morphology and appearance, ice content, isotopic and geochemical characteristics, and ice crystallographic analyses (oriented block samples) will form the basis of stratigraphic and paleoenvironmental reconstructions. Laboratory-based analyses of sediment characteristics, ice chemistry, and petrography will be carried out at McGill University during the winter. Shallow drilling will be carried out (using a permafrost coring kit) to assess shallow ground ice distribution and the size and extent of ice wedges. Selection of drill sites will be based on reconnaissance observations from 1991 and 1992. Deep drilling would provide considerable information on materials underlying massive ground ice.

Expected benefits

Research focusing on massive ground ice in Fosheim Peninsula will contribute to a better understanding of permafrost conditions and the environments under which permafrost formed and evolved. In addition, the information collected will contribute to the growing database on ground ice for the Canadian Arctic. It will therefore be useful in the interpretation of current geomorphic processes and landforms (e.g., retrogressive thaw slumps and active layer slides) as well as predicting terrain responses to climate change. Accordingly, the results of this study should also provide useful inputs into other research concerned with the impacts of global change.

ACKNOWLEDGMENTS

Funding for this research was provided by a grant from the Natural Sciences and Engineering Research Council of Canada. Logistical support on Fosheim Peninsula was provided by the Polar Continental Shelf Project (Project 165-87). I would like to acknowledge Dr. Alan Morgan (Terrain Sciences Division and the University of Waterloo) for collaboration in the field and Dr. Sylvia Edlund (Terrain Sciences Division) for helpful comments, suggestions, and hospitality at Hot Weather Creek. I also wish to acknowledge Dr. David Harry (GSC) who initiated this project and generously provided source materials and information on locations of possible study sites. Dr. Sylvia Edlund and Dr. Larry Dyke provided helpful comments on the manuscript. This research will be continued under EMR Research Agreement 227-4-91.

REFERENCES

Dallimore, S.A and Wolfe S.
1988: Massive ground ice associated with glaciofluvial sediments, Richards island, N.W.T., Canada; in Permafrost, Fifth International Conference Proceedings, v.I,, Tapir Publishers, Trondheim, Norway, p. 127-131.

Demek, J.
1978: Periglacial geomorphology: present problems and future prospects; in Geomorphology, (ed.) C. Embelton, D. Brunsden and D. Jones, Oxford University Press, p. 139-153.

Edlund, S.A., Alt, B.T., and Young, K.L.
1989: Interaction of climate, vegetation, and soil hydrology at Hot Weather Creek, Fosheim Peninsula, Ellesmere Island, Northwest Territories; in Current Research Part D; Geological Survey of Canada, Paper 89-1D, p. 125-133.

Egginton, P. and Hodgson, D.
1990: Preliminary assessment of selected drainage basins in western Fosheim Peninsula, Ellesmere Island, as sites for global change studies; in Current Research, Part D; Geological Survey of Canada, Paper 90-1D, p. 71-77.

French, H.M., Bennet, L., and Hayley, D.W.
1986: Ground ice conditions at Rae Point and Sabine Peninsula, Eastern Melville Island; Canadian Journal of Earth Sciences, v. 22, p. 1389-1400.

French, H.M., Harry, D.G., and Clark, M.J.
1982: Ground ice stratigraphy and late Quaternary events, south-west Banks Island, Canadian Arctic; in Proceedings, Fourth Canadian Permafrost Conference, National Research Council of Canada, Ottawa, p. 81-90.

Harry, D.G., French, H.M., and Pollard, W.H.
1988: Massive ground ice and ice-cored terrain near Sabine Point, Yukon Coastal Plain; Canadian Journal of Earth Sciences, v. 25, p. 1846-1856.
Hodgson, D.A.
1985: The last glaciation of west-central Ellesmere Island, Arctic Archipelago, Canada; Canadian Journal of Earth Sciences, v. 22, p. 347-368.
Houghton, J.T., Jenkins, G.J., and Ephraums, J.J.
1990: Climate Change: The IPCC Scientific Assessment; published for the Intergovernmental Panel on Climate Change, Cambridge University Press, Cambridge, 364 p.
Lamonthe, C. and St-Onge, D.
1961: A note on a periglacial erosional process in the Isachsen area, Northwest Territories; Geographical Bulletin, no. 16, p. 104-113.
Lorrain, R.D. and Demeur, P.
1985: Isotopic evidence for relic Pleistocene glacier ice on Victoria Island, Canadian Arctic archipelago; Arctic and Alpine Research, v. 17, p. 89-98.
Mackay, J.R.
1963: The Mackenzie Delta area, N.W.T.; Geographical Branch, Memoir 5, 202 p.
1966: Segregated epigenetic ice and slumps in permafrost, Mackenzie Delta area, N.W.T.; Geographical Bulletin, v. 8, p. 59-80.
1971: The origin of massive icy beds in permafrost, western Arctic, Canada; Canadian Journal of Earth Sciences, v. 8: p. 397-422.
1973: Problems in the origin of massive icy beds, Western Arctic, Canada; in Permafrost: North American Contribution to the Second International Conference, Washington, D.C., National Academy of Sciences, p. 223-228.
1974: Reticulate ice veins in permafrost, Northern Canada: Reply; Canadian Geotechnical Journal, v. 12, p. 163-165.
1989: Massive ice some field criteria for the identification of ice types; in Current Research, Part G; Geological Survey of Canada, Paper 89-1G, p. 5-11.
Permafrost Subcommittee
1988: Glossary of Permafrost and Related Ground-ice Terms; Associate Committee on Geotechnical Research, National Research Council of Canada, Ottawa, 156 p.
Pihlainen, J.A. and Johnston, G.H.
1963: Guide to a field description of permafrost; National Research Council of Canada, Technical Memorandum No. 79, 21 p.
Pollard, W.H.
1990: The nature and origin of ground ice in the Herschel Island area, Yukon Territory; in Permafrost Canada, Proceedings of the Fifth Canadian Permafrost Conference Collection Nordicana, Centre d'étude nordique, Université Laval, p. 23-30.
Pollard, W.H. and Dallimore, S.R.
1988: Petrographic characteristics of massive ground ice, Yukon Coastal Plain, Canada; in Permafrost, Fifth International Conference Proceedings, v. I,, Tapir Publishers, Trondheim, Norway, p. 224-229.
Pollard, W.H. and French, H.M.
1980: A first approximation of the volume of ground ice, Richard Island, Pleistocene Mackenzie delta, NWT; Canadian Geotechnical Journal, v. 17, p. 509-516.
Schlesinger, M.E. and Mitchel, J.F.B.
1987: Climate model simulations of equilibrium climate response to increased carbon dioxide; Review of Geophysics, v. 25, p. 760-798.
Woo, M.K., Young, K.L, and Edlund, S.A.
1990: 1989 observations of soil, vegetation, and microclimate, and effects on slope hydrology, Hot Weather Creek basin, Ellesmere Island, Northwest Territories; in Current Research, Part D; Geological Survey of Canada Paper 90-1D, p. 85-93

Precambrian structure and stratigraphy based on seismic interpretation, Colville Hills region, Northwest Territories: Discussion

Frederick A. Cook[1]

Cook, F.A., 1991: Precambrian structure and stratigraphy based on seismic interpretation, Colville Hills region, Northwest Territories: Discussion; in Current Research, Part E; Geological Survey of Canada, Paper 91-1E, p. 233-238.

INTRODUCTION

Interpretations of seismic reflection data from the Anderson Plains in the Northwest Territories (Fig. 1, 2) have significant implications for the Proterozoic tectonic development of northwestern Canada. The purpose of this Discussion is to elaborate on our views for these data and to present interpretations that differ significantly from those of D.G. Cook and I.R. Mayers (1990) for the same area.

An evaluation is important because the Anderson Plains have few good exposures of features observed on the seismic data, and, therefore, because it is tempting to consider that subsurface data from the area have a multitude of interpretations. An evaluation is also important because the area is not well known, and the large seismic database provides a unique opportunity to image previously unseen Proterozoic structures.

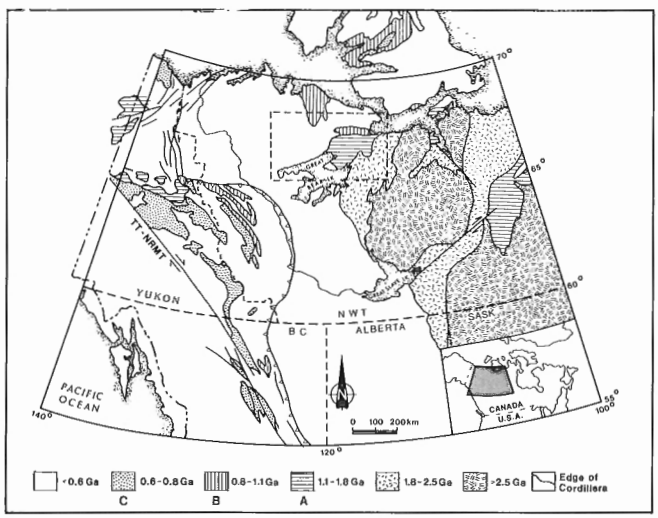

Figure 1. General map of northwestern Canada with the location of Figure 2 outlined.

As additional data are released for the area, it is clear that the potential for mapping these deep Proterozoic structures is perhaps the most outstanding in the world.

However, because most of the structures observed are in the subsurface, the approach that must be taken requires input from a variety of techniques, both geophysical (primarily seismic) and geological. I believe that if standard interpretational techniques are followed, the conclusions will be significantly different from those presented by Cook and Mayers (1990). I begin by addressing the question of data precision in velocity estimation.

DATA PRECISION

Cook and Mayers (1990) used seismic velocity information to attempt to constrain their interpretation. This approach is unlikely to produce any useful information for the existing

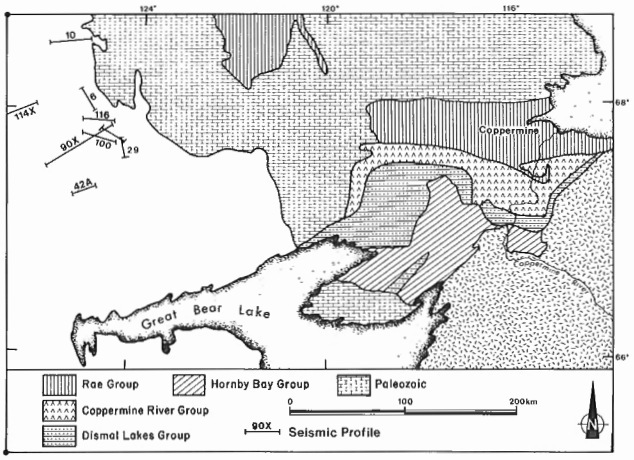

Figure 2. Enlargement of eastern portion of the Anderson Plains and the locations of some of the data discussed in the text.

[1] Department of Geology and Geophysics, University of Calgary, Calgary, Alberta T2N 1N4

data because the source-receiver offsets are far too small to provide sufficient moveout (difference in arrival times for a reflection at different source-receiver offsets) to determine reasonable velocity estimates. Over the maximum offsets utilized in acquiring these data (about 1600 m), the moveout for a reflection at even 1.0 s is insufficient to distinguish between about 5.0 and 7.0 km/s stacking velocity (Sengbush, 1983, p. 5). Even if velocity could be determined from the data, the fact that many different lithologies have identical p-wave velocities (Press, 1966) make this parameter of little use by itself in constraining lithology.

GEOMETRIC AND GEOLOGICAL INFORMATION

The style of faulting

The fundamental structural information provided by seismic reflection data is subsurface geometry. A variety of features on these data led me to interpret layer-parallel thrust faults within the Proterozoic (Cook, 1988a,b). These include:

1. Observations of apparent hanging wall cutoffs,
2. Observations of apparent footwall cutoffs,
3. Observations of apparent repetition of layers with nearly identical seismic character,
4. Observations of apparent duplex geometry, and
5. Observations of possible backthrust structures.

Although Cook and Mayers (1990) claimed not to recognize some of the specific faults that I proposed (Cook, 1988a,b), they showed data (their Fig. 4) that clearly exhibit a geometric cutoff at 3.0-4.0 s between an overlying arched and uplifted sequence (their sequence 1b) and an underlying horizontal sequence (their sequence 1a). I believe this is an outstanding example of a footwall cutoff and that their figure has thus imaged the position of one of the thrust faults (or a strikingly similar one) described in Cook (1988a,b). Cook and Mayers (1990) interpreted these horizontal layers (their sequence 1a) as post-orogenic intrusives.

Contrary to the assertions of Cook and Mayers (1990, p. 346), the horizontal reflections below the cutoff (their sequence 1a) do not cut discordantly across the west dipping panel. Rather, with the exception of some unmigrated time domain reflection data, the deep horizontal reflections always terminate at the dipping panel(s). Many examples are obvious on the data; some of these include lines 42a and G9 (Fig. 6 and 7 of Cook, 1988b), lines 6 (Fig. 3 here), and 90x (Fig. 4a). Even the example that Cook and Mayers (1990) use (their Fig. 4) clearly shows that the sequence 1a reflections terminate at the west dipping ramp. The statements by Cook and Mayers (1990) appear to be in conflict with the observations.

Thin-skin thrusting is clearly compatible with the geometric cutoffs (Cook, 1988a,b; Cook and Mayers, 1990, p. 346) and provides a simple explanation for many of the uplifts such as that seen on the east side of line 114x (Fig. 4 of Cook and Mayers, 1990); they were caused by migration of thrust sheets

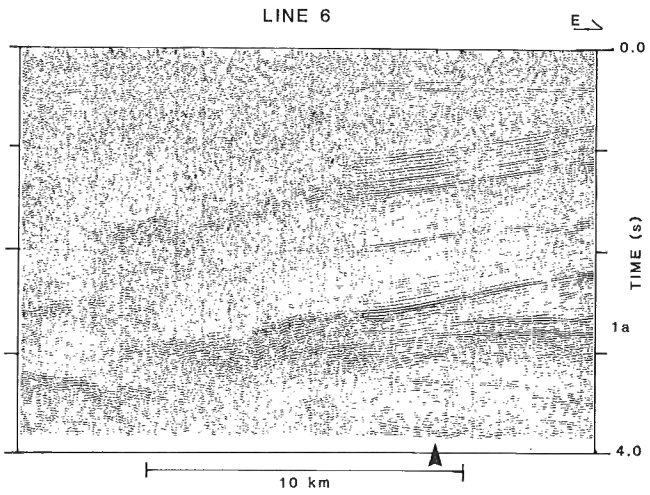

Figure 3. Line 6 (Simpson Lake) imaging cutoffs (at 2.7 to 2.9 s above arrow) of deep layers (1a) with no evidence of crosscutting.

over footwall ramps. An alternative explanation, for example by steeply dipping faults, conflicts with the existing geometries and thus requires a model in which older structures (steep faults?) are completely masked by post-orogenic "intrusives". I believe such an interpretation is internally inconsistent, is not supported by any of the geometric information, and is inconsistent with available geological data. Let us consider each of these difficulties.

The interpretation is internally inconsistent for the following reason

On one hand Cook and Mayers (1990) interpret some seismic reflectors as pre-orogenic stratigraphy and, with no independent verification, interpret some others as post-orogenic intrusives. Such an approach essentially negates most of the constraints imposed by the geometry. For example, if some layers (especially those that exhibit thin-skinned ramp and flat geometry) on the east are interpreted as post-orogenic intrusives, then some or all of the layers observed in the Proterozoic to the west could also be interpreted as post-orogenic intrusives, depending on one's wishes. The use of geometric cutoffs to map faults or unconformities is no longer valid under these circumstances, and any subsequent interpretation that attempts to relate reflections to regional stratigraphy must be questioned.

The interpretation of the deep layering as post-orogenic intrusives is not supported by the geometric information

As I recognized (Cook, 1988a,b) and as noted by Cook and Mayers (1990, p. 346), layer-parallel thrusting is required if these deep layers are pre-orogenic layering. A large quantity, and great variety, of ancillary data lead to the conclusion that these layers are pre-orogenic and that layer-parallel faults with large displacements exist in the area. Some of these observations include:

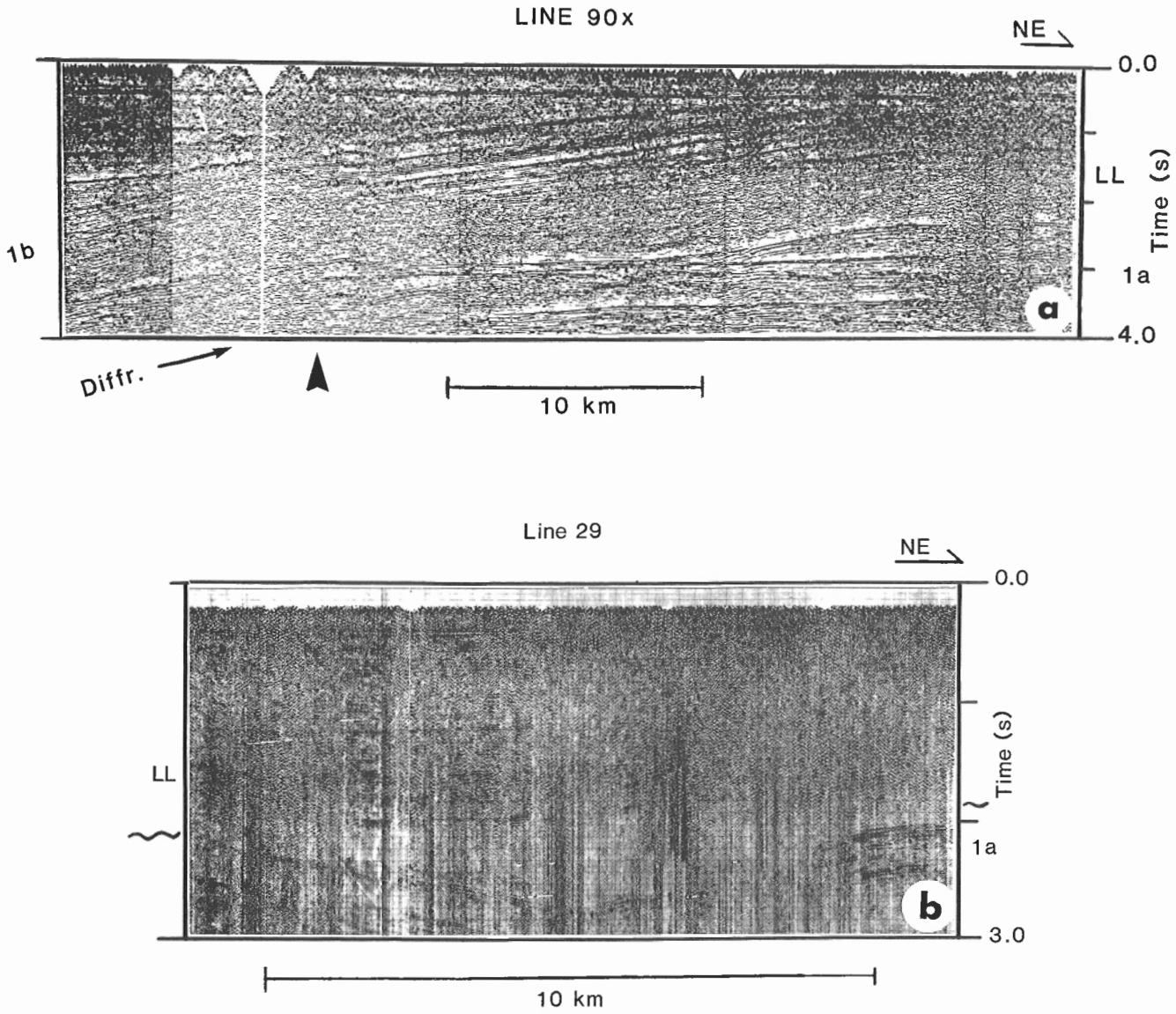

Figure 4. **a**) Line 90x across cutoffs (between 3.0 and 3.6 s above large arrow) of deep layers (1a). Some weak, apparent crosscutting events are diffractions (labeled 'Diffr'). Sequence 1b is seen as a west dipping zone of reflections that truncates sequence 1a, and layers LL are followed eastward where they are situated above deformed layers of sequence 1a. **b**) Line 29 east of 90x illustrates both layers LL and sequence 1a. Along this profile, sequence 1a is deformed and is overlain by LL with angular unconformity (curved line). Thus 1a was deformed prior to the formation of LL, and is therefore not post-orogenic layering.

1. Deformation of the deep layers (sequence 1a of Cook and Mayers, 1990) that shows they are pre-orogenic (layer L in Fig. 4, 5, 6, and 7 of Cook, 1988a).
2. Repetition of layers with nearly identical seismic character (particularly the deep layering; Fig. 4 of Cook, 1988b) indicating repetition of stratigraphy,
3. Apparent hanging wall cutoffs (Fig. 4 and 5 of Cook, 1988a, and Fig. 4 of Cook, 1988b),
4. Apparent footwall cutoffs as discussed above (Fig. 4 of Cook, 1988b)
5. Delineation of piggyback basins based on observations of layers that onlap the dip slope of the uplifts and were then carried and themselves uplifted as deeper faulting occurred (Cook and Clark, 1990). Reconstruction of the piggyback basin geometry shows the faults were subhorizontal (F. Cook and E. Clark, 1990).

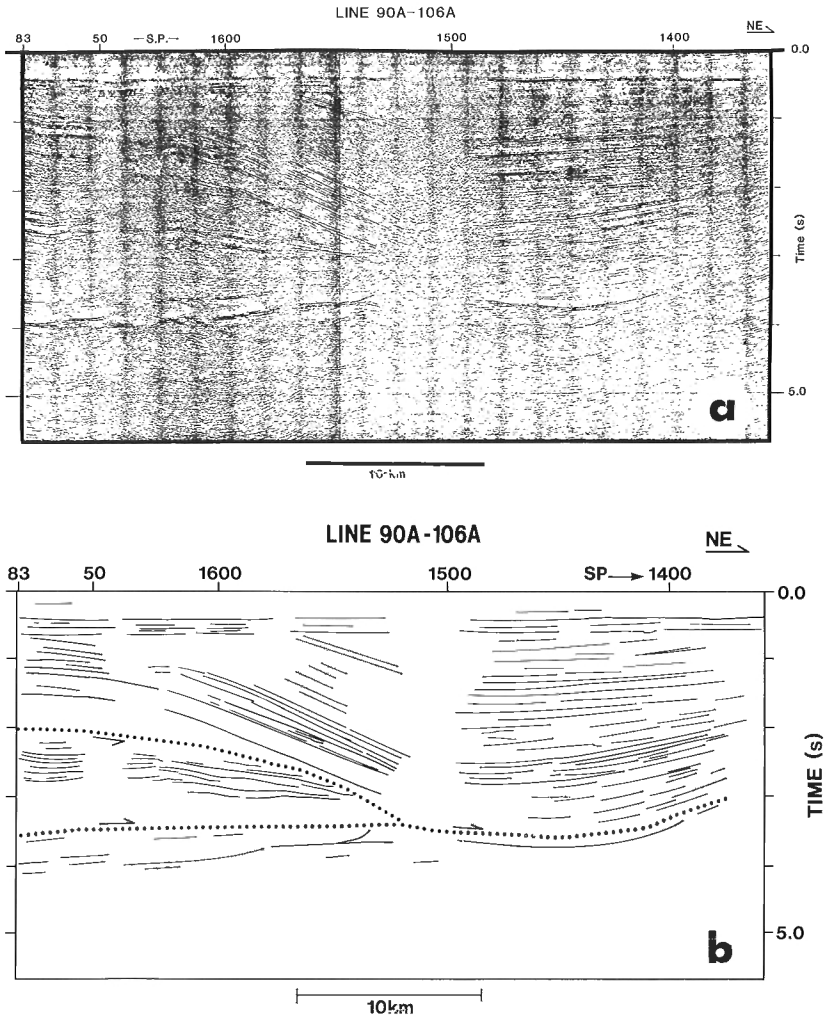

Figure 5. **a**) Line 90A-106A located about 40 km south of line FR-14 (Fig. 2). Note the similarity of the first 3.0 s of this profile to line FR-14 (Cook and Mayers, 1990 their Fig. 3). Data are displayed to 6.0 s showing a nearly continuous, sub-horizontal reflection at about 4.0 s that underlies the east-dipping structure. **b**) An interpretation with a west-verging thrust caused by west-to-east shortening. The vertical band of no reflections around shotpoint 1500 is due to poor data quality; additional parallel profiles establish the continuity of reflections between 2.0 and 3.0 s through this zone.

Indeed, the deep layers (sequence 1a in Fig. 4) can be traced continuously eastward from the point of truncation by overlying west-dipping reflectors (1b in Fig. 4a) to the east where they are deformed and unconformably overlain by intervening layers (LL in Fig. 4). Layers LL are also truncated against 1b on the west. Therefore, sequence 1a was structurally deformed following its formation, was unconformably overlain by LL, and was then truncated against 1b. It is clear that reflectors of sequence 1a are not post-orogenic intrusives.

The interpretation of the deep layers as post-orogenic intrusives is not consistent with geological data

The deep layering (sequence 1a of Cook and Mayers, 1990) is interpreted by them to be intrusive into the Proterozoic Dismal Lakes and Hornby Bay groups. These rocks are exposed within 100 km of the easternmost seismic profile. Two independent geological observations conflict with the interpretation of the deep layers as post-orogenic intrusives:

1. Correlation of a synthetic seismic trace based upon the stratigraphy in the Coppermine Homocline to the reflection data indicates the deep layers are likely the pre-orogenic Dismal Lakes and Hornby Bay group strata, not intrusives (Cook and Taylor, in press), and

2. There is no geological evidence for intrusives of the age (younger than Coppermine volcanics) and stratigraphic position (within the Dismal Lakes and Hornby Bay groups) predicted by the interpretation in Cook and Mayers (1990, p. 346). No sills that are younger than the tilted panel (interpreted to be Coppermine volcanics) have been observed in exposures of the Dismal Lakes and Hornby Bay groups where these rocks are exposed to the east (Kerans et al., 1981; Kerans, 1982; Ross, 1983). No such sills have been observed in wells that likely penetrate the Dismal Lakes and/or Hornby Bay groups (Aitken and Pugh, 1984), and no such sills have been described in exposures of Dismal Lakes and Hornby Bay strata that occur in uplifts near the front of the Cordillera (Aitken and Pugh, 1984; G. M. Ross, pers. comm., 1990). Thus no sills with the appropriate post-Coppermine age are to be expected in the stratigraphic position interpreted by Cook and Mayers(1990).

The interpretation of these layers is critical to a fundamental understanding of the structural style. However, any hypothesis for the structural development of this area must accommodate geometric and geological observations such as those listed above. Even when considered individually, each of these observations provides a clear indication that the deep layering is pre-orogenic; taken together, the evidence is compelling.

The orientation of faulting

Cook and Mayers (1990, their Fig. 3) interpreted a reflection record to image a high angle, west-verging structure. I believe that their assertion (Cook and Mayers, 1990, p. 345) that this fault is incompatible with a regional, thin-skin, east-directed thrust belt (Cook, 1988a,b) is incorrect and misleading in two ways.

First, the structure occurs near the base of the seismic section so that the deep geometry of the fault is impossible to determine. An interpretation with a west-verging, layer-parallel fault that flattens immediately below the limit of the section is just as reasonable as that presented by Cook and Mayers (1990); there is no evidence based on this line alone that the fault must be a deeply penetrating, steep fault. Indeed, about 40 km to the south of line FR-14 a very similar feature illustrates this point (Fig. 5). Here, data were recorded to about 6.0 s, rather than 3.0 s. An interpretation that is nearly identical to that described by Cook and Mayers (1990) could easily be made based upon the first 3.0 s. However, as the additional data to 6.0 s indicate, the structure is underlain by subhorizontal reflections at about 4.0 s that show no expression of the overlying steep dips (Fig. 5). Although alternative interpretations may be possible, a logical interpretation that is consistent with thin-skin thrusting is that the east dipping structure was caused by west-east shortening, perhaps including backthrusting, above a subhorizontal detachment (Fig. 5b).

Second, the west-verging orientation of the structure on line FR-14 has no bearing on compatibility with regional east-directed thin-skinned thrusting. Structures that verge in the opposite direction of regional transport are extremely common at all scales in thrust and fold belts. Some examples from North America include the Appalachian structural front (Gwinn, 1970), triangle zones and backthrusts in the thrust and fold belt in Alberta (Jones, 1982; Price, 1986), the Porcupine Creek anticlinorium in southern British Columbia (Price, 1986), and the suture between accreted terranes and North America in south-central British Columbia (Brown et al., 1986; Price, 1986). Until data are available that establish the deep structure and regional setting of features such as that shown in Figure 3 of Cook and Mayers (1990), their tectonic significance is uncertain.

Stratigraphic interpretation

The stratigraphic interpretation of the seismic layering depends on correlating the reflection sequences with known interfaces. An initial, albeit general, attempt was made by Cook (1988b) based upon reflection character and regional stratigraphy. However, the only available ties were from wells that, with one exception, penetrated to the Proterozoic immediately beneath the Paleozoic and provided some information that the uppermost (probably post-orogenic) Proterozoic layers are part of the Mackenzie Mountains Supergroup and the equivalent Rae Group (Aitken and Pugh, 1984; Cook, 1988a).

One well, the Tweed Lake M-47, penetrated through the basal Mackenzie Mountains Supergroup sedimentary rocks, interpreted in wells near the M-47 (Aitken and Pugh, 1984), into basalt (Cook, 1988b) within or above Cook and Mayers (1990) sequence II. Some or all of their sequence II, therefore, must be older than, or coeval with, the basalt which, in turn, is older than the drilled Mackenzie Mountains Supergroup strata. For these reasons, I interpreted the basalt as part of the Coppermine lavas (Cook, 1988b). This interpretation has recently been supported by geochemical analyses (Sevigny et al., in press). An interpretation of much of sequence II as Mackenzie Mountains Supergroup strata is not consistent with the available stratigraphic, and more recently, geochemical, data.

CONCLUSIONS

The recognition of major, previously unseen, Proterozoic structures beneath the Interior Platform in northwest Canada provides exciting new insight into a poorly understood area. As new data become available and as new techniques are applied, interpretations will be modified and enhanced. However, any interpretation must be within the precision of the data, must honour the available geometric information, and must be consistent with available geological information. Application of standard interpretation techniques shows that reflection stacking velocity information is not useful for constraining subsurface lithology, that reflection geometries are most consistent with pre-orogenic layering and thus thin-skin thrusting, and that drilling data provide important limits on subsurface stratigraphic correlations.

ACKNOWLEDGMENTS

This research is supported by a Research Agreement (No. 90-4-14) from the Department of Energy Mines and Resources.

REFERENCES

Aitken, J. and Pugh, D.
1984: The Fort Norman and Leith Ridge structures: major, buried, Precambrian features underlying Franklin Mountains and Great Bear and Mackenzie plains; Canadian Petroleum Geology, Bulletin, v. 32, p. 139-146.

Brown, R., Journeay, J., Lane, L., Murphy, D., and Rees, C.
1986: Obduction, backfolding, and piggyback basin thrusting in the metamorphic hinterland of the Southern Canadian Cordillera; Journal of Structural Geology, v. 8, p. 255-268.

Cook, D.G. and Mayers, I.R.
1990: Precambrian structure and stratigraphy based on seismic interpretation, Colville Hills region, Northwest Territories; in Current Research, Part C, Geological Survey of Canada, Paper 90-1C, p. 339-348.

Cook, F.
1988a: Proterozoic thin skinned thrust and fold belt beneath the Interior Platform in Northwest Canada; Geological Society of America, Bulletin, v. 100, p. 877-890.
1988b: Middle Proterozoic compressional orogen in northwestern Canada; Journal of Geophysical Research, v. 93, p. 8985-9005.

Cook, F., and Clark, E.
1990: Middle Proterozoic piggyback basin in the subsurface of northwestern Canada; Geology, v. 18, p. 662-664.

Cook, F., and Taylor, G.
in press: Seismic reflection trace synthesized from Proterozoic outcrop and its correlation to seismic profiles in northwestern Canada; Tectonophysics.

Gwinn, V.
1970: Kinematic patterns and estimates of lateral shortening, Valley and Ridge and Great Valley Provinces, Central Appalachians, south-central Pennsylvania; in Studies of Appalachian Geology, Central and Southern, (ed.) G. Fisher, F. Pettijohn, J. Reed, Jr., and K. Weaver; J. Wiley and Sons, p. 127-146.

Jones, P.
1982: Oil and gas beneath east-dipping underthrust faults in the Alberta foothills; in Geologic Studies of the Cordilleran Thrustbelt, (ed.) R. Powers; Rocky Mountain Association of Geologists, v. 1, p. 61-74.

Kerans, C.
1982: Sedimentology and stratigraphy of the Dismal Lakes Group, Northwest Territories; PhD Thesis, Carleton University, Ottawa, 323 p.

Kerans, C., Ross, G., Donaldson, J., and Geldsetzer, H.
1981: The Helikian Hornby Bay and Dismal Lakes groups, District of Mackenzie; in Proterozoic Basins of Canada, (ed.) F.H.A. Campbell; Geological Survey of Canada, Paper 81-10, p. 157-182.

Press, F.
1966: Seismic velocities; in Handbook of Physical Constants, (ed.) S. Clark, Jr.; Geological Society of America, Memoir 97, p.195-218.

Price, R.
1986: The southeastern Canadian Cordillera: thrust faulting, tectonic wedging, and delamination of the lithosphere; Journal of Structural Geology, v. 8, p. 239-254.

Ross, G.
1983: Geology and depositional history of the Hornby Bay Group, Northwest Territories, Canada; PhD Thesis, Carleton University, Ottawa, 326 p.

Sengbush, R.
1983: Seismic Exploration Methods; International Human Resources Development Corporation, Boston, 296 p.

Sevigny, J., Cook, F., and Clark, E.
in press: Geochemical signature and seismic stratigraphic setting of Coppermine basalts drilled beneath the Anderson Plains in northwest Canada; Canadian Journal of Earth Sciences.

Precambrian structure and stratigraphy based on seismic interpretation, Colville Hills region, Northwest Territories: Reply

Donald. G. Cook and I. Richard Mayers[1]
Institute of Sedimentary and Petroleum Geology, Calgary

Cook, D.G. and Mayers, I.R., 1991: Precambrian structure and stratigraphy based on seismic interpretation, Colville Hills region, Northwest Territories: Reply; in Current Research, Part E; Geological Survey of Canada, Paper 91-1E, p. 239-241.

Instead of working through an item by item, detailed reply to F.A. Cook's Discussion of our work on the Colville Hills region (Cook and Mayers, 1990a), we offer a few general comments. Cook's Discussion falls in five areas which, in order of increasing importance, are:

a) The use of processing velocities to calculate P-wave velocities, and his implication that we use those velocities "for constraining subsurface lithology",

b) Our suggestion that a pair of deep parallel reflections might represent intrusive sheets,

c) Stratigraphic correlations,

d) Westward versus eastward thrusting, and

e) Our interpretation that bedding plane thrust-faults previously interpreted by him do not exist.

(a) Velocities

We are puzzled by his suggestion that we used velocity data to constrain our lithological interpretation. We calculated Dix interval velocities, presented them for information in Figure 5, and used them to calculate approximate stratigraphic thicknesses and depth conversions, but we made little or no use of them to infer lithologies. We noted (Cook and Mayers, 1990a, p. 343) that seismic processing velocities at times greater than 2.5 s are often unreliable.

F.A. Cook's discussion of source-receiver offsets, moveouts etc., seems to serve little purpose other than to obfuscate the real issue, which is the degree to which strata in the region are repeated on low-angle thrust faults.

(b) Intrusive sheets

In our preliminary work we were impressed by the remarkable parallelism of two deep reflections and the manner in which they seem to terminate abruptly westward. Because we do not see them repeated in overlying reflections, and do not see hangingwall geometries requisite to a thrust interpretation, we reject F.A. Cook's suggestion that the abrupt terminations represent footwall cutoffs. We offered an alternative suggestion that the parallel reflections might represent intrusive sheets or sills. Further work, however, (D. G. Cook and B. C. MacLean, unpublished results) shows them to be part of a stratigraphic sequence, and we no longer believe that they represent sills. Nonetheless, for reasons outlined below we still reject the westward terminations as representing footwall cut-offs, and we retract our statement "The lower of his two thrusts is required if a set of sub-horizontal reflections, here considered to represent intrusive sheets, in fact represent stratigraphic layering" (Cook and Mayers 1990a, p.346)

(c) Stratigraphy

Our tentative correlations were broadly similar to those suggested by F. A. Cook (1988a) with important differences regarding the upper part of the sequence and the placement of the "sub-Rae Group" unconformity. Those correlations are currently being overhauled in line with alternatives suggested by D.G. Cook and Mayers (1990b). Our current stratigraphic rationale (Cook and MacLean, 1990; MacLean and Cook, 1990) relies heavily on the correlation (Sevigny et al., 1991) of basalts drilled in the Tweed Lake area with the exposed Coppermine basalts. We differ significantly with F.A. Cook and associates, in that we see the basalts as the youngest Proterozoic strata

[1]Geophysical Consultant, 2216 Longridge Drive S.W., Calgary, Alberta T3E 5N6

over most of the area. Precambrian rocks penetrated by wells northward of Tweed Lake were assigned by Aitken and Pugh (1984) to Mackenzie Mountains Supergroup (MMS). In our interpretation, however, these wells penetrate strata older than Tweed Lake basalts. F.A. Cook, on the other hand, sees MMS strata overlying the basalts, and endorses the Aitken and Pugh assignments. A key well is Tweed Lake M-47, wherein F.A. Cook and Coflin (1990, p. 312), and Sevigny et al. (1991, p. 185-189) attributed the presence of MMS units to Aitken and Pugh (1984). These authors need some other reference because the well was not spudded until 1985. Moreover, examination of the well cuttings reveals that basal Cambrian sandstone directly overlies basalt.

Because well control for the Proterozoic is minimal, and the publicly available seismic control does not reach Proterozoic outcrop, stratigraphic concepts will continue to evolve. In the meantime, the resolution of the presence or absence of layer-parallel faults is dependant on interpreting the continuity of stratigraphic units, geometric relationships among units, and the seismic character of the sequences themselves, and is independant of what those sequences are named.

(d) Westward vs eastward thrusting

We (Cook and Mayers, 1990a) do know that asymmetric thrust systems can include back-thrusts with the opposite sense of transport to the norm, and acknowledged (p. 346) "that the large reverse fault interpreted in Figure 3 could, no doubt, be accommodated in a primarily eastward-directed kinematic system". We nonetheless stand by our assertion (p. 345) that a westward-directed, intra-cratonic crustal-scale block-uplift appears to be incompatible with the thin-skinned eastward directed thrust belt conceived by F.A. Cook. Further elaboration seemed unnecessary considering that, in our view, the thrust belt does not exist.

(e) Layer-parallel thrust faults

Our summary interpretation (Cook and Mayers, 1990a) was based on the examination of regional cross-sections which have since been presented in Cook and Mayers (1990b). F.A. Cook's Figure 4 (Cook, 1988a) is based on Petro-Canada Line 120A, a line that appears at the eastern end of our transect B2-B' (Cook and Mayers, 1990b, Fig. 5). It is fascinating that the same data have resulted in two irreconcilably different interpretations. In F.A. Cook's (1988a) interpretation, a seismic unit, repeated on two bedding-parallel thrust-faults, appears three times in vertical succession; in our interpretation the three "repeats" are part of a stratigraphic sequence, punctuated by regional unconformities, that has been subjected to regional tilting and erosional truncation. Thrust-faults are present, but are minor relative to those envisioned by F.A. Cook. The following comparisons are best understood if the reader has two references in hand (F.A. Cook, 1988a, Fig 4; and D.G. Cook and Mayers, 1990b, Fig. 5). For comparison purposes, note that our marker A corresponds to a strong reflection in the middle of his sequence M, and our marker B occurs at or near the base of his sequence U. We outline the fundamental differences in the two interpretations below:

1. Despite F.A. Cook's assurances, we find little similarity in the seismic character of his U, M, and L (upper, middle and lower) layered reflection sequences. Moreover, the upper boundary of his M sequence is not, in our view, geologically significant; on Lines 120 and 116 (Fig. 4, 5) he has picked the top of a white band which, in our opinion, is a processing artifact, caused by automatic gain control (AGC) in response to the very strong reflection which occurs in the middle of his sequence M; on Lines 104 and 100 (Fig. 6, 7) he has picked the contact at a higher level, but not at any distinctive reflection. Because we see inconsistencies, and in particular we believe F.A. Cook, on some lines, has misinterpreted a processing artifact to be a geologically significant contact, we reject the possibility that his sequence M is a repeat of his sequence L, and that his sequence U is a repeat of his sequence M. In 2 recent papers (F.A. Cook, 1991a, Fig. 3; 1991b, Fig. 4a) F.A. Cook appears to have recognized a problem, because in his interpretation of line 90-X, which intersects lines 104 and 100 noted above, he has no middle sequence, and only one thrust. Direct comparisons can be made of those interpretations of a segment of line 90-X and our interpretation of the full line (Cook and Mayers, 1990b, Fig. 7).
2. We have examined upwards of 4000 line kilometres of data, and find that the reflections comprising F.A. Cook's sequence U (reflection band above our marker B), and the strong reflection in the middle of his sequence M, (our reflection A) are regionally continuous. Although each of these elements is locally broken by thrust faults, there is no possibility that one can be a thrust-repeat of a package containing the other.

SUMMARY COMMENTS

The fundamental difference between our interpretation and that of F.A. Cook is that he sees significant regional horizontal shortening amounting to 50 to 90 km (F. A. Cook, 1988b) and more recently 150 to 200 km (Clark and Cook, 1990), whereas we see much more moderate shortening of an intracratonic nature (Cook and Mayers, 1990b; MacLean and Cook, 1990). Resolution of this discrepancy will have profound significance for our understanding of Proterozoic history of northwestern Canada. Because we and F.A. Cook have both published uninterpreted data with the interpreted, readers are invited to compare interpreted sections with the raw data and form their own opinions.

We do not claim that we fully understand the stratigraphic and structural relationships of this region, and our understanding will certainly continue to evolve. Nonetheless we have developed a regionally consistent rationale which we are confident is more viable than are the various spot solutions offered by F.A. Cook and his associates.

REFERENCES

Aitken, J.D. and Pugh, D.C.
1984: The Fort Norman and Leith Ridge structures: major, buried, Precambrian features underlying Franklin Mountains and Great Bear and Mackenzie Plains; Bulletin of Canadian Petroleum Geology, v. 32, no. 2 , p. 139-146.

Clark, E.A. and Cook, F.A.,
1990: Cross section across a Proterozoic compressional orogen in the Anderson Plains, Northwest Territories (abstract); G.A.C./M.A.C. Program with Abstracts, Vol. 15.

Cook, D.G., MacLean, B.C.
1990: Three phases of reactivation of an earlier fault; two compressional, one extensional (abstract); Geological Society of America, 1990 Annual Meeting, Abstracts with Programs.

Cook, D.G. and Mayers, I.R.
1990a: Precambrian structure and stratigraphy based on seismic interpretation, Colville Hills region, Northwest Territories; in Current Research, Part C, Geological Survey of Canada, Paper 90-1C, p. 339-348.
1990b: Reflection seismic interpretation of the Proterozoic Geology, Colville Hills Region, Northwest Territories; Geological Survey of Canada, Open File 2254, 25 p., plus figures.

Cook, F.A.
1988a: Proterozoic thin-skinned thrust and fold belt beneath the Interior Platform in northwest Canada; Geological Society of America Bulletin, v. 100, p. 877-890.
1988b: Middle Proterozoic compressional orogen in Northwestern Canada; Journal of Geophysical Research, v. 93, p. 8985-9005.
1991a: Was the Coppermine Homocline of northwestern Canada uplifted as part of a middle Proterozoic forebulge; Geophysical Research Letters, v. 18, p. 101-104.
1991b: Precambrian structure and stratigraphy based on seismic interpretation, Colville Hills region, Northwest Territories: Discussion; in Current Research, Part E, Geological Survey of Canada, Paper 91-1E.

Cook, F.A. and Coflin, K.C.
1990: Reactivation tectonics in the Arctic of western Canada; Marine Geology, v. 93, p. 303-316.

MacLean, B.C. and Cook, D.G.
1990: Reflection seismic interpretation of two cross-sections in the Colville Hills region, Northwest Territories Canada (abstract); Geological Society of America, 1990 Annual Meeting, Abstracts with Programs.

Sevigny, J.H., Cook F.A., and Clark, E.A.
1991: Geochemical signature and seismic stratigraphic setting of Coppermine basalts drilled beneath the Anderson Plains in northwest Canada; Canadian Journal of Earth Sciences, v. 28, p. 184-194.

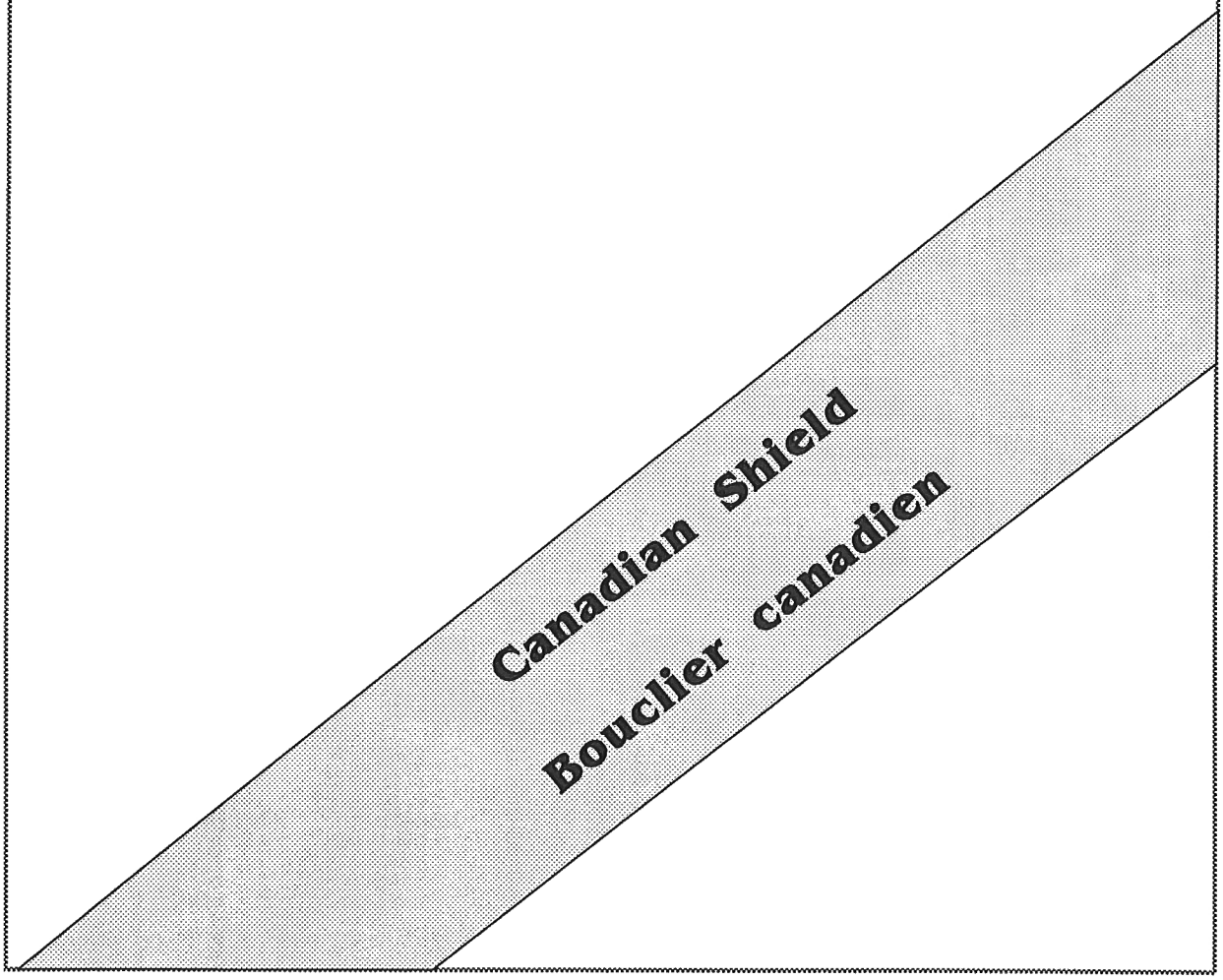
Canadian Shield
Bouclier canadien

Preliminary notes on the geology of the St. Maurice tectonic zone, Grenville orogen, Quebec

L. Nadeau and D. Corrigan[1]
Quebec Geoscience Centre, Sainte-Foy

Nadeau, L. and Corrigan, D., 1991: Preliminary notes on the geology of the St. Maurice tectonic zone, Grenville orogen, Quebec; in Current Research, Part E; Geological Survey of Canada, Paper 91-1E, p. 245-255.

Abstract

The Grenville orogen in the Portneuf-St. Maurice region comprises three contrasting lithotectonic entities; from west to east 1) the Mékinac domain, underlain by granulite-facies migmatitic granodioritic gneiss, a possible extension of the Allochthonous Monocyclic Belt to the west; 2) the St. Maurice tectonic zone, an easterly-dipping mid- to deep crustal anastomosing shear zone which comprises a variety of lithologies, including rocks of supracrustal and plutonic origin; and 3) the Laurentides Park plutonic complex, which is part of the Allochthonous Polycyclic Belt.

A steeply-dipping shear zone with a sinistral shear-component marks the east margin of the St. Maurice tectonic zone. Farther west, dips become shallower and the shear zone projects above Mékinac domain in the west. Current tectonic model for the Grenville orogen in southwestern Quebec shows the Allochthonous Monocyclic Belt to be overthrust onto the Allochthonous Polycyclic Belt. Our observations show that this model cannot be extended to the St. Maurice tectonic zone.

Résumé

Dans la région de Portneuf-Saint-Maurice, l'orogène de Grenville comprend trois entités lithotectoniques contrastantes. Ce sont, de l'ouest vers l'est 1) le domaine de Mékinac, dont le sous-sol est composé de gneiss migmatitiques granodioritiques, qui représente possiblement le prolongement de la zone monocyclique allochtone à l'ouest; 2) la zone tectonique du Saint-Maurice, une zone de cisaillement anastomosée à pendage est, développée dans le niveau crustal moyen à profond, et comprenant une variété de lithologies d'origine supracrustale et plutonique; et 3) le complexe du parc des Laurentides, qui fait partie de la zone polycyclique allochtone.

Une zone de cisaillement senestre sub-horizontal à pendage fort marque la marge est de la zone tectonique du Saint-Maurice. Vers l'ouest, les pendages de direction est deviennent progressivement plus faibles et la zone de cisaillement surplombe le domaine de Mékinac. Le modèle le plus récent de l'évolution tectonique de l'orogène de Grenville montre la zone allochtone monocyclique chevauchant la zone allochtone polycyclique. Nos observations montrent que ce modèle ne peut être étendu à la zone tectonique du Saint-Maurice.

[1] Department of Earth Sciences, Carleton University and Ottawa-Carleton Geoscience Centre, Ottawa, Ontario K1S 5B6

INTRODUCTION

Current tectonic models for the Grenville orogen in central Quebec postulate the presence of regionally extensive structures. These models are based on the distribution of lithotectonic packages. While two sutures between three continental blocks, Proto-Laurentia, Grenvillia, and Quebecia, are suggested by Rondot (1978, 1986; Fig. 1) to be located in the Portneuf-St. Maurice region, Rivers et al. (1989) describe this area as forming the eastern margin of the Allochthonous Monocyclic Belt (Fig. 2). Rondot's model for a collisional suture between Grenvillia and Quebecia hinges on the interpretation that metasedimentary rocks of the Montauban group were deposited in a rift environment and that the La Bostonnais complex is a relict ophiolite. In southeastern Ontario and western Quebec, the Allochthonous Monocyclic Belt has been thrust to the northwest onto the Allochthonous Polycyclic Belt (Culshaw et al., 1983; Hanmer and Ciesielski, 1984; Hanmer, 1988; McEachern, 1990; S. Hanmer and S. McEachern, pers. comm., 1991). Extension of this thrust event to the eastern margin of the Allochthonous Monocyclic Belt would require the occurrence of a west-dipping shear zone in the St. Maurice region. However we here recognize a major east-dipping mid- to deep crustal shear zone, hereafter called the St. Maurice tectonic zone, which possibly represents a major tectonic feature of the Grenville orogen in central Quebec. This paper reports on eight weeks of regional mapping of the St. Maurice tectonic zone and is intended as a summary of our preliminary observations. We highlight some of the structural, metamorphic and chronological elements which any successful tectonic model for the Grenville orogen in central Quebec must satisfy.

PREVIOUS STUDIES AND PROJECT SCOPE

Previous geological mapping in the Portneuf-St. Maurice region includes early 1:63 360 scale mapping by Tiphane (1954), Klugman (1956, 1963), Newman (1973), Pyke (1967), Rondot (1976a, b, c) and the regional synthesis by Rondot (1978) at a scale 1:100 000. This pioneer work succeeded in establishing the distribution of the principal lithologies which characterize the region, such as anorthosite, gabbro, late-metamorphic granitoids, amphibolite, marble, and quartzite. In contrast, much of the high grade, intensely-deformed gneisses of the intervening areas have been grouped in composite map units, presumably representing an older basement. The "distinctive association" of marble, quartzite and pelitic gneiss (Wynne-Edwards, 1972) and the mineralogical and textural similarities between these rocks and paragneisses of the Central Metasedimentary Belt have constituted the basis for the correlation of the metasupracrustal rocks of the Montauban area with the Grenville Supergroup (Gauthier et al., 1985; Bernier et al., 1987). This correlation was also predicated on the interpretation that the Grenville orogen is entirely ensialic, with the Grenville Supergroup representing an Early to Middle Proterozoic, regionally extensive, platform-type cover resting on a largely Archean, cratonic basement (Wynne-Edwards, 1972).

Conversely, Rondot (1978) recognized that correlation of all the metasedimentary rocks of the Montauban area with the Grenville Supergroup is unjustified. His regional lithostratigraphic synthesis resulted in the identification of three contrasting crustal blocks: Laurentia, Grenvillia, and Quebecia

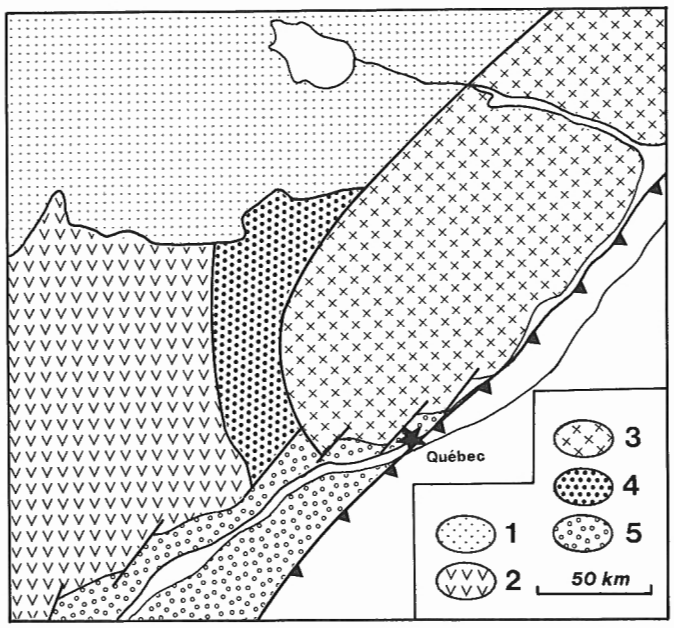

Figure 1. Tectonic model for the Portneuf-St. Maurice region after Rondot (1978, 1986). (1) Laurentia; (2) Grenvillia; (3) Quebecia; (4) Relict ophiolite, collisional suture between Grenvillia and Laurentia; (5) fault bounded Paleozoic cover. The thrust symbol marks the Appalachian front.

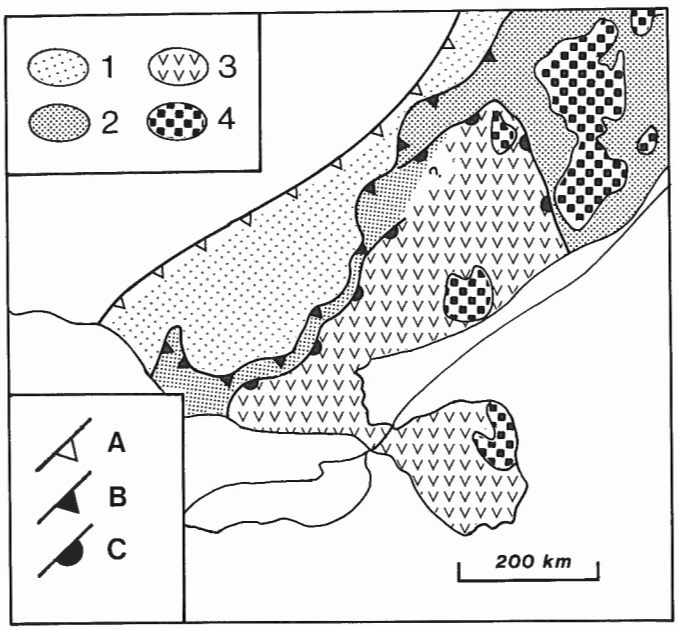

Figure 2. Tectonic model for the Portneuf-St. Maurice region after Rivers et al. (1989). (1) Parautochthonous Belt; (2) Allochthonous Polycyclic Belt; (3) Allochthonous Monocyclic Belt; (4) Anorthosite-mangerite-charnockite-granite suite; [A] Grenville Front; [B] Allochthon boundary thrust; [C] Monocyclic belt boundary thrust.

(Fig. 1). These blocks were viewed as distinct continental segments juxtaposed along collisional sutures (Rondot, 1978, 1986; Anderson and Burke, 1983).

Previous mapping highlighted the orientations of compositional layering and mineral foliation. Lineations were only rarely recorded. Although high grade regional metamorphism was recognized by most workers, the associated structural effects were not appreciated; compositional layering was interpreted as bedding and the rock succession described in stratigraphic terms (e.g. Rondot, 1978; Jourdain et al., 1987).

The present study aims at a better understanding of the tectonic evolution of the Grenville orogen of central Quebec and determining the nature, regional context, and tectonic significance of the La Bostonnais complex and of the associated supracrustal rocks. This work is part of a joint Ministère de l'Energie et des Ressources du Québec (MERQ) - Centre géoscientifique de Québec (CGQ/GSC) mapping project (1:50,000 scale) of the La Bostonnais complex (Nadeau and Hébert, 1990; Hébert and Nadeau, 1990a, 1990b). It follows two decades of major advances in our understanding of the Grenville orogen (compare Wynne-Edwards, 1972 with Moore et al., 1986 and Rivers et al., 1989) and is spurred by a better appreciation of the origin and tectonic significance of high grade tectonites (e.g. Davidson et al., 1982; Davidson, 1984; Nadeau, 1984, 1990; Hanmer, 1988).

LITHOTECTONIC SUBDIVISIONS

The geology of the Portneuf-St. Maurice region is summarized in sketch maps of the main lithologic units, of the foliations and of the extension lineations (Fig. 3, 4, and 5). In this region, the Grenville orogen is not a uniform geological entity (compare Wynne-Edwards, 1972 with Rondot, 1978, 1986 and Rivers et al., 1989). It comprises three contrasting lithotectonic subdivisions with distinctive aeromagnetic signatures. From west to east, these subdivisions are hereafter informally referred to as the Mékinac domain, St. Maurice tectonic zone, and Laurentides Park complex.

Mékinac domain

Mékinac domain extends westward from the west margin of the map area. It is underlain by homogeneous, fine- to medium-grained, buff to brown, granulite-facies granodioritic gneisses (Fig. 3, unit 1). These rocks contain less than 20% mafic minerals, including hypersthene, augite, hornblende, and biotite. They commonly exhibit weakly contrasting centimetre-thick migmatitic segregations that parallel the well developed mineral foliation. A plutonic protolith for these gneisses is suggested by their homogeneous composition and by the absence, except for ubiquitous, sparse, metre-thick, discontinuous mafic layers and boudins, of layering in the mesosome. These monotonous gneisses also host a number of kilometre-scale masses and lenses of metagabbro and tracts of migmatitic pelitic (sillimanite-garnet-biotite) gneiss, quartzite and marble tectonic mélange.

Although having a generally northerly orientation, structural trends within Mékinac domain are irregular and define shallowly-plunging open folds and broad domes. Sub-horizontal structures typical of Mékinac domain are only present in the southwestern corner of the map area (Fig. 4). Although locally variable, northeast-trending lineations are characteristic (Fig. 5). This structural grain and the homogeneity of the component gneisses give Mékinac domain its distinctive regional-scale aeromagnetic signature.

The rocks underlying Mékinac domain in the study area have been described by Rondot (1978) as forming the lower three members of the Mékinac group. Farther west, these rocks give way to the highly migmatitic, pink and grey, amphibolite-facies granitic and granodioritic gneisses of the Chapeau de Paille complex (Rondot, 1978). Mékinac domain also corresponds to the eastern extension of Morin terrane and Allochthonous Monocyclic Belt of Rivers et al. (1989).

St. Maurice tectonic zone

Identification of mid- to deep crustal shear zones is based on the recognition of high-strain tectonites. Such tectonites have recently been described from thrust zones in the Central Gneiss Belt and the Central Metasedimentary Belt boundary thrust zone of Ontario (Davidson et al., 1982; Davidson, 1984; Hanmer and Ciesielski, 1984; Nadeau, 1984, 1990; Hanmer, 1988). These tectonites exhibit a variety of structural and textural attributes, indicative of intense ductile deformation. The widespread occurrence of similar tectonites in the map area constitutes the basis for defining the St. Maurice tectonic zone.

The St. Maurice tectonic zone comprises two structurally juxtaposed contrasting rock packages hereafter referred to as the lower and the upper belts (Fig. 3). It features a shallowly to moderately east-dipping foliation (Fig. 4) with an easterly to southeasterly plunging extension lineation (Fig. 5). Below we first examine the regional-scale structural elements which mark the margins of the tectonic zone, and then briefly describe the geological features which distinguish the upper and lower belts.

Western margin

The western margin of the St. Maurice tectonic zone is approximately located along the west edge of the map area. It is structurally defined by the first appearance of continuous, regionally distributed north-trending and moderately east-dipping planar structures (Fig. 4). The changes in style and orientation of the structural grain occur within intensely-deformed granulite-facies gneisses of eastern Mékinac domain (Fig. 3, unit 1). Eastward across the western margin of the St. Maurice tectonic zone, the shallow-dipping open structures, typical of Mékinac domain, give way to progressively steeper, easterly-dipping, homoclinal structures (Fig. 4). An abrupt swing in the lineation trends toward east-southeasterly-plunging directions is associated with the transposition of the planar fabric (Fig. 5). These structural

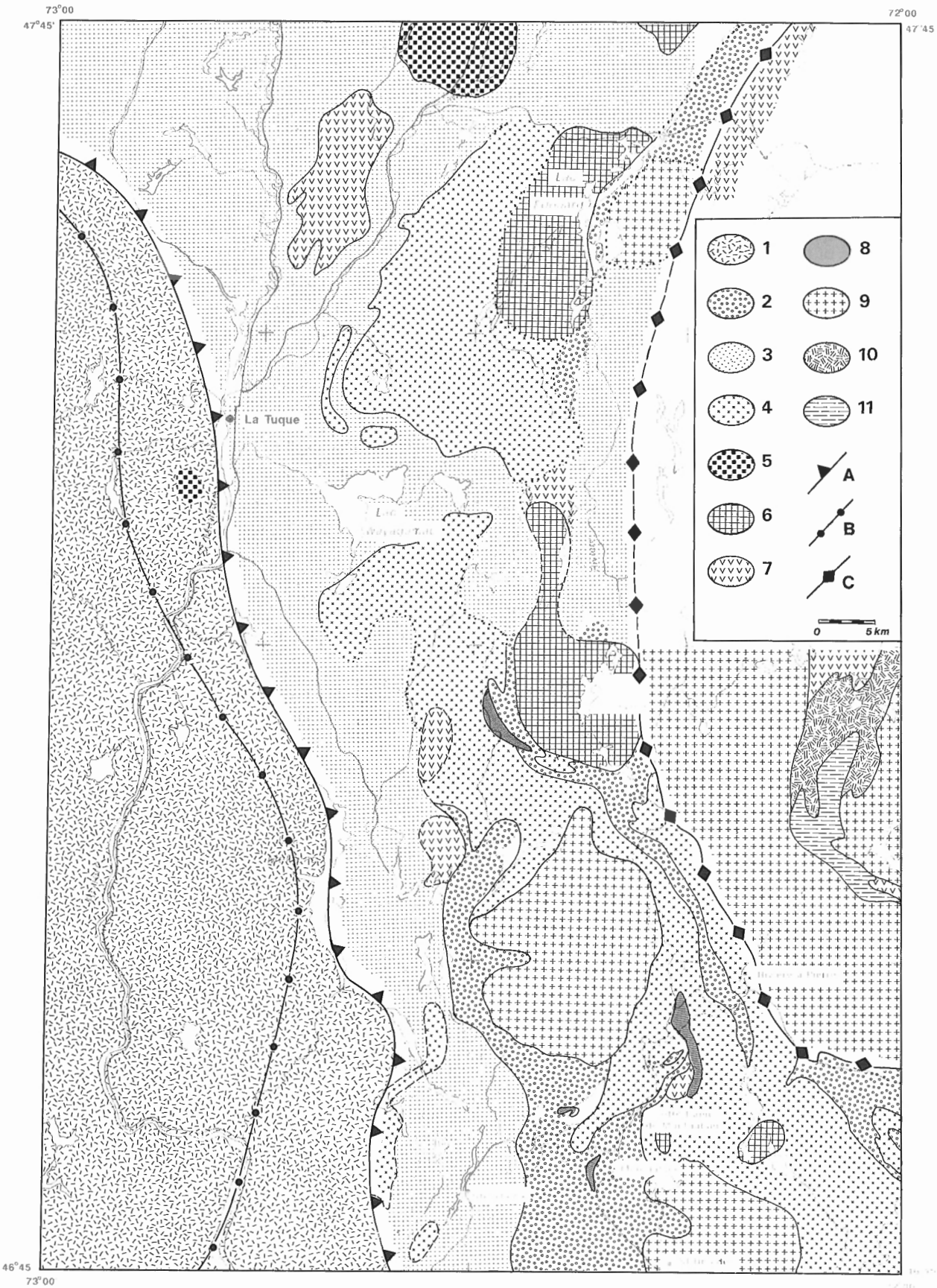
73°00
72°00
47°45'
47°45
La Tuque
1
2
3
4
5
6
7
8
9
10
11
A
B
C
0
5 km
46°45
73°00

modifications are accompanied by a marked change in the pattern, orientation, and intensity of the aeromagnetic signature.

Eastern margin

A north-northeasterly-trending arcuate ductile shear zone marks the eastern margin of the St. Maurice tectonic zone with the Laurentides Park complex (Fig. 3). Whereas steep dips with a sinistral strike-slip component characterize the southern part of the shear zone, shallower southeasterly dips and shear-sense indicators, consistent with northwest-directed thrusting, are observed along the northeastern extension (Fig. 4, 5, and 6a). Major changes in structural style and rock assemblages occur across this zone. The steep and irregular structures of the Laurentides Park complex to the east contrast sharply with the homoclinal easterly-dipping structures of the adjacent St. Maurice tectonic zone (Fig. 4). While lithological diversity characterizes the St. Maurice tectonic zone, mangerites, charnockites, and granites dominate in the Laurentides Park complex. The eastern margin of the St. Maurice tectonic zone is also marked by a sharp and regionally extensive break in the orientation and intensity of the aeromagnetic pattern.

The lower belt

The structurally lower part of the St. Maurice tectonic zone consists of tectonically transposed units from the underlying Mékinac domain (Fig. 3). These consist chiefly of granulite-facies straight gneisses (Davidson et al., 1982; Hanmer, 1988) of granodioritic composition. The straight gneisses include i) centimetre to decametre-thick concordant mafic layers and boudins, ii) a number of kilometre-wide masses of metagabbro and meta-anorthosite, and iii) concordant lenses and sheets of pelitic and calc-silicate gneiss, quartzite and marble tectonic mélange.

The granulite-facies granodioritic straight gneiss is fine- to medium-grained, well foliated, granoblastic and contains less than 10% mafic minerals, including orthopyroxene, augite, hornblende, and subordinate biotite and magnetite. They typically host attenuated and weakly contrasting medium grained migmatitic segregations, which parallel foliation.

Proportion, thickness, and continuity of the concordant mafic layers and boudins enclosed in the granulite-facies straight gneisses vary greatly. The thickness typically ranges from a few centimetres to a few tens of metres. Meso-scale layers are commonly folded isoclinally and some of the thicker layers can be traced for several kilometres along strike. Ophitic and subophitic textures are preserved locally in some of the thickest layers. Thinner layers are totally recrystallised and strongly foliated.

Primary igneous textures are also preserved in the larger metagabbro and meta-anorthosite masses and lenses, but these bodies also exhibit ubiquitous meso-scale boudinage, contain shear zones, mylonitic layering and porphyroclastic pegmatites (Fig. 6b; Davidson et al., 1982; Hanmer, 1988), indicative of intense but heterogeneous penetrative ductile deformation. The occurrence of such structures within kilometre-size coherent plutonic masses is an indication of the high intensities of ductile deformation accommodated by the wall rocks.

Marble tectonic mélange, quartzite, pelitic and calcsilicate gneisses form concordant and discontinuous sheets within granulite-facies straight gneisses. These sheets are typically less than a few hundred metres thick and extend for up to a few kilometres along strike. Their frequency increases structurally up section. Pelitic and semipelitic gneisses are well foliated and lineated and commonly exhibit a mylonitic textures (Fig. 6c). Migmatitic segregations are transposed along the mineral foliation. The mylonitic structure along with the occurrence of marble tectonic mélange and of sheath folds in associated calc-silicate gneiss (Fig. 6d) indicate that the paragneiss sheets have accommodated intense ductile deformation and that they represent mechanically weak zones (Hanmer, 1988). Accordingly, the sequence of alternating sheets of paragneiss and granulite-facies straight gneiss is interpreted as having resulted from tectonic interleaving.

The upper belt

Lithologic diversity makes the upper belt of St. Maurice tectonic zone distinct from both the lower belt and the Laurentides Park complex to the east. The upper belt is underlain by a wide variety of migmatitic, upper amphibolite-facies gneisses of supracrustal and plutonic origin (Fig. 3, units 2 to 9). Supracrustal rocks include the metasedimentary rocks of the Montauban group and correlative paragneisses (Nadeau and Hébert, 1990; Hébert and Nadeau, 1990a, 1990b). These

---

Figure 3. (opposite) Geological sketch map of the Grenville orogen in the Portneuf-St. Maurice region.

[A] lithotectonic break between the "lower" and "upper" belts of the St. Maurice tectonic zone; [B] aeromagnetic discontinuity between the St. Maurice tectonic zone and the Mékinac domain; and [C] shear zone marking the west margin of the Laurentides Park complex.

From west to east, lithotectonic subdivision includes: the Mékinac domain, {.?.[B]}; the "lower" and "upper" belts of the St. Maurice tectonic zone, {.?.[B][A]} and {[A][C]} respectively; and the Laurentides Park complex {[C]...}.

Major map units comprise: (1) mainly migmatitic granodioritic orthogneiss, granulite facies; (2) aluminous paragneiss, minor quartzite, calcsilicate and mafic tracts and boudins; (3) undivided high-grade para- and orthogneisses; (4) dominantly dioritic to granodioritic orthogneiss and gneissic equivalents, La Bostonnais complex; (5) meta-anorthosite; (6) meta-gabbro; (7) biotite granitic orthogneiss; (8) mafic gneiss; (9) hornblende-biotite porphyritic granite; (10) charnockitic orthogneiss; and (11) alaskitic gneiss.

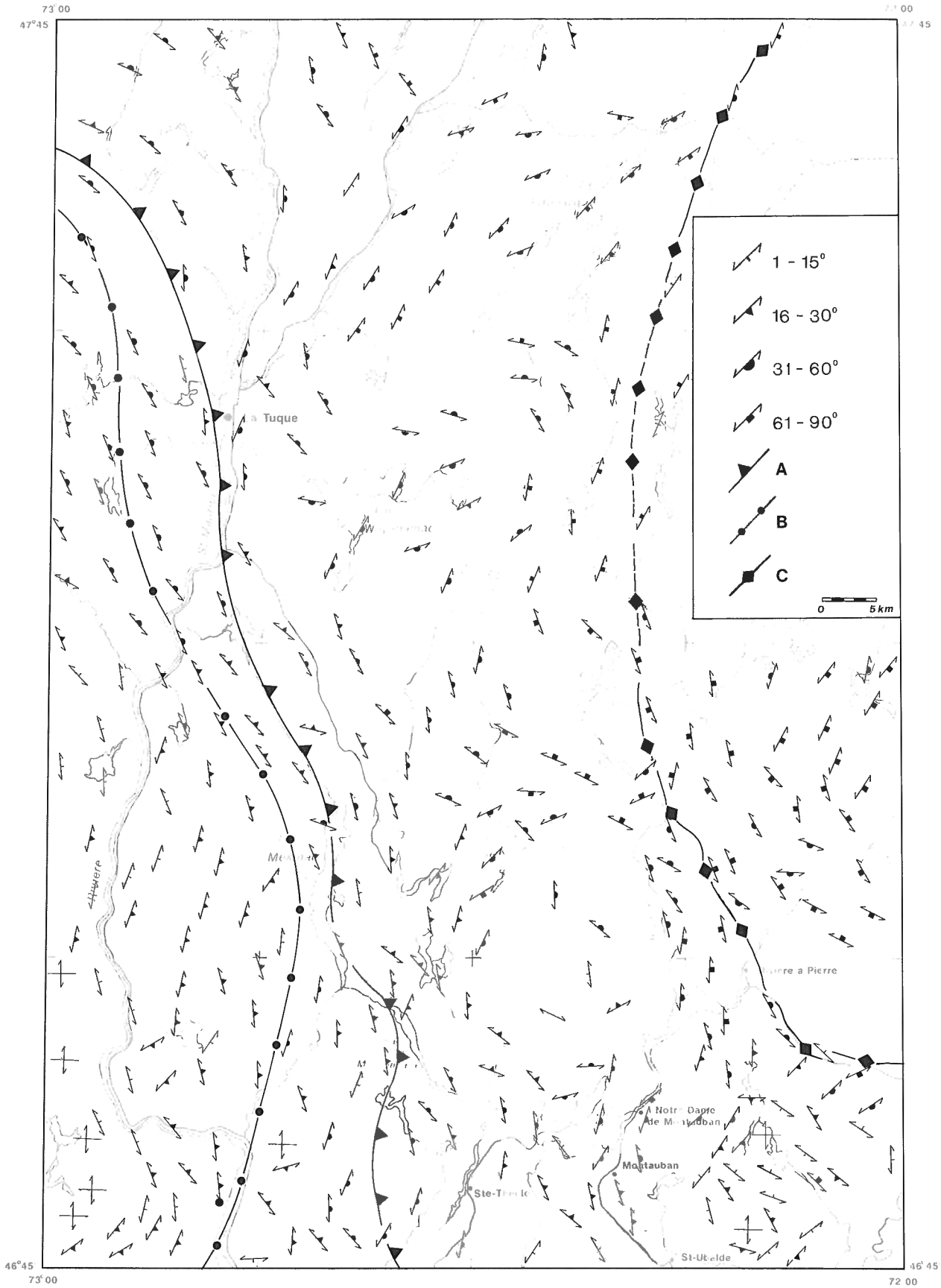

Figure 4. Generalized map of orientations of mineral foliation and layering.

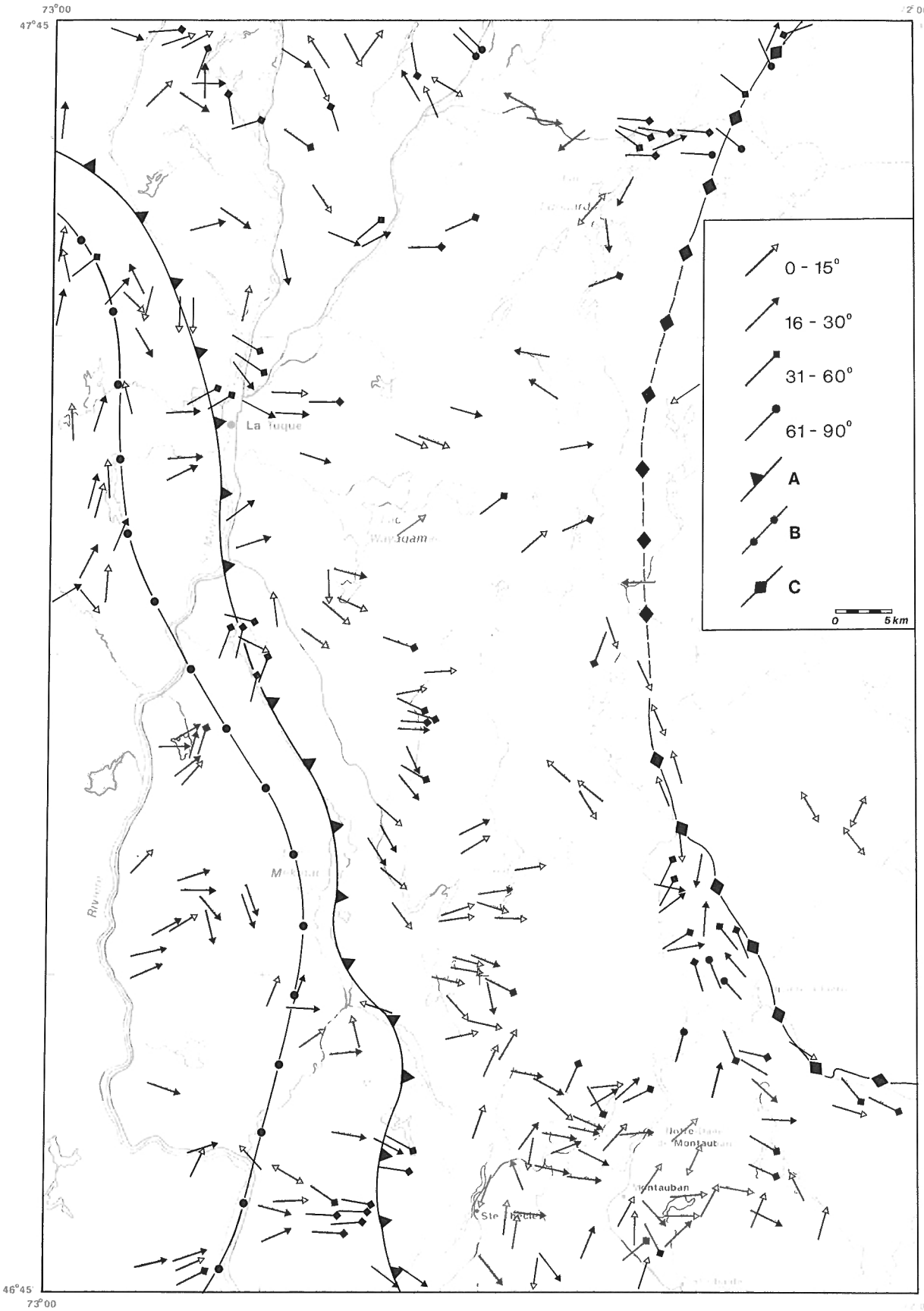

Figure 5. Generalized map of extension lineations.

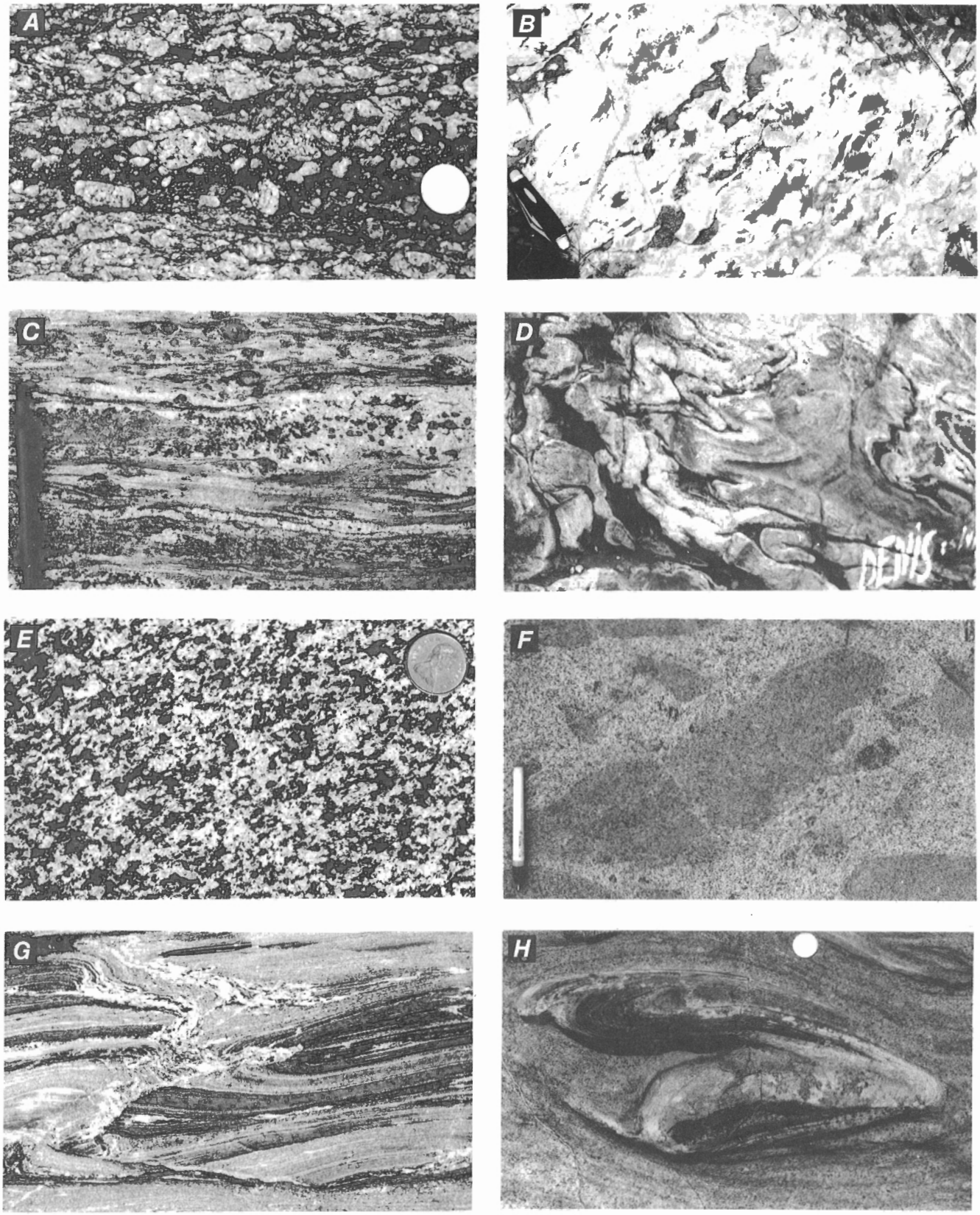
A
B
C
D
E
F
G
H

gneisses host discrete metaplutonic bodies including anorthosite, gabbro, porphyritic granite, and the dioritic to granodioritic rocks of the La Bostonnais complex.

Pelitic and semipelitic gneisses are widespread (Fig. 3, unit 2). They are locally associated with quartzite, calc-silicate gneiss, and amphibolite. Pelitic gneisses are migmatitic and consist of medium grained biotite-garnet-sillimanite-feldspar-quartz paleosome with 20-30% coarser grained granitic leucosome (Fig. 6c). Common accessory minerals include graphite and pyrite. Although relict primary layering, represented by variations in the proportions of mafic minerals or by trails of calc-silicate boudins, is locally recognizable, stratigraphic relationships are obliterated.

These migmatitic paragneisses have been tentatively correlated with the presumably lower grade metasediments of the Montauban group on the basis of observed field continuity (Nadeau and Hébert, 1990a; Hébert and Nadeau, 1990). While muscovite, locally in the form of vermicular intergrowths with quartz, is ubiquitous in the lower amphibolite-facies aluminous metasediments of the Montauban group, this mineral is absent in the correlative migmatitic pelitic gneisses described above. The low-grade metamorphic assemblages of the Montauban area appear to be retrograde effects. Perhaps the retrogression is related to sulphide mineralization.

Figure 6. (opposite) Characteristic structures of high grade rocks from the Portneuf-St. Maurice region.

A. Mylonitic porphyritic granite. C/S fabric, shear-band foliation and rotated porphyroclasts indicate senestral shear-sense. East margin, St. Maurice tectonite zone, scale = 2.5 cm.

B. Gneissic meta-anorthosite. Upper belt, St. Maurice tectonic zone, scale = 10cm.

C. Typical appearance of migmatitic, high strain, pelitic gneiss, (garnet-biotite-sillimanite-feldspar-quartz), scale = 15 cm.

D. Sheath-like fold in high strained calc-silicate gneiss (deeply weathered) adjacent to a mafic boudin and to granulite-facies granodioritic gneiss (upper right corner). Fold axes are parallel to the stretching direction. Lower belt, St. Maurice tectonic zone, scale = 30 cm high.

E. Characteristic texture of low strain, medium grained, pyroxene-hornblende quartz-diorite, La Bostonnais complex, scale = 2.5 cm.

F. Crosscutting relationship of quartz-diorite and granodiorite, La Bostonnais complex, scale = 13 cm.

G. Contrasting metamorphic structure of biotite-hornblende gneiss, expressed via secondary layering and injection of migmatitic leucosome, La Bostonnais complex, scale = 15 cm.

H. Isoclinal folding and boudinage of competent calc-silicate layer in fine grained mylonitic aluminous paragneiss. Upper belt of the St. Maurice tectonic zone, scale = 2.5 cm.

The La Bostonnais complex is composed of metaplutonic rocks, ranging from pyroxene-hornblende diorite to hornblende-biotite granodiorite with 40 to 15% mafic minerals (Fig. 3, unit 4; Fig. 6e). These rocks host small hornblendite and pyroxenite masses which may represent products of early crystal segregation. In their less-deformed state, these rocks show crosscutting relationships indicative of sequential intrusion from diorite to granodiorite (Fig. 6f). All the rocks of the La Bostonnais complex have undergone highgrade metamorphism and tectonism. While the meta-diorites have retained traces of their igneous textures, the granodiorites are recrystallised, largely migmatitic and heterogeneously deformed (Fig. 6g).

In contrast with the dioritic to granodioritic rocks described above, the gabbroic masses are homogeneous in composition, primary textures and structures are well preserved (Fig. 3, unit 6). These rocks contain 40-60% ortho- and clinopyroxene and subordinate hornblende. They exhibit medium grained ophitic to subophitic textures and primary flow structures are preserved locally. The effects of ductile deformation are limited to the margins of the bodies where the rocks are recrystallized and well foliated. Contact relationships with the adjacent La Bostonnais complex have not been established. The contrasting field and petrographical characteristics of the gabbroic rocks, with respect to the rocks of the La Bostonnais complex, suggest that the two rock groups belong to distinct plutonic suites.

Several discrete masses of augen and/or porphyritic granitic orthogneiss are present in the upper belt of the St. Maurice tectonic zone (Fig. 3, unit 7 and 9). Among them, the two masses of porphyritic granite, which outcrop in the southeast corner of the map area, are remarkable by their structural setting (Fig. 4). These rocks are identical to the hornblende-biotite porphyritic granite which, immediately to the east, dominates the Laurentides Park complex. Away from their contacts these granitic masses show little evidence of penetrative ductile deformation. However the western contact of these bodies with the underlying paragneisses is well exposed at several places. The contact dips gently to the east and is marked by an abrupt strain gradient in the granite. Moreover, the mylonitic fabric of the granite is concordant with the ductile structure of the underlying paragneisses. These two granite bodies are tentatively interpreted as thrust sheets detached from the Laurentides Park complex to the east.

Deformation in the upper belt of the St. Maurice tectonic zone is less homogeneous than in the lower belt. It is emphasized that the interior of some plutonic bodies shows little evidence of penetrative ductile deformation whereas abrupt strain gradients are developed along contacts. The following observations suggest that the para- and orthogneisses intervening between the discrete plutonic masses have experienced intense strain. In low strain zones, the rocks show abrupt strain gradients and boudinage structures. At higher strain, the gneisses are invariably recrystallized to fine grain size, mylonitic, thinly foliated, and well lineated. They include ubiquitous boudins of the more competent rock types and tight to isoclinal folds with axes parallel to the stretching lineation (Fig. 6h). Metamorphic segregations and pegmatites are disaggregated and transposed.

At regional scale the internal structure of the upper belt of the St. Maurice tectonic zone is that of an anastomosing network of high strain zones that isolate less deformed, discrete meta-plutonic bodies.

Laurentides Park complex

The Laurentides Park complex extends from the eastern part of the map area to the Saguenay-Charlevoix region, approximately 100 km to the east. The complex has not been mapped in detail. It consists dominantly of mangeritic, charnockitic, and granitic orthogneisses (Avramtchev and Piché, 1981). Some of these plutonic rocks may be part of the anorthosite-mangerite-charnockite-granite suite associated with the Lac St.Jean complex (e.g. Emslie and Hunt, 1990).

In the map area, the Laurentides Park complex includes large bodies of leucocratic, porphyritic granite and quartz-monzonite (Fig. 3, unit 9; Nadeau and Hébert, 1990). Pink and grey hornblende-biotite varieties grade locally into olive-green to brown orthopyroxene-augite charnockite and mangerite. Perthitic feldspar megacrysts commonly exceed 3 cm. Rapakivi textures are present in places. Although a foliation is locally developed, chiefly near contacts, the interior of these bodies are massive and nonmigmatitic. In addition, tracts of paragneiss, fine- to medium-grained equigranular and well-foliated migmatitic charnockitic orthogneiss (Fig. 3, unit 10), alaskitic gneiss (Fig. 3, unit 11), and pink migmatitic biotite granitic gneiss (Fig. 3, unit 7) locally form mappable units (Nadeau and Hébert, 1990).

In contrast with the shallow to moderately easterly-dipping structural grain of the St. Maurice tectonic zone, steep dips (>70°) and more variable structural trends characterize the Laurentides Park complex in the study area (Fig. 4; Nadeau and Hébert, 1990). The regional structural pattern is controlled by the vast and relatively rigid plutonic masses.

METAMORPHIC ZONATION

The distribution of regional metamorphic zones coincides with the lithotectonic subdivisions. From west to east, mineral assemblages indicate regional metamorphic conditions of: 1) granulite facies in Mékinac domain and in the lower belt of the St. Maurice tectonic zone; 2) uppermost amphibolite facies in the upper belt of the St. Maurice tectonic zone; and 3) alternating granulite and amphibolite facies in the Laurentides Park complex. The metamorphic assemblages observed in the lower belt of the St. Maurice tectonic zone, combined with pressure and temperature estimates of 900 ± 50 MPa and 820 ± 40° C for associated sapphirine-garnet-orthopyroxene-sillimanite-plagioclase-phlogopite (Herd et al., 1986) indicate a tectonically thickened crust.

The causes for the change in metamorphic mineral assemblages from granulite facies in the lower belt of the St. Maurice tectonic zone, to amphibolite facies in the upper belt, are unknown. Widespread occurrence of granitic leucosomes in the gneisses of the upper belt suggests that these rocks attained granulite-facies temperatures. Therefore, the changes of metamorphic assemblages possibly reflect a gradient in the activity of metamorphic fluids rather than in regional metamorphic pressure and temperature conditions.

In addition to little-deformed and nonmigmatitic mangerite, charnockite, and hornblende-biotite granite, the Laurentides Park complex contains migmatitic and penetratively deformed granulite-facies orthogneiss. The rock association indicates that the juxtaposition of amphibolite and granulite-facies rocks is probably the result of the emplacement of plutonic masses at amphibolite-facies conditions, after the attainment of granulite-facies conditions.

AGE RELATIONS

There are no geochronological age constraints on the lithotectonic evolution of the Portneuf-St. Maurice region. However, the relative ages of some of the major rock units have been deduced from crosscutting relationships. The occurrences of paragneiss xenoliths and of hornblende-biotite porphyritic granite dykes in the plutonic rocks of the La Bostonnais complex indicate that the latter is younger than the supracrustal assemblage, but predates the porphyritic granite. The hornblende-biotite porphyritic granite appears to constitute the latest major intrusive phase in the Laurentides Park complex.

Moreover, in the absence of geochronological data, it is stressed that the effects of highgrade metamorphism and ductile deformation on the paragneisses of the Portneuf-St. Maurice region preclude stratigraphic correlations with the Grenville Supergroup based on lithological similarities.

CONCLUDING REMARKS

Our observations in the Portneuf-St. Maurice region support the following preliminary conclusions:

1) The Grenville orogen in the Portneuf-St. Maurice region comprises three contrasting lithotectonic entities; from west to east, the Mékinac domain, the St. Maurice tectonic zone, and the Laurentides Park plutonic complex.

2) The St. Maurice tectonic zone is a regional-scale easterly-dipping mid- to deep crustal ductile shear zone that separates the Mékinac domain, a possible extension of the Allochthonous Monocyclic Belt to the west, from the Laurentides Park complex, which is part of the Allochthonous Polycyclic Belt, to the east.

3) The lower belt of the St. Maurice tectonic zone comprises tectonically transposed footwall structures and lithologies. The west margin of the zone is structurally defined by the first appearance of regionally distributed north-trending and easterly moderately-dipping homoclinal planar fabric and by east- southeasterly-plunging lineations.

4) Deformation in the upper belt of the St. Maurice tectonic zone is less homogeneous than in the lower belt. At regional-scale, high strain gneisses define an anastomosing network of high strain zones which includes less deformed, discrete meta-plutonic bodies.

5) A north-northeasterly-trending steep to southeasterly-dipping arcuate ductile shear zone with a northwest-directed thrust-component marks the eastern margin of the St. Maurice tectonic zone with the Laurentides Park complex.

6) Current regional interpretations of the Grenville orogen in southwestern Quebec show the Allochthonous Monocyclic Belt to be overthrusted onto the Allochthonous Polycyclic Belt. Although overthrusting is well established in western Quebec and Ontario, our observations at the St. Maurice tectonic zone show that the structural development of the eastern margin of the Allochthonous Monocyclic Belt does not fit this simple model.

ACKNOWLEDGMENTS

Sylvie Lévesque and Michel Dion are gratefully acknowledged for their support during field mapping. Pierre Brouillette (CGQ) helped greatly with the drafting of the figures. The original manuscript was much improved by the critical review of G. Lynch (CGQ) and T. Feininger (CGQ) and A. Davidson (CGD). This study benefits from discussions with C. Hébert (MERQ).

REFERENCES

Anderson, S.L. and Burke, K.
1983: A Wilson Cycle approach to some Proterozoic problems in eastern North America; Geological Society of America, Memoir 161, p. 75-93.

Avramtchev, L. and Piché, G.
1981: Cartes des gîtes minéraux du Quebec, région de Laurentie - Saguenay; Ministère de l'Énergie et des Ressources du Québec, DPV-809.

Bernier, L., Pouliot, G., and MacLean, W.H.
1987: Geology and metamorphism of the Montauban North Gold Zone: a metamorphosed polymetallic exhalation deposit, Grenville Province, Québec; Economic Geology, v. 82, p. 2076-2090.

Culshaw, N.G., Davidson, A., and Nadeau, L.
1983: Structural subdivisions of the Grenville Province in the Parry Sound - Algonquin region, Ontario; in Current Research, Geological Survey of Canada, Paper 83-1B, p. 243-252.

Davidson, A.
1984: Identification of ductile shear zones in the southwestern Grenville Province of the Canadian Shield; in Precambrian tectonics illustrated, (ed.) A. Kröner and R. Greiling; E. Schweitzerbart'sche Verlagsbuchhandlung (Nägele u. Obermiller), Germany, Stuttgart, p. 207-235.

Davidson, A., Culshaw, N.G., and Nadeau, L.
1982: A tectono-metamorphic framework for part of the Grenville Province, Parry Sound region, Ontario; in Current Research, Geological Survey of Canada, Paper 82-1A, p. 175-190.

Emslie, R.F. and Hunt, P.
1990: Ages and petrogenetic significance of igneous mangerite-charnockite suites associated with massif anorthosites, Grenville Province; Journal of Geology, v. 98, p. 213-231.

Gauthier, M., Morin, G., and Marcoux, P.
1985: Minéralisations aurifères de la partie centrale de la Province de Grenville, Bouclier Canadien; Canadian Mining and Metallurgical Bulletin, v. 78, no. 874, p. 60-69.

Hanmer, S.
1988: Ductile thrusting at mid-crustal level, southwestern Grenville Province; Canadian Journal of Earth Sciences, v. 25, p. 1049-1059.

Hanmer, S.K. and Ciesielski, A.
1984: A structural reconnaissance of the northwest boundary of the Central Metasedimentary Belt, Grenville Province, Ontario and Quebec; in Current Research, Geological Survey of Canada, Paper 84-1B, p. 121-131.

Hébert, C., and Nadeau, L.
1990a: Géologie du feuillet SNRC 31 P/1 (Talbot): implications tectoniques et économiques; in Rapport d'activités 1990, Ministère de l'Énergie et des Ressources du Québec, DV 90-10, p. 16-17.
1990b: New exploration targets for polymetallic sulfides (Zn, Cu, Pb, Au, Ag) Grenville Province, Portneuf Area, Quebec; Ministère de l'Énergie et des Ressources du Québec, PRO 90-08, 5 p.

Herd, R.K., Ackermand, D., Windley, B.F., and Rondot, J.
1986: Sapphirine - garnet rocks, St. Maurice area, Québec: petrology and implications for tectonics and metamorphism; in The Grenville Province, (ed.) J.M. Moore, A. Davidson, and A.J. Baer; Geological Association of Canada, Special Paper 31, p. 241-253.

Jourdain, V., Roy, D.W., and Simard, J.-M.
1987: Stratigraphy and structural analysis of the North Gold Zone at Montauban-les-mines, Quebec; Canadian Mining and Metallurgical Bulletin, v. 80, no. 906, p. 61-66.

Klugman, M.A.
1956: La Tuque Area (West half), Rapport géologique; Ministère des richesses naturelles du Québec, DPV-370, 45 p.
1963: Boucher-Carignan Area, Rapport géologique; Ministère des richesses naturelles du Québec, DPV-371, 51 p.

McEachern, S.J.
1990: Structure and U-Pb geochronology of the Pembroke thrust stack, Central Metasedimentary Belt boundary thrust zone; M.Sc. thesis, Carleton University, 156 p.

Moore, J.M., Davidson, A., and Baer, A.J., (ed.)
1986: The Grenville Province; Geological Association of Canada, Special Paper 31, 358 p.

Nadeau, L.
1984: Deformation of leucogabbroic rocks at Parry Sound, Ontario; M.Sc. thesis, Carleton University, Ottawa, Ontario, 191 p.
1990: Tectonic, thermal and magmatic evolution of the Central Gneiss Belt, Huntsville region, southwestern Grenville orogen; Ph.D. thesis, Carleton University, Ottawa, Ontario, 270 p.

Nadeau L. and Hébert, C.
1990: Déformation et extension de l'assemblage métasédimentaire de Montauban dans la réserve de Portneuf; dans Nouveaux horizons pour l'exploration 1990, Ministère de l'Énergie et des Ressources du Québec, DV 90-40, p. 11-14.

Newman, W.D.N.
1973: Interim Report on Chaumonot Area; Ministère des Richesses naturelles du Québec, GM. 28633, 37 p.

Pyke, D.R.
1967: Geology of the Montauban Area; Ph.D. thesis, McGill University, Montreal, 197 p.

Rivers, T., Martignole, J., Gower, C.F., and Davidson, A.
1989: New tectonic divisions of the Grenville Province, southeast Canadian Shield; Tectonics, v. 8, p. 63-84.

Rondot, J.
1976a: Géologie de la région de Mattawin - Lac Chat Est; Ministère des Richesses naturelles du Québec, DPV-373, 249 p.
1976b: Rapport géologique de la région de la rivière aux Rats; Rapport géologique; Ministère des Richesses naturelles du Québec, DPV-440, 92 p.
1976c: Rapport géologique de la région de la Croche; Ministère des Richesses naturelles du Québec, DPV-372, 90 p.
1978: Stratigraphie et métamorphismes de la région du Saint-Maurice; in Metamorphism in the Canadian Shield, (ed.) J.A. Fraser and W.W. Heywood; Geological Survey of Canada, Paper 78-10, p.329-352.
1986: Géosutures dans le Grenville; in Geological Association of Canada, Special Paper 31, p. 313-325

Tiphane, M.
1954: La Tuque Area (east half), Rapport géologique; Ministère des Richesses naturelles du Québec, DPV-369, 29 p.

Wynne-Edwards, H.R.
1972: The Grenville Province; in Variations in tectonic styles in Canada, (ed.) R.A. Price and R.J.W. Douglas; Geological Association of Canada, Special Paper 11, p. 263-334.

Electrical characteristics of a graphitic rock from the Kapuskasing Structural Zone, Ontario

T.J. Katsube, M. Mareschal[1] and F. Aucoin[1]
Mineral Resources Division

Katsube, T.J., Mareschal, M., and Aucoin, F., 1991: Electrical characteristics of a graphitic rock from the Kapuskasing Structural Zone, Ontario; in Current Research, Part E; Geological Survey of Canada, Paper 91-1E, p. 257-263.

Abstract

Electrical properties of a surface rock sample, a paragneiss containing grain-boundary graphite, from the Kapuskasing Structural Zone have been measured to obtain information that might help explain the origin of high electrical conduction in the lower continental crust. Five rectangular specimens were cut out from the sample for petrophysical measurements in three directions, including complex electrical resistivity.

The bulk resistivity and surface resistivity values are in the range of 2000-5500 Ωm, values 5 to 10 times smaller than those usually observed for similar rocks in the literature, indicating the possibility of electrically conductive minerals lining the pores. Complex resistivity plots indicate pore surface polarization parallel to the foliation, likely due to an electronically conductive mineral lining. These results will be used to study the "broken conductor model" developed to represent the physical process by which electrically conductive rocks from the lower crust lose conductivity during uplift to the surface.

Résumé

Les propriétés électriques d'un échantillon de roche de surface, un paragneiss contenant des grains de graphite périphériques, de la zone structurale de Kapuskasing ont été mesurées dans le but de connaître l'origine de la forte conduction électrique dans la croûte continentale inférieure. Cinq éprouvettes rectangulaires ont été découpées dans l'échantillon pour des mesures pétrophysiques dans trois directions, notamment pour des mesures de résistivité électrique complexe.

La résistivité apparente et la résistivité superficielle sont de l'ordre de 2000 à 5000 Ω-m, valeurs de 5 à 10 fois inférieures à celles normalement observées pour des roches semblables, indiquant la possibilité que les interstices soient occupés par des minéraux électriquement conducteurs. Les tracés de résistivité complexe révèlent une polarisation superficielle parallèle à la foliation, qui est probablement due à la présence de minéraux intersticiels électroniquement conducteurs. Ces résultats serviront à étudier le "modèle des conducteurs brisés", mis au point pour représenter le phénomène physique par lequel les roches électroniquement conductrices de la croûte inférieure perdent de leur conductivité lorsqu'elles atteignent la surface.

[1] Ecole Polytechnique, C.P. 6079, Succ. A, Montreal, Quebec, Canada H3C 3A7.

INTRODUCTION

Electrical properties of a surface rock sample from the Kapuskasing Structural Zone (KSZ; Ontario, Canada) have been measured. The zone is considered to be a relict of an Archean uplift (Percival and Card, 1983, 1985) having brought to the present surface rocks formed in the intermediate to lower continental crust. Although the present upper crust of the KSZ is very resistive ($4x10^4$ Ωm) and only includes two zones of very weak subhorizontal electrical anomalies, probably unrelated to the uplift itself (Bailey et al., 1989), its lower crust is characterized by a bulk resistivity of a few 100 Ωm at the most (Kurtz et al., 1989) and may show signs of electrical anisotropy (Mareshal, 1990, and references therein).

The purpose of this study is to determine whether the surface rock sample can provide any information on the source of electrical conductivity commonly observed in most lower crusts (Haak and Hutton, 1986), and on the reason why this conductivity disappears once the rocks are uplifted to the surface. The presence of brine in pores has been offered as an explanation for the electrical conduction (e.g., Hyndman, 1988), but suffers from lack of petrological evidence. Furthermore, an electrical anisotropy such as that possibly observed in the present lower crust of the Kapuskasing uplift may be more easily explained by the presence of solid conductors organized in a preferred direction than by brine which at the prevailing temperature and pressure would re-equilibrate isotropically in a matter of seconds. Although the exposed lower crustal rocks of the Kapuskasing uplift may be very resistive, there is a possibility that petrophysical studies can find indications of previous solid conduction. According to the "broken conductor model" (Katsube and Mareschal, unpub. rep.), even if an electrically conducting rock with resistivities as low as 10^{-2} - 10 Ωm is formed in the lower crust, the rock will no longer be conductive by the time it is uplifted to the surface, as suggested by Frost et al. (1989).

The rock sample under study is a paragneiss (Percival, 1983, Sample number PG-16 [GSC No. PBA79-32]) containing grain-boundary graphitic carbon identified by Auger spectrometry (W.S. Fyfe, pers. comm., 1990; Mareschal, et al., 1990). The graphite content is thought to be less than 5%

Table 1. Mineral composition of sample, GSC no. PBA79-32 (J.A. Percival, pers. comm., 1991)

Minerals	Composition (%)
Plagioclase (An_{35})	60
Quartz	5
K-Feldspar	1
Apatite	1
Garnet	5
Hornblende	10
Biotite	6
Orthopyroxene	7
Opaque	5
Chlorite	tr

tr = trace amounts

Table 2. Dimensions of specimens cut from sample no. PBA79-32

Specimens	MM-1	MM-2	MM-3	MM-4	MM-5
Length					
a_1 (cm)	1.828	2.209	1.445	1.486	1.505
a_2 (cm)	1.735	1.493	1.144	1.459	1.460
Thickness					
ℓ (cm)	0.780	0.561	0.605	0.690	0.411
weight					
w (g)	6.8269	4.9903	2.6812	4.1005	2.3957
K_G (x0.01)	4.08	5.88	2.71	3.15	5.35
δ (g/mL)	2.75	2.70	2.68	2.74	2.65

K_G: geometric factor
δ : specific density

(J.A. Percival, pers. comm., 1991), as shown in Table 1. Five rectangular specimens were cut out from the sample for petrophysical measurements in three directions. Complex electrical resistivity, formation-factor and pore surface electrical resistivity measurements have been made on all five rectangular specimens, and the effective porosity determined from a remaining chip from the same sample. This paper reports the results of the electrical and porosity measurements.

METHOD OF INVESTIGATION

Sample preparation

The geometric characteristics of the specimens are listed in Table 2, their dimensions being of the order of (1.5-2.0) by (1.5-2.0) cm for the cross-section, and 0.4 to 0.8 cm in thickness. A remaining chip from the same sample was prepared for effective porosity measurements. The geometric factor, K_G, calculated for all of the rectangular specimens prior to the electrical measurements is derived from

$$K_G = A/\ell \qquad A = a_1 a_2, \tag{1}$$

where a_1 and a_2 are the lengths of the two sides of the rectangular specimen, and ℓ is its thickness. Specimens MM-1 to MM-3 are cut so that the electrical measurements will be parallel to the foliation, and MM-4 and MM-5 vertical to the foliation as described in Figure 1.

Effective porosity measurements

Effective porosity in principle includes the pore volume of all connected pores, and is determined from the difference in weight between the oven-dried and water saturated rock specimen (Katsube, 1981). The effective porosity, ϕ_E, is derived using the following equation:

$$\phi_E = (W_w - W_D) / W_D \tag{2}$$

where W_w, W_D and δ are the wet weight, dry weight and specific density of the rock sample, respectively. A separate study shows the porosity variation within a sample to be 10% for gneisses (Wadden and Katsube, 1982). Further details of the measuring procedures can be found in Katsube and Salisbury (this volume).

Complex resistivity measurements

The techniques used for the complex electrical resistivity and formation-factor measurements have been described previously (Katsube, 1981; Katsube and Walsh, 1987). First, the specimens are placed under vacuum for 15 minutes and then immersed in distilled water (still under vacuum) for 15 minutes. The specimens are then allowed to stand in the distilled water (in covered beakers) for 24 hours under atmospheric pressure. Subsequently, they are placed in a capacity type sample-holder (Katsube and Collett, 1973) with a graphite electrode covering each face. The surfaces of the sides of the specimen are dried before measurement, to eliminate any specimen surface electrical conduction due to moisture. The sample-holder is then placed in an enclosed space in order to reduce movement of air around it. This is a precautionary measure to minimize evaporation of fluid from the rock pores. The sample holder is connected to an automatic electrical impedance system which measures the in-phase and out-of-phase components of the impedance at frequencies of 1.0 - 10^6 Hz, as described in Gauvreau and Katsube (1975). The complex resistivity, ρ^* (Katsube, 1975):

$$\rho^* = \rho_R + i\rho_I, \tag{3}$$

where ρ_R is the real resistivity and ρ_I is the imaginary resistivity, is derived from the impedance by

$$\rho^* = ZK_G. \tag{4}$$

When electrical resistivity is measured over these frequencies, dielectric polarization, Warburg impedance and electrode polarization affects are reflected in the measurements (Katsube, 1975, 1977). A simple method applied to distinguish different mechanisms for improvement of the electrical resistivity measurement accuracy is to use Cole-Cole plots where imaginary-resistivity (ρ_I) is plotted against real-resistivity (ρ_R) (Katsube and Walsh, 1987). Katsube (1975) considered plots consisting of three arcs (Fig. 2) and suggested that each arc includes the effect of different groups of electrical polarization mechanisms. It was proposed that the left-most arc characterizes the effects of the dielectric constant, double layer, pore structure, and pore water chemistry. According to this model, bulk rock resistivity, ρ_r, is determined from the point where the right-hand side of the left-most arc intersects the horizontal axis. It reflects the pore structure and the pore-water chemistry or pore-water resistivity of the rock.

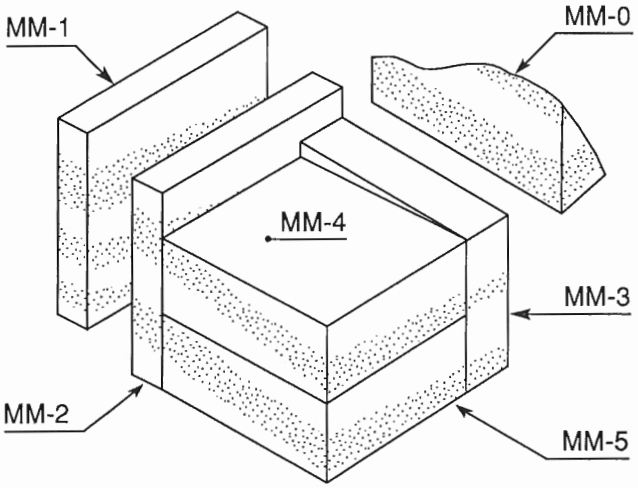

Figure 1. Descriptions of specimens (MM-0 to MM-5) cut from sample no. PBA79-32.

Formation-factor measurements

The formation-factor, F, is defined by the ratio of the bulk rock resistivity (ρ_r) over the pore fluid resistivity, ρ_w (Archie, 1942), and is a parameter representing one of the pore structure characteristics of the rock. Bulk rock resistivity (ρ_r) is a function of both pore structure and pore water resistivity (ρ_w). However, in order to eliminate the pore surface electrical conductivity effect (Patnode and Wyllie, 1950), F is actually derived by measuring the bulk resistivity (ρ_r) of the

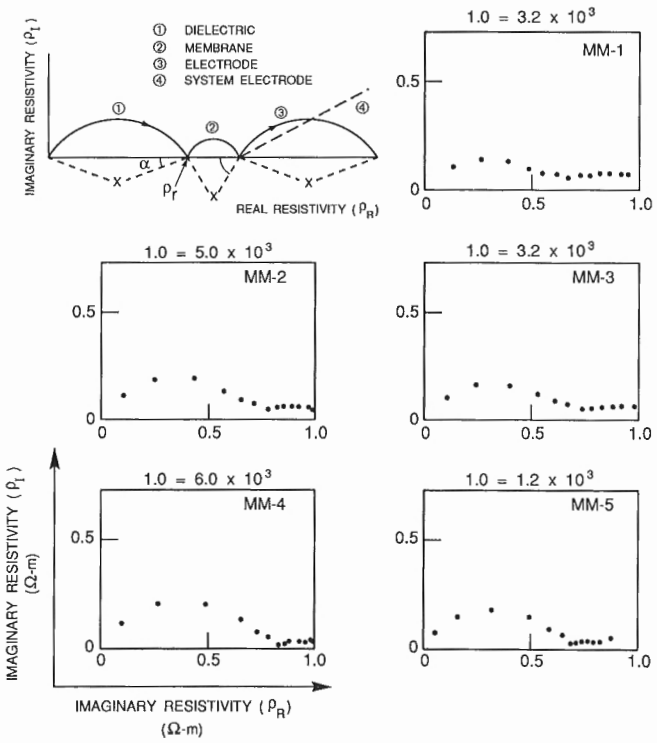

Figure 2. Three Electrical Polarization Mechanism model (after Katsube, 1975) and complex resistivity plots (1 - 10^6 Hz) for the 5 specimens, MM-1 to MM-5. Parameters and ρ_r are the distribution angle and bulk electrical resistivity, respectively. The error range for ρ_r is estimated to be 10-20%. The resistivity scales are indicated above each box containing the complex resistivity plots. For example, the scale of 1.0 for specimen MM-2 is equal to 5×10^3 Ωm.

rock for solutions of different salinities (NaCl: 0.02, 0.05, 0.10, 0.20 and 0.50 N), and then inserting the results into an equation derived from the Patnode and Wyllie (1950, Equation 1) equation:

$$1/F_a = 1/F + \rho_w/\rho_c \quad (5)$$

where

$F_a = \rho_r/\rho_w$

$\rho_c = F\rho_s d$

F_a = apparent formation-factor

ρ_c = bulk surface resistivity

ρ_s = surface resistivity

d = pore aperture.

Effective porosity, complex resistivity, and formation-factor were determined at room temperature conditions. The errors for these parameters are estimated to be generally in the ranges of 10%, 10 to 20%, and 20 to 40%, respectively (Wadden and Katsube, 1982; Katsube, 1981). The main source of error for determination of formation-factor is in the resistivity measurements and in the regression analysis when using equation (5). Further details of the measuring procedures can be found elsewhere (Katsube, 1981; Katsube and Walsh, 1987; Katsube and Salisbury, this volume).

EXPERIMENTAL RESULTS

The effective porosity (ϕ_E) is 3.25% (W_w=6.1967 g, W_D=6.1241 g, δ=2.740.04). Three sets of complex resistivity measurements were carried out on the five rectangular specimens. The results are listed in Table 3. Typical examples of the complex resistivity data are shown in Figure 2.

Bulk resistivity measurements at five different NaCl concentration were also carried out on all five rectangular specimens for formation-factor (F) determinations. Bulk resistivity measurements for specimen MM-3 were repeated at NaCl concentration of 0.5N and 0.02N due to concern of possible experimental procedural error. Results of all these measurements are listed in Table 4. First, the apparent formation-factor (F_a) was derived for each specimen. Then these values with the pore fluid resistivity values were inserted into equation (5) for determination of formation-factor (F) and surface resistivity (ρ_c) by use of the reduced major axis, RMS (Davis, 1986; Katsube and Agterberg, 1990). The results are shown in Figure 3, and the formation-factor values are listed in Table 5. The small differences seen between the RMS and the normal regression lines, NRL, reflect the relatively small errors for F and ρ_c. The data for the two resistivities, ρ_r and ρ_c, are also listed in Table 5. Similar data obtained by others for gneisses are listed in Table 6 for the purpose of comparison.

Table 3. Outline of bulk resistivity data

Specimens	Bulk Resistivity, ρ_r (10^3 Ωm)/t) Measurement (No. 1)	Measurement (No. 2)	Measurement (No. 3)	Mean
MM-1	1.73 (44:30)	2.15 (23:50)	2.36 (92:00)	2.1 ± 0.3
MM-2	2.58 (45:00)	3.92 (24:20)	3.95 (92:20)	3.5 ± 0.6
MM-3	2.38 (45:40)	2.38 (22:40)	2.64 (92:40)	2.5 ± 0.1
MM-4	7.46 (46:00)	5.05 (23:10)	4.40 (93:10)	5.5 ± 1.4
MM-5	0.396 (46:20)	0.837 (23:30)	0.419 (93:30)	0.55 ± 0.2

ρ_r : Determined where ρ_i shows a minimum closest to the left-most arc, since the right-hand side of the left-most arc never clearly intersected the horizontal axis for these measurements. The minimum was always at 1000 Hz, except for MM-4 (No. 1) which was at 300 Hz.

t : Saturation time (hours) prior to measurement.

Table 4. Bulk resistivities of the specimens, MM-1 to MM-5, for different NaCl solutions

(a): Formation-Factor Data

ρ_w	NaCl	Bulk Resistivity ρ_r (Ωm)				
(Ωm)	(N)	MM-1 (x10^3)	MM-2 (x10^3)	MM-3 (x10^3)	MM-4 (x10^3)	MM-5 (x10^3)
0.302	0.5	0.096	0.193	0.278*	0.426	0.035
0.602	0.2	0.215	0.341	0.372	0.670	0.086
1.37	0.1	0.317	0.618	0.772	0.906	0.129
2.32	0.05	0.750	1.241	1.041	1.895	0.215
5.46	0.02	1.076	1.601	1.359*	2.773	0.262

ρ_w: Fluid resistivity
N : NaCl concentration
* : Initial measurements were 0.152 and 1.066 for 0.5N and 0.2N, respectively.

(b): Error Data

ρ_w	NaCl	Error for ρ_r (Ωm)				
(Ωm)	(N)	MM-1 (x10^3)	MM-2 (x10^3)	MM-3 (x10^3)	MM-4 (x10^3)	MM-5 (x10^3)
0.302	0.5	0.004	0.01	0.02	0.01	0.001
0.602	0.2	0.02	0.04	0.02	0.05	0.004
1.37	0.1	0.04	0.04	0.05	0.09	0.03
2.32	0.05	0.1	0.2	0.05	0.3	0.02
5.46	0.02	0.4	0.4	0.3	0.1	0.02

Table 5. Formation-factor and other petrophysical data for sample no. PBA79-32, specimens MM-1 to MM-5

		ρ_r (x10^3 Ωm).					
Specimens	δ (g/mL)	mean	max.	min.	F (x10^2)	ρ_c (x10^3 Ωm)	ρ_c/F (Ωm)
MM-1 pf	2.75	2.1 ± 0.3	2.4	1.7	3.6 ± 0.4	2.1 ± 0.6	5.9
MM-2 pf	2.70	3.5 ± 0.6	4.0	2.6	6.9 ± 0.2	2.8 ± 0.2	4.1
MM-3 pf	2.68	2.5 ± 0.1	2.6	2.4	9.4 ± 0.1	1.8 ± 0.0	2.0
MM-4 vf	2.74	5.5 ± 1.4	7.5	4.0	12.9 ± 1.0	4.2 ± 0.5	3.2
MM-5 vf	2.65	5.3 ± 0.2	8.0	3.8	15.1 ± 0.4	3.7 ± 0.1	2.4

pf : measurements parallel to foliation
vf : measurements perpendicular to foliation
δ : specific density
ρ_r : bulk resistivity of the rock sample
F : formation-factor
ρ_c : bulk surface resistivity

DISCUSSION AND CONCLUSIONS

The effective porosity (ϕ_E) of 3.25% is a value rather large for a crystalline rock (Katsube, et al., 1985), probably a result of weathering. The bulk resistivity, formation-factor and surface resistivity values are in the range of 2000 to 5500 Ωm, 400 to 1500 and 2000 to 4500 Ωm, respectively, about 5 to 10 times smaller than those usually observed for these types of rocks (Table 6; Katsube et al., 1985; Katsube and Hume, 1987a,b, 1989). This indicates the possibility of strong surface conduction either due to electrically conductive minerals or clays lining the pores. The clay lining could be a result of weathering.

The values of all three parameters are generally 1.5 to 2 times larger in the direction perpendicular to the foliation compared to the other directions, clearly indicating a directional effect. These values of 1.5-2.2 exceed the error ranges for the three parameters (Table 5), particularly for formation-factor (F). The surface resistivities indicate a pore surface conduction effect in all three directions, an effect likely due to electronically conductive or clay minerals lining the pore surfaces. The complex resistivity plots indicate a strong pore surface polarization effect in the directions of the foliation. This effect is probably due to electronically conductive minerals lining the pores, most likely the grain boundary graphitic carbon previously recognized by Auger spectrometry. The strong pore surface polarization is identified by indications of large distribution angles, of the left-most arcs for some of the specimens in Figure 2.

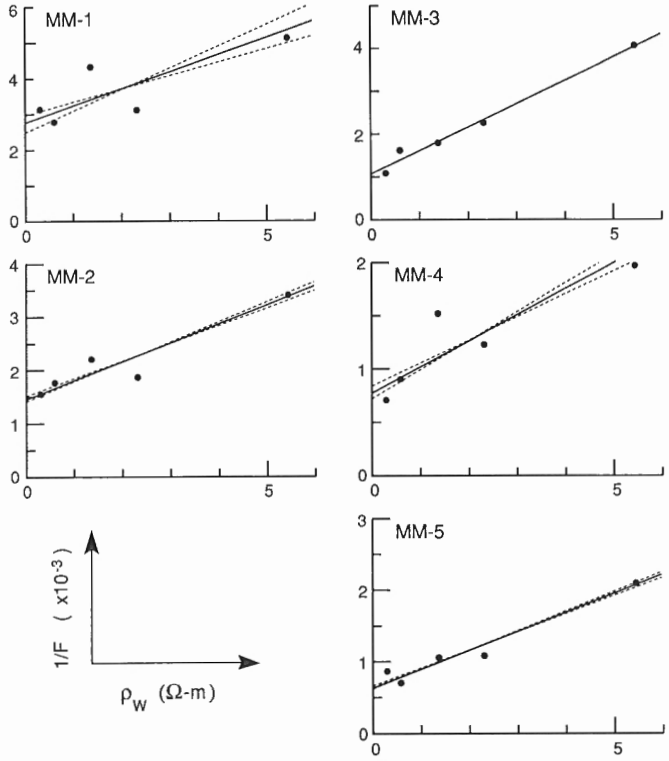

Figure 3. Reciprocal of apparent formation-factor (F_a) as a function of pore fluid resistivity (ρ_w). The solid lines are the reduced major axis (RMS) and the broken lines are the normal regression lines (NRL).

Table 6. Petrophysical properties of a suite felsic to mafic gneisses (Katsube and Hume, 1989)

Sample No.	F	ρ_r	ρ_c	ρ_s	Mineral Composition				
	- ($x10^3$) -				KF	PC	QZ	MAF	OP
CR 6-086	110	280	610	48.2	24.7	31.6	tr	36.4	3.9
6-093	13	7	7.5	8.6	15.3	55.0	7.1	21.9	0.,4
6-143	25	83	34	17.4	39.8	42.4	3.7	12.9	0.8
6-166	8.1	8.4	5.3	14.9	49.4	38.4	1.8	9.7	0.5
6-193	2.6	28	18	113	36.7	32.8	25.8	4.5	tr
6-227	33	200	170	40.9	0.0	54.9	tr	38.4	6.2
6-237	530	290	320	2.4	0.0	53.6	tr	40.4	5.4
6-245	0.2	0.14	0.29	0.24	0.0	50.0	5.0	35.0	5.0
6-286	230	350	490	12.8	0.0	48.9	0.0	45.3	5.5
6-301	2.0	2.8	2.4	2.17	11.4	54.7	7.1	24.4	tr
Units		(Ωm)	(Ωm)	(Ω)	(%)	(%)	(%)	(%)	(%)

F = Formation-factor
ρ_r = Bulk resistivity
ρ_c = Bulk surface resistivity
ρ_s = surface resistivity
KF = Potassium feldspars
PC = Plagioclase
QZ = Quartz
MAF = Mafic minerals
OP = Opaque minerals

Results of interest have been obtained by these measurements and will be used for studying the "broken conductor model" (Katsube and Mareschal, unpub. rep.), a model developed to represent the physical process by which an electrically conductive rock from the lower crust loses its conductivity as it is uplifted to the surface. The anisotropy observed in the Kapuskasing area will be addressed in the future, most likely when discussing the broken conductor model.

ACKNOWLEDGMENTS

Complex resistivity measurements were carried out by J. Frechette. The authors thank J.A. Percival (Geological Survey of Canada) for providing the sample and its mineral composition data used in this study, and for his constructive comments on this paper. The authors are grateful to W.S. Fyfe (University of Western Ontario) for the Auger spectrometry showing the existence of grain-boundary graphite films. The authors are also grateful to R.D. Kurtz (Geological Survey of Canada) for critically reviewing this paper and for his very helpful comments. Part of this study was supported by a "Quebec/Other Provincial" grant.

REFERENCES

Archie, G.E.
1942: The electrical resistivity log as an aid in determining some reservoir characteristics; Transactions of the American Institute of Mining, Metallurgical and Petroleum Engineers, v. 146, p. 54-67.

Bailey, R.C., Craven, J.A, Macnae, J., and Polzer, B.
1989: Imaging deep fluids in Archean crust; Nature, v. 340, p. 136-138.

Davis, J.C.
1986: Statistics and Data Analysis in Geology; John Wiley & Sons, p. 200-204.

Frost, B.R., Fyfe, W.S., Tazaki, K., and T. Chan
1989: Grain-boundary graphite in rocks and implications for high electrical conductivity in the lower crust; Nature, v. 340, p. 134-136.

Gauvreau, C. and Katsube, T.J.
1975: Automation in electrical rock property measurements; Report of Activities, Part A, Geological Survey of Canada, Paper 75-1A, p. 83-86.

Haak, V. and Hutton, R.
1986: Electrical resistivity in continental lower crust, in "The Nature of the Lower Continental Crust", (ed.) J.B. Dawson et al.; Geological Society of London Special Publications, v. 24, p. 35-49.

Hyndman, R.D.
1988: Dipping seismic reflectors, electrically conductive zones, and trapped water in the crust over a subducting plate; Journal of Geophysics Research, v. 93, p. 13391-13405.

Jones, A.G.
1981: On a type classification of lower crustal layers under precambrian regions; Journal of Geophysics, v. 49, p. 226-233.

Katsube, T.J.
1975: The electrical polarization mechanism model for moist rocks; Geological Survey of Canada, Paper 75-1C, p. 353-360.
1977: Electrical properties of rocks; in "Induced Polarization for Exploration Geologists and Geophysicists", Short Course Presented by the University of Arizona, Tucson, March 14-16, p. 15-44.
1981: Pore structure and pore parameters that control the radionuclide transport in crystalline rocks; Proceedings of the Technical Program, International Powder and Bulk Solids Handling and Processing, Rosemont, Illinois, p. 394-409.

Katsube, T.J. and Agterberg, F.P.
1990: Use of statistical methods to extract significant information from scattered data in petrophysics; in Statistical Applications in the Earth Sciences, (ed.) F.P. Agterberg and G.F. Bonham-Carter; Geological Survey of Canada, Paper 89-9, p. 263-270.

Katsube, T.J. and Collett, L.S.
1973: Measuring techniques for rocks with high permittivity and high loss; Geophysics, v. 38, p. 92-105.

Katsube, T.J. and Hume, J.P.
1987a: Pore structure characteristics of granitic rock samples from Whiteshell Research Area; in Geotechnical Studies at Whiteshell Research Area (RA-3), CANMET, Report MRL 87-52, p. 111-158.
1987b: Electrical properties of granitic rocks in Lac du Bonnet batholith; in Geotechnical Studies at Whiteshell Research Area (RA-3), CANMET, Report MRL 87-52, p. 205-220.
1989: Electrical resistivity of rocks from Chalk River; in Workshop Proceedings on "Geophysical and Related Geoscientific Research at Chalk River, Ontario", Atomic Energy of Canada Limited, Report AECL-9085, p. 105-114.

Katsube, T.J. and Salisbury, M.
1991: Petrophysical characteristics of surface core samples from the Sudbury structure; in Current Research, Part E; Geological Survey of Canada, Paper 91-1E.

Katsube, T.J. and Walsh, J.B.
1987: Effective aperture for fluid flow in microcracks; International Journal of Rock Mechanics and Mining Sciences and Geomechanics Abstracts, v. 24, p. 175-183.

Katsube, T.J., Percival, J.B., and Hume, J.P.
1985: Characterization of the rock mass by pore structure parameters; Atomic Energy of Canada Limited Technical record, TP-299, p. 375-413.

Kurtz, R.D., Macnae, J.C., and West, G.F.
1989: A controlled source, time-domain electromagnetic survey over an upthrust section of Archean crust in the Kapuskasing Structural zone; Geophysical Journal International, p. 195-203.

Mareschal, M.
1990: Electrical conductivity: the story of an elusive parameter, and of how it possibly relates to the Kapuskasing uplift (Lithoprobe, Canada); Exposed Cross-Sections of the Continental Crust, (ed.) M.H. Salisbury and D.M. Fountain; Kluwer Academic Publishers, Netherland, p. 453-468.

Mareschal, M., Smith, T., Macnae, J., Chakridi, R., and Aucoin, F.
1990: Conductivity model of the Groundhog River Block (Kapuskasing Uplift, Canada) based on a joint interpretation of MT, UTEM and Auger spectroscopy analysis of exposed rocks; presented at the 10th Workshop on Electromagnetic Induction in the Earth and Moon, August, Ensenada, Mexico, p. 429.

Patnode, H.W. and Wyllie, M.R.J.
1950: The presence of conductive solids in reservoir rocks as a factor in electric log interpretation; Transactions of the American Institute of Mining, Metallurgical and Petroleum Engineers, v. 189, p. 47-52.

Percival, J.A.
1983: High-grade metamorphism in the Chapleau-Foleyet area, Ontario; American Mineralogist, v. 68, p. 667-686.

Percival, J.A. and Card, K.D.
1983: Archean crust as revealed in the Kapuskasing uplift, Superior Province, Canada; Geology, v. 11, p. 323-326.
1985: Structure and evolution of Archean crust in central Superior Province, Canada; in Evolution of Archean Supercrustal Sequences, (ed.) L.D. Ayres, P.C. Thurston, K.D. Card, and W. Weber; Geological Association of Canada Special Paper, v. 28, p. 179-192.

Wadden, M.M. and Katsube, T.J.
1982: Radionuclide diffusion rates in crystalline rocks; Chemical Geology, v. 36, p. 191-214.

Petrophysical characteristics of surface core samples from the Sudbury structure, Ontario

T.J. Katsube and M. Salisbury[1]
Mineral Resources Division

Katsube, T.J. and Salisbury, M., 1991: Petrophysical characteristics of surface core samples from the Sudbury structure, Ontario; in Current Research, Part E; Geological Survey of Canada, Paper 91-1E, p. 265-271.

Abstract

Petrophysical properties of 14 surface rock samples representing north and south ranges of the four major lithologies in the Sudbury complex (Chelmsford, Onaping, Micropegmatite, and Norite) have been measured to assist geophysical interpretation and the understanding of the Sudbury structure.

Porosities are in the range of 0.1 to 1.7%, values common for igneous crystalline rocks (Norite and Micropegmatite) but very low for sedimentary rocks (Chelmsford and Onaping). Resistivities are in the range of 10^4 to $5x10^4$ Ωm for all formations except the Chelmsford, values common for igneous crystalline rocks but high for sedimentary rocks. They are very low (15 to 1400 Ωm) for the Chelmsford formation. Formation-factor and apparent tortuosity values increase towards the deeper formations, reflecting a more complex geological history. The low resistivity of the Chelmsford formation is due to electronic conduction of the pore surfaces, most likely a continuous inter-connected graphite lining.

Résumé

Les propriétés pétrophysiques de 14 échantillons de roche superficielle représentatifs des parties nord et sud des quatre grandes lithologies du complexe de Sudbury (grauwacke de Chelmsford, tuf de Onaping, micropegmatite et norite) ont été mesurées pour faciliter l'interprétation géophysique et l'étude de la structure de Sudbury.

Les porosités vont de 0,1 à 0,7 %, valeurs courantes pour des roches cristallines ignées (norite et micropegmatite), mais très faibles pour des roches sédimentaires (Chelmsford et Onaping). Les résistivités varient de 10^4 à 5 x 10^4 Ωm pour toutes les formations sauf celle de Chelmsford, valeurs courantes pour des roches cristalline ignées, mais élevées pour des roches sédimentaires. Les résistivités sont faibles, de 15 à 1400 Ωm, pour la formation de Chelmsford. Les valeurs du facteur de formation et de la tortuosité apparente augmentent avec la profondeur des formations, dénotant une histoire géologique plus complexe. La faible résistivité de la formation de Chelmsford est due à la conduction électrique des surfaces intersticielles, par la présence vraisemblablement d'un revêtement de graphite interconnecté.

[1] Atlantic Geoscience Center, Geological Survey of Canada, Bedford Institute of Oceanography, P.O. Box 1006, Dartmouth, N.S. B2Y 4A2

INTRODUCTION

Petrophysical properties of 14 rock samples representing north and south ranges of the four major lithologies in the Sudbury complex (sedimentary rocks: Chelmsford graywack and Onaping tuff; igneous rocks: Micropegmatite and Norite) have been measured. These samples are cores from the surface which have been used for magnetic studies (E.I. Tanczyk, pers. comm., 1991). The measurements consist of porosity, complex resistivity, bulk electrical resistivity, and pore surface electrical resistivity for all samples, and formation-factor for 8 of the 14 samples. The purpose of this study is to assist geophysical interpretation and improve the understanding of the geological structure of the Sudbury basin. This paper reports the results of these measurements which will be used for future analysis and interpretation related to the Sudbury structure.

METHOD OF INVESTIGATION

Mineralogy and sample preparation

Two cylindrical specimens were cut out from each of the 14 samples. The geometric characteristics of the specimens used for electrical measurements are listed in Table 1, their dimensions in the ranges of 2.4-2.5 cm for diameter and 0.4-0.9 cm for thickness. The geometric factor, K_G, is calculated for all specimens used for the electrical measurements:

$$K_G = (r_D/2)^2\pi/\ell \quad (1)$$

where r_D is the diameter and ℓ is the thickness of the specimen. The specimen not used for the electrical measurements is prepared for the effective porosity measurement.

Effective porosity measurements

Effective porosity in principle includes the pore volume of all interconnected pores, and is determined from the difference in weight between the oven-dried and water-saturated rock specimen (Katsube, 1981). Initially, a room-dried specimen is placed in a beaker in a vacuum chamber and vacuum is applied (10^{-4} Torr Hg) for 15 minutes in order to remove trapped air and gases. Then the specimen is vacuum-saturated with deionized-distilled water and immersed under vacuum for another 15 minutes in the same set up. After immersing the specimen for another 60 minutes under atmospheric pressure, it is removed from the water, and the surfaces are dried with tissue before its weight measured, using an analytical balance with a sensitivity of 0.1 mg. Subsequently, the specimen is heated at 105°C for 4 hours and then placed in a desiccator to cool to room temperature before its weight is measured again. The effective porosity, ϕ_E, is derived using the following equation:

$$\phi_E = \delta\,(W_w - W_D) / W_D \quad (2)$$

where W_w, W_D, and δ are the wet weight, dry weight and specific density, respectively. The dry weight (W_D) of the specimen and the weight difference between its wet and dry state are in the order of 7.0-10.7 g and 3-50 mg, respectively, so that the error for the porosity is less than 10%. A separate study showed the porosity variation within a sample to be 10% (Wadden and Katsube, 1982). Therefore, 10% is used to represent the error range for porosity.

Table 1. Dimensions of specimens cut out from the Sudbury samples for electrical measurements

Sample No.	r_D (cm)	ℓ (cm)	W (gm)	K_G (m)	δ (g/mL)
Sx,28-71	2.475	0.774	10.6178	0.062	2.86
Sx,27-62	2.480	0.708	9.6734	0.068	2.83
Sx,36-21	2.460	0.741	9.4054	0.064	2.67
Sx,37-51	2.485	0.693	9.0645	0.070	2.70
Sx,56-11	2.485	0.819	10.7151	0.059	2.70
Sx,51-41	2.493	0.818	10.6386	0.060	2.66
Sx,55-32	2.465	0.723	9.2855	0.066	2.69
BSW,139-A	2.470	0.724	9.6906	0.066	2.79
BSY,74-B	2.375	0.824	10.0169	0.054	2.73
Sx 76-31	2.463	0.463	5.7800	0.103	2.63
Sx 77-71	2.485	0.616	8.0960	0.079	2.70
Sx 78-61	2.475	0.940	12.1026	0.051	2.67
Sx,73-72	2.410	0.771	9.6547	0.059	2.74
Sx,75-72	2.475	0.681	9.0036	0.071	2.75

r_D = diameter
ℓ = thickness
W = weight
K_G = geometric factor
δ = specific density

Table 2. Results of the effective porosity measurements

Sample No.	Formation Name	δ (g/cc)	W_w (g)	W_D (g)	ϕ_E (%)
Sx,28-71	S-Nor	2.86	10.6184	10.6146	0.102
Sx,27-62		2.83	9.5577	9.5491	0.255
Sx,36-21	S-MP	2.67	9.4106	9.4002	0.295
Sx,37-51		2.70	9.0669	9.0621	0.143
Sx,56-11	S-Onp	2.70	10.7187	10.7125	0.156
Sx,51-41	Chl	2.66	10.6557	10.6367	0.476
Sx,55-32		2.69	9.3087	9.2813	0.794
BSW,139-A	N-Onp	2.79	7.2316	7.2268	0.185
BSY,74-B		2.73	5.3989	5.3917	0.365
Sx 76-31	N-MP	2.63	7.2276	7.1820	1.670
Sx 77-71		2.70	7.0159	7.0073	0.331
Sx 78-61		2.67	9.8728	9.8423	0.827
Sx,73-72	N-Nor	2.74	-	-	-
Sx,75-72		2.75	8.8320	8.8293	0.084

$\phi_E = \delta(W_w - W_D) / W_D$
W_w = wet weight
W_D = dry weight
δ = specific density
ϕ_E = effective porosity

N,S-Nor = north and south range Norite formations
N,S-MP = north and south range Micropegmatite formations
N,S-Onp = north and south range Onaping formations
Chl = Chelmsford formation

Complex resistivity measurements

The techniques used for the complex electrical resistivity and formation-factor measurements have been described previously (Katsube, 1981; Katsube and Walsh, 1987). First, the specimens are placed under vacuum for 15 minutes and then immersed in distilled water (still under vacuum) for 15 more minutes. The specimens are then allowed to stand in the distilled water (in covered beakers) for 24 hours under atmospheric pressure. Subsequently, they are placed in a capacity type sample-holder (Katsube and Collett, 1973) with a graphite electrode covering the two faces. The surfaces of the sides of the specimen are dried before measurement.

Table 3. Bulk resistivity data for the Sudbury samples

Sample No.	Name	Formation	ρ_r ($\times 10^4$ Ωm)	f (Hz)	N
Sx,28-71		S-Nor	4.9 ±1.2	3-10	3
Sx,27-62			1.2 ±20%	3	1
Sx,36-21		S-MP	1.8 ±0.8	3-10	3
Sx,37-51			3.2 ±1.1	3-30	3
Sx,56-11		S-Onp	0.95 ±0.23	100	3
Sx,51-41		Chl	0.015±0.004	-	3
Sx,55-32			0.141±0.006	1000	3
BSW,139-A		N-Onp	4.1 ±0.3	300-1000	3
BSY,74-B			1.9 ±20%	100	1
Sx 76-31		N-MP	1.1 ±20%	10	1
Sx 77-71			1.5 ±20%	10	1
Sx 78-61			3.9 ±20%	100	1
Sx,73-72		N-Nor	5.0 ±0.5	3-10	3
Sx,75-72			4.7 ±0.5	10	3

ρ_r = Bulk resistivity
F = Frequency at which ρ_r was determined
N = Number of measurements

N,S-Nor = north and south range Norite formations
N,S-MP = north and south range Micropegmatite formations
N,S-Onp = north and south range Onaping formations
Chl = Chelmsford formation

Table 4. Formation-factor, surface resistivity and bulk resistivities for different NaCl solutions for the Sudbury samples

Samples	ρ_{rn} ($\times 10^3$ Ωm)					F ±% ($\times 10^3$)	ρ_c ±% ($\times 10^4$) (Ωm)
ρ_w (Ωm)	0.302	0.602	1.37	2.32	5.46		
NaCl (N)	0.5	0.2	0.1	0.05	0.02		
Sx,28-71	6.6	13.6	7.0*	20.1*	48.6	28.0 ±10	6.3 ±10
Sx,36-21	1.4	3.0	3.8	9.0	9.4*	5.9 ±8.2	1.3 ±8.5
Sx,37-51	1.7	3.2	4.7	8.7	15.4	5.5 ±5.1	2.8 ±12
Sx,56-71	0.96	1.7	3.24	9.2	10.3	3.7 ±22	1.9 ±48
Sx,51-41	0.012	0.011	0.013	0.014	0.014	0.11±0.5	0.0014±0
Sx,55-32	0.50	0.7	0.99	2.8	3.6	1.5 ±30	0.53±40
Sx,73-72	4.2	9.2	31.4	39.2	67.2	19.7 ±44	14.7 ±110
Sx,75-72	5.5	10.8	21.0	57.6	69.4	22.1 ±26	14.7 ±68

ρ_w = pore fluid resistivity
ρ_{rn} = bulk resistivity of the rock for solutions of different salinities
F = formation-factor
ρ_c = surface resistivity
* : Initial results were 32.770, 24.700 and 8.412 for 0.1N, 0.05N and 0.02N.

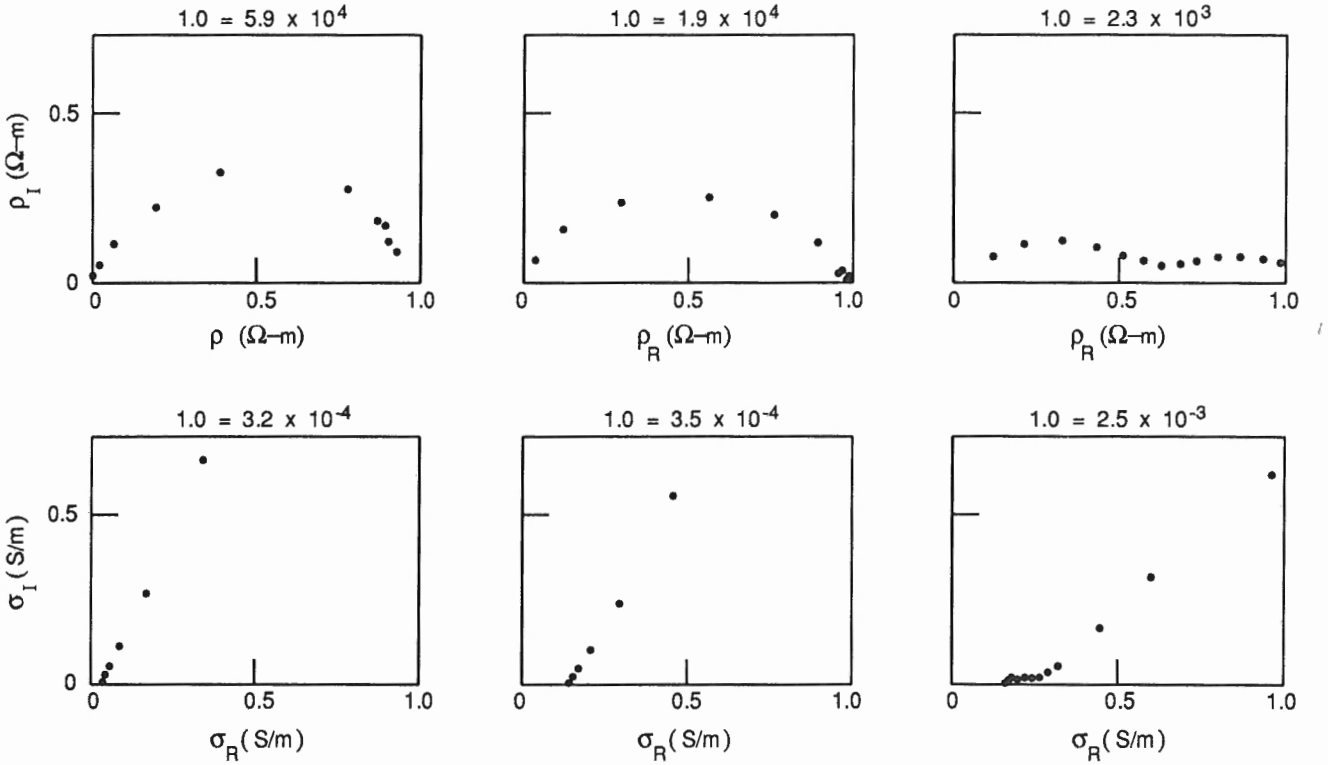

(a) Sx, 73-72 (b) Sx, 36-21 (c) Sx, 55-32

a - sample number Sx,73-72
b - sample number Sx,36-21
c - sample number Sx,55-32.

ρ_R = real resistivity
ρ_I = imaginary resistivity
σ_R = real conductivity

Figure 1. Typical examples of the complex resistivity plots for samples showing large, medium, and small values of bulk resistivity:

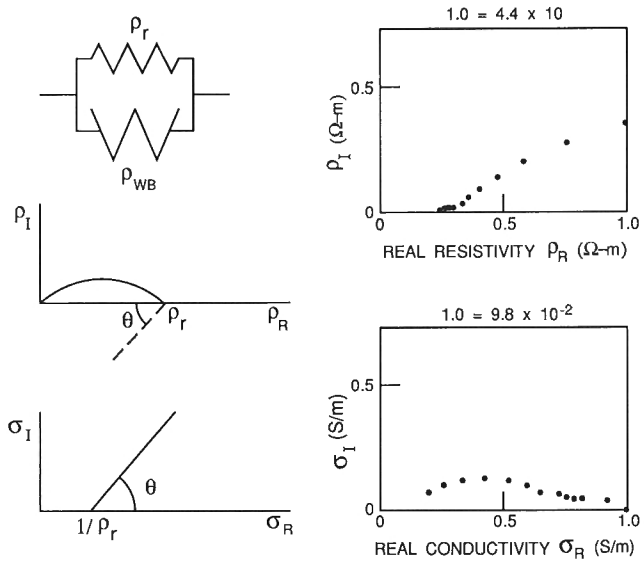

a - complex resistivity model (after Katsube, 1977),
b - complex resistivity plot for sample number Sx,51-41.

WB= Warburg impedance
ρR = real resistivity
σ_r = bulk rock resistivity
ρI = imaginary resistivity
σ_R = real conductivity
σ_I = imaginary conductivity
θ = distribution angle

Figure 2. Complex resistivity model and complex resistivity plot for a sample showing a very small value of bulk resistivity.

The sample-holder is then placed in an enclosed space in order to reduce movement of air around it. This is a precautionary measure to minimize evaporation of fluid from the rock pores. The sample holder is connected to an automatic electrical impedance system which measures the in-phase and out-of-phase components of the impedance at frequencies of 1.0 - 10^6 Hz, as described in Gauvreau and Katsube (1975). The complex resistivity, ρ* (Katsube, 1975) is equal to:

$$\rho^* = \rho_R + i\,\rho_I, \tag{3}$$

where ρ_R is the real resistivity and ρ_I is the imaginary resistivity, and is derived from the impedance measurement by

$$\rho^* = ZK_G. \tag{4}$$

When electrical resistivity is measured over these frequencies, dielectric polarization, Warburg impedance, and electrode polarization effects are reflected in the measurements (Katsube, 1975, 1977). A simple method applied to distinguish different mechanisms for improvement of the measurement accuracy is to use Cole-Cole plots where imaginary-resistivity (ρ_I) is plotted against real-resistivity (ρ_R) (Katsube and Walsh, 1987). Katsube (1975) considered plots consisting of three arcs (Fig. 2) and suggested that each arc includes the effect of different groups of electrical conduction mechanisms. It was proposed that the left-most arc reflects the effects of the dielectric constant, double layer, pore structure,

Table 5. Petrophysical data for the Sudbury samples

Sample No,Name	Formation	δ (g/c)	ϕ_e (%)	ρ_r (Ωm) x10^4	F x10^3	τ_a	ρ_c/ρ_r	ρ_c/F (Ωm)
Sx28-71	S-Nor	2.86	0.102	4.9	28.0	5.3	1.3	2.3
Sx27-62		2.83	0.255	1.2				
Sx36-21	S-MP	2.67	0.295	1.8	5.9	4.2	1.0	2.2
Sx37-51		2.70	0.143	3.2	5.5	2.8	1.0	5.1
Sx56-11	S-Onp	2.70	0.156	0.95	3.7	2.4	2.0*	5.1*
Sx51-41	Chl	2.66	0.476	0.0015	0.11	1.0	1.0	0.13
Sx55-32		2.69	0.794	0.14	1.5	3.5	3.8*	3.5*
BSW139A	N-Onp	2.79	0.185	4.1				
BSY74-B		2.73	0.365	1.9				
Sx76-31	N-MP	2.63	1.670	1.1				
Sx77-71		2.70	0.331	1.5				
Sx78-61		2.67	0.827	3.9				
Sx73-72	N-Nor	2.74		5.0	19.7*	-	2.9*	7.5*
Sx75-72		2.75	0.084	4.7	22.1	4.3	3.1*	6.7*

* : Error over 40%.
δ = specific density
ρ_r = bulk resistivity of the rock sample
ρ_c = surface resistivity
ϕ_e = effective porosity
F = formation factor
τ_a = apparent tortuosity

N,S-Nor = north and south range Norite formations
N,S-MP = north and south range Micropegmatite formations
N,S-Onp = north and south range Onaping formations
Chl = Chelmsford formation

and pore water chemistry. In accordance with this model, bulk rock resistivity, ρ_r, is determined from the point where the left arc intersects the horizontal axis.

Formation-factor measurements

The formation-factor, F, is derived by, measuring the bulk resistivity, ρ_{rn}, of the rock for solutions of different salinities, deriving F_a by taking the ratio of ρ_{rn} over ρ_W (Archie, 1942) for each saturating solution, and then inserting F_a and ρ_w into an equation derived from the Patnode and Wyllie (1950, Equation 1) equation:

$$1/F_a = 1/F + \rho_w/\rho_c \tag{5}$$

where

$F_a = \rho_{rn}/\rho_w$

$\rho_c = Fd\rho_s$

F_a = apparent formation-factor

ρ_w = pore fluid resistivity

ρ_c = bulk surface resistivity

ρ_s = surface resistivity

d = pore aperture.

The formation-factor is determined using this equation in order to eliminate the erroneous effect of the conductive layer on the pore surfaces that are present not only in sedimentary rocks, but also in crystalline rocks (Brace et al., 1965). Patnode and Wyllie (1950) and Waxman and Smits (1968) used NaCl solutions with concentrations ranging from 1N to distilled water, and 6.14 to 0.018N, respectively. The specimens for this study are placed under vacuum for 15 minutes, vacuum-saturated, and immersed in the saline

solution for 60 minutes. This procedure is similar to that used for the effective porosity measurements. The resistivities are measured over a frequency range of 10-10^3 Hz (Katsube, 1981; Katsube and Walsh, 1987). After the measurement is completed, the specimens are soaked in distilled water for approximately 5 to 10 hours several times (until the resistivity of the rinsed rock specimen generally rises to more than 10 times that of the rock saturated with the saline solutions) to rinse the saline solution from the rock pores, and then air-dried. The procedure described above is repeated using 0.02, 0.05, 0.10, 0.20 and 0.50 N NaCl solutions. The errors for the formation-factor measurements are generally estimated to be in the order of 20-40% (Katsube, 1981), with the main sources being in the resistivity measurements and in the regression analysis when using equation (5). The correlation coefficient, r, for the reciprocal of the apparent formation-factor ($1/F_a$) over the resistivity of the saturating fluids is generally in the order of 0.80 to 0.95. Measurements resulting in $r<0.8$, or that show a lack of linearity between the two parameters are usually eliminated. Values of F are determined by linear regression analysis, using the reduced major axis (Davis, 1986), RMA. The error range is determined by use of the two normal regression lines, NRL, y on x and x on y (Katsube and Agterberg, 1990).

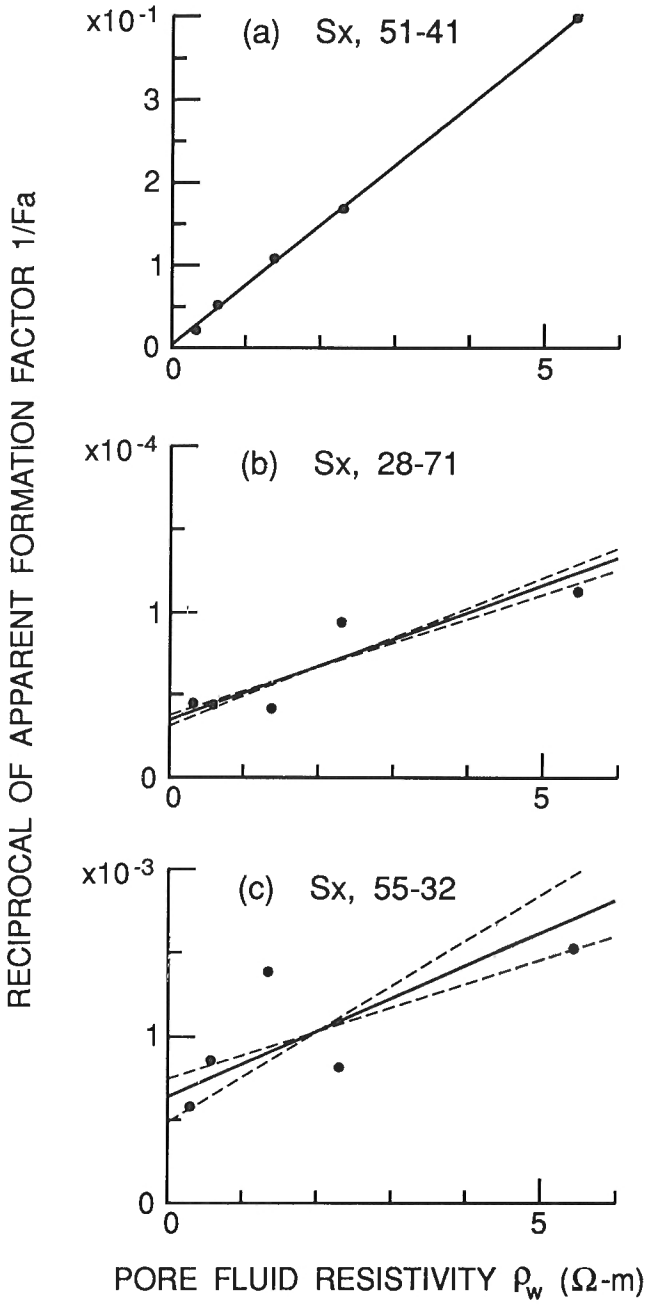

Figure 3. Typical examples of reciprocal of apparent formation-factor (F_a) as a function of pore fluid resistivity (ρ_w):

(a): sample number Sx,51-41 (r = 1.000)
(b): sample number Sx,28-71 (r = 0.905)
(c): sample number Sx,55-32 (r = 0.718).

Derived parameters

Another parameter found to be useful in studying the relationship between the physical and geological characteristics of rocks is the apparent tortuosity, τ_a. It is derived from the following equation (Ward and Fraser, 1967; Wadden and Katsube, 1982):

$$\tau_a = \sqrt{F\phi_E} \qquad (6)$$

Table 6. Resistivities of granites (Katsube and Hume,1989)

Rock Type	N	Resistivities Min.	Max.	($x10^4$, Ωm) Mean	Reference
WN	34	0.063	8.98	4.16	Katsube et al. (1985)
URL	65	0.504	6.14	2.48	Katsube et al. (1985)
Granite Azerbaidjan		-	-	3.0x10	Parkhomenko, (1967)
Granites	-	0.016	$3.6x10^2$	-	Beblo, (1982)
Aplite Granite (Boulder, Colorado)			-	$4.35x10^7$	Olhoeft, (1981)
Biotite Granite	-	-	-	$8.33x10^6$	Olhoeft, (1981)
Granite	-	-	-	$3.03x10^6$	Olhoeft, (1981)
Rhodonite- Wollastonite Garnet Skarn				1.4	Rzhevsky & Novik, (1971)
Quartz-porphyry				2.5	Rzhevsky & Novik, (1971)
Syenite	-	-	-	7.1	Rzhevsky & Novik, (1971)
Tremolite-Wollastonite Skarn	-	-	-	0.0154	Rzhevsky & Novik, (1971)

N = Number of Samples
Min. = Minimum values
Max. = Maximum values

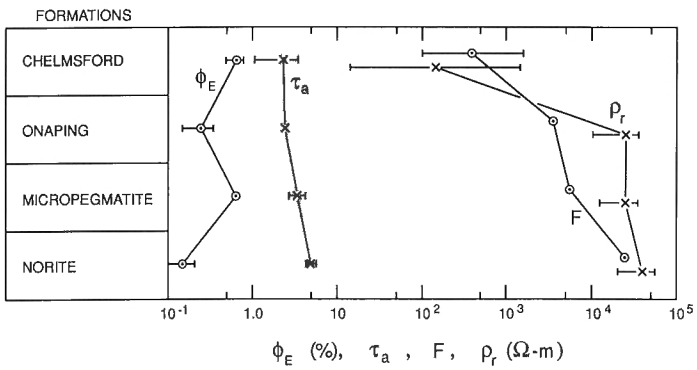

Figure 4. Effective porosity (ϕE), bulk resistivity (ρ_r), formation-factor (F) and apparent tortuosity (τ_a) for the four major formations of the Sudbury structure.

Measurement errors

Effective porosity, complex resistivity and formation-factor were determined at room temperature. The errors for these parameters are estimated to be generally in the ranges of 9 to 10%, 10 to 20% and 20 to 40%, respectively.

EXPERIMENTAL RESULTS

Effective porosity measurements were carried out on all 14 samples, and the results are listed in Table 2. Their values are in the range of 0.1-1.7%. Bulk resistivity (ρ_r) was also determined for all 14 samples. It was determined from complex resistivity measurements made over a frequency range of 1 to 10^6 Hz. These measurements were made on different specimens from those used for porosity measurements. The results are listed in Table 3. Typical examples of the complex resistivity plots are shown in Figure 1 and 2.

Bulk resistivity (ρ_r) measurements at five different NaCl concentrations (0.02 to 0.5N) were carried out on 8 of the samples for formation-factor (F) determinations. Measurements for sample Sx,28-71 were repeated at NaCl concentration of 0.05N and 0.1N, and at 0.02N for sample Sx,36-21. The results are listed in Table 4. The apparent formation-factor (F_a) was derived for each measurement of bulk resistivity (ρ_r) for all five NaCl solutions. Then, their values with the pore-fluid resistivity values were inserted into equation (5) for determination of formation-factor (F) and surface resistivity (ρ_c) by regression analysis using the reduced major axis. The results are listed in Table 4, and some of the results are shown in Figure 3.

It should be noted that the complex resistivity plot shown in Figure 2b for sample Sx,51-41 is very unusual. A comparison is made with the conventional equivalent circuit for a rock and its complex resistivity plot, which is shown in Figure 2a. Results of all the measurements are compiled in Table 5. Values obtained by other investigators for granites and gneisses are listed in Table 6 and 7 for the purpose of comparison.

DISCUSSION AND CONCLUSIONS

The porosities range from 0.16 to 0.79% for samples from the Chelmsford and Onaping formations, values very low for sedimentary rocks (Freeze and Cherry, 1979; Daly et al., 1966). The porosities of samples from the micro-pegmatite and Norite formations range from 0.1 to 1.7%, values common for igneous crystalline rocks (Katsube et al., 1985; Katsube and Hume, 1987). Bulk resistivities range from 10^4 to 5×10^4 Ωm for the samples from all formations except the Chelmsford, values common for igneous crystalline rocks but high for sedimentary rocks (Table 6 and 7). The values are very low for the Chelmsford formation: 15 to 1400 Ωm.

Effective porosities of the samples from the south range formations tend to be slightly lower than those from the north range samples (Table 2 and 5), suggesting that the south range formations may be tighter. Formation-factor (F) and apparent tortuosity (τ_a) values increase towards the deeper formations

Table 7. Petrophysical properties of a suite of felsic to mafic gneisses (Katsube and Hume, 1987)

Sample No.	F	ρ_r	ρ_c $-(\times10^3)-$	ρ_s	Mineral Composition KF	PC	QZ	MAF	OP
CR6-086	110	280	610	48.2	24.7	31.6	tr	36.4	3.9
6-093	13	7	7.5	8.6	15.3	55.0	7.1	21.9	0.4
6-143	25	83	34	17.4	39.8	42.4	3.7	12.9	0.8
6-166	8.1	8.4	5.3	14.9	49.4	38.4	1.8	9.7	0.5
6-193	2.6	28	18	113	36.7	32.8	25.8	4.5	tr
6-227	33	200	170	40.9	0.0	54.9	tr	38.4	6.2
6-237	530	290	320	2.4	0.0	53.6	tr	40.4	5.4
6-245	0.2	0.14	0.29	0.24	0.0	50.0	5.0	35.0	5.0
6-286	230	350	490	12.8	0.0	48.9	0.0	45.3	5.5
6-301	2.0	2.8	2.4	2.17	11.4	54.7	7.1	24.4	tr
Units		(Ωm)	(Ωm)	(Ω)	(%)	(%)	(%)	(%)	(%)

F = Formation-factor
ρ_r = Bulk resistivity
ρ_c = Bulk surface resistivity
ρ_s = surface resistivity
KF = Potassium feldspars
PC = Plagioclase
QZ = Quartz
MAF = Mafic minerals
OP = Opaque minerals

(Fig. 4), suggesting a more complex pore structure for the deeper rocks, probably reflecting the more complex geological history of the older rocks.

The fact that bulk resistivity (ρ_r) and surface resistivity (ρ_c) show very similar values for the samples with low error ranges (see ρ_r/ρ_c values in Table 5), suggests that the pore surface conduction plays a dominant role in determining the bulk resistivity (ρ_r) values of these rocks. Although this is the case for the samples from the south range formations, it may not be the case for those from the north range formations. The measurement errors for the south range samples are too large to confirm such a suggestion. The significant pore surface conduction in some of these rocks could be due to either electronically conductive minerals or clay lining the pore surfaces. Clay lining could be a result of weathering.

The very low resistivities of sample Sx,51-41 (Chelmsford formation) is likely due to strong pore surface conduction. Considering the very low bulk resistivity (ρ_r) and surface resistivity (ρ_c) values of 14-15 Ωm (Table 5) that are produced, electronically conductive minerals may be lining the pore surfaces. Since the density (δ = 2.66) of this sample is not particularly large, graphite lining is suggested. The unusual complex resistivity plot (Figure 2) for this sample is another possible indication of the existence of electronically conductive minerals in this sample.

These measurements contain interesting results that will be useful for future analysis and interpretations of geological and geophysical data (e.g., surface electromagnetic surveys) related to the Sudbury structure.

ACKNOWLEDGMENTS

Complex resistivity measurements were carried out by J. Frechette (Geological Survey of Canada) and F. Aucoin (Ecole Polytechnique), and the formation-factor measurements were carried out by F. Aucoin. We thank E.I. Tanczyk (Geological Survey of Canada) for supplying the samples used in this study. The authors are grateful to C.J. Mwenifumbo (Geological Survey of Canada) for critically reviewing this paper.

REFERENCES

Archie, G.E.
1942: The electrical resistivity log as an aid in determining some reservoir characteristics; Transactions of the American Institute of Mining, Metallurgical and Petroleum Engineers, v. 146, p. 54-67.

Beblo, M.
1982: Electrical properties; in Landolt-Bornstein Numerical Data and Functional Relationships in Science and Technology, Physical Properties of Rocks, v. 1, Subvolume b, G. Angenheister, New York, p. 239-307.

Brace, W.F., Orange, A.S., and Madden, T.R.
1965: The effect of pressure on the electrical resistivity of water-saturated crystalline rocks; Journal of Geophysical Research, v. 70 (22), p. 5669-5678.

Daly, R.A., Manger, E.G., and Clark, S.P. Jr.
1966: Density of rocks Sec.4 (p.23); in Handbook of Physical Constants; Geological Society of America, Inc. Memoir 97, p. 19-26.

Davis, J.C.
1986: Statistics and Data Analysis in Geology; John Wiley & Sons, p. 200-204.

Freeze, R.A. and Cherry, J.A.
1979: Groundwater; Prentice Hall, New Jersey, 604 p.

Gauvreau, C. and Katsube, T.J.
1975: Automation in electrical rock property measurements; Report of Activities, Part A, Geological Survey of Canada, Paper 75-1A, p. 83-86.

Katsube, T.J.
1975: The electrical polarization mechanism model for moist rocks; Geological Survey of Canada, Paper 75-1C, p. 353-360.

1977: Electrical properties of rocks; in "Induced Polarization for Exploration Geologists and Geophysicists", Short Course Presented by the University of Arizona, Tucson, March 14-16, p. 15-44.

1981: Pore structure and pore parameters that control the radionuclide transport in crystalline rocks; Proceedings of the Technical Program, International Powder and Bulk Solids Handling and Processing, Rosemont, Illinois, p. 394-409.

Katsube, T.J. and Agterberg, F.P.
1990: Use of statistical methods to extract significant information from scattered data in petrophysics; in Statistical Applications in the Earth Sciences, (ed.) F.P. Agterberg and G.F. Bonham-Carter; Geological Survey of Canada, Paper 89-9, p. 263-270.

Katsube, T.J. and Collett, L.S.
1973: Measuring techniques for rocks with high permittivity and high loss; Geophysics, v. 38, p. 92-105.

Katsube, T.J. and Hume, J.P.
1987a: Pore structure characteristics of granitic rock samples from Whiteshell Research Area; in Geotechnical Studies at Whiteshell Research Area (RA-3), CANMET, Report MRL 87-52, p. 111-158.

1987b: Electrical properties of granitic rocks in Lac du Bonnet batholith; in Geotechnical Studies at Whiteshell Research Area (RA-3), CANMET, Report MRL 87-52, p. 205-220.

1989: Electrical resistivity of rocks from Chalk River; in Workshop Proceedings on "Geophysical and Related Geoscientific Research at Chalk River, Ontario", Atomic Energy of Canada Limited, Report AECL — 9085, p. 105-114.

Katsube, T.J. and Walsh, J.B.
1987: Effective aperture for fluid flow in microcracks; International Journal of Rock Mechanics and Mining Sciences and Geomechanics Abstracts, v. 24, p. 175-183.

Katsube, T.J., Percival, J.B., and Hume, J.P.
1985: Characterization of the rock mass by pore structure parameters; Atomic Energy of Canada Limited Technical record, TP-299, p. 375-413.

Olhoeft, G.R.
1981: Electrical properties of rocks; in Physical Properties of Rocks and Minerals, v. II-2, (ed.) Y.S. Touloukian, W.R. Judd, and R.F. Roy; New York, p. 257-329.

Parkhomenko, E.I.
1967: Electrical Properties of Rocks; Plenum Press, New York, N.Y., 277 p.

Patnode, H.W. and Wyllie, M.R.J.
1950: The presence of conductive solids in reservoir rocks as a factor in electric log interpretation; Transactions of the American Institute of Mining, Metallurgical and Petroleum Engineers, v. 189, p. 47-52.

Rzhevsky, V. and Novik, G.
1971: The physics of rocks; MIR Publishers, Moscow, 320 p.

Wadden, M.M. and Katsube, T.J.
1982: Radionuclide diffusion rates in crystalline rocks; Chemical Geology, v. 36, p. 191-214.

Ward, S.H. and Fraser, D.C.
1967: Conduction of electricity in rocks; in Mining Geophysics, Volume II, Society of Exploration Geophysics, and Mining Geophysics Volume Editing Committee, Society of Exploration Geophysics, Tulsa, Oklahoma, p. 197-223.

Waxman, M.H. and Smits, L.J.M.
1968: Electrical conductivities in oil-bearing shaly sands; transactions of the Society of Petroleum Engineers Journal, v. 243, p. 107-122.

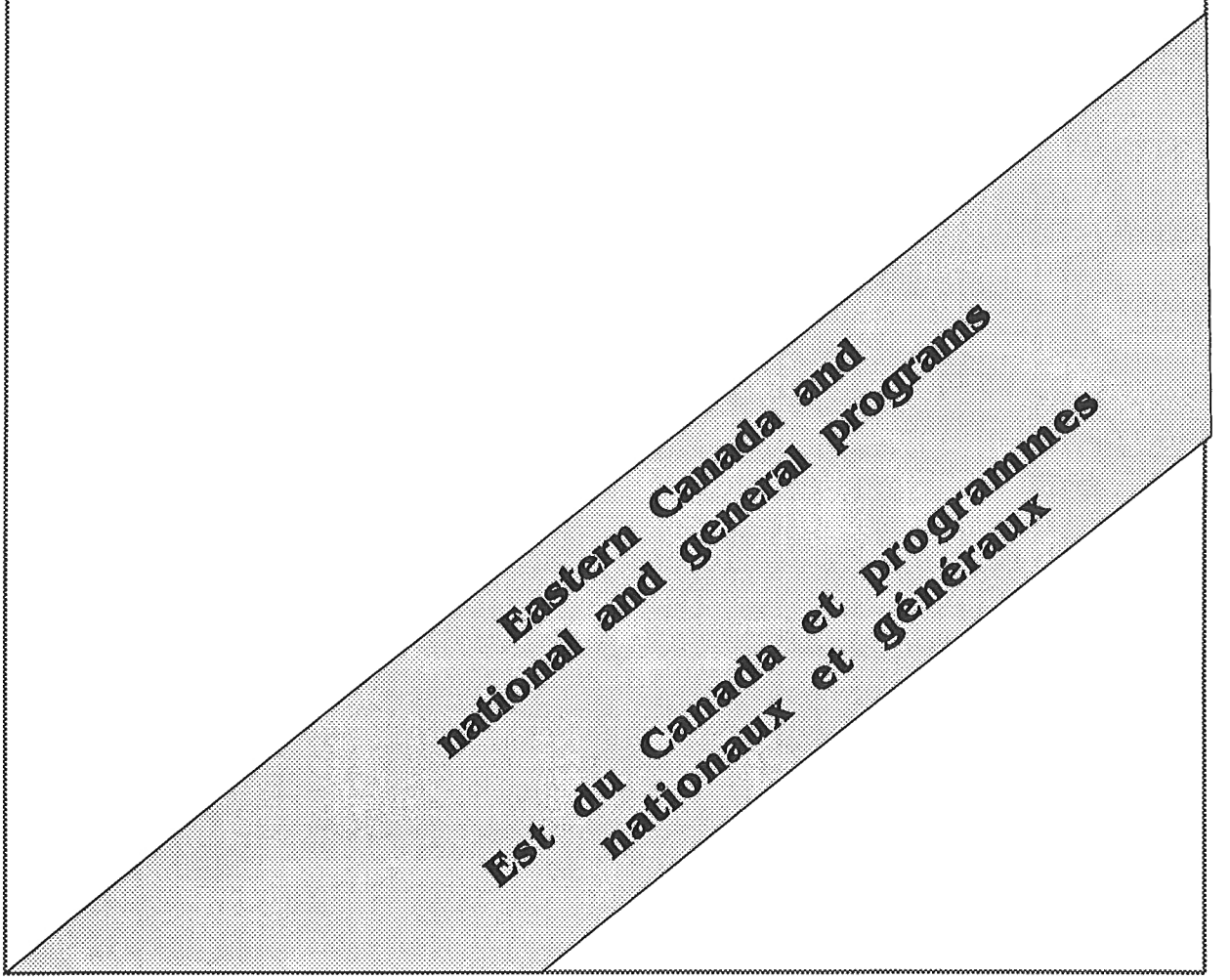
Eastern Canada and
national and general programs
Est du Canada et programmes
nationaux et généraux

The Canadian geomagnetic reference field 1990

L.R. Newitt and G.V. Haines
Geophysics Division

Newitt, L.R. and Haines, G.V., 1991: The Canadian geomagnetic reference field 1990; in Current Research, Part E; Geological Survey of Canada, Paper 91-1E, p. 275-281.

Abstract

The 1990 revision of the Canadian Geomagnetic Reference Field (CGRF) has been produced using the technique of spherical cap harmonic analysis over a spherical cap of half angle 30° centred over Canada. The secular variation was modelled with a spatial index of 7 and a temporal degree of 3. All main field data, consisting of Canadian vector aeromagnetic and MAGSAT vector satellite data, were updated to 1990 using the integrated secular variation model. The main field analysis was carried out with spatial index 16, after values of the International Geomagnetic Reference Field (IGRF), evaluated at 1990, were subtracted from the updated data. The CGRF 1990 is applicable to the time interval 1960 to 1995.

Résumé

La révision en 1990 du Champ géomagnétique canadien de référence (CGCR) s'est faite à l'aide de la technique d'analyse par harmoniques sphériques en calotte, la calotte considérée ayant un demi-angle de 30° et étant centrée sur le Canada. La variation séculaire a été modélisée selon un indice spatial de 7 et un degré temporel de 3. Toutes les valeurs de champ principal, à savoir les données vectorielles canadiennes mesurées à l'aide des méthodes aéromagnétiques et les données vectorielles MAGSAT enregistrées par satellite, ont été mises à jour pour l'année 1990 en utilisant le modèle intégré de variation séculaire. L'analyse du champ principal s'est faite selon un indice spatial de 16, une fois que les valeurs du Champ géomagnétique international de référence (IGRF), ramenées à 1990, aient été retranchées des données mises à jour. Le CGCR de 1990 peut être utilisé sur l'intervalle de temps s'étendant de 1960 à 1995.

INTRODUCTION

Information about magnetic declination has been presented in the form of contour charts since at least the eighteenth century. Edmund Halley's declination chart of the Atlantic Ocean, published in 1701, is a prime example.

The first magnetic charts of what is now Canada were published by J.H. Lefroy based primarily on his epic magnetic survey from 1842 to 1844 (Lefroy, 1883). However, it was not until 1922 that magnetic declination charts of Canada were produced on a regular basis (Dawson and Dalgetty, 1966). Regular charting of the other elements of the magnetic field did not start until much later; inclination and total intensity charts have been produced regularly only since 1955 (Dawson and Dalgetty, 1966).

All early magnetic charts of Canada were produced by hand-contouring observations which had been updated in some manner to the epoch of the chart. The 1965 magnetic charts were the first to be produced with the aid of a computer (Dawson and Dalgetty, 1966). However, the computer was used only to facilitate the jobs of updating and gridding the data. The gridded data were still hand-contoured.

The charts of 1970 were the first to be produced from a prior mathematical analysis of the data; in this case, a spherical harmonic analysis was used (E. Dawson, pers. comm., 1973). These charts also saw the first application of machine contouring of the grid values derived from the model. For the 1975 charts, polynomial models were derived for four overlapping areas before contouring (Dawson and Newitt, 1977). However, in both these cases, the production of a mathematical model was viewed primarily as an intermediate step toward the production of the charts.

By the time the 1980 magnetic declination chart was produced, it was realized that users needed better information than could be obtained by hand-scaling a chart. This requirement could be fulfilled by providing them with values derived directly from a mathematical model of the magnetic field. The 1980 declination chart was based on spherical harmonic analyses of the north (X) and east (Y) components of the magnetic field separately (Dawson et al., 1981). By performing the analyses on gridded data, a maximum degree and order of 180 was obtained, enabling considerable detail to be shown on the resultant chart. However, since the resultant models each contained 32 760 coefficients, it was too cumbersome to use them for the routine calculation of magnetic declination values. The method also suffered from another serious difficulty. It was not a spherical harmonic analysis in the normally accepted sense; that is, it was not an expansion of the potential from which the magnetic field elements could be obtained through derivation. Rather, it was a method of function fitting which required each element to be fitted separately. Thus three models would be required for a full description of the field, and the mathematical relationships which apply to potential fields were ignored.

The development of spherical cap harmonic analysis (SCHA) by Haines (1985a) enabled for the first time the production of a mathematical model of the magnetic field and its secular variation over Canada which could easily be used for routine calculations. The method was used to produce the Canadian Geomagnetic Reference Field for 1985 (Haines and Newitt, 1986) and its successor, the Canadian Geomagnetic Reference Field 1987.5 (Newitt and Haines, 1989).

With the advent of SCHA, the model, rather than the chart, became the primary product and source of information. The model allows the quick and automatic determination of precise values of the magnetic field elements at any point and time.

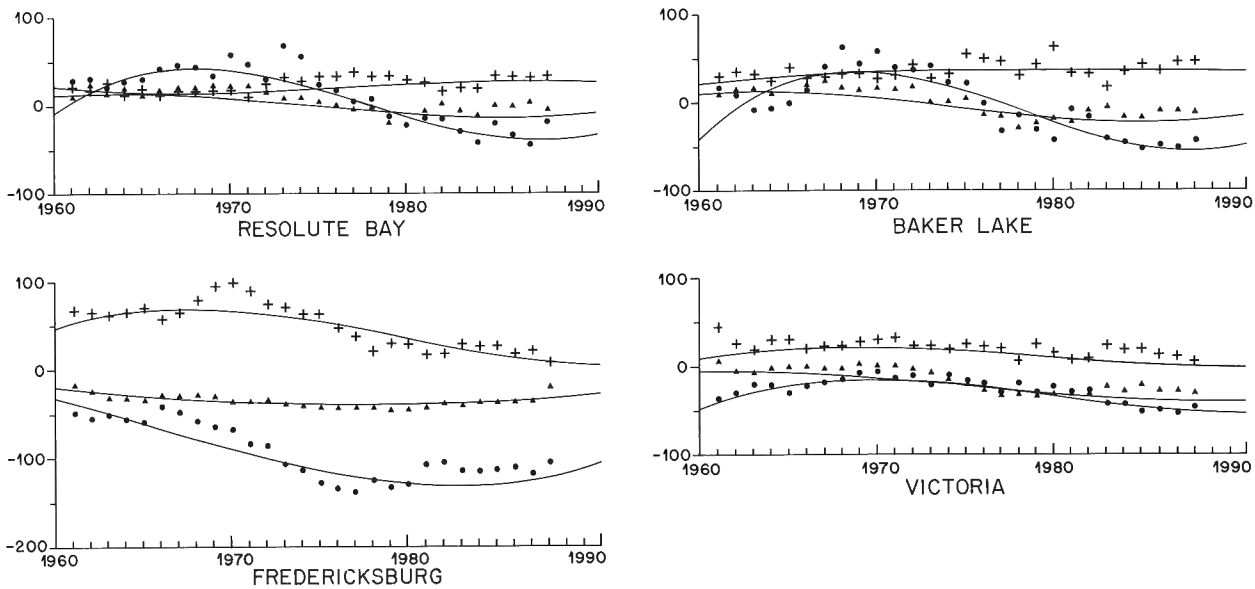

Figure 1. First differences of the X (pluses), Y (triangles), and Z (circles) components from four North American observatories. The corresponding secular variation curves derived from the spherical cap harmonic model are given by the solid lines.

Table 1. Coefficients of spherical cap harmonic fit to aeromagnetic and Magsat data over Canada and adjacent areas updated to 1990.0, after subtraction of IGRF 1985 extrapolated to 1990. Coefficients $g^m_{k,0}$ and $h^m_{k,0}$ refer to index k and order m. "Constant" is the Schmidt normalizing constant for the associated Legendre function of order m and degree $n_k(m)$.

k	m	$n_k(m)$	Constant	$g^m_{k,0}$	$h^m_{k,0}$
0	0	0.0000	0.100000E+01	0.000	
1	0	4.0837	0.100000E+01	3.940	
1	1	3.1196	0.253621E+01	-152.553	-35.097
2	0	6.8354	0.100000E+01	0.000	0.000
2	1	6.8354	0.517746E+01	452.437	50.750
2	2	5.4928	0.612537E+01	13.280	-188.386
3	0	10.0385	0.100000E+01	0.000	
3	1	9.7121	0.721601E+01	-768.652	-77.446
3	2	9.3733	0.170110E+02	-17.157	569.208
3	3	7.7524	0.154891E+02	17.085	-3.330
4	0	12.9083	0.100000E+01	0.000	
4	1	12.9083	0.947928E+01	995.386	63.632
4	2	12.3720	0.290691E+02	8.303	-1134.270
4	3	11.8074	0.533354E+02	-23.412	0.000
4	4	9.9589	0.398615E+02	0.000	-5.590
5	0	16.0248	0.100000E+01	1.027	
5	1	15.8215	0.115415E+02	-1013.290	-38.237
5	2	15.6154	0.456895E+02	0.000	1778.610
5	3	14.9180	0.105995E+03	13.549	0.000
5	4	14.1778	0.162625E+03	0.000	0.000
5	5	12.1334	0.103486E+03	-2.005	0.000
6	1	18.9364	0.137460E+02	779.207	12.382
6	2	18.5830	0.641554E+02	0.000	-2174.680
6	3	18.2219	0.190927E+03	-4.100	-3.710
6	4	17.3910	0.364976E+03	2.530	0.000
6	5	16.5041	0.486587E+03	0.000	0.000
6	6	14.2861	0.270001E+03	0.000	-4.668
7	1	21.8702	0.158221E+02	-464.803	0.000
7	2	21.7210	0.870680E+02	0.000	2110.870
7	3	21.2461	0.300181E+03	0.000	0.000
7	4	20.7588	0.734755E+03	0.000	0.000
7	5	19.8121	0.121018E+04	0.000	2.819
7	6	18.7979	0.143591E+04	-4.561	2.365
8	1	24.9514	0.180025E+02	182.408	0.000
8	2	24.6858	0.111915E+03	0.000	-1657.320
8	4	23.8390	0.126951E+04	0.000	0.663
8	7	21.0663	0.419235E+04	-1.344	0.000
8	8	18.5472	0.185281E+04	0.000	-2.073
9	1	27.8979	0.200874E+02	-40.888	0.000
9	2	27.7807	0.141168E+03	0.000	988.606
9	4	27.0470	0.209140E+04	4.014	0.000
9	5	26.3784	0.501966E+04	0.000	-1.434
10	2	30.7474	0.172387E+03	0.000	-455.496
10	3	30.5325	0.876491E+03	0.000	-0.757
10	4	30.0829	0.318566E+04	-2.590	0.000
10	8	26.8711	0.384162E+05	1.551	0.000
10	10	22.7683	0.127842E+05	0.000	-2.293
11	0	34.0120	0.100000E+01	1.234	
11	2	33.8193	0.207993E+03	5.647	137.241
11	4	33.2235	0.471946E+04	0.000	-0.417
11	9	29.1761	0.117952E+06	0.000	1.589
11	10	27.7627	0.996787E+05	1.350	0.000
12	1	36.9669	0.265041E+02	2.769	0.000
12	2	36.7886	0.245582E+03	0.000	-21.831
12	6	35.2710	0.625103E+05	1.710	0.000
12	8	33.7718	0.242271E+06	0.000	0.795
12	12	26.9619	0.884337E+05	0.000	-3.108
13	0	40.0102	0.100000E+01	-0.531	
13	4	39.3438	0.922032E+04	4.287	0.000
13	6	38.4664	0.104918E+06	-0.684	0.000
13	9	36.1810	0.834895E+06	-0.588	0.000
13	12	32.1619	0.802105E+06	4.442	0.000
14	1	42.9715	0.307525E+02	-1.029	-0.401
14	3	42.6643	0.236389E+04	0.000	-0.779
14	4	42.3494	0.123446E+05	-9.722	0.000
14	5	42.0320	0.506746E+05	-0.410	0.000
14	6	41.5359	0.165915E+06	0.000	1.029
14	8	40.3169	0.100244E+07	0.000	-2.027
14	9	39.5844	0.188373E+07	0.000	1.777
14	12	35.9940	0.321758E+07	-8.887	-1.727
14	13	34.3470	0.226154E+07	-1.043	0.000
15	2	45.8662	0.379827E+03	-0.607	0.000
15	4	45.4313	0.163099E+05	9.922	-0.730
15	7	44.1294	0.751154E+06	0.528	0.000
15	8	43.5694	0.186492E+07	0.000	1.617
15	9	42.7989	0.381372E+07	0.000	-3.841
15	10	42.0100	0.667923E+07	0.000	0.396
15	11	40.9382	0.938057E+07	1.989	0.000
15	12	39.8232	0.111063E+08	9.418	0.000
15	13	38.2408	0.953823E+07	0.000	-1.786
15	14	36.5239	0.635452E+07	0.000	-0.582
15	15	33.2160	0.161204E+07	0.000	-0.919
16	0	48.9749	0.100000E+01	0.307	
16	1	48.9749	0.350000E+02	0.000	0.598
16	3	48.7056	0.350375E+04	0.000	-0.391
16	4	48.4311	0.210193E+05	-4.529	1.219
16	5	48.1549	0.995458E+05	0.000	0.280
16	6	47.7278	0.380260E+06	0.000	0.281
16	7	47.2962	0.121828E+07	0.000	0.965
16	9	46.0801	0.742617E+07	0.000	2.693
16	11	44.4162	0.232234E+08	-1.497	0.799
16	12	43.2911	0.307483E+08	-5.299	0.000
16	13	42.1198	0.345010E+08	0.000	1.852
16	14	40.4771	0.281031E+08	0.924	0.000
16	15	38.6935	0.178002E+08	-1.073	0.000

However, charts still have their uses. They form a visual presentation of the magnetic field pattern (at a given epoch and altitude) and their continued publication is likely for the foreseeable future.

The 1990 revision of the Canadian Geomagnetic Reference Field (CGRF) is described in this paper. The methods used are similar to those described by Haines (1985b) and Haines and Newitt (1986). The computer programs used for the following analysis have been described by Haines (1988).

SECULAR VARIATION MODEL

The secular variation model serves two purposes: it permits the updating of data gathered at different times to a common epoch for the main field analysis; it also allows the main field model to be extrapolated forward and backward in time.

The secular variation model produced for the CGRF 1985 was a spherical cap harmonic model of maximum spatial index 4 and temporal degree 2 (Haines, 1985b). The area of the analysis was a spherical cap of 30° radius centred at 65°N, 85°W, and the input data comprised first differences of the north (X), east (Y), and vertical (Z) component values from 24 North American observatories and 138 North American repeat stations in the time span 1960 to 1983.

The secular variation model for the CGRF 1987.5 followed the same basic procedure but with the following differences introduced to improve the fit and to improve spatial and temporal interpolation and extrapolation in areas of sparse data (Newitt and Haines, 1989): (i) The number of observatories and repeat stations used in the analysis increased from 24 to 29 and from 138 to 150 respectively, and included some stations outside the cap boundary.

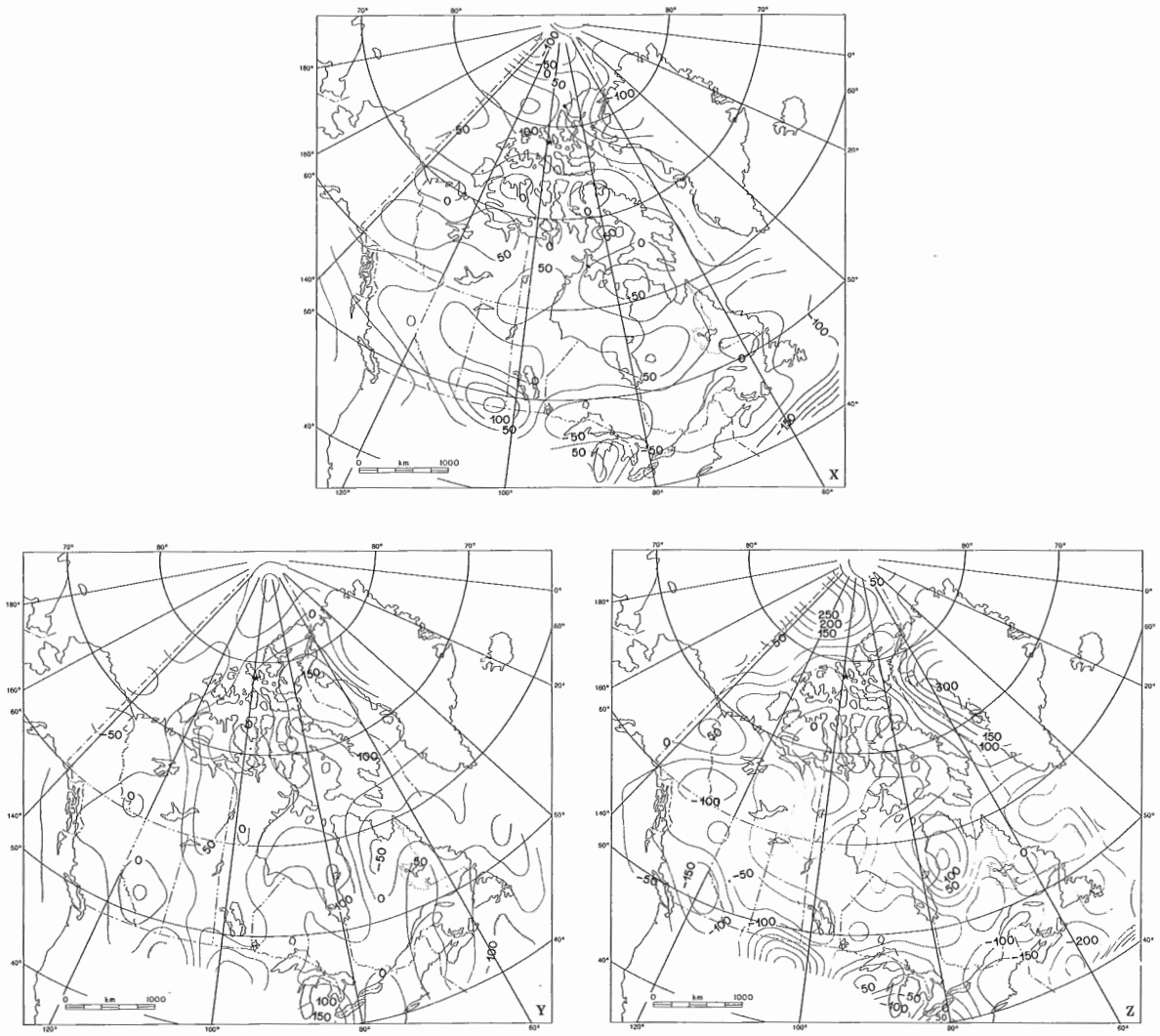

Figure 2. North (X), east (Y), and vertical (Z) residuals at sea level derived from the spherical cap analysis of aeromagnetic and Magsat data. Values are relative to the IGRF 1985 evaluated at 1990.

(ii) Simulated observatories, whose first differences were derived from the DGRF/IGRF models (IAGA Division 1 Working Group 1), were added at 16 locations in oceanic areas where there were no data. (iii) The spatial index was increased from 4 to 5.

A concern with both the 1985 and 1987.5 models has been the rather poor predictive capability of either model past its epoch. This is a common problem when extrapolating on the basis of a polynomial, and it limits the useful lifetime of the model. In an attempt to improve both the fit of the new model near 1990 and its ability to extrapolate reasonably beyond 1990 the following modifications were made for the present analysis.

i) The data set was supplemented by the addition of the latest observatory annual means and repeat station values. In addition, several new U.S. observatories were added to the data set, along with some previously unused repeat station observations. In all, data from 33 observatories and 155 repeat stations were used. The time span of the data was from 1960 to 1989; observatory annual means for 1988 were available from 26 of the observatories; 1989 values were available from 11 Canadian repeat stations. In all, there were 3444 component first differences. As for the 1987.5 model, 16 simulated observatories with data ranging from 1960 to 1985 were added to the data set.

ii) The data series for each observatory were artificially extended by repeating the 1988 first difference values from 1989 to 1993. This "encourages" the model to give a more linear prediction of the secular variation in the time period 1988 to 1993 than it would otherwise give. Comparing secular variation plots from models derived from data with and without these additions showed that adding these artificial data resulted in a more reasonable extrapolation in the time period 1988 to 1993. However, it must be realized that this procedure is subjective since it is based on the assumption that the secular variation will remain constant over the time interval 1988 to 1993.

iii) Because of the improved fit in the time interval 1988-1993 it was practicable to perform the final analysis with a spatial index of 7 and a temporal index of 3. This compares with a spatial index of 5 and a temporal index of 2 used for the 1987.5 model. The standard error of estimate was 10.1 nT/a.

Sample secular variation curves for four sample observatories are shown in Figure 1. These may be compared to similar plots given by Newitt and Haines (1989).

UPDATING MAIN FIELD DATA

The main field data are the same as those used for the production of both the CGRF 1985 and the CGRF 1987.5 and have been described in detail by Haines and Newitt (1986). Briefly, they consist of two data sets: 3 component aeromagnetic observations made between 1965 and 1976 averaged in 127 km x 127 km cells, a total of 4350 component observations; and selected quiet time Magsat data, a total of 5662 component observations. To update these data, the secular variation model coefficients were first integrated. Then, for each observation location, the difference was

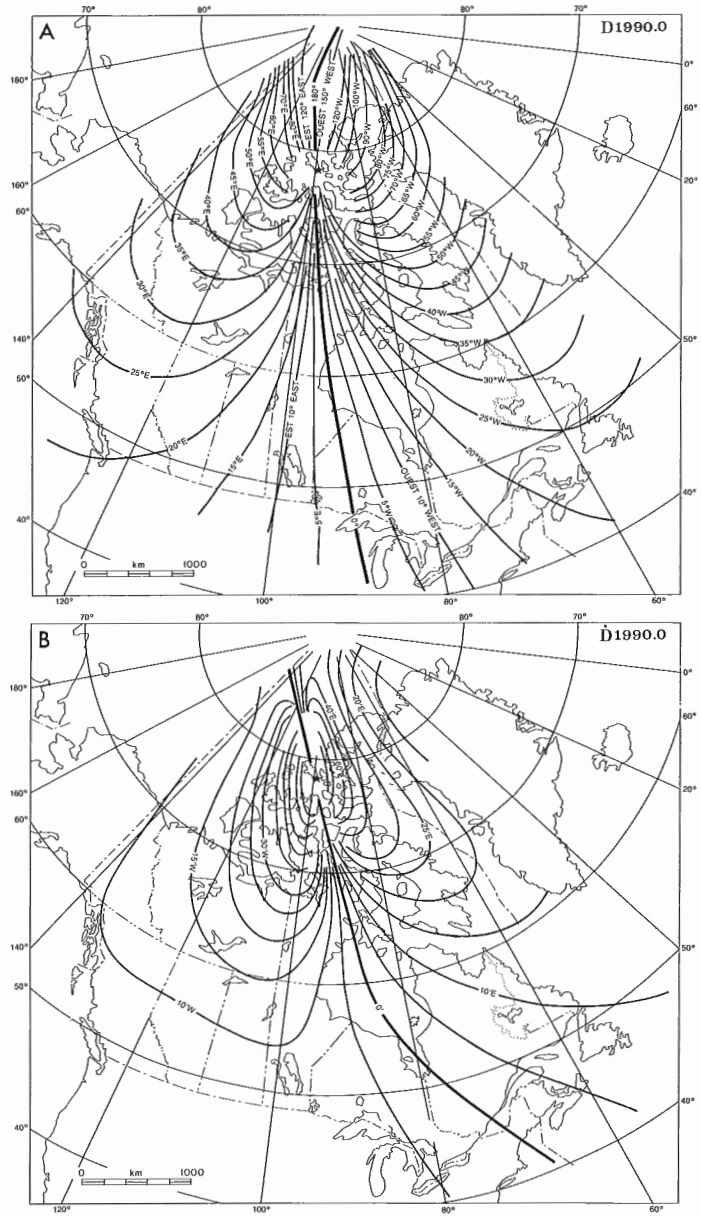

Figure 3. (**A**) Magnetic declination (D) at 1990.0 in degrees east or west of true north and (**B**) annual change (Ḋ) in minutes per year east or west, at sea level, from the CGRF 1990.

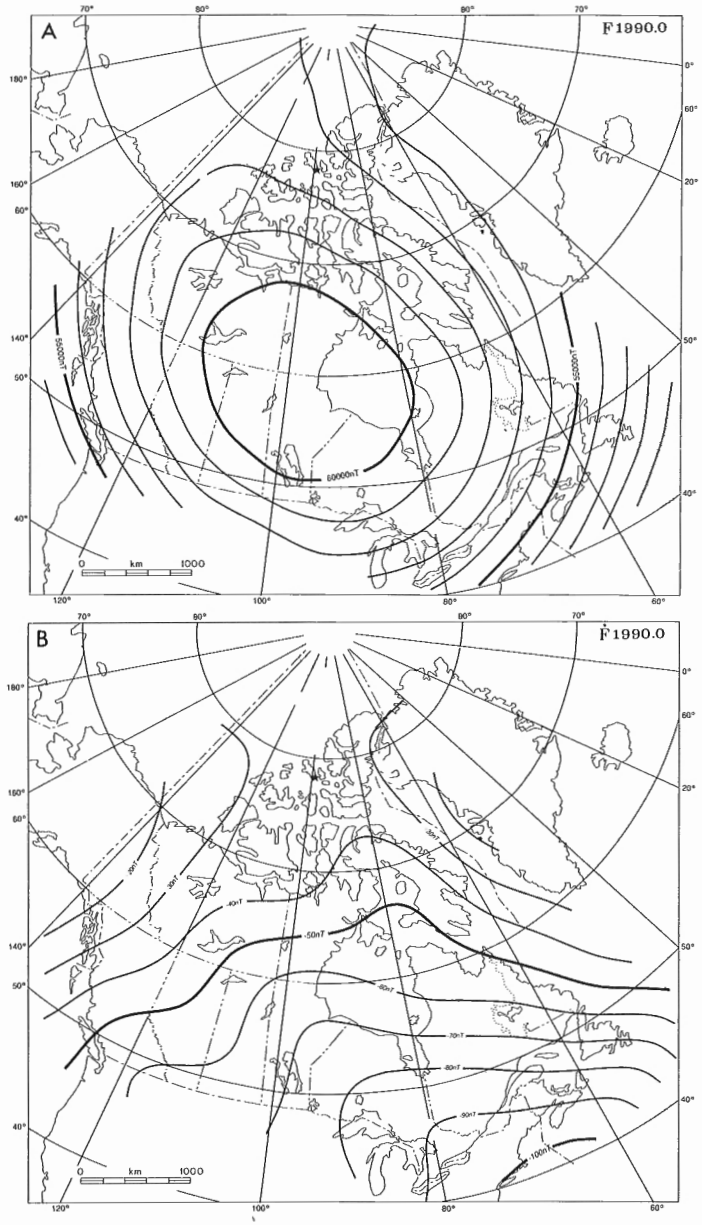

Figure 4. (**A**) Magnetic total intesity (F) at 1990.0 in nanoteslas and (**B**) annual change (F) in nanoteslas per year, at sea level, from the CGRF 1990.

calculated between the values given by the integrated model at 1990 and at the time of the observation. This difference was added to the observation to update it to 1990.

MAIN-FIELD ANALYSIS

The method used for the main-field analysis is similar to that described by Haines and Newitt (1986). First, residual values were calculated by subtracting from each observation the corresponding value calculated from the IGRF 1985 (IAGA Division 1, Working Group 1, 1986) updated to 1990. The resulting residuals were then transformed to a new spherical co-ordinate system centred on a pole at 65°N, 85°W.

The maximum spatial indéx of the spherical harmonic analysis was set at 16, the same as for the previous two models. At an F level of 3, 87 of the 289 possible coefficients were found to be significant. The standard error of estimate for the model was 66.8 nT. The model coefficients are given in Table 1. The coefficients of the integrated secular variation model, which are combined with the main field coefficients, are given in Table 2.

Plots of the X, Y, and Z component residuals derived from the model are given in Figure 2. These plots show short-wavelength core fields as well as broad scale crustal anomalies which are not depicted by world models such as the IGRF. The Canadian Geomagnetic Reference Field 1990 is a combination of the IGRF 85, evaluated at 1990, and the spherical cap harmonic model of the residual field along with the integrated secular variation terms. Charts of the declination (D) and total intensity (F) and inclination (I) components are shown in Figures 3 and 4 and 5. Charts of D, F, and I have been published as part of the Geophysical Atlas of Canada series at a scale of 1:10 000 000 (Newitt and Haines, 1990a,b,c).

The pole position derived from the CGRF 1990, and shown on the charts is 78.26°N, 104.00°W. This compares with a position of 77.76°N, 103.69°W derived from the IGRF 1985 updated to 1990. The last observed position was 77.0°N, 102.3°W in 1983.9 (Newitt and Niblett, 1986).

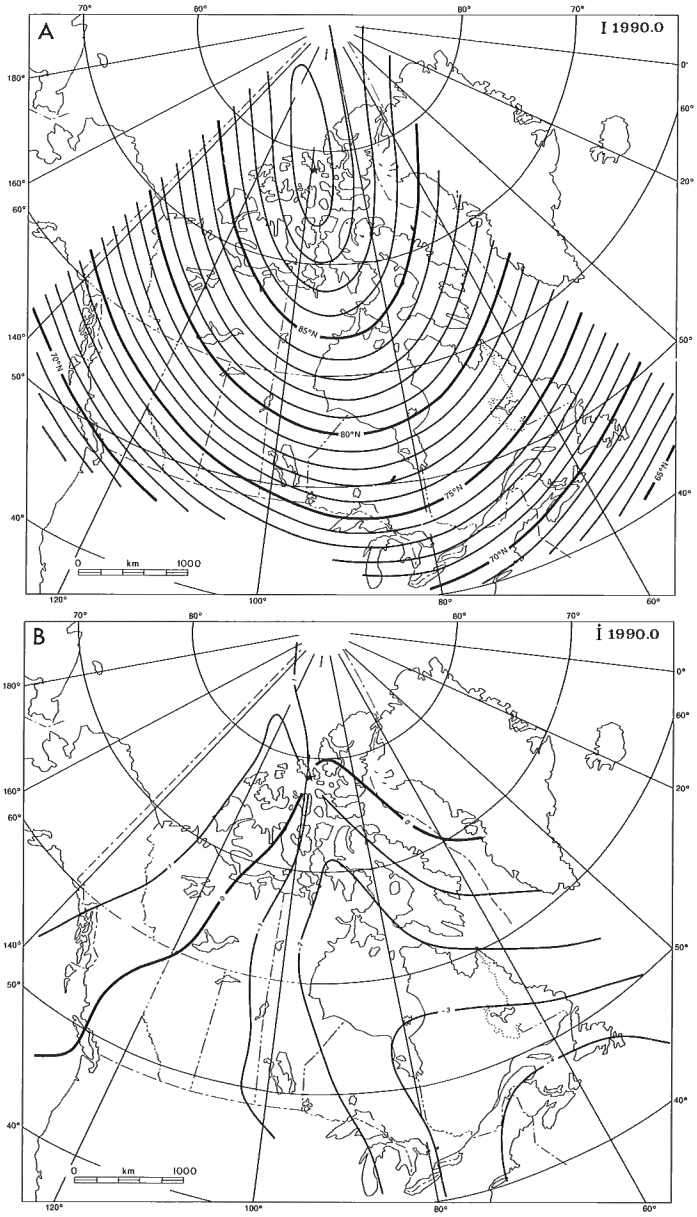

Figure 5. **(A)** Magnetic inclination (I) at 1990 in degrees north or downward and (**B**) annual change (İ), in minutes per year, at sea level, from CGRF 1990.

MAGNETIC INFORMATION RETRIEVAL PROGRAM

Information concerning the magnetic field, derivable from main field models, is required by a variety of users such as federal and provincial government agencies, educational institutions, industry, and the general public. The information is used in a variety of ways: for example, on aeronautical, topographic, marine, and geological charts; for runway headings and navigational aids; in land and legal surveys; in directional drilling and in aligning satellite receivers.

The Magnetic Information Retrieval Program (MIRP) has been developed to enable users to obtain magnetic field values quickly and easily. MIRP is an interactive computer program resident on one of the Geophysics Division's computers. It is accessible using a microcomputer and modem over the commercial telephone network.

MIRP is able to provide the user with values of any magnetic field element and its annual change calculated from the CGRF 1990 for locations within Canada and adjacent areas. Optionally, the IGRF can be used to calculate magnetic field values for points outside Canada. A complete description of MIRP is given in Newitt et al. (1990).

Table 2. Coefficients of (integrated) spherical cap harmonic fit to secular variation of Canada and adjacent areas relative to 1990.0. Second subscript of coefficient refers to degree of temporal polynomial.

k	m	$g^m_{k,1}$	$h^m_{k,1}$	$g^m_{k,2}$	$h^m_{k,2}$	$g^m_{k,3}$	$h^m_{k,3}$	$g^m_{k,4}$	$h^m_{k,4}$
0	0	805.212		-2133.660		-4421.170		-2317.480	
1	0	288.157		276.897		-643.388		-480.977	
1	1	658.761	333.090	-169.371	-304.683	0.000	-493.076	136.406	-159.062
2	0	-124.345		-223.119		-208.055		-122.209	
2	1	-291.487	-382.857	0.000	-48.698	0.000	-133.601	123.905	-74.194
2	2	142.083	282.898	0.000	-175.786	-59.083	0.000	0.000	95.623
3	0	29.354		47.095		0.000		0.000	
3	1	256.738	366.483	0.000	0.000	-106.881	0.000	-78.383	0.000
3	2	0.000	-244.150	0.000	72.497	0.000	-66.128	-3.400	-69.561
3	3	-187.627	74.974	-88.767	7.293	0.000	0.000	0.000	0.000
4	0	0.000		0.000		14.485		0.000	
4	1	-154.933	-291.324	0.000	0.000	9.635	0.000	0.000	0.000
4	2	0.000	248.416	0.000	-37.845	0.000	0.000	0.000	12.272
4	3	122.009	-38.062	0.000	0.000	0.000	0.000	32.344	0.000
4	4	-13.660	27.663	17.835	0.000	0.000	-6.712	0.000	0.000
5	0	0.000		0.000		0.000		0.000	
5	1	75.023	191.267	0.000	0.000	0.000	0.000	0.000	0.000
5	2	0.000	-187.180	0.000	0.000	11.590	0.000	13.765	0.000
5	3	-104.855	23.509	0.000	0.000	0.000	0.000	-26.096	0.000
5	4	24.706	-4.576	0.000	0.000	0.000	0.000	0.000	0.000
5	5	0.000	0.000	0.000	0.000	0.000	0.000	0.000	0.000
6	1	-22.441	-85.714	0.000	0.000	0.000	0.000	0.000	0.000
6	2	0.000	99.458	0.000	0.000	0.000	0.000	0.000	0.000
6	3	64.295	-9.445	0.000	0.000	-18.297	0.000	0.000	0.000
6	4	-18.847	0.000	0.000	0.000	0.000	0.000	0.000	0.000
6	5	0.000	2.672	0.000	0.000	0.000	0.000	0.000	0.000
6	6	0.000	-4.098	3.912	0.000	0.000	0.000	0.000	-5.269
7	1	0.000	25.882	0.000	0.000	0.000	0.000	0.000	0.000
7	2	0.000	-30.595	0.000	0.000	0.000	0.000	0.000	0.000
7	3	-24.774	0.000	-7.320	0.000	0.000	0.000	0.000	0.000
7	4	9.818	0.000	0.000	0.000	0.000	0.000	0.000	0.000
7	5	0.000	0.000	0.000	0.000	0.000	0.000	0.000	0.000
7	6	0.000	0.000	0.000	0.000	0.000	0.000	0.000	0.000

REFERENCES

Dawson, E. and Dalgetty, L.C.
1966: Magnetic charts of Canada for epoch 1965.0; Publications of the Dominion Observatory, v. 31, no. 9.

Dawson, E. and Newitt, L.R.
1977: An analytical representation of the geomagnetic field in Canada for 1975. Part I: The main field; Canadian Journal of Earth Sciences, v. 14, p. 477-487.

Dawson, E., Newitt, L.R., Nandi, A., and Nagy, D.
1981: A spherical harmonic approach to mapping the magnetic declination in Canada for 1980; Earth Physics Branch Geomagnetic Series no. 21.

Haines, G.V.
1985a: Spherical cap harmonic analysis; Journal of Geophysical Research, v. 90, p. 2583-2591.
1985b: Spherical harmonic analysis of the geomagnetic secular variation over Canada 1960-1983; Journal of Geophysical Research, v. 90, p. 12563-12574.
1988: Computer programs for spherical cap harmonic analysis of potential and general fields; Computers and Geosciences, v. 14, p. 413-447.

Haines, G.V. and Newitt, L.R.
1986: Canadian geomagnetic reference field 1985; Journal of Geomagnetism and Geoelectricity, v. 38, p. 895-921.

IAGA Division 1, Working Group 1
1986: International Geomagnetic Reference Field revision 1985; Geophysical Journal of the Royal Astronomical Society, v. 85, p. 217-220.

Lefroy, J.H.
1883: Diary of a magnetic survey of a portion of the Dominion of Canada; Longmans, Green and Company, London, 192 p.

Newitt, L.R. and Haines, G.V.
1989: A Canadian geomagnetic reference field for epoch 1987.5; Journal of Geomagnetism and Geoelectricity, v. 41, p. 249-260.
1990a: Magnetic declination chart of Canada 1990; Geological Survey of Canada, Canadian Geophysical Atlas — Map 10 scale 1:100 000 000.
1990b: Total intensity chart of Canada 1990; Geological Survey of Canada, Canadian Geophysical Atlas — Map 8, scale 1:100 000 000.
1990c: Magnetic inclination chart of Canada 1990; Geological Survey of Canada, Canadian Geophysical Atlas — Map 9, scale 1:10 000 000.

Newitt, L.R. and Niblett, E.R.
1986: Relocation of the north magnetic dip pole; Canadian Journal of Earth Sciences, v. 23, p. 1062-1067.

Newitt, L.R., Haines, G.V., and Coles, R.L.
1990: The magnetic information retrieval program; Geophysics Division, Geological Survey of Canada, Internal Report no. 90-3, 78 p.

Radon decay products over Canadian lakes

R.L. Grasty, P.B. Holman, and A.B. Silis
Mineral Resources Division

Grasty, R.L., Holman, P.B., and Silis, A.B., 1991: Radon decay products over Canadian lakes; in Current Research, Part E; Geological Survey of Canada, Paper 91-1E, p. 283-289.

Abstract

Radon (^{222}Rn) daughter concentrations over Canadian lakes have been calculated from airborne gamma ray survey data. The airborne system was calibrated at three airports on large areas of uniform ground whose uranium concentrations were determined using a calibrated portable gamma ray spectrometer.

Daytime summer airborne measurements showed regional differences in ^{222}Rn daughter concentrations. Measurements over lakes in the prairie regions of Manitoba and Saskatchewan gave mean values of approximately 4 to 5 Bq/m^3, significantly higher than the levels of 1 to 2 Bq/m^3 found in eastern Canada. Small concentrations of decay products of thoron (^{220}Rn) were also found over all lakes surveyed.

Résumé

Les concentrations des produits de filiation du radon (^{222}Rn) au-dessus de lacs canadiens ont été calculées à partir de données de levé aériens gamma. Le système aéroporté a été étalonné dans trois aéroports sur des grandes étendues de terrain uniforme dont les concentrations d'uranium ont été déterminées à l'aide d'un spectromètre gamma portatif étalonné.

Les mesures aériennes diurnes d'été ont révélé des écarts régionaux entre les concentrations des produits de filiation du ^{222}Rn. Les mesures au-dessus de lacs de la régions des prairies du Manitoba et de la Saskatchewan ont révélé des titres moyens d'environ 4 à 5 Bq/m^3, valeurs sensiblement plus élevées que celles de 1 à 2 Bq/m^3 observées dans d'autres régions du Canada. De faibles concentrations de produits de désintégration du thoron (^{220}Rn) ont aussi été observées au-dessus de tous les lacs survolés.

INTRODUCTION

In airborne gamma ray surveys there are three sources of background radiation that contribute to the airborne measurement. They are the radioactivity of the aircraft and its equipment, cosmic radiation, and airborne radioactivity due to decay products of ^{222}Rn.

In monitoring background radiation, the standard Geological Survey of Canada (GSC) procedure has been to fly over lakes at the beginning and end of each survey flight. Since the concentrations of radioactive nuclides in lakes are several orders of magnitude lower than in most crustal material, the activity measured over a lake will be the total background contribution from all three sources. Fortunately, in most of Canada, lakes are abundant and the background values can be updated during the course of the survey.

In the last few years, the GSC has carried out a variety of different research programs in airborne gamma ray spectrometry which have involved surveys in the prairie regions of Manitoba and Saskatchewan where lakes are not so abundant. The GSC is also frequently involved in airborne gamma ray surveys overseas where there are few lakes. An alternative procedure for measuring atmospheric background was therefore required.

In 1987, upward-looking detectors, shielded from ground radiation by the main detectors were installed in the GSC aircraft for continuously monitoring atmospheric backgrounds. Measurements over lakes were still carried out, as part of the upward detector calibration procedure (IAEA, 1991). Figure 1 shows a schematic diagram of the detector assembly flown by the GSC. Three standard energy windows from the main downward-looking detectors are used for monitoring potassium, uranium, and thorium in the ground (IAEA, 1976). A uranium window from the upward-looking detectors monitors background variations in the air during the course of the survey flight. A cosmic ray window which records all interactions above 3 MeV in the main detectors is used to monitor cosmic ray increases of the potassium, uranium, and thorium windows with aircraft altitude (IAEA, 1991).

Evidence for the presence of ^{222}Rn decay products in the air is clearly shown in Figure 2. The measurements were taken over lakes during the course of an airborne survey flown in northern Manitoba in 1990. The slope of the line, the increase in the potassium window count rate per unit increase in the uranium window count rate, has a value of 0.8. This is the same as the potassium-to-uranium window ratio for a pure uranium spectrum (commonly called the stripping ratio) (Løvborg, 1984). The potassium and uranium window count rate variations are due to changes in the concentration of ^{214}Bi, a decay product of ^{222}Rn in the uranium decay chain which emits gamma ray photons at several energies around 1760 keV.

This paper describes the procedure to convert the airborne gamma-ray measurements over lakes to standard units of Becquerels per cubic meter (Bq/m^3) for ^{222}Rn decay products. The procedures are then applied to overwater gamma ray measurements from different areas of Canada made during the last three years.

CALIBRATION - THEORY

Introduction

This section describes the theoretical approach to converting the overwater background measurements to standard units of Bq/m^3 of ^{222}Rn decay products. The procedure is to

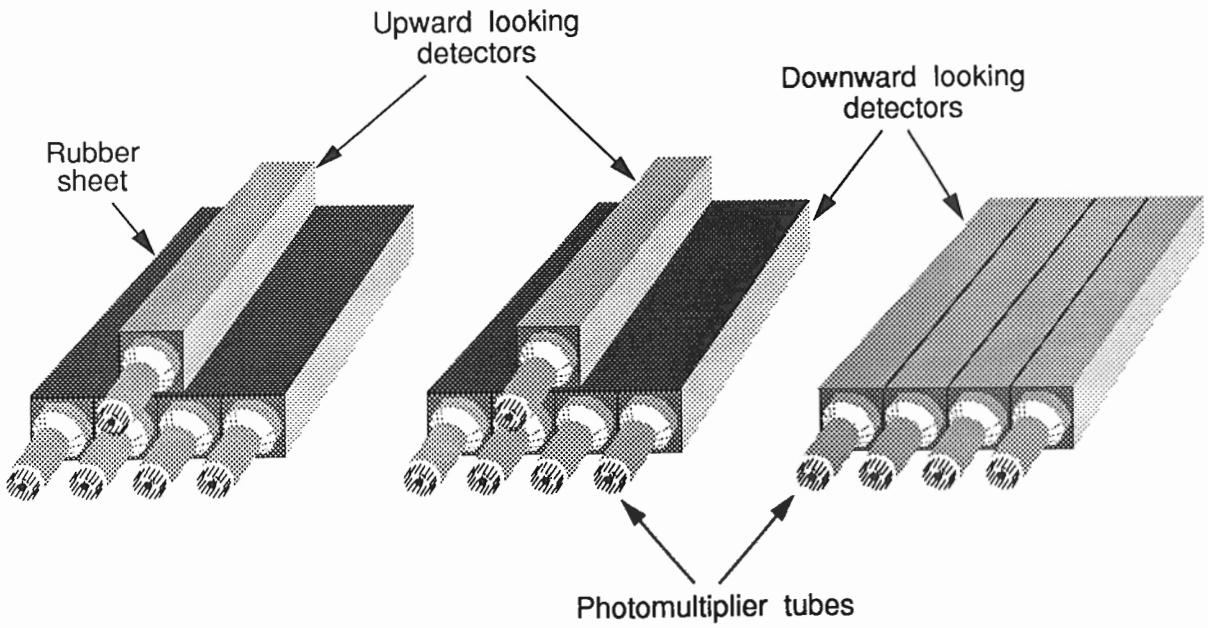

Figure 1. A schematic diagram showing the configuration of the downward- and upward-looking detectors.

determine the sensitivity of the spectrometer to a known concentration of uranium in the ground which can then be converted to ^{222}Rn decay products in the air.

In making the conversion of count rates to Bq/m^3, one important assumption is that the distribution of ^{214}Bi in the air is uniform. This assumption appears to be valid, at least over lakes and large bodies of water. Figure 3 shows a plot of the upward detector uranium window count rates compared to those from the downward window using measurements over lakes. The results are from the same survey as the data presented in Figure 2.

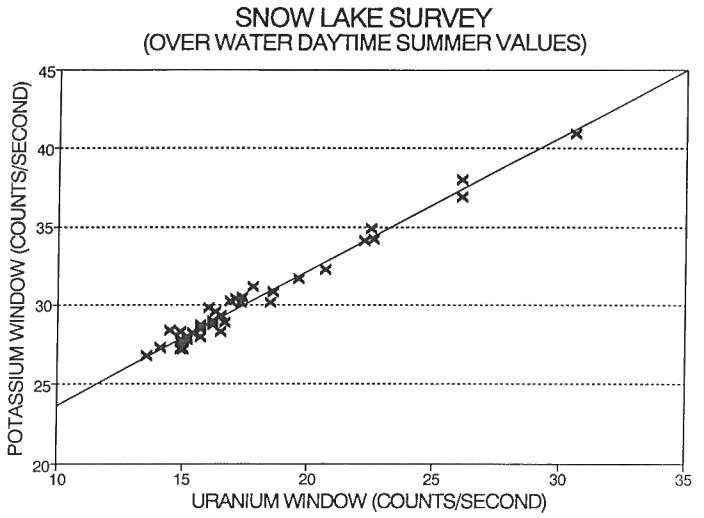

Figure 2. Variation of the potassium and uranium window count rates over lakes in northern Manitoba. One sigma errors in the potassium and uranium window count rates are approximately 0.3 counts per second.

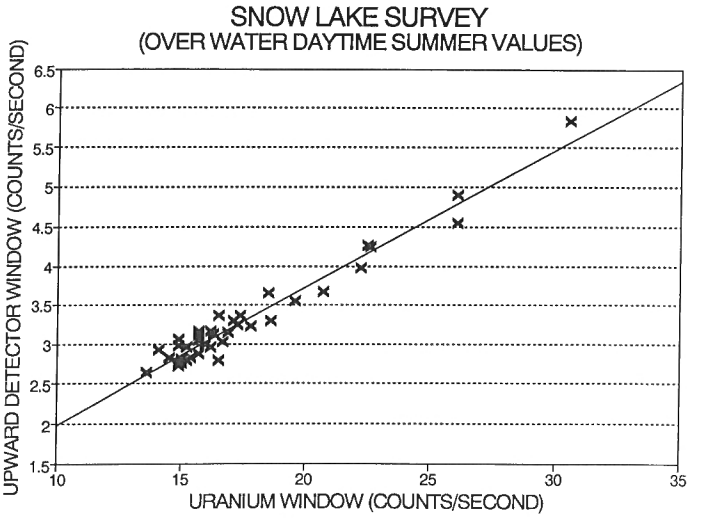

Figure 3. Variation of the upward and downward uranium window count rates over lakes in northern Manitoba. One sigma errors in the upward and downward uranium window count rates are approximately 0.15 and 0.3 counts per second, respectively.

In Figure 3 the upward detectors are measuring airborne radioactivity predominantly from the air above the aircraft. The downward detectors, however, are measuring radiation both from above and below the aircraft. Plots such as these are used to calibrate the upward-looking detectors (Grasty et al., 1988; IAEA, 1991). The fact that the data in Figure 3 closely fit a straight line implies that the distribution of ^{214}Bi in the air has remained the same throughout these flights. If, on some occasions, the ^{214}Bi was concentrated below the aircraft, the counts would increase in the downward-looking detectors whereas there would only be a small increase in the count rate of the upward detectors.

Since the upward-looking detectors were installed in the GSC aircraft in 1987, no measurable inhomogeneities in the distribution of ^{214}Bi in the air over lakes or large bodies of water have been found. This is probably because the airborne survey flights are carried out during daylight hours, when the air is well mixed. In addition, the ^{214}Bi must have originated from ^{222}Rn which emanated from the ground and then travelled some distance over the lake. In travelling this distance, some additional mixing would have occurred.

Theory

For an airborne gamma ray spectrometer at an altitude, h, above the ground, Grasty (1975) has shown that the number of unscattered photons detected per second, N, is given by:

$$N = \frac{n}{2\lambda} \int_1^{\infty} \frac{A\varepsilon e^{-\mu h \sec\theta}\, d(\sec\theta)}{(\sec\theta)^2} \qquad (1)$$

where,

n is the number of primary photons emitted from the ground per unit volume per second,

A is the cross-sectional area of the detector,

ε is photopeak efficiency, defined as the number of photons that are completely absorbed divided by the total number striking the detector

μ is the linear attenuation coefficient of gamma radiation in the air,

λ is the linear attenuation coefficient of gamma radiation in the ground and

θ is the angle of incidence of the primary gamma ray photon as measured from the vertical.

For a spherical detector, A and ε are independent of θ, consequently:

$$N = \frac{nA\varepsilon}{2\lambda} \int_1^{\infty} \frac{e^{-\mu h \sec\theta}\, d(\sec\theta)}{(\sec\theta)^2} \qquad (2)$$

Equation (2) for a spherical detector is commonly simplified to:

$$N = N_o E_2(\mu h) \quad (3)$$

where N_0 is the count rate at ground level and is given by

$$N_o = A\varepsilon n/2\lambda \quad (4)$$

and,

$$E_2(\mu h) = \int_1^\infty \frac{e^{-\mu h x}\, dx}{x^2} \quad (5)$$

where, E_2 is the exponential integral of the second kind and commonly called King's Function (King, 1912).

However, equation (2) has been computed for a spherical detector in which $A\varepsilon$ in equation (1) is independent of the angle of incidence of the gamma radiation. This is clearly not the case for the detector arrays shown in Figure 1 which are much more efficient in detecting gamma radiation travelling vertically compared to those travelling in a horizontal direction. To simplify the computation, we have assumed that the GSC system only records gamma ray photons striking the bottom surface of the detectors.

In this case,

$$A\varepsilon = a \cos\theta \quad (6)$$

where a is a constant.

As shown by Kogan et al. (1971), the count rate at an altitude h for this particular detector is given by:

$$N = N_o E_3(\mu h) \quad (7)$$

where as before N_0 is the count rate from an infinite source at ground level. Using data presented by Grasty et al. (1988), the E_3 function has been found to provide a good representation of the variation of count rate with aircraft altitude.

The count rate at ground level, N_0, does not depend on the density of the material as is more apparent when equation (4) is converted to one involving the mass attenuation coefficient, λ_m of the gamma radiation in the ground. Equation (4) then becomes:

$$N_o = n_g A\varepsilon/2\lambda_m \quad (6)$$

where n_g is now the number of gamma ray emitted per unit mass of material. Since λ_m is independent of density, the count rate at the surface of the ground will also be independent of the density of the medium.

For air and most rocks and soils, the mass attenuation coefficients for gamma ray energies in the region of 0.4 to 3.0 Mev are almost identical (Hubbel and Berger, 1968). This is because Compton scattering is the dominant attenuation process for most rocks, soils, and the air which all have similar average atomic numbers. Therefore, from equation (6) a gamma ray spectrometer will record the same count rate from air or ground with the same specific activity. An airborne gamma ray spectrometer can therefore be calibrated for ^{222}Rn decay products in the air using measurements on the ground where the concentration of uranium is known.

When flying at the standard airborne survey altitude of 123 m (400 feet), the detectors are receiving radiation from ^{222}Rn decay products (^{214}Bi) in the air above the aircraft as well as from the 123 m of air below the aircraft. For all practical purposes, the air above the aircraft can be considered an infinite source.

The relationship between the count rate, N_h from the air layer of depth h and the count rate N_0 from an infinitely thick layer will be given by:

$$N_h/N_o = (1 - E_3(\mu h)) \quad (7)$$

The linear attenuation coefficients for gamma radiation of energy 1.76 MeV in air at 20°C and 76mm of Hg is 0.00577/m (Grasty,1979). Using this value in equation (7) for a survey altitude of 123m, we find that the ratio of the gamma-ray count rates from ^{214}Bi in the air below the aircraft to that produced by an infinite source is 0.836.

The count rate of the main detectors from radiation above the aircraft will be reduced from that produced by an infinite source at ground level because of the shielding effect of the two upward detectors (Fig. 1). Since there are 12 individual detectors in the main array, the resultant count rate from radiation above the aircraft will be reduced by a factor of approximately 10/12 (0.833).

The total uranium window count rate from air both above and below the aircraft (N_T) compared to that produced by an infinite source measured at ground level (N_0) will then be given by:

$$(N_T/N_o) = (0.836 + 0.833) = 1.669 \quad (8)$$

This ratio can be used to convert the sensitivity of the uranium window to 1 ppm eU (1 ppm of uranium in equilibrium with its decay products) in the ground to the sensitivity to 1 ppm eU in the air. By recalculating this ratio for a spherical detector using the E_2 function (equation 3), the error in this ratio 1.669 was estimated to be less than 3%.

CALIBRATION - PRACTICE

Calibration at ground level

In the standard calibration procedure for an airborne gamma ray spectrometer, measurements are made on large concrete calibration pads with known concentrations of potassium, uranium, and thorium (Løvborg, 1984). However, these

Table 1. Measured concentration of calibration sites

Airport	Potassium (%)	Uranium (eU ppm)	Thorium (eTh ppm)	Number of measurements
Carp	1.09 ± 0.01	1.10 ± 0.04	3.80 ± 0.09	41
Uplands	2.23 ± 0.02	4.17 ± 0.08	11.56 ± 0.17	40
St. Leonards	1.23 ± 0.01	1.53 ± 0.05	6.08 ± 0.10	36

N.B. Errors indicated are one sigma errors on the mean value and take into consideration the number of measurements.

Table 2. Sensitivity of airborne system at ground level

Airport	Potassium Counts/s/%	Uranium Counts/s/ppm	Thorium Counts/s/ppm
Carp	310.1	26.8	17.0
Uplands	313.7	28.9	16.1
St. Leonards	304.1	28.4	16.9
Mean value	309.3	28.0	16.7

concrete pads are not sufficiently large to give the sensitivities of the system to an infinite source. Measurements on the pads are only used to derive the shapes of the potassium, uranium, and thorium spectra. In practice, the system sensitivities are measured by flying over a calibration range with known concentrations of the three radioactive elements.

In order to determine the system sensitivity at ground level to an effectively infinite source of radioactivity, it is necessary to locate a large area of uniform radioactivity. Fortunately, most airports have large parking ramps that are ideal for this purpose. In 1988, the sensitivities of the GSC airborne system to potassium, uranium, and thorium in the ground were measured at three airports. The airports were Ottawa International airport; Carp airport, about 40 km west of Ottawa; and St. Leonard's airport in New Brunswick. At all three airports, an area at least 60 m by 60 m of uniform radioactivity could be found. It was calculated that errors incurred in using these sites as infinite sources could be neglected.

Measurements of the potassium, uranium and thorium concentrations of these three sites were made using a portable gamma ray spectrometer calibrated on concrete pads of known radioelement concentration (Grasty et al., 1991). Approximately 40 two minute measurements were taken at each site. Most of the measurements were concentrated towards the centre of the calibration site since the central area has a greater contribution to the count rate of the airborne spectrometer. The entire area surveyed typically covered an area of 25 m by 25 m. Backgrounds for the portable spectrometer were obtained from measurements over nearby rivers.

Table 1 gives the portable spectrometer analyses for the three airport calibration sites. Analysis of the portable spectrometer total count window rate showed that any inhomogeneities in the calibration sites were less than 3% (Glynn and Grasty, 1990).

In order to determine the airborne spectrometer system sensitivities for an infinite source of uranium in the ground, the system must be calibrated to separate the interfering effects of potassium, uranium, and thorium in the three spectrometer windows. This calibration was performed in Ottawa using the same concrete pads that were used for calibrating the portable spectrometer. Each box of 4 detectors was calibrated separately to reduce spectral distortion due to high count rates. Measurements with the airborne system at each of the calibration sites were also carried out using the individual detector boxes. Measurements were taken for approximately 5 minutes at the centre of each site. This time was found to be sufficient to reduce errors due to counting statistics to negligible proportions. Backgrounds for the airborne spectrometer were determined from measurements over nearby lakes or large rivers.

Following the standard stripping procedure, the airborne spectrometer measurements at ground level were corrected to give the count rates in the potassium, uranium, and thorium windows from pure sources of potassium, uranium, and thorium in the ground at the three calibration sites. From a knowledge of the potassium, uranium, and thorium concentrations in the ground at these sites, the sensitivity of the airborne spectrometer to unit concentration of the three radioelements was determined. These results are presented in Table 2, together with the mean value for all three calibrations. The potassium and thorium sensitivity are also indicated.

From the calculated system sensitivity for uranium, the count rate in the uranium window can be converted to Bq/m^3 of uranium decay products in the air. For the uranium series,

1 Bq/g of material = 81.04 ppm of uranium.

Since 1 cubic metre of air at 20°C weighs 1205 g, then,

1 Bq/m^3 = 1/1205 Bq/g = 81.04/1205 ppm

i.e. 1 Bq/m^3 of air = 0.0673 ppm eU

From Table 2, the count rate in the uranium window from 1 ppm eU is 28.0 counts per second. We have already shown that the count rate in the uranium window for an equivalent concentration of 1 ppm eU in the air above and below the aircraft will be 1.67 times this value. Therefore, a uniform source of ^{222}Rn decay products in the air with a concentration of 1 Bq/m^3 will produce a count rate in the uranium window given by:

$$1 \text{ Bq/m}^3 \text{ (eU)} = 0.0673 \times 28.0 \times 1.67 = 3.15 \text{ counts/second} \quad (9)$$

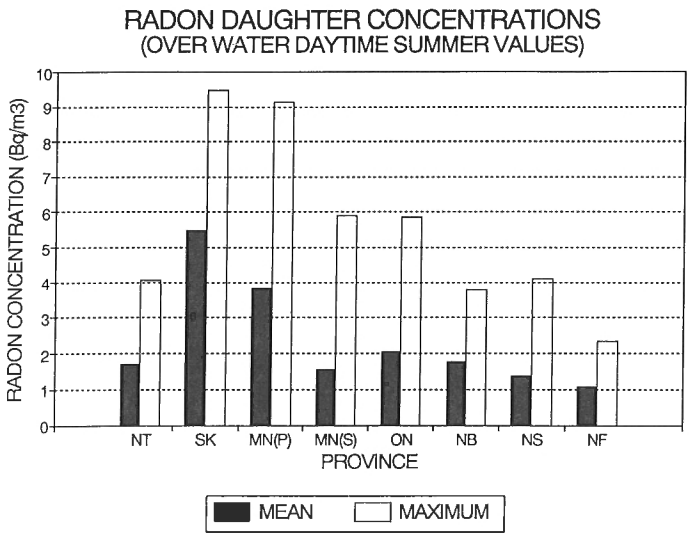

Figure 4. Summer daytime ^{222}Rn daughter concentrations over Canadian lakes. NT = Northwest Territories; SK = Saskatchewan; MN(P) = Manitoba (Prairie); MN(S) = Manitoba (Shield); ON = Ontario; NB = New Brunswick; NS = Nova Scotia; NF = Newfoundland.

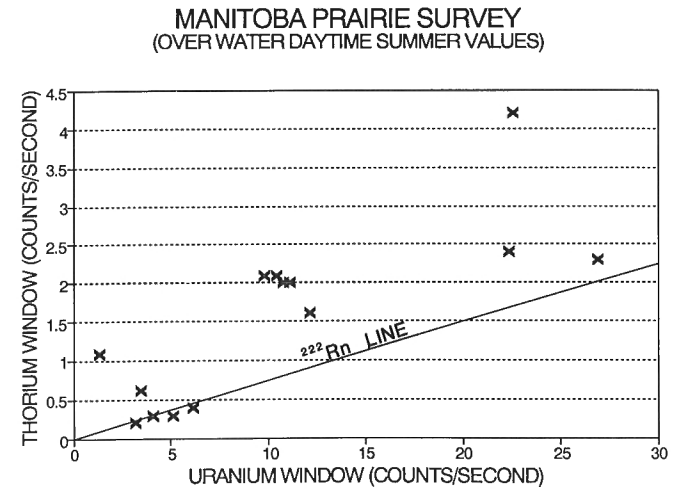

Figure 5. Variation of the thorium and uranium window count rates over lakes in the prairie regions of Manitoba and Saskatchewan. One sigma errors in the thorium and uranium window count rates are approximately 0.3 counts per second.

RESULTS

Before the count rates in the uranium window can be converted to Bq/m^3 of ^{222}Rn decay products, they must first be corrected for cosmic radiation and the aircraft background. Based on measurements over the sea and from high altitude flights, the uranium window background count rate due to cosmic radiation and the aircraft and its equipment is estimated to be 13.6 counts per second at sea level. To simplify the computations, we have assumed this value is constant for all lakes surveyed, irrespective of their elevation above sea level.

The highest elevation of any lake surveyed was 600 m above sea level. Using an exponential relationship between altitude and window count rate (Grasty et al., 1988) the count rate in the uranium window 600 m above sea level will increase by 0.7 counts per second. This will correspond to an apparent increase of 0.2 Bq/m^3 in the measurement of ^{214}Bi (Equation 9). Since almost all lakes surveyed were less than 250 m above sea level, errors arising from the assumption that all the lakes are at sea level will be significantly less than 0.2 Bq/m^3.

Figure 4 shows the calculated ^{222}Rn daughter concentrations from 404 background flights over lakes which have been carried out over the last 3 years. The arithmetic mean and maximum value are presented for each province. For the province of Manitoba (MN), the data has been subdivided into measurements over the shield regions - MN(S) and the prairie regions - MN(P). For Saskatchewan, all measurements were carried out over lakes in the prairie regions.

The results clearly show that there are regional differences in daughter concentrations over lakes. Measurements over the prairie regions of Manitoba and Saskatchewan are significantly higher than in other parts of Canada. The mean levels over the prairie lakes are also significantly higher than the value of 1 Bq/m^3 quoted by Health and Welfare, Canada (1989).

Analysis of the overwater backgrounds has also shown evidence for decay products of ^{220}Rn (thoron) in the thorium decay series.

Figure 5 shows a plot of the thorium and the uranium window count rates for all flights over prairie lakes in Manitoba and Saskatchewan. Due to a small contribution of high energy gamma ray photons from ^{214}Bi which are detected in the thorium window, the thorium window will show a small increase as the ^{222}Rn concentration increases. The thorium-to-uranium window ratio due to ^{222}Rn decay products will be the same as the ratio from a pure uranium source. From measurements on calibration pads this ratio was found to be 0.075 and was used to plot the ^{222}Rn line shown in Figure 5. In this figure, the background contribution from the aircraft and cosmic radiation has been subtracted from the measured data.

The results in Figure 5 show that the increase in the thorium window count rate cannot be explained solely by increases in ^{222}Rn daughter concentrations. However, the results can be explained by an additional contribution from

decay products of ^{220}Rn from the thorium decay series. The detection of decay products of ^{220}Rn was initially somewhat of a surprise since ^{220}Rn has a half life of only 55 seconds. However ^{212}Pb, its longest lived decay product has a half life of approximately 10.5 hours and depending on the wind conditions can travel considerable distances. Measurements of the concentration of ^{220}Rn at ground level have also shown it to have a comparable activity to ^{222}Rn (Israelsson et al., 1973).

The highest ^{220}Rn concentration, corresponding to the thorium window count rate of approximately 4 counts per second in Figure 5, was measured over Last Mountain Lake, near Regina, Saskatchewan. This lake is long and narrow therefore higher concentrations of ^{220}Rn would be expected over this lake, since the aircraft would never be far from the shore. We have calculated that the thorium window count rate over Last Mountain Lake corresponds to a ^{220}Rn daughter concentration of approximately 0.5 Bq/m^3. Similar results showing the presence of small concentrations of decay products of ^{220}Rn have been obtained from measurements over lakes in all parts of Canada.

CONCLUSIONS

Analysis of airborne gamma ray surveys over Canadian lakes carried out in the years 1987 to 1990 have shown the following:

1) There are regional differences in ^{222}Rn daughter concentrations over Canadian lakes.

2) Summer daytime measurements over lakes in the prairie regions of Manitoba and Saskatchewan have mean values of approximately 4 to 5 Bq/m^3 which are significantly higher than the levels of 1 to 2 Bq/m^3 found in other parts of Canada.

3) A comparison of upward- and downward-looking detector data for overwater daytime measurements showed no evidence for inhomogeneity in the distribution of ^{222}Rn decay products.

4) Measurements over lakes in Canada showed the presence of small concentrations of ^{220}Rn daughters with a maximum value of 0.5 Bq/m^3 being measured over a narrow lake near Regina, Saskatchewan.

REFERENCES

Health and Welfare, Canada
1989: Radon - you and your family - a personal perspective; Information booklet, Environmental Health Directorate, National Health and Welfare, Canada, p. 20.

Glynn, J.E. and Grasty, R.L.
1990: Counting statistics: is anything really there?; Nuclear Geophysics, v. 4, p. 493-498.

Grasty, R.L.
1975: Atmospheric absorption of 2.62 MeV gamma-ray photons emitted from the ground; Geophysics, v. 40(6), p. 1058-1065.
1979: Gamma ray spectrometric methods in uranium exploration - theory and operational procedures; in Geophysics and Geochemistry in the Search for Metallic Ores, (ed.) Peter J. Hood; Geological Survey of Canada, Economic Geology Report 31, p. 147-161.

Grasty, R.L., Holman, P.B., and Blanchard, Y.
1991: Transportable calibration pads for ground and airborne gamma-ray spectrometers; Geological Survey of Canada, Paper 90-23, 26 p.

Grasty, R.L., Wilkes, P.G., and Kooyman, R.
1988: Background measurements in gamma-ray surveys; Geological Survey of Canada, Paper 88-11, 31 p.

Hubbell, J.H. and Berger, M.J.
1968: Attenuation coefficients, energy absorption coefficients, and related quantities; Engineering Compendium on Radiation Shielding, v. 1, Springer Verlag, Berlin, p. 167-202.

IAEA
1976: Radiometric reporting methods and calibration in uranium exploration; Technical Report Series, no. 174 (International Atomic Energy Agency, Vienna), 57 p.
in press: Airborne gamma-ray spectrometer surveying; Technical Report Series (International Atomic Energy Agency, Vienna).

Israelsson, S., Knudsen, E., and Ungethm, E.
1973: Simultaneous measurement of radon (Rn^{222}) and thoron (Rn^{220}) in the atmospheric surface layer; Tellus 25, p. 281-290.

King, L.V.
1912: Absorption problems in radioactivity; Philosophical Magazine, v. 23, p. 242.

Kogan, R.M., Nazarov, I.M., and Fridman, Sh.D.
1971: Gamma spectrometry of natural environments and formations - theory of the method, applications to geology and geophysics; Israel Program for Scientific Translations, 5778, Jerusalem, 337 p.

Løvborg, L.
1984: The calibration of portable and airborne gamma-ray spectrometers - theory, problems and facilities; Risø Report M-2456, 207 p.

Effective porosity measuring procedure for low porosity rocks

T.J. Katsube and N. Scromeda[1]
Mineral Resources Division

Katsube, T.J. and Scromeda, N., 1991: Effective porosity measuring procedure for low porosity rocks; in Current Research, Part E; Geological Survey of Canada, Paper 91-1E, p. 291-297.

Abstract

A porosity measuring procedure for low porosity (0.1-1.0%) rocks (granites, gabbros and a shale) has been studied to determine measurement accuracy of low porosities.

Low porosity rocks are being considered for hosting radioactive waste and their petrophysical properties are also being used for modelling of sedimentary basin development (shales). These porosities are 10-100 times smaller than those of common reservoir rocks and are beyond the lower limit of many porosity measuring techniques. A commonly used technique to determine low porosities takes the weight difference between a water-saturated and oven-dried sample. The optimum times required for saturation and oven-drying have been studied.

Results show that a saturation time of 140 minutes will ensure a 95% saturation, and an oven drying time of 180 minutes for the granites and 300-1000 minutes for others will ensure dry state. Shorter duration times, such as 30 and 250 minutes for saturation and drying will reduce measurement accuracy to 30%.

Résumé

Les méthodes de mesure de la porosité des roches peu poreuses (0,1 - 1,0 %) (granites, gabbros et schistes argileux) ont été étudiées dans le but de déterminer la précision des mesures des faibles porosités.

La possibilité d'utiliser des roches de faible porosité pour enfouir des déchets radioactifs et pour modéliser la formation des bassins sédimentaires (schistes argileux) est à l'étude. Ces porosités sont de 10 à 1000 fois inférieures à celles des roches réservoirs courantes et peuvent être mesurées que par un nombre restreint de méthodes de mesure de la porosité. Une méthode répandue mesure la différence de poids entre la roche saturée d'eau et la même roche séchée au four. Les temps optimaux de saturation et de séchage au four ont été étudiés.

Les résultats montrent qu'un temps de saturation de 140 minutes assure une saturation de 95 % et que des temps de séchage au four de 180 minutes pour les granites et de 300 à 1000 minutes pour les autres matériaux assurent un état sec. Des temps plus courts, par exemple 30 minutes pour la saturation et 250 pour le séchage, diminuent l'exactitude des mesures à ± 40 %.

[1] McGill University, Montreal, Quebec.

INTRODUCTION

The significance of porosity for non-reservoir low porosity rocks has increased considerably over the last 10 years due to these rock types being considered as host rocks for radioactive and other waste disposal (e.g., granites, gabbros, shales) and for modelling of sedimentary basin development (shales). The porosity of crystalline rocks such as granites, gabbros, and gneisses have been reported to be as low as 0.01-0.8% (Table 1; Katsube and Hume, 1989; Katsube et al., 1991), and 0.8-3.0% for shales (Daly et al., 1966; Katsube et al., 1990). These porosities are generally 10 to 100 times smaller than those of common reservoir rocks, which vary from 4.0 to 40% (Levorsen, 1967). These low porosity values often exceed the lower limit of most porosity measuring methods (Johnson and Olhoeft, 1984).

The effective porosity measuring procedures for low porosity rocks (0.1 to 1.0%) have been studied, using a suite of six rock samples representing three rock types (granites, gabbros, and shales), for the purpose of obtaining basic information on measurement accuracy and reliability of low porosity values.

Effective porosity, ϕ_E, is the porosity of all interconnected pores in a rock, and total porosity, ϕ_T, is the porosity of all pores including those sealed-off from the interconnected pore network (Daly et al., 1966). A simple and commonly used technique to determine the effective porosity, particularly for low porosity (<1.0%) rocks (Katsube, 1981; Melnyk and Skeet, 1986), takes the weight difference between a water saturated and dry rock sample and derives the porosity from the following equation:

$$\phi_E = \delta (W_W - W_D) / W_D \quad (1)$$

where W_w, W_D and δ are the wet weight, dry weight, and bulk density of the rock sample, respectively.

The procedure commonly used to determine W_w and W_D follow the next three steps:

(1) dry and degas a rock sample under vacuum at room temperature,

(2) saturate the sample by introducing water into the vacuum chamber, and then by leaving the sample immersed under atmospheric pressure before measuring W_W,

(3) driving out the water by heating the saturated sample, before measuring W_D.

It is important to know the optimum length of time needed for drying and degassing under vacuum, t_I, for saturating under atmospheric pressure, t_s, and for heat treatment, t_D. This is because durations long enough to reach steady state are often used to determine W_w and W_D, which could take days. The main purposes of this study is to find out what effect the difference in times has on measurement accuracy. This paper reports results of a laboratory study for six rock samples.

METHOD OF INVESTIGATION

Samples

Three granites, two gabbros, and one shale sample were used in this study. The dimensions of these samples are listed in Table 2. Petrophysical information related to these samples is available in Katsube and Hume (1987) for the granites, in Hume and Katsube (1987) for the gabbros, and in Katsube et al. (1990) for the shale.

Table 1. Porosities (%) of some low-porosity rocks (granites)

Locations	N	Min.	Max.	Mean	Reference
Lac du Bonnet, Man.	101	0.16	0.67	0.36	Katsube et al. (1985)
Barre, VT	1			0.079	Hanley et al. (1978)
Westerly, RI.	1			0.106	Hanley et al. (1978)
Stone Mt., GA.				0.30	Brace (1965)
-	45			0.40	Franklin & Hoecke (1970)
Tucson, AZ.	1			0.611	Norton & Knapp (1977)
-	6			0.7	Mellor (1971)
-	26	0.4	4.8	0.9	Izett (1960)
Laramie, WY.	1			1.08	Norton & Knapp (1977)
Westerly, RI.				1.1	Brace (1965)
- MD.	17	0.44	3.98	1.11	Houser (1962)
Troy, AZ.	1			1.36	Norton & Knapp (1977)
-	322	0.1	11.2	1.40	Kessler et al. (1940)
Globe-Miami, AZ.	1			1.77	Norton & Knapp (1977)
Canyon, AZ.	1			2.96	Norton & Knapp (1977)
-	9	0.7	5.5	3.0	Norton & Knapp (1977)
Altnabieac, ALA	32	0.39	2.67	0.56	Alexander et al. (1981)
Finnsjon, Sweden	30	0.18	0.54	0.29	Skagius & Neretnieks (1985)

N = Number of Samples

Table 2. Basic information on the rock samples

Sample No.	Rock Type	h (m)	Shape	r_D (cm)	ℓ (cm)	A (cm^2)	W (g)
W-1	GR	124	HD	4.42	0.91	7.74	18.77
W-2	GR	564	HD	4.56	1.05	8.04	22.38
W-3	GR	906	HD	4.16	1.00	7.16	19.05
E-1	GB	201	HD	4.12	0.97	7.07	20.07
E-2	GB	342	HD	4.10	1.01	7.02	20.46
S-#6	Sh	5132	D	2.48	0.55	4.83	8.31

GR = granite (Katsube and Hume, 1987)
GB = gabbro (Hume and Katsube, 1987)
Sh = shale (Katsube et al., 1990)
h = depth
HD = half disc
D = disc
r_D = diameter of sample
ℓ = thickness of sample
A = area of flat surfaces
W = weight of sample

Table 3a. Vacuum pumping results of air-dried granite samples

Sample	t_l (min)	W_r (g)	ΔW_r (mg)	S_r (%)
W-1	0	18.7690	4.4	15.1
	45	18.7688	4.2	14.4
	120	18.7684	3.8	13.0
	240	18.7682	3.6	12.3
	300	18.7680	3.4	11.6
	390	18.7678	3.2	11.0
	4270	18.7678	3.2	11.0
W-2	0	22.3847	5.5	12.7
	60	22.3843	5.1	11.8
	120	22.3839	4.7	10.9
	240	22.3837	4.5	10.4
	300	22.3834	4.2	9.7
	360	22.3834	4.2	9.7
	1396	22.3834	4.2	9.7
W-3	0	19.0477	5.8	12.0
	60	19.0476	5.7	11.8
	120	19.0474	5.5	11.4
	240	19.0474	5.5	11.4
	300	19.0471	5.2	10.8
	360	19.0471	5.2	10.8
	1396	19.0471	5.2	10.8

t_l : Vacuum pumping time
W_r : Weight of specimen at time t
ΔW_r: Weight difference between W_r and W_D of the oven-dried specimen
S_r : degree of saturation

Table 3b. Vacuum pumping results of air-dried gabbro and shale samples

Sample	t_l (min)	W_r (g)	ΔW_r (mg)	S_r (%)
E-1	0	20.0661	4.5	46.9
	30	20.0659	4.3	44.8
	60	20.0659	4.3	44.8
	90	20.0658	4.2	43.8
	120	20.0658	4.2	41.8
	150	20.0656	4.0	41.7
	210	20.0656	4.0	41.7
	270	20.0656	4.0	41.7
	330	20.0656	4.0	41.7
	390	20.0656	4.0	41.7
E-2	0	20.4565	4.9	22.8
	30	20.4565	4.9	22.8
	60	20.4563	4.7	21.9
	90	20.4563	4.7	21.9
	120	20.4563	4.7	21.9
	150	20.4561	4.5	20.9
	210	20.4558	4.2	19.5
	270	20.4557	4.1	19.1
	330	20.4557	4.1	19.1
	390	20.4557	4.1	19.1
S-#6	0	8.3096	23.5	83.5
	15	8.3092	23.1	82.1
	30	8.3087	22.6	80.3
	60	8.3083	22.2	78.9
	90	8.3082	22.1	78.5
	135	8.3075	21.4	76.0
	210	8.3068	20.7	73.5
	270	8.3064	20.3	72.1
	330	8.3062	20.1	71.4
	390	8.3059	19.8	70.3

t_l : Vacuum pumping time
W_r : Weight of specimen at time t
ΔW_r: Weight difference between W_r and W_D of the oven-dried specimen
S_r : degree of saturation

Experimental procedure

The three steps in this experimental procedure are described below in detail:

(1)Vacuum drying

An air dried (room temperature) sample was placed in a glass beaker using tweezers. The beaker was then placed in a vacuum chamber with vacuum applied for periods varying from 15 to about 4000 minutes. At the end of a specified period, the sample was removed from the chamber and weighed. The sample was then returned to the vacuum chamber and vacuum applied again for the duration of the next period. This procedure was repeated until a constant weight was obtained. A Mettler 10 TW balance (sensitivity: ±0.1 mg) was used for the weight measurements.

(2)Vacuum saturation

Vacuum was applied for 15 minutes to degas the sample before it was saturated by introducing deionized, distilled water (DDW) into the vacuum chamber. After saturation,

Table 4a. Extent of saturation with time under atmospheric pressure, following vacuum saturation of the granite samples

Sample	t_s (min)	W_r (g)	ΔW_r (mg)	S_r (%)
W-1	0	18.7670	2.4	8.2
	1	18.7887	24.1	82.5
	10	18.7891	24.5	83.9
	25	18.7900	25.4	79.0
	40	18.7906	26.0	89.0
	55	18.7910	26.4	90.4
	70	18.7911	26.5	90.8
	140	18.7928	28.2	96.6
	180	18.7938	29.2	100
	240	18.7938	29.2	100
	300	18.7938	29.2	100
W-2	0	22.3844	5.2	12.0
	1	22.4191	39.9	91.9
	10	22.4214	42.2	97.2
	25	22.4223	43.1	99.3
	40	22.4223	43.1	99.3
	70	22.4223	43.1	99.3
	100	22.4223	43.1	99.3
	160	22.4226	43.4	100
	190	22.4226	43.4	100
	220	22.4226	43.4	100
	250	22.4226	43.4	100
W-3	0	19.0477	5.8	12.0
	1	19.0892	47.3	97.9
	10	19.0894	47.5	98.3
	25	19.0894	47.5	98.3
	40	19.0902	48.3	100
	70	19.0902	48.3	100
	100	19.0902	48.3	100
	160	19.0902	48.3	100
	190	19.0902	48.3	100
	220	19.0902	48.3	100
	250	19.0902	48.3	100

t_s : Saturation time
W_r : Weight of specimen at time t
ΔW_r: Weight difference between W_r and W_D of the oven-dried specimen
S_r : degree of saturation

Table 4b. Extent of saturation with time under atmospheric pressure, following vacuum saturation of the gabbro and shale samples

Sample	t_s (min)	W_r (g)	ΔW_r (mg)	S_r (%)
E-1	0	20.0657	4.1	42.7
	1	20.0694	7.8	81.3
	10	20.0694	7.8	81.3
	25	20.0704	8.8	91.7
	40	20.0711	9.5	99.0
	70	20.0711	9.5	99.0
	120	20.0711	9.5	99.0
	180	20.0712	9.6	100
	210	20.0712	9.6	100
	240	20.0712	9.6	100
	270	20.0712	9.6	100
	330	20.0712	9.6	100
E-2	1	20.4562	4.5	20.9
	10	20.4668	15.1	70.2
	20	20.4690	17.3	80.5
	25	20.4709	19.2	89.3
	40	20.4709	19.2	89.3
	70	20.4711	19.4	90.2
	120	20.4719	20.2	94.0
	180	20.4732	21.5	100
	210	20.4732	21.5	100
	240	20.4732	21.5	100
	270	20.4732	21.5	100
	330	20.4732	21.5	100
S-#6	0	8.3105	24.4	86.7
	1	8.3136	27.5	97.7
	20	8.3136	27.5	97.7
	25	8.3138	27.7	98.4
	40	8.3138	27.7	98.4
	70	8.3139	27.8	98.8
	120	8.3139	27.8	98.8
	180	8.3144	28.3	100.5
	240	8.3137	27.6	98.0
	300	8.3144	28.3	100.5
	360	8.3152	29.1	103.4

t_s : Saturation time
W_r : Weight of specimen at time t
ΔW_r: Weight difference between W_r and W_D of the oven-dried specimen
S_r : degree of saturation

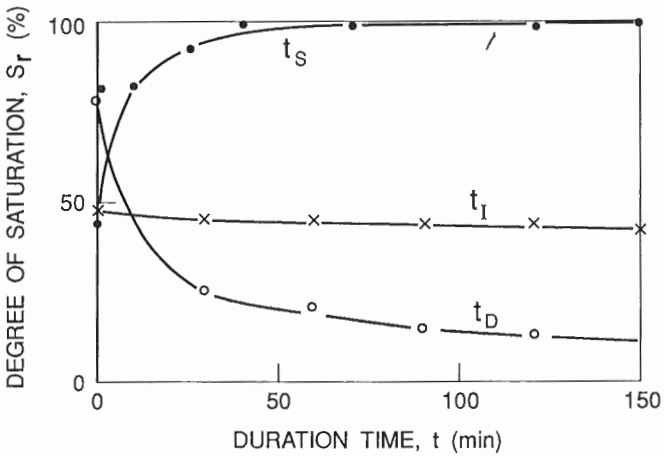

Figure 1. Typical examples of vacuum drying (air-dried sample), saturating (under atmospheric pressure), and oven- drying curves, for sample E-1 (gabbro).

Table 5a. Results of oven-drying the saturated granite samples

Sample	t_D (min)	W_r (g)	ΔW_r (mg)	S_r (%)
W-1	0	18.7892	24.6	84.2
	30	18.7670	2.4	8.2
	60	18.7656	1.0	3.4
	105	18.7650	0.4	1.4
	180	18.7646	0.0	0.0
	240	18.7646	0.0	0.0
	300	18.7646	0.0	0.0
W-2	0	22.4205	41.3	95.4
	30	22.3808	1.6	3.7
	60	22.3797	0.5	1.2
	105	22.3796	0.4	0.9
	180	22.3793	0.1	0.2
	240	22.3792	0.0	0.0
	300	22.3792	0.0	0.0
W-3	0	19.0871	45.2	93.6
	30	19.0422	0.3	0.6
	60	19.0419	0.0	0.0
	105	19.0419	0.0	0.0
	180	19.0419	0.0	0.0
	240	19.0419	0.0	0.0
	300	19.0419	0.0	0.0

t_D : Oven-drying time
W_r : Weight of specimen at time t
ΔW_r: Weight difference between W_r and W_D, which is W^r at the maximum value of t
S_r : degree of saturation

vacuum was applied for another 15 minutes for degassing before the immersed sample was left under atmospheric pressure for periods varying from 1 to 60 minutes. The sample was weighed after each period. Before weighing, the sample was removed from the beaker and dried using a kimwipe until the surface did not shine due to surface moisture films. Considerable care was taken to keep the surface-drying process consistent. The sample was returned to the beaker and the procedure was repeated until a constant weight was obtained.

(3)Oven drying

Once saturation was completed, the sample was placed in a beaker and heated in an oven set at 100-105°C for periods varying from 30 to about 1000 minutes. After each period, the sample and beaker were removed from the

Table 5b. Results of oven-drying the saturated gabbro and shale samples

Sample	t_D (min)	W_r (g)	ΔW_r (mg)	S_r (%)
E-1	0	20.0691	7.5	78.1
	30	20.0640	2.4	25.0
	60	20.0636	2.0	20.8
	90	20.0630	1.4	14.6
	120	20.0629	1.3	13.5
	180	20.0626	1.0	10.4
	240	20.0623	0.7	7.3
	300	20.0620	0.4	4.2
	1320	20.0616	0.0	0.0
	1440	20.0616	0.0	0.0
E-2	0	20.4732	21.6	97.7
	30	20.4580	6.4	29.8
	60	20.4568	5.2	24.2
	90	20.4559	4.3	20.0
	120	20.4555	3.9	18.1
	180	20.4548	3.2	14.9
	240	20.4546	3.0	14.0
	300	20.4533	1.7	7.9
	1320	20.4516	0.0	0.0
	1440	20.4516	0.0	0.0
S-#6	0	8.3144	28.3	100.5
	30	8.3022	16.1	57.2
	60	8.2991	13.0	46.2
	90	8.2973	11.2	39.8
	120	8.2959	9.8	34.8
	180	8.2937	7.6	27.0
	270	8.2920	5.9	21.0
	330	8.2912	5.1	18.1
	1290	8.2861	0.0	0.0
	1320	8.2861	0.0	0.0

t_D : Oven-drying time
W_r : Weight of specimen at time t
ΔW_r: Weight difference between W_r and W_D, which is W^r at the maximum value of t
S_r : degree of saturation

Table 6. Results of the effective porosity measurements

Sample No.	δ (g/cc)	W_W (g)	W_D (g)	ΔW (mg)	ϕ_E (%)
W-1	2.66	18.7938	18.7646	29.2	0.41
W-2	2.65	22.4226	22.3792	43.3	0.51
W-3	2.66	19.0902	19.0419	48.3	0.67
E-1	2.93	20.0712	20.0616	9.6	0.14
E-2	2.88	20.4732	20.4516	21.5	0.30
S-#6	2.73	8.3143	8.2861	28.2	0.93

$\phi_E = \delta (W_W - W_D) / W_D$ $\quad \Delta W = W_W - W_D$
W_W = wet weight $\quad \delta$ = bulk density
W_D = dry weight $\quad \phi_E$ = effective porosity

oven and placed in a desiccator to cool for 7 to 20 minutes before the weight was measured. Longer cooling times were required for longer heating periods.

Considerable care was taken to minimize any deviation from these procedural steps, in order to ensure consistency in the measurements.

Definition of parameters used in the measurements

Duration times, t_I, t_s, and t_D are expressed in minutes. Duration of saturation, t_s, is measured from the point that the 15 minutes of vacuum drying and 15 minutes of vacuum degassing the immersed sample is completed. The weight of a specimen at any given time is represented by W_r in grams. When W_r reaches a constant value during the saturation process, the sample is considered to be fully saturated and its weight is represented by W_W. When W_r reaches a constant value during oven drying, the sample is considered to be completely dried and its weight is represented by W_D. The weight difference between W_r and W_D is ΔW_r:

$$\Delta W_r = W_r - W_D \quad (2)$$

The degree of saturation, S_r, is the weight of the water content (ΔW_r) at any given duration time over the weight of the maximum water content ($W_W - W_D$), and is expressed as follows:

$$S_r = \Delta W_r (W_W - W_D) \quad (3)$$

EXPERIMENTAL RESULTS

Results of vacuum drying and degassing of air dried samples are listed in Table 3a and 3b. It is not certain whether the constant values of W_r reached over long time intervals are the irreducible water saturation (Levorsen, 1967) of the samples, because it is not known whether these samples were fully saturated before being left in the room to dry.

Results of saturation under atmospheric pressure are listed in Table 4a and 4b. The constant values reached over long time intervals are used to determine W_W. Since the values of W_r for sample S-#6 were unstable at the longer time periods, W_W was determined by averaging W_r over the duration times from 70 to 360 minutes.

The results of oven-drying the saturated samples are listed in Table 5a and 5b. The constant values reached over long time intervals were used to determine W_D. The results for W_W and W_D are listed in Table 6. The effective porosities (ϕ_E) derived using equation (1) are also listed in Table 6. The degree of saturation (S_r) has been calculated (equation (3)) for every measurement of W_r and is listed in Tables 3a to 5b. A typical example of the three curves: vacuum drying of the air dried sample, saturation under atmospheric pressure, and oven-drying, is shown in Figure 1. The vacuum drying curve expressed by t_I in Figure 1 decreases slightly with time. The saturation curve expressed by t_s increases rapidly with time and reaches a constant value. The oven-drying curve expressed by t_D decreases with time and eventually also reaches a constant value.

DISCUSSIONS AND CONCLUSIONS

Vacuum drying and degassing of air-dried samples show very little change in degree of saturation (S_r), as seen in Tables 3a and 3b. Therefore, this is not an effective method for evacuating moisture from a rock. However, the 15 minute period of vacuum pumping prior to saturation should still be applied, since it is necessary to degas the sample.

The time required for a sample to remain immersed in water under atmospheric pressure to saturate is surprisingly short (Table 4a and 4b). All granite samples and the shale sample are 80% saturated within 1.0 minute, and two of the granites and the shale sample are also 90% saturated within the same time. The gabbros took longer to saturate, but were 80% saturated within 20 minutes, and 90% saturated within 70 minutes. A saturation time of 140 minutes was required for 95% saturation, for all six samples.

The oven-drying time (t_D) required to dry a sample was relatively short for the granites, but was longer than expected for the others (Table 5a and 5b). The degree of saturation (S_r) is almost zero within 180 minutes for the granites. For the other three samples more than 300 minutes are required for S_r to reach that level. These results show that the samples are dry after 1000 minutes, but indicate that there is a lack of data between 300 and 1000 minutes. Further experiments are required to determine the optimum length of time for oven-drying of the gabbro and shale samples.

In conclusion, a time of 15 minutes for the initial vacuum drying and degassing, and 140 minutes for the immersing in water under atmospheric pressure, appears to be adequate for saturating these samples. A time of 180 minutes for oven-drying is adequate to dry the granites, but 300-1000 minutes is required for the gabbros and shale. The optimum oven-drying time for latter three rocks has still to be determined.

However, slight diversions from the optimum times appear to be only moderately significant. According to these results, a 25 minute saturation and a 180 minute oven-drying, for example, would cause a maximum error of 30% (about 20% for granites) for porosity measurements, the effect of oven-drying being rather significant. This error is calculated for sample S-#6 (for example) as follows:

(1) At $t_S = 25$ (min) $S_r = 98.4\%$ (Table 4b), 1.6% under fully saturated condition required for determining W_W.

(2) At $t_D = 180$ (min) $S_r = 27.0\%$ (Table 5b), 27.0% above completely dried condition required for determining W_D.

(3) The combination of the two deviated values is 28.6%.

The porosity values obtained in this study (Table 6) are in the same range (0.3-1.5), as those reported for similar rocks (Table 1; Hume and Katsube, 1987; Katsube and Hume, 1987).

Acknowledgments

The authors are grateful to J.B. Percival (Geological Survey of Canada) for critically reviewing this paper and for her very constructive comments. Previous studies by S.W. Adcock (Geological Survey of Canada) have contributed to certain approaches adopted in this study. The authors also thank M.E. Best (Geological Survey of Canada) for allowing the shale sample to be used in this study.

REFERENCES

Alexander, J., Hall, D.H., and Storey, B.C.
1981: Porosity measurements of crystalline rocks by laboratory and geophysical methods; Report on the Institute of Geological Sciences, ENPU81-10, 45 p.

Brace, W.F.
1965: Some new measurements of linear compressibility of rocks; Journal of Geophysical Research, v. 70, p. 391-398.

Daly, R.A., Manger, E.G., and Clark, S.P. Jr.
1966: Density of rocks; Sec. 4 (p. 23) in Handbook of Physical Constants; The Geological Society of America Inc., Memoir 97, p. 19-26.

Franklin, J.A. and Hoecke, E.
1970: Developments in triaxial testing technique; Rock Mechanics, v. 2, p. 223-228.

Hanley, E.J., Dewitt, D.P., and Roy, R.F.
1978: The thermal diffusivity of eight well-characterized rocks for the temperature range 300-1000K; Engineering Geology, v. 12, p. 31-47.

Houser, F.N.
1962: Some physical property data of samples from UI5A site, Nevada test site; United States Geological Survey Technical Letter, area 15-2, 4 p.

Hume, J.P. and Katsube, T.J.
1987: Pore structure characteristics; in Geotechnical Studies at East Bull Lake Research Area (ed.) A.G. Latham; Canada Centre for mineral and Energy Technology, Report MRL 87-94, p. 39-66.

Izett, G.A.
1960: Granite exploration hole, area 15, Nevada test site, Nye County, NV; Interim report, Part C, United States Geological Survey Trace Elements Memorandum Report 836-C, 3 p.

Johnson, G.R. and Olhoeft, G.R.
1984: Density of rocks and minerals; in CRC Handbook of Physical Properties of Rocks, Volume 3, CRC Press Inc., p. 2-38.

Katsube, T.J.
1981: Pore structure and pore parameters that control the radionuclide transport in crystalline rocks; Proceedings of the Technical Program, International Powder and Bulk Solids Handling and Processing, Rosemont, Illinois, p. 394-409.

Katsube, T.J. and Hume, J.P.
1987: Pore structure characteristics of granitic rock samples from Whiteshell Research Area; in Geotechnical Studies at Whiteshell Research Area (RA-3), CANMET, Report MRL 87-52, p. 111-158.
1989: Electrical resistivity of rocks from Chalk River; in Workshop Proceedings on "Geophysical and Related Geoscientific Research at Chalk River, Ontario", Atomic Energy of Canada Limited Report AECL-9085, p. 105-114.

Katsube, T.J., Murphy, T.B., Best, M.E., and Mudford, B.S.
1990: Pore structure characteristics of low permeability shales from deep formations; in Proceedings of the 1990 SCA (Society of Core Analysts) 4th Annual Technical Conference, August, 1990, Dallas, Texas, SCA-9010, p. 1-21.

Katsube, T.J., Mareschal, M., and Aucoin, F.
1991: Electrical characteristics of a graphitic rock from the Kapuskasing Structural zone; Part E; Geological Survey of Canada, Paper 91-1E.

Katsube, T.J., Percival, J.B., and Hume, J.P.
1985: Characterization of the rock mass by pore structure parameters; Atomic Energy of Canada Limited Technical record, TP-299, p. 375-413.

Kessler, D.W., Insley, H., and Sligh, W.H.
1940: Physical, mineralogical and durability studies on the building and monumental granites of the United States; Journal of Research of the National Bureau of Standards, v. 25, p. 161-206.

Levorsen, A.I.
1967: Geology of Petroleum; W.H. Freeman and Company, San Francisco, 723 p.

Mellor, M.
1971: Strength and deformability of rocks at low temperatures; Cold Regions Research and Engineering Laboratory (Hanover, NH) Report CORRELL-RR-294, 73 p.

Melnyk, T.W. and Skeet, A.M.M.
1986: An improved technique for the determination of rock porosity; Canadian Journal of Earth Sciences, v. 23, p. 1068-1074.

Norton, D. and Knapp, R.
1977: Transport phenomena in hydrothermal systems; the nature of porosity: American Journal of Sciences, v. 277, p. 913-936.

Skagius, K. and Neretnieks, I.
1985: Porosities and diffusivities of some non-sorbing species in crystalline rocks; KBS Technical report 85-03, 62 p.

Optical texture in coal subjected to spontaneous combustion

Thomas Gentzis[1] and Fariborz Goodarzi
Institute of Sedimentary and Petroleum Geology

Gentzis, T. and Goodarzi, F., 1991: Optical texture in coal subjected to spontaneous combustion; in Current Research, Part E, Geological Survey of Canada, Paper 91-1E, p. 299-304.

Abstract

Samples taken from coal that has undergone spontaneous combustion in a waste pile at Coleman, Alberta, were examined under the microscope using reflected light. Thermally altered coal macerals and their byproducts (i.e., pyrolytic carbon and tar) in these samples were observed to have optical textures and properties that differ from those of ordinary coal. Anisotropic pyrolytic carbon, showing a granular mosaic, botryoidal, and cenospheric morphology, was present, an indication that heat generated from coal combustion has resulted in the thermal cracking of the coal under locally elevated temperatures (<600°C).

The coals from the Coleman waste pile are compared with those from other carbonized and combusted coal seams in Western Canada, and the various similarities and differences are discussed.

Résumé

Des échantillons de charbon ayant été soumis à une combustion spontanée dans une pile de résidus à Coleman (Alberta) ont été examinés au microscope en lumière réfléchie. On a observé que les macéraux de charbon altérés par la chaleur et leurs sous-produits (charbon et goudron pyrolytiques), contenus dans ces échantillons, avaient des textures et des propriétés optiques différentes de celles du charbon ordinaire. Du charbon pyrolytique anisotrope, présentant une morphologie botryoïdale et cénosphérique à mosaïque granulaire, a été observé, indiquant que la chaleur produite par la combustion du charbon a entraîné la fissuration thermique du charbon à des températures élevées par endroits (plus de 600 °C).

Les charbons de la pile de résidus de Coleman sont comparés à ceux d'autres couches de charbon carbonisé et brûlé de l'Ouest canadien, et les diverses ressemblances et différences sont analysées.

[1] Alberta Research Council, Coal Research Centre Devon, 1 Oil Patch Drive, Devon, Alberta T0C 1E0

INTRODUCTION

Heat treatment of coal (carbonization) results in its destructive distillation, producing solid (semicoke and coke), liquid (tar), and gases (volatile matter) (Berkowitz, 1985). The same byproducts can also be produced by heat generated by the spontaneous combustion of coal (as shown by Gentzis and Goodarzi, 1989), as exemplified in a coal waste pile at Coleman, Alberta. Coal macerals develop an isotropic to anisotropic optical texture due to an increase in temperature during thermal treatment in processes such as carbonization, combustion, or liquefaction (hydrogenation) (Brown et al., 1964; Chandra and Taylor, 1982; Shibaoka et al., 1984; Goodarzi, 1986). The isotropic or anisotropic nature of the optical texture is dependent upon the reactivity of the coal macerals. The reactive macerals (liptinite, vitrinite) develop an anisotropic texture in response to artificial heating, but the texture of the non-reactive macerals (inertinite, weathered vitrinite) remains isotropic. Anisotropy can be either basic (strain anisotropy) similar to that developed in low-rank coals or near oxidation rims of reactive macerals that have been pre-oxidized and subsequently carbonized (Goodarzi et al., 1975; Goodarzi, 1986) or granular, showing a fine- to coarse-grained mosaic that develops in higher-rank coals, such as those described by Grint and Marsh (1981) and Goodarzi et al. (1988).

Different types of optical texture, as described by Grint and Marsh (1981) (Table 1), have been observed in self-ignited coal seams. The texture is related to coal rank and the combustion temperature of either the coal seam or coal waste pile (Goodarzi, 1987; Goodarzi et al., 1988; Gentzis and Goodarzi, 1989). One type of secondary optical texture formed as the result of thermal treatment of coal is that of pyrolytic carbon. Pyrolitic carbon normally forms as a result of thermal cracking of volatile matter (Goodarzi, 1986), and is known to occur in heat-modified coal seams, and coke and hydrogenation residues (Brown et al., 1964; Chandra and Taylor, 1982; Shibaoka et al., 1984; Goodarzi, 1986). It also occurs as part of the maceral composition of coals of subbituminous to meta-anthracite rank (0.5 to 7.3% R_o max) (Lemos de Sousa, 1973; Goodarzi, 1985a, b, 1986).

Table 1. Classification of the optical texture in cokes (After Grint and Marsh, 1981)

Classification of optical texture		Description of optical texture
Basic anisotropy	(B)	A flat featureless anisotropy associated with the parent uncarbonized vitrain from anthracites. This changes little (apparently) during carbonization.
Isotropic	(1)	
Fine grained mosaics	(Mf)	0.5-1.5 μm in diameter
Medium grained mosaics	(Mn)	1.5-5.0 μm in diameter
Coarse grained mosaics	(Mc)	5.0-10.0 μm in diameter
Coarse-flow anisotropy	(CF)	30-60 μm length; 5-10 μm width
Flow domain	(FD)	> 60 μm length; >10 μm width
Domains	(D)	Large rectangular shaped units >60.0 μm in diameter. D_1 is from the basic anisotropy of low volatile caking vitrains. D_2 is by the growth of mesophase from liquid pitch.

Goodarzi (1985a,b, 1986), Goodarzi et al. (1988), and Gentzis and Goodarzi (1989) have described the optical texture of pyrolytic carbon present in coals, naturally burning coal seams, and waste piles in Western Canada. The coal seams referred to are of different ranks (subbituminous C to medium volatile bituminous; 0.50 to 1.1% R_o max) and it was concluded from these studies that the pyrolytic carbon developed as a result of locally elevated temperatures (<600°C), resulting from either frictional heat generated during folding and faulting (i.e., at Byron Creek, British Columbia), or thermal events (i.e., Highvale, Alberta). These findings are in agreement with those of Shibaoka et al. (1984).

Both isotropic and anisotropic pyrolytic carbon have been identified in western Canadian coals, each having a distinct morphology and optical properties. The isotropic pyrolytic carbon has no fixed forms and occurs as either irregular masses or interlayered with anisotropic pyrolytic carbon. The latter exhibits two morphologies, conical or lamellar, and spherulitic. The reflectance and thickness of lamellae increase with temperature. At 500°C the lamellar thickness is only a few microns, whereas at 1000°C this thickness is 100 microns (Brown et al., 1964). The spherulitic carbon appears at temperatures exceeding 700°C and the size of the spheres is approximately 10 to 20 microns (Goodarzi, 1985b).

EXPERIMENTAL

The samples from the Coleman self-ignited coal waste pile were collected from a channel 4.4 m deep. Hot samples were cooled in water immediately to prevent further oxidation and combustion, and were then dried and crushed to -20 mesh (850 μm) and prepared into pellets following the method of Mackowsky (1982). The samples were studied petrologically using a Zeiss MPM II microscope, fitted with a Zonax microcomputer. Photomicrographs were taken using plane polarized light or with partly crossed polars.

RESULTS AND DISCUSSION

Examination of the organic matter from the self-ignited coal waste pile at Coleman, Alberta (Fig. 1) reveals the presence of both isotropic and anisotropic pyrolytic carbon. Heat generated from the spontaneous combustion of the waste pile carbonized the coal and produced tar. This tar subsequently escaped upward toward the roof of the waste pile, and was deposited in the interstices of the coal and coke fragments, effectively briquetting them.

Pyrolytic carbon is believed to form in the gas phase only (Shibaoka et al., 1984), and the thick, well developed, pyrolytic carbon masses seen in the Coleman waste pile indicate either the existence of gas for a long period of time, or rapid carbon formation. The most likely source of the pyrolytic carbon is the carbon dioxide that was generated during

dissolution of the coal in the waste pile. Usually, carbon dioxide is reduced to carbon monoxide, which can be thermally cracked to form pyrolytic carbon (Shibaoka et al., 1984).

In the Coleman waste pile, pyrolytic carbon consists of anisotropic layers coating semicoke fragments (Fig. 2a), or penetrating parallel fractures and veins inside cavities (Fig. 2b). This type of pyrolytic carbon forms under relatively low temperatures (<500°C). Anisotropic pyrolytic carbon forms large domains, which may be either "Y"-shaped (Fig. 2c) or nodal-shaped (Honda et al., 1971; Ragan and Goodarzi, 1985) (Fig. 2d). The latter authors observed "X"- and "Y"-shaped domains in a high rank vitrinite coke and a petroleum needle coke. They suggested that the presence of this type of optical texture is strong evidence of the formation of mesophase and a fast rate of heating. In addition, another type of anisotropic texture present resembles cenospheres, as shown in Figure 3a. The fragment illustrated is highly reflecting, rounded, contains devolatilization vacuoles, and is somewhat similar to pyrosclerotinite (Goodarzi, 1985b). The byproducts, which show a morphology similar to that of sclerotinite, were probably formed by the carbonization of reactive coal macerals (i.e. resinite) at temperatures around 500°C. Similarly, the temperature of formation of the nodal and Y-shaped domains is estimated at 400 to 500°C.

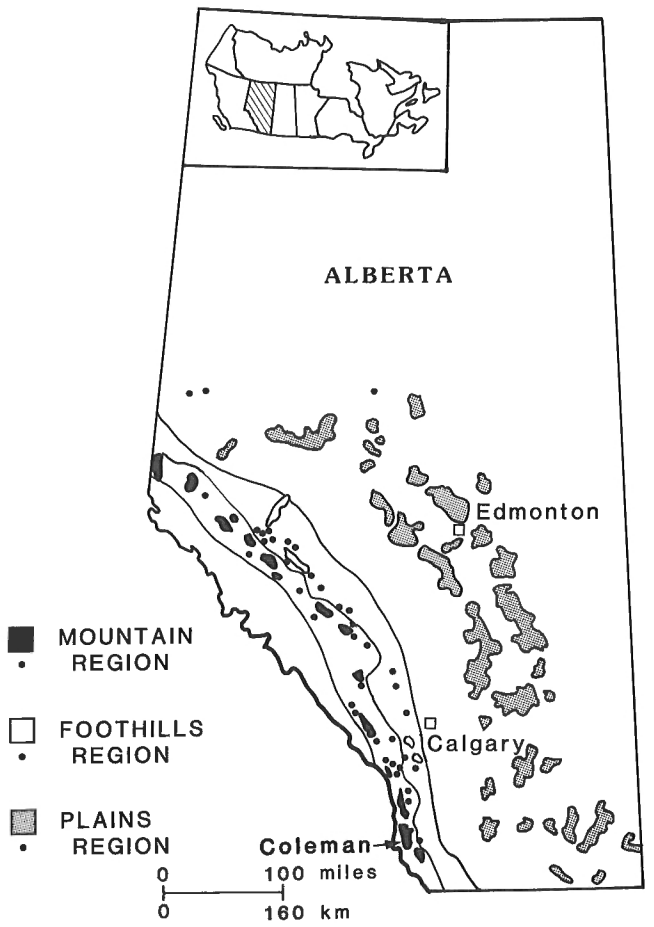

Figure 1. Location map of the study area. (After Gentzis and Goodarzi, 1989).

Brown et al. (1964) divided pyrolytic carbon into different types, based on the temperature of their formation. Pyrolytic carbon showing a coarse grained mosaic texture, similar to the texture commonly found in the vicinity of devolatilization vacuoles (Fig. 3b), was formed at a temperature of 500°C. This type of pyrolytic carbon shows that the volatile matter from which it originated penetrated cracks in pre-carbonized residues or in non-reactive coal macerals. Another type of pyrolytic carbon present in the Coleman waste pile shows high anisotropy, botryoidal structure, and cross extinction when the microscope stage is rotated (Fig. 3c, d). It also exhibits zonal texture, possibly due to variations in the degree of compaction and the size of the spheres. Particles of this type of pyrolytic carbon are up to 50 μm long, were produced at high temperatures (500°C), and formed from volatile matter (tar) deposited as penetrative material far away from the source of heat.

Apart from pyrolytic carbon that originates from the gaseous components of combustion, pitch-like solids (tar) can form from the liquid components. Different types of tar may be distinguished, based on morphology and optical texture. The isotropic texture of some of the tar is an indication that it originated from the cooler liquids, whereas the granular texture of other tars indicates that they formed from the hottest liquids. Figure 3e illustrates the coexistence of two types of optical texture a low-reflectance, low temperature (<500°C), isotropic phase, and a higher temperature (650°C), anisotropic phase that penetrated semi-coke fragments in the carbonization zone of the waste pile. The resulting structure is indicative of the zonation of optical texture formed by the interaction of two phases of tar.

Comparison with pyrolytic carbon in other deposits

Pyrolytic carbon has been observed in a partly combusted and coked bituminous coal seam at Aldridge Creek, British Columbia (Goodarzi et al., 1988). The rank of the unaltered coal at Aldridge Creek is 1.1% R_0 max, very similar to that of the Coleman waste pile (1.07% R_0 max) and, at both localities, tar produced by carbonization moved downward through the "deposit".

One of the main differences between the Coleman and Aldridge cases is a difference in byproducts. The burning coal at Coleman produced subangular coke fragments (showing basic anisotropy due to weathering prior to burning) that had been briquetted by coal-tar pitch. At Aldridge Creek, the burning of the coal produced a metallic, porous coke. Combustion temperature at Aldridge Creek is estimated to have been 1100°C, compared to 550 to 600°C at Coleman. Pyrolytic carbon in the Aldridge Creek samples is anisotropic and formed as the result of penetration of the semi-coke subzone by hot gases.

Goodarzi (1986) also found that coals in tectonically disturbed seams (e.g., Byron Creek Collieries, at Mist Mountain, British Columbia) commonly contain anisotropic, pyrolytic carbon showing lamellar structure. Heat generated by friction and burial during faulting produced locally elevated temperatures of up to 600°C (Bustin, 1983), resulting in the formation of lamellar pyrolytic carbon. Lamellar pyrolytic

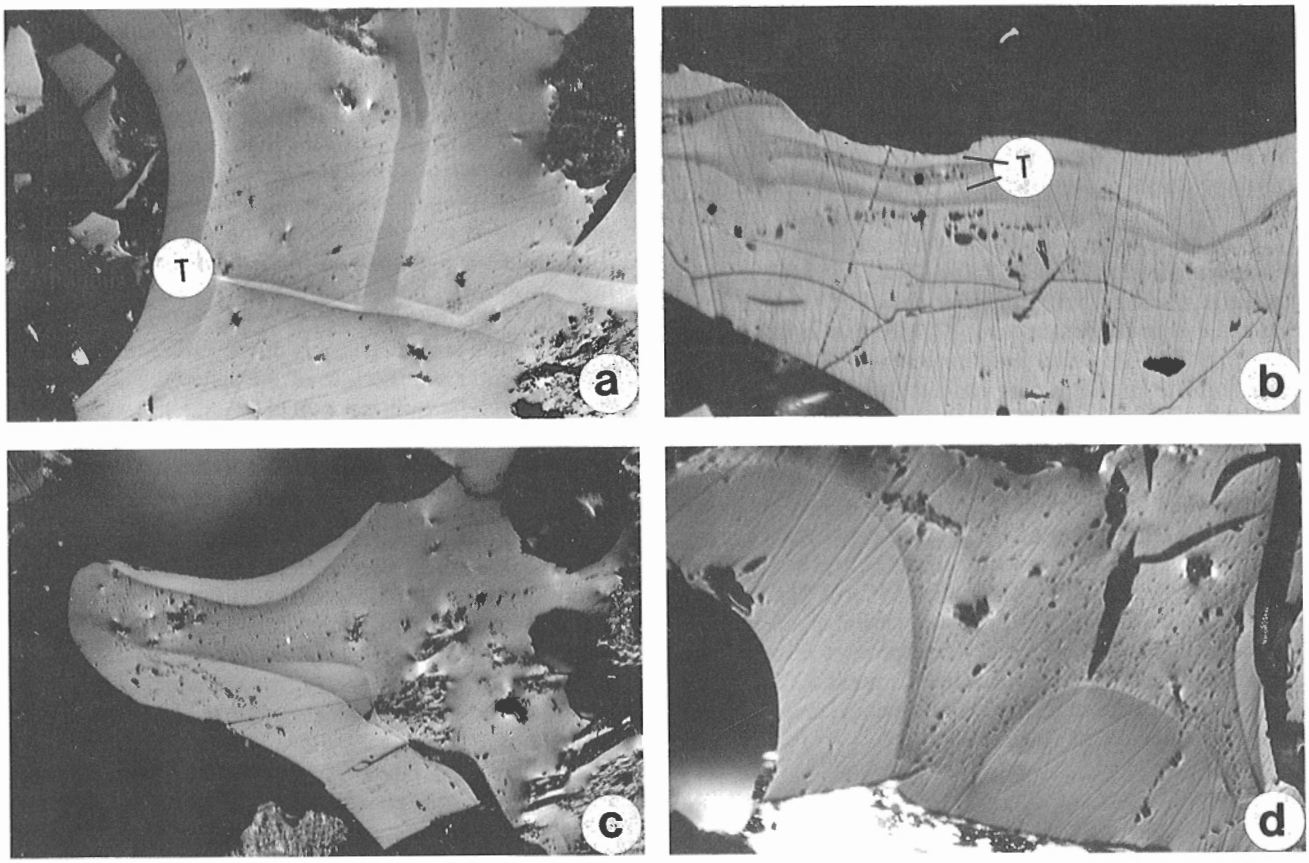

a - Anisotropic tar (T) coating organic fragments and filling cracks.

b - Anisotropic tar (T) growing parallel to edge of cavity.

c - A "Y"-shaped domain of a 2-type anisotropic pyrolytic carbon.

d - A nodal-shaped domain of anisotropic pyrolytic carbon.

Figure 2. Photomicrographs of samples from Coleman, Alberta. All photomicrographs were taken using black and white film, oil immersion, plane polarized light. Magnification is x500.

carbon, from a heat-modified (the result of a lightning strike) bituminous coal seam in the Eagle Mountain Coalfield, British Columbia, was classified into four morphological types by Gentzis and Goodarzi (1990). The four types are: i) granular, ii) simple spherulitic, iii) conical-laminated, and iv) thin lining. All these types are anisotropic and their development followed distinct paths during carbonization of the seam. The morphological and optical properties of the four types were used to estimate the range of temperatures responsible for their genesis. Therefore, pyrolytic carbon can be produced by heat generated not only by spontaneous combustion of a coal waste pile or seam, but also as the result of either tectonic activity (faulting) or a lightning strike.

Goodarzi (1985b) observed pyrolytic carbon in a subbituminous coal ($\%R_o$ max = 0.70) at Highvale, Alberta. This pyrolytic carbon has a rosette structure and formed from the condensation of volatile products generated during combustion of carbonaceous material. Highvale coal is the lowest rank coal found to contain pyrolytic carbon. Its occurrence is considered unusual and it is believed that its origin was allochthonous (detrital). Pyrolytic carbon in the Highvale coal is indicative of temperatures in the order of 500°C (Goodarzi, 1985b). A thermal event such as a forest or swamp fire could have been responsible for its formation, because of the high temperatures associated with such a fire (800 to 1000°C). The occurrence of pyrolytic carbon in such a low rank coal demonstrates that it can be produced by a forest (bush) fire, and then be transported to the site of peat formation and thus be incorporated in the coal.

Pyrolytic carbon with a lamellar morphology has also been observed in a high volatile bituminous coal seam ($\%R_o$ max = 0.70) at Coalspur, Alberta (Goodarzi, 1985c). Because of the non-coking properties of the coal relative to the coking coal at Aldridge Creek, coal from Coalspur was converted to non-porous, oxidized and combusted residue (char). The transformation of coal to ash resulted in an almost complete loss of seam morphology (Goodarzi and Gentzis, in press). In contrast, the coking coal at Aldridge Creek was transformed into hard, cohesive coke retaining the original coal seam morphology (texture) (Goodarzi et al., 1988). It is obvious that pyrolytic carbon can form in both coking and

non-coking coal seams as well as in coal waste piles, and that the morphology and optical texture of pyrolytic carbon are functions of the temperature responsible for its formation.

SUMMARY

This paper focuses on the optical textures present in a self-ignited coal in a waste pile at Coleman, Alberta, with particular emphasis on the resulting byproducts, especially pyrolytic carbon. The pyrolytic carbon from this "deposit" showed granular mosaic, botryoidal, and cenospheric morphology, indicating localized combustion temperatures in the order of 600°C. The morphology and temperature of formation of pyrolytic carbon depend on parameters such as coal rank (coking versus non-coking), coal morphology (seam or waste pile), and the origin of the heat (spontaneous combustion, forest fire, lightning strike, or tectonic activity).

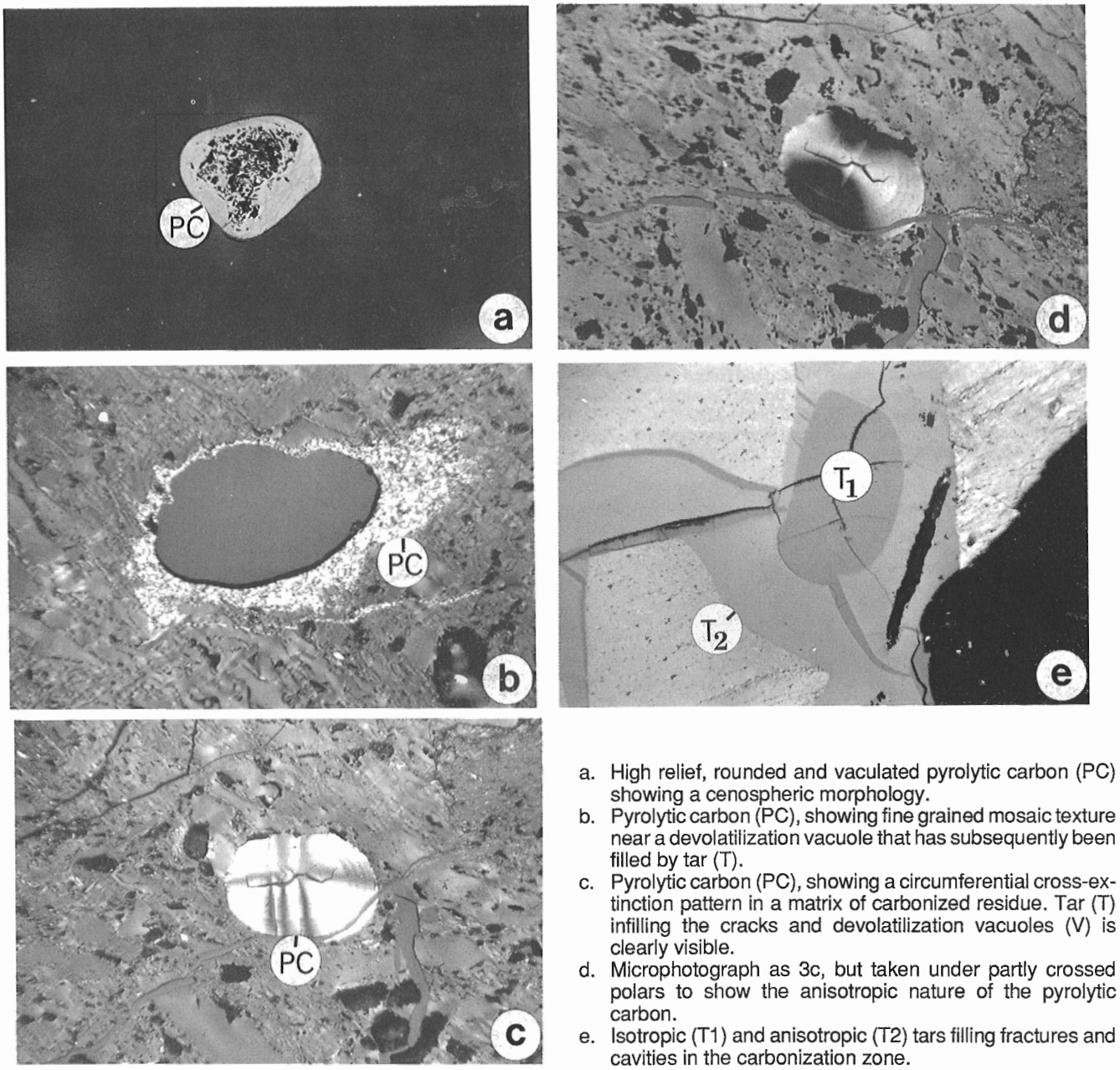

a. High relief, rounded and vaculated pyrolytic carbon (PC) showing a cenospheric morphology.
b. Pyrolytic carbon (PC), showing fine grained mosaic texture near a devolatilization vacuole that has subsequently been filled by tar (T).
c. Pyrolytic carbon (PC), showing a circumferential cross-extinction pattern in a matrix of carbonized residue. Tar (T) infilling the cracks and devolatilization vacuoles (V) is clearly visible.
d. Microphotograph as 3c, but taken under partly crossed polars to show the anisotropic nature of the pyrolytic carbon.
e. Isotropic (T1) and anisotropic (T2) tars filling fractures and cavities in the carbonization zone.

Figure 3. Photomicrographs of samples from Coleman, Alberta. All photomicrographs were taken using black and white film, oil immersion, plane polarized light, except 3d, which was taken under partly crossed polars. Magnification is x500.

ACKNOWLEDGMENTS

The manuscript benefitted from critical reading by A.R. Cameron, Geological Survey of Canada.

REFERENCES

Berkowitz, N.
1985: Some aspects of coal carbonization: coal tar processing; in The Chemistry of Coal, (ed.) N. Berkowitz; Elsevier, Amsterdam, p. 341-350.

Brown, H.R., Taylor, G.H., and Cook, A.C.
1964: Prediction of coke strength from the rank and petrographic composition of Australian coals; Fuel, v. 43, p. 43-54.

Bustin, R.M.
1983: Heating during thrust faulting in the Rocky Mountains: friction or fiction? Tectonophysics, v. 95, p. 309-328.

Chandra, D. and Taylor, G.H.
1982: Thermally altered coals; in Coal Petrology, (ed.) E. Stach et al.; Gebrüder Borntraeger, Berlin-Stuttgart, p. 206-218.

Gentzis, T. and Goodarzi, F.
1989: Organic petrology of a self-burning coal wastepile from Coleman, Alberta, Canada; International Journal of Coal Geology, v. 11, p. 257-271.

Goodarzi, F.
1985a: Optical properties of vitrinite carbonized at different pressures; Fuel, v. 64, p. 156-162.
1985b: Optically anisotropic fragments in a western Canadian subbituminous coal; Fuel, v. 64, p. 1294-1300.
1985c: Characteristics of pyrolytic carbon in Canadian coals; Fuel, v. 64, p. 1672-1675.
1986: Anisotropic fragments in strongly folded and faulted coals from the Rocky Mountain area of southeast British Columbia; Canadian Journal of Earth Sciences, v. 23, no. 2, p. 254-258.
1987: Reflectance and petrology of a burning bituminous coal seam; Fuel, v. 66, p. 1073-1078.

Goodarzi, F. and Gentzis, T.
1990a: The lateral and vertical reflectance and petrological variation of a heat-affected bituminous coal seam from southeastern British Columbia, Canada; International Journal of Coal Geology, v. 15, p. 317-339.
1990b: Natural coprocessing of coal and tar; in Proceedings of the American Chemical Society Division of Fuel, 200th National Meeting, Washington, D.C., v. 35, no. 4, p. 1071-1079.
in press: Geological controls on coal seams burning "in place"; American Association of Petroleum Geologists.

Goodarzi, F., Gentzis, T., and Bustin, R.M.
1988: Reflectance and petrology profile of a partially combusted and coked bituminous coal seam from British Columbia; Fuel, v. 67, p. 1218-1222.

Goodarzi, F., Hermon, G., Iley, M., and Marsh, H.
1975: Carbonization and liquid-crystal (mesophase) development. Part 6. Effects of pre-oxidation on vitrinites upon coking properties; Fuel, v. 54, p. 105-112.

Grint, P. and Marsh, H.
1981: Carbonization of coal blends: mesophase formation and coke properties; Fuel, v. 60, p. 1115-1120.

Honda, H., Kimura, H., and Sanada, Y.
1971: Changes of pleochroism and extinction contours in carbonaceous mesophase; Carbon, v. 9, p. 695-697.

Lemos de Sousa, M.J.
1973: Sur la presence du pyrocarbone dans quelques carbon; International Committee for Coal Petrology, Meeting, Lille, France, 18 p.

Mackowsky, M. M-Th.
1982: Methods and tools of coal examination; in Coal Petrology, (ed.) E. Stach et al.; Gebrüder Borntraeger, Berlin-Stuttgart, p. 295-300.

Ragan, S. and Goodarzi, F.
1985: Disclinations in the optical texture of a high-rank vitrinite coke and a petroleum needle-coke; Fuel, v. 63, p. 1382-1384.

Shibaoka, M.F., Foster, W.R., Okada, K., and Clark, K.N.
1984: Formation of pyrolytic carbon in a continuous reaction for coal hydrogenation; Fuel, v. 63, p. 169-173.

Investigations of the Quaternary geology of Hudson Strait and Ungava Bay, Northwest Territories

B. MacLean, G. Vilks, A. Aitken[1], V. Allen[2], W. Briggs[3], D. Bruneau[4], A. Doiron[5], M. Escamilla[6], I. Hardy, J. Miner[6], W. Mode[7], R. Powell[6], M. Retelle[8], J. Stravers[6], A. Taylor[2], and N. Weiner[3]
Atlantic Geoscience Centre, Dartmouth

MacLean, B., Vilks, G., Aitken, A., Allen, V., Briggs, W., Bruneau, D., Doiron, A., Escamilla, M., Hardy, I., Miner, J., Mode, W., Powell, R., Retelle, M., Stravers, J., Taylor, A., and Weiner, N., 1991: Investigations of the Quaternary geology of Hudson Strait and Ungava Bay, Northwest Territories; in Current Research, Part E; Geological Survey of Canada, Paper 91-1E, p. 305-315.

Abstract

Investigations of the Quaternary geology of Hudson Strait and Ungava Bay were carried out from ***CSS Hudson*** *between September 24 and October 16, 1990. The studies were conducted mainly by means of geophysical profiling with acoustic systems, sediment coring, and grab sampling. They provide information on sediment distribution, depositional environments, late glacial- deglacial- postglacial history, and proxy data relating to global change.*

The thickest accumulations of Quaternary sediments (up to 130 m) are in three main basins, one in the east, and two in the west, and locally in bays and fiords along the south coast of the strait and in the channel marginal to the central platform in Ungava Bay. Glacial, glaciomarine, and postglacial sediments are represented.

Résumé

Des recherches sur la géologie du Quaternaire du détroit d'Hudson et de la baie d'Ungava ont été menées à partir du ***CSS Hudson*** *entre le 24 septembre et le 16 octobre 1990. Les études ont été réalisées principalement en établissant des profils géophysiques à l'aide de systèmes acoustiques et en prélevant des carottes de sédiments et des échantillons au hasard. Elles ont fourni des renseignements sur la distribution des sédiments, les milieux de sédimentation, l'histoire de la fin du glaciaire, de la déglaciation et du post-glaciaire, et des données approximatives sur le changement planétaire.*

Les couches les plus épaisses de sédiments du Quaternaire (jusqu'à 130 m) se trouvent dans trois principaux bassins, un dans l'est et deux dans l'ouest, et par endroits dans des baies et des fjords le long de la côte méridionale du détroit et dans le chenal en bordure de la plate-forme centrale dans la baie d'Ungava. Des sédiments glaciaires, glaciomarins et postglaciaires sont représentés.

[1] Queen's University, Kingston, Ontario
[2] Terrain Sciences Division, Ottawa
[3] University of Colorado, Boulder, Colorado
[4] University of Montreal, Montreal, Quebec
[5] Centre Geoscientifique de Quebec, Sainte-Foy, Quebec
[6] Northern Illinois University, DeKalb, Illinois
[7] University of Wisconsin, Oshkosh, Wisconsin
[8] Bates College, Lewiston, Maine

INTRODUCTION

An investigation of the Quaternary geology of Hudson Strait and Ungava Bay was carried out from **CSS Hudson** from September 23 to October 16, 1990 during cruise 90-023. This was a collaborative program with participating researchers from nine institutions who have been studying the Quaternary geology onshore and offshore in this region. Prior to commencing investigations in Hudson Strait, work relating to other programs was carried out in Frobisher Bay and adjacent offshore areas (see J. Stravers in MacLean et al., 1991).

During the Wisconsinan, Hudson Strait was a major distributory route for glacial ice, and it is thought also to have been a major meltwater discharge route. Objectives of the studies in Hudson Strait — Ungava Bay were to examine the record of glacial — deglacial — postglacial events, conditions, and environments to further delineate the Quaternary history of the region and to obtain data relating to studies of global change. The study was also concerned with acquiring further regional information regarding distribution of the sediment units, their composition, depositional environments, stratigraphic and facies relationships, chronologies, and relationships with onshore deposits.

Generalized bathymetry of Hudson Strait — Ungava Bay is shown in Figure 1. Greatest water depths in Hudson Strait occur in three half-graben basins: one in the eastern part of the Strait north of Ungava Bay where depths exceed 900 m; and in two basins in the western part of the Strait, north and southwest of Charles Island, where depths exceed 400 m. The broad zone enclosed by the 200 m isobath in the central region of the Strait reflects the synclinal bedrock structure in that region (MacLean et al., 1986).

In Ungava Bay a shallow platform, with depths from 53 m to about 135 m, occupies the central part of the Bay. This is bounded to the west, south, and east by a marginal channel with maximum depths of 250 m in the west to 365 m in the east.

METHODS

Investigations carried out from **CSS Hudson** cruise 90-023 included the collection of both geophysical data and samples. Geophysical data were obtained with a Huntec high resolution seismic reflection system; hull-mounted 3.5 kHz system; single channel seismic reflection system using a 655 cm^3 compressed air source and Nova Scotia Research Foundation

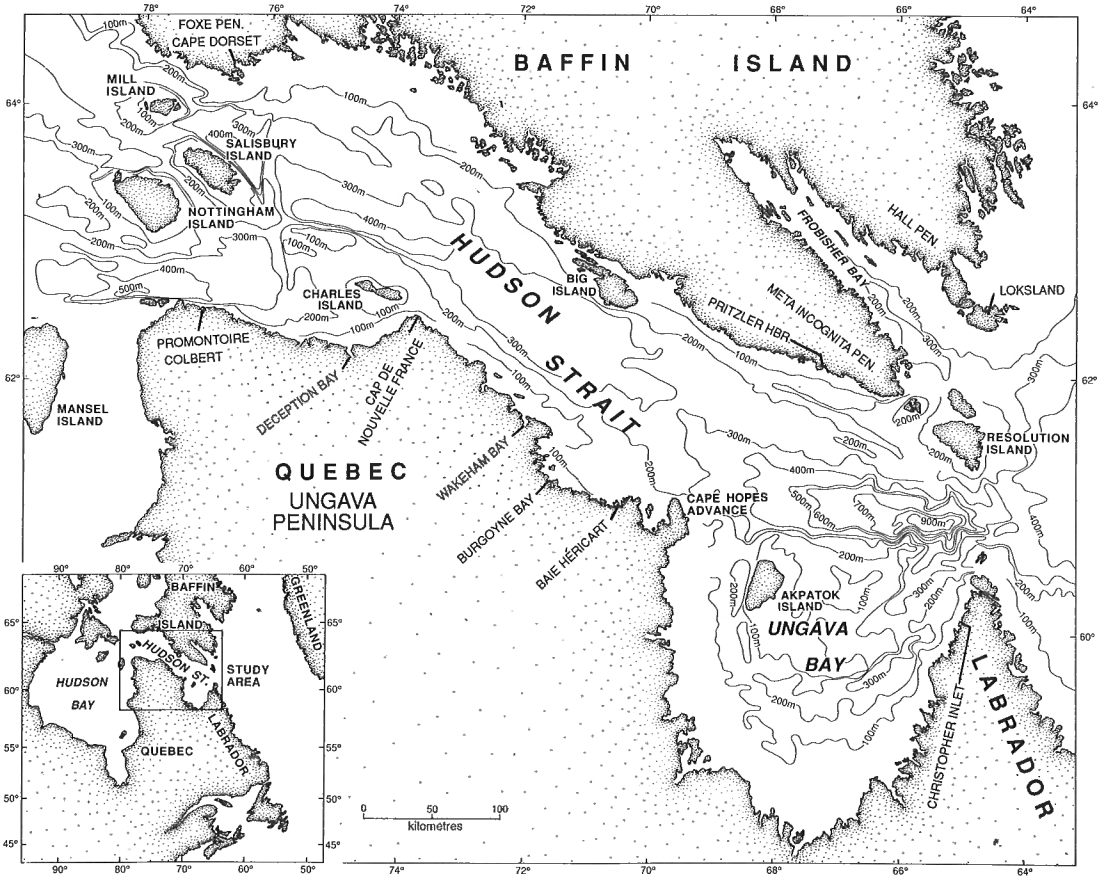

Figure 1. Bathymetry of Hudson Strait and Ungava Bay.

hydrophone; Bedford Institute of Oceanography sidescan sonar, and a Barranger magnetometer. Survey tracks are shown in Figure 2.

Sediment samples were obtained by means of the AGC large diameter piston corer, IKU clam shell sampler, Van Veen grab sampler, and by box coring (Table 1, Fig. 3).

Measurements of in situ temperature and pore pressure were conducted at selected stations by means of an instrumented core cutter on the piston corer.

Vertical plankton tows provided data on modern microfaunal populations within the water column.

Nearshore geological surveys were carried out in Deception Bay from a launch fitted with small profiling and sampling systems.

Preliminary measurements and processing of sediment cores and samples were carried out at sea. These included thermal conductivity, magnetic susceptibility, physical property (shear vane) measurements, core splitting and visual logging, core photography, and subsampling that included micro- and macro- fossils, palynology, texture, water content - bulk density, and gas. Selected cores were also subsampled for paleomag, ostracods, diatoms, thermo-luminescence, and consolidation studies.

Bulk samples from IKU and Van Veen grabs and from box cores were washed and sieved to provide data on gravel lithologies, and also contributed specimens for studies of seabed and subsurface biota.

Navigational positioning was primarily by Navstar GPS, which was available approximately 20 hours per day, supplemented by Lorac-C, NNSS TRANSIT satellite, and log and gyro data.

Further details regarding cruise procedures may be obtained from the 90-023 cruise report (MacLean et al., 1991).

PREVIOUS STUDIES

The following summary is derived from selected studies in the region and in relevant adjacent areas. On southern Baffin Island, studies by Blake (1966) and Clark (1985) indicated southward ice flow toward Hudson Strait with impingement of eastward flowing Hudson Strait ice in a narrow zone along the coast, and northeasterly flow across eastern Meta Incognita Peninsula. Deglaciation had progressed to the Big Island area by ca. 8000 B.P.

Studies of eastern Meta Incognita Peninsula (Stravers, 1986; Miller et al., 1988) indicated multiple glaciations, and evidence of northeasterly flowing ice which overrode the

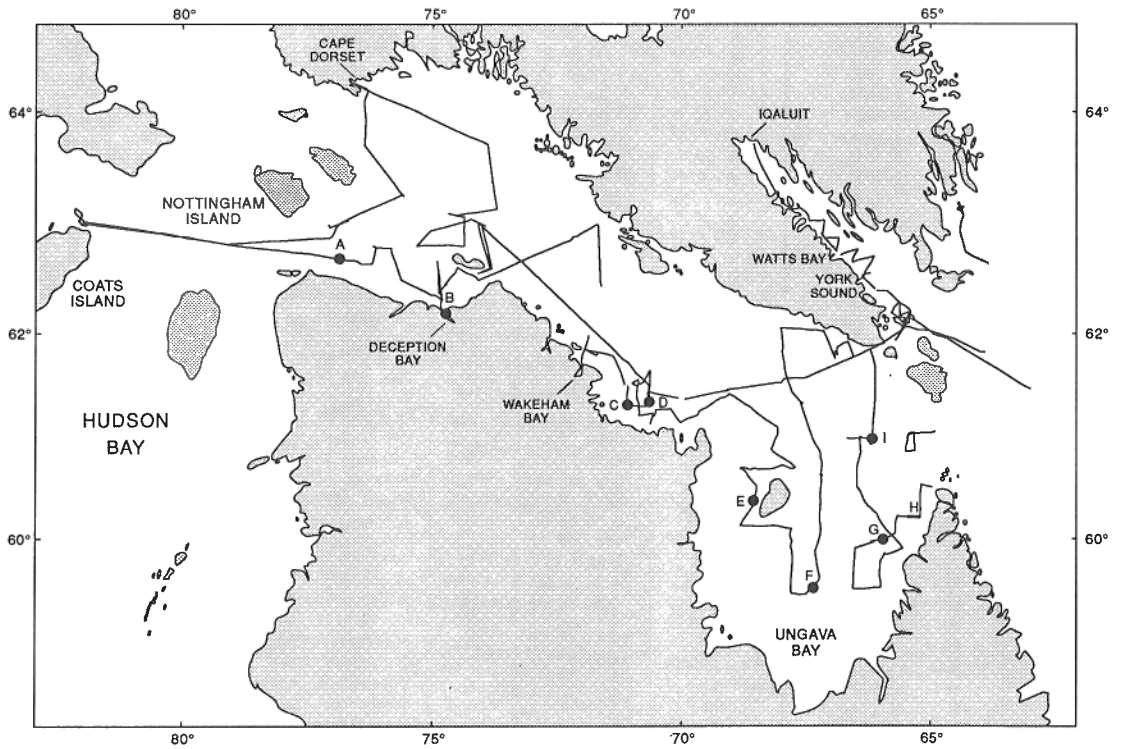

Figure 2. Survey tracks.

Table 1. 90-023 Stations

Station Number	Sample Type	Latitude	Longitude	Depth (m)	Geographic Location
031	core	60 57.10 N	62 26.70 W	872	Hudson Strait
032	grab	60 57.30 N	65 29.70 W	872	Hudson Strait
033	grab	60 09.75 N	65 11.22 W	112	Ungava Bay
034	core	59 59.41 N	65 44.03 W	112	Ungava Bay
035	grab	59 59.35 N	65 44.00 W	336	Ungava Bay
036	core	59 57.81 N	65 53.89 W	332	Ungava Bay
037	grab	59 51.00 N	66 29.69 W	108	Ungava Bay
038	grab	59 26.17 N	66 32.88 W	245	Ungava Bay
039	core	59 47.06 N	65 55.82 W	387	Ungava Bay
040	grab	59 47.00 N	65 55.79 W	408	Ungava Bay
041	grab	60 31.80 N	66 28.30 W	149	Ungava Bay
042	core	60 57.01 N	66 36.95 W	761	Eastern Hudson Strait
043	grab	60 57.03 N	66 36.95 W	729	Eastern Hudson Strait
044	boxcore	60 56.97 N	66 08.92 W	844	Eastern Hudson Strait
045	core	60 56.80 N	66 08.28 W	845	Eastern Hudson Strait
046	water	60 55.48 N	66 08.64 W	200	Eastern Hudson Strait
047	water	60 54.73 N	66 08.76 W	200	Eastern Hudson Strait
048	grab	61 48.29 N	66 11.78 W	226	Eastern Hudson Strait
049	IKU	61 47.37 N	66 51.62 W	223	Eastern Hudson Strait
050	grab	61 58.80 N	67 06.96 W	87	Eastern Hudson Strait
051	grab	62 00.95 N	67 57.34 W	150	Eastern Hudson Strait
052	core	61 19.48 N	67 36.21 W	402	Eastern Hudson Strait
053	grab	61 19.31 N	67 36.01 W	400	Eastern Hudson Strait
054	grab	60 34.98 N	67 10.47 W	137	Ungava Bay
055	camera	60 34.85 N	67 09.26 W	141	Ungava Bay
056	grab	60 15.90 N	67 12.15 W	111	Ungava Bay
057	grab	59 50.19 N	67 17.75 W	57	Ungava Bay
058	camera	59 50.45 N	67 16.50 W	82	Ungava Bay
059	core	59 32.01 N	67 13.26 W	290	Ungava Bay
060	grab	59 31.60 N	67 12.63 W	294	Ungava Bay
061	grab	60 02.89 N	67 45.78 W	72	Ungava Bay
062	core	60 15.76 N	68 32.97 W	234	Ungava Bay
063	grab	60 15.55 N	68 32.89 W	232	Ungava Bay
064	core	60 07.50 N	70 34.60 W	196	Baie Héricart
065	grab	61 08.10 N	70 34.00 W	196	Baie Héricart
066	core	61 27 82.N	70 51.00 W	193	Baie Héricart-Wakeham Bay
067	grab	61 27.29 N	70 52.12 W	193	Baie Héricart-Wakeham Bay
068	core	61 26.58 N	71 02.39 W	157	Baie Héricart-Wakeham Bay
069	grab	61 26.39 N	71 02.98 W	150	Baie Héricart-Wakeham Bay
070	IKU	61 26.21 N	71 03.34 W	149	Baie Héricart-Wakeham Bay
071	core	61 46.72 N	71 56.65 W	110	Wakeham Bay Area
072	grab	61 46.72 N	71 56.20 W	111	Wakeham Bay Area
073	IKU	62 25.17 N	71 34.63 W	333	Central Hudson Strait
074	IKU	62 44.28 N	72 42.26 W	358	Central Hudson Strait
075	IKU	62 27.90 N	74 03.11 W	86	Western Hudson Strait
076	core	62 09.70 N	74 42.28 W	67	Deception Bay
077	grab	62 09.58 N	74 42.14 W	69	Deception Bay
078	camera	62 21.24 N	74 48.19 W	110	Western Hudson Strait
079	IKU	62 21.31 N	74 48.37 W	115	Western Hudson Strait
080	grab	62 08.47 N	74 38.56 W	40	Deception Bay
081	grab	62 08.20 N	74 38.42 W	70	Deception Bay
082	core	62 08.20 N	74 38.42 W	70	Deception Bay
083	IKU	62 46.71 N	76 05.34 W	315	Western Hudson Strait
084	grab	62 46.72 N	76 05.27 W	315	Western Hudson Strait
085	core	62 36.95 N	76 22.53 W	380	Western Hudson Strait
086	grab	62 37.01 N	76 22.54 W	390	Western Hudson Strait
087	core	62 38.90 N	76 39.77 W	390	Offshore Promontoire Colbert
088	grab	62 38.95 N	76 39.97 W	390	Offshore Promontoire Colbert
094	core	63 00.97 N	76 38.61 W	320	Western Hudson Strait
095	grab	63 01.01 N	76 38.56 W	320	Western Hudson Strait
096	IKU	62 57.45 N	76 59.91 W	275	Western Hudson Strait
097	core	63 14.96 N	75 32.68 W	427	Western Hudson Strait
098	grab	63 14.83 N	75 32.40 W	427	Western Hudson Strait
099	core	63 03.90 N	74 33.96 W	386	Western Hudson Strait
100	grab	63 04.07 N	74 34.00 W	393	Western Hudson Strait
101	core	63 02.99 N	74 18.24 W	389	Western Hudson Strait
102	grab	63 03.07 N	74 18.31 W	421	Western Hudson Strait
103	water	63 02.89 N	74 18.05 W	200	Western Hudson Strait
104	core	62 59.50 N	74 00.04 W	410	Western Hudson Strait
105	grab	62 59.57 N	73 59.90 W	410	Western Hudson Strait
106	core	62 59.30 N	73 59.90 W	412	Western Hudson Strait
107	core	61 20.67 N	70 37.77 W	182	Baie Héricart-Wakeham Bay
108	grab	61 20.70 N	70 37.67 W	182	Baie Héricart-Wakeham Bay
109	IKU	61 24.17 N	70 37.35 W	152	Baie Héricart-Wakeham Bay
110	IKU	61 19.90 N	69 54.80 W	210	Cape Hopes Advance Area
111	grab	61 19.75 N	69 54.54 W	214	Eastern Hudson Strait
112	IKU	61 32.06 N	67 28.07 W	265	Eastern Hudson Strait

southeastern part of the peninsula and deposited till whose provenance suggested a source in the Ungava Peninsula. From this evidence and data from Loksland and Hall Peninsula (Miller, 1985) and from the continental shelf (Praeg et al. 1986; Josenhans et al., 1986) ice from Ungava/Labrador was postulated to have crossed Hudson Strait and to have overridden southeastern Meta Incognita Peninsula and parts of eastern Baffin Island and adjacent shelf to the north (Osterman et al., 1985; Stravers, 1986, Miller et al., 1988; Andrews, 1989). Miller and Kaufman (1990) suggested three such advances onto Meta Incognita between 11 500 and 8000 B.P.

The Late Quaternary geology of northern Labrador has also been studied in various areas (see Clark, 1988; 1990). Relationships associated with glacial lakes indicate that glacial ice remained in Ungava Bay after part of the Labrador Peninsula had become ice-free (Klassen, 1990).

On Akpatok Island investigations by Løken (1978) and Gray et al. (1990) provided evidence of: eastward moving ice in the west that retreated before 7200 B.P.; impingement of northward moving ice in the southeast; emergence in an open marine environment had begun by 6900 to 6500 B.P.; and postglacial tilting of the island.

Ice flow from Ungava Peninsula into Ungava Bay was convergent; northerly in the southwest, and northeasterly along the west coast. The southern part of the bay was not deglaciated until ca. 7300-7000 B.P. and ice lingered nearby until 6500 and later (Gray and Lauriol, 1985; Lauriol and Gray, 1987; Allard et al., 1989).

On the northern coast of Ungava Peninsula west of Ungava Bay northward ice flow in the region bordering Hudson Strait appears to have merged with eastward flowing ice which slightly overrode the coast (see Gray and Lauriol, 1985; Bruneau et al., 1990). Withdrawal of ice from the Deception Bay — Cap de Nouvelle-France coastal region occurred as early as ca. 10 000 to 9500 B.P. Flow was also eastward on northern Charles Island.

At the western end of the strait flow was convergent: predominantly northward on northern Ungava Peninsula; southward on southern Foxe Peninsula, except eastward on the tips of both; and eastward on Nottingham, Salisbury, and Mill islands. Deglaciation of the islands and the adjacent part of Ungava Peninsula did not occur before 8100 B.P., and the southern coast of Foxe Pensinsula not until 7700 B.P. (Laymon, 1988).

The Quaternary history of much of Hudson Strait is intimately related to that of Hudson Bay and Foxe Basin, which has been the subject of much debate (see review references below).

Previous marine investigations included: studies by Grant and Manchester (1970) that provided data on bedrock and surficial sediments in eastern Hudson Strait and Ungava Bay; coring by Fillon and Harmes (1982) provided initial age dates of 9100 ± 480 and 8730 ± 250 on sediments in the eastern part of the strait; reconnaissance investigations of Hudson Strait by MacLean et al. (1986) outlined and sampled Quaternary sediments in three principal basins and indicated the bedrock

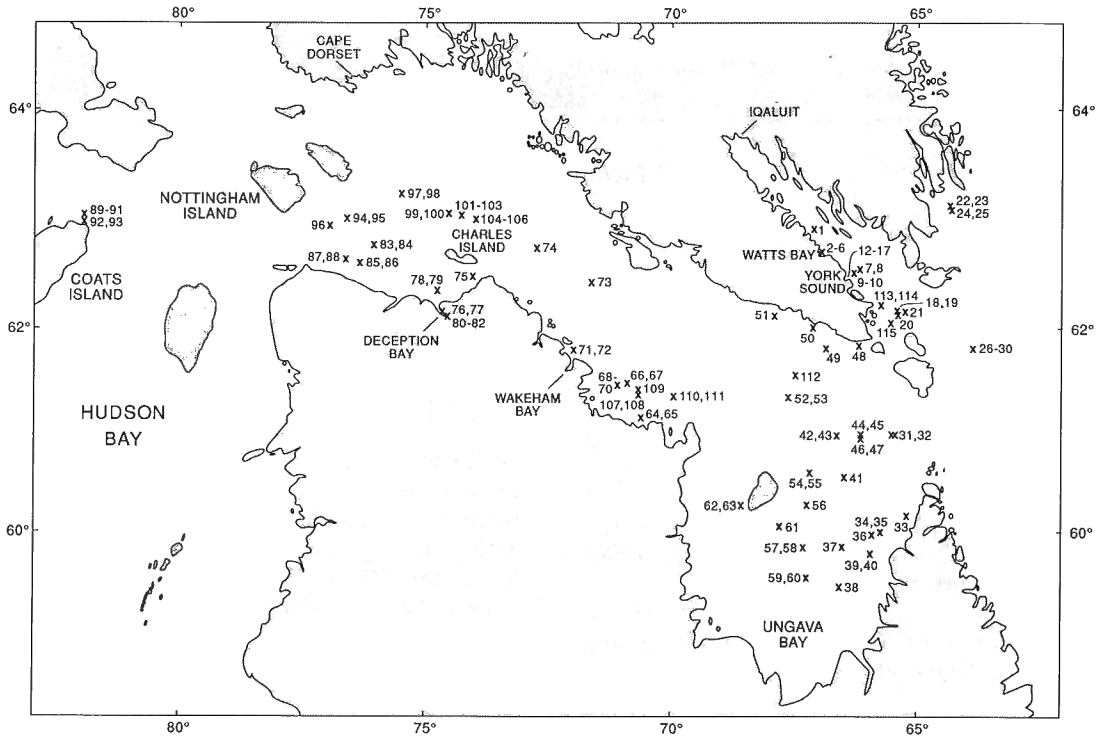

Figure 3. Sample station locations.

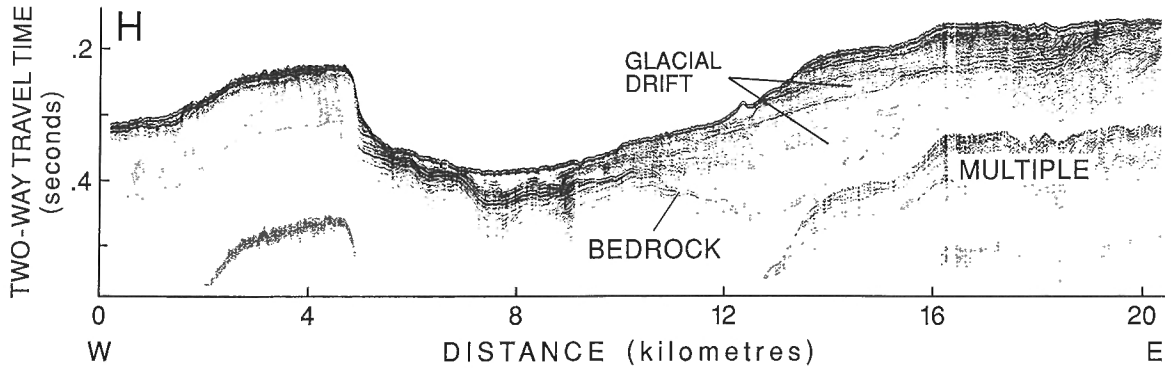

Figure 4. Section H, Seismic reflection profile illustrating multiple glacial drift sequences overlying bedrock in the marginal channel in eastern Ungava Bay. (see Fig. 2 for location)

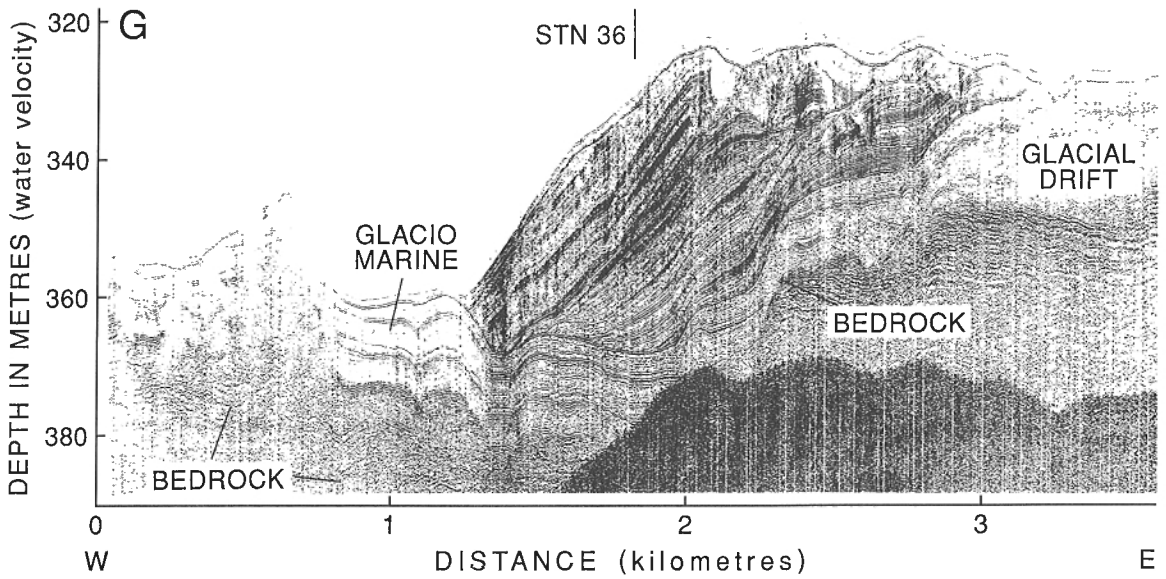

Figure 5. Section G, Huntec seismic reflection profile showing a wedge of prograded sediments in the marginal channel in eastern Ungava Bay. Underlying acoustically stratified sediments appear to be transitional to glacial drift 2 to 3 km along section.

geology and structure; from these cores Vilks et al. (1989) outlined depositional and paleoceanographic conditions, and biostratigraphic framework which indicated ice distal conditions in the eastern basin while ice proximal conditions still prevailed in the western part of the strait ca. 7900 B.P. Studies in Hudson Bay by Josenhans and Zevenhuizen (1990) suggest deglaciation of that region was rapid and dynamic. For further regional information readers are referred to: Dyke and Prest (1987), Andrews et al. (1982), Andrews (1989), and to relevant sections of Piper et al. (1990).

RESULTS

Sediments in the three main basins include glacial drift[1], glaciomarine ice proximal and ice distal, and postglacial sediments which locally total 130 m in thickness. Debris flow sediments may also be represented (MacLean et al., 1986; Vilks et al., 1989). This report provides a preliminary overview of the geological setting in areas investigated in 1990.

[1] The term glacial drift is used to describe sediments that we consider were deposited beneath grounded glacial ice, including till and other ice contact sediments not resolved by acoustic profiles.

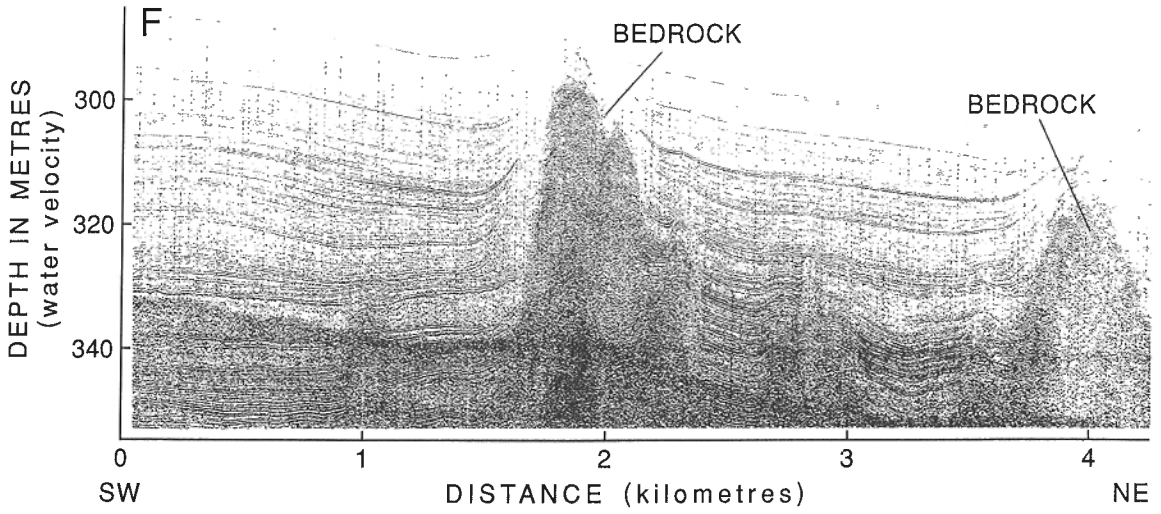

Figure 6. Section F, Huntec seismic reflection profile showing thick sediment deposits overlying an irregular surface on Precambrian rocks in the marginal channel in southern Ungava Bay.

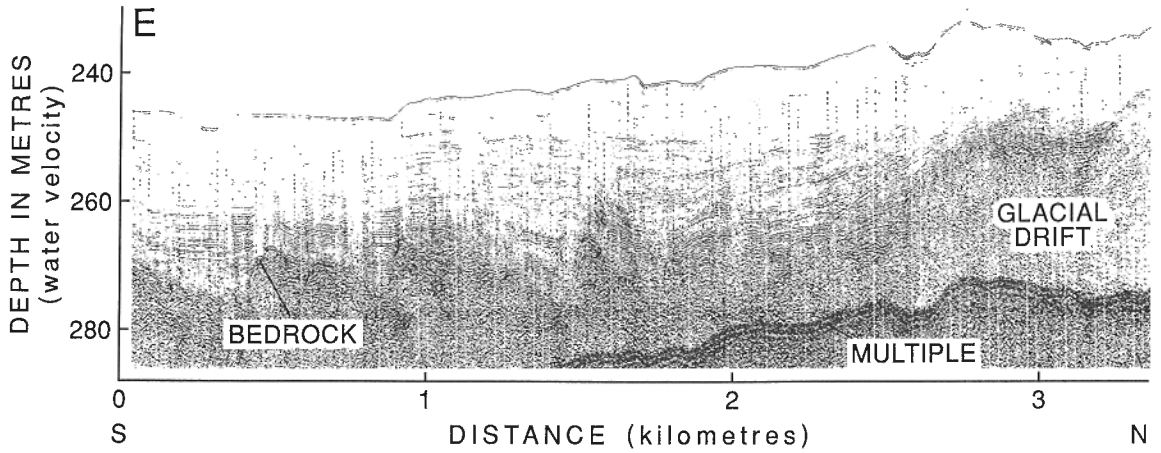

Figure 7. Section E, Huntec seismic reflection profile showing sediments in the marginal channel west of Akpatok Island. In the northern part of the section, later drift or ice keel turbate overlie the acoustically stratified glaciomarine sediments.

Eastern Hudson Strait

In the eastern part of the Strait, acoustically stratified sediments of the eastern basin give way northward to acoustically unstratified ice scoured sediments above 200 m water depth. Sediments interpreted to be glacial drift form what may be a moraine in 95 to 110 m water depth 9 km southeast of Pritzler Harbour (Fig. 1). Sidescan sonograms from areas southeast and southwest of Pritzler Harbour display numerous aligned ice scours (sole marks ?) that appear to trend slightly south of east.

Ungava Bay

In eastern Ungava Bay glacial drift deposits comprising up to six multiple sequences, totalling 150 m in thickness, extend some 20 km northwestward from the coast near Christopher Inlet (Fig. 4). Thirty-eight kilometres to the southwest, glacial drift interfingers with acoustically stratified sediments inferred to represent glaciomarine deposits (Fig. 5). The sediments at that locality are unconformably overlain by a westerly facing wedge of prograding younger sediments (outwash delta?) (Fig. 5). Water depth at this locality is 330 m.

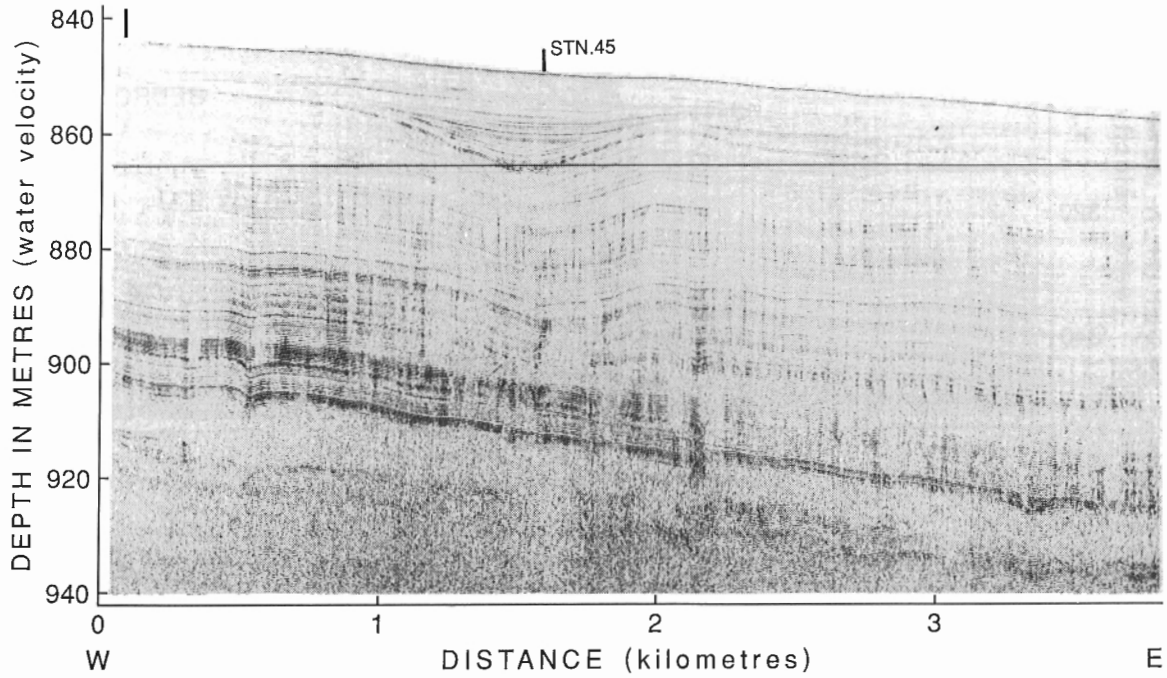

Figure 8. Section I, Huntec profile showing part of the thick sediment deposit in the eastern basin in Hudson Strait.

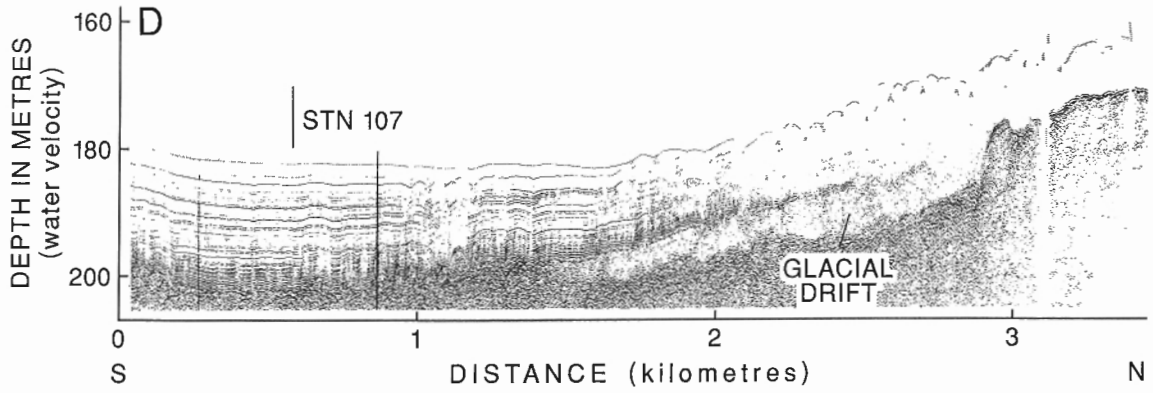

Figure 9. Section D, Huntec seismic reflection profile showing the transition of aoustically stratified glaciomarine sediments to unstratified sediments interpreted to represent glacial drift and/or ice keel turbate in Baie Héricart - Wakeham region.

Foraminifera from 20 cm intervals of Core 90-023-36 in the prograding sediments indicate assemblages that correspond to faunal zones C and D of Vilks et al. (1989) in the eastern basin of Hudson Strait. The top is dominated by the cold water species *Islandiella helenae* and the remainder by *Elphidium excavatum* and *Cassidulina reniforme*. Dominance down core of the latter assemblages suggests reduced salinities and fast sedimentation rates normally associated with proglacial environments. The presence of planktonic foraminifera and a few offshore species indicate a faunal connection to the Labrador Sea through Hudson Strait.

Sediments in the marginal channel in the southern part of Ungava Bay principally comprise acoustically stratified sediments, 20 to 40 m thick, that infill and cover a very irregular surface across Precambrian rocks (Fig. 6). In the southeast these sediments in places are overlain by unstratified sediments.

Acoustically stratified sediments also occur in the marginal channel west of the platform where, as in the south, they infill depressions, but are less continuous. Sediments in this area have been extensively ice scoured except in the deepest

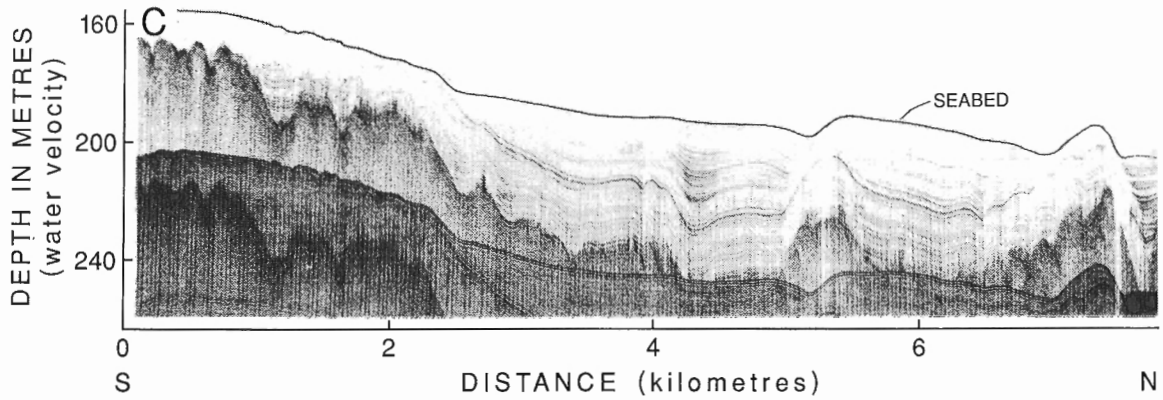

Figure 10. Section C, Huntec seismic reflection profile showing thick sediments off Burgoyne Bay in Baie Héricart-Wakeham region.

part of the marginal channel west of Akpatok Island. Northward the upper part of the sequence is overlain by turbate or glacial drift (Fig. 7).

In contrast to those in the marginal channel, sediments on the central plateau in Ungava Bay are generally thin except in the southeast where they range from <5 to 10 m in thickness. Sediments in all areas on the plateau have been intensely ice scoured and are acoustically unstratified, except in a few localities in the southeast where remnant stratification is evident. This suggests those deposits include reworked glaciomarine sediments.

Central Hudson Strait

The region on the south side of Hudson Strait from Baie Héricart westward towards Wakeham Bay contains important accumulations of acoustically stratified sediments that laterally are transitional to sediments interpreted to be glacial drift (Fig. 9, 10), which locally form moraines (MacLean et al., 1986). Cores collected at several localities in this region (Fig. 3 and Table 1) are expected to provide significant information on environments and chronologies. Andrews et al. (this volume) present magnetic susceptibility data from the sediments in Core 90-023-64 from this region and compare those data with results from Core 90-023-45 in postglacial sediments in the eastern basin of Hudson Strait (Fig. 8).

Deposits within Wakeham Bay comprise up to 50 m of acoustically stratified and unstratified sediments. These, and thick deposits in Deception Bay in the western part of the strait, indicate the presence of substantial amounts of sediment in the fiords along the south coast of Hudson Strait.

In Hudson Strait north of Wakeham Bay and westward to Charles Island acoustically unstratified sediments are the principal sediment unit, except west of Big Island where acoustically stratified sediments up to 15 m thick locally overlie glacial drift. Between Charles Island and Cap de Nouvelle France acoustically unstratified sediments up to 60 m thick, which appear to comprise several individual units, flank both the north and south sides of a bedrock ridge.

Western Hudson Strait

The thick acoustically unstratified sediments between Charles Island and Cap de Nouvelle France thin westerly south of Charles Island, but thicken to 50 m and possibly substantially more northwest of the entrance to Deception Bay. Deposits within Deception Bay comprise up to 40 m or more of mainly acoustically stratified sediments (Fig. 11).

Westward in the basin southwest of Charles Island up to 12 m of acoustically stratified sediments and 7 m of acoustically transparent (postglacial) sediments overlie unstratified sediments interpreted to comprise multiple glacial drift units that reach 80 m in total thickness. The stratified sediments intertongue with the uppermost drift unit 30 km northeast of Promontoire Colbert (Fig. 12). Acoustically stratified sediments also appear to interfinger with glacial drift 37 km southeast of Nottingham Island in the northwestern part of this basin.

The basin north of Charles Island contains up to 40 m of acoustically stratified sediments that overlie up to 90 m of unstratified sediments thought to consist mainly of glacial drift, but possibly including some debris flow sediments (Vilks et al., 1989). The acoustically stratified sediments appear to be laterally transitional to unstratified sediments on both the north and south sides of the basin.

In the northwestern part of the Strait, little to no sediment is evident over an irregular surface on Precambrian rocks in the region southeast of Cape Dorset.

Clast lithology and provenance

Clast lithology and provenance were investigated in a series of grab samples of bottom sediments. Samples included clasts of Paleozoic sedimentary rocks and Precambrian crystalline rocks and were subdivided into 25 lithologic classes. Possible source areas of Paleozoic rocks are mainly the floors of Ungava Bay, Hudson Strait, Foxe Basin, and Hudson Bay. Paleozoic rock types include limestone, dolostone, mudstone, siltstone, and sandstone. A preliminary assessment indicates that Paleozoic rocks represent 54% of the total clasts collected.

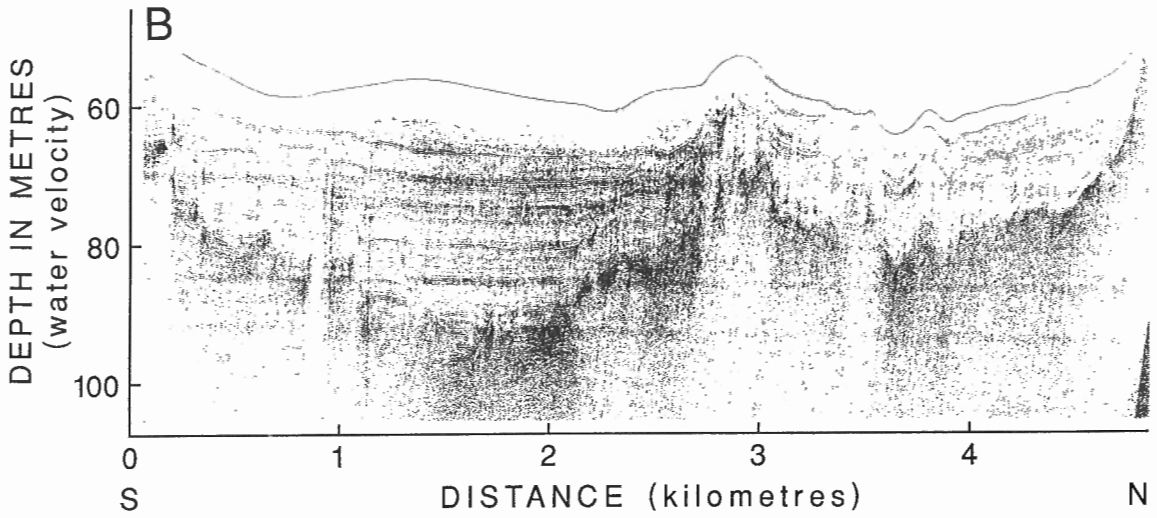

Figure 11. Section B, Huntec seismic reflection profile showing thick deposits of sediments in Deception Bay.

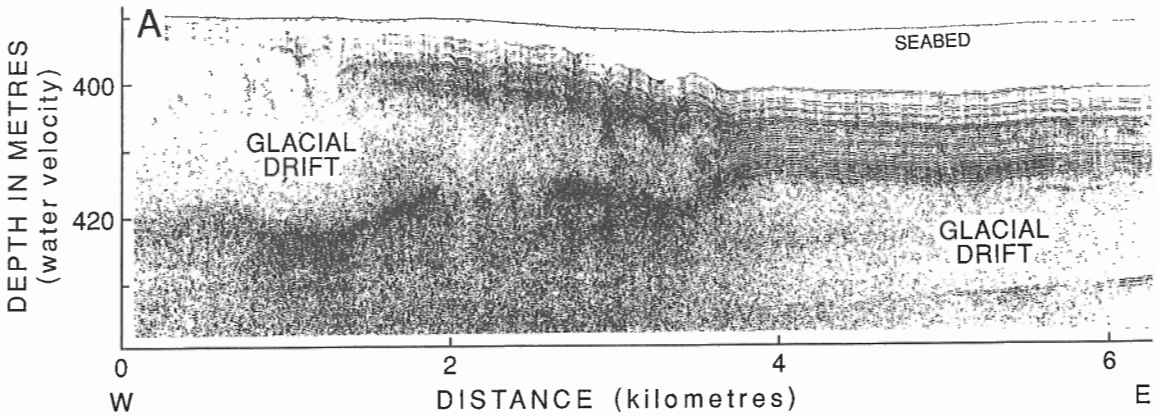

Figure 12. Section A, Huntec profile showing acoustically stratified sediments tonguing with unstratified sediments inferred to be glacial drift 30 km northeast of Promontoire Colbert.

Possible source areas for Precambrian rocks form a vast region that includes Baffin Island, Labrador, Ungava as well as areas surrounding Foxe Basin and Hudson Bay. Precambrian rock types include various igneous and metamorphic rocks associated with both Archean and Proterozoic suites. Of the 25 rock types, none can be considered as a distinctive lithological indicator with a well defined, unique source area. Even iron-formation clasts which have commonly been utilized as source indicators may be derived from sources located either on the south shore of Hudson Strait (New-Quebec Orogen, Cape Smith Thrust Belt or Sugluk Terrane), or on the north shore of the Strait (Dorset Orogen). Iron-formation clasts were recovered from 23 sample sites scattered throughout the strait. Stations with the highest iron-formation percentages are 51 (23%), 112 (9%), 77 (7%), and 37 (4%) (see Fig. 3 and Table 1 for locations).

Acoustic profiles and sample composition suggest that sediments at the stations sampled represent a variety of depositional settings including ice contact, proglacial and postglacial environments. Results outlined in this preliminary report thus may include components deposited at the base of a grounded ice sheet, rain-out sediments from an ice shelf, and ice-rafted material, as well possibly as material deposited by sediment gravity flows. A more definitive assessment of the facies and origin of the collected sediments will be possible later when results of all the various studies of the cruise data become available.

ACKNOWLEDGMENTS

The authors are grateful to Captain L. Strum, officers, and crew of **CSS Hudson**; to A. Boyce, B. Chapman, G. Fenn, R. Howie, R. Murphy, R. Potter, and R. Sparkes of Atlantic Geoscience Centre, G. Standen of Seachem/Star Ltd., and H. Boudreau of Canadian Hydrographic Service for their excellent support and cooperation at sea, to L. Whitman for laboratory support, and to H.W. Josenhans and A.C. Grant for critical review of the manuscript.

REFERENCES

Allard, M., Fournier, A., Gahé, E., and Seguin, M.K.
1989: Le Quaternaire de la côte sud-est de la Baie D'Ungava, Québec nordique; Géographie Physique et Quaternaire, v. 43, p. 325-336.

Andrews, J.T.
1989: Quaternary geology of the northeastern Canadian Shield; in Chapter 3 of Quaternary Geology of Canada and Greenland, (ed.) R.J. Fulton; Geological Survey of Canada, Geology of Canada, no. 1, p. 276-317 (also Geological Society of America, The Geology of North America, v. K-1).

Andrews, J.T., Briggs, W.M., and Weiner, N.
1991: Rock and paleo-magnetic studies of cored sediments during Hudson Cruise HU 90-023 in Frobisher Bay, Ungava Bay, and Hudson Strait; in Current Research, Part E; Geological Survey of Canada, Paper 91-1 (this volume).

Andrews, J.T., Shilts, W.W., and Miller, G.H.
1982: Multiple deglaciations of the Hudson Bay Lowlands, Canada, since deposition of the Missinaibi (last interglacial) Formation; Quaternary Research, 19, p. 18-37.

Blake, W., Jr.
1966: End moraines and deglaciation chronology in northern Canada with special reference to southern Baffin Island; Geological Survey of Canada, Paper 66-26, 31 p.

Bruneau, D., Gray, J.T., and Lauriol, B.
1990: Glacial flow patterns and chronology of ice retreat in the Charles Island - Cap de Nouvelle France sector of Hudson Strait; 19th Arctic Workshop, Boulder, Colorado, March 1990, Program and Abstracts, p. 15-17.

Clark, P.U.
1985: A note on the glacial geology and postglacial emergence of the Lake Harbour region, Baffin Island, N.W.T.; Canadian Journal of Earth Sciences, v. 22, p. 1864-1871.
1988: Glacial geology of the Torngat Mountains, Labrador: Canadian Journal of Earth Sciences, v. 25, p. 1184-1198.
1990: Reconnaissance study of the glacial geology of northernmost Labrador; 19th Arctic Workshop, Boulder, Colorado, March 1990, Program and Abstracts, p. 19.

Dyke, A.S. and Prest, V.K.
1987: Late Wisconsinan and Holocene history of the Laurentide Ice Sheet; Géographie physique et Quaternaire, 41, p. 237-263.

Fillon, R.H. and Harmes, R.A.
1982: Northern Labrador shelf glacial chronology and depositional environments; Canadian Journal of Earth Sciences, 19, p. 162-192.

Grant, A.C. and Manchester, K.S.
1970: Geophysical investigations in the Ungava Bay-Hudson Strait region of northern Canada; Canadian Journal of Earth Sciences, v. 7, p. 1062-1076.

Gray, J.T. and Lauriol, B.
1985: Dynamics of the Late Wisconsin ice sheet in the Ungava Peninsula interpreted from geomorphological evidence; Arctic and Alpine Research, v. 17, p. 289-310.

Gray, J.T., Lauriol, B., and Sloan, V.
1990: Geomorpological evidence for the partial overriding of Akpatok Island, Ungava Bay, by two lobes of Laurentide Ice; 19th Arctic Workshop, Boulder, Colorado, March 1990, Program and Abstracts, p. 27-30.

Josenhans, H.W. and Zevenhuizen, J.
1990: Dynamics of the Laurentide Ice Sheet in Hudson Bay, Canada; Marine Geology, 92, p. 1-26.

Josenhans, H.W., Zevenhuizen, J., and Klassen, R.A.
1986: The Quaternary geology of the Labrador Shelf; Canadian Journal of Earth Sciences, v. 23, p. 1190-1213.

Klassen, R.A.
1990: The glacial history of the Labrador Peninsula and Ungava Bay region; the glacial lake enigma; 19th Arctic Workshop, Boulder, Colorado, March 1990, Program and Abstracts, p. 43.

Lauriol, B. and Gray, J.T.
1987: The decay and disappearance of the Late Wisconsin Ice Sheet in the Ungava Peninsula, northern Quebec, Canada; Arctic and Alpine Research, v. 19, p. 109-126.

Laymon, C.A.
1988: Glacial geology of western Hudson Strait, Canada, with reference to Laurentide Ice Sheet dynamics; PhD thesis, University of Colorado, 345 p.

Løken, O.H.
1978: Postglacial tilting of Akpatok Island, Northwest Territories; Canadian Journal of Earth Sciences, v. 15, p. 1547-1553.

MacLean, B., Vilks, G., Aitken, A., Boudreau, H., Briggs, W., Bruneau, D., Doiron, A., Hardy, I., Mode, W., Powell, R., Retelle, M., Stravers, J., Taylor, A., and Allen, V.
1991: Cruise report CSS Hudson cruise 90-023, Marine geological investigations in Hudson Strait, Ungava Bay and Frobisher Bay; Geological Survey of Canada, Open File 2372, 152 p.

MacLean, B., Williams, G.L, Sanford, B.V., Klassen, R.A., Blakeney, C., and Jennings, A.
1986: A reconnaissance study of the bedrock and surficial geology of Hudson Strait, N.W.T.; in Current Research, Part B; Geological Survey of Canada, Paper 86-1B, p. 617-635.

Miller, G.H.
1985: Moraines and proglacial lake shorelines, Hall Peninsula, Baffin Island; in Quaternary Environments, Eastern Canadian Arctic, Baffin Bay, and Western Greenland: (ed.) J.T. Andrews; Allen and Unwin, London, p. 546-557.

Miller, G.H. and Kaufman, D.S.
1990: Rapid fluctuations of the Laurentide Ice Sheet at the mouth of Hudson Strait: new evidence for ocean/ice-sheet interactions as a control on the Younger Dryas; Paleoceanography, v. 5, p. 907-919.

Miller, G.H., Hearty, P.J., and Stravers, J.A.
1988: Ice-sheet dynamics and glacial history of southeasternmost Baffin Island and outermost Hudson Strait; Quaternary Research, 30, p. 116-136.

Osterman, L.E., Miller, G.H., and Stravers, J.A.
1985: Late and mid-Foxe glaciation of southern Baffin Island, N.W.T.; in Quaternary Environments, Eastern Canadian Arctic, Baffin Bay, and western Greenland, (ed.) J.T. Andrews; Allen and Unwin, London, p. 520-545.

Piper, D.J.W., Mudie, P.J., Fader, G.B., Josenhans, H., MacLean, B., and Vilks, G.
1990: Quaternary geology: Chapter 10; in Geology of the Continental Margin of Eastern Canada, (ed.) M.J. Keen and G.L. Williams; Geological Survey of Canada, Geology of Canada, no. 2, p. 475-607 (also Geological Society of America, The Geology of North America, v. I-2).

Praeg, D.B., MacLean, B., Hardy, I.A., and Mudie, P.J.
1986: Quaternary geology of the southeast Baffin Island continental shelf; Geological Survey of Canada, Paper 85-14, 38 p.

Stravers, J.A.
1986: Glacial geology of outer Meta Incognita Peninsula, southern Baffin Island, Arctic Canada; PhD thesis, University of Colorado, 251 p.

Vilks, G., MacLean, B., Deonarine, B., Currie, C.G., and Moran, K.
1989: Late Quaternary paleoceanography and sedimentary environments in Hudson Strait; Géographie physique et Quaternaire, v. 43, p. 161-178.

Rock and paleomagnetic studies of cored sediments during Hudson Cruise HU90-023 in Frobisher Bay, Ungava Bay, and Hudson Strait, Northwest Territories

J.T. Andrews[1], W.M. Briggs[1] and N. Weiner[1]
Atlantic Geoscience Centre, Dartmouth

Andrews, J.T., Briggs, W.M., and Weiner, N., 1991: Rock and paleomagnetic studies of cored sediments during Hudson Cruise HU90-023 in Frobisher Bay, Ungava Bay, and Hudson Strait, Northwest Territories; in Current Research, Part E; Geological Survey of Canada, Paper 91-1E, p. 317-320.

Abstract

Whole core analysis of the magnetic susceptibility was carried out on all the cores collected during ***Hudson*** *cruise HU90-023. Throughout the region surveyed during this cruise magnetic susceptibility varied between ca. 2 and 600 x 10^{-5} SI units. Two cores (HU90-023-045 and HU90-023-064) were selected to illustrate some of the significant changes in downcore magnetic susceptibility. Paleomagnetic measurements are being carried out on five cores and one NRM record is illustrated from HU90-023-045.*

Résumé

Une analyse de susceptibilité magnétique de carottes entières a été effectuée sur toutes les carottes prélevées pendant la sortie 90-023 de l' ***Hudson****. Sur toute l'étendue de la région étudiée au cours de cette sortie, la susceptibilité magnétique a varié entre 2 et 600 x 10^{-5} unités SI environ. Deux carottes (HU 90-023-045 et HU90-023-064) sont choisies pour illustrer certains changements importants de la susceptibilité magnétique en fonction de la profondeur. Des mesures paléomagnétiques sont effectuées sur cinq carottes et un enregistrement NRM provenant de la carotte HU90-023-045 est illustré.*

[1] INSTAAR and Department of Geological Sciences, Box 450, University of Colorado, Boulder, CO 80309

INTRODUCTION

Variations in magnetic susceptibility (MS) reflect changes in sediment density, texture and mineralogy (Thompson and Oldfield, 1986). Patterns of regional and temporal MS variations give us insight into lithofacies and sediment sources (Andrews and Jennings, 1987). Core logging and the measurement of "wet" sediment produces a measure of volume MS whose units are 10^{-5} SI (dimensionless). This note is a companion to the report by MacLean et al. (1991) which gives additional data on the cruise objectives and data.

On cruise HU90-023 (Fig. 1) all the Long-core Facility (LCF) and trigger cores were measured for volume magnetic susceptibility (MS) with two major objectives: 1) to assist in describing and understanding sedimentation processes; and 2) to document changes in sediment source(s).

We measured MS with a Bartington MS-1 meter and an 11.5 cm loop. Samples were taken every 5 cm along the length of a core. In addition, a number of split cores were sampled with 8 cc plastic boxes for additional laboratory study. These samples were shipped to the University of Colorado where research on the samples will include measurement of the paleomagnetic remanance magnetization, saturation isothermal remanant magnetization, and magnetic susceptibility. These studies will be carried out in combination with investigations of sediment texture, mineralogy, and biotic components.

RESULTS

There are substantial regional and temporal variations in MS (Fig. 2). For example, significant downcore changes in MS occur in cores from two areas of Hudson Strait that experienced complex and rapidly changing glaciological regimes during the last deglaciation (Josenhans et al., 1986; Miller et al., 1988). The MS variations will thus provide information on characteristics of sediment sources that may lead to discrimination between sediments derived from different glacial centres, for example, central Labrador versus Hudson Bay (Andrews et al., 1990; Miller et al., 1988; Miller and Kaufman, 1990; Praeg et al., 1986; Stravers, 1986). In addition, the data will add to information collected during an earlier (1985) cruise (MacLean et al., 1986).

Core HU90-023-064 is from near the south coast of Hudson Strait west of Ungava Bay (Fig. 1). The susceptibility record indicates two major sources contributed sediment to the site. Between the base of the core and ca. 3 m the susceptibility averages around 120 (x 10^{-5} SI) with three well-defined peaks. Thereafter, the magnetic susceptibility decreases sharply and in the upper 3 m averages about 15 (x 10^{-5} SI) (Fig. 2).

In Eastern Basin, Hudson Strait, core HU90-023-045 (Fig. 1) shows a different sequence of MS units. In this core the lowermost 4 m is characterized by relatively low MS values and there is a progressive increase between 6 and 4 m

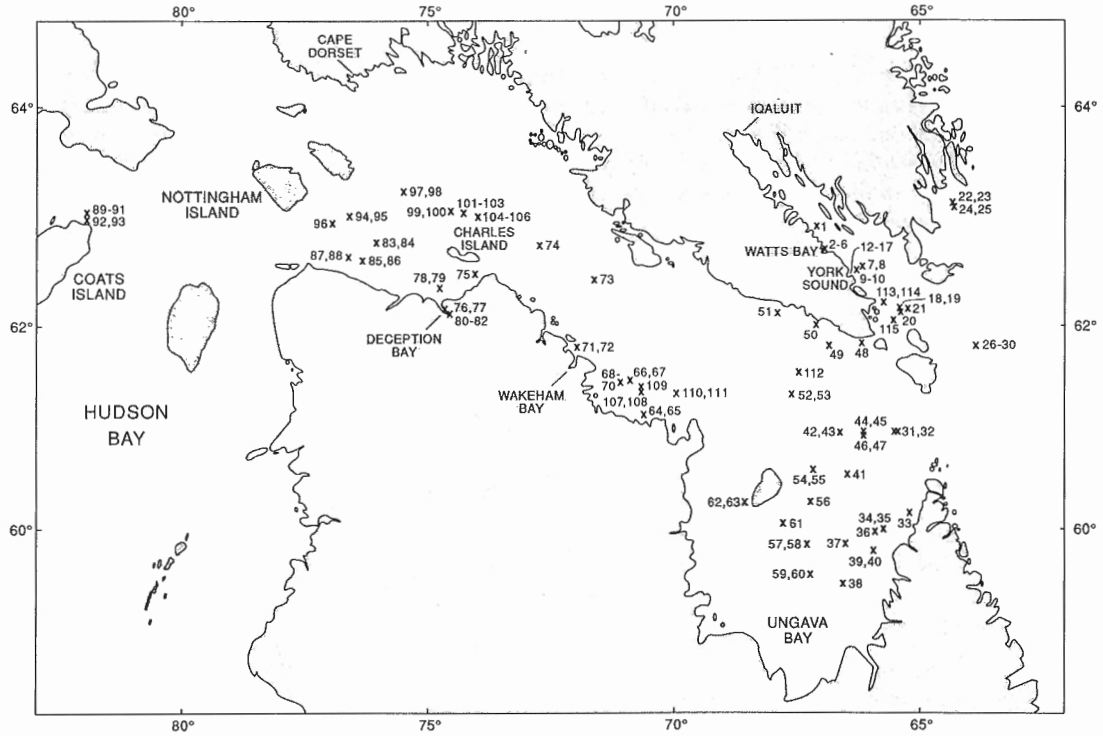

Figure 1. Stations occupied during cruise HU90-023 (see MacLean et al., 1991). Sites HU90-023-045 and -064 (Fig. 2) are located in Eastern Basin, Hudson Strait, and from near the south coast of Hudson Strait west of Ungava Bay.

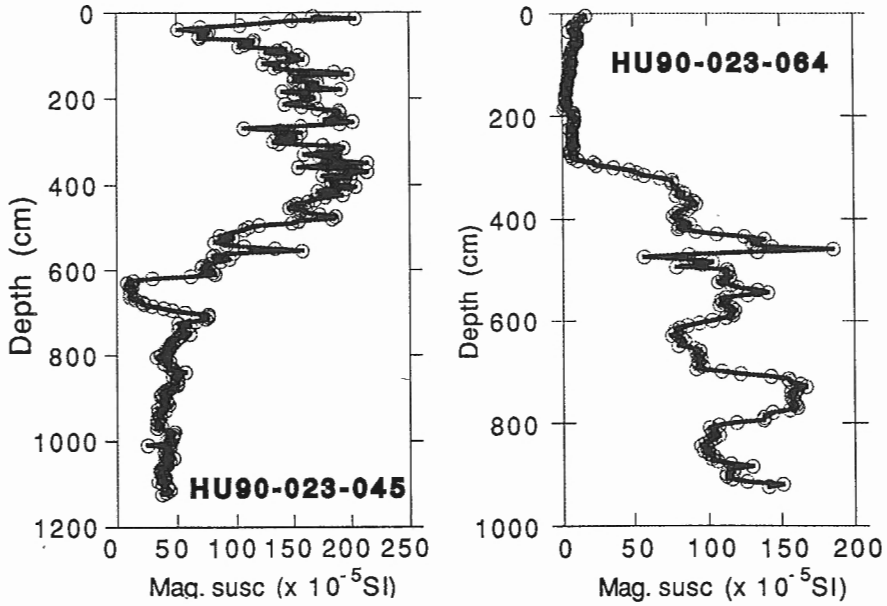

Figure 2. Wholecore volume magnetic susceptibility measurements, taken every 5 cm on cores HU90-023-045 and -064 (Fig. 1). Units are 10^{-5} SI units (Thompson and Oldfield, 1986).

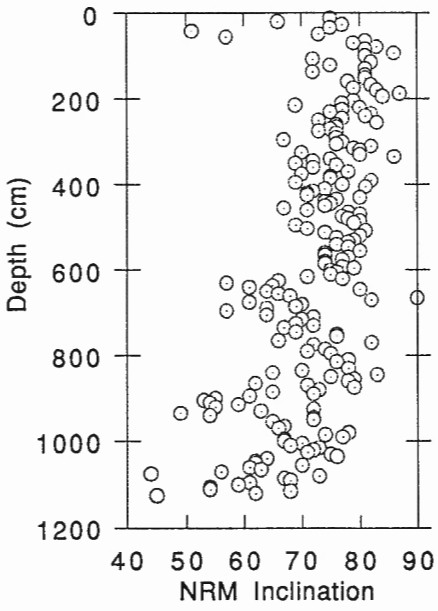

Figure 3. NRM data from HU90-023-045 showing inclination. Samples were taken in 8 cc plastic boxes and processed on a spinner magnetometer at the United States Geological Survey, Denver.

when readings reached ca. 200 (x 10^{-5} SI) (Fig. 2). This core was taken from the youngest part of the stratigraphic section within Eastern Basin.

Until more research is conducted on the mineralogy and rock magnetics of these cores the explanation for these changes remains uncertain. Low MS readings have been noted in sediments from areas of the Precambrian Canadian Shield that consist mainly of quartzites (Andrews and Jennings, 1987), but low MS readings coincide in Resolution Basin sediments with intervals of high detrital carbonate content (Andrews et al., 1990; Evans, 1990). The cores with the highest MS readings on cruise HU90-023 were taken from outer Frobisher Bay and western Ungava Bay and may be associated with the advance of ice across Hudson Strait and southeastern Baffin Island (Miller et al., 1988).

When the various submitted ^{14}C dates on foraminifera and molluscs are available, the MS data (e.g. Fig. 2) will provide a valuable key to interpreting both spatial and temporal shifts in the patterns of major sediment-bearing meltwater systems associated with the retreat of the Laurentide Ice Sheet between ca. 13 and 8 ka.

Figure 3 shows the NRM inclination, from HU90-023-045. The average inclination of 74° is close to that expected for this latitude. The data will have to undergo Af demagnetization before more can be said, although it is tempting to correlate the steep inclination peak at ca. 150 cm with event #2 in the Baffin Island fiords (Andrews and Jennings, 1990).

ACKNOWLEDGMENTS

We would like to acknowledge financial assistance from National Science Foundation grant DPP 88 22022.

REFERENCES

Andrews, J. T., Evans, L. W., Williams, K. M., Briggs, W. M., Jull, A. J. T., Erlenkeuser, H., and Hardy, I.
1990: Cryosphere/ocean interactions at the margin of the Laurentide Ice Sheet during the Younger Dryas Chron: SE Baffin Shelf, Northwest Territories; Paleoceanography, v. 5, p. 921-935.

Andrews, J. T. and Jennings, A. E.
1987: Influence of sediment source and type on the magnetic susceptibility of fiord and shelf deposits, Baffin Island and Baffin Bay, N.W.T.; Canadian Journal Earth Sciences, v. 24, p. 1386-1401.
1990: Geomagnetic secular variations (inclination) of high latitude fiord cores: eastern Canadian Arctic; Polar Research, v. 8, p. 245-259.

Evans, L.W.
1990: Late Quaternary stratigraphy of the Hatton and Resolution Basins, Southeast Baffin Island Shelf, N.W.T., Canada; MSc thesis, University of Colorado, Boulder, 188 p.

Josenhans, H.W., Zevenhuizen, J., and Klassen, R.A.
1986: The Quaternary geology of the Labrador Shelf; Canadian Journal of Earth Sciences, v. 23, p. 1190-1214.

MacLean, B., Williams, G. L., Sanford, B. V., Klassen, R. A., Blakeney, C., and Jennings, A. E.
1986: A reconnaissance of the bedrock and surficial geology of Hudson Strait. Preliminary results; in Current Research, Part B; Geological Survey of Canada, Paper 86-1B, p. 154-177.

MacLean, B., Vilks, G., Aitken, A., Allen, V., Briggs, W., Bruneau, D., Doiron, A., Escamilla, M., Hardy, I., Miner, J., Mode, W., Powell, R., Retelle, M., Stravers, J., Taylor, A., and Weiner, N.
1991: Investigations of the Quaternary geology of Hudson Strait and Ungava Bay, Northwest Territories; in Current Research, Part E; Geological Survey of Canada, Paper 91-1E.

Miller, G. H. and Kaufman, D. S.
1990: Rapid fluctuations of the Laurentide Ice Sheet at the mouth of Hudson Strait: New evidence for ocean/ice-sheet interactions as control on the Younger Dryas; Paleoceanography, v. 5, p. 907-919.

Miller, G. H., Hearty, P. J., and Stravers, J. A.
1988: Ice-sheet dynamics and glacial history of southeasternmost Baffin Island and outermost Hudson Strait; Quaternary Research, v. 30, p. 116-136.

Praeg, D. B., MacLean, B., Hardy, I. A., and Mudie, P. J.
1986: Quaternary geology of the southeast Baffin Island continental shelf; Geological Survey of Canada, Paper 85-14, 13 p. (with maps).

Stravers, J. A.
1986: Glacial Geology of the outer Meta Incognita Peninsula, Southern Baffin Island, Arctic Canada; PhD thesis, University of Colorado, Boulder, 231 pp.

Thompson, R. and Oldfield, F.
1986: Environmental Magnetism. Winchester, Mass.; Allen & Unwin, 219 p.

Radiocarbon chronology of late Quaternary sections on the inner and middle Scotian Shelf, south of Nova Scotia

David J. W. Piper and Steven D. Fehr[1]
Atlantic Geoscience Centre, Dartmouth

Piper, D.J.W. and Fehr, S.D., 1991: Radiocarbon chronology of late Quaternary sections on the inner and middle Scotian Shelf, south of Nova Scotia; in Current Research, Part E; Geological Survey of Canada, Paper 91-1E, p. 321-325.

Abstract

Ten new AMS (accelerator mass spectrometry) radiocarbon dates are reported on molluscs from Emerald Basin and the inner Scotian Shelf off Lunenburg. These show that the base of the LaHave Clay on the Scotian Shelf is diachronous and that in Emerald Basin there is an acoustic signature to the Younger Dryas cooling event. Dates on the inner shelf suggest that the "Late Till" south of Lunenburg is older than 14.3 ka; and that substantial amounts of pre-Late Wisconsinan proglacial sediment are preserved in tunnel valleys on the inner shelf.

Résumé

Dix nouvelles dates ont été établies au carbone radioactif par AMS pour des mollusques du bassin Emerald et de l'intérieur du plateau Néo-Écossais au large de Lunenbourg. Elles révèlent que la base de l'argile LaHave sur le plateau Néo-Écossais est diachrone et que le bassin Emerald présente une signature acoustique de l'épisode de refroidissement Younger Dryas. Les dates pour l'intérieur du plateau indiquent que le "till récent" au sud de Lunenbourg est âgé de plus de 14,3 ka; et que des quantités importantes de sédiments proglaciaires antérieurs au Wisconsinien supérieur sont conservées dans des ravins sous-glaciaires à l'intérieur du plateau.

[1] Department of Oceanography, Dalhousie University, Halifax N.S. B3H 3J4

INTRODUCTION

Accelerator mass spectrometry radiocarbon dating has permitted dating of mollusc shells in glaciomarine sediments, providing for the first time a reliable chronology for offshore glaciomarine deposits. Gipp and Piper (1989) reported a chronology for the older part of the Emerald Silt section on the Scotian Shelf. King and Fader (1988a) report dates for the upper part of the Emerald Silt and the lower LaHave Clay in northeast Emerald Basin, to the south of Chedabucto Bay. There is no continuity in seismic reflections between this area and southwest Emerald Basin, where Gipp (1989) has erected a detailed sequence stratigraphy. Therefore, we have dated samples from southwest Emerald Basin (Fig. 1) to provide a chronology for the sequence stratigraphy of Gipp (1989).

In addition, we have obtained a new core to date a possible glacial re-advance on the inner shelf off the South Shore of Nova Scotia (Piper et al., 1986). This site also provides constraints to sea level in the late Pleistocene.

EMERALD BASIN

Seven dates have been obtained from mollusc shells in the upper part of the Emerald Silt section and the LaHave Clay in core 87003-04 (Table 1 and Fig. 2). Samples were obtained from sand-sized residues of grain size analysis. Although the autochthonous setting of the cores cannot be proven, the fragile nature of the shells and the overall muddy deep-water depositional setting suggests that they are unlikely to be reworked. The dates show progressive downcore increase in age and, where seismic correlation exists, are completely consistent with previous dates (Gipp and Piper, 1989). The dates provide estimates for the age of boundaries between depositional sequences 3, 4 and 5 of Gipp (1989) (Fig. 3). Correlation of the seismic profile and the core is based on physical properties variation (Moran et al., 1989; Fehr, 1991) and correlation of the trigger weight core with the piston core (Fehr, 1991) that indicates insignificant sediment loss at the top of the core.

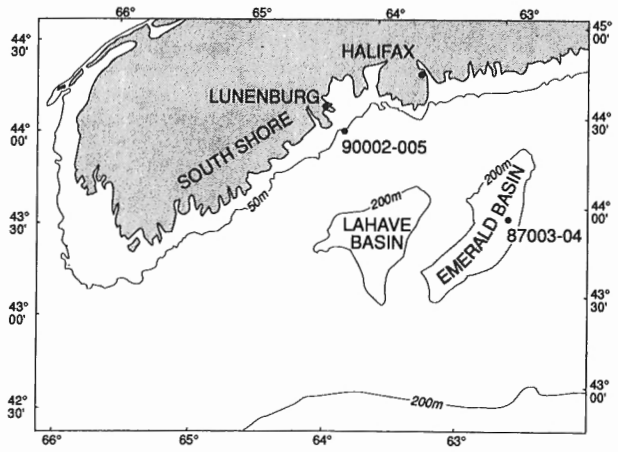

Figure 1. Map of the western Scotian Shelf showing location of cores studied.

INNER SHELF OFF LUNENBURG

Core 90002-05 is located in 71 m water depth in a basin 5 km offshore from Cross Island, near Lunenburg. It is an approximate duplicate of core 77-15 of Piper et al. (1986): the location, seismic stratigraphy and lithology of core 77-15 are illustrated in Fig. 20, 21, 42, and 43 of Piper et al. (1986). Core 77-15 contains a surface sand layer overlying dark, rather gassy muds in which the sparse foraminiferal assemblage suggests a bay environment with exchange with the open sea. A total organic carbon date of 14 ka was obtained from the lower part of core 77-15. Piper et al. (1986) used this date to constrain sea level to about -60 m (the depth required to produce a sheltered basin with exchange with the open sea). This muddy unit corresponds to acoustic unit d1. At a distance of only 2 km, the underlying unit c interfingers with a late till ridge that overlies unit b (Fig. 18 of Piper et al., 1986).

Core 90002-05 contains three sedimentary units (Fig. 4). The upper 95 cm consists of medium and fine sand, with common *Modiolus* shells probably eroded off the adjacent rocky banks. From 95-154 cm, the sediments consist of grey muds with a 10 cm muddy sand at the base containing slate pebbles and granules. Petrographically, this resembles the late till ridge, the coarse fraction of which consists principally of slate. The sand appears to overlie a bioturbated possibly erosional surface at the top of a sequence of brownish muds 278 cm thick. These muds show silty laminae and near the base contain slate granules. On the basis of the on-site 3.5 kHz profile, correlated with the regional seismic lines (Fig. 20 of Piper et al., 1986), the upper unit corresponds to acoustic unit d2 of Piper et al. (1986), the middle unit to d1, and the lower unit, which was not sampled in core 77-15, is interpreted as correlating with seismic unit c, which passes laterally into the late till. The unconformity overlying units a and b occurs at about 5 m subbottom.

Paired valves of *Tellina agilis* from the grey muds (seismic unit d1) yielded an age of 14.05 ka; paired valves of *Nucula tenuis* from the underlying brownish muds (seismic unit c) an age of 14.19 ka, implying that the late till dates from before 14.3 ka. The occurrence of *Tellina agilis*, which has a present range of intertidal to -20 m and occurs only as far north as the Gulf of St. Lawrence, is consistent with deposition distant from an ice margin in shallow water depths.

The *Modiolus modiolus* specimen from the upper sandy unit yielded an age of 28 ka. This age clearly indicates reworking. This sample must have been preserved in a site protected from ice erosion on rocky banks near the core site. Its age suggests ice-free conditions on the inner shelf at 28 ka.

DISCUSSION

In northeast Emerald Basin, King and Fader (1988a) bracketed the unconformity between the LaHave Clay and Emerald Silt to between 9.5 and 10.5 ka and the contact between facies

Table 1. New radiocarbon dates

Core depth cm	Age	Material	Lab No
87003-04			
185	5245±80	*Dentalium occidentale*	Beta 36342, ETH 6458
290	8675±90	*Astarte undata*, 1v	Beta 36343, ETH 6459
432	10480±80	Pelecypod fragments	TO 1920*
604	11900±310	*Nucula tenuis*, 1v	TO 1921*
667	13910±120	*Nucula tenuis*, 1v	Beta 36344, ETH 6460
855	14870±130	*Margarites helicina*, 1v	Beta 36445, ETH 6461
948	15110±140	*Portlandia arctica*, pv	Beta 36446, ETH 6462
90002-05			
74-75	27990±220	*Modiolus modiolus*, 1v	TO 2038
138	14050±100	*Tellina agilis*, pv	TO 2039*
222	14190±100	*Nucula tenuis*, pv	TO 2040

pv = paired valves, 1v = one valve, * = sample too small to preleach

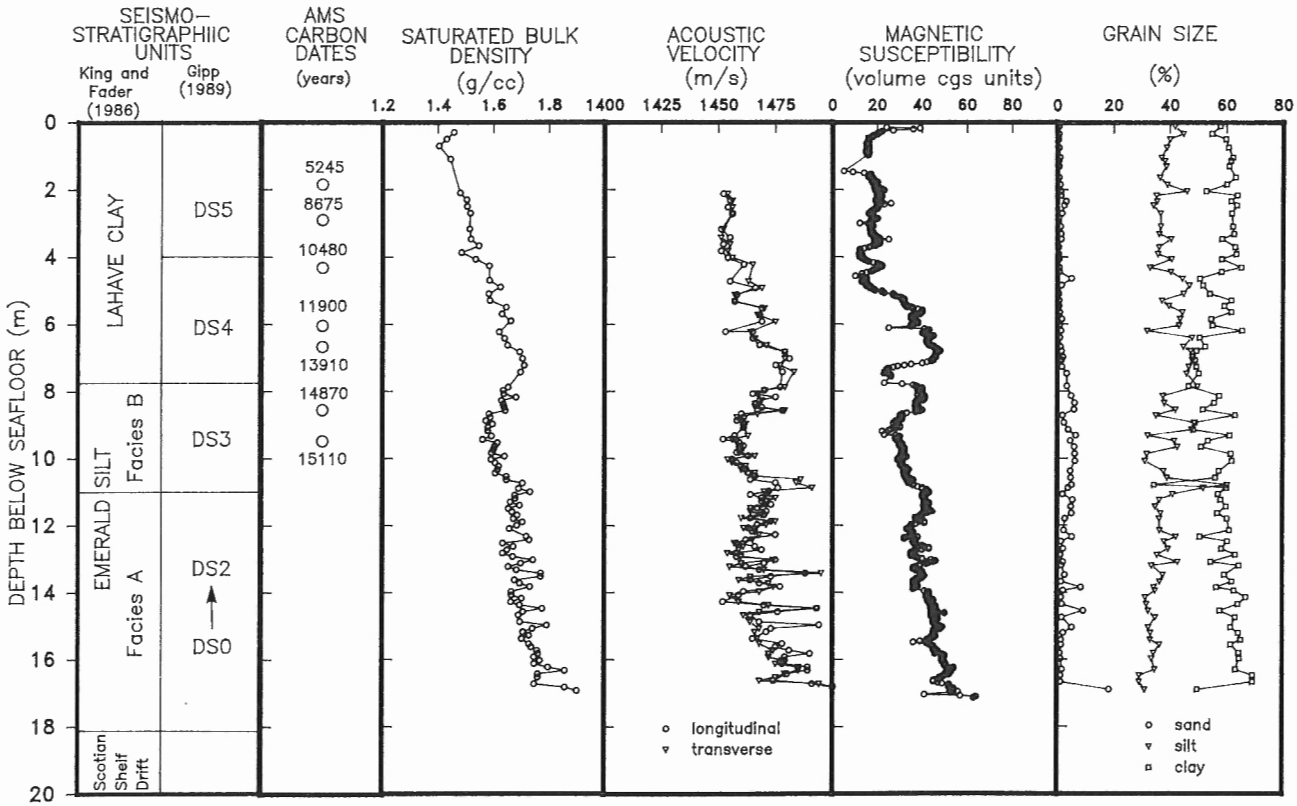

Figure 2. Plot of downcore variation in physical properties and grain size for core 87003-04 (from Fehr, 1991) showing radiocarbon chronology and correlation with seismostratigraphic units of King and Fader (1986) and the sequence stratigraphy of Gipp (1989).

A and B of Emerald Silt to between 14.3 and 14.6 ka. Our data suggests that the Emerald Silt - LaHave Clay boundary in southwest Emerald Basin is substantially older, being bracketed by 13.7 and 14.4 ka dates by Gipp and Piper (1989) and by 13.9 and 14.9 dates in this study. The depositional sequence 4/5 boundary (within the LaHave Clay) in southwest Emerald Basin appears to be about the same age as the top of the Emerald Silt in northeast Emerald Basin, suggesting that the LaHave Clay sediment facies is diachronous between the inner and outer shelf. The boundary between depositional sequences 2 and 3 (equivalent to facies A - B boundary) was bracketed to between 14.9 and 15.1 ka by Gipp and Piper (1989), older than the ages of King and Fader (1988a) further to the northeast.

Within the LaHave Clay, the top of depositional sequence 4 is marked by a strong reflection over much of the northern part of southwest Emerald Basin (Fig. 3). This has an extrapolated age of about 10.2 ka and may thus correspond approximately to the Younger Dryas cooling event. The sparse dates are also consistent with a higher sedimentation rate at around this time, but more dates would be needed to confirm this. There is no evidence that the late till in the Lunenburg area represents a Younger Dryas advance: it appears to date from before 14.3 ka and may represent a local readvance following the main late Wisconsinan retreat from the outer shelf (Mosher et al., 1989). King and Fader (1988b), however, did recognise an erosional Younger Dryas event in northeast Emerald Basin that they interpreted to result from readvance of ice on the offshore banks.

The new radiocarbon dating on the inner Scotian Shelf confirms that the muddy unit with shallow-water foram and mollusc faunas dates from about 14 ka. The physiographic setting of the core (Piper et al., 1986) would require a -50 to -60 m sea level at that time. The new dates also suggest that sea level was at least as high and the area ice free at about 28 ka. Between these two dates, there was a rapid ice advance to the shelf break through Emerald and LaHave basins, that must have crossed the Lunenburg area. Although the age of this advance was estimated at 25 ka by Mosher et al. (1989), the oldest date on proglacial sediments on the upper continental slope, well above the base of the section, is only 20 ka. Ice lifted off from Emerald Basin at about 18 ka (Gipp and Piper, 1989).

The new dates reported here and the outer shelf chronology of Gipp and Piper (1989) provide an opportunity to reconsider the sea level curves proposed by Piper et al. (1986, their Fig. 44). The unconformity between acoustic units a+b and c, on the basis of distribution and morphology, was interpreted as corresponding to the late Wisconsinan lowstand of sea level and the subsequent transgression. The new evidence for late Wisconsinan ice crossing the shelf suggests that subglacial erosion could have formed this unconformity.

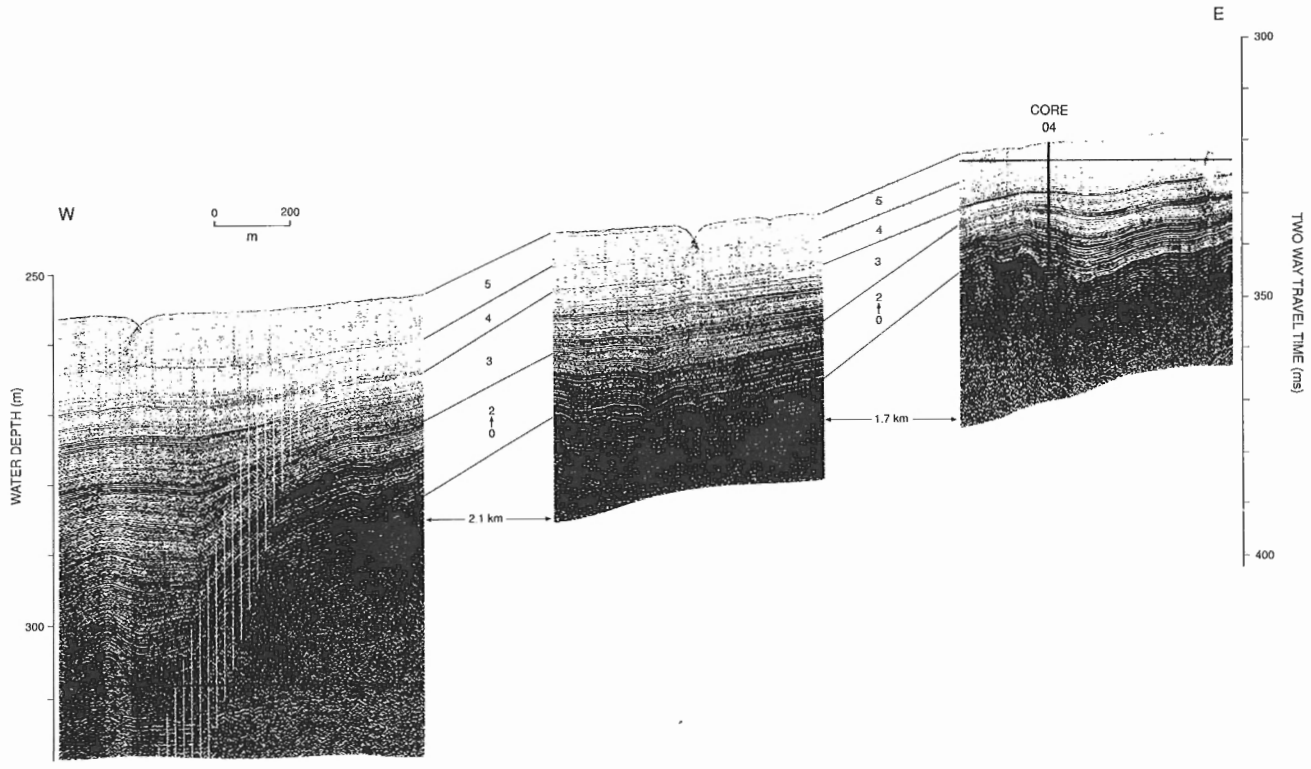

Figure 3. East-west Huntec DTS profile through core site 87003-04 showing acoustic stratigraphy of Gipp (1989).

This would imply substantial preservation of pre-late Wisconsinan sediment in tunnel valleys on the inner shelf. Such a hypothesis is consistent with the 28 ka date on the *Modiolus* shell and is also consistent with G.B. Fader's (pers. comm, 1991.) evidence for similarly old shell dates (24-26 ka) from Georges Basin in the Gulf of Maine. The pre-late Wisconsinan high stand of sea level could account for the sediments of unit a, deposited in areas with water depths as little as 58 m, and the occurrence of proglacial muds in water depths as little as 27 m in Lunenburg Bay (core 78005-100; Fig. 44 of Piper et al., 1986).

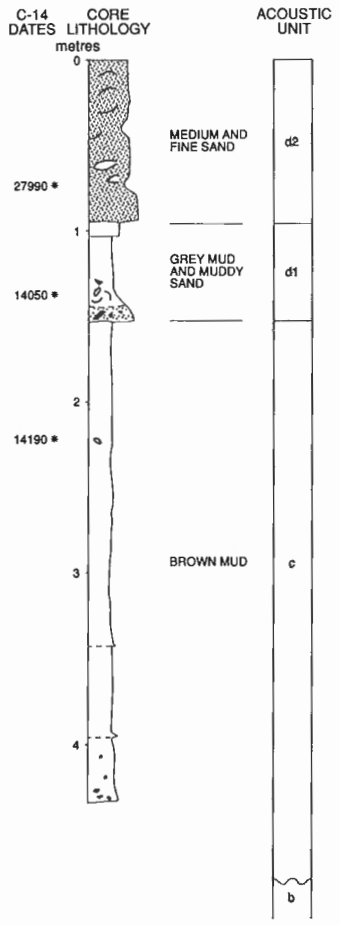

Figure 4. Core log for 90002-05 showing radiocarbon dates and correlation with acoustic stratigraphy of Piper et al. (1986).

If glacial erosion rather than marine transgression caused the widespread unconformity between acoustic units a+b and c, then the argument of Piper et al. (1986, their Fig. 44) for a -120 m lowstand of sea level on the inner shelf is invalid. On the Eastern Shore of Nova Scotia, Forbes et al. (in press) present evidence for a maximum lowering of sea level of about -50 m preceded by a high relative sea level during the early stages of glacial recession. The change in physiography at about -60 m off Lunenburg (Piper et al., 1986, their Fig. 5) suggests that there may have been a similar lowstand of sea level at -50 to -60 m on the South Shore. There is no evidence to determine whether this was preceded by a higher sea level, or represents the effects of the change in rate of sea level rise at about 14-13 ka that has been recognised in nonglacial regions.

ACKNOWLEDGMENTS

Molluscs were identified by F. Cole. This study has been assisted by the work of L. Mayer and K. Moran. The manuscript was reviewed by Mike Gipp, Don Forbes, and Gordon Fader. S.D. Fehr's work was partly supported by NSERC grants to L. Mayer.

REFERENCES

Fehr, S.
1991: A geoacoustic model for the upper sediments of Emerald Basin. M.Sc. thesis, Dalhousie University, Halifax, Nova Scotia, 241 p.

Forbes, D.L., Boyd, R., and Shaw, J.
in press: Late Quaternary sedimentation and sea-level changes on the inner shelf near Halifax, Nova Scotia; Continental Shelf Research.

Gipp, M.R.
1989: Late Wisconsinan deglaciation of Emerald Basin, Scotian Shelf; M.Sc. thesis, Memorial University of Newfoundland, St. John's, 219 p.

Gipp, M.R. and Piper, D.J.W.
1989: Chronology of Late Wisconsinan glaciation, Emerald Basin, Scotian Shelf; Canadian Journal of Earth Sciences, v. 26, p. 333-335.

King, L.H. and Fader, G.B.
1986: Wisconsinan glaciation of the continental shelf, southeastern Atlantic Canada. Geological Survey of Canada, Bulletin 363, 72 p.
1988a: A comparison between the Late Wisconsinan history of southwest and northeast Emerald Basin; Geological Survey of Canada, Open File 2060, 12 p.
1988b: Late Wisconsinan ice on the Scotian Shelf; Geological Survery of Canada, Open File 1972, 15 p.

Moran, K., Piper, D.J.W., Mayer, L.A., Courtney, R.C., Driscoll, A.H., and Hall, F.R.
1989: Scientific results of long coring on the eastern Canadian continental margin; 21st Offshore Technology Conference, paper 5963, p. 65-71.

Mosher, D.C., Piper, D.J.W., Vilks, G., Aksu, A.E., and Fader, G.B.
1989: Evidence for Wisconsinan glaciations in the Verrill Canyon area, Scotian Slope; Quaternary Research, v. 31, p. 27-40.

Piper, D.J.W., Mudie, P.J., Letson, J.R.J., Barnes, N.E., and Iuliucci, R.J.
1986: The marine geology of the inner Scotian Shelf off the South Shore, Nova Scotia; Geological Survey of Canada, Paper 85-19, 65 p.

Clay mineralogy in Devonian-Carboniferous basins, mainland Nova Scotia, and its bearing on the genesis of sediment-hosted mineralization

Q. Gall[1] and D.F. Sangster
Mineral Resources Division

Gall, Q. and Sangster, D.F., 1991: Clay mineralogy in Devonian-Carboniferous basins, mainland Nova Scotia, and its bearing on the genesis of sediment-hosted mineralization; in Current Research, Part E, Geological Survey of Canada, Paper 91-1E, p. 327-335.

Abstract

A preliminary study of phyllosilicates, including illite crystallinity, in Devonian-Carboniferous basins of mainland Nova Scotia was undertaken to determine the level of thermal maturation of the sedimentary rocks with a view to determining areas or zones through which heated mineralizing fluids could have migrated. The majority of the sample localities contain diagenetic illite and/or smectitic phyllosilicates, suggesting that strata of the Horton and upper Windsor groups in these areas have remained within the diagenetic realm. The study indicates that, for the areas which were sampled, there is no indication of wholesale migration of heated mineralizing fluids through either the Horton Group or Windsor Group strata. Fluid movement along the Meguma Group - Horton Group unconformity, however, is not precluded by the data.

Résumé

Une étude préliminaire des phyllosilicates, et de la cristallinité de l'illite, dans les bassins du Dévono-Carbonifère de la partie continentale de la Nouvelle-Écosse a été menée pour déterminer le niveau de maturation thermique des roches sédimentaires en vue d'établir les trajectoires de migration des fluides minéralisants chauds. La majorité des endroits échantillonnés contiennent de l'illite diagénétique et (ou) des phyllosilicates smectitiques, ce qui indique que les couches du groupe de Horton et du groupe supérieur de Windsor dans ces endroits sont demeurées dans le contexte diagénétique. L'étude indique que, dans les endroits échantillonnés, il n'y a aucun signe de migration globale de fluides minéralisants chauds, soit par les couches du groupe de Horton, soit par les couches du groupe de Windsor. Un déplacement de fluide le long de la discordance entre le groupe de Méguma et le groupe de Horton n'est toutefois pas impossible selon les données.

[1] Ottawa-Carleton Geoscience Centre, Dept. of Earth Sciences, Carleton University, Ottawa, Ontario K1S 5B6

INTRODUCTION

Within mainland Nova Scotia, numerous sediment-hosted Pb-Zn and barite deposits, such as the Gays River and Walton deposits (Fig. 1), as well as smaller occurrences (e.g., Brookfield, Smithfield, Pembroke), are located within Lower Carboniferous carbonate units of Devonian-Carboniferous basins and show similarities to Mississippi Valley or sedex type deposits (Boyle, 1972; Lydon, 1978; Ravenhurst et al., 1989, Sangster, 1986). Vitrinite reflectance measurements on organic material found close to mineralization suggest that the material is more mature than organic material found elsewhere in the basins (Ravenhurst, 1987). Fluid inclusions within sphalerite, calcite, barite, and fluorite from the deposits yield a range of homogenization temperatures between 138°C and 250°C (Akande, 1982; Ravenhurst et al., 1989).

Clay minerals and the crystallinity of illite are known to be sensitive indicators of physico-chemical changes within sedimentary sequences during burial diagenesis and low grade metamorphism (Dunoyer De Segonzac, 1970; Kisch, 1983; Kubler, 1967). Diagenetic clay minerals, brought into contact with migrating ore fluids at these elevated temperatures, might be expected to recrystallize to more highly-ordered states and so be identified by standard illite crystallinity techniques. Mineralizing fluids of the temperature indicated by fluid inclusions in ore and associated minerals (138°C to 250°C), might be expected to produce anchimetamorphic illite within the strata through which the fluids migrated.

We conducted a preliminary study of the clay mineralogy and illite crystallinity of the Horton Group and upper Windsor Group sedimentary rocks within the Kennetcook, Shubenacadie, Musquodoboit, and Antigonish basins and the Rawdon Hills area to (a) investigate the thermal maturation of the basin sediments adjacent to the Pb-Zn mineralization, and, (b) identify areas or zones within the Devonian-Carboniferous basins through which heated mineralizing fluids may have migrated (Fig. 1). Through such an investigation we are also documenting for the first time, to our knowledge, the clay mineralogy of Horton Group and upper Windsor Group sedimentary rocks over a large area. Results of such a study may serve as a basis for a variety of further geological investigations.

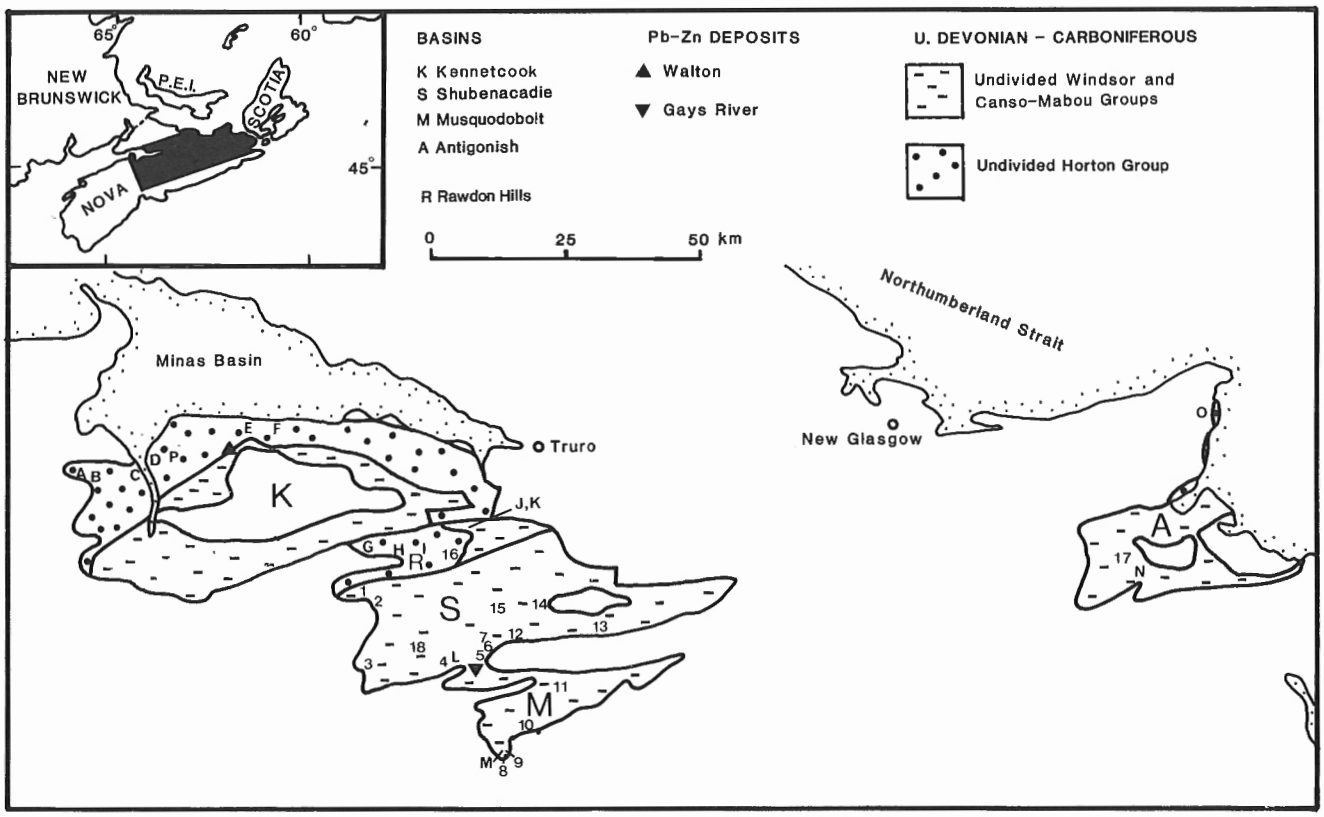

Figure 1. Location of Horton Group (H) and Windsor Group (W) samples collected from outcrop (letters) or drill core (numbers) in four Late Devonian to Carboniferous age basins in Nova Scotia. Letters and numbers centred on sample locality. Outcrop sampled from: A= Harding Brook (H); B= Curry Brook (H); C= Blue Beach (H); D= Cheverie Point (H); E= Walton Beach (H); F= Tennycape Beach (H); G & H & I= Rawdon Hills (H); J & K= Green Creek (W); L= Milton Station (H); M= Meaghers Grant (W); N= Glen Road (W); O= Wilkie Brook (H); P= Bar S Ranch (W). Drill core sampled from: 1= UR-2 (H, W); 2= NM-29 (H); 3= HP-7 (W); 4= M-1 (W); 5= MA-73-1 (H); 6= MA-73-4 (H); 7= MA-73-9 (H); 8= MG-2 (W); 9= MG-15 (W); 10= MG-43 (W); 11= 208-3 (W); 12= C-15 (H); 13= W-3 (W); 14= 153-3 (W); 15= SB-1 (H, W); 16= BP-6 (H); 17= GR-83-1 (W); 18= NM-19 (W).

ANALYTICAL METHODS

To avoid variations in clay mineralogy attributable to lithologic variation, and in order to extract enough clay-size material to analyze, we restricted our sampling to fine grained siliciclastic sedimentary rocks (i.e., claystone, mudstone, and siltstone) of the Tournasian Horton Group and Visean Windsor Group (Table 1). The scarcity of fine grained siliciclastic sediments in the lower and middle Windsor Group in Nova Scotia (Giles, 1981) precluded sampling of this interval. However, the Green Oaks Formation in the upper part of the Windsor Group contains a higher proportion of fine grained siliciclastic sediments and is widely distributed in the Shubenacadie and Musquodoboit basins (Giles and Boehner, 1982; R. Boehner, pers. comm. 1990), and so was sampled for this study. In the Musquodoboit Basin the Horton Group does not outcrop, nor was it found in any of the available drill core. In lieu of this, the Meaghers Grant Formation of the Windsor Group was sampled as it contains a high proportion of fine grained siliciclastic sediments and occurs near the bottom of the basin sequence, stratigraphically above the Gays River Formation (Table 1), but close (~30 km) to the reefoid part of the Gays River Formation where the Pb-Zn mineralization is located.

In the Kennetcook Basin the Murphy Road Formation is roughly time equivalent to the Green Oaks Formation (Giles, 1981) (Table 1), however there were no fine grained siliciclastic sediments available for sampling from drill core, and only a few small outcrops near the Bar S Ranch could be sampled. In the Antigonish Basin fine grained siliciclastic Horton Group sediments (Keppie et al., 1978) could only be sampled from shoreline outcrop immediately south of Cape George. Also in the Antigonish Basin the Visean Hood Island Formation was sampled due to its general lithologic and stratigraphic similarities to the Green Oaks Formation in the Shubenacadie and Musquodoboit basins (B. Boehner, pers. comm. 1990).

Unweathered material was sampled from outcrop wherever it was available, and from all available drill core stored at the Provincial Core Library in Stellarton and at Acadia University in Wolfville. A total of 86 samples were collected from the following localities: Kennetcook Basin (n=22), Rawdon Hills (n=7), Shubenacadie Basin (n=33), Musquodoboit (n=13), and Antigonish Basin (n=11). After breaking into centimetre-size pieces, the samples were individually washed in sodium metaphosphate to disperse the phyllosilicates. Distilled water was then added to each sample before being centrifuged for 14 minutes at 2800 rpm to extract the <2 μm (clay) fraction. Aliquots of each sample were then placed on a glass disk and allowed to air dry to make oriented mounts for X-ray diffraction analysis.

Table 1. Table of formations and correlation between Horton Group and Windsor Group strata for the study area in mainland Nova Scotia. Stratigraphic position of the Walton (W) and Gays River (GR) deposits are indicated. Simplified from Giles (1981), Boehner and Giles (1982), Ferguson (1983), and Moore and Ferguson (1986).

	KENNETCOOK BASIN	RAWDON HILLS	SHUBENACADIE BASIN	MUSQUODOBOIT BASIN	ANTIGONISH BASIN
VISEAN WINDSOR GROUP (800–1000 m)	Murphy Road Fm.		Green Oaks Fm.	Green Oaks Fm.	Hood Island Fm.
	Pesaquid Fm.		MacDonald Road Fm.	Elderbank Fm.	Addington Fm.
	Wentworth Station Fm.				Wallace Brook Fm.
	Miller Creek Fm.				Lakevale Fm.
	Tennycape Fm.		Stewiacke Fm.		Hartshorn Fm.
	White Quarry Fm.		Carrolls Corner Fm.	Carrolls Corner Fm.	Bridgeville Fm.
				Meaghers Grant Fm.	
	Macumber Fm. (W)		Gays River Fm. (GR)	Gays River Fm.	Gays River Fm. Macumber Fm
TOURNASIAN HORTON GROUP (0–1500 m)	Cheverie Fm.	Undivided Horton Group	Coldstream Fm. Undivided Cheverie Fm. and	Coldstream Fm. Undivided Cheverie Fm. and	Wilkie Brook Fm.
	Horton Bluff Fm.		Horton Bluff Fm.	Horton Bluff Fm.	

All diffractograms were made using a Philips PW 1830/1710 generator and diffractometer control operating at 50 kV 30 mA, using Ni-filtered CuKα radiation, a scanning speed of 3°/minute, slits of 1°-0.1 mm-1°, a chart speed of 1 cm/°2θ, and a time constant of 2. Diffractogram mineral peaks were then identified but not quantified. Samples were also glycolated for 24 hours, and heat treated for 2 hours at 550°C to aid in phyllosilicate mineral identification. Using the pre-treatment diffractograms, illite crystallinity (Kubler, 1967) (10Å peak width at half height measured in Δ°2θ) was determined for all the samples which produced well defined 10Å and 5Å peaks. The crystallinity of illite increases (and the half-height 10Å peak width decreases) as diagenetic conditions proceed into the metamorphic realm. Illite crystallinity measurements were determined from diffractograms using a magnifying glass and precision rule. As there is no standard illite sample available for direct interlaboratory comparison, and therefore no standard Δ°2θ values are available for our particular upper and lower anchizone boundaries, instrumental settings were compared with those recently compiled by Kisch (1983, 1990) from a number of illite crystallinity studies. Our instrumental settings are most similar to Kubler's Neuchatel settings, which place the diagenetic zone - anchizone boundary at 0.42 Δ°2θ, and the anchizone - epizone boundary at 0.25 °2 (Fig. 2).

Esquevin (1969) found that the crystallinity of illites not only depended on recrystallization temperature but also on the composition of the micas' octahedral layer. Esquevin determined that aluminous (dioctahedral) micas would reflect changing temperatures much more efficiently than ferromagnesian (trioctahedral) micas, and that the relative intensity of the 5Å (002) peak and 10Å (001) peak could be used to distinguish dioctahedral and trioctahedral micas respectively, as originally determined by Nagelschmidt (1937). Therefore the I(002)/I(001) peak ratio is greater for micas of muscovite composition than for those of biotite or phengite composition. The majority of micas in the samples are of aluminous muscovite composition (i.e. I(002)/I(001) >0.4; Fig. 2 and 3), and therefore the octahedral layer composition is not affecting the illite crystallinity indices.

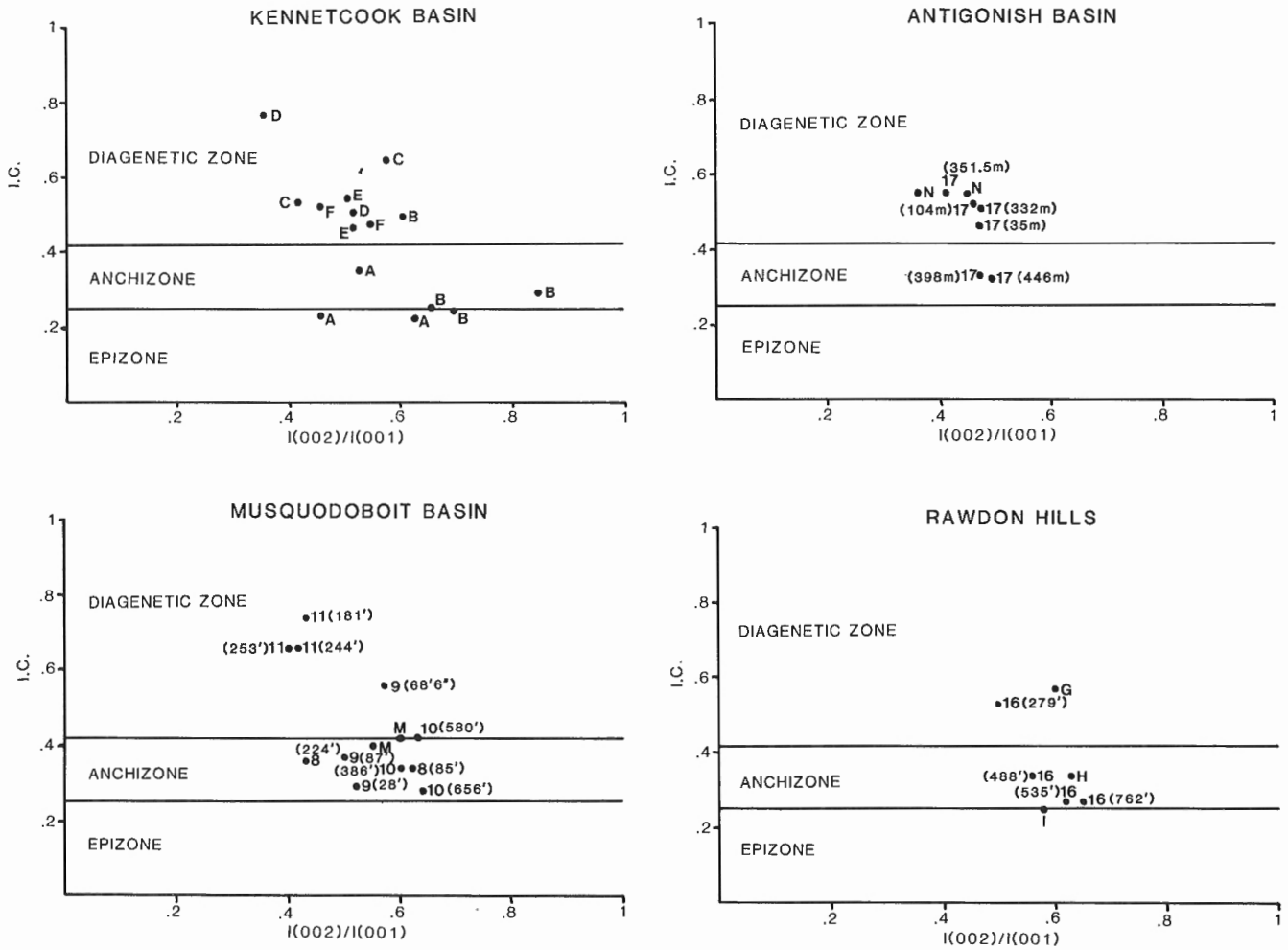

Figure 2. Illite crystallinity (I.C.) versus intensity ratio of 5Å to 10Å peaks (I(002)/I(001)) for outcrop and drill hole samples collected in the Kennetcook Basin, Musquodoboit Basin, Antigonish Basin, and Rawdon Hills. Sample numbers and letters correlate with those listed for Figure 1. Sample depth is indicated beside drill core samples.

RESULTS

Kennetcook Basin

In the Kennetcook Basin the high concentration of drilling in the vicinity of clay-poor Windsor Group sulphate deposits dictated that fine grained siliciclastic samples in the basin be collected from outcrop exposures along the coast and a few brooks. A majority of samples are from the Horton Bluff and Cheverie formations of the Horton Group; a few were collected from the Murphy Road Formation (locality P, Fig. 1).

The Horton Group samples consist of interbedded black to grey-green fissile claystone and mudstone, and grey to pale-red siltstone. In the Curry Brook and Harding Brook area there is commonly a high proportion of detrital white mica in the basal sediments of Horton Bluff Formation, with noticeably less detrital micas at other sample localities. The abundance of this detrital mica increases towards the unconformity with the underlying phyllitic Meguma Group rocks, from which the mica was probably derived. Ripple and wave laminae, parting lineations, trails and burrows, ostracods, plant debris, pyrite nodules, and concretions were all noted in the fine grained sedimentary rocks. The Murphy Road Formation samples consist of micaceous, noncalcareous red siltstone, interbedded with minor sandstone.

The clay size material of the Horton Group samples contains mica, chlorite, kaolinite, feldspar, and quartz. Minor amounts of smectite were detected in some of the Horton Bluff Formation lacustrine sediments (Martel, 1990) at Blue Beach. Illite and kaolinite X-ray peaks of samples from the Murphy Road Formation showed only poor crystallinity. Figure 2 shows that all the micas are aluminous, and that the majority of the illite crystallinity (I.C.) measurements fall within the diagenetic zone suggesting that authigenic illite is present in the samples. Interestingly, most of the samples from Harding Brook and Curry Brook yield I.C. values within the anchizone and epizone. These lower I.C. values likely reflect the high proportion of detrital muscovite from the Meguma Group, which have retained their high metamorphic crystallinity and have not been degraded during sedimentary diagenesis to high I.C. values. Away from the metamorphosed 'basement', towards areas of thicker sediment accumulation in the Kennetcook Basin, the mica appear to be less crystalline and are likely diagenetic illites formed from degraded detrital mica or illitization of feldspar. The presence of detrital muscovite, fibrous authigenic illite on altered feldspar, plus interstitial kaolinite, was observed in thin section.

Musquodoboit Basin

In the Musquodoboit Basin fine grained siliciclastic sediments of the Meaghers Grant Formation were collected from one road cut locality and from core from three holes drilled along the southern margin of the basin (Fig. 1). The samples consist of thin bedded to planar-laminated mudstone and siltstone. Some samples are calcareous and interbedded with minor calcarenite and anhydrite. The fissile mudstone at localities 8 and 9 (Fig. 1) is dark grey to black, very indurate and contains abundant finely disseminated sulphides. In thin section abundant quartz, carbonate, detrital muscovite, and authigenic illite is evident. Small opaque grains are sulphide minerals and, possibly, detrital organic material. The clay-fraction mineralogy for the Meaghers Grant Formation samples is muscovite, illite (based on I.C. plots), chlorite, kaolinite, smectite, and minor quartz, feldspar, and dolomite. Figure 2 shows that all the micas are aluminous and that most of the samples fall within the anchizone I.C. field, reflecting the high proportion of detrital mica in these samples.

The only samples which could be collected from the Green Oaks Formation in the Musquodoboit Basin came from drill core near the northern margin of the basin (Fig. 1). They consist of red noncalcareous siltstone interbedded with micritic carbonate sediments. Detrital mica is evident in hand samples. The clay-fraction mineralogy consists of muscovite, illite, chlorite, kaolinite, smectite, hematite, and lesser amounts of dolomite. All the I.C. values for these samples fall well within the diagenetic field (Fig. 2), suggesting that the majority of the mica in these samples is authigenic illite.

Shubenacadie Basin

Samples of fine grained siliciclastic rock from the Horton Group and Green Oaks Formation were collected from drill hole and outcrop localities located on Figure 1, as well as on Map 82-4 (Giles and Boehner, 1982). In the Shubenacadie Basin the Horton Group samples consist of red siltstone to dark green mudstone. The samples are laminated with some fissility, noncalcareous, micaceous and, in the reddened samples, display some beige reduction mottling. Some desiccation and soft sediment deformation structures were visible in drill core samples. Clay-fraction mineralogy consists of mica (muscovite and illite), chlorite and kaolinite, and minor quartz, feldspar, and hematite. Two samples (locations 1 and 6, Fig. 1) contained minor amounts of smectite.

The Green Oaks Formation samples consist of red to green-grey siltstone and mudstone. They are massive to laminated, and may contain moderate amounts of detrital mica, fractures and vugs filled and lined by calcite, and reduction mottling. The clay-fraction mineralogy consists of illite and muscovite, kaolinite and chlorite, and variable amounts of quartz, feldspar, hematite, dolomite, smectite, and irregular mixed-layered illite-smectite. Figure 3 shows that the mica is aluminous, and a scattering of I.C. values between the diagenetic zone, anchizone, and upper epizone for both the Horton Group and Green Oaks Formation samples. This scattering of points cannot be related to the degree of burial diagenesis of the sediments as samples from the same drillhole do not show systematic I.C. increase with depth; in some cases just the opposite trend is shown. The only plausible explanation for this distribution of points is that samples with high proportions of detrital muscovite (and high inherited crystallinity) have masked the signature of any diagenetic illite that might be present. The samples with a high proportion of detrital muscovite plot in or close to the anchizone field.

The only locality within our study area where other thermal maturation indicators had been measured and could be compared with our data (Fig. 4), was drillhole SB-1 (Fig. 1 locality 15). The vitrinite reflectance measurements for DH SB-1, reported by Utting (1980), indicate a uniform reflectance

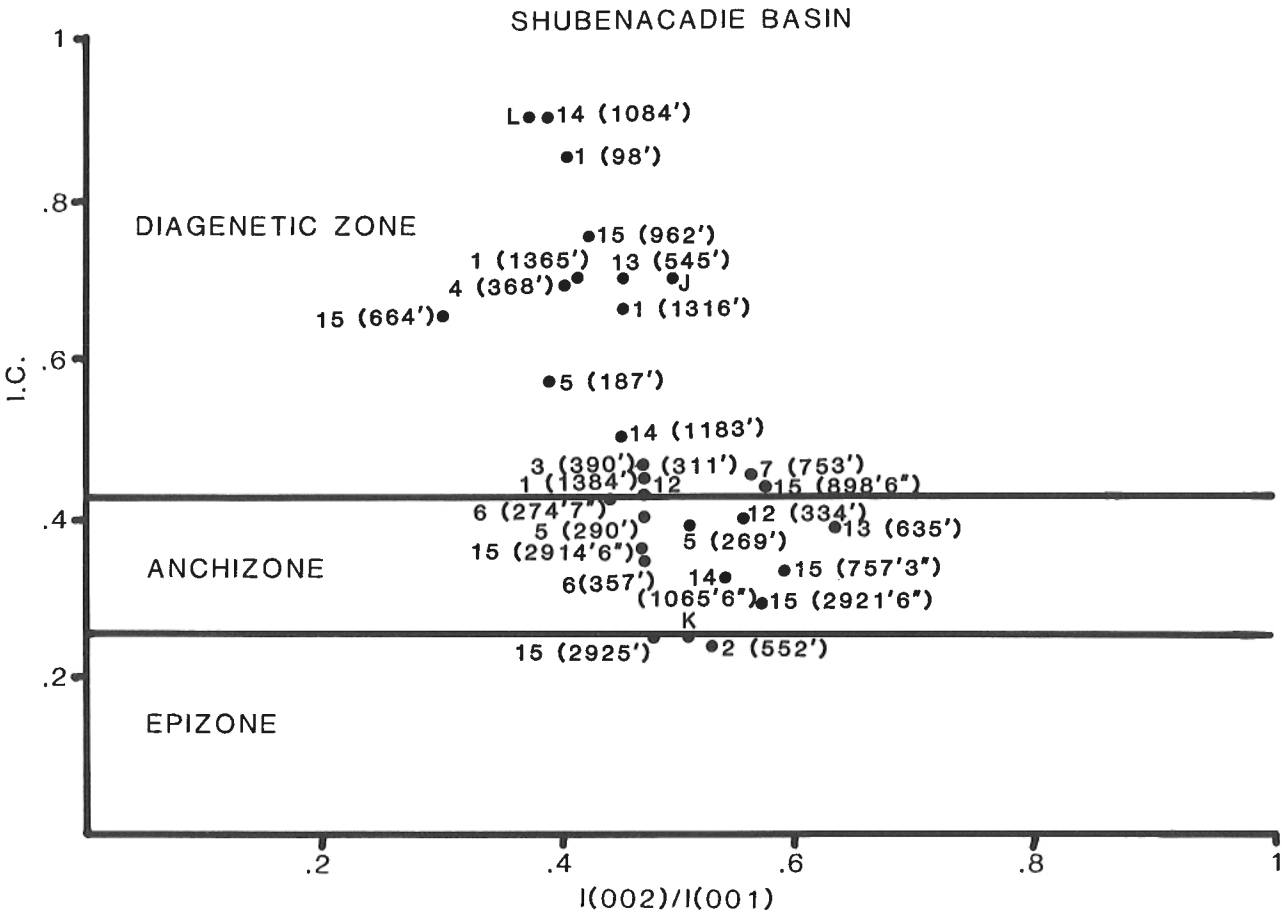

Figure 3. Illite crystallinity (I.C.) versus intensity ratio of 5Å to 10Å peaks (I(002)/I(001)) for outcrop and drill hole samples collected in the Shubenacadie Basin. Sample numbers and letters correlate with those listed for Figure 1. Sample depth is indicated beside drill core samples.

within the Windsor Group, with a slight increase within the Horton Group. The Thermal Alteration Index (TAI) determined on palynomorphs by Utting (1980, 1987) for DH SB-1 suggests an increase in organic maturation with depth within the Windsor Group, although all samples plot within the TAI catagenic zone. Our I.C. results for DH SB-1, taken over a greater stratigraphic interval with fewer samples, fall within the I.C. diagenetic zone except for four samples. These latter samples may contain a higher proportion of detrital illite.

Antigonish Basin

The Wilkie Brook Formation of the Horton Group was sampled from shoreline outcrop at the type section between Wilkie Brook and Marsh Cove. The samples consist of black fissile claystones containing abundant calcareous concretions, and dull red siltstone with detrital white mica and minor calcite. The fine grained siliciclastic sediments together with algal limestones have been interpreted as being lacustrine in origin (Boehner and MacBeath, 1989), and are interbedded with alluvial fan sandstone and conglomerate. The clay-fraction mineralogy consists of illite, chlorite, kaolinite, smectite, and minor quartz. The I.C. of these samples could not be adequately measured as the 10Å diffraction peaks were broad and display shoulders, possibly due to interference with the smectite peaks at lower 2θ angles.

Samples from the Hood Island Formation, representing the uppermost stratigraphic unit of the Windsor Group in the basin (Table 1), could only be obtained from a few poor outcrop localities and one cored drill hole near Glen Road (Fig. 1). The samples consist of massive red to dark-green siltstone and some mudstone. Minor detrital white micas are evident as are a few calcite veins. The clay-fraction mineralogy consists of muscovite, illite, chlorite, and kaolinite, and lesser amounts of quartz, feldspar, and dolomite. One of the eight samples contained minor smectite. Most of the samples contain diagenetic illite (Fig. 2) although there is no systematic I.C. increase with drill core sample depth, as seen in thicker 'shale' sequences undergoing burial diagenesis (e.g., Dunoyer De Segonzac, 1969).

Rawdon Hills Area

The Rawdon Hills area is a fault-bounded hilly region, between the Kennetcook Basin and Shubenacadie Basin, consisting of undivided interlayered conglomerate, sandstone,

and minor finer grained siliciclastic sediments of the Horton Group (Giles and Boehner, 1982). The samples consist of black to green grey, laminated and pyritic claystone and mudstone, and grey micaceous siltstone. The clay-fraction mineralogy consists of mica, kaolinite, chlorite, feldspar, and quartz. Figure 2 shows an aluminous mica composition, and that most I.C. values plot in the anchizone field. One outcrop sample (G) is a mudstone compared to the other two (H, I) which are more micaceous mudstone to siltstone. Also, the I.C. values for DH BP-6 (16) systematically increase with

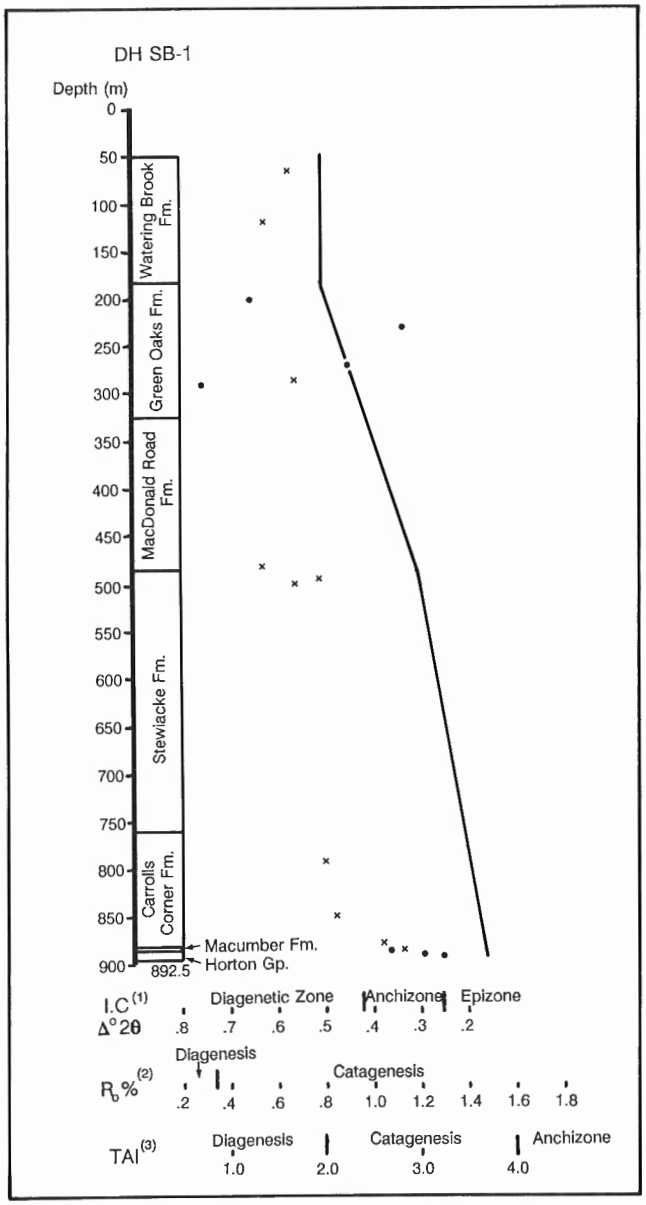

Figure 4. Comparison of thermal maturation indicators for DH SB-1 in the Shubenacadie Basin. Vitrinite reflectance and TAI maturation zone terminology and boundaries based on general compilation table by Héroux et al. (1979) for thermal maturation indicators. Data obtained from: (1) I.C. this study, point symbols; (2) R_o% Utting (1980), cross symbols; (3) TAI Utting (1980), continuous line.

Table 2. Clay-fraction mineralogy for the samples collected for this study and described in the text. Sample localities are shown in Figure 1. Abbreviations as follows: M=mica; C=chlorite; K=kaolinite; S=smectite; ML=mixed-layered phyllosilicate; Q=quartz; F=feldspar; D=dolomite; H=hematite.

LOCALITY	SAMPLE	CLAY-FRACTION MINERALOGY								
		M	C	K	S	ML	Q	F	D	H
	KENNETCOOK BASIN									
A	HB-90-1b	X		X						
	-2	X	X	X						
	-3	X	X	X						
B	CB-90-1	X		X				X		
	-2a	X		X				X		
	-2b	X		X				X		
	-3	X		X						
C	BB-90-1	X	X	X						
	-2	X	X	X						
	-3a	X	X	X		X				
	-3b	X	X	X						
	-4	X		X						
	-5	X	X	X		X				
D	CP-90-1	X		X			X			
	-2	X		X						
E	WB-90-1	X	X	X						
	-2	X	X	X						
F	TB-90-1	X	X	X						
	-2	X	X	X			X	X		
P	NS-90-22	X	X	X						
	-23	X	X	X						
	-24	X	X	X						
	MUSQUODOBOIT BASIN									
M	NS-90-3	X	X	X	X					
	-4	X	X	X	X					
11	208-3-181′	X		X	X			X	X	X
	-244′	X	X	X						
	-253′	X	X	X	X					
8	MG-2-85′	X	X	X	X					
	-244′	X	X	X			X	X	X	
9	MG-15-28′	X	X	X			X	X		
	-68′6"	X	X	X						
	-87′	X	X	X						
10	MG-43-386′	X	X	X						
	-580′	X	X	X						
	-656′	X	X	X						
	SHUBENACADIE BASIN									
18	NM-19-140′	X	X	X		X				
	-160′	X	X	X						
2	NM-29-552′	X	X	X						
L	NS-90-5	X		X						
J	-8	X	X	X						
K	-9	X	X	X					X	
14	153-3-1065′6"	X		X			X			
	-1084′	X		X						
	-1183′	X	X	X						
13	W-3-545′	X		X						
	-635′	X	X	X						
4	M-1-323′	X	X	X		X				
	-368′	X	X	X	X					
15	SB-1-664′	X	X	X				X		X
	-757′3"	X	X	X				X	X	X
	-898′6"	X		X						
	-962′	X		X						X
	-2914′6"	X		X						
	-2921′6"	X		X						
	-2925′	X		X			X	X	X	X
3	HP-7-390′	X	X	X						
12	C-15-311′	X		X						X
	-334′	X		X						
5	MA-73-1-187′	X		X						
	-269′	X	X	X			X			
	-290′	X	X	X						
6	MA-73-4-274′7"	X		X	X					
	-357′	X	X	X						
7	MA-73-9-753′	X	X	X						
1	UR-2-98′	X	X	X	X		X	X		
	-1316′	X	X	X			X			X
	-1365′	X	X	X	X		X			
	-1384′	X	X	X			X			
	ANTIGONISH BASIN									
N	NS-90-11	X	X	X			X	X		X
	-12	X	X	X						
O	NS-90-13	X	X	X	X		X			
	-14	X	X	X	X					
	-15	X	X	X						
17	GR-83-1-35m	X	X	X			X			
	-104m	X	X	X						
	-332m	X	X	X						
	-351.5m	X	X	X						
	-398m	X	X	X			X	X	X	X
	-446m	X	X	X				X		
	RAWDON HILLS									
G	NS-90-2	X		X						
I	-6	X		X				X		
H	-7	X		X				X		
16	BP-6-279′	X	X	X						
	-488′	X	X	X				X		
	-535′	X	X	X						
	-762′	X	X	X						

stratigraphic depth. This suggests once more that, as the basal Horton Group unconformity is approached, or as micaceous siltstones are encountered, the higher proportion of detrital mica masks any diagenetic illite signature and results in higher I.C. values being recorded.

CONCLUSIONS

This study of the regional distribution and character of clay-fraction minerals, particularly phyllosilicates, in Carboniferous age sedimentary rocks of mainland Nova Scotia permits the following conclusions:

1. Despite the separation of the clay fraction (<2 μm), it was not possible to eliminate detrital mica (in theory generally larger than authigenic illite) before analyzing the samples using X-ray diffractometry. However, in samples where detrital micas were subordinate, the I.C. values indicate that the authigenic illite falls within the diagenetic zone.

2. This suggests that the rocks, at these localities at least, have not been subjected to anchimetamorphic conditions (>200°C; Kisch, 1987) since deposition.

3. Smectite, or smectite-bearing mixed-layered phyllosilicates, have been identified at several localities indicated in Figure 1. Within the Horton Group: minor amounts of irregular mixed-layered illite - smectite exists in locality C (Kennetcook Basin); smectite exists in localities 1 and 6 (Shubenacadie Basin); and smectite exists in locality O (Antigonish Basin). Within the Windsor Group: minor amounts of irregular mixed-layered illite - smectite and smectite exists in locality 4; smectite exists in locality 1 (Shubenacadie Basin) and in localities M, 8, and 11 (Musquodoboit Basin). The presence of smectite and irregular mixed-layered illite - smectite suggests that the sediments in those areas have not been subjected to temperatures >150°C (Kisch, 1983; Singer and Muller, 1983; Frey, 1987). This is very similar to the diagenetic state of coeval Carboniferous sedimentary rocks in the Deer Lake Basin of western Newfoundland (Gall and Hiscott, 1986).

4. Samples from localities A, G, H, I, K, 2, 10, and 12 (Fig. 1) do not contain diagenetic illite or smectitic phyllosilicates. One explanation for this is that heated mineralizing fluids may have selectively affected the sedimentary rocks at these localities and resulted in neomorphic illite with high I.C. accompanied by destruction of smectitic phyllosilicates. An alternate possibility is that no authigenic phyllosilicates existed and that all micas are detrital in origin. Further petrographic studies might resolve this uncertainty.

5. Although sampling was widely spaced and many gaps remain, the study indicates that for the areas which were sampled there is no indication that heated mineralizing fluids migrated through either the Horton Group or upper Windsor Group strata and contributed to the genesis of known Pb-Zn deposits. It is possible, however, that mineralizing fluids migrated along the Meguma Group - Horton Group unconformity or directly through the Meguma Group 'basement'. Neither situation would have been detected by the methods employed in this study but either would have resulted in the 'B'-type lead isotope signature of the Gays River mineralization (Sangster, 1990).

ACKNOWLEDGMENTS

This study benefited greatly from in-house technical assistance offered by Jean Hsieh, Bob DeLabio, and Meriam Wygergangs. We are also grateful to Bob Boehner, Bob Ryan, and Jim Languille of the Nova Scotia Department of Mines and Energy for guidance in unravelling the stratigraphy of the study area and in granting us permission to sample, and directing us to, suitable drill core. Our thanks to Jack Coldwell and Reg Moore of Acadia University for allowing us to sample drill core and for guidance to sample localities in the Kennetcook Basin. Constructive comments by Bob Ryan (NSDME) and Jean Percival (GSC) improved the manuscript.

REFERENCES

Akande, S.O.
1982: Genesis of the lead and zinc mineralization at Gays River, Nova Scotia, Canada; Ph.D. thesis, Dalhousie University, Halifax, 349 p.

Boehner, R.C. and Giles, P.S.
1982: Geological map of the Antigonish Basin, Nova Scotia; Nova Scotia Department of Mines and Energy, Map 82-2, 1:50 000.

Boehner, R.C. and MacBeath, B.E.
1989: A lacustrine limestone mound (algal reef) in the Wilkie Brook Formation (Horton Group), Cape George area, northeastern mainland Nova Scotia; in Reefs, Canada and adjacent area, (ed.) H.H.J. Geldsetzer, N.P. James, and G.E. Tebbutt; Canadian Society of Petroleum Geologists, Memoir 13, p. 626-630.

Boyle, R.W.
1972: The geology, geochemistry, and origin of the barite, manganese, and lead-zinc-copper-silver deposits of the Walton-Cheverie area, Nova Scotia; Geological Survey of Canada, Bulletin 166, 181 p.

Dunoyer De Segonzac, G.
1969: Les minéraux argileux dans la diagenèse - passage au métamorphisme; Mémoires du Service de la Carte Géologique d'Alsace et de Lorraine, Vol. 29, 317 p.
1970: The transformation of clay minerals during diagenesis and low grade metamorphism: a review; Sedimentology, v. 15, p. 281-346.

Esquevin, J.
1969: Influence de la composition chimique des illites sur leur cristallinité; Bulletin du Centre de Recherches de Pau - SNPA, Vol. 3, p. 147-153.

Ferguson, S.A.
1983: Geological map of the Hantsport area Nova Scotia; Nova Scotia Department of Mines and Energy, Map 83-1, scale 1:25 000.

Frey, M.
1987: Very low-grade metamorphism of clastic sedimentary rocks; in Low temperature metamorphism; (ed.) M. Frey, Blackie, p. 9-48.

Gall, Q. and Hiscott, R.H.
1986: Diagenesis of locally uraniferous sandstones of the Deer Lake Group, and sandstones of the Howley Formation, Carboniferous Deer Lake subbasin, western Newfoundland; Bulletin of Canadian Petroleum Geology, v. 34, p. 17-29.

Giles, P.S.
1981: Major transgressive-regressive cycles in Middle to Late Visean rocks of Nova Scotia; Nova Scotia Department of Mines and Energy, Paper 81-2, 27 p.

Giles, P.S. and Boehner, R.C.
1982: Geological map of the Shubenacadie and Musquodoboit Basins central Nova Scotia; Nova Scotia Department of Mines and Energy, Map 82-4, scale 1:250 000.

Héroux, Y., Chagnon, A., and Bertrand, R.
1979: Compilation and correlation of major thermal maturation indicators; The American Association of Petroleum Geologists Bulletin, v. 63, p. 2128-2144.

Keppie, J.D., Giles, P.S., and Boehner, R.C.
1978: Some Middle Devonian to Lower Carboniferous rocks of Cape George, Nova Scotia; Nova Scotia Department of Mines, Paper 78-4, 37 p.

Kisch, H.J.
1983: Mineralogy and petrology of burial diagenesis (burial metamorphism) and incipient metamorphism in clastic rocks; in Diagenesis in sediments and sedimentary rocks. (ed.) G. Larsen and G.V. Chilingar; Developments in Sedimentology, Elsevier, v. 25B, p. 289-493.
1987: Correlation between indicators of very low-grade metamorphism; in Low temperature metamorphism, (ed.) M. Frey; Blackie, p. 227-300.
1990: Calibration of the anchizone: a critical comparison of illite 'crystallinity' scales used for definition; Journal of Metamorphic Geology, v. 8, p. 31-46.

Kubler, B.
1967: Anchimétamorphisme et schistosité; Bulletin du Centre de Recherches de Pau - SNPA, Vol. 1, p. 259-278.

Lydon, J.W.
1978: Observations on some lead-zinc deposits of Nova Scotia; Geological Survey of Canada, Paper 78-1A, p. 293-298.

Martel, A.T.
1990: Stratigraphy, fluviolacustrine sedimentology and cyclicity of the Late Devonian/Early Carboniferous Horton Bluff Formation, Nova Scotia, Canada; Ph.D. thesis, Dalhousie University, Halifax, Nova Scotia, 297 p.

Moore, R.G. and Ferguson, S.A.
1986: Geological map of the Windsor area Nova Scotia; Nova Scotia Department of Mines and Energy, Map 86-2, scale 1:25 000.

Nagelschmidt, G.
1937: X-ray investigation on clays; Zeitschrift Für Kristallographie, v. 97, p. 514-521.

Ravenhurst, C.E.
1987: An isotopically and thermochronologically constrained model for lead-zinc and barium mineralization related to Carboniferous basin evolution in Nova Scotia, Canada; Ph.D. thesis, Dalhousie University, Halifax, Nova Scotia, 251 p.

Ravenhurst, C.E., Reynolds, P.H., Zentilli, M., Krueger, H.W., and Blenkinsop, J.
1989: Formation of Carboniferous Pb-Zn and barite mineralization from basin-derived fluids, Nova Scotia, Canada; Economic Geology, v. 84, p. 1471-1488.

Sangster, D.F.
1986: Classification, distribution and grade-tonnage summaries of Canadian lead-zinc deposits; Geological Survey of Canada, Economic Geology Report 37, 68 p.
1990: Mississippi Valley-type and sedex lead-zinc deposits: a comparative examination; Transactions of the Institution of Mining and Metallurgy, Section B, v. 99, p. B21-B42.

Singer, A. and Muller, G.
1983: Diagenesis in argillaceous sediments; in Diagenesis in sediments and sedimentary rocks, 2; (ed.) G. Larsen and G.V. Chilinger; Developments in Sedimentology, Elsevier, v. 25B, p. 115-212.

Utting, J.
1980: Palynology of the Windsor Group (Mississippian) in a borehole at Stewiacke, Shubenacadie Basin, Nova Scotia; Canadian Journal of Earth Sciences, v. 17, p. 1031-1045.
1987: Palynology of the lower Carboniferous Windsor Group and Windsor-Canso boundary beds of Nova Scotia, and their equivalents in Quebec, New Brunswick and Newfoundland; Geological Survey of Canada, Bulletin 374, 93 p.

Notes on the use and performance of thermal instrumentation: experience from the Norman Wells pipeline ground temperature monitoring program

M.M. Burgess and V.S. Allen
Terrain Sciences Division

Burgess, M.M. and Allen, V.S., 1991: Notes on the use and performance of thermal instrumentation: experience from the Norman Wells pipeline ground temperature monitoring program; in Current Research, Part E; Geological Survey of Canada, Paper 91-1E, p. 337-345.

Abstract

Since 1984, over 150 multithermistor temperature cables have been installed at some 30 sites along the Norman Wells to Zama Pipeline as part of a Permafrost and Terrain Research and Monitoring Program. The performance of over 1400 temperature sensors, the majority of which are YSI44033 thermistors, has been excellent. As of December 1990, 97% of the sensors continued to function well. Multi-channel data loggers have been installed at 8 of the monitoring sites. Data recovery has been high at 82%, with only 6.4% data loss due to logger failure or malfunction. Moisture in the temperature cable connector may lead to erroneously warm readings, by as much as 1°K.

Résumé

Depuis 1984, plus de 150 câbles de mesure de la température à plusieurs thermistors ont été installés en quelque 30 endroits le long du pipeline allant de Norman Wells à Zama dans le cadre d'un programme d'étude et de contrôle du pergélisol et du relief. Le rendement de plus de 1 400 sondes de température, dont la majorité sont des thermistors YSI44033, a été excellent. En décembre 1990, 97 % des sondes fonctionnaient toujours bien. On a installé des enregistreurs de données multibandes à huit des endroits qui ont été identifiés comme points de contrôle. Le taux de récupération des données a été élevé, atteignant 82 %, et à peine 6,4 % des données ont été perdues à cause de pannes ou du mauvais fonctionnement des enregistreurs. L'humidité dans le raccord du câble de sondage de la température peut fausser les mesures et mener à l'enregistrement de températures trop élevées d'au plus 1°K.

INTRODUCTION

The federal Departments of Energy, Mines and Resources (EMR) and Indian and Northern Affairs (INAC) have established several instrumented study sites along Mackenzie Valley as part of a Permafrost and Terrain Research and Monitoring Program along the Norman Wells, NWT to Zama, Alberta pipeline corridor. The 869 km pipeline is the first fully buried oil pipeline in permafrost terrain in Canada, traversing the discontinuous permafrost zone in a more or less north-south direction.

A major component of the research program is the quantification and analysis of changes in the ground thermal regime. EMR (initially the Earth Physics Branch and later the Geological Survey of Canada) took the lead in the design, selection, and thermal instrumentation of the monitoring sites. Thermistor sensors were used in the construction of the ground temperature cables — there are over 150 cables installed at some 30 sites. At several locations cables have been connected to 64 channel data loggers (SEADATA model 1250B).

This report presents selected statistical highlights of the performance of the thermal instrumentation and data acquisition systems adopted for the EMR/INAC project. Some of the difficulties (pitfalls and/or surprises) in automating the temperature measurements are outlined. Finally, recommendations are provided for the continued handling of data from the existing project as well as for future projects.

Qualitative and quantitative performance information on instruments used in research and monitoring programs unfortunately is not often reported, since most publications focus on the presentation and analyses of results rather than on the details of instrumentation (DiBiagio, 1990). This paper is intended to help fill this void and to provide observations useful to regulators and industry as well as researchers.

BACKGROUND

The small diameter, buried, uninsulated and "ambient" temperature pipeline has been in operation since April 1985 and is owned by Interprovincial Pipe Line (NW) Ltd (IPL). Several novel engineering approaches were implemented in order to limit energy exchange with the environment, minimize terrain disturbance and assure pipe integrity (Nixon et al., 1984; McRoberts et al., 1985; MacInnes et al., 1989).

Monitoring the ground thermal regime forms part of the larger multidisciplinary Permafrost and Terrain Research and Monitoring (PTRM) Program established by INAC in 1983 following the signing of an Environmental Agreement with IPL. The overall program objectives include: assessing the impacts of construction and operation of the pipeline on permafrost terrain, recommending improvements in the design and construction of future projects, and increasing the knowledge of the regional environmental framework and the terrain response to climate change as well as man-induced disturbances.

A description of the PTRM program, the selection, location and layout of monitoring sites, and a discussion of observations and analyses from 1983 to 1988 are outlined in greater detail in two volumes by MacInnes et al. (1989, 1990). The discussion of instrumentation performance that follows in this report is restricted to the EMR/INAC ground temperature project. Thermal instrumentation that is part of a separate project within the PTRM program involving Agriculture Canada is not discussed here; nor is the instrumentation installed as part of IPL's geotechnical monitoring program.

GROUND TEMPERATURE MEASUREMENT PROGRAM

Twenty three of the EMR/INAC monitoring sites consist of an instrumented cross-section, called a thermal fence. Thermal instrumentation is designed to document changes in the ground temperature regime, both on and off the right-of-way (ROW) to depths ranging from 5 to 20 m, as well as changes in the pipe temperature regime. Typically, 5 temperature sensors are strapped to the outside of the pipe, 3 temperature cables are located on-ROW, and 1 cable is positioned off-ROW. A site establishment report (Pilon et al., 1989) provides detailed information on the establishment of each thermal fence. Additional ground temperature cables have been installed at select fences as well as at other locations along the route, for example at IPL thaw settlement monitoring sites, and at 4 permafrost and climate change study sites.

Since pipeline operation began, data collection has been generally undertaken on a monthly to bi-monthly schedule. (For a discussion and an analysis of data frequency requirements, see Burgess and Riseborough, 1989). Summer readings are taken by various PTRM researchers, while winter readings are primarily undertaken by INAC district staff from Norman Wells and Fort Simpson. Compilations of the data are published annually as GSC Open Files (e.g. Burgess and Naufal, 1990); these include listings of all cables at thermal fences and at any additional sites.

Temperature instrumentation

The EMR/INAC ground temperature cables are installed in boreholes cased with small diameter (25-38 mm) PVC tubes filled with an environmentally safe nonfreezing silicone oil to allow for thermal equilibration with the surrounding soil, as well as for cable removal or replacement. Silicone fluid viscosity was selected to minimize convective overturn in the boreholes.

Shorter cables generally contain 10 temperature sensors spaced every 50 cm; longer cables generally contain 11 thermistor sensors spaced every metre near the surface and then every 2 or 3 m at depth. The temperature sensors are negative temperature coefficient thermistors, semi-conductor devices in which electrical resistance varies inversely as a function of temperature. Three types of thermistor have been used: 1) YSI44033 (Yellow Springs Inc. type 44033), the most common; 2) YSI44032, at two fences in northern

Alberta and a few additional cables; and 3) ATKINS, for 1984 pipe temperature sensors. The YSI sensors have a manufacturer's specified interchangeability of ± 0.1 K.

The ground temperature cables were manufactured with 22 conductor cable, so that paired wiring could be used to minimize sensor loss should a few conductors fail. The more conservative paired wiring uses two conductors per thermistor. Although a single common for all sensors could have been used to reduce the number of conductors, damage to the common conductor could have resulted in loss of data for the entire cable. The thermistor bead enclosures were completed by injection molding using polyurethane to provide waterproof installation. Each cable has a 2 m lead-in protected with braided shielding to minimize damage from small animals and terminated with a 24 pin military specification (MS) connector. The pipe thermistor sensors are individually wired with 2 conductor cable and connected to a switch box completed with a phone jack connector.

Measurements are taken manually using a digital multimeter (Fluke model 8062A). Sixty-four channel automatic data acquisition systems (SEADATA logger model 1250, discussed below) were later connected at select monitoring sites. The resolution of both these measurement systems is on the order of 0.01 to 0.02 K.

Automatic temperature data acquisition: SEADATA loggers

In 1983, at the time of the initial planning for the instrumentation of the Norman Wells pipeline thermal monitoring sites, the use of multiple channel temperature data loggers in cold region environments was in its infancy in the northern geothermal group of EMR. The thermal monitoring program was therefore designed essentially for manual data collection.

In the mid 1980's, tests by EMR of the 64 channel SEADATA tape cassette logger (model 1250) were promising in arctic environments. Plans were made to purchase three loggers for installation at the remote monitoring sites drilled in the winter of 1985 in the Wrigley area. Initially, it was anticipated that the more remote sites would not be visited during the winter months.

From the fall of 1985 through 1988, a total of 8 loggers were installed. Loggers were specified for YSI44033 thermistor sensors and with four MS input connectors. They are located at the following kilometrepost sites along the pipeline (km 0 is the northern end of the route in Norman Wells): 19.0, 79.2, 271.2, 272.0, 272.3, 608.7 and 783.3, and on Kee Scarp (about 5 km north of Norman Wells). The frequency of data acquisition was set to 8 hours and 20 minutes. The original configuration of the logger field installation involved connecting the appropriate extension cables and storing the logger in a wooden box placed at the edge of the right-of-way. Field trips by GSC personnel are required twice a year for servicing the loggers (battery change: 24 D cells).

Several modifications were required to the temperature cables and logger system to either adapt the cables to the loggers or adapt the data acquisition system to the needs of the monitoring program. These are outlined briefly in a subsequent section.

PERFORMANCE HIGHLIGHTS

Thermistors

Table 1 summarizes, by year since the program began in 1984, the cumulative number and type of temperature cables and associated thermistors in use on the EMR/INAC project. As of December 1990, there was a total 154 temperature cables, with 1461 thermistor sensors (the 5 pipe temperature sensors at a thermal fence were called a cable for this analysis). YSI44033 thermistors account for 86% of the sensors.

Table 2 presents the statistics on sensor failure. For each year the total number of failures to date is given, that is, 1985 failures include 1984, etc. As of December 1990, a total of 45 sensors had failed; this represents 3.1% of the sensors in use.

Thermistor failures have been of two types: i) sudden large drift or offset and ii) the most frequent, a gradual drift. Slow drifts in pipe thermistor sensors are often more difficult to identify, as these may be confused with or obscured by the sensors possibly moving relative to the pipe (i.e., if a sensor is pulled away from the pipe, and no longer strapped, then the thermal regime would change). This difficulty, along with

Table 1. Statistical summary - thermistor sensor performance

INSTALLATION STATISTICS - CUMULATIVE NUMBER OF CABLES AND NUMBER OF SENSORS								
YEAR	ALL SENSOR TYPES		YSI44033		YSI44032		ATKINS	
	cables/sensors		cables/sensors		cables/sensors		cables/sensors	
1984	58	535	33	334	14	146	11	55
1985	121	1130	97	939	13	136	11	55
1986	132	1248	107	1047	14	146	11	55
1987	141	1338	120	1179	10	104	11	55
1988	141	1338	120	1179	10	104	11	55
1989	154	1461	129	1260	14	146	11	55
1990	154	1461	129	1260	14	146	11	55

the different wiring of pipe temperature sensors, may explain why the failure rate of Atkins sensors (used in 1984 pipe sensors) is greater at 7.3%. Figure 1 shows an example of a possible failure in a pipe thermistor sensor at site 85-10B, km 588.7. This temperature versus time plot shows the general agreement amongst three pipe sensors prior to 1988; however, as of mid 1988 sensor 1 begins to drift and could be failing. A small consistent offset between sensor 2 and sensor 3 appears as of late 1988 and may reflect sensor movement.

SEADATA loggers

Over the years several modifications were made to accommodate the temperature cables to the requirements of data loggers or the data loggers to the needs of the monitoring program. These modifications and the constraints that they have placed on the performance of the instrumentation are discussed below.

1. Extension cables and conversion to single common wiring

The standard 2 m lead in termination of the temperature cables was too short for connection to the data logger, which was generally positioned at the edge of the right-of-way and as much as 10-20 m away from a particular borehole. Extension cables were thus required. These cables also used 22 conductor cable and 24 pin MS connectors.

The four ground temperature cables at a thermal fence generally had a total of 42 sensors with two conductors per sensors. The SEADATA loggers are, however, single common input. In order to install a logger, each temperature cable had to be converted to single common wiring. This conversion was incorporated into the extension cables. The dual purpose extension cables were protected with braided metal shielding.

2. Nonenvironmental connectors

All the ground temperature cables originally installed in 1984 and 1985 were terminated with nonenvironmental connectors. These are quite adequate for manual data collection but may lead to moisture problems for more sensitive automatic data acquisition. Environmental connectors would help ensure these problems are avoided. Environmental connectors have been used subsequently on several extension cables as well as on replacement cables, however the bulk of the ground temperature cables do not have them.

Figures 2 and 3 give two examples of problems that were likely due to moisture in connectors. Data files are maintained for the manual data collected from each cable. Where these cables are/or have been subsequently connected to data loggers, manual readings have been continued but at a lower frequency. Gaps of several months between manual readings have been filled in using data from the logger. Figure 2 shows combined manual/logger data for the 3 m sensor on cable T3 at site 85-7A, km 271.2. Note the large warm spikes of over 1 K in 1988. These warmer readings were taken from the data logger tape.

Figure 3 plots the temperature for three sensors on cable T4 at site 84-2A, km 19.0; this cable was connected to a logger in October 1988. Note the sudden increase in the 4 m sensor and its spikiness from that point onwards; the higher values are logger readings, the lower ones are manual. By contrast the 3 m sensor does not seem affected, while the 5 m sensor seems to show a much reduced effect.

Problems with moisture in the connectors may thus not necessarily affect all pins, and therefore not all sensors, on the cable. The presence of moisture generally seems to create an apparent capacitive effect. This means that a reading takes more time to stabilize, with an initially lower resistance (hence higher temperature) drifting towards a higher resistance (hence lower temperature) stable reading. This effect

Table 2. Sensor failure statistics - cumulative sensor failures

YEAR	ALL SENSOR TYPES		YSI44033		YSI44032		ATKINS	
	#sensors	%	#sensors	%	# sensors	%	# sensors	%
1984	2	0.4	1	0.3	-	0	1	1.8
1985	7	0.6	6	0.6	-	0	1	1.8
1986	10	0.8	9	0.9	-	0	1	1.8
1987	19	1.4	18	1.5	1	1.0	1	1.8
1988	25	1.9	22	1.9	1	1.0	3	5.5
1989	36	2.5	33	2.6	1	1.0	3	5.5
1990	45	3.1	41	3.3	1	1.0	4	7.3

TOTAL FAILURE RATE AS OF DECEMBER 1990: 3.1 %

can clearly be seen while taking manual readings. However, the automatic logger measurements are taken too quickly for the effect to have dissipated, and thus the temperatures tend to be too "high".

Figure 4 shows the temperature-time plot for the combined manual and logger data of the 3.5 m sensor on cable T1 at site 85-7A. Throughout the length of the record, a difference between manual and logger readings of 0.1 to 0.4 K is apparent and likely due to moisture in the connector. In addition, however, an apparent cooling trend as of approximately mid-1988 may be a drifting sensor. This sensor drift is suspected since the time series of the sensors above and below (e.g., combined manual and logger data from 4 m sensor plotted in Fig. 5) show a warming trend from 1988 onwards.

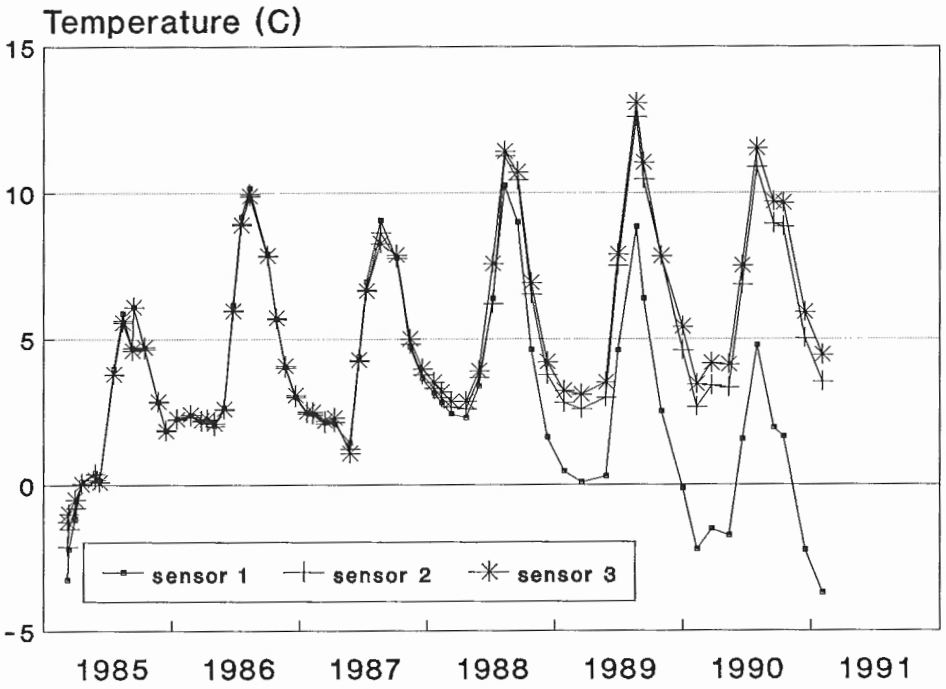

Figure 1. Temperature-time plot for three pipe sensors at site 85-10B, km 588.7. The sensors are strapped to the outside of the pipe and positioned as follows: #1 on the top of the pipe, #2 on the side, and #3 on the bottom.

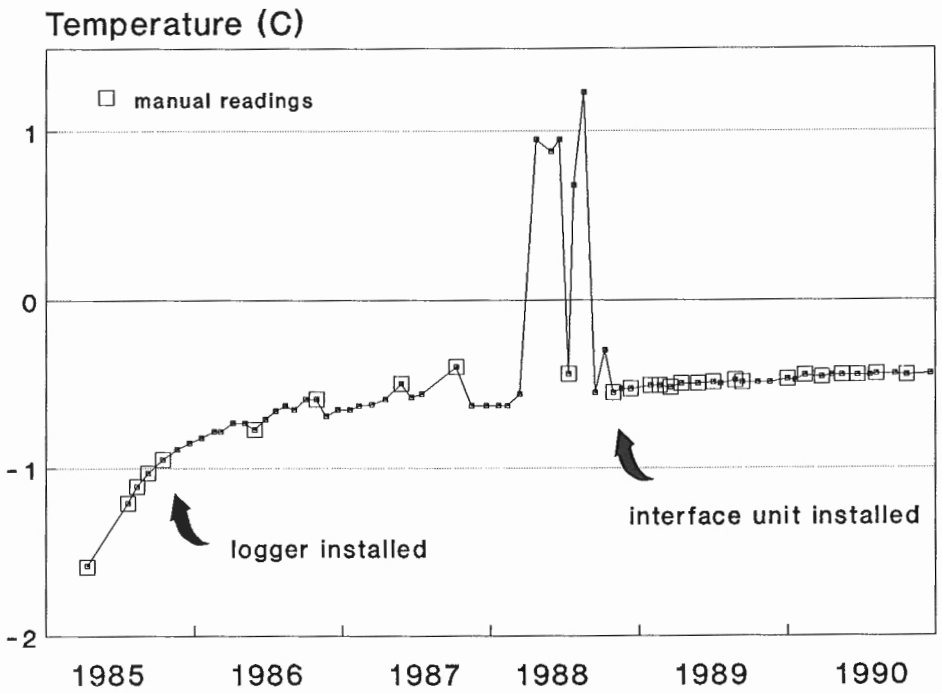

Figure 2. Temperature-time plot for the 3 m sensor on ground temperature cable T3 located on the right-of-way at site 85-7A, km 271.2.

3. Acquisition of both manual and logger data

The Seadata loggers store data on a cassette tape which must be returned to the laboratory for processing with a tape reader, adding a cumbersome step to the data processing. The data cannot be easily examined nor the loggers queried in the field. Software for processing the data tapes is specialized, written by the authors in-house in Rocky Mountain Basic for Hewlett Packard Series 200/300 computers.

The only means initially of obtaining real time knowledge of temperature readings when at a site was to disconnect the cables and read them manually using a multimeter. Since real time data was desirable, especially during the early years of the monitoring program and particularly from INAC's regulatory perspective to address concerns about environmental and engineering performance on a real time basis, cables were disconnected and reconnected several times. This could, and did, lead to a variety of problems with the logger data

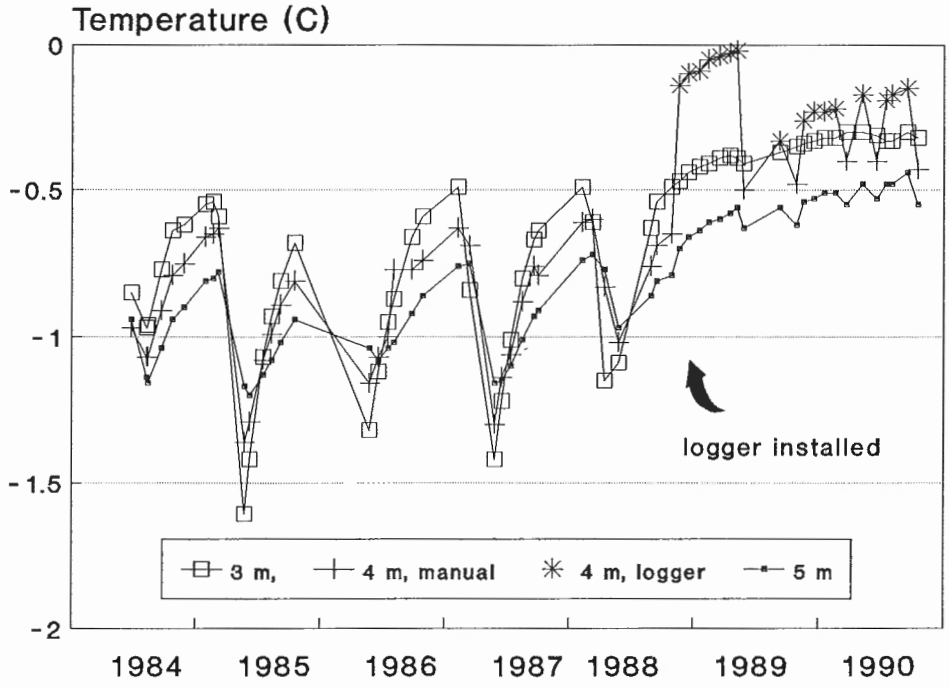

Figure 3. Temperature-time plot for three sensors on ground temperature cable T4 located off the right-of-way at site 84-2A, km 19.0.

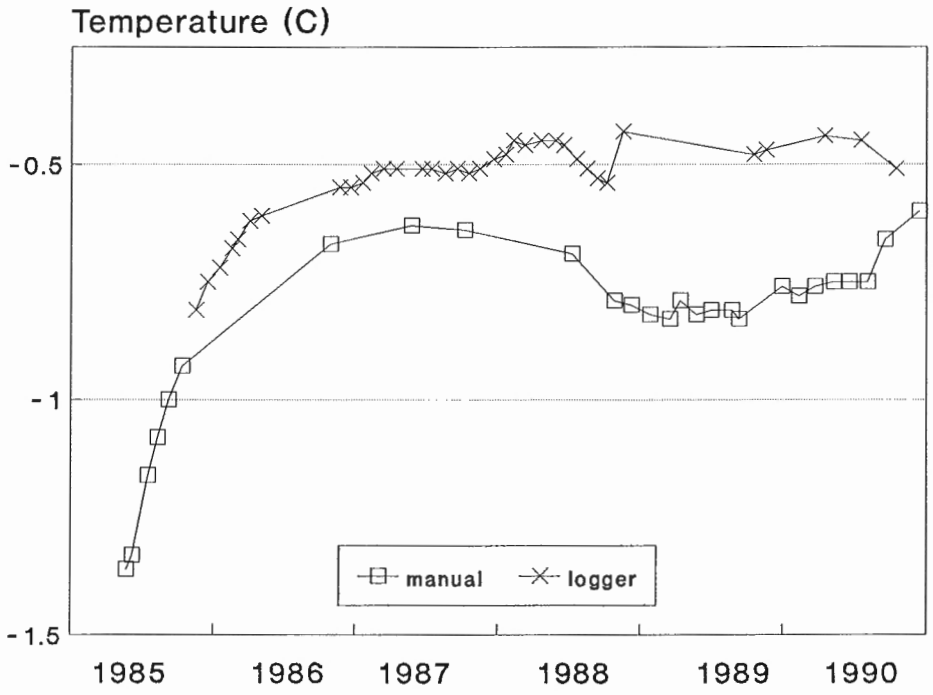

Figure 4. Temperature-time plot for the 3.5 m sensor on cable T1, located on the right-of-way at site 85-7A, km 272.0. The data have been graphed as two curves to highlight the difference between the concurrent manual and logger measurements.

collection: 1) water in the connectors, 2) wires sheared in the connectors interrupting data collection on some channels, and 3) cables not always properly reconnected, hence contact was not always achieved on all channels.

4. 1986 modifications to connect soil probes at select sites

Several channels remained available on each of the four logger inputs. However, these channels were not readily accessible since the four temperature cables occupied the four input connectors. In 1986, Agriculture Canada, as part of their separate project to study in detail the soil temperatures in the upper 1.5 m, installed seven sensor probes (one on and one off the right-of-way) at several thermal fences (Tarnocai and Kroetsch, 1990.) At those sites were SEADATA loggers were installed, the automatic acquisition of temperature data from these probes was desired and modifications were designed for the SEADATA system. A new connecting box, built by Richard Brancker Research (RBR), converted six cable inputs to four outputs, distributing the soil probe sensors into the available logger channels. The use of the box was discontinued after a few years, when the entire soil probe program was converted to its own dedicated data loggers (RBR 8 channel XL-800 loggers).

5. Interface unit for manual readings and connecting additional cables

In response to the problems identified above in points 1, 3 and 4, a system was designed to allow for manual readings in the field without disconnecting cables and to allow the option of connecting 2 additional cables of up to 7 sensors each (i.e, up to 6 cables, 4 with a maximum of 11 sensors, and 2 with up to 7 sensors). These "interface units" were also designed to convert the paired sensor wiring to single common, so that any extension cable required would be strictly a straight extension. A benefit of the interface units was that manual data could be collected by non-GSC personnel during other field trips, and should a logger have failed between servicing there would not be a complete data gap or loss. The interface units were installed in October 1988 and May 1989 (km 783.3 and Kee Scarp remain on the old system). Since 1989 pipe thermistors and shallow temperature probes placed near the pipe have been connected through these interface units at a number of sites.

The interface units have, however, also introduced some problems of their own. For example, the units were not built with environmental enclosures and moisture in the manual cable selection switches has caused some of them to freeze or give erratic readings. The installation of the interface units also required the design of new field boxes.

Performance and data recovery

Despite the difficulties and constraints noted above, the performance of the SEADATA loggers on the Norman Wells pipeline has been very good, with 82% data recovery. Table 3 details by month, the quality of the data recovered at each site from the time of logger installation until October 1990. The statistical analysis of this performance used a unit defined as a "cable-month", i.e., one cable connected to a logger for one month. The total number of cables-months is 1619 and the number of cable-months with data loss or data gaps is 292. This represents an 18% data loss which can be broken down as follows: 1) 6.4% due to logger failure or malfunction, 2) 2.5% due to human errors in the field, 3) 3.2% due to errors in tape processing or glitches in tapes, and 4) 5.9% due to extension cable problems or moisture problems.

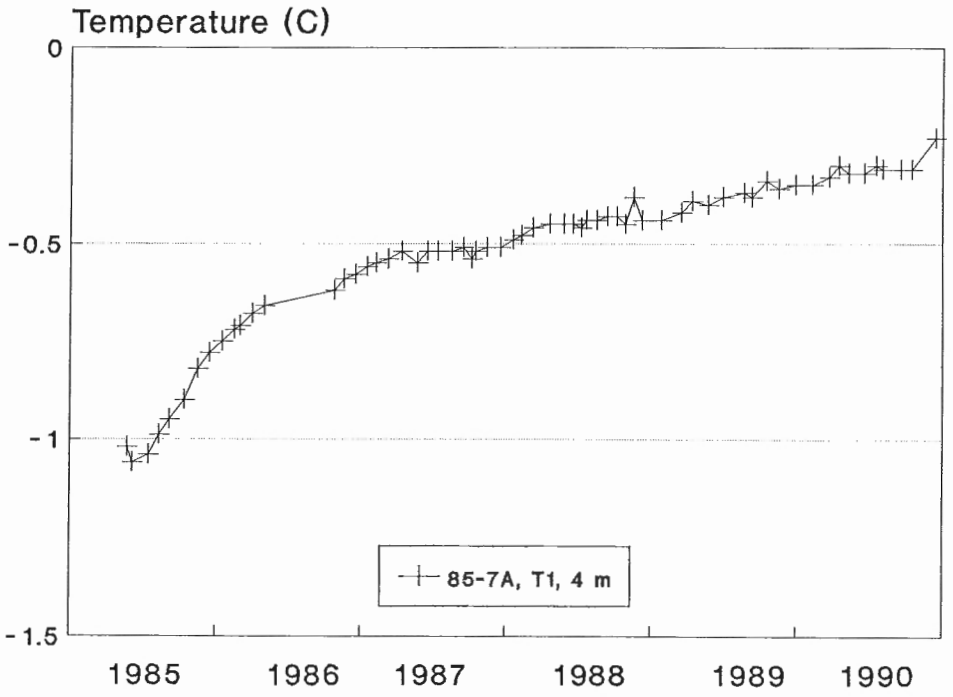

Figure 5. Temperature-time plot for the 4 m sensor on cable T1, site 85-7A, km 271.2.

Table 3. Seadata logger performance and data recovery - Norman Wells Pipeline

```
SITE  LOCATION  | CABLE | 1985 |     1986 |     1987 |     1988 |     1989 |     1990
                        MJJASONDJFMAMJJASONDJFMAMJJASONDJFMAMJJASONDJFMAMJJASONDJFMAMJJASOND

84-2A, km  19.0 ...T1      AAAAAAAAAAAAAAAAAAAAAAAAAAAAAAAAddbbbAAAAAAAAAAAAAAAAAAAAAAAA
                   T2      AAAAAAAAAAAAAAAAAAAAAAAAAAAAAAAAAAAAAAAAAAAAAAAAAAAAAAAAAAAAA
                   T3      AAAAAAAAAAAAAAAAAAAAAAAAAAAAeeeeeeeeeeAAAAAAAAeeeAAAAAAAAAAAAA
                   T4                                                AAAAAAAAAAAAAAAAAAAAAAA
                  2810                                                     AAAAAAAAbAAAAAA
                  2812                                                     AAAAAAAAAAAAAAA

84-3A, km  79.2 ...T1      AAAAAAAAggggggAAAAbbAAAeeeeeffffffeeeAAAAAAAAAAAAAAAAAAbbAAAAA
                   T2      AAAAAAAAggggggAAAAAAAAAAAAAAAffffffAAddAAAAAAAAAAAAAAAAAAAAAAA
                   T3      AAAAAAAAggggggAAAAAAAAddddAAAffffddddAAAAAAAAAAbbAAAAAddddddd
                   T4      dddddAAAggggggddddddAAAAAAAdddffffddddddAAAAAAAAddddddddddddc

85-7A, km 271.2 ...T1      AAAAAAAAeeeeeAAAAAAAAAAAAAAAAAAAAAAAAAAAAAAAAAAAAAAAAAAAAAAAA
                   T2      AAAAAAAAeeeeeAAAAAAAAAAAAAAAAAAAAAAAAAAAAAAAAAAAAAAAAAAAAAAAA
                   T3      AAAAAAAAeeeeeAAAAAAAddddddddddddddddAAAAAAAAAAAAAAAAAAAAAAAA
                   T4      AAAAAAAAeeeeeAAAAAAAAAAAAAAAAAAAAAAAAAAAAAAAAAAAAAAAAAAAAAAAA
                   T5                                                AAAAAAAAAAAAAAAAA

85-7B, km 272.0 ...T1      AAAAAAAAeeeeeAAAAAAAAAAAAAAAAAAAAAAAAAAAAAAAAAAAAAAAAAAAAAAAA
                   T2      AAAAAAAAeeeeeAAAAAAAAAAAAAAAAAAAAAAAAAAAAAAAAAAAAAAAAAAAAAAAA
                   T3      AAAAAAAAeeeeeAAAAAAAAAAAAAAAAAAAAAAAAAAAAAAAAAAAAAAAAAAAAAAAA
                   T4      AAAAAAAAeeeeeAAAAAAAAAAAAAAAAAAAAAAAAAAAAAAAAAAAAAAAAAAAAAAAA
                   PT                                                AAAAAAAAAAAAAAAAA

85-7C, km 272.3 ...T1                                  AAAAfffffffff------AAAAAAAAAffAAAAAAA
                   T2                                  AAAAfffffffff------AAAAAAAAAffAAAAAAA
                   T3                                  AAAAfffffffff------AAAAAAAAAffAAAAAAA
                   T4                                  AAAAfffffffff------AAAAAAAAAffAAAAAAA
                   T5                                                AAAAAAAAAffAAAAAAA
                   2813                                                 AAAAAAffAAAAAAA

85-12B, km 608.7 ..T1                                                AAAAAAcAAAAAAAAAAAAAAAA
                   T2                                                AAAAAAcAAAAAAAAAAAAbbbbb
                   T3                                                AAAAAAAAAAAAAAAAAAAAAAA
                   T4                                                AAAAAAAAAAAAAAAAAAAAAAA
                   2811                                                   AAAAAAAAAAAAAAA
                   PT                                                AAAAAAAAAAAAAAAAA

84-5B, km 783.3 ...T1                                  AAAAAAAAAAAAAAAAAAAAAgggggggggAAAAAAA
                   T2                                  AAAAAAAAAAAAAAAAAAAAAgggggggggAAAAAAA
                   T3                                  AAAAAAAAAAAAAAAAAAAAAgggggggggAAAAAAA
                   T4                                  AAAAAAAAAAAAAAAAAAAAAgggggggggAAAAAAA

KEE SCARP          139                                       AAAAAAAAddAAAAAAAAAA

AG-CAN soil probes

84-3A              T5                  AAAAAAAAAAAAAAAfffffAAAA........disconnected....
                   T6                  AAAAAAAAAAAAAAAfffffAAAA........disconnected....
85-7A              T5                  AAAAAAAAAAAAAAAAAAAAAAAA........disconnected....
                   T6                  AAAAAAAAAAAAAAAAAAAAAAAAAAAA...disconnected....
85-7B              T5                  AAAAAAAAAAAAAAAAAAAA............disconnected....
                   T6                  AAAAAAAAAAAAAAAAAAAA............disconnected....

CODES:  A: good data recovery                      e: field error/extension cable problem
        b: minor noise                             f: power supply problem/ malfunction
        c: bad data/no data                        g:  glitch in tape/error in processing
        d: lots of noise (moisture problems)     - : logger removed for servicing
        months not in bold:  represent actual gap in data
```

SUMMARY AND RECOMMENDATIONS

Thermistors and temperature cables

The performance of the temperature cables and sensors has been excellent. Only 3.1% of thermistors have failed over 1984 to 1990. To ensure high data quality, constant comparison with adjacent sensors and examination of the temperature-time series and temperature-depth profiles is necessary. In future programs, we would recommend 1) the method of cable fabrication used here and cable installation in silicone filled PVC tubes, 2) standardizing the type of sensor (YSI44033), and 3) the use environmental connectors. To provide greater flexibility, if data loggers are to be possibly later installed, common wiring of thermistors could be used rather than paired.

SEADATA loggers

The SEADATA logger use is continuing and has proven to be successful with 82% data recovery. Quality control is an important and integral component of the logger measurement program.

The logger program has evolved over several years. Each alteration has added a level of complexity and thus the possibility for additional things to go wrong. Software changes were usually needed as a result of a modification. Perhaps the best rule of thumb for field data loggers in cold environments, particularly where there are many different data collectors, is to keep things simple. Or conversely, it is better to deal with the loggers as they were designed, that is, to not expect what they cannot produce. Minimize the number of extensions, connections and modifications, and recognize, as is the case of for the SEADATA loggers, that they may not be designed for real time data gathering.

Moisture in connectors may offset the logger temperature readings. This offset, particularly if all channels in a connector are affected, may not be evident when examining logger data in isolation. If only a few channels are affected then a comparison of the logger data from these sensors relative to the others on the cable may indicate there is a problem. To ensure that there is no potential moisture problem, manual readings should be taken periodically (at least twice a year, at the time of logger servicing), checked for stability, and compared to logger readings. In the worst case illustrated in this report, reliance on logger data would have indicated temperatures 1K warmer than they actually were (which would have meant unfrozen conditions rather than frozen).

Some of the logger problems outlined above are not inherent to the SEADATA logger and could occur no matter what kind of automatic data acquisition system was used. For future multi-site and multi-cable measurement programs, newer solid state loggers would be recommended rather than cassette tape loggers. The solid state loggers are microprocessor based, can thus be monitored in the field, and have lower power requirements. One logger recently used elsewhere is the 64 channel solid state unit from RBR (model RDL-100). This logger uses solar battery charging and can be equipped with a modem for remote data acquisition and control.

ACKNOWLEDGMENTS

The Permafrost and Terrain Research and Monitoring Program is coordinated by Kaye MacInnes, Indian and Northern Affairs (INAC), Yellowknife. The monitoring has been primarily funded by INAC's Northern Affairs Program, with contributions from the Northern Oil and Gas Action Program (NOGAP). Additional funding and other assistance has been provided by the former Earth Physics Branch of EMR, the Geological Survey of Canada, the Federal Panel on Energy Research and Development, and IPL.

Many individuals within INAC, EMR, IPL, Agriculture Canada and the National Research Council have provided cooperation and support. We thank all those who helped, and continue to help, with aspects of the program, in particular the field data collection. Janice Naufal has provided an invaluable service with the data management and quality control. We also thank Murray Mitchell, formerly of Hardy BBT and currently with M Squared Ltd., for his refinements to the temperature cable fabrication technique.

REFERENCES

Burgess, M.M. and Naufal, J.A.
1990: Norman Wells Pipeline monitoring sites ground temperature data file: 1988; Geological Survey of Canada, Open File 2155, 203 p.

Burgess, M.M. and Riseborough, D.W.
1989: Measurement frequency requirements for permafrost ground temperature monitoring: analysis of Norman Wells pipeline data, Northwest Territories and Alberta; in Current Research, Part D, Geological Survey of Canada, Paper 89-1D, p. 69-75.

DiBiagio, E.
1990: The performance of instruments and the success of monitoring programs in the offshore environment; in Proceedings Workshop Ice Scouring and the Design of Offshore Pipelines, Calgary, April 1990.

MacInnes, K.L., Burgess, M.M., Harry, D.G., and Baker, T.W.H.
1989: Permafrost and Terrain Research and Monitoring: Norman Wells Pipeline, Volume I Environmental and Engineering Considerations; Department of Indian and Northern Affairs Canada, Northern Affairs Program, Environmental Studies Report No. 64, 132 p.

1990:
Permafrost and Terrain Research and Monitoring: Norman Wells Pipeline, Volume II Research and Monitoring Results: 1983-1988; Department of Indian and Northern Affairs Canada, Northern Affairs Program, Environmental Studies Report No. 64, 204 p.

McRoberts, E.C., Hanna, A.J., and Smith, J.
1985: Monitoring of thawing permafrost slopes: Interprovincial Pipe Line; National Research Council Canada, Proceedings of Workshops on Subsea Permafrost and pipelines in Permafrost, Nov. 1985, NRCC Technical Memorandum 139, p. 133-151.

Nixon, J.F., Stuchly, J., and A.R. Pick.
1984: Design of Norman Wells pipeline for frost heave and thaw settlement; Third International Symposium on Offshore Mechanics and Arctic Engineering, New Orleans, Feb. 12-16, 1984, Paper No. 83-OMA-303.

Pilon, J.A., Burgess, M.M., Judge, A.S., Allen, V.S., MacInnes, K.L., Harry, D.G., Tarnocai, C., and Baker, H.
1989: Norman Wells to Zama pipeline permafrost and terrain research and monitoring program: site establishment report; Geological Survey of Canada, Open File 2044, 332 p.

Tarnocai, C. and Kroetsch, D.J.
1990: Site and soil descriptions for the Norman Wells Pipeline soil temperature study; Land Resources Research Centre, Agriculture Canada, Contribution Number 89-56, 46 p.

Baseline marine geological studies off Grande Rivière de la Baleine and Petite Rivière de la Baleine, southeastern Hudson Bay

H. Josenhans[1], J. Zevenhuizen[2], and J. Veillette[3]

Josenhans, H., Zevenhuizen, J., and Veillette, J., 1991: Baseline marine geological studies off Grande Rivière de la Baleine and Petite Rivière de la Baleine, southeastern Hudson Bay; in Current Research, Part E; Geological Survey of Canada, Paper 91-1E, p. 347-354.

Abstract

A dense seismic coverage seaward of Grande Riviere de la Baleine and Petite Riviere de la Baleine is being compiled to map the thickness, lateral distribution, and mode of deposition of the Quaternary sediments. The seismic data indicate that not all sediments transported to the deltas by these rivers settle out proximally. Slumping at the delta front off Petite Riviere de la Baleine has produced sediment flows that extend up to 7.5 km seaward of the delta. The modern marine/estuarine sediment fractions found in the offshore basins appear to be heavily influenced by bottom currents. These bottom currents form sedimentary furrows, and erode and transport sediments from the basins in a southwesterly direction.

Résumé

Une couverture sismique dense de la région au large de l'embouchure de la Grande rivière de la Baleine et de la Petite rivière de la Baleine a été entreprise dans le but de porter sur carte l'épaiseur, la répartition latérale et le mode de sédimentation des sédiments du Quaternaire. Les données sismiques révèlent que les sédiments transportés jusque dans les deltas par ces rivières ne se déposent pas tous à proximité. L'affaissement du front du delta au large de la Petite rivière de la Baleine a produit des écoulements de sédiments qui s'étendent sur des distances atteignant 7,5 km vers le large du delta. Les fractions modernes de sédiments marins et estuariens observées dans les bassins extracôtiers semblent fortement liées aux courants de fond. Ces derniers forment des sillons sédimentaires, et érodent et transportent les sédiments des bassins vers le sud-ouest.

[1] Atlantic Geoscience Centre, Dartmouth, Nova Scotia
[2] Orca Marine Geological Consultants, 3609 Rosemeade Avenue Halifax, Nova Scotia B3K 4L8
[3] Terrain Sciences Division, Ottawa

INTRODUCTION

We illustrate and briefly describe the highlights of the CSS Baffin marine survey 90-024, designed to collect base line surficial geological environmental data near the Grande Riviere de la Baleine (Great Whale River) and Petite Riviere de la Baleine (Little Whale River) estuaries (Fig. 1) in anticipation of the proposed diversion of these rivers for hydroelectric development. The seismic and sample data will be interpreted and analyzed in order to prepare a series of 1:50,000 maps illustrating the geological conditions and seafloor processes in the vicinity of the river mouths. This preliminary report illustrates the marine geology and active sediment transport observed in the region.

METHODS

More than 856 line kilometres of seismic and sidescan sonar data were collected in 1990 (Fig. 2, 3) as well as 8 Leheigh cores, 11 benthos gravity cores and 8 Van Veen grab samples (Josenhans and Johnston, 1991). Surface towed Huntec Sea Otter boomer data and Ratheon 3.5 kHz subbottom profiler data were collected to provide seismostratigraphic information and sediment thickness data. A Klein 100 kHz sidescan sonar was used for surficial feature identification and determination of seabed processes. GPS navigation with on board recording facilities provided accuracies of ±50 m.

REGIONAL BEDROCK GEOLOGY

The bedrock of the onshore areas bordering Manitounuk Sound (Fig.1) is composed of Proterozoic interbedded volcanics and carbonates, forming a series of cuesta ridges. These have low relief on the western side with steep slopes on the eastern side. Geophysical data indicate that submerged cuesta ridges, with a similar orientation, extend offshore for at least 20 km.

REGIONAL SURFICIAL GEOLOGY: NEARSHORE AND OFFSHORE

Unconsolidated sediments in the Grande Riviere de la Baleine and Petite Riviere de la Baleine basins, and Manitounuk Sound region (Fig. 1) are interpreted to represent, from base to top: till, glaciolacustrine sediments associated with the glacial Lake Ojibway, ice proximal glaciomarine sediments associated with the invasion of the Tyrrell Sea, ice distal glaciomarine/Tyrrell Sea sediments, postglacial marine sediments, and in the nearshore, deltaic-estuarine sediments. The onshore stratigraphic succession is well preserved in outcrop in both the Grande Riviere de la Baleine and Petite Riviere de la Baleine valleys (Bilodeau et al., in press) with equivalent offshore sections displayed by the seismic/core data (Bilodeau et al., 1990). The eastern limit of Lake Ojibway sediments is marked by the Sakami Moraine, which terminates just southeast of Grande Riviere de la Baleine estuary (Vincent, 1989). The Sakami Moraine was formed when the Labradorean Ice Sheet retreated eastward to this position. Subsequent incursion of marine waters from Hudson Strait penetrated Hudson and James bays draining glacial Lake Ojibway (Hardy, 1976). At the time of the Tyrrell Sea invasion, sea levels were substantially higher than present. Maximum recorded marine limit in the area is 315 m above present-day sea level (Vincent, 1989). The area is rapidly emerging. A minimum emergence curve for Richmond Gulf (Hilliare-Marcel, 1976, 1979) indicates that at the time of deglaciation uplift was 10.0-6.5 m/century decreasing linearly to 1.1 m/century for the present. Deglaciation for the area west of the Sakami Moraine (Vincent, 1989) is estimated at 8100 YBP (Hilliare-Marcel, 1976).

SURFICIAL MARINE GEOLOGY: SEAWARD OF GRANDE RIVIERE DE LA BALEINE AND PETITE RIVIERE DE LA BALEINE

The surficial marine geology east of the Belcher Islands is locally complex and only surveyed in detail off Grande Riviere de la Baleine, Petite Riviere de la Baleine, and Manitounuk Sound. Offshore geophysical and bottom sample data (Fig. 2, 3) have recently been collected in this area (Henderson, 1989; Grant and Sanford, 1989; Zevenhuizen and Josenhans, 1989; Josenhans and Johnston, unpublished report, 1991; Josenhans and Moir, 1991) but has not been interpreted and mapped in detail.

Seismostratigraphic interpretations seaward of the Grande Riviere de la Baleine mouth indicate three seismically defined units overlying bedrock (see Fig. 4, sections 4, 7, and 9, and Fig. 3 for core 69 location). The basal seismic unit (1) immediately overlying bedrock is homogenoeus and generally unstratified, the overlying seismic unit 2 appears as a series of conformably draped, evenly spaced, fairly high amplitude reflectors, and unit 3 consists of weakly stratified, low amplitude, and nearly transparent reflectors. Piston core 69 (Fig. 3) reveals that sediments representative of seismic unit 1 consists of poorly sorted gravelly muds interpreted to represent glacial till/ice contact deposits. Sediments of seismic unit 2 consists of laminated clays, at times faulted and very disaggregated. The disaggregated material resembles previously ice bonded sediments (Chamberlain and Gow, 1979), suggesting that pore waters of low salinity, associated with glaciolacustrine conditions, were previously frozen. Sediments representative of seismic unit 3 grade from sandy

silty sediments at the base to bioturbated mud. Detailed analysis of the lithological, micropaleoentological, and palynological properties of the piston core 69 are presented by Marsters (1988), Henderson (1989), and Bilodeau et al. (1990).

The offshore Grande Riviere de La Baleine section can be readily correlated on the basis of sedimentological character with the sections exposed along the river banks near the estuaries. The seismic coverage offshore allows us to define the broader regional extent of these units.

SCIENTIFIC HIGHLGHTS

The seismic coverage seaward of the deltas (Fig. 2) allows us to determine the thickness and lateral distribution of the Quaternary sediments. At some locations where the basal unit (till/ice contact) outcrops, elongated ridges trending west/southwest are observed. The ridges are similar in scale to fluted tills (section 6) and essentially trend parallel to the regional glacial striae. We tentatively interpret these ridges to represent fluted till deposits formed by a late glacial flow trending in a west-southwesterly direction.

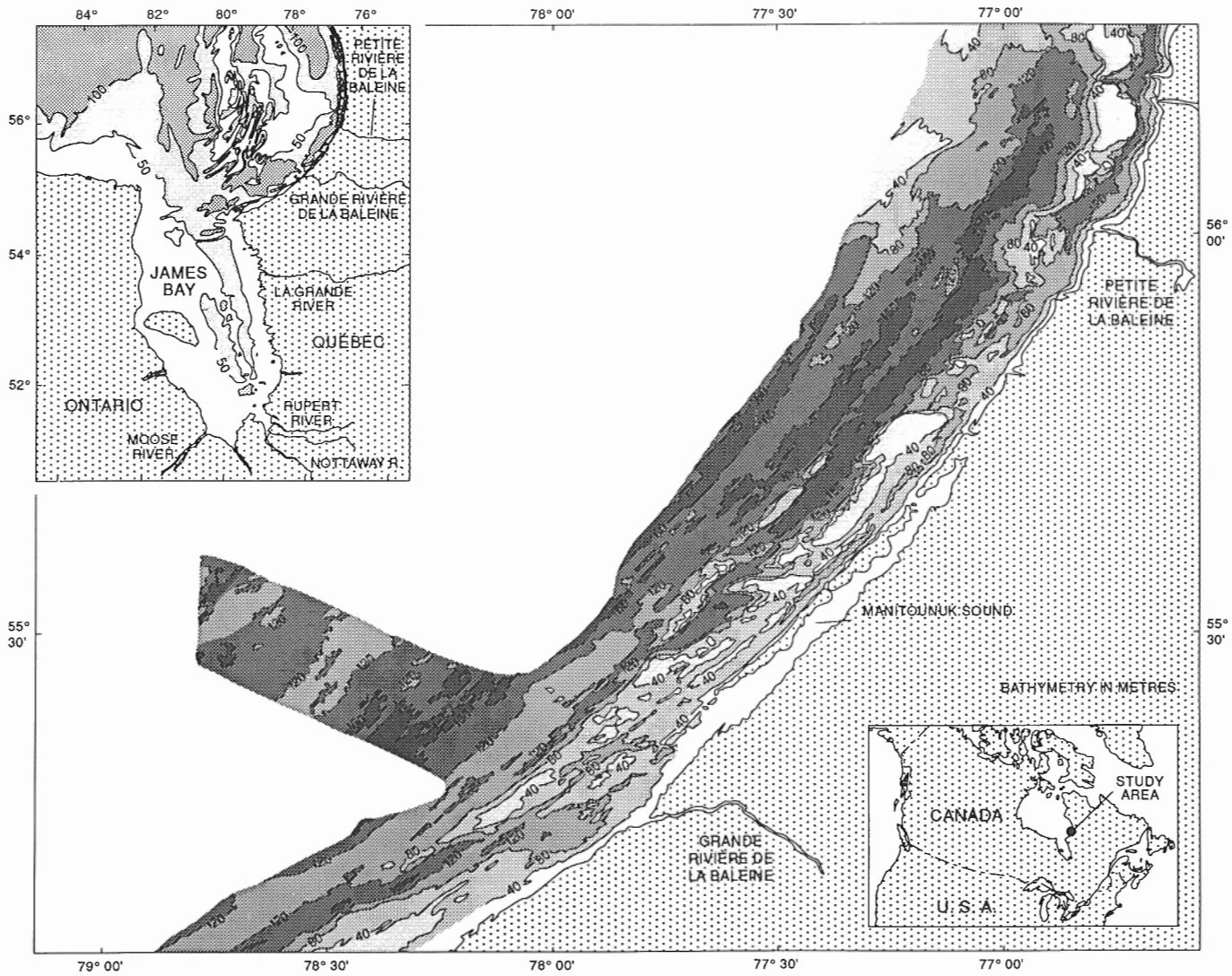

Figure 1. Index map and bathymetry of study area showing the location of major rivers that may be affected by hydroelectric development.

Acoustically well stratified sediments (sections 4, 7) are observed below the modern sediments and immediately overlying the till/ice contact deposits. They are generally less than 4 m thick and are thought to have been deposited in an ice proximal setting in deeper water before onset of isostatic rebound. These acoustically well stratified sediments correlate with the possible frozen sediments observed in piston core 69 and may represent the former glaciolacustrine Lake Ojibway sediments.

Seaward of Petite Riviere de la Baleine delta front, we observe sediment failure (section 8) and westward (seaward) thinning density flow deposits that may be attributed to sediment loading by river output. These density flows extend and wedge out over a very gently sloping seafloor approximately 7.5 km seaward of the delta front.

The uppermost stratigraphic unit is acoustically weakly stratified. The unit is characterized by an asymmetric depositional style (section 7) indicative of current influence on deposition.

Within the deep (bedrock controlled) basins, the modern muddy sediment surface is scoured by erosional channels up to 1.5 m in depth. These features, named sedimentary furrows by Flood (1983), have been observed within muddy sediments throughout the world's oceans. They are interpreted as being formed by recurring, directionally stable and episodically strong currents (±50 cm/sec) that erode the fine grained cohesive sediments. These sedimentary furrows (sections 2, 4) are aligned parallel to the dominant (bedrock controlled) physiographic features. In some instances (section 4, 0.5 km along sidescan profile) the furrows are seen to coalesce or

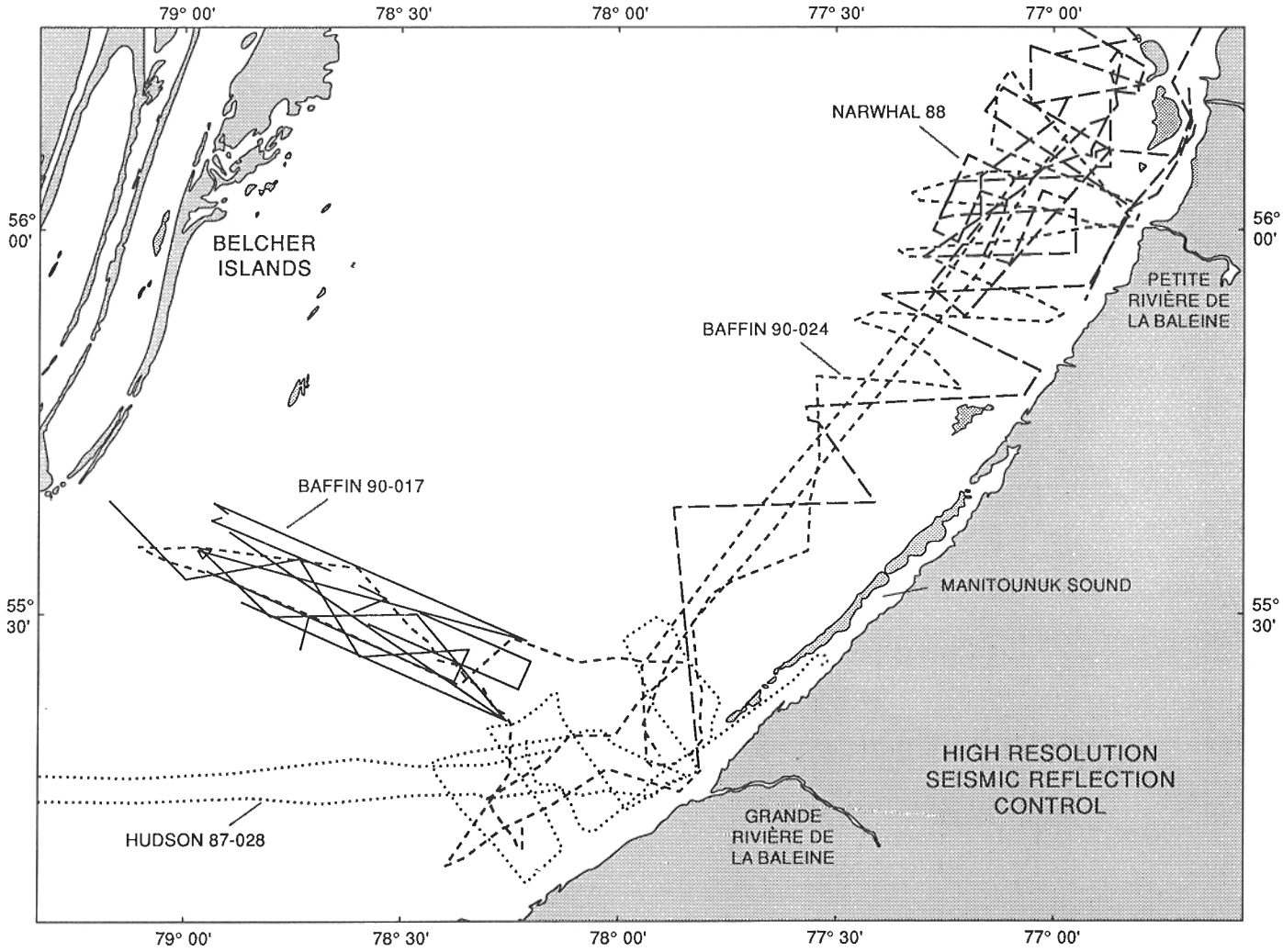

Figure 2. Seismic track map.

bifurcate. According to Flood (1983) "sedimentary furrows come together in the direction of the measured near-bottom currents". The direction of bifurcation can be used in this instance to infer current transport of seafloor sediments toward the southwest.

SUMMARY

Preliminary review of the seismic data indicates that not all sediments transported to the deltas by the Grande Riviere de la Baleine and Petite Riviere de La Baleine settle out proximally. Slumping at the delta front off Petite Riviere de la Baleine has produced sediment flows that extend up to 7.5 km seaward of the delta. The modern marine/estuarine sediment fractions found in the offshore basins appear to be heavily influenced by bottom currents and in some instances by sedimentary furrows that erode and transport these sediments in a southwesterly direction.

ACKNOWLEDGMENTS

We thank the officers and crew of the C.S.S. Baffin for their willing and able support at sea and Don Locke and Larry Johnston for their dedicated technical support in the acquisition of this excellent data set. We also thank Debbie Smith, Valerie Sloan, Bill Leblanc, and the Canadian Hydrographic Service staff for collection of the 3.5 kHz profiles and bottom samples on Baffin 90-017.

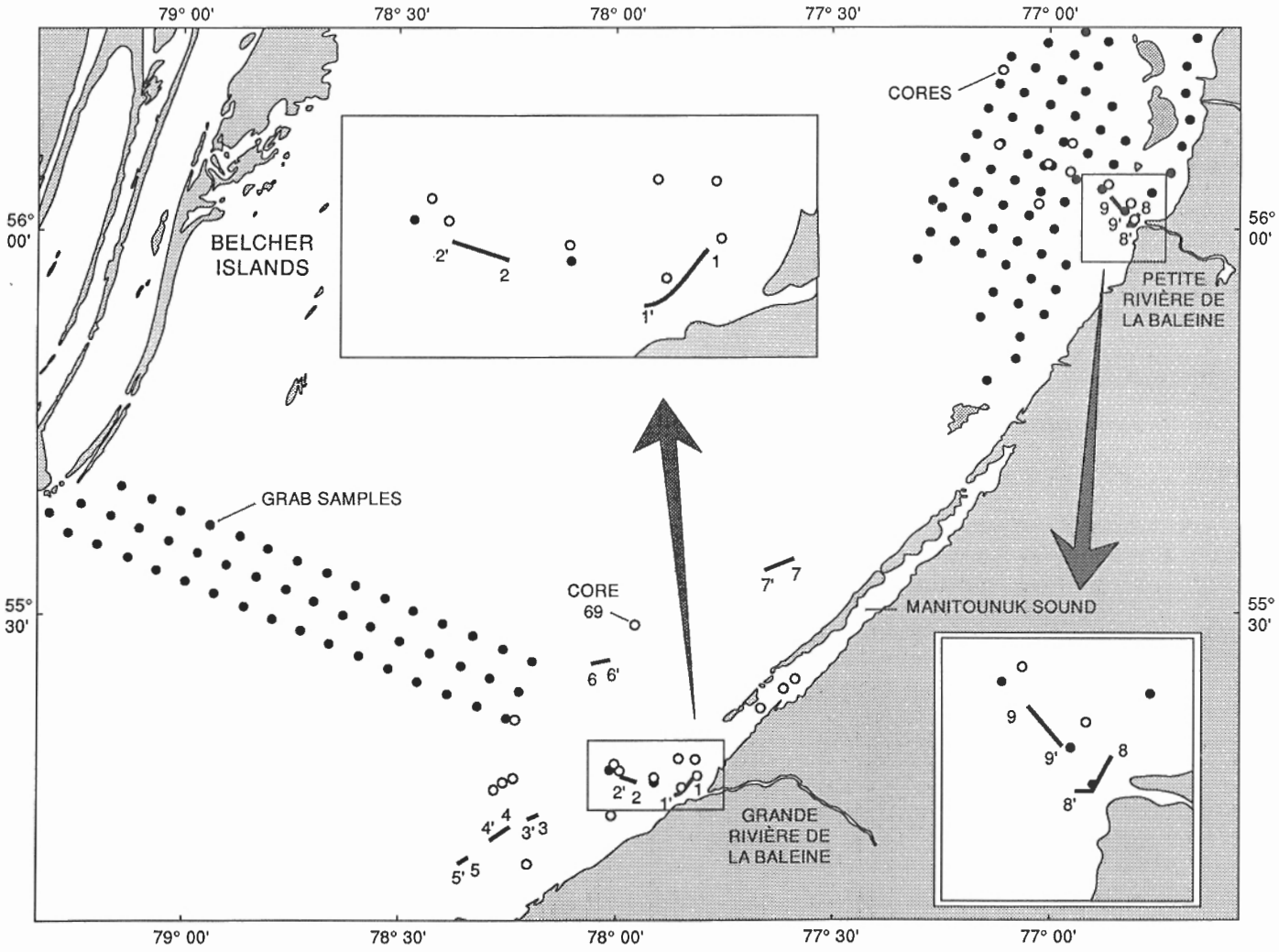

Figure 3. Location map of bottom samples and seismic sections: 1-1' to 9-9'. Core 69 is representative of the seismic type section and is described in the text.

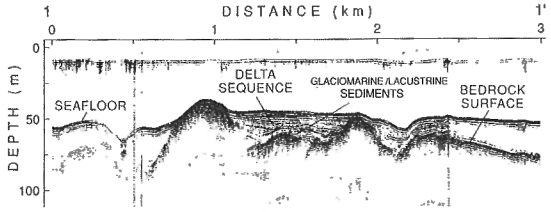

Huntec boomer subbottom profile of undisturbed deltaic sediments seaward of Great Whale River estuary. The relatively thin deltaic sequence is deposited on top of conformably draped glaciomarine sediments.

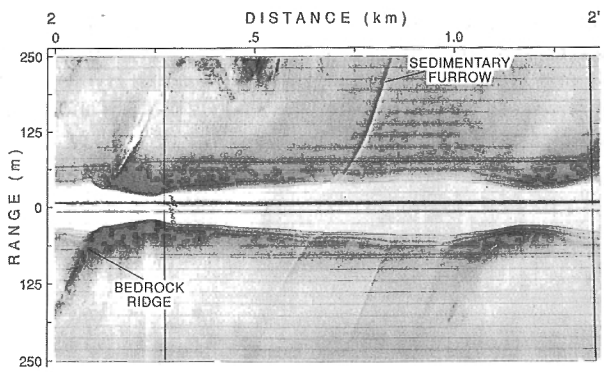

Sidescan sonogram (100 kHz) taken seaward of the Great Whale River delta. Note the outcropping bedrock ridge and current formed sedimentary furrows in the trough which are oriented parallel to the ridge.

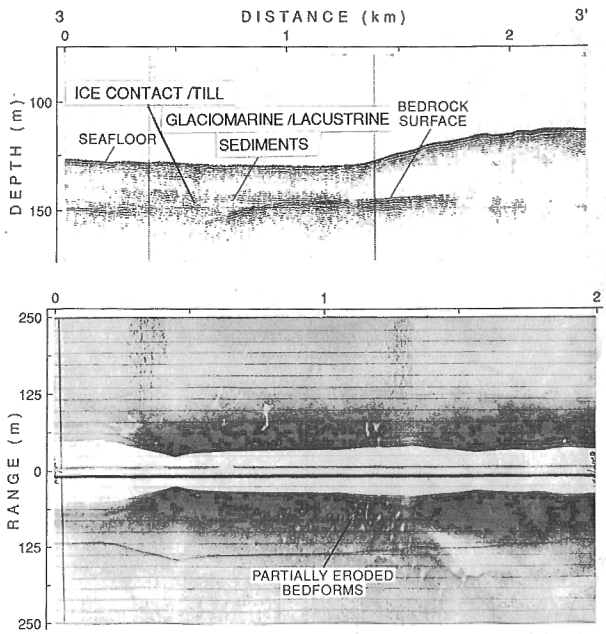

Sidescan sonogram and Huntec boomer profile of partially eroded bedforms. These features indicate a non-depositional to partly erosional setting in the proximity of the Great Whale River delta.

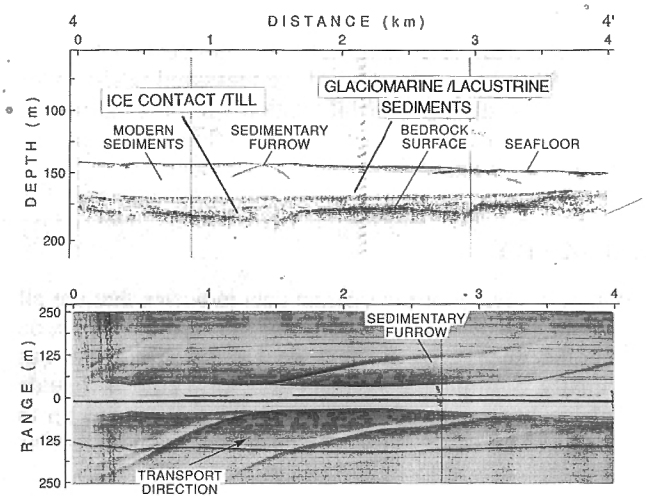

Sidescan sonogram and Huntec boomer profile of sedimentary furrows. These erosional furrows are formed in the modern muddy sediments by localized currents. The arrow indicates the direction of current flow and resultant sediment transport in a southwesterly direction.

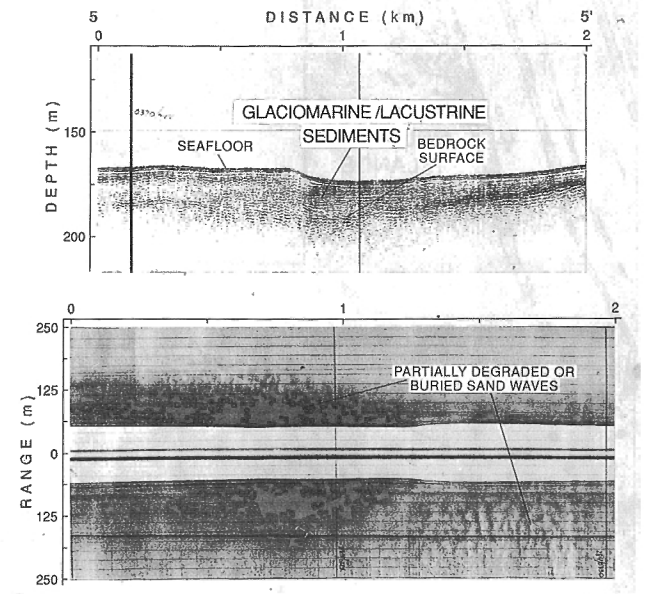

Sidescan sonogram and Huntec boomer profile of degraded sandwave field partially buried by modern muds. Presence of the mud veneer may indicate episodic stronger current flows or a recent reduction in current strength.

Figure 4. Seismic and sidescan sonar sections 1 to 9 with explanatory text and labels. Location of sections is shown on Figure 3).

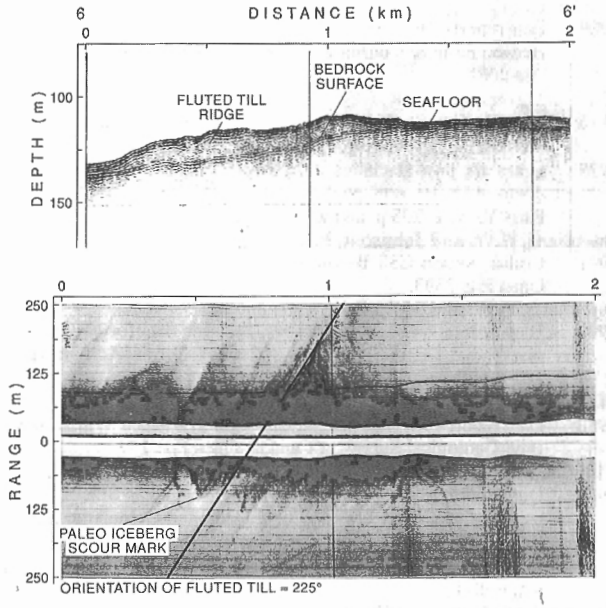

Sidescan sonogram and Huntec boomer profile of 10 m thick till ridge with fluted and iceberg scoured surface. Flute orientation is approximately 225°. Similar fluted till outcrops occur throughout the study area and indicate a regional southwesterly ice flow which deposited flow parallel till ridges up to 70 m in thickness.

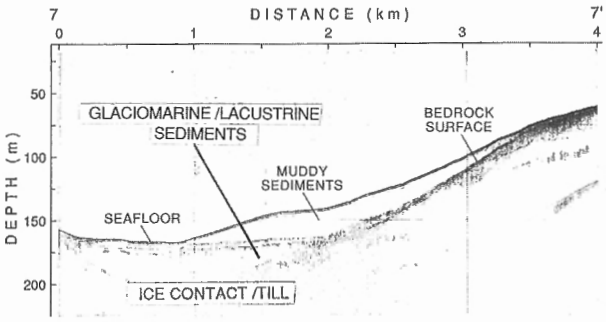

Huntec boomer profile of asymmetric wedge of modern muddy sediment deposited against bedrock ridge. The profile illustrates the irregular depositional pattern of modern sediments within the study area. Note the absence of modern sediments in the deepest area.

Figure 4 (cont'd.)

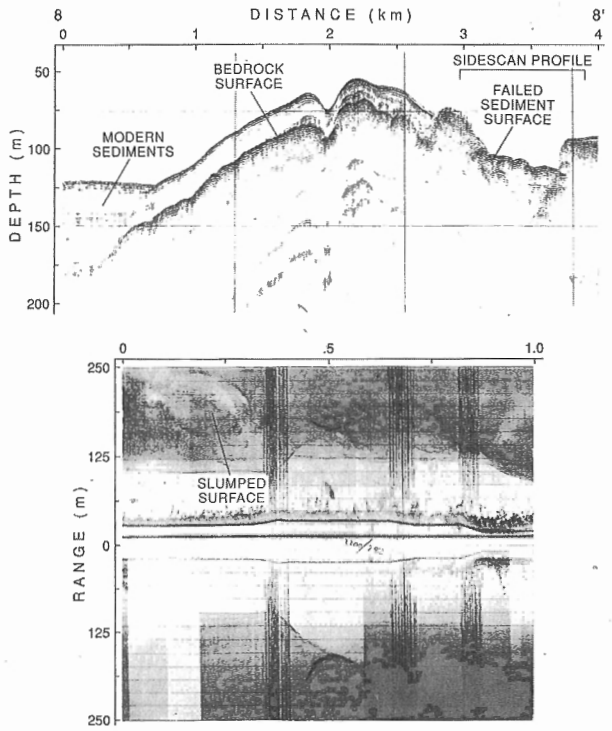

Sidecan sonogram and Huntec boomer profile parallel to delta front off Little Whale River. The sidescan profile illustrates an area of sediment failure near the delta front.

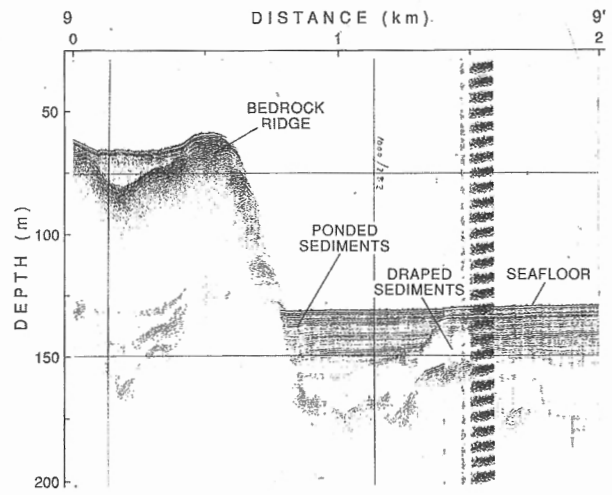

Huntec boomer profile of thick sediment sequence deposited in a bedrock low just seaward of Little Whale River. Note the conformable sequence above bedrock which is thought to have been deposited in deeper water (>400 m) during late glacial times (8000 ybp). The thick ponded sequences are restricted to the Manitounuk and Nastapoka Sounds.

REFERENCES

Bilodeau, G., de Vernal, A., Hilliare-Marcei, C., and Josenhans, H.W.
1990: Postglacial paleoceanography of Hudson Bay: stratigraphy, microfaunal and palynological evidence; Canadian Journal of Earth Sciences, v. 27, p. 946-963.

Bilodeau, G., de Vernal, A., Hilliare-Marcel, C., et Vincent, J-S.
in press: Stratigraphie holocène du sud-est de la baie d'Hudson: correlations micropaléontologiques entre une coupe des terrasses de la Grande Rivière de la Baleine et une carotte marine (87-028-069); Géographie physique et Quaternaire.

Chamberlain, E.J. and Gow, A.J.
1979: Effects of freezing and thawing on the permeability and structure of soils; Engineering Geology, v. 13, p. 73-92.

Flood, R.F.
1983: Classification of sedimentary furrows and a model for furrow initiation and evolution; Geological Society of America Bulletin, v. 94, p. 630-639.

Grant, A.C. and Sanford, B.V.
1989: Bedrock geological mapping and basin studies in the Hudson Bay region; in Current Research, Part B, Geological Survey of Canada, Paper 88-1B, p. 287-296.

Hardy, L.
1976: Contribution à l'étude géomorphologique de la portion quebecoise des basses terres de la baie James; thèse de doctorat non publiée Université McGill, Montréal, 264 pages.

Henderson , P.J.
1989: Data report - description and composition of cores and grab samples, Hudson 87-028, Hudson Bay; Geological Survey of Canada, Open File 2081.

Hilliare-Marcel, C.
1976: La déglaciation et le relèvement isostatique sur la côte est de la baie d'Hudson; Cahiers de géographie de Québec, v. 20, p. 185-20.
1979: Les mers post-glaciaires du Québec: quelques aspects; thèse de doctorat d'état non publiée, Université Pierre et Marie Curie, Paris VI, v. 1, 293 p. and v. 2, 249 p.

Josenhans, H.W. and Johnston, B.L.
1991: Cruise Report CSS Baffin 90-024; Geological Survey of Canada, Open File 2393.

Josenhans, H.W. and Moir, P.
1991: High resolution seafloor surveys; baseline data for environmental assessment; Geological Survey of Canada, Current Activities Forum - 01991, Program with Abstracts, p. 11.

Marsters, J.C.
1988: Data report - physical properties program, Hudson 87-028, Hudson Bay; Geological Survey of Canada, Open File 1593.

Vincent, J-S.
1989: Quaternary geology of the southeastern Canadian Shield; in Chapter 3 in Quaternary Geology of Canada and Greenland; (ed.) R.J. Fulton; Geological Survey of Canada, Geology of Canada, no. 1 (also Geological Society of America, the Geology of North America, v. K-1).

Zevenhuizen, J. and Josenhans, H.W.
1989: Surficial Geology of Hudson Bay; Geological Survey of Canada, Open File Report 2215, 5 maps, scale 1:2 000 000.

A bibliography and inventory of tree-ring studies in Canada

B.H. Luckman[1] and T.A. Innes[2]
Terrain Sciences Division

Luckman, B.H. and Innes, T.A., 1991: A bibliography and inventory of tree-ring studies in Canada; in Current Research, Part E; Geological Survey of Canada, Paper 91-1E, p. 355-361.

Abstract

This paper briefly describes a bibliography and data base for tree-ring studies in Canada that has recently been completed and integrated into the Geological Survey's National Paleoecological Data Base. The bibliographic data base includes 561 titles of papers, reports and abstracts that refer to tree-ring studies in Canada. Each entry consists of full reference information and (where appropriate) details on geographic location, species, techniques used, area of application and summary comments. The chronology data base lists 396 tree-ring chronologies (over 350 in Canada and a further 93 under development) with information on site, species used, collector, geographic location, parameters measured and length of chronology. A selective overview of the data is presented including a listing of the 71 Canadian ring-width chronologies that extend back prior to 1652.

Résumé

Le présent rapport fait état de manière concise d'une bibliographie et d'une base de données colligées à partir des études des anneaux de croissance des arbres au Canada qui ont été récemment effectuées et intégrées à la Base nationale de données paléoécologiques de la Commission géologique. La base de donnéees bibliographiques comprend 561 titres d'études, de rapports et de résumés se rapportant à des études d'anneaux de croissance au Canada. Chaque entrée comprend une information bibliographique complète et (le cas échéant) des détails sur le lieu géographique, l'espèce, les techniques utilisées, le domaine d'application et de brefs commentaires. La base de données chronologiques répertorie 396 chronologies d'anneaux de croissance (plus de 350 au Canada et 93 autres à l'étude) et renferme de l'information sur l'endroit, l'espèce utilisée, le collectionneur, le lieu géographique, les paramètres mesurés et la longueur de la chronologie. Un choix de données est présenté, dont une liste des 71 chronologies canadiennes de largeurs d'anneaux de croissance antérieures à 1652.

[1] Department of Geography, University of Western Ontario, London N6A 5C3
[2] Faculty of Forestry, University of New Brunswick, Fredericton E3B 5A3

INTRODUCTION

The core International Geosphere-Biosphere Progamme (IGBP) project on Past Global Changes (PAGES) has identified the development of a global data set of proxy data with annual resolution for the last 2000 years as one of two priority areas for proxy data studies within IGBP (ICSU 1990). Such data sets are necessary to understand and model the natural decennial to centennial variations in climate on which recent and predicted anthropogenic impacts are superimposed. In Canada the instrumental record of climate is short (Toronto, the oldest record, dates back to 1840), geographically biassed (few northern stations have records of more than 40 years), and few documentary sources are available to extend these records prior to 1800. The obvious natural archives for high resolution proxy climate data in Canada are ice cores, lacustrine and nearshore marine sediments, and tree rings. Tree rings are the most widely distributed and accessible of these sources and therefore have the greatest potential for development as proxy climate records with annual resolution over most of Canada.

Until very recently, dendrochronological studies received little attention in Canada. The literature is scattered, mainly originating from the United States, and few major facilities and scientists were domiciled in Canada. Although tree-ring studies have been carried out in Canada for over 60 years, there has been no comprehensive attempt to pull this material together on a national basis to examine the available data. One of the projects initiated under the Global Change program in Terrain Sciences Division was to compile a data base of available literature and chronology holdings for dendrochronological work in Canada.

This is an important preliminary step in the evaluation of the potential role of tree-ring studies in the Canadian IGBP and provides an inventory of available materials on which future studies can build. The project was initiated in February 1989 and the initial phase completed in October 1990 (Luckman and Innes,1991a). The bibliography and chronology data bases, plus supporting documentation, have subsequently been integrated into the Geological Survey's National Paleoecological data base (see Jetté,1990) and will shortly be available to potential users upon request.

THE BIBLIOGRAPHY DATA BASE

The bibliography provides a semi-annotated data base and is a first step towards a national compendium of tree-ring research pertinent to Canada. It is unique in attempting to cover all Canadian environments and all holdings of Canadian data although some earlier regional reviews have been published(e.g.,Cropper and Fritts,1981; Jacoby,1982). In selecting entries, primary emphasis was placed upon tree-ring studies carried out within Canada or by researchers living in Canada with specific emphasis on dendrochronology, dendroclimatology,and dendrogeomorphology. The ecological and physiological literature on tree rings may therefore be incompletely captured because of this paleoenvironmental bias. Additional North American literature is also included if it contains material that deals with (i) tree-ring sites in immediately adjacent areas of the United States; (ii) large-scale (hemispheric or global) climatic analysis involving Canadian data or regions;and (iii) topics of direct interest to Canadian researchers (e.g. similar species or discussion of the development of appropriate techniques). The effective cut-off date for this literature review was material published prior to August, 1989 although some later material (up to March, 1990) is also included.

The bibliographic data base contains 561 titles with full reference, information on (where appropriate) geographic location, species, techniques used, applications,and a brief commentary in a data base (dBASE IV) format. The citations follow a standard pattern as illustrated in Table 1. Over 450 of these references are of Canadian origin or contain Canadian data. All items containing references to tree-rings studies in Canada were included and classified as to whether the tree-ring material is an incidental, significant (24% of entries),or central (63% of entries) component of the source document (see Scope, Table 1).

Table 1. Sample entry from the bibliographic data base

162. FILION, L., S. PAYETTE, L. GAUTHIER and Y. BOUTIN. 1986.
Light rings in subarctic conifers as a dendrochronological tool. Quaternary Research 26: 272-279.

Scope: **Focus**
Region: **Bush Lake, Québec**
Species: ***Picea mariana***
Application: **Dendrochronology, dendroclimatology, dendroecology.**
Techniques: **Crossdating, earlywood, latewood, light rings, ring width.**
Comments:
- Light rings in black spruce are evaluated as diagnostic tools for effective establishment of cross-dates in tree-ring studies.
- A master chronology of the years of light-ring formation was superimposed on the tree growth curve for Bush Lake presented in Payette et al. (1985) for the years 1398 to 1982.
- Causes of light-ring formation are discussed.

The literature search began with obvious sources such as Fritts (1976) and Hughes et al. (1982), Schweingruber (1987), and several journals (e.g. Tree-Ring Bulletin and Canadian Journal of Forest Research) were examined in their entirety. Coverage of unpublished theses, government and other institutional reports is more selective because of difficulties of access to materials. Figure 1 shows the date of publication of the Canadian sources listed in the data base and is an effective summary of the growth of the literature and interest in tree-rings in Canada. A more detailed discussion of this material is given in Luckman and Innes (1991b).

The major uses for tree-ring data in Canada to date have been for the interpretation of past climatic conditions, providing dating for geomorphic or hydrological events (e.g., moraines, landslides, ice-scars, floods, lake-level fluctuations,and snow avalanches) and for a variety of dendroecological studies (e.g., insect infestations, fires, population dynamics, tree growth and development).

CHRONOLOGY DATA BASE

A primary aim of this project was to assemble an initial listing of available tree-ring chronologies for Canada and present the sources for these data in a single document and standard format. This proved a difficult task and was only partially completed. The present chronology data base contains material from many sources and even simple standardized data, such as species, number of samples, dates of chronology, are not available for all entries. The major sources used were the literature in the bibliographic data base; the Tree-Ring Laboratory Collections (TRRL) of the University of Arizona at Tucson; the International Tree-Ring Data Bank at the University of Arizona; Lamont-Doherty Geological Observatory, Columbia University (Dr. G. Jacoby, personal communication); Forintek Canada Corporation, Vancouver (data file of 50 chronologies held at the National Archives, Ottawa); Dr. F.H. Schweingruber (Swiss Federal Forestry Institute, Birmensdorf, personal communication) plus personal research files and responses to a questionnaire survey circulated to Canadian scientists in 1989.

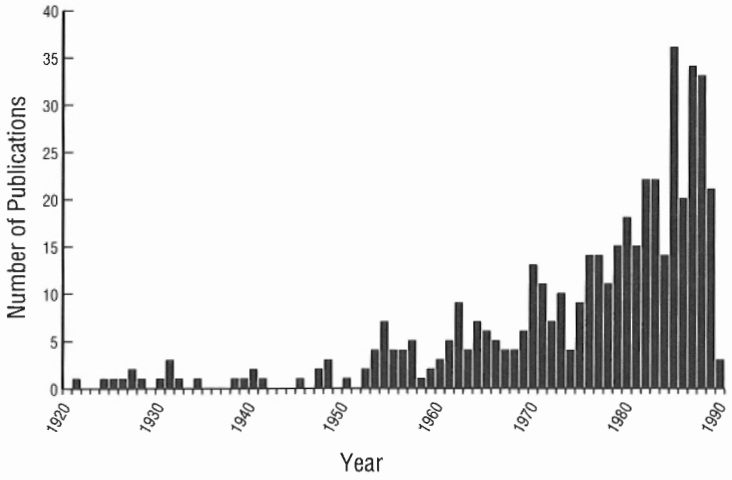

Figure 1. Date of publication for papers on tree rings in Canada.

The data base includes all publications, excluding abstracts (articles, reports, theses, etc.) referring to tree rings in Canada (453 entries) listed in Luckman and Innes (1991a). The criteria for inclusion are broad, including paleoclimate reviews, use of tree rings as dating techniques, methods of measurement, statistical techniques, stand dynamics studies, etc. As these data were complied in Fall 1989, the 1989 and 1990 data are incomplete.

Table 2. Sample entry from the chornology data base

Chronology Number:	15
Site name:	BANFF
Province:	Alberta
Latitude:	051011042N
Longitude:	115029032W
Elevation:	1430 m
Species:	*Pseudotsuga menziesii*
Collector:	L.A. Jozsa and N.B. Schultz
Date of sample collection:	September, 1979
Number of trees sampled:	10
Number of cores used:	20
Application:	Dendroclimatology
Techniques:	Ring width, density, volume; earlywood width, density and volume, latewood width, density and volume, maximum and minimum density.
Chronology coverage:	1550-1978.
Reference:	Jozsa and Oguss (1985), Robertson and Jozsa (1988)

Table 3. Canadian tree-ring chronologies that extend back prior to 1650

[1]No.	LOCALITY / NAME	COORDINATES		COLLECTOR	TAXA	YEARS
	Yukon Territory:					
	Cornwall River	66° 48'	136° 22'	LDGO	*Picea glauca*	1568-1987
	McMillan Pass	63° 11'	130° 12'	LDGO	*Picea glauca*	1494-1987
A1708	River Crag	65° 40'	138° 00'	LDGO	*Picea glauca*	1635-1975
A1703	Spruce Creek	68° 38'	138° 38'	Church	*Picea glauca*	1570-1977
A1613	Terasmae	64° 05'	138° 19'	LTRR	*Picea glauca*	1624-1964
A1707	TTHH	65° 00'	138° 20'	LDGO	*Picea glauca*	1459-1975
	TTHH Revisited	65° 00'	138° 20'	LDGO	*Picea glauca*	1499-1987
	Northwest Territories:					
	Big Bend	66° 49'	116° 04'	LDGO	*Picea glauca*	1525-1977
	Coppermine	67° 14'	115° 55'	LDGO	*Picea glauca*	1428-1977
	Finnie Flats	64° 09'	102° 35'	LDGO	*Picea glauca*	1516-1983
	Franklin Mountains	65° 21'	126° 42'	LDGO	*Picea glauca*	1615-1983
	Hornby Cabin	64° 02'	103° 52'	LDGO	*Picea glauca*	1491-1983
	Mack Mountain	65° 00'	127° 50'	LDGO	*Picea glauca*	1626-1983
	Mackenzie Delta	67° 43'	135° 23'	Giddings	*Picea glauca*	1357-1946
	September Mountain	67° 11'	116° 08'	LDGO	*Picea glauca*	1340-1977
	Soapberry Hill	64° 17'	103° 32'	LDGO	*Picea glauca*	1495-1983
I182	Thelon Game Sanctuary	63° 05'	104° 12'	Dennis	*Picea glauca*	1574-1969
	Ennadai Lake	61° 00'	101° 00'	EFisk	*Larix lariciana*	1638-1977
	British Columbia:					
	Bennington Glacier	52° 42'	118° 20'	UWO	*Pinus albicaulis*	1112-1985
	Bull Canyon	52° 06'	123° 13'	Desloges	*Pseudotsuga menziesii*	1650-1985
	Gang Ranch	51° 32'	122° 16'	FOR	*Pseudotsuga menziesii*	1590-1968
	Haney	49° 01'	133° 03'	FOR	*Pseudotsuga menziesii*	1590-1975
I343	Kamloops	50° 45'	120° 23'	LTRR	*Pseudotsuga menziesii*	1420-1965
I379	Kamloops	50° 45'	120° 23'	LTRR	*Pseudotsuga menziesii*	1505-1965
I346	Naramata	49° 36'	119° 35'	LTRR	*Pseudotsuga menziesii*	1415-1965
I339	Pavillion Lake	50° 45'	121° 33'	LTRR	*Pseudotsuga menziesii*	1460-1960
	Pavillion Lake	50° 45'	121° 41'	LTRR	*Pseudotsuga menziesii*	1480-1965
	Stuie	52° 25'	126° 03'	Desloges	*Pseudotsuga menziesii*	1579-1983
A376	Fraser River	52° 00'	122° 00'	LTRR	*Pinus ponderosa*	1420-1944
I437	Kamloops	50° 45'	120° 33'	LTRR	*Pinus ponderosa*	1590-1960
I345	Naramata	49° 36'	119° 35'	LTRR	*Pinus ponderosa*	1500-1965
	Bugaboo Glacier	50° 54'	117° 47'	FOR	*Picea engelmannii*	1590-1975
	Floe Lake	51°.03'	116° 08'	UWO	*Larix lyallii*	1523-1987
	Alberta:					
	Banff	51° 11'	115° 29'	FOR	*Pseudotsuga menziesii*	1550-1978
A132	Banff	51° 09'	115° 29'	LTRR	*Pseudotsuga menziesii*	1461-1950
A111	Exshaw	51° 04'	115° 11'	LTRR	*Pseudotsuga menziesii*	1560-1965
A131	Jasper	52° 54'	118° 04'	LTRR	*Pseudotsuga menziesii*	1537-1947
	Kananaskis	51° 05'	115° 00'	FOR	*Pseudotsuga menziesii*	1630-1979
A109	Powerhouse	51° 12'	115° 31'	LTRR	*Pseudotsuga menziesii*	1410-1965
	Pyramid and Patricia	52° 54'	118° 05'	LTRR	*Pseudotsuga menziesii*	1540-1965
	Pyramid Lake	52° 54'	118° 06'	LTRR	*Pseudotsuga menziesii*	1630-1960
I350	Tunnel Mountain	51° 10'	115° 33'	LTRR	*Pseudotsuga menziesii*	1460-1965
	Athadome	52° 13'	117° 14'	UWO	*Picea engelmannii*	1646-1980
	Columbia Icefield	52° 13'	117° 14'	FOR/UWO	*Picea engelmannii*	1323-1981
	Larch Valley	51° 20'	116° 13'	UWO	*Picea engelmannii*	1638-1986
	Robson Glacier	53° 09'	119° 07'	UWO	*Picea engelmannii*	1569-1982
	Swan Hills	55° 25'	115° 25'	FOR	*Picea glauca*	1651-1978
	Athabasca Snag	52° 13'	117° 14'	UWO	*Picea engelmannii*	1293-1898
	Peyto Lake	51° 45'	116° 13'	FHS	*Picea engelmannii*	1634-1983

Table 3. (cont.)

[1]No.	LOCALITY / NAME	COORDINATES		COLLECTOR	TAXA	YEARS
Alberta: (cont.)						
	Nakiska	50° 50'	115° 15'	UWO	*Picea engelmannii*	1616-1987
	Tyrwhitt	50° 36'	114° 59'	UWO	*Picea engelmannii*	1613-1987
	Larch Valley	51° 20'	116° 13'	UWO	*Larix lyallii*	1538-1986
	Sunshine	51° 04'	115° 47'	UWO	*Larix lyallii*	1440-1987
	Marmot Basin	50° 50'	115° 15'	UWO	*Larix lyallii*	1650-1987
	Nakiska	50° 50'	115° 15'	UWO	*Larix lyallii*	1563-1987
	Highwood	50° 36'	114° 59'	UWO	*Larix lyallii*	1559-1987
Manitoba:						
	Churchill	58° 43'	94° 04'	LDGO	*Picea glauca*	1650-1978
Ontario:						
	Dixon Lake	45° 17'	78° 02'	Cook	*Pinus resinosa*	1550-1982
	Pot Lake	45° 17'	79° 00'	Cook	*Tsuga canadensis*	1641-1982
Québec:						
	Grande Rivière de la Baleine	55° 17'	77 °47'	CEN	*Picea glauca*	1640-1986
	Richmond Gulf	56° 09'	76° 34'	LDGO	*Picea glauca*	1628-1982
	Boniface-Bush	57° 05'	76° 00'	CEN	*Picea mariana*	1305-1803
	Bush Lake	57° 47'	75° 45'	CEN	*Picea mariana*	1398-1982
	Clearwater Lake	56° 03'	75° 03'	CEN	*Picea mariana*	1630-1982
	Fort Chimo 4-L (Kuujjuaq)	58° 22'	68° 23'	LTRR	*Larix lariciana*	1650-1974
	Rivière aux feuilles	58° 15'	72° 00'	Arquiller	*Larix lariciana*	1596-1978
	Gaspé	48° 35'	65° 55'	LDGO	*Thuja occidentalis*	1404-1982
	Lac Duparquet	48° 26'	79° 21'	Archambault	*Thuja occidentalis*	802 years
	Rivière du Moulin	46° ?	71° ?	Cook	*Tsuga canadensis*	1524-1982
Labrador:						
	Saltwater Pond	56° 31'	61° 55'	LDGO	*Picea glauca*	1602-1988
	Nain	56° 27'	62° 05'	LDGO	*Picea glauca*	1574-1986

NOTES:

Archambault= S. Archambault, University of Montreal (presently CEN)
Arquilliere= S. Arquiller, Centre d'études nordiques, Université Laval
CEN = Centre d'études nordiques, Université Laval
Church = M. Church, Geography, University of British Columbia
Dennis = J. Dennis
Desloges= J. Desloges, Geography, University of Toronto
EFisk = D. Elliot-Fisk
Cook = E.R. Cook, Lamont-Doherty Geological Observatory
FOR = Forintek Canada Corporation (L. Jozsa / M. Parker)
FHS= F.H. Schweingruber
FOR/UWO= L. Jozsa / B.H. Luckman
Giddings= J. Giddings
LDGO= Lamont Doherty Geological Observatory (G. Jacoby)
LTRR= Laboratory of Tree-Ring Research, Tucson
UWO = Department of Geography, University of Western Ontario
?= data not available

[1]No.: Numbers refer to chronologies listed in either the files of the Laboratory of Tree-Ring Research at Tucson, Arizona (e.g. A376) or the International Tree-Ring Data Base (e.g. I182, also held at Tucson) for which printouts were kindly provided for Dr. M.K. Hughes in May 1989. If the chronology is listed in both only the ITRDB number is given.

The chronology data base lists 355 Canadian, 39 Alaskan and 2 Greenland chronologies (plus 93 others under development) with information (where available) on site, collector, species used, geographic location, number of samples and first and last dates of chronologies. A sample, fairly complete entry is given as Table 2. Given such a variety of sources and multiple references to sites and chronologies by authors, it is very difficult to verify discrepancies between cited chronologies without access to the original data. In some cases there are multiple chronologies from the same site (or closely adjacent sites) whereas in other cases authors may use slightly different versions of the same chronology in different papers. Attempts have been made to remove the most obvious duplication but, when in doubt, duplication has been preferred to removal. Over 300 sites have fairly complete documentation. However, the primary goal in attempting this compilation was to indicate what data are potentially available rather than to provide a data set of uniform high quality for immediate analysis. Reduction of possible errors, inconsistencies, or omissions from this data base are seen as the task of individual researchers or subsequent projects with a more specialised focus. Space does not permit a full discussion of this data

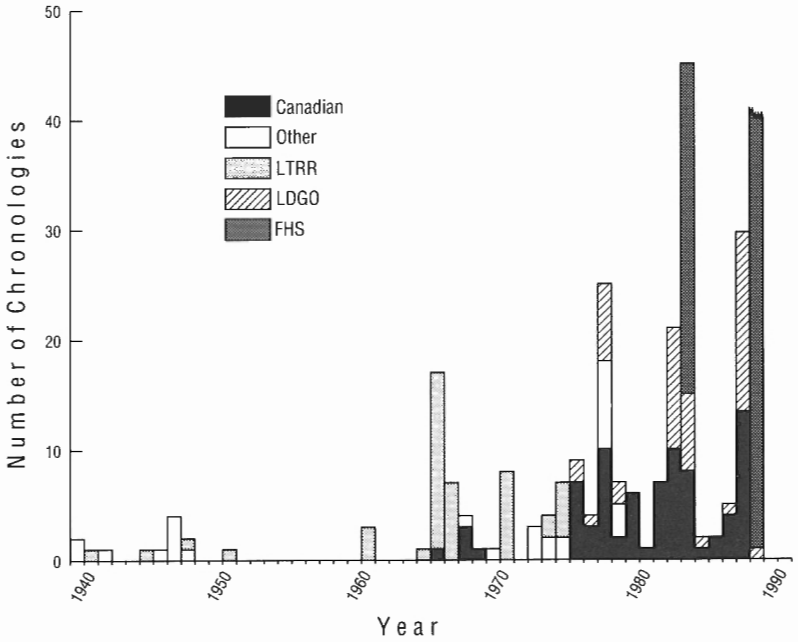

Figure 2. Last date of Canadian tree-ring chronologies.

Abbreviations used are: LTRR = Laboratory of Tree-Ring Research, Tucson; LDGO = Lamont-Doherty Geological Observatory, New York; FHS = F.H. Schweingruber, Swiss Federal Forestry Institute. The data base is the 273 chronologies listed by Luckman and Innes (1991a) for which the final date is available. The data for 1987 include 8 LDGO chronologies being processed in 1990 and the 1988 data include 40 chronologies, collected on a transect of the northern tree line between Fort Simpson and Labrador by Schweingruber and Jacoby in 1988, that had been processed by January 1991. Where multiple chronologies of the same species have been listed for a site only one is included. As the last year of the chronology is usually the year prior to collection, this distribution reflects the development of the chronology data base over time.

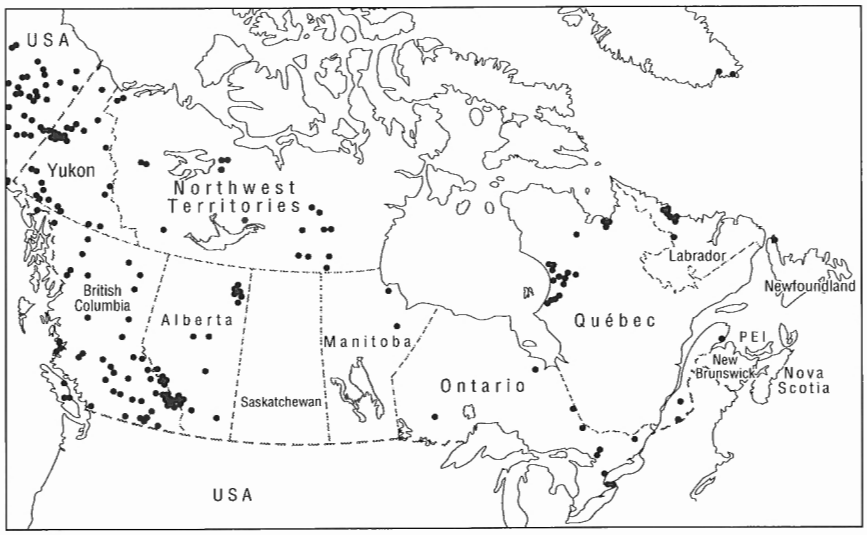

Figure 3. Distribution of Canadian tree-ring chronology sites. The data base used is the 162 Canadian sites (245 chronologies) listed in Luckman and Innes (1991a) for which latitude and longitude are given, plus some adjacent sites in Alaska and two from Greenland. These sites do not include those sampled by Schweingruber in 1988 or 8 LDGO sites collected in the Yukon and being processed in mid-1989.

base (see Luckman and Innes, 1991a, b) but, despite the imperfections, it provides a broad overview of the available data base for Canada and offers some interesting insights into the way it has been accumulated. Figure 2 shows the last date of 230 Canadian tree-ring chronologies. In most cases the last year of the chronology can be assumed to represent the year before data collection and, therefore, this figure provides a measure of chronology acquisition and, indirectly, changes in the level of interest in dendrochronology in Canada over the period shown. The geographical distribution of sites is shown in Figure 3. These two diagrams show the important contribution and spatial biasses of individual and institutional research programs that have dominated the development of this data base. About 52% of the chronologies shown in Figure 2 (excluding chronologies under development) were collected by the Laboratory of Tree-Ring Research (Tucson, 22%), Lamont-Doherty Geological Observatory (G. Jacoby, about 18%) and F.H. Schweingruber (Swiss Federal Forestry Institute, about 13%). The Canadian contribution is dominated by the work of M. Parker and Forintek Canada Corporation (about 13%) and, more recently, contributions from the Centre d'études nordiques, Université Laval (Québec-Labrador) and Department of Geography, University of Western Ontario (Canadian Rockies). The spatial biasses of the present data base are well shown in Figure 3. There are, for example, no chronologies listed from Saskatchewan or the Maritimes (Nova Scotia, Prince Edward Island, and New Brunswick), very few from southern Ontario or Quebec, and little explicit attention has been given to sampling in the west coast forests where the oldest Canadian trees occur.

A useful indicator of the paleoenvironmental potential of tree-ring series in Canada is the data shown in Table 3. Although there has been little work to date on subfossil wood, several Canadian species provide living tree chronologies in excess of 500 years. There has been little attempt to explore systematically the potential of all species or environments in Canada. Most attention has focused on spruce (61% of all chronologies) and Douglas fir, but there is considerable scope for the development of long records using larch, various pines, cedar and hemlock from a range of environments across the country. The material presented in Table 3 indicates there is excellent potential to build up regional chronologies for several areas of Canada that could span the last 500-1000 years using a variety of species.

CONCLUDING REMARKS

The bibliography and chronology data bases (Luckman and Innes, 1991a) discussed here are a first attempt to summarize the published Canadian tree-ring literature; they can clearly be expanded and improved in the future but such inventory studies are a vital prerequisite to long-term research programmes such as are envisaged in Global Change. Consolidation of available data can eliminate duplication of effort, highlight areas where data are needed (or adequate sources are already available), and may lead to the retrieval of significant information that has lain fallow for long periods of time and would be expensive or impossible to replace. National or regional data bases can also be used to address much broader issues than those for which the data were originally gathered. Growing concern about the importance of anthropogenic forcing on present and future global environmental changes, and the need for rapid action to assess the situation, underscores the need to manage existing scientific data effectively and clearly identify those areas where critical new data are needed.

ACKNOWLEDGMENTS

This project was initiated when the senior author was seconded to Terrain Sciences Division, Geological Survey of Canada and was supported under the Global Change Program of the Division. We acknowledge and thank D.A. St-Onge, D.G. Harry and R. McNeely for their advice and support. We also thank many scientists who contributed data and information incorporated into the original report; the Department of Geography, University of Western Ontario for the provision of facilities and G. Shields (UWO) for drafting the figures.

REFERENCES

Cropper, J.P. and Fritts, H.C.
1981: Tree-ring width chronologies from the North American Arctic; Arctic and Alpine Research, v. 13, p. 245-260

Fritts, H.C.
1976: Tree Rings and Climate; Academic Press, New York.

Hughes, M.K., Kelly, P.M., Pilcher, J., and LaMarche, V.C., Jr.
1982: Climate from Tree Rings; Cambridge University Press, Cambridge.

ICSU
1990: Global Change, Report no. 12 "The Initial Core Projects"; IGBP, Stockholm, Sweden.

Jacoby, G.C.
1982: The Arctic, in Climate from Tree Rings, M.K. Hughes et al.; Cambridge University Press, Cambridge, p. 107-114

Jetté, H.
1990: Geological Survey of Canada Paleoecological Data Base (abstract); in Programme and Abstracts, First Joint CANQUA-AMQUA meeting, University of Waterloo, June 4-6, 1990, p. 21

Jozsa, L.A. and Oguss, E.
1985: Climatic reconstruction from tree-rings; Forintek Canada Corp. Report to Canadian Forestry Service, Hull, Québec, 02-80-12-018, 30 p.

Luckman, B.H. and Innes, T.A.
1991: Tree-Ring studies in Canada: A bibliography and data base; Geological Survey of Canada, Open File 2379.
in press: Dendrochronology in Canada; Dendrochronologica

Payette, S., Filion, L., Gauthier, L., and Boutin, Y.
1985: Secular climate change in old-growth tree-line vegetation of northern Québec; Nature, v. 315, p. 135-138.

Robertson, E.O. and Jozsa, L.A.
1988: Climate reconstruction from tree-rings at Banff; Canadian Journal of Forest Research, v. 18, p. 888-900.

Schweingruber, F.H.
1987: Tree Rings; D. Reidel Co., Boston, 276 p.

AUTHOR INDEX

NOTE TO CONTRIBUTORS

Submissions to the Discussion section of Current Research are welcome from both the staff of the Geological Survey of Canada and from the public. Discussions are limited to 6 double-spaced typewritten pages (about 1500 words) and are subject to review by the Chief Scientific Editor. Discussions are restricted to the scientific content of Geological Survey reports. General discussions concerning sector or government policy will not be accepted. All manuscripts must be computer word-processed on an IBM compatible system and must be submitted with a diskette using WordPerfect 5.0 or 5.1. Illustrations will be accepted only if, in the opinion of the editor, they are considered essential. In any case no redrafting will be undertaken and reproducible copy must accompany the original submissions. Discussion is limited to recent reports (not more than 2 years old) and may be in either English or French. Every effort is made to include both Discussion and Reply in the same issue. Current Research is published in January and July. Submissions should be sent to the Chief Scientific Editor, Geological Survey of Canada, 601 Booth Street, Ottawa, Canada, K1A 0E8.

AVIS AUX AUTEURS D'ARTICLES

Nous encourageons tant le personnel de la Commission géologique que le grand public à nous faire parvenir des articles destinés à la section discussion de la publication Recherches en cours. Le texte doit comprendre au plus six pages dactylographiées à double interligne (environ 1500 mots), texte qui peut faire l'objet d'un réexamen par le rédacteur scientifique en chef. Les discussions doivent se limiter au contenu scientifique des rapports de la Commission géologique. Les discussions générales sur le Secteur ou les politiques gouvernementales ne seront pas acceptées. Le texte doit être soumis à un traitement de texte informatisé par un système IBM compatible et enregistré sur disquette WordPerfect 5.0 ou 5.1. Les illustrations ne seront acceptées que dans la mesure où, selon l'opinion du rédacteur, elles seront considérées comme essentielles. Aucune retouche ne sera faite au texte et dans tous les cas, une copie qui puisse être reproduite doit accompagner le texte original. Les discussions en français ou en anglais doivent se limiter aux rapports récents (au plus de 2 ans). On s'efforcera de faire coïncider les articles destinés aux rubriques discussions et réponses dans le même numéro. La publication Recherches en cours paraît en janvier et en juillet. Les articles doivent être envoyés au rédacteur en chef scientifique, Commission géologique du Canada, 601, rue Booth, Ottawa, Canada, K1A 0E8.

Geological Survey of Canada Current Research, is released twice a year. Paper 91-1, parts A to D were published in January 1991 and Paper 91-1 Part E (this volume) was published in July 1991.

Recherches en cours, une publication de la Commission géologique du Canada, est publiée deux fois par année. Les parties A à D de l'Étude 91-1 ont été publiées en janvier 1991 tandis que le partie E de l'Étude 91-1 (le présent volume) l'a été en juillet 1991.

Part A, Cordillera and Pacific Margin
Partie A, Cordillère et marge du Pacifique

Part B, Interior Plains and Arctic Canada
Partie B, Plaines intérieures et région arctique du Canada

Part C, Canadian Shield
Partie C, Bouclier canadien

Part D, Eastern Canada and national and general programs
Partie D, Est du Canada et programmes nationaux et généraux

Part E (this volume)
Partie E (ce volume)